

Synthesis and applications of poly(trisulfides)

By

Jasmine Pople

*Thesis
Submitted to Flinders University
for the degree of*

Doctor of Philosophy
Collage of Science and Engineering
11th November 2024

Contents

Abstract	II
Declaration	IV
Acknowledgements	V
Publications from work described in this thesis	VI
Chapter 1: Advances in the synthesis of high sulfur content polymers	1
Chapter 2: Electrochemical synthesis of poly(trisulfides)	24
Chapter 3: Large scale electrochemical synthesis of poly(trisulfides) and their applications	112
Chapter 4: Photochemical synthesis of poly(trisulfides) in continuous flow	172
Chapter 5: Antimicrobial and antifungal activity of poly(trisulfide)	252
Chapter 6: Conclusions and future work	286

Abstract

High sulfur content polymers have garnered significant interest in the past decade due to their excellent properties including high refractive index and electrochemical capacitance, and their low-cost feedstocks. These polysulfides are predominantly synthesised through inverse vulcanisation, an operationally simple polymerisation technique. Through inverse vulcanisation, a range of high-value polysulfides with applications in gold sorbents and lenses for infrared thermal imaging can be produced. However, inverse vulcanisation presents several challenges, including operational hazards and the production of ill-defined materials, making it difficult to scale up the production of polysulfides.

This thesis reports a novel method to produce poly(trisulfides), using electrochemistry to achieve mild and safe reaction conditions. Using well-defined sulfur containing monomers, linear poly(trisulfides) were produced through an electrochemically-initiated ring-opening polymerisation. Through computational and experimental studies, the synthesis of linear poly(trisulfides) with a known sulfur rank of three was demonstrated for the first time. Additionally, a key poly(trisulfide) was shown to be fully recyclable back to its monomer unit, allowing for a closed-loop recycling system.

Upscaling of the electrochemical synthesis of poly(trisulfides) was validated through the design of large-scale batch and continuous flow electrochemical reactors, achieving a 20-fold increase in reaction output. With sustainability in mind, the electrolyte solution was shown to be recyclable.

High sulfur content polymers have shown excellent metal binding properties. A water-soluble poly(trisulfide) with a known sulfur rank was produced for the first time and exhibited enhanced metal binding properties compared to non-water soluble polysulfides. Another key poly(trisulfide) was explored as a fully recyclable gold sorbent. This development was a significant achievement in polysulfide applications, as typical polysulfides produced through inverse vulcanisation cannot be recycled due to cross-linking and their ill-defined structure.

The photochemical production of linear poly(trisulfides) was developed to establish a method for producing high molecular weight materials. This was achieved by controlling the amount of light irradiation through a continuous flow photochemical reactor. Photochemical continuous flow synthesis offered the production of poly(trisulfides) on a large scale.

Water-soluble poly(trisulfides) were shown to exhibit antimicrobial and antifungal properties. This marked the first exploration of the biocidal properties of high sulfur content polymers with a well-defined structure and a known sulfur rank of three.

These achievements demonstrated the ability to produce polysulfides using safe and sustainable techniques that employ electrochemical or photochemical initiation. By polymerising fully characterised sulfur-containing monomers, well-defined polysulfides with a known sulfur rank of three were produced. The recyclability of poly(trisulfides) and their abundant starting material enhances the sustainability of these polysulfides. Key poly(trisulfides) were validated in a range of applications which was enabled by their well-defined linear structure. The upscaling of both electrochemical and photochemical polymerisation resulted in the safe multi-gram production of poly(trisulfides).

Declaration

I certify that this thesis does not incorporate without acknowledgment any material previously submitted for a degree or diploma in any university; and the research within will not be submitted for any other future degree or diploma without the permission of Flinders University; and that to the best of my knowledge and belief it does not contain any material previously published or written by another person except where due reference is made in the text.

Signed: Jasmine Pople

Date: 17th July 2024

Acknowledgement

I want to thank my supervisor Professor Justin Chalker for the opportunity to complete my PhD under his guidance. Over the past four years, your innovative ideas, captivating talks and discussions, and meticulous attention to detail have truly inspired me. You have shaped me into the person I am today, constantly encouraging and supporting me to seize every opportunity. I cannot thank you enough for all you have done. I want to thank my co-supervisor Associate Professor Mike Perkins for his continued guidance and assistance. I would also like to thank Dr. Tom Hasell for welcoming me into his lab at Liverpool University to complete part of my PhD research.

I want to thank all of the larger synthesis group for their friendship and support. It has been a pleasure to work alongside you all. A special thank you to Dr Thomas Nicholls for your mentorship and guidance.

I want to thank my family and my partner, without their love and support I could not have made this journey.

I would like to acknowledge the Australian Government for providing an Australian Government Research Training Program Scholarship.

Lastly, I want to thank all the people and staff at Flinders University and Liverpool University for their assistance, knowledge and willingness to help.

Publications from work described in this thesis

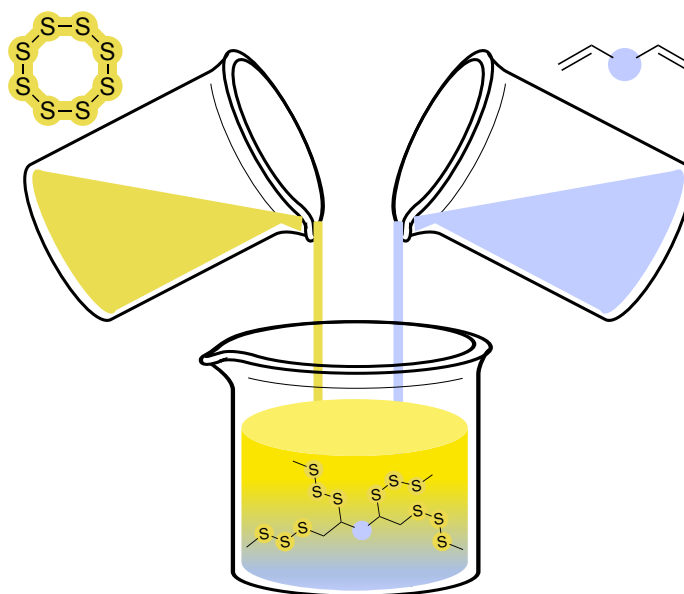
Electrochemical synthesis of poly(trisulfides)

Pople, J. M. M.; Nicholls, T. P.; Pham, L. N.; Bloch, W. M.; Lisboa, L. S.; Perkins, M. V.; Gibson, C. T.; Coote, M. L.; Jia, Z.; Chalker, J. M. J. *Am. Chem. Soc.* 2023, 145, 11798-11810

Chapter 1

Advances in the synthesis of high sulfur content polymers

This chapter highlights the challenges associated with high sulfur content polymer synthesis, including high temperature processes which can result in dangerous runaway reactions. Several new methods of polysulfide synthesis are showcased, addressing some of these concerns by introducing milder and safer reaction conditions. However, one challenge that has yet to be addressed is the synthesis of well-defined high sulfur content polymers.



Abundance of elemental sulfur and its applications

Elemental sulfur is a vibrant yellow, naturally occurring eight-membered heterocycle (Figure 1.1).^[1] Elemental sulfur is highly abundant in nature in geological deposits. However, it is not commonly mined due to the production of millions of tons of elemental sulfur by the oil and natural gas industries.^[2] Elemental sulfur is the product of crude oil and natural gas desulfurisation processes. It is important to reduce the content of sulfur compounds in crude oil to reduce emissions during fuel combustion, such as sulfur oxides (SO_x).^[3] Additionally, it is essential to remove sulfur by-products like H_2S from natural gas due to its toxicity, unpleasant odour, and corrosive nature.^[4] The removal of sulfur compounds from crude oil and natural gas is a two-step process. First, sulfur compounds are converted into H_2S through hydrodesulfurisation.^[5] Next, H_2S is combined with SO_2 and converted into elemental sulfur and water through the Claus process.^[6-7] Stockpiles of elemental sulfur now exist around the world due to its large-scale production from these industries (Figure 1.1).

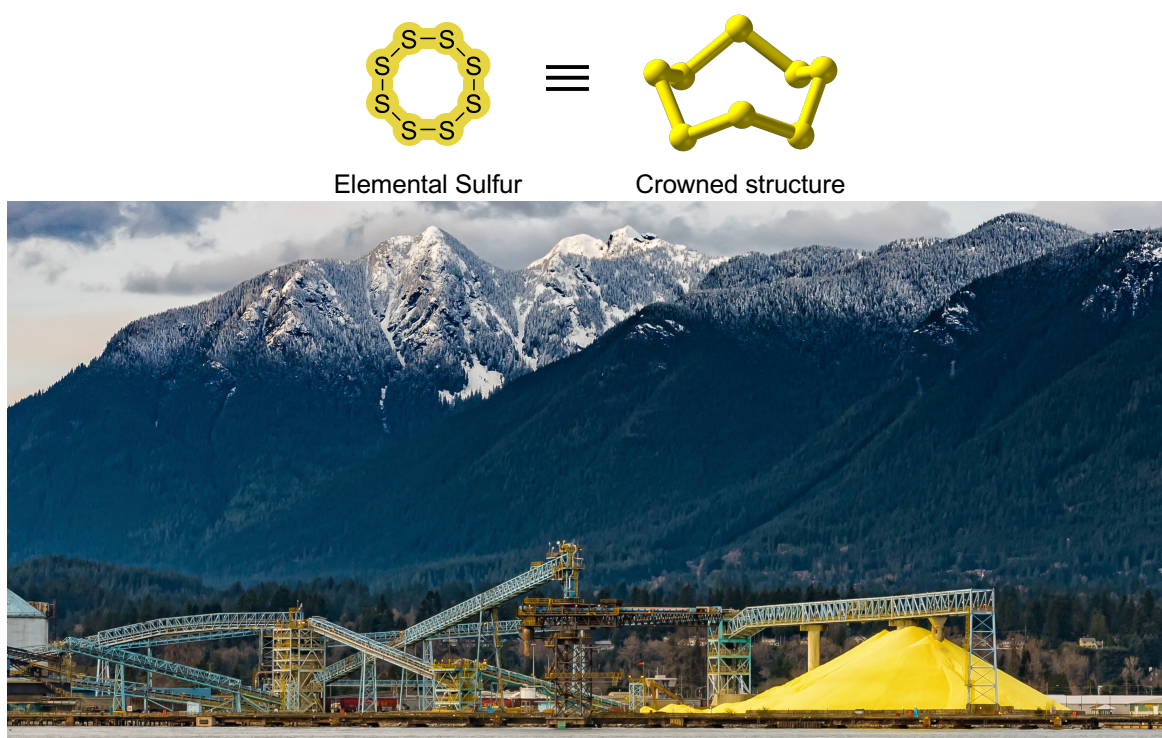
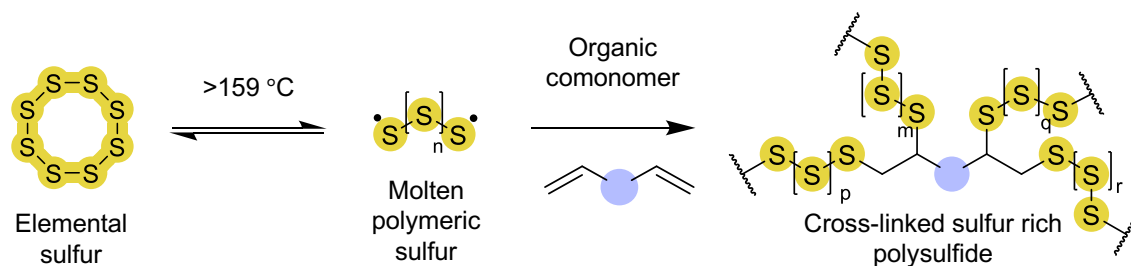


Figure 1.1: Structure of elemental sulfur (top). Stockpile of elemental sulfur at a shipping yard (bottom). Image credit: Coral Norman. This image was reproduced under a Creative Commons License: CC BY 4.0.

The most common application for elemental sulfur is the production of sulfuric acid.^[8] Sulfuric acid is produced on a scale of hundreds of millions of tons yearly and used in a range of applications including fertilisers and batteries.^[9] Although the demand for sulfuric acid is forecast to increase in the coming years, its demand is not as much as the billions of tons of elemental sulfur being produced. The build-up of elemental sulfur stockpiles can be detrimental to the environment if not stored and maintained correctly. Negative impacts can be caused by oxidation of sulfur to sulfuric acid, which can then enter groundwater, or the spreading of sulfur ‘dust’ into the environment.^[10]

A potential outlet for elemental sulfur is the production of high sulfur content polymers (polysulfides).^[11] Over the past decade, there has been increased interest in the research and development of polysulfide synthesis and applications.^[12] Converting elemental sulfur into useful chemical substances like polysulfides is an efficient use of the by-product and provides an outlet for the growing stockpiles of elemental sulfur.

The use of sulfur in polymers began more than a century ago when Charles Goodyear developed the method of vulcanisation by treating rubber (i.e. polyisoprene) with sulfur at high temperatures.^[13] This produced a material with improved chemical and physical properties. However, the process of vulcanisation only incorporated small amounts of sulfur (approximately 3-5 wt.%) into a premade polymeric material. To truly harness the desired properties of sulfur-containing polymers, such as its high refractive index and electrochemical activity, a higher weight percent of sulfur must be incorporated. Pure elemental sulfur has been known to self-polymerise under high temperature, resulting in an unstable polysulfide made from 100% sulfur.^[14] When elemental sulfur is heated above 159 °C, it becomes a molten liquid, and the S–S bonds undergo homolytic cleavage, revealing thiyl radicals (Scheme 1.1). These radicals attack and open the ring of neighbouring sulfur molecules, leading to ring-opening polymerisation. However, polymerised sulfur is not stable and depolymerises back to elemental sulfur due to backbiting of unquenched terminal sulfur radicals.^[14] In 2013, Pyun and co-workers developed the method of inverse vulcanisation to produce high sulfur content polymers (30–90 wt.% sulfur) with the aim of making functional polysulfides while utilising elemental sulfur as a feedstock.^[11] The synthesis of polysulfides via inverse vulcanisation was achieved by introducing alkene containing comonomers to molten sulfur to react with and quench the thiyl radical groups, producing a stable, high sulfur content polymer (Scheme 1.1). Possible routes of termination for the polymerisation could be radical recombination.



Scheme 1.1: Reversible ring-opening polymerisation of elemental sulfur at high temperature followed by irreversible crosslinking of polymeric sulfur with an organic comonomer.

Applications of polysulfides

In recent years, the field of sulfur polymer chemistry has developed rapidly with an influx of innovative strategies to produce high sulfur content polymers that harness the chemical and physical properties of sulfur to create functional materials. Elemental sulfur possesses high electrochemical capacitance and a high refractive index. Through the synthesis of polysulfides, these properties can be combined with improved chemical and processing characteristics inherent to their polymeric structure.

Several groups have been using inverse vulcanisation to produce high sulfur content polysulfides that act as cathode materials in lithium-sulfur batteries.^[15-18] Using polysulfides over pure elemental sulfur helps to prevent capacity decline by securing the sulfur adducts in a polymer network. Pyun and co-workers showed the electrochemical performance of poly(sulfur-*r*-1,3-diisopropenylbenzene), which was reported to contain 90 wt.% sulfur.^[17, 19] They found the material to have a stable capacity of 1005 mAhg⁻¹ after 100 cycles and battery lifetimes over 500 cycles at a 10-hour discharge. Several other research groups have improved the capacity and lifetime of batteries made with polysulfides by altering the organic comonomer used.^[15, 18]

Organic polymeric materials with high refractive indices ($n > 1.75$) are difficult to produce and usually exhibit strong absorbance in the mid-wave (3–5 microns) and long-wave (8–12 microns) infrared window due to strong C–H stretching and bending signals.^[20] A solution to this problem is the incorporation of large amounts of elemental sulfur into polymeric material, reducing the absorbance in the infrared window while providing a high refractive index. Polysulfides made by inverse vulcanisation, such as poly(sulfur-*r*-1,3-diisopropenylbenzene) have been reported to have a refractive index of $n = 1.75$ – 1.85 and sufficient transparency in the infrared window to make a suitable lens for infrared thermal imaging.^[21] Modern advancements to traditional inverse vulcanisation have widened the scope of organic comonomers that can be polymerised with elemental sulfur to produce exceptional lenses for infrared thermal imaging ($n = 1.85$ – 1.90 at 1 mm

thick).^[22] These lenses offer a low-cost alternative compared with traditional infrared imaging lenses like germanium, which are many times more expensive.^[22]

Another valuable property of sulfur is its ability to bind to soft metals.^[23] Polysulfides act as excellent sorbents for the remediation of toxic metals like mercury from the environment.^[24] Polysulfides also show high selectivity for gold from complex metal mixtures, making them inexpensive and environmentally friendly gold sorbents for the mining and electronic waste recycling industries.^[25] Polysulfides have also been shown to have high strength and resistance against solvents and acids, making them suitable materials for adhesives and composites^[25-27]. These polysulfides contain many S–S covalent bonds that are dynamic and can be cleaved chemically,^[28-29] thermally,^[30] or via UV/visible irradiation.^[31] This allows polysulfides to be restored if damaged or molded into new shapes. These are just a few of the applications that polysulfides with high sulfur content can provide.

Challenges of high sulfur content polysulfide synthesis

The production of functional sulfur rich polysulfides creates an outlet for the millions of tons of elemental sulfur produced every year by the petroleum and related industries. Yet, high sulfur content polysulfide synthesis is challenging due to the insolubility of elemental sulfur in common organic solvents and the limited range of chemical substances that are miscible in molten elemental sulfur.^[32] The recent discovery of inverse vulcanisation, which allows the use of molten elemental sulfur to act as a reaction medium and comonomer in the process to form chemically stable polysulfides, helps to overcome this long standing challenge.^[11] Despite the effectiveness of inverse vulcanisation and related methods to produce high sulfur content polymers, there still remains several challenges related to this method.

There have been several reports of polysulfide synthesis via inverse vulcanisation that led to dangerous runaway reactions caused by autoacceleration, known as the Trommsdorf effect.^[16] The Trommsdorf effect causes rapid overheating of the polymerisation mixture, leading to copolymer decomposition and the vigorous production of toxic gaseous by-products such as H₂S. Dangerous runaway reactions that occur during inverse vulcanisation have been reported on several occasions.^[33] A classic example of this effect is the inverse vulcanisation of elemental sulfur and dicyclopentadiene. At high temperatures, this polymerisation can produce an exotherm that leads to an uncontrollable spike in reaction temperature, resulting in a hazardous runaway reaction (Figure 1.2). Increasing the scale of these reactions also increases the likelihood of runaway reactions to occur, making the large-scale production of polysulfides challenging. Another limitation of inverse vulcanisation, associated with its high temperature, is its incompatibility with many organic

comonomers, many of which are volatile.^[34] The incompatibility may also be caused by immiscibility of organic comonomers with molten sulfur, leading to phase separation and incomplete reactions.^[29] Inverse vulcanisation is a highly energy intensive process due to high temperatures required to form molten sulfur and induce its ring-opening polymerisation (typically 160 °C or higher).^[11]

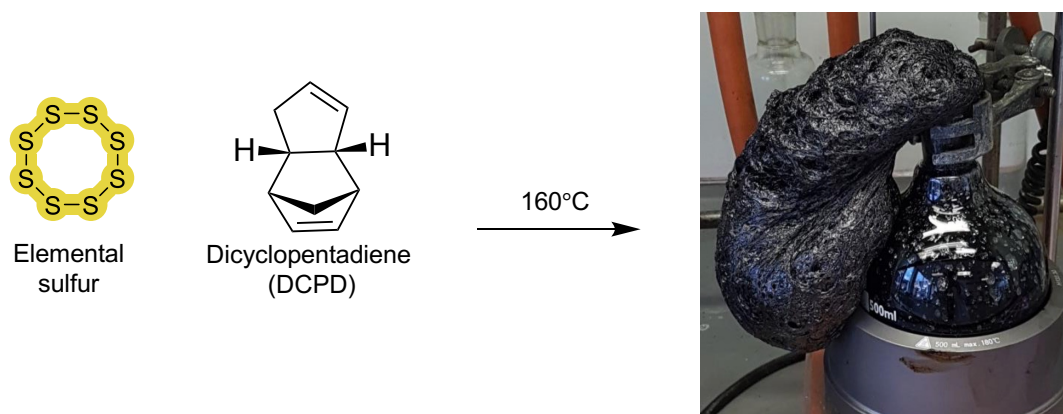


Figure 1.2: Autoacceleration reaction between sulfur and dicyclopentadiene. According to the authors, ‘Within a few seconds it boiled up violently to overflow the container, venting gas, and volatilised monomer, before rapidly setting as a solid.’^[35] © 2019, Xiaofeng Wu et al, Nature Communications. This image was reproduced under a Creative Commons License: CC BY 4.0.^[35]

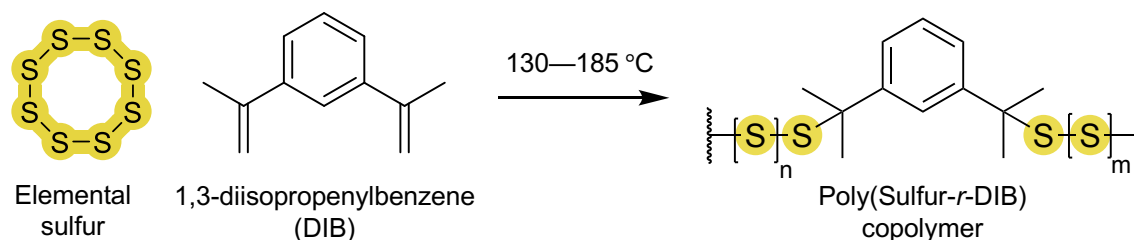
Polysulfide synthesis through inverse vulcanisation with dienes or polyenes leads to highly crosslinked polymeric structures, making many of these materials insoluble in organic solvents. This makes it challenging to characterise their structure using standard solution-based techniques such as Nuclear Magnetic Resonance (NMR) and Gel Permeation Chromatography (GPC). Additionally, there is limited control over polymer molecular weight, stereochemistry, and sulfur rank (the number of sulfur atoms that connect each organic monomer).^[36] Control over these features is important for regulating the chemical and physical properties of the material. For instance, it is known that sulfur rank influences the strength of S–S bonds.^[37-38] Therefore, controlling sulfur rank will lead to controlling the strength of the material along with other properties.

Several research groups have developed innovative solutions to address some of the above challenges. This includes alternative procedures to achieve high sulfur content polysulfide synthesis such as reducing reaction temperature,^[16] addition of catalysts,^[35] sulfur chemical vapour deposition,^[39] initiation by mechanochemical forces^[34] or UV light,^[31] and the strategic design of a polymer reactor compatible with gaseous monomers.^[22] Polysulfide synthesis through ionic pathways has also seen advancements in recent years, resulting in mild synthesis conditions.^[40-41]

In this review, the focus will be on atom-economical inverse vulcanisation processes and so related processes like poly-condensation polysulfide synthesis methods will not be covered.

High temperature inverse vulcanisation

The method of inverse vulcanisation, developed by Pyun and co-workers in 2013, uses molten elemental sulfur at high temperature to achieve stable high sulfur content polysulfides.^[11] Molten elemental sulfur acts as the solvent, initiator and comonomer, resulting in an operationally simple polymerisation process. Pyun and co-workers demonstrated the copolymerisation of 1,3-diisopropenylbenzene (DIB) and molten sulfur at 185 °C within 10 minutes, leading to complete vitrification (Scheme 1.2).^[11, 42] DIB is added after the sulfur is melted to intercept the thiyl radical chain ends. DIB was chosen as it is miscible in molten sulfur and not volatile at the high temperatures, resulting in homogenous polymerisation. In the pursuit of kilogram-scale production of polysulfides via inverse vulcanisation, the reaction temperature must be reduced to moderate the risk of dangerous runaway reactions. Pyun and co-workers lowered the reaction temperature from 185 °C to 130 °C for the 1 kg production of poly(sulfur-*r*-DIB) (Scheme 1.2).^[16] Lowering the reaction temperature proved successful for producing a stable polysulfide material, but internal temperature measurements showed the reaction reached 160 °C. Therefore, there still remains the danger of internal temperature spiking for large-scale polymerisations leading to run-away reactions.

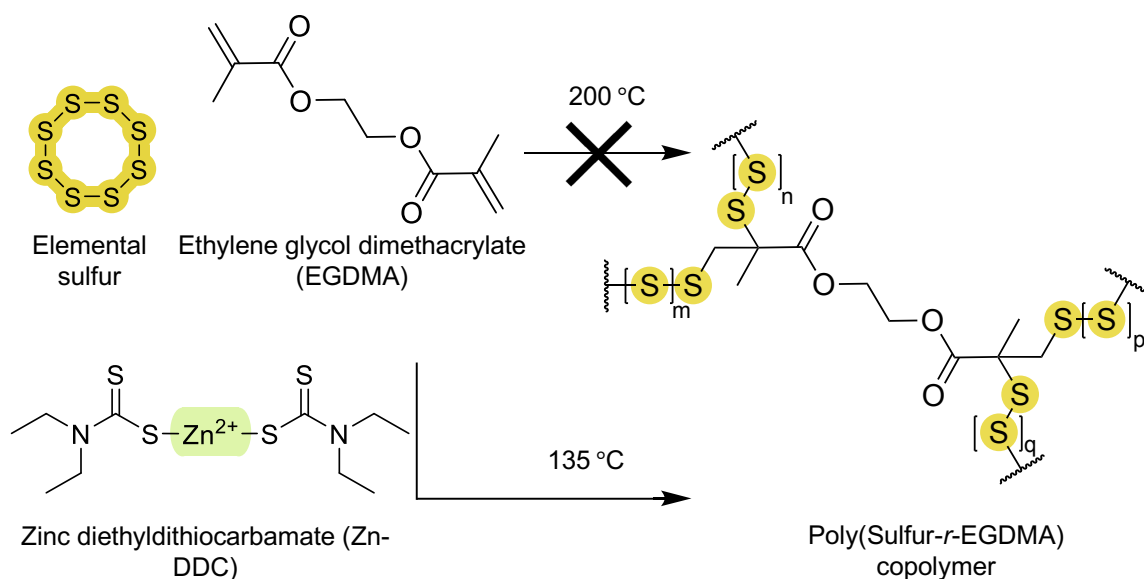


Scheme 1.2: Copolymerisation of elemental sulfur and DIB via inverse vulcanisation.

Catalytic inverse vulcanisation

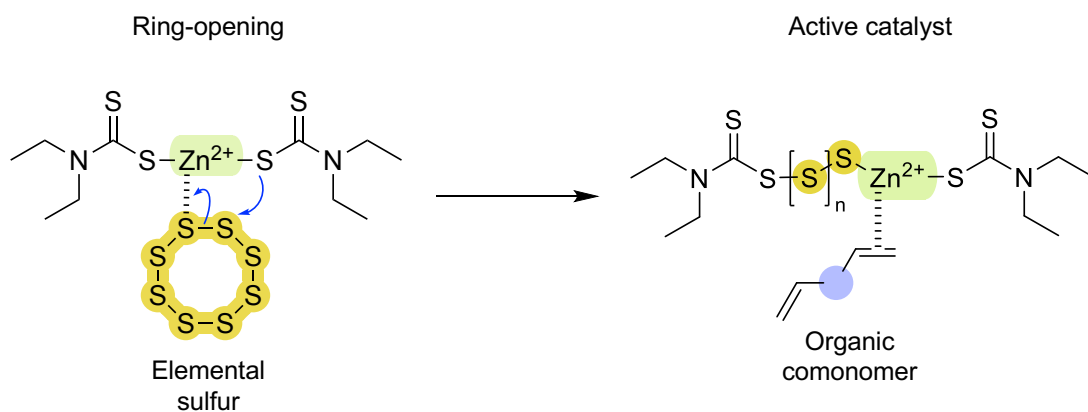
The range of organic comonomers for polymerisation through inverse vulcanisation is limited to non-volatile species due to the high temperature required to achieve ring-opening polymerisation of elemental sulfur. To include species with lower boiling points and less reactive monomers, catalysts have been introduced to reduce the temperature required to achieve inverse vulcanisation. Catalytic inverse vulcanisation allows for the reduction of reaction temperature by lowering activation energy as well as reducing the formation of toxic H₂S gas.^[35] In 2019, Hasell and co-workers achieved inverse vulcanisation between 100–135 °C via the addition of metal diethyldithiocarbamate (DDC) catalysts (1 wt.%) (Scheme 1.3).^[35] Through the addition of Zn-DDC

catalyst, ethylene glycol dimethacrylate (EGDMA) can be copolymerised with elemental sulfur – a comonomer that was previously unreactive with sulfur at temperatures below 200 °C. Addition of metal-DDC catalysts also allowed for reaction time to be drastically reduced.^[35, 43]



Scheme 1.3: Copolymerisation of elemental sulfur and EGDMA via inverse vulcanisation. Uncatalyzed at 200 °C the reaction does not proceed. Addition of Zn-DDC results in copolymerisation at 135 °C.

The mechanistic details for how the catalyst aids in the polymerisation are not fully clarified. However, several mechanistic suggestions have been made. It is proposed that the metal-DDC catalysts aid in the ring-opening of elemental sulfur at reduced temperature by weakening S–S bonds.^[35] The sulfur can coordinate with the metal centre in the catalyst, activating it, and transferring the sulfur in-between the metal and ligand (Scheme 1.4). This brings the sulfur into proximity with the crosslinker, followed by bond formation between the two. It is also proposed that the ligand can act as a nucleophile, aiding in the cleavage of S–S and C=C bonds.^[44] Another proposal is that the metal-DDC catalysts, after reaction with sulfur (Scheme 1.4), acts as a phase transfer agent shuttling sulfur into the organic monomer phase.^[44]



Scheme 1.4: Proposed mechanism of sulfur ring-opening and coordination to comonomer via Zn-DDC catalyst.

Catalytic inverse vulcanisation has advanced high sulfur content polysulfide synthesis by allowing inverse vulcanisation to occur below the melting point of sulfur. Research has been conducted into different types of catalysts to reduce the temperature of inverse vulcanisation reactions. However, catalytic inverse vulcanisation still requires high temperatures (100–135 °C), limiting the library of organic comonomers to those that are not volatile or thermally sensitive.

Sulfur chemical vapour deposition

Sulfur chemical vapor deposition (sCVD) was developed by Im and co-workers in 2020 as a method to achieve high refractive index polysulfides for applications in optoelectronic devices.^[39] A high refractive index is considered to be $n > 1.8$ for inorganic semiconductors used in advanced optical devices.^[39] During sCVD, vaporised sulfur and vinyl comonomer are sprayed onto a substrate where they undergo thermally induced inverse vulcanisation to form a thin film. Through bulk inverse vulcanisation of elemental sulfur and organic monomers such as DIB or norbornadiene, polysulfides with $n > 1.8$ can be produced.^[45-46] However, these polysulfides exhibit strong absorption in the visible range, resulting in their opaque appearance. Through sCVD, high refractive index polysulfides with full transparency over the visible spectrum can be achieved. Bulk inverse vulcanisation also results in rapid vitrification making polymer processing highly challenging. On the other hand, sCVD allows for the direct deposition of thin, uniform, and homogeneous films onto a substrate, which is advantageous for polysulfide film generation (Figure 1.3).

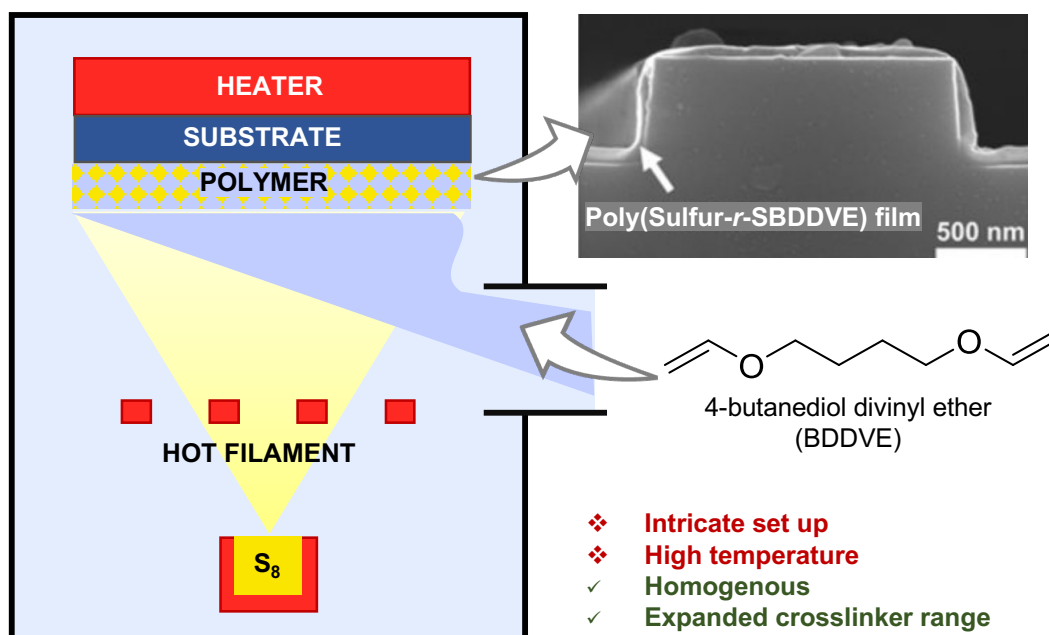


Figure 1.3: Illustration of the sCVD system (left). A scanning electron microscope image of the 1600-nm nanopatterned Si wafer coated conformally with 60-nm-thick poly(Sulfur-*r*-SBDDVE) film (right). © 2020 Kim et al, Science advances. This image was reproduced under a Creative Commons License: CC BY 4.0.^[39]

The equipment and set-up involved in polysulfide synthesis through sCVD is complex, requiring temperature controlled heated sources, heating filaments, and vaporisers to spray elemental sulfur and the desired comonomer onto a substrate (Figure 1.3). The substrate requires a specific temperature window (110–135 °C) to ensure monomer/oligomer adsorption and polymer propagation. The heated filaments are maintained at 350 °C for the constant generation of sulfur radicals produced through homolytic ring-opening. Vaporised comonomers from an adjacent cell saturate the sulfur radicals as they are deposited onto the substrate resulting in a homogenous polysulfide thin film. This method allows the polymerisation of vinyl-containing comonomers which have not been previously successful via inverse vulcanisation due to their immiscibility in liquid elemental sulfur. For example, 1,4-butanediol divinyl ether (BDDVE) (Figure 1.3) and di(ethylene glycol)divinyl ether (DEGDVE) were copolymerised with elemental sulfur for the first time using sCVD. The film produced via sCVD from BDDVE showed a refractive index of 1.91 at a width of 632.8 nm and had high optical transparency in the entire visible light region.

sCVD is a unique method to produce high refractive index, transparent, and homogenous polysulfide films directly onto a substrate. Im and co-workers developed this method to allow the homogenous polymerisation of monomers which are otherwise immiscible in elemental sulfur during bulk inverse vulcanisation. However, a drawback of sCVD is the specialised equipment required to achieve this polymerisation which is not typically found in research laboratories. The

high temperature needed to maintain the production of sulfur radicals is energy intensive and hazardous. However, sCVD may be necessary for specific applications requiring thin polysulfide films with high refractive indices and optical transparency.

Mechanochemical inverse vulcanisation

In 2022, Hassell and co-workers used the concept of mechanochemistry to synthesise crosslinked polysulfides at room temperature.^[30] The purpose of this room temperature approach to polysulfide synthesis was to reduce the risk of runaway reactions, H₂S gas production, and polymer degradation present in high temperature inverse vulcanisation. Using mechanical energy rather than thermal energy provides a safer and environmentally friendly approach to polysulfide synthesis which is reported to have shorter reaction times, homogeneity and high atom economy.^[30] Additionally, room temperature synthesis allows for a broad range of organic comonomers to be used including volatile species.

Using a commercially available ball mill, Hassell and co-workers combined elemental sulfur and organic crosslinkers such as DIB and styrene along with steel milling balls which agitate the monomers with mechanical force, causing them to react (Figure 1.4).^[30] It was hypothesised that the polysulfide structure produced during ball milling would be complementary to inverse vulcanised polysulfides. Therefore, to test this theory, polysulfides containing the same monomers were synthesised by inverse vulcanisation and their physical and chemical properties were compared. They found crosslinked polysulfides such as poly(sulfur-*r*-DIB) made through ball milling had a much lower glass transition temperature compared to the relevant inverse vulcanised polysulfide. Whereas linear or branched polysulfides such as poly(sulfur-*r*-styrene) had slightly higher glass transition temperature values. All polysulfides produced by ball milling were insoluble in THF and chloroform regardless of their linear or cross-linked structure, which is unusual. Therefore, to understand the insolubility of polysulfides produced via ball milling, energy dispersive spectroscopy (EDS) of the polysulfides was conducted and revealed a significant presence of iron in the polymers indicating iron filings from the steel milling balls are present within the polysulfide network (Figure 1.4).

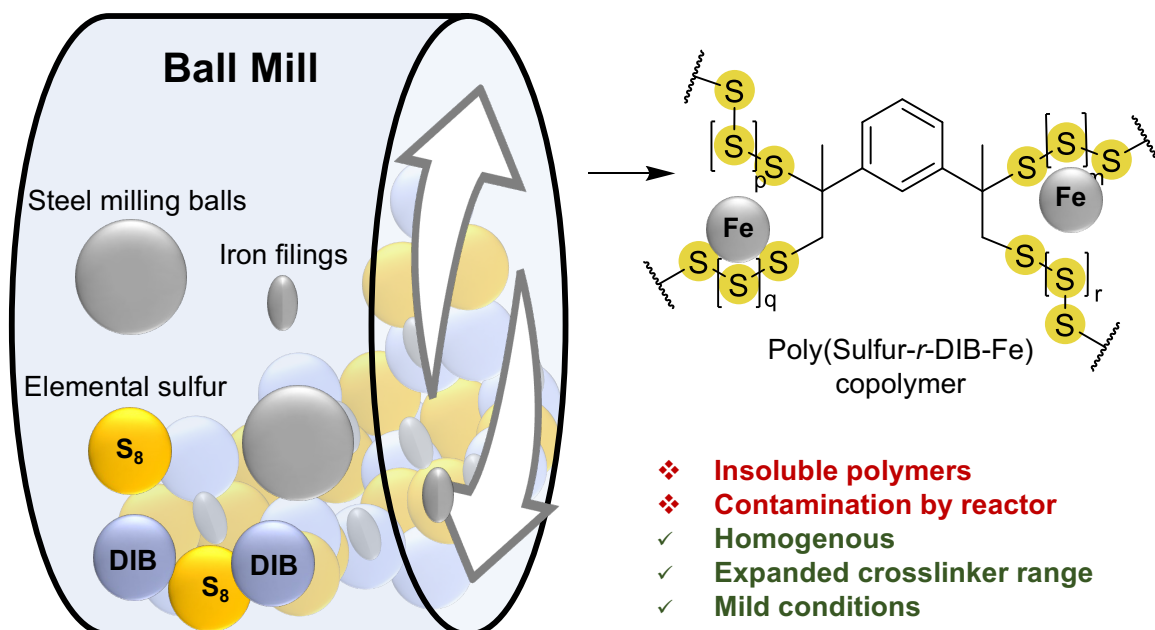


Figure 1.4: Illustration of ball mill and the contamination of iron fillings into the polysulfide network.

The presence of iron in the polysulfides prevents characterisation by solid state NMR spectroscopy, which is a drawback for structure analysis. Additionally, the insolubility of the polysulfides results in greater processing challenges when trying to scale up the reaction. However, it is worth noting that volatile monomers such as isoprene (b.p. 34 °C) were successfully polymerised in the ball mill reactor, a polysulfide synthesis which would not be possible via high temperature inverse vulcanisation. The mild, simple, and rapid conditions of polysulfide synthesis through ball milling are highly attractive for potential large-scale polysulfide applications.

Photoinduced inverse vulcanisation

There is longstanding precedence for photochemical synthesis of polysulfides.^[47-48] However, little research has been done since these initial studies. This was until Hasell, Quan, and co-workers used photochemistry for the copolymerisation of elemental sulfur and organic comonomers in 2022.^[31] They developed a synthetic method which allowed a diverse range of crosslinkers with low boiling points to be polymerised with sulfur which is not possible by high temperature inverse vulcanisation. Photoinduced polysulfide synthesis is also favourable because it can be conducted under ambient conditions, reducing the dangers associated with high temperature inverse vulcanisation including runaway reactions and H₂S gas production, while also being less energy intensive.

The photopolymerisation reactions were conducted in a small quartz cell lined with a mixture of elemental sulfur and organic comonomer (Figure 1.5). The photopolymerisation was

tested at 520 nm, 380 nm, 435 nm, with 435 nm being the most effective, while no polymerisation occurred at 520 nm. To test the homogeneity of the polymerisation, polymer samples were taken from different areas in the reaction vessel and analysed by thermal gravimetric analysis. The authors found that different areas in the vessel had different thermal stability, indicating different levels of polymerisation. This is likely due to different levels of light intensity at different locations in the vessel.

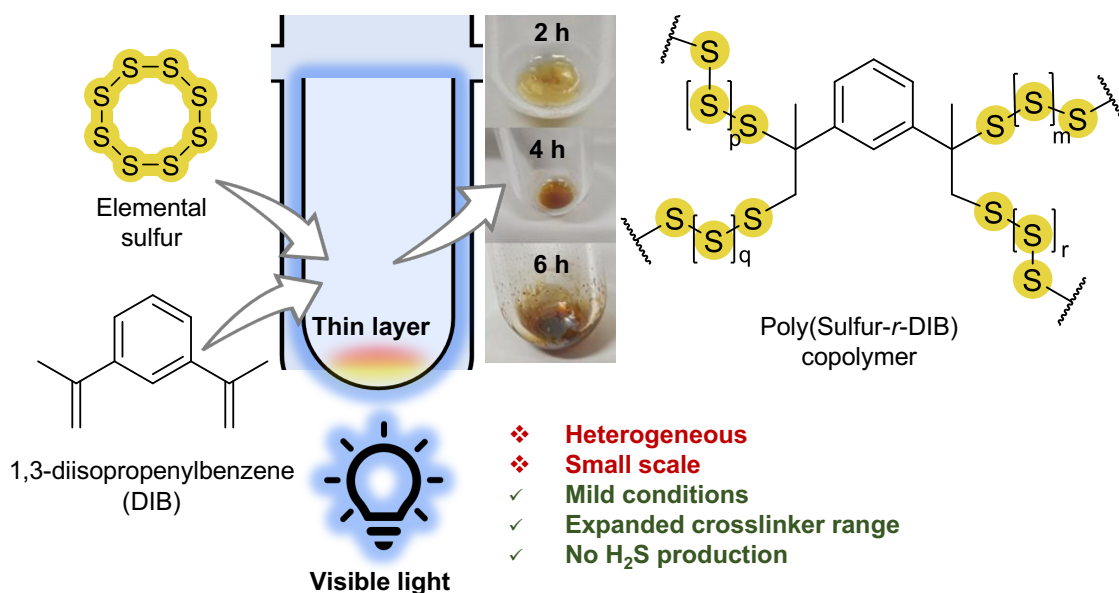


Figure 1.5: Illustration of photoreactor used to produce a thin layer of poly(sulfur-*r*-DIB). Images show appearance of reaction mixture over time. © 2022, Jinhong Jia et al, Springer Nature Limited, Nature Chemistry. This image was reproduced under a Creative Commons License: CC BY 4.0.^[31]

UV-visible spectroscopy of elemental sulfur shows broad absorption between 200–450 nm, while DIB absorbs UV light below 350 nm. It is proposed that light irradiation induces homolytic ring-opening of elemental sulfur, forming free radicals that can then react with alkene or alkyne groups on the organic comonomer. It is hypothesised that the reaction proceeds less efficiently at 380 nm compared to 435 nm due to competing reactions. Photopolymerisation at 435 nm was tested on a range of low-boiling point alkenes and alkynes such as vinyl chloride and propyne. ¹H NMR spectra of the reactions showed close to, or complete conversion of the low boiling point monomers, validating the method and aims of the authors. The room temperature polymerisation of low-boiling point monomers expands the library of sulfur-rich polymers for potential applications.

Inverse vulcanisation using gaseous organic monomers

In 2023, Chalker and co-workers designed a novel reaction set up to achieve high temperature inverse vulcanisation with a volatile comonomer.^[22] Their aim was to incorporate cyclopentadiene (b.p. 42.5 °C) as the comonomer for the synthesis of a polysulfide with application as a lens material for infrared optical devices. Cyclopentadiene was chosen as the organic comonomer as it would provide limited modes of vibration, especially in the long wave infrared region, leading to increased transparency. Through a standard reaction set up, cyclopentadiene copolymerises poorly with molten sulfur due to its high volatility and spontaneously undergoes a Diels–Alder reaction with itself, forming dicyclopentadiene, which has a higher boiling point and will copolymerise with elemental sulfur.^[22] Therefore, Chalker and co-workers developed a reaction set up where gaseous cyclopentadiene is pumped directly into molten sulfur resulting in homogenous copolymerisation (Figure 1.6).

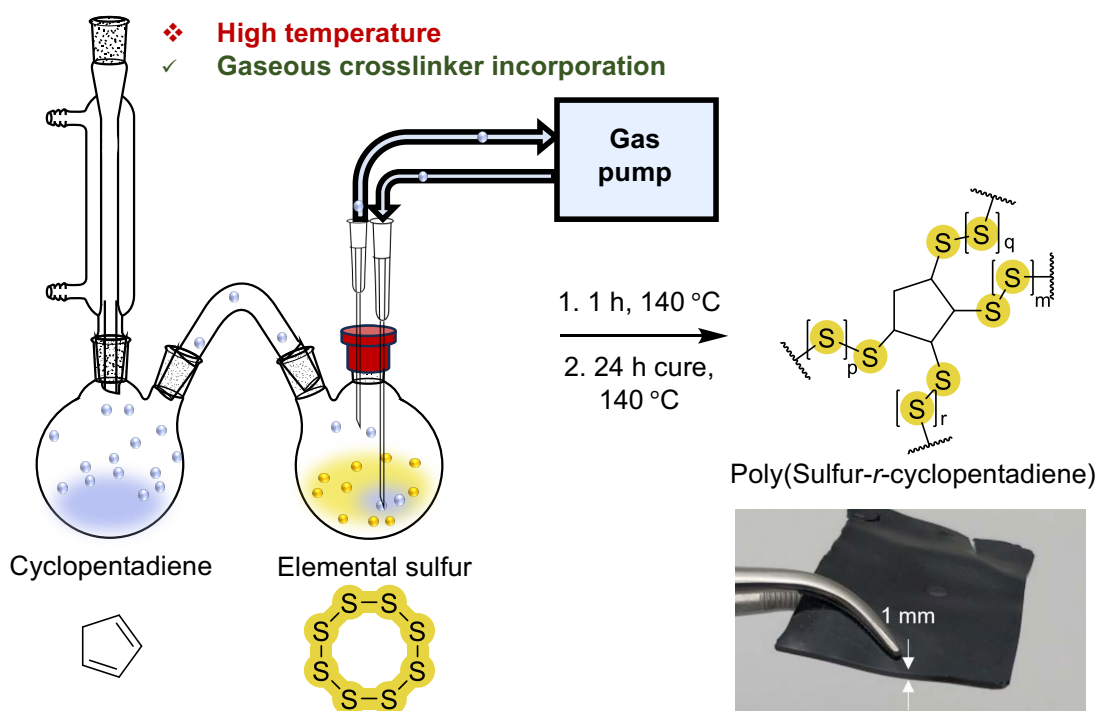


Figure 1.6: Illustration of gas pumped inverse vulcanisation of cyclopentadiene with elemental sulfur. Image shows 1 mm thick poly(Sulfur-*r*-cyclopentadiene) window. © 2023 Tonkin et al, Advanced Optical Materials, Wiley-VCH GmbH. This image was reproduced under a Creative Commons License: CC BY 4.0.^[22]

Figure 1.6 shows the design for the copolymerisation of sulfur and cyclopentadiene. One round bottom flask contains refluxing cyclopentadiene. The gaseous cyclopentadiene then travels to an adjacent round bottom flask which contains molten sulfur and a gas pump via a glass connecting

tube. The inlet of the gas pump is in the headspace of the flask and the outlet pumps the gaseous cyclopentadiene into the molten sulfur at a rate of 500 mL/min. After 60 minutes of reaction, the resulting viscous black solution is poured into a silicon mould and cured for 24 hours at 140 °C. The cured poly(sulfur-*r*-cyclopentadiene) can be produced as free-standing windows (1 mm thick). The transmittance of the polymer windows in the mid wave infrared region was among the highest reported for synthetic polymers at the time and its refractive index was between $n = 1.85\text{--}1.90$.^[22] Using this method, the Chalker lab showed for the first time, bulk copolymerisation of sulfur with a gaseous monomer via thermal inverse vulcanisation. This new reaction design is highly useful for polysulfide synthesis with volatile organic comonomers which previously could not be used. However, the procedure is run at high temperature, which is energy intensive, potentially leading to the production of H₂S gas, and can lead to runaway reactions.

Ionic polysulfide synthesis

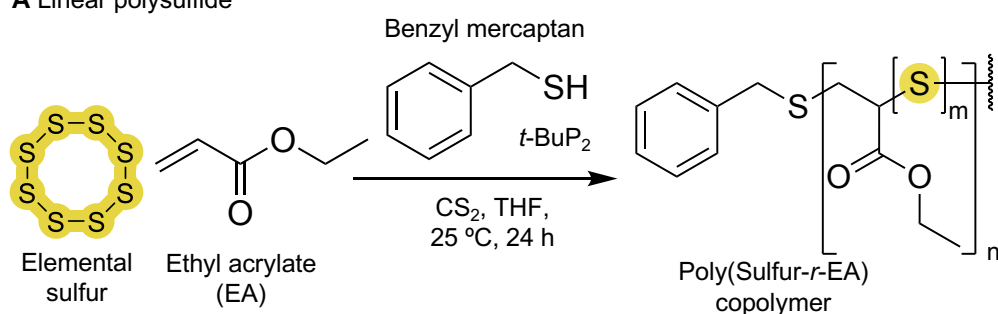
Ionic polysulfide synthesis through the copolymerisation of elemental sulfur and cyclic monomers was studied over 40 years ago.^[49] Anionic polysulfide synthesis of elemental sulfur with episulfides was demonstrated by Duda, Penczek, and co-workers in 1978^[50] and 1982.^[51] Cationic polysulfide synthesis of elemental sulfur and cyclic thianes was demonstrated by Schmidt and co-workers in 1978.^[52] Ionic polysulfide synthesis has provided important insights into polysulfide chemistry, but limited availability of episulfide monomers have discouraged more extensive applications of these polymerisations.^[40] However, recent advancements have been made in ionic polysulfide synthesis.

In 2023, Zhang and co-workers demonstrated the anionic hybrid copolymerisation of elemental sulfur with acrylates and diacrylates.^[40] These organic comonomers are low cost and the authors report excellent mechanical properties for the polysulfides. Anionic hybrid copolymerisation refers to the copolymerisation between cyclic and vinyl monomers which can be difficult due to the difference in reactivity and mechanisms of the two species. Zhang and co-workers propose a hybrid mechanism of ring-opening polymerisation of elemental sulfur and the stepwise polyaddition of acrylamides to produce homogeneous polysulfides. Through chain transfer reactions, the polysulfide network is regulated to contain short polysulfide segments. The authors show the synthesis of both linear and crosslinked polysulfides through this method (Figure 1.7). Although, the method was limited to vinyl monomers which contained carboxyl functional groups. The polymerisation is initiated by benzyl mercaptan which is deprotonated by *t*-BuP₂ resulting in the thiolate anion. The reaction is conducted in a mixture of organic solvents at room temperature under an inert atmosphere. The resulting crosslinked poly(sulfur-*r*-1,4-butanediol diacrylate) had the highest

reported tensile strength of 10.7 MPa, with a breaking strain at 22% when compared to other polysulfides produced through the copolymerisation of elemental sulfur and vinyl co-monomers.^[40]

The authors were successful at producing polysulfides through the hybrid anionic copolymerisation of elemental sulfur with acrylates and diacrylates. The resulting polysulfides had high mechanical properties, with an ultimate tensile strength as high as 10.7 MPa attributed to their short polysulfide segments. However, this synthesis requires an inert atmosphere resulting in a more challenging set up.

A Linear polysulfide



B Cross-linked polysulfide

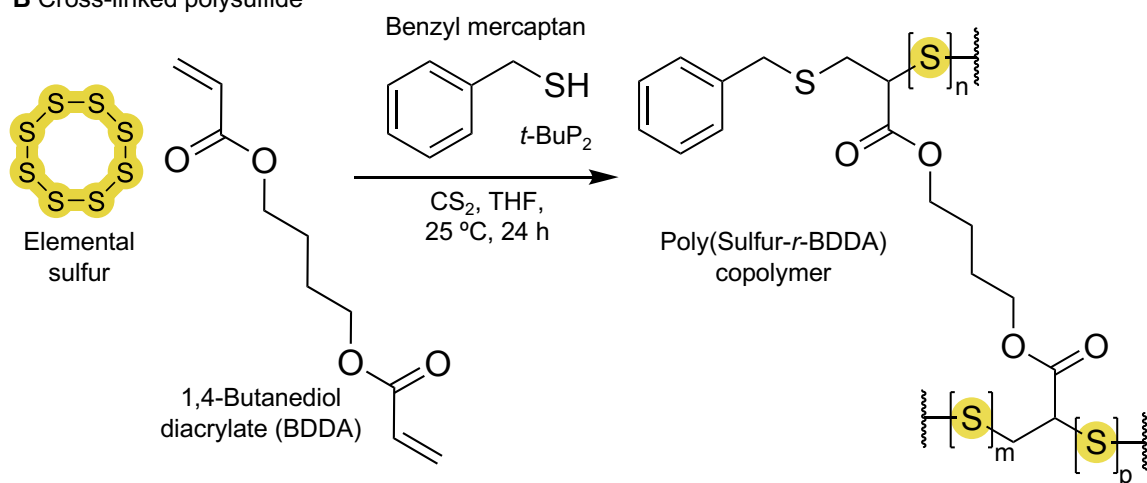
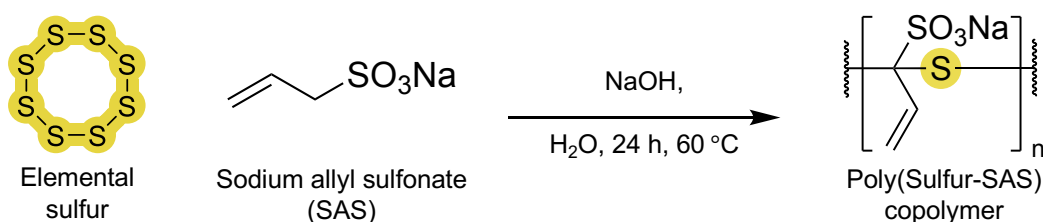


Figure 1.7: (A) Anionic copolymerisation of elemental sulfur and ethyl acrylate resulting in a linear polysulfide. (B) Anionic copolymerisation of elemental sulfur and 1,4-butanediol diacrylate resulting in a crosslinked polysulfide.

Another recent advancement in the ionic synthesis of polysulfides was shown by Hasell and co-workers in 2024.^[41] They show copolymerisation of elemental sulfur with sodium allyl sulfonate (SAS) initiated ionically by hydroxide under mild reaction conditions (Figure 1.8 A). At 60 °C, the reaction is run in water under atmospheric conditions. The addition of NaOH results in the formation of sodium polysulfides which are fully soluble under the reaction conditions. This is highly attractive

as high temperature, and organic solvents are not required to solubilise elemental sulfur. Also, the reaction proceeds without the need of air sensitive ionic initiators. The mild conditions avoid the dangerous associated with high temperature inverse vulcanisation such as H₂S gas production and runaway reactions. The resulting poly(sulfur-SAS) was water soluble and showed impressive application as a desiccant with a sorption maximum of 345 w/w % and excellent metal sorption abilities.^[41] The authors found that the electron withdrawing sulfonate group promotes the removal of the alpha protons adjacent to the sulfonate group under basic conditions (Figure 1.8 B). The resulting carbon centred anion can then undergo nucleophilic attack on the polysulfide chain. Although this is an exciting new method to produce polysulfides under mild conditions, the product reported has a 37 wt.% of sulfur, making its sulfur content relatively low compared to polysulfides synthesised through inverse vulcanisation.

A Polysulfide synthesis



B Proposed mechanism

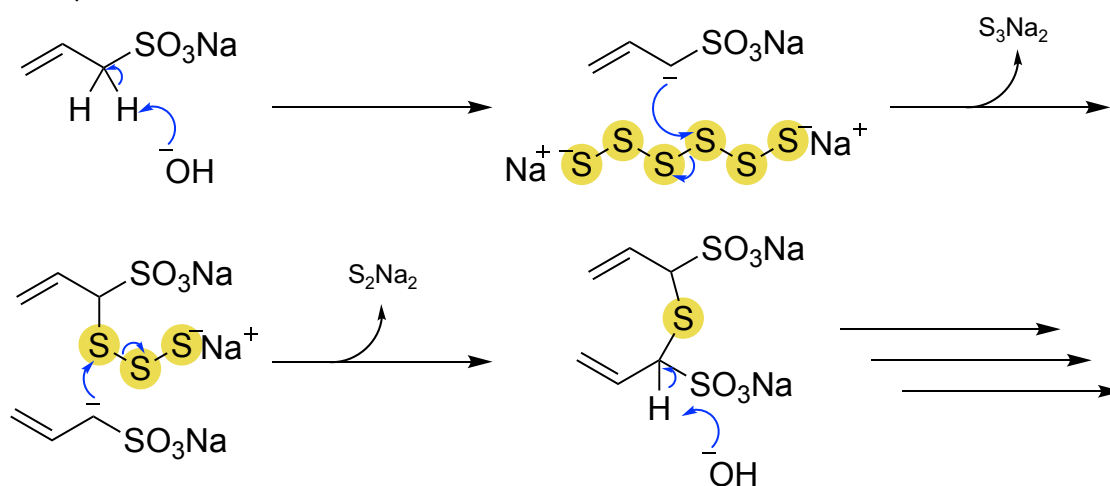


Figure 1.8: (A) Copolymerisation of elemental sulfur and sodium allyl sulfonate. Elemental sulfur is converted into sodium polysulfides. (B) Proposed mechanism for anionic process.

Conclusion

Elemental sulfur can be converted into functional polysulfide materials through its copolymerisation with organic monomers. Over the past decade, there have been several major developments in polysulfide synthesis. This includes the reduction in temperature of inverse

vulcanisation via the addition of catalysts. Polysulfides can be produced as homogeneous thin films through sCVD. Inverse vulcanisation of gaseous organic monomers has also been demonstrated with specialised reactors. Room temperature polysulfide synthesis have been shown to occur via mechanochemical forces from ball milling or via UV irradiation in a photoreactor. Recent advancements in ionic polysulfide synthesis has allowed for the copolymerisation of cost-friendly vinyl comonomers with elementals sulfur under mild reaction conditions. Alternative modes of polysulfide synthesis at low temperature reduce or eliminate the risk of runaway reactions, H₂S gas production and reduce the energy cost associated with high temperature inverse vulcanisation. Through the advances in polysulfide synthesis a broader library of organic comonomers can be copolymerised with elemental sulfur such as volatile and unreactive molecules. These advances allow for the design of functional polysulfides which could not previously be produced by conventional inverse vulcanisation.

With many polysulfides showing promise in commercial and large-scale applications, it is important that they can be produced in a hazard-free and efficient manner. Polysulfide processability is an important feature for polysulfide synthesis on a large-scale. Also, control over polysulfide structure has shown to be important for determining their physical properties. Therefore, the continued research and development into high sulfur content polymer synthesis is necessary.

Research aims and summary of research in thesis

There is a current demand for the safe, scalable, and processable production of high sulfur content polysulfides. Over recent years, there have been several advances in this area to mitigate hazards and improve scalability. However, polysulfide synthesis still faces many challenges such as random copolymerisation, distribution of sulfur ranks, uncontrolled stereochemistry, and poor processability. The aim of the research in this thesis was to address these challenges through the development of novel methods to produce high sulfur content polymers. Ideally, these polymerisation methods would be low temperature, safe, and scalable, and also produce polysulfides which are well-defined and processable. Well-defined, high sulfur content polymers have not yet been studied in detail and provide many advantages such as control of sulfur rank, controlled C–S stereochemistry, and regioselective propagation.

Chapter 2 describes a novel method to produce high sulfur content polymers through the electrochemically induced ring-opening polymerisation of 1,2,3-trithiolane monomers. A library of norbornane-based 1,2,3-trithiolane monomers was synthesised, including one monomer containing a carboxylic acid functional group which could be later modified to produce a water-soluble polysulfide. The redox activity of the monomers was investigated using electrochemical techniques

and validated by computational studies. The redox information was then utilised to selectively induce anionic ring-opening polymerisation of the monomers. This innovative method results in the production of linear high sulfur content poly(trisulfides) at room temperature and open to atmosphere, with electricity being the key energy source. The kinetics and mechanism of the polymerisation were studied, revealing that the polymer is produced rapidly and has a sulfur rank of three. Having a known and well-defined sulfur rank is rare for high sulfur content polymers and represents a milestone in the area of inverse vulcanisation and related reactions.

Chapter 3 focuses on the applications of poly(trisulfides) synthesised in Chapter 2. This is followed by studies to scale-up the electrochemical polymerisation. One poly(trisulfide) was shown to bind to gold in aqueous solution. The gold bound poly(trisulfide) could then be thermally recycled to recover both the monomer and gold in high yield. A water-soluble poly(trisulfide) was shown to have a greater ability to bind to copper in aqueous solution compared with water-insoluble poly(trisulfides). Another application explored was the crosslinking of linear poly(trisulfides) to produce a material with higher thermal stability and solvent resistance. Upscaling the electrochemical poly(trisulfide) synthesis is then described. Through the design of a large-scale electrochemical batch reactor, the poly(trisulfide) was produced on a scale 20 times that of the original method. Alternative cost-effective electrode materials were investigated, and the electrolyte solution was shown to be recyclable. The electrochemical polymerisation using a continuous flow process is also briefly investigated.

Chapter 4 explores the photoinduced ring-opening polymerisation of 1,2,3-trithiolane monomers, a phenomenon that is known to occur, but only produces low molecular weight oligomers. Through the application of a continuous flow photoreactor, the amount of UV irradiation to the reaction solution was controlled, resulting in the control of poly(trisulfide) molecular weight. A range of polymerisation conditions were explored resulting in high molecular weight linear poly(trisulfides). Under ambient conditions, solution processable, linear poly(trisulfides) were produced solely through light irradiation. Running the reaction in continuous flow provided the possibility for large scale production of the polymer. The poly(trisulfides) were then shown to be rapidly photodegradable into low molecular weight species. Photodegradable sulfur-rich polymers have potential applications in photodegradable films and coatings.

Chapter 5 investigates the antimicrobial and antifungal activity of poly(trisulfides). Water-soluble poly(trisulfides) are used to determine minimum inhibitory concentration (MIC) against clinically relevant bacteria (*Staphylococcus aureus* and *Escherichia coli*) and fungi (*Candida albicans*). Poly(trisulfide) **Na-poly-3** had a MIC for *Staphylococcus aureus* at $\leq 256 \mu\text{g/mL}$ and a

MIC for *Candida albicans* at $\leq 16 \mu\text{g/mL}$. **Na-poly-3** was less effective against *Escherichia coli*, only inhibiting some bacterial growth likely due to the bacteria's more complex outer membrane. These experiments explored the antimicrobial and antifungal activity for high sulfur content polymers resulting in MIC values for the first time. The MIC values obtained are significant in comparison to commercially available antimicrobial and antifungal agents, warranting further investigation.

In conclusion, this thesis studies the synthesis of linear poly(trisulfides) through mild and safe conditions. Through computational and experimental studies, the synthesis of a well-defined polysulfide with a known sulfur rank of three was shown for the first time. A novel electrochemical poly(trisulfide) synthesis was developed and shown to be scalable for the multi-gram production of poly(trisulfides). The photochemical synthesis of poly(trisulfides) was revisited, and a continuous flow photochemical reactor was used to selectively control the molecular weight. Continuous flow synthesis also offered the multi-gram production of poly(trisulfides). Several high value applications were then explored including metal binding, biocidal activity and post-polymerisation modifications. For the first time, a fully recyclable polysulfide was shown in an application as a gold sorbent, resulting in the recovery of both gold and the recycled monomer. These results have helped advance the synthesis and use of polysulfides, and the development of sustainable polymers. Poly(trisulfide) production using these safe and sustainable methods is now underway and they are being used in new applications such as fungicides, recyclable gold sorbents, and photodegradable films.

References

- [1] B. Meyer, *Chemical Reviews* **1976**, 76, 367-388.
- [2] G. Kutney, *Sulfur: history, technology, applications and industry*, Elsevier, **2023**.
- [3] C. Song, X. Ma, *Applied Catalysis B: Environmental* **2003**, 41, 207-238.
- [4] B. O. Al Sasi, A. Demirbas, *Petroleum Science and Technology* **2016**, 34, 1550-1555.
- [5] S. Schuman, H. Shalit, *Catalysis Reviews* **1971**, 4, 245-318.
- [6] M. P. Elsner, M. Menge, C. Müller, D. W. Agar, *Catalysis Today* **2003**, 79-80, 487-494.
- [7] A. De Angelis, *Applied Catalysis B: Environmental* **2012**, 113, 37-42.
- [8] M. King, M. Moats, W. G. Davenport, *Sulfuric acid manufacture: analysis, control and optimization*, Newnes, **2013**.
- [9] I. E. Apodaca, *US Geological Survey* **2021**.
- [10] T. Rappold, K. Lackner, *Energy* **2010**, 35, 1368-1380.
- [11] W. J. Chung, J. J. Griebel, E. T. Kim, H. Yoon, A. G. Simmonds, H. J. Ji, P. T. Dirlam, R. S. Glass, J. J. Wie, N. A. Nguyen, *Nature chemistry* **2013**, 5, 518-524.
- [12] J. M. Chalker, M. J. Worthington, N. A. Lundquist, L. J. Esdaile, *Sulfur Chemistry* **2019**, 125-151.
- [13] M. Raue, M. Wambach, S. Glöggler, D. Grefen, R. Kaufmann, C. Abetz, P. Georgopoulos, U. Handge, T. Mang, B. Blümich, *Macromolecular Chemistry and Physics* **2014**, 215, 245-254.
- [14] R. Steudel, S. Passlack-Stephan, G. Holdt, *Zeitschrift für anorganische und allgemeine Chemie* **1984**, 517, 7-42.
- [15] I. Gomez, D. Mecerreyes, J. A. Blazquez, O. Leonet, H. Ben Youcef, C. Li, J. L. Gómez-Cámer, O. Bondarchuk, L. Rodriguez-Martinez, *Journal of Power Sources* **2016**, 329, 72-78.
- [16] J. J. Griebel, G. Li, R. S. Glass, K. Char, J. Pyun, *Journal of Polymer Science Part A: Polymer Chemistry* **2015**, 53, 173-177.
- [17] A. G. Simmonds, J. J. Griebel, J. Park, K. R. Kim, W. J. Chung, V. P. Oleshko, J. Kim, E. T. Kim, R. S. Glass, C. L. Soles, Y.-E. Sung, K. Char, J. Pyun, *ACS Macro Letters* **2014**, 3, 229-232.
- [18] Y. Zhang, J. J. Griebel, P. T. Dirlam, N. A. Nguyen, R. S. Glass, M. E. Mackay, K. Char, J. Pyun, *Journal of Polymer Science Part A: Polymer Chemistry* **2017**, 55, 107-116.
- [19] P. T. Dirlam, A. G. Simmonds, R. C. Shallcross, K. J. Arrington, W. J. Chung, J. J. Griebel, L. J. Hill, R. S. Glass, K. Char, J. Pyun, *ACS Macro Letters* **2015**, 4, 111-114.
- [20] H. Dislich, *Angewandte Chemie International Edition in English* **1979**, 18, 49-59.

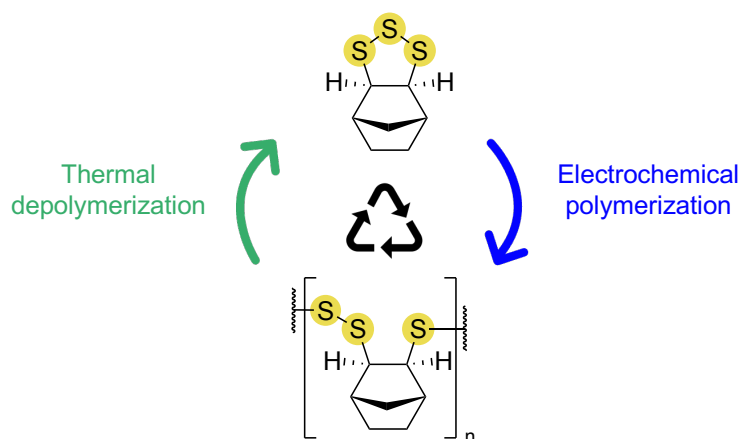
- [21] J. J. Griebel, S. Namnabat, E. T. Kim, R. Himmelhuber, D. H. Moronta, W. J. Chung, A. G. Simmonds, K.-J. Kim, J. van der Laan, N. A. Nguyen, E. L. Dereniak, M. E. Mackay, K. Char, R. S. Glass, R. A. Norwood, J. Pyun, *Advanced Materials* **2014**, *26*, 3014-3018.
- [22] S. J. Tonkin, L. N. Pham, J. R. Gascooke, M. R. Johnston, M. L. Coote, C. T. Gibson, J. M. Chalker, *Advanced Optical Materials* **2023**, *11*, 2300058.
- [23] F. G. Müller, L. S. Lisboa, J. M. Chalker, *Advanced Sustainable Systems* **2023**, *7*, 2300010.
- [24] J. M. Chalker, M. Mann, M. J. Worthington, L. J. Esdaile, *Organic Materials* **2021**, *3*, 362-373.
- [25] M. M. a. J. M. Chalker, *Vol. WO2020198778.*, **2019**.
- [26] M. Mann, B. Zhang, S. J. Tonkin, C. T. Gibson, Z. Jia, T. Hasell, J. M. Chalker, *Polymer Chemistry* **2022**, *13*, 1320-1327.
- [27] C. Herrera, K. J. Ysinga, C. L. Jenkins, *ACS Applied Materials & Interfaces* **2019**, *11*, 35312-35318.
- [28] Y. Zhang, N. G. Pavlopoulos, T. S. Kleine, M. Karayilan, R. S. Glass, K. Char, J. Pyun, *Journal of Polymer Science Part A: Polymer Chemistry* **2019**, *57*, 7-12.
- [29] M. Mann, P. J. Pauling, S. J. Tonkin, J. A. Campbell, J. M. Chalker, *Macromolecular Chemistry and Physics* **2022**, *223*, 2100333.
- [30] P. Yan, W. Zhao, F. McBride, D. Cai, J. Dale, V. Hanna, T. Hasell, *Nature Communications* **2022**, *13*, 4824.
- [31] J. Jia, J. Liu, Z.-Q. Wang, T. Liu, P. Yan, X.-Q. Gong, C. Zhao, L. Chen, C. Miao, W. Zhao, *Nature Chemistry* **2022**, *14*, 1249-1257.
- [32] J. J. Griebel, R. S. Glass, K. Char, J. Pyun, *Progress in Polymer Science* **2016**, *58*, 90-125.
- [33] D. J. Parker, H. A. Jones, S. Petcher, L. Cervini, J. M. Griffin, R. Akhtar, T. Hasell, *Journal of Materials Chemistry A* **2017**, *5*, 11682-11692.
- [34] L. He, J. Yang, H. Jiang, H. Zhao, H. Xia, *Industrial & Engineering Chemistry Research* **2023**, *62*, 9587-9594.
- [35] X. Wu, J. A. Smith, S. Petcher, B. Zhang, D. J. Parker, J. M. Griffin, T. Hasell, *Nature communications* **2019**, *10*, 647.
- [36] T. Lee, P. T. Dirlam, J. T. Njardarson, R. S. Glass, J. Pyun, *Journal of the American Chemical Society* **2022**, *144*, 5-22.
- [37] S. J. Tonkin, C. T. Gibson, J. A. Campbell, D. A. Lewis, A. Karton, T. Hasell, J. M. Chalker, *Chemical Science* **2020**, *11*, 5537-5546.
- [38] N. A. Lundquist, A. D. Tikoalu, M. J. H. Worthington, R. Shapter, S. J. Tonkin, F. Stojcevski, M. Mann, C. T. Gibson, J. R. Gascooke, A. Karton, L. C. Henderson, L. J. Esdaile, J. M. Chalker, *Chemistry – A European Journal* **2020**, *26*, 10035-10044.

- [39] D. H. Kim, W. Jang, K. Choi, J. S. Choi, J. Pyun, J. Lim, K. Char, S. G. Im, *Science advances* **2020**, *6*, eabb5320.
- [40] H. Yang, J. Huang, Y. Song, H. Yao, W. Huang, X. Xue, L. Jiang, Q. Jiang, B. Jiang, G. Zhang, *Journal of the American Chemical Society* **2023**, *145*, 14539-14547.
- [41] J. J. Dale, M. W. Smith, T. Hasell, *Advanced Functional Materials* **2024**, *n/a*, 2314567.
- [42] J. Bao, K. P. Martin, E. Cho, K.-S. Kang, R. S. Glass, V. Coropceanu, J.-L. Bredas, W. O. N. Parker, Jr., J. T. Njardarson, J. Pyun, *Journal of the American Chemical Society* **2023**, *145*, 12386-12397.
- [43] B. Zhang, H. Gao, P. Yan, S. Petcher, T. Hasell, *Materials Chemistry Frontiers* **2020**, *4*, 669-675.
- [44] L. J. Dodd, Ö. Omar, X. Wu, T. Hasell, *ACS Catalysis* **2021**, *11*, 4441-4455.
- [45] T. S. Kleine, R. S. Glass, D. L. Lichtenberger, M. E. Mackay, K. Char, R. A. Norwood, J. Pyun, *ACS Macro Letters* **2020**, *9*, 245-259.
- [46] T. S. Kleine, T. Lee, K. J. Carothers, M. O. Hamilton, L. E. Anderson, L. Ruiz Diaz, N. P. Lyons, K. R. Coasey, W. O. Parker Jr., L. Borghi, M. E. Mackay, K. Char, R. S. Glass, D. L. Lichtenberger, R. A. Norwood, J. Pyun, *Angewandte Chemie International Edition* **2019**, *58*, 17656-17660.
- [47] J. Emsley, D. W. Griffiths, *Phosphorus and Sulfur and the Related Elements* **1980**, *9*, 227-230.
- [48] S. Inoue, T. Tezuka, S. Oae, *Phosphorus and Sulfur and the Related Elements* **1978**, *4*, 219-221.
- [49] S. Penczek, A. Duda, *Phosphorus, Sulfur, and Silicon and the Related Elements* **1991**, *59*, 47-62.
- [50] S. Penczek, R. ŚLazak, A. Duda, *Nature* **1978**, *273*, 738-739.
- [51] A. Duda, S. Penczek, *Macromolecules* **1982**, *15*, 36-40.
- [52] E. Weissflog, M. Schmidt, *Zeitschrift für anorganische und allgemeine Chemie* **1978**, *445*, 175-183.

Chapter 2

Electrochemical synthesis of poly(trisulfides)

Given the increasing interest in high sulfur content polymers, new methods for their synthesis that feature improved safety and control of structure are needed. This chapter describes the development of a novel electrochemical procedure for the synthesis of linear poly(trisulfides). Through the electrochemical ring-opening polymerisation of 1,2,3-trithiolane monomers, a library of well-defined, solution processable, linear poly(trisulfides) were produced and characterised. The electrochemical synthesis featured improved safety, operational simplicity, and control of polymer structure. Computational studies revealed an intriguing “self-correcting” mechanism that ensures trisulfide linkages between monomer units. This control over sulfur rank is a new benchmark for high sulfur content polymers and creates opportunities to better understand the effects of sulfur rank on polymer properties. Thermal depolymerisation of the poly(trisulfide) was shown to deliver the pure monomer in high yields, which is remarkable for a high sulfur content polymer.



Acknowledgments

Thomas Nicholls and Zhongfan Jia for electrochemical training and guidance

Witold Bloch for X-ray crystallography

Le Nhan Pham and Michelle Coote for DFT calculations

Christopher Gibson for Raman analysis

Introduction

Sulfur is a highly abundant, low-cost feedstock for polymeric materials. A common method of high sulfur content polymer synthesis is through inverse vulcanisation where organic dienes or polyenes are copolymerised with elemental sulfur (Figure 2.1 A).^[1] Despite the utility of inverse vulcanisation to produce polysulfides, there remain drawbacks to the synthetic method. These include limited or no control of polymer molecular weight, mechanical properties, sulfur rank, and C–S stereochemistry. Regulation of these properties is important for understanding and tuning the relationship between polymer structure and function. Organic molecules such as dicyclopentadiene (DCPD), which contain more than one alkene group can form a crosslinked structure when copolymerised with elemental sulfur through inverse vulcanisation (Figure 2.1 A).^[2] Polysulfides with crosslinked structures often have poor processability and are difficult to characterise through solution-based techniques such as Nuclear Magnetic Resonance (NMR) spectroscopy and Gel Permeation Chromatography (GPC). Other molecules such as 1,3-diisopropenylbenzene (DIB) which contain two alkene groups have been reported to form a crosslinked structure by multiple research groups.^[1, 3] However, over a decade later since the structure was first reported, the correct linear structure was described by Pyun and co-workers after in-depth studies using solid state ¹³C NMR, synthesis of sulfurated DIB small molecules, and mechanistic studies aided by density functional theory (DFT) calculations.^[3] This recent discovery highlights the challenges and lack of knowledge of the structure of polysulfides produced via inverse vulcanisation. It has been reported that the large-scale production of polysulfides by inverse vulcanisation can lead to dangerous runaway reactions that cause decomposition and the vigorous production of gaseous by-products such as H₂S gas.^[4-5] Alternative routes to high sulfur content polysulfide synthesis using catalysts,^[6] mechanochemistry^[7] or UV light^[8] have made progress towards safer synthetic procedures. However, there remain challenges associated with structural characterisation and processability of polysulfides produced by these methods.

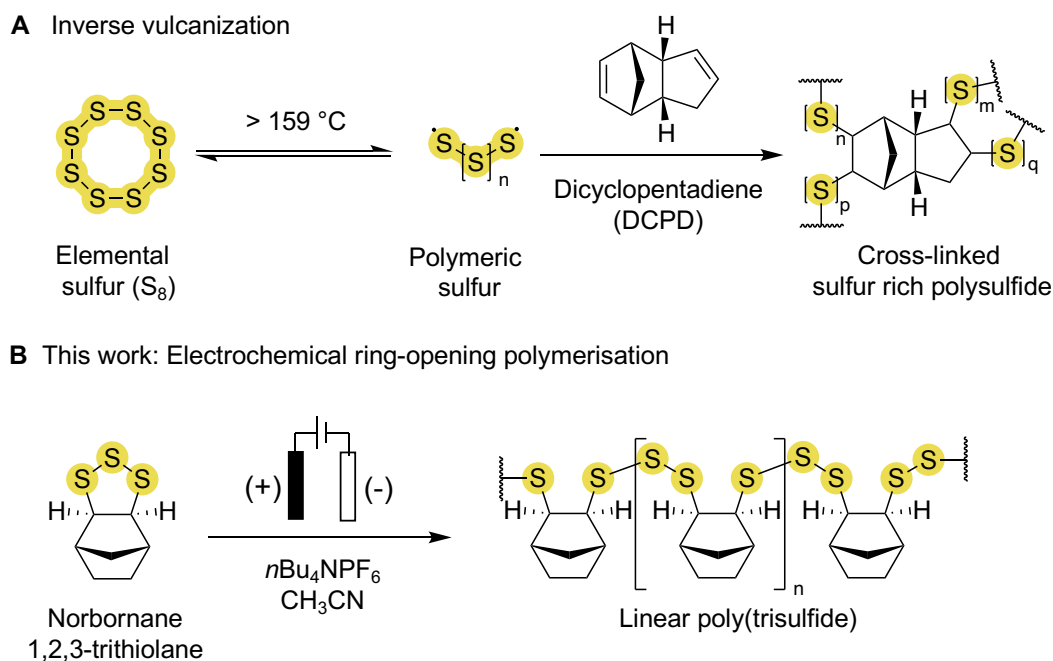


Figure 2.1: (A) Inverse vulcanization. (B) This work: electrochemically induced ring-opening polymerisation providing linear polysulfides with regular sulfur rank.

In this chapter, an alternative synthetic method to safely produce high sulfur content polymers with controlled C–S stereochemistry and sulfur rank is described. Room temperature polysulfide synthesis is achieved by initiating polymerisation using electrochemistry. This is done through the electrochemically initiated ring-opening polymerisation (ROP) of 1,2,3-trithiolanes to produce sulfur rich polymers with a linear structure (Figure 2.1 B). 1,2,3-Trithiolanes are synthesised from norbornene-based molecules and elemental sulfur (S_8), providing an outlet for the waste stream of sulfur.^[9] Electrochemical ROP is environmentally sustainable as it doesn't require energy-intensive conditions or chemical initiation. The electrochemical ROP method described in this chapter is conducted in open air, making it operationally simple. The mild reaction conditions avoid the potential dangers of runaway reactions and toxic gas production that occur during high temperature inverse vulcanisation.

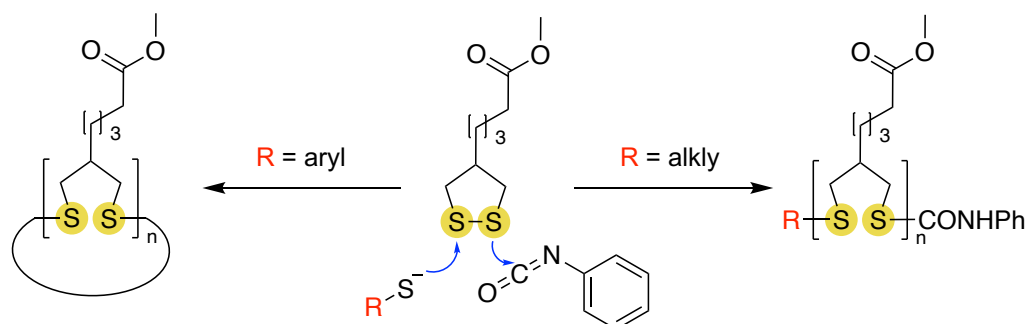
Using electrochemistry to initiate ROP provides a sustainable and safe route to produce high sulfur content polymers with increased selectivity and control over the polymer structure. The control of sulfur rank delivered from electrochemical ROP of 1,2,3-trithiolanes is beneficial for the fundamental understanding of polysulfides and their associated properties. Polysulfides produced by this method will exhibit properties complementary to those produced via inverse vulcanisation. This includes redox activity, high refractive indices, and affinity for metals.

Ring-opening polymerisation

ROP is a commonly used chain-growth polymerisation technique that harnesses the ability of an initiating species to activate a cyclic monomer, causing ring-opening and subsequent propagation. ROP was first utilised in 1906 by Hermann Leuchs for the synthesis of polypeptides.^[10] The use of ROP underwent rapid expansion in the 1960's after the mechanisms of ROP were established over the previous decade.^[11-12] The major driving force for ROP is release of ring strain and associated steric considerations.^[13] Over recent years, the use of ROP has seen continuous growth and is responsible for the large scale production of common materials such as nylon-6,^[14] polyglycolides and polylactides.^[15] There are several ways in which ROP can be initiated including anionic and cationic species, light, thermal and electrochemical initiation. The growing chain can proceed by radical, anionic, or cationic intermediates.

Anionic ring-opening polymerisation

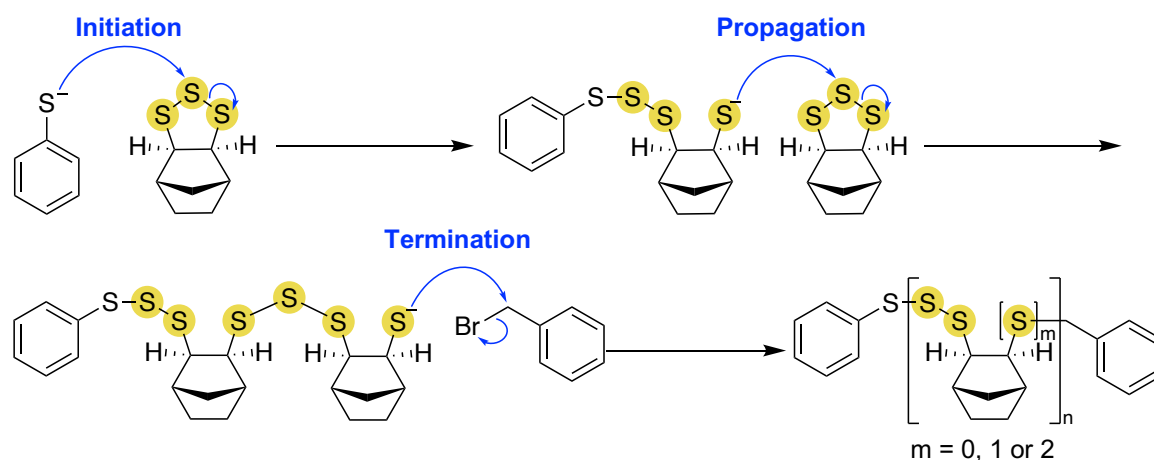
Anionic ring-opening polymerisation (AROP) is described as the nucleophilic attack of a growing-chain end on a cyclic monomer. Poly(disulfides) can be produced by AROP from common dithiolanes such as lipoic acid.^[16] In 2019, Moore and co-workers used thiols and base to initiate the synthesis of poly(disulfides) (Scheme 2.1).^[17] They achieved selectivity over the formation of cyclic or linear chains through selective initiators that are also good leaving groups, resulting in polymer ring formation after backbiting.^[17] Poly(disulfide) synthesis has been widely investigated. However, with our focus on polymers with high sulfur content, our interest steered us towards 1,2,3-trithiolanes as monomers.



Scheme 2.1: Anionic ROP of lipoic acid methyl ester with control over linear or cyclic polymer structure.^[17]

In 1984, Penczek and co-workers described the AROP of norbornane- and dicyclopentadiene-1,2,3-trithiolane monomers, producing poly(trisulfides).^[18] This paper sparked our interest due to the high sulfur content of the poly(trisulfides) which are comparable to polysulfides produced by inverse vulcanisation. The linear structure of the poly(trisulfides) aided

their solubility in common organic solvents. Penczek and co-workers report the bulk or in solvent polymerisation of 1,2,3-trithiolanes using sodium thiophenolate activated by complexation of crown ether with the sodium cation and later termination by benzyl bromide (Scheme 2.2).



Scheme 2.2: Anionic ring-opening polymerisation of 1,2,3-trithiolane.

Principles of electrochemical synthesis

Electrochemistry has emerged as a powerful tool that has seen a surge in use by synthetic chemists in the past decade.^[19] Electrochemical synthesis offers a range of advantages over conventional synthetic techniques that rely on reducing or oxidising agents. This stems from its use of an applied electrical potential to achieve reduction or oxidation reactions. Other advantages of electrochemical synthesis also include mild and ‘green’ reaction conditions, selectivity, and high atom economy.

There are several key components that make up a simple electrochemical cell (Figure 2.2 A). A power supply connects the two electrodes, which are submerged in the reaction solution. The reaction solution contains an electrolyte made of electrically conductive ions. The power supply delivers electrons from the anode to the cathode. The movement of charged species through the reaction solution completes the electrical circuit. Oxidation will occur at the anode, while reduction occurs at the cathode. The electrodes are also identified as the working electrode and the counter electrode; the working electrode is where the reaction of interest occurs. The current of a reaction refers to the rate of electron transfer, while the reaction potential describes the energy by which they are moved.

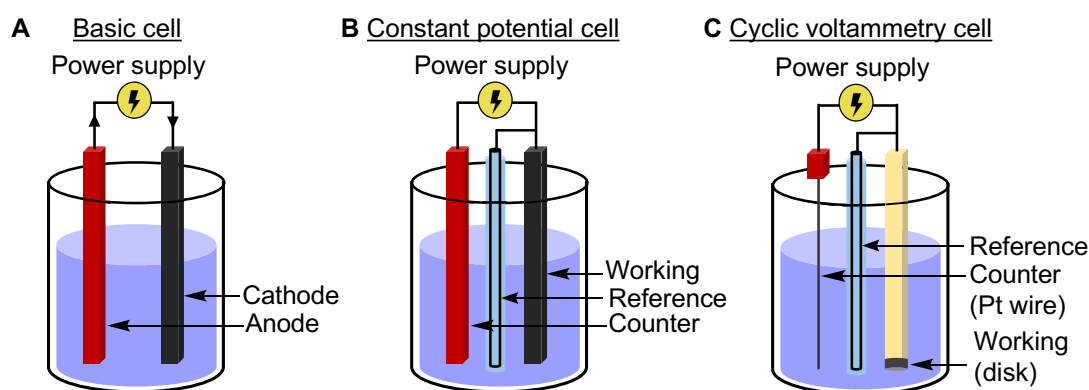


Figure 2.2: (A) Simple two-electrode cell. (B) Three-electrode cell used for constant potential reactions. (C) Three-electrode cell used for cyclic voltammetry reactions.

There are two main types of electrochemical reactions used in electrochemical synthesis. The first type is a constant current reaction where galvanostatic conditions are applied. Constant current reactions require a simple set up consisting of a two-electrode cell (Figure 2.2 A). These reactions are supplied with a constant current, and the potential may vary. The lack of control over potential is a drawback for reactions that require selectivity and may lead to undesired redox processes occurring. The second type of reaction is called a constant potential reaction, which is run under potentiostatic conditions. Potentiostatic conditions require a reference electrode which measures the potential at the working electrode (Figure 2.2 B). This allows for a specific reaction potential to be applied to the working electrode, resulting in high selectivity for the desired redox process. To determine the redox potential required for a desired chemical transformation, cyclic voltammetry is used. Cyclic voltammetry is an analytical tool which requires a three-electrode cell (Figure 2.2 C). A potential window is scanned in a cyclic manner, while changes in current are detected. If a change in current is observed at a particular potential, it means a redox process is happening, allowing current to flow. If this is the redox process of interest, the potential at which has peak current can be applied to a constant potential cell.

Results and discussion

Monomer synthesis

Sulfurisation of C=C double bonds using S_8 was an operationally simple approach to gain access to 1,2,3-trithiolanes. The sulfurisation of strained olefins such as norbornene has been reported in the literature to produce 1-thiolanes, 1,2,3-trithiolanes and 1,2,3,4,5-pentathiolanes.^[18,20] Nickel(II) complexes act as a catalyst for the sulfurisation of norbornene, giving good selectivity for the synthesis of the 1,2,3-trithiolanes.^[21] Heating norbornene in dimethylformamide (DMF) at 120 °C in the presence of S_8 and a catalytic amount of $[Ni(NH_3)_6]Cl_2$ for 16 hours afforded a 57% isolated

yield of norbornane-*exo*-1,2,3-trithiolane (**1**) and 10% isolated yield of norbornane-*exo*-1,2,3,4,5-pentathiolane (**2**) (Figure 2.3 A). The lower yields were attributed to the formation of a mixture of oligomeric and polymeric material. After column chromatography of the crude material, monomer **1** contained trace impurities of monomer **2**. Vacuum distillation of the column fraction provided monomer **1** as a yellow oil with high purity, as observed by ^1H NMR spectrometry analysis. Monomer **2** was a white crystalline solid suitable for analysis by single crystal X-ray diffraction (Figure 2.3 B).

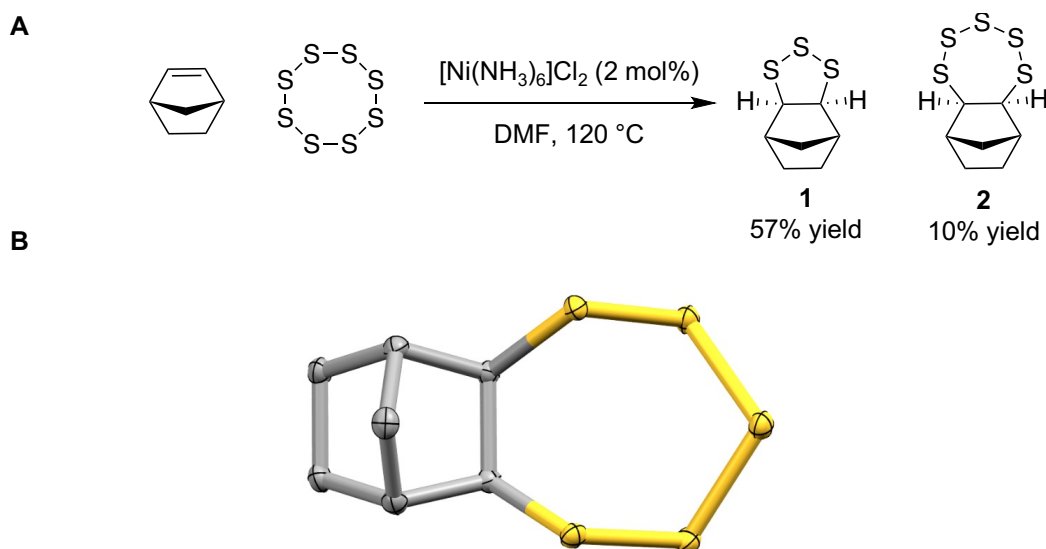


Figure 2.3: (A) Reaction of sulfur and norbornene to form monomer **1** and **2**. (B) X-ray crystal structure of monomer **2**.

Under the same reaction conditions, a small library of 1,2,3-trithiolanes was prepared. 1,2,3-Trithiolanes containing different functional groups were synthesised to assess the functional group tolerance of the polymerisation method and to produce polymers with different properties. 1,2,3-Trithiolanes **3** and **4** were also crystalline, and their structures were determined unambiguously by single crystal X-ray diffraction (Figure 2.4). In all cases, the monomers were isolated as the *exo* isomers in which the two C–S bonds have a *cis* relationship on the same face as the bridgehead methylene group. All monomers were characterised by proton NMR (^1H NMR), carbon NMR (^{13}C NMR), correlation spectroscopy (COSY), heteronuclear multiple quantum correlation (HMQC), Fourier-transform infrared spectroscopy (FTIR) and Raman spectroscopies as well as high-resolution mass spectrometry (HRMS) or gas chromatography–mass spectrometry (GC-MS), and elemental analysis. 1,2,3-Trithiolanes **1**, **3** and **4** contain high sulfur percentages of 50%, 44% and 42% respectively, which was comparable to many sulfur polymers made by inverse vulcanisation.

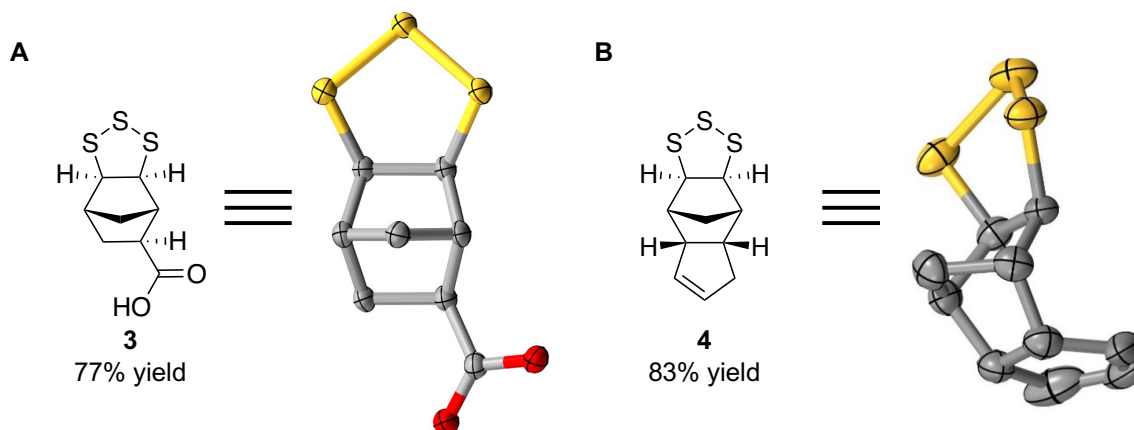
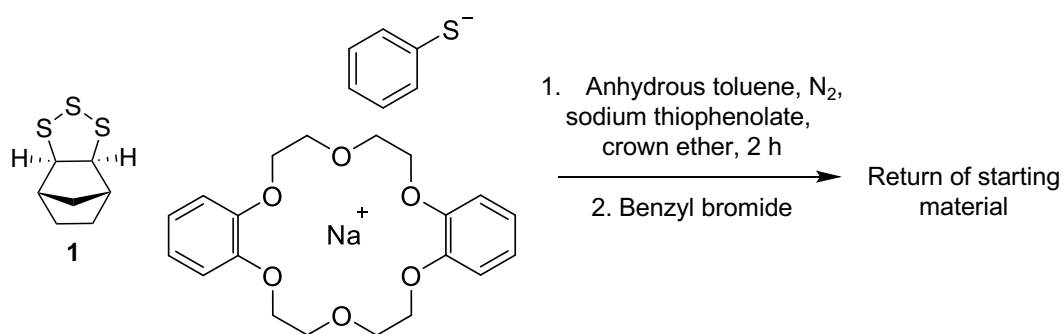


Figure 2.4: (A) X-ray crystal structure of monomer **3**. (B) X-ray crystal structure of monomer **4**.

Anionic polymerisation

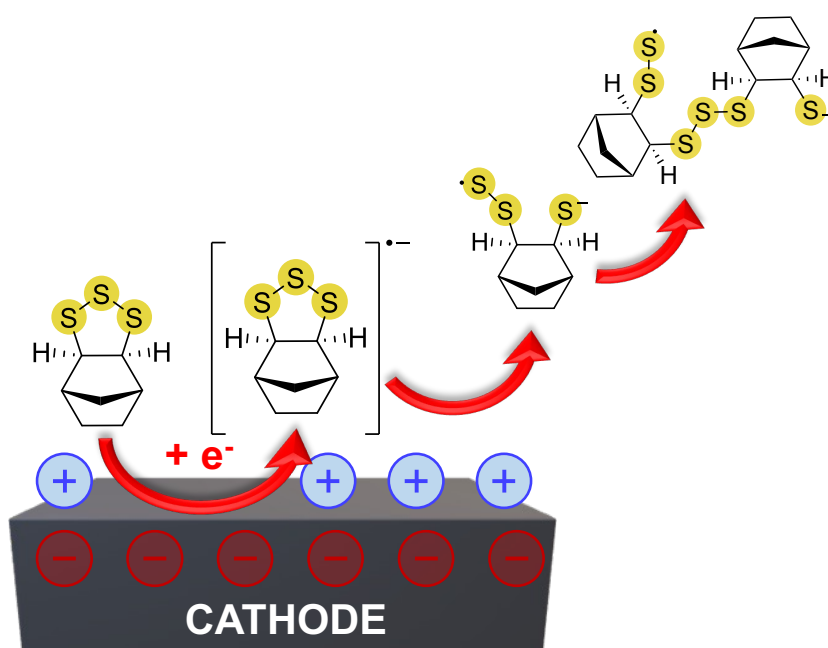
The AROP of monomer **1** produced high molecular weight polymers as described by Penczek and co-workers.^[18] The AROP of monomer **1** was initiated by sodium thiophenolate activated by complexation of crown ether with the sodium cation (Scheme 2.3). The reaction had to be kept dry and under an atmosphere of nitrogen as oxygen and water impurities inhibit the polymerisation by reacting with the growing polymer chain or quenching the initiator. After repeating the literature method on monomer **1** (1.0 M, toluene) under an inert atmosphere for 2 hours, the reaction was quenched by addition of benzyl bromide before workup and analysis. GPC and ¹H NMR spectroscopy analysis resulted in the return of starting material only. AROP of monomer **1** proved to be challenging and highly sensitive method to produce poly(trisulfides). The challenges associated with AROP of **1** prompted us to develop alternative electrochemical initiation methods that are more operationally simple.



Scheme 2.3: AROP of **1** using sodium thiophenolate activated by complexation of crown ether with the sodium cation as the initiator.

Electrochemical polymerisation

An alternative, chemical initiator-free method to induce ROP was by harnessing electrochemistry to add an electron to the 1,2,3-trithiolane monomer, provoking ring-opening of the putative radical anion species (Scheme 2.4). The radical anion formed in the electrode double layer can diffuse away, allowing for chain growth without further reduction at the electrode (Scheme 2.4). This differed from AROP, which consists of a homogenous solution of initiating species that can react with and cleave the growing polymer chain. To test the hypothesised electrochemical polymerisation method, the potential required to reduce the 1,2,3-trithiolane monomers was investigated using cyclic voltammetry.



Scheme 2.4: Initiation of ROP at electrode surface followed by diffusion of the growing polymer chain away from electrode surface.

Monomer redox activity – cyclic voltammetry

Cyclic voltammetry was used to investigate the electrochemical redox behaviour of monomers **1**, **2**, **3**, and **4**. A three-electrode cell was charged with the monomer (5 mM) in an electrolyte solution of 0.1 M *n*Bu₄NPF₆ in acetonitrile. This electrolyte and solvent solution are commonly used in electrochemical synthesis and analysis due to their redox stability across a broad potential range. At a scan rate of 100 mV/s, the current was measured between -3.0 and +1.5 V versus Fc/Fc⁺ (Figure 2.5). The cyclic voltammogram of **1** shows two distinct redox peaks: a cathodic peak at -2.2 V versus Fc/Fc⁺, and an anodic peak at +1.0 versus Fc/Fc⁺. These redox features were also found in the cyclic voltammograms of **3** and **4**. The cyclic voltammogram for **2** exhibits

additional redox features at -1.6 and -0.8 V versus Fc/Fc^+ . These additional features were likely derived from more complex redox activity of monomer **2**.

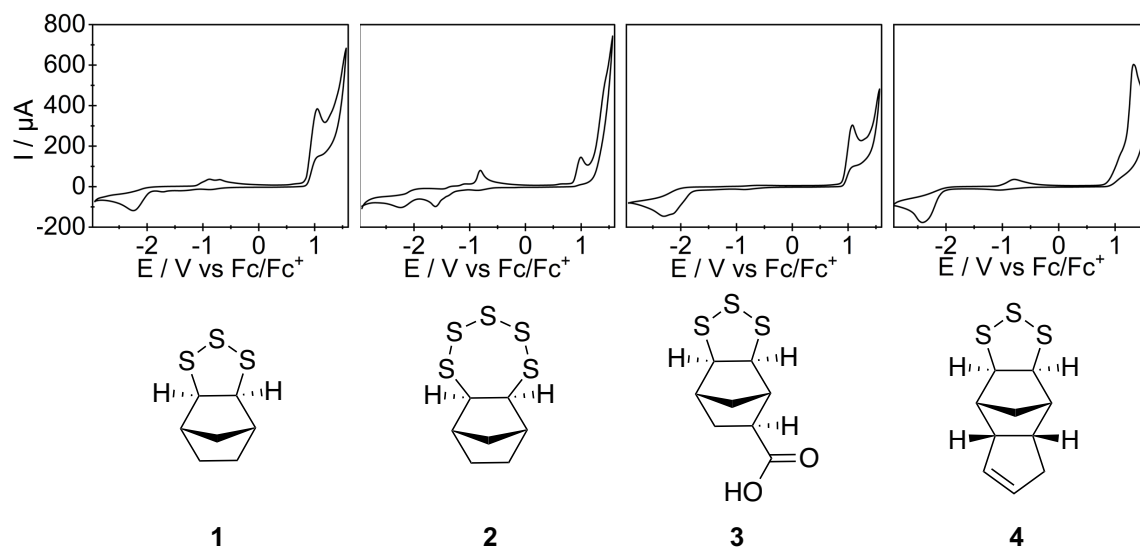


Figure 2.5: Cyclic voltammograms of monomers (5 mM) were measured in a potential window of -3.0 and $+1.5$ V versus Fc/Fc^+ at 100 mV/s showing the third cycle. The supporting electrolyte was a solution of 0.1 M $n\text{Bu}_4\text{NPF}_6$ in acetonitrile (10 mL).

The cathodic peak at -2.2 V versus Fc/Fc^+ provided the initial evidence to support the hypothesised electrochemically induced ROP, with the initiation step resulting from reduction of the monomer. The reversibility of the peak was investigated by running cyclic voltammograms at scan rates between 50 mV/s to 1000 mV/s on monomer **1** (Figure 2.6). Even at these rapid scan rates, no corresponding oxidation peak was observed for the proposed reduction that occurs at -2.2 V versus Fc/Fc^+ . The irreversibility suggests a chemical reaction occurs immediately following reduction, consistent with ring-opening of the radical anion species.

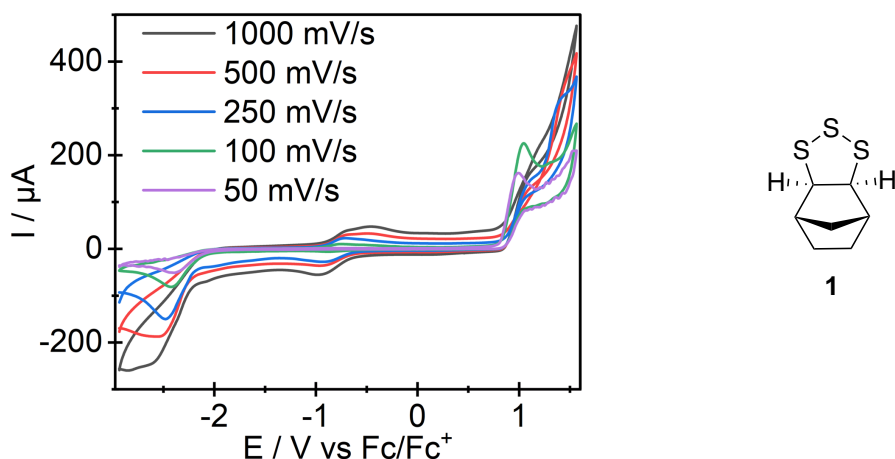


Figure 2.6: Cyclic voltammograms of monomer **1** (5 mM) were measured in a potential window of -3.0 and $+1.5$ V versus Fc/Fc^+ showing the third cycle at different scan rates (50, 100, 250, 500 and 1000 mV/s). The supporting electrolyte was a solution of 0.1 M $n\text{Bu}_4\text{NPF}_6$ in acetonitrile (10 mL).

Next, monomer **4** was investigated for its redox activity in different solvents by cyclic voltammetry. Tetrahydrofuran (THF), Dimethylformamide (DMF), and dichloromethane (DCM) were selected as the monomers were soluble, and the solvents are inert under reductive redox conditions (Figure 2.7). In THF and DCM, no significant change in current was observed in the cathodic region on the cyclic voltammogram, indicating less efficient reduction. In DMF, the cathodic peak was shifted to -2.6 V versus Fc/Fc^+ , and the current was reduced, also indicating a less efficient reduction. As such, acetonitrile was used in subsequent experiments.

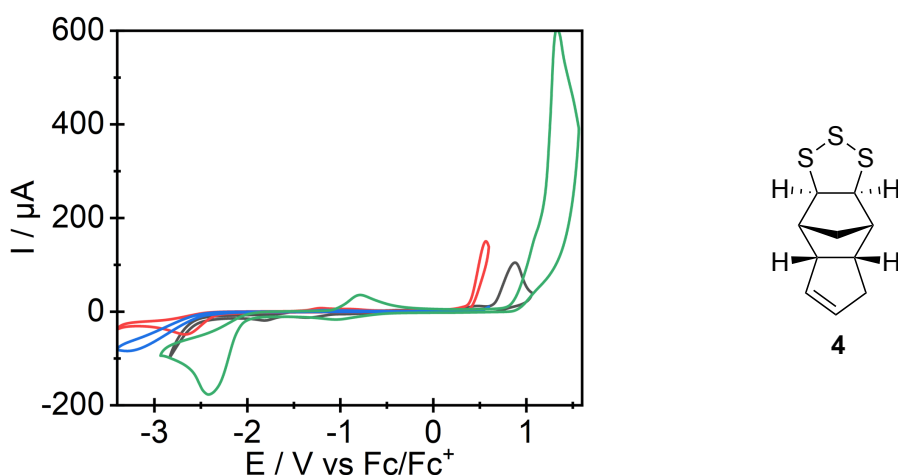


Figure 2.7: Cyclic voltammograms of monomer **4** (5 mM) measured in different solvents at 100 mV/s showing the third cycle. The supporting electrolyte was a solution of 0.1 M $n\text{Bu}_4\text{NPF}_6$ in solvent (10 mL).

Monomer redox activity – chronoamperometry

Following the investigation of the monomer's redox activity by cyclic voltammetry, chronoamperometry experiments were conducted with both positive and negative applied potentials. These experiments were performed in a divided cell containing monomer **1** (5 mM) in an electrolyte solution of 0.1 M $n\text{Bu}_4\text{NPF}_6$ in acetonitrile. When a potential of -2.0 V versus Ag/AgCl was applied to the working electrode, a current response was observed (Figure 2.8). However, when a potential of $+2.0$ V versus Ag/AgCl was applied to the working electrode, no current was observed (Figure 2.8). To investigate this further, the concentration of monomer was increased (0.04 M) in both sides of the divided cell. The cathodic potential of -2.0 V versus Ag/AgCl was applied for 4 hours. A build-up of precipitate was observed in the cathodic chamber of the cell, while no precipitate was observed in the anodic chamber. The precipitate was later identified as polymeric material. These experiments provided motivation to explore the polymerisation by reductive electrochemical initiation.

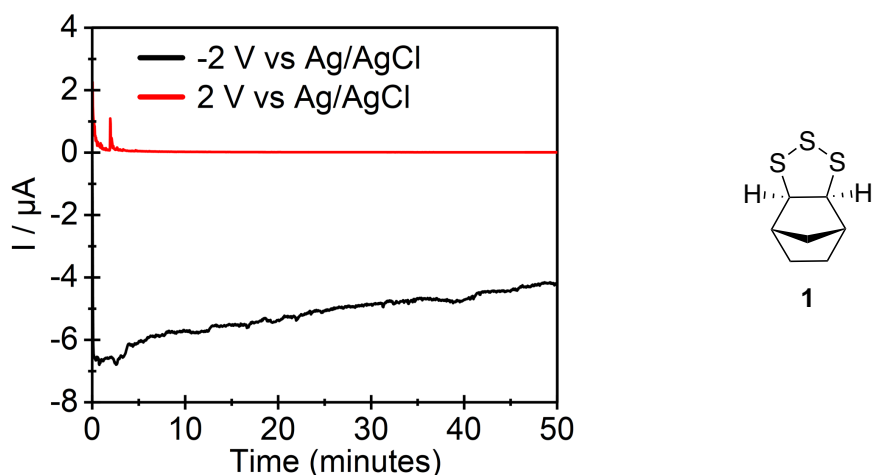


Figure 2.8: Chronoamperogram of monomer **1** (5 mM), $n\text{Bu}_4\text{NPF}_6$ (0.1 M in MeCN, 50 mL) at a constant potential of 2.0 V or -2.0 V versus Ag/AgCl for 50 minutes.

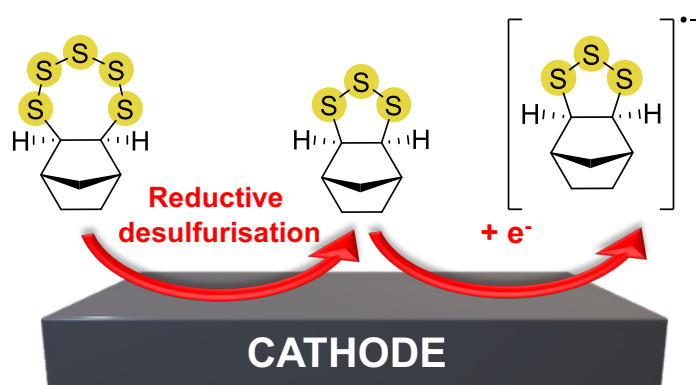
Monomer redox activity – DFT calculations

To further investigate the monomer's redox activity, DFT calculations were performed to determine the reduction potentials of monomers **1**, **2**, **3**, and **4**. The theoretical reduction potential calculated for each monomer closely matched the experimental values obtained (Table 2.1). These calculations were simulated in the same electrolyte solution of 0.1 M $n\text{Bu}_4\text{NPF}_6$ in acetonitrile. The similarity of the calculated values to the experimentally obtained values for monomers **1**, **3**, and **4** provided support for their accuracy, as further calculations were continued later for a mechanistic study. The results also corroborate the hypothesis that addition of an electron to the trithiolane monomer formed the initiating species.

Table 2.1: Summary of DFT calculated reduction potentials, and comparison to the experimentally measured reduction potentials (V versus Fc/Fc⁺).

Monomer	1	2	3	4
DFT Calculated (vs. Fc/Fc ⁺)	-2.29 V	-2.05 V	-2.24 V	-2.28 V
Measured by CV (vs. Fc/Fc ⁺)	-2.22 V	-2.21 V, -1.60 V	-2.27 V	-2.30 V

The outlier was monomer **2**, which did not match the experimental value obtained (Table 2.1). A more complex processes was observed for the reduction of monomer **2** during cyclic voltammetry. The cyclic voltammogram of monomer **2** shows a cathodic peak at -1.6 V versus Fc/Fc⁺ and at -2.2 V versus Fc/Fc⁺ (Figure 2.5). Interestingly, the second peak at -2.2 V versus Fc/Fc⁺ closely matches the experimentally and computationally obtained value for the reduction of monomer **1**. It was hypothesised that the first cathodic peak at -1.6 V versus Fc/Fc⁺ relates to the desulfurisation of monomer **2** and formation of monomer **1**, which was then reduced at -2.2 V versus Fc/Fc⁺ (Scheme 2.5). This hypothesis was later confirmed by ¹H NMR analysis of monomer **2** under reductive electrochemical conditions.



Scheme 2.5: Proposed cathodic reduction of monomer **2** undergoing reductive desulfurisation forming monomer **1** before reduction to radical anion species.

Based on the experimental results obtained using cyclic voltammetry and the supporting computational results, further investigation into the polymerisation of monomers **1**, **2**, **3**, and **4** was

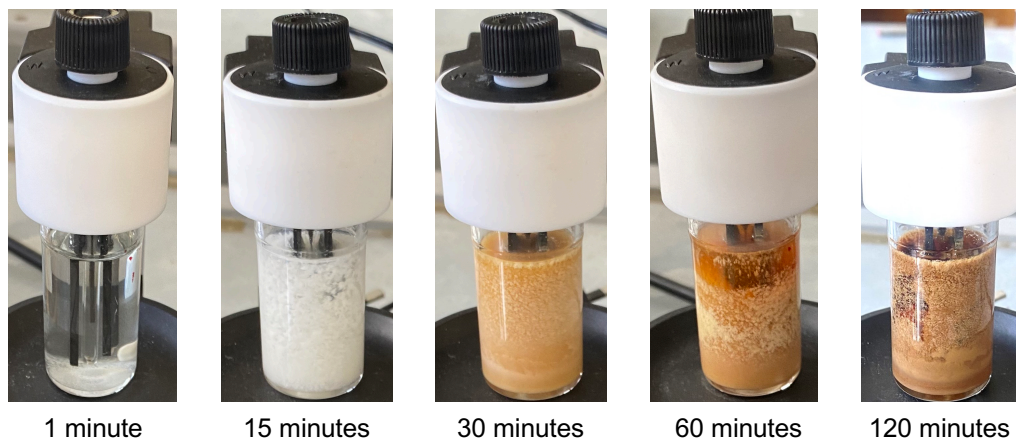
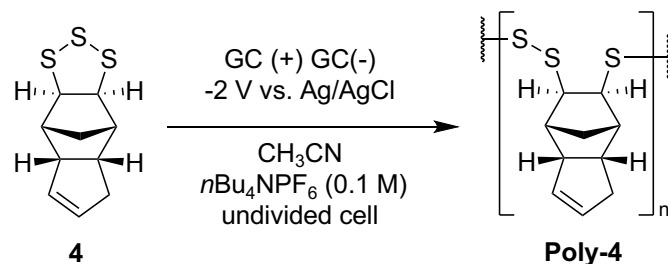
conducted. Reduction of the monomers was targeted to initiate ROP by way of a putative radical anion intermediate.

Electrochemical polymerisation

After investigating the potential required to reduce monomers **1**, **2**, **3**, and **4**, this potential was applied to an electrochemical cell containing a monomer and electrolyte solution to induce polymerisation. For these reactions, an IKA ElectraSyn was used, which was a commercially available benchtop electrochemical reactor. The ElectraSyn also came with a range of standard electrodes, which facilitates reproducibility across other labs.

It was hypothesised that the cathodic reduction of 1,2,3-trithiolanes formed a radical anion that can act as the initiating species for ROP. To test this hypothesis, monomer **4** was targeted, as its proton signals in the ^1H NMR spectra were further downfield than the proton signals from the electrolyte $n\text{Bu}_4\text{NPF}_6$, which were in a much higher concentration than the monomer. Therefore, integration of the monomer signals against the electrolyte was used to calculate the conversion of the monomer into polymer.

To a 20 mL ElectraSyn cell, monomer **4** (160 mg) was loaded along with a small stir bar. The cell was then filled with $n\text{Bu}_4\text{NPF}_6$ acetonitrile solution (0.1 M, 15 mL). The lid of the cell was fitted with two glassy carbon electrodes and a Ag/AgCl reference electrode. While stirring at 1500 rpm, a constant potential of -2.0 V versus Ag/AgCl was applied to the cell resulting in the immediate formation of precipitate (Scheme 2.6). The reaction was stirred at the maximum speed to prevent the build-up of precipitate on the electrode surface, which can result in decreased current due to the reduction of electrode surface area. After 4 hours the precipitate had changed from white to brown (Scheme 2.6). The reaction was stopped and purified by filtration. The presence of precipitate in the filtrate was observed, which indicated some of the polymeric material was passing through the filter. Instead, the polymer was purified by successive dissolution in chloroform (10 mL) and precipitation with acetonitrile (30 mL). The resulting suspension was centrifuged at 5000 rpm for 5 minutes, forming a pellet of the precipitate. The supernatant was decanted, and the process was repeated three times to purify the precipitate from the electrolyte and the remaining monomer. Based on this method of purification, the precipitate was insoluble in acetonitrile but soluble in chloroform. The precipitate was also partially soluble in THF. The solubility of the product in different organic solvents was a significant achievement, as most sulfur-based polymers are insoluble in organic solvents, making solution-based characterisation unfeasible.



Scheme 2.6: Conditions for electrochemical polymerisation of monomer **4** (top). Precipitation occurring in the reaction mixture over the course of the reaction (bottom).

Polymer characterisation

Because the precipitate formed during the electrochemical polymerisation of monomer **4** was soluble in a range of organic solvents, a range of solution-based characterisation could be conducted. ^1H NMR analysis of the precipitate in chloroform showed broad peaks, which is typical of polymeric material (Figure 2.9). Integration of the alkene signals from the precipitate between $\delta = 5.6\text{--}5.8$ ppm (2H) compared to the integration of the alkene signals of monomer **4** ($\delta = 5.5\text{--}5.8$ ppm, 2H) indicate that the alkene moiety was unreactive under the reaction conditions. This supported the hypothesis that a linear polymer was produced, and no crosslinking had occurred. This was an important result as it provided evidence that the constant potential reaction was chemoselective.

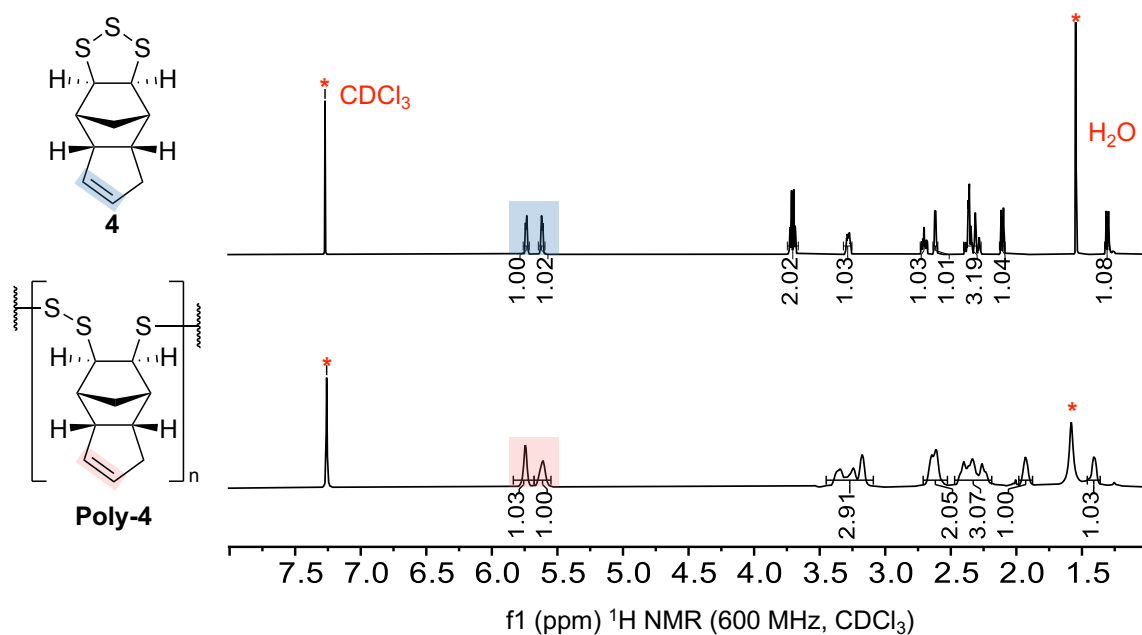


Figure 2.9: ¹H NMR spectra of monomer **4** (top) and precipitate (**poly-4**, bottom).

To provide further evidence that polymeric material had formed, GPC was used to analyse the precipitate. GPC is an important tool for characterising polymeric material based on their molecular weight. However, very few examples of sulfur polymers have been characterised by GPC due to their insolubility in organic solvents. Therefore, it was advantageous that this precipitate was soluble in THF and able to be analysed by GPC. For molecular weight assignment, a series of polystyrene standards were used to calibrate the instrument. The GPC data showed the precipitate had a weight-average molecular weight (M_w) of 3900 g/mol and a dispersity (D) of 1.91 (Figure 2.10). This indicates the precipitate formed from the reaction was polymeric and had a moderately broad dispersity. Dispersity refers to the polymer size distribution with a dispersity of 1 indicating all polymer chains are the same length (uniform). To accurately determine the molecular weight range of the polymer, mass spectrometry techniques were employed.

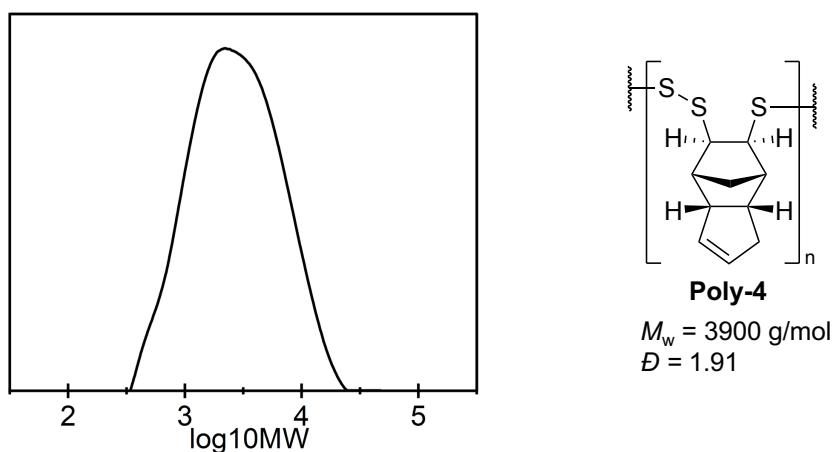


Figure 2.10: GPC (THF) trace of precipitate (**poly-4**).

Matrix-assisted laser desorption/ionization-time of flight (MALDI-TOF) is a commonly used technique to determine the mass of polymeric materials as it provides the absolute molecular weight compared to relative molecular weight as determined by GPC. MALDI-TOF offers the ability to ionise polymeric material without the need for it to be solution processable, as samples can be coated with an energy-absorbing matrix. The coated sample is then ionised by a laser. The precipitate was prepared for analysis by MALDI-TOF by loading the sample on the target plate and coating it with and without a matrix. The spectrum for all samples revealed a mixture of peaks all containing a mass difference of 32 mass-to-charge ratio (m/z), the atomic weight of sulfur. This indicated polymer decomposition caused by the technique leading to the release of sulfur atoms. Polysulfides have been shown to be modified by low powered lasers.^[22] Therefore, it was not surprising that MALDI-TOF led to polymer breakdown and the technique was not investigated further. Although knowing the mass range of the polymers being produced would be interesting, it is not essential for polymer applications and polymerisation optimisation.

The FTIR spectrum of the precipitate from the reaction shows broadened peaks compared to monomer **4** (Figure 2.11). The medium signal at 1444 cm^{-1} in the monomer **4** spectrum was assigned to the cyclic C=C group. The same region in the spectrum of the precipitate contains several broad peaks at 1431 cm^{-1} , 1518 cm^{-1} and 1629 cm^{-1} . These peaks were assigned to the C=C bonds present in the polymeric material. The additional C=C signals in the polymer might have been caused by the moderate dispersity of the material, resulting in different chemical environments.

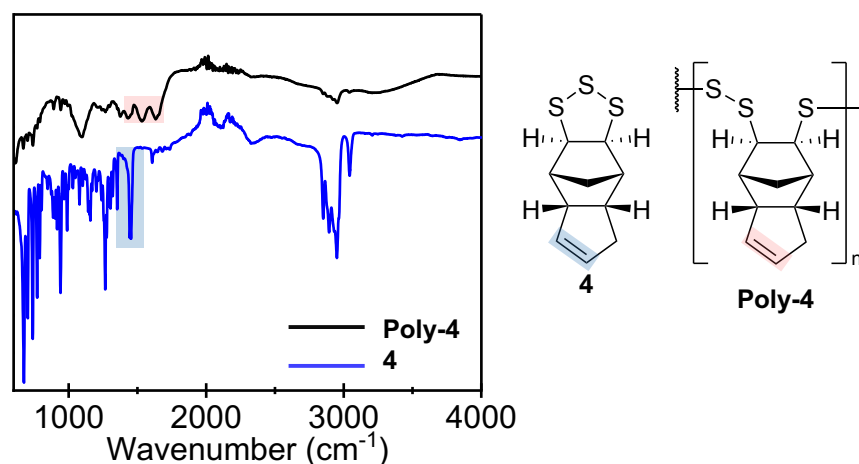


Figure 2.11: FTIR spectra of monomer **4** and precipitate (**poly-4**).

Raman spectroscopy was also used to analyse the material. However, fluorescence interference was observed while using either a 532 nm laser or a 785 nm laser (Figure 2.12). The presence of fluorescence interference in Raman spectroscopy was known to occur for dicyclopentadiene-sulfur copolymers.^[23] It had been reported recently that this fluorescence can be minimised using a lower-powered laser to run the analysis.^[23] Therefore, using a 1064 nm laser, a Raman spectrum of the polymer was obtained (Figure 2.12). The spectrum shows some fluorescence interference. However, the signals in the S–S region at 425–550 cm^{-1} and C–S region at 670–780 cm^{-1} were observed in both the monomer **4** and polymer (**poly-4**) spectra.

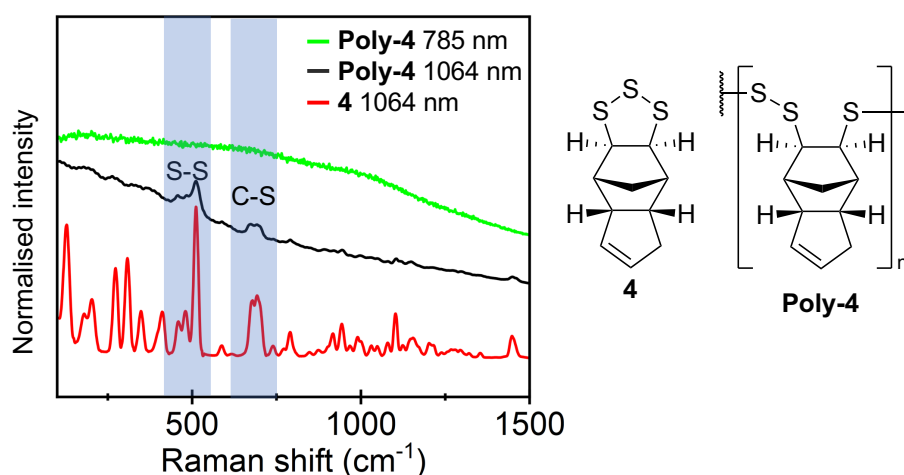


Figure 2.12: Raman spectra of monomer **4** (1064 nm laser) and precipitate (**poly-4**) using a 1064 nm and a 785 nm laser.

A commonly used technique to analyse polymeric materials are degradation studies to investigate the structural composition of the polymer. This technique has been used to analyse the structure of an insoluble dicyclopentadiene-sulfur copolymer that was synthesised through inverse vulcanisation at 140 °C.^[2] The degradation of the copolymer by LiAlH_4 reduction was conducted at

different stages during thermal mixing and curing. At earlier stages in the polymerisation process, the reduced dicyclopentadiene species contained one or two thiol groups and an intact alkene group, indicating a linear polymer structure. After the polymer was cured at 140 °C for 24 h, the reduced dicyclopentadiene species contained between one and four thiol groups, indicating crosslinking had occurred. LiAlH₄ reduction of the electrochemical polymerisation product (**poly-4**) revealed dicyclopentadiene dithiol (**5**) as a clean product after hexane extraction of the mixture shown in the ¹H NMR spectrum (Figure 2.13). This product corroborates the proposed linear structure of the polymer and provides evidence that the alkene remains intact, and no cross-linking occurs. This experiment also suggested that the C–S bonds retain the same stereochemistry as the original monomer.

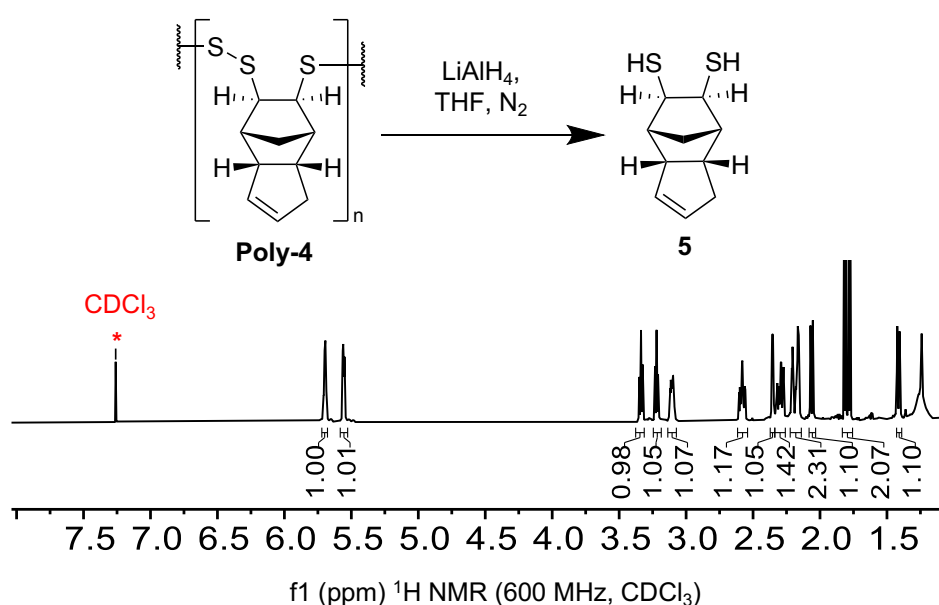


Figure 2.13: ¹H NMR spectrum of hexane extract showing high purity for dithiol **5**.

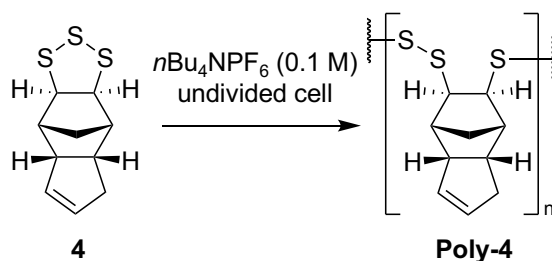
Several important conclusions were drawn from this initial study of the polymerisation of monomer **4**. First, cathodic reduction of monomer **4** rapidly produced polymer, as evidenced by ¹H NMR spectroscopy, GPC, FTIR, and Raman spectroscopy. Second, the polymer was soluble in several organic solvents — an advantageous property for polymer processing. Third, the reaction was chemoselective: no reaction occurred at the alkene, and polymerisation was therefore due to a ring-opening reaction of the 1,2,3-trithiolane functional group. Finally, the C–S stereochemistry is selectively installed in the monomer synthesis and retained in the polymer.

Electrochemical polymerisation optimisation

After successfully achieving electrochemically induced ROP of monomer **4**, polymerisation optimisation studies were conducted (Table 2.2). Several variables were investigated, including

changing electrode material, solvent, electrolyte concentration, monomer concentration, atmosphere, constant current, applied potential, and reaction time. Each reaction was run for 30 minutes unless otherwise specified. At the end of each reaction, an aliquot of the crude mixture was taken, concentrated under reduced pressure, and analysed by ^1H NMR spectroscopy to measure monomer conversion. For this reason, monomer **4** was selected as an ideal monomer for optimisation experiments, as its proton signals did not overlap with the electrolyte ($n\text{Bu}_4\text{NPF}_6$) proton signals. This allowed the comparison of the integration of the resonances of the monomer and electrolyte to determine monomer conversion. Each reaction was then purified using centrifugation to determine polymer yield. The polymer was then analysed using GPC to determine M_w and \bar{D} . All reactions were run in a 20 mL undivided cell containing monomer **4** dissolved in an electrolyte solution (15 mL, 0.1 M $n\text{Bu}_4\text{NPF}_6$).

Table 2.2: Summary of optimisation of monomer **4** polymerisation.



	Variation	Conversion (%)	Yield (%)	M_w	\bar{D}
1	Glassy Carbon	66	32	3370	2.14
2	Graphite	66	44	3960	4.20
3	RVC	34	21	3580	6.05
4	BDD	73	45	3350	4.12
5	DCM*	0	0	-	-
6	THF	0	0	-	-
7	DMF	0	0	-	-
8	4 (0.02 M)	97	26	2160	3.74
9	4 (0.06 M)	80	21	3920	3.74
10	Argon	62	34	3110	3.88
11	-1.6 V	44	25	6030	4.47
12	-2.4 V	78	28	2760	3.20
13	10 mA	68	12	3990	9.98
14	60 minutes	66	32	3370	2.14
15	120 minutes	66	24	3920	2.01
16	240 minutes	99	74	3890	2.01

Entry 1 was run under the previously successful conditions for 30 minutes. Specifically, at a monomer concentration of 0.04 M in acetonitrile (15 mL, 0.1 M $n\text{Bu}_4\text{NPF}_6$). The reaction was run under a constant potential of -2.0 V versus Ag/AgCl, which was the peak potential observed during cyclic voltammetry of monomer **4**. The electrode material used was glassy carbon, which was used for the other entries unless otherwise specified. Glassy carbon electrodes were selected as they were

known to be inert across a wide potential range, have chemical stability, are highly impermeable, and have high durability. The reaction resulted in a monomer conversion of 66% and an isolated polymer yield of 32%. The difference in monomer conversion and isolated polymer yield was attributed to the purification method by successive precipitation, which excludes lower molecular weight polymers. The isolated product had a M_w of 3370 g/mol and a D of 2.14.

Graphite is a cheaper carbon-based material than glassy carbon, therefore acting as a more cost-effective electrode material. Entry 2 shows graphite electrodes perform similarly to glassy carbon in terms of monomer conversion and a slightly higher yield of 44%. However, electrode degradation was observed during the reaction, likely caused by the permeation of the reaction mixture into the more porous electrode surface. The degradation caused cracking and breaking of the graphite electrodes, which made them unusable for further reactions. Therefore, it was not feasible to use graphite electrodes for the polymerisation.

Reticulated vitreous carbon (RVC, entry 3), another carbon-based electrode material was assessed due to its remarkably high void volume and surface area. With higher surface area, it was hypothesised that a higher monomer conversion would be observed due to increased activity. However, this was not the case, as a decrease in conversion (34%) and isolated polymer yield (21%) was found. RVC electrodes are also very brittle, which resulted in electrode contamination into solution.

Boron-doped diamond (BDD) electrodes were investigated next due to their high durability and superior electrochemical stability (entry 4). A monomer conversion of 73% and isolated polymer yield of 45% was observed, slightly outperforming the glassy carbon electrodes (entry 1). BDD electrodes were not used further due to their high cost. Therefore, glassy carbon electrodes were used for subsequent reactions.

DCM, THF, and DMF were previously investigated for monomer redox activity using cyclic voltammetry due to their monomer solubility properties. Significant redox activity was not observed in these solvents, but they were still tested under the polymerisation condition (entry 5, 6, and 7). DCM has low conductivity for supporting ions due to its low permittivity and ionization properties. Due to these factors, it was not surprising that no polymerisation occurred when a potential of -2.0 V versus Ag/AgCl was applied. THF also has poor permittivity, making it a poor solvent for electrochemistry. When the reaction was run in THF, no polymerisation occurred. The permittivity of DMF is comparable to that of acetonitrile. Also, a subtle change in redox activity was observed when cyclic voltammetry of monomer **4** was conducted in DMF. However, under the reaction conditions used in entry 7, no polymerisation occurred. It is likely that applying a stronger reduction

potential would cause ring-opening of monomer **4**. However, a harsher reductive potential can cause damage to the electrodes and electrolyte. Therefore, acetonitrile was used for subsequent reactions.

Next, the optimal monomer concentration was investigated. It was hypothesised that increasing monomer concentration would lead to higher molecular weight polymers. Entry 8 had a reduced monomer concentration from 0.04 M to 0.02 M. As expected, an increase in conversion was observed but unexpectedly there was a decrease in isolated polymer yield. It was suspected this is due to formation of smaller polymer chain lengths caused by the decrease in monomer concentration. The molecular weight of the isolated polymer material confirmed this as it was lower (2160 g/mol) than the polymer collected from the 0.04 M reaction (entry 1, 3370 g/mol). By increasing the monomer concentration (entry 9, 0.06 M) greater conversion (80%) was observed compared to the reaction run at 0.04 M (entry 1, 66%). The inflated conversion value was due to the insolubility of the monomer in acetonitrile at the increased concentration. A crude aliquot was taken at the end of the reaction to determine conversion, which does not consider monomer that had precipitated out of solution. At the higher monomer concentration, the polymer had a M_w of 3920 g/mol. This molecular weight was not significantly different than the molecular weight of the polymer run at 0.04 M (entry 1, 3370 g/mol). It was believed to achieve a higher molecular weight, the monomer concentration must be significantly higher to have an effect. However, the solubility of the monomer in acetonitrile limits this approach. Based on the solubility of monomer **4** in acetonitrile, a concentration of 0.04 M was used for subsequent reactions.

An inert atmosphere of Argon (entry 10) was investigated next to see how it affected the polymerisation reaction. Using rigorously dried reagents and glassware and under an atmosphere of argon, no significant change in conversion, yield and molecular weight was observed compared to the same reaction run under atmosphere (entry 1). This indicated that the electrochemical process did not require an inert atmosphere which simplified the method. In comparison, the anionic polymerisation of 1,2,3-trithiolanes was highly sensitive to moisture and oxygen and requires tedious preparation of initiators.^[18]

For entry 11 and 12, the potential applied to the cell was changed to either side of the reductive redox peak (-2.0 V versus Ag/AgCl) observed during cyclic voltammetry. At -1.6 V versus Ag/AgCl (entry 11), a decrease in monomer conversion (44%) and polymer yield (25%) was observed. This result was anticipated because less efficient reduction of the monomer was expected at this potential. Interestingly, a larger M_w of 6030 g/mol and a broader \mathcal{D} were obtained at this potential in comparison to the standard reaction at -2.0 V versus Ag/AgCl (entry 1). Relatedly, at -2.4 V versus Ag/AgCl (entry 12) there was an increase in monomer conversion (78%) and a decrease in polymer yield (28%). At this potential, a lower M_w of 2760 g/mol was obtained.

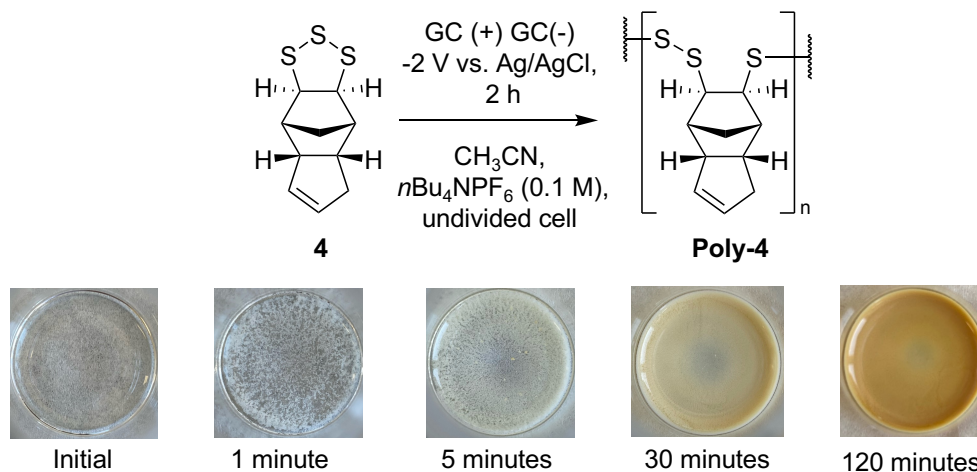
Together, these results suggest that changing the reactor potentials can be used for control over the molecular weight of the polymer.

Another type of electrochemical technique called a galvanostatic reaction is where a constant current is applied to the cell instead of a constant potential. Galvanostatic or constant current reactions are commonly used in electrochemical synthesis as they can be run without the need for cyclic voltammetry studies and are often run without a reference electrode. This makes galvanostatic reactions simpler to set up and run, but not as tailorable to the desired redox reaction. Using a cell containing two glassy carbon electrodes a galvanostatic reaction was carried out on monomer **4** at a current of 10 mA (entry 14). This resulted in a 68% conversion of monomer and a 12% polymer yield with a D of 9.98. Low polymer yield and broad D were expected for the constant current reaction because it did not target the precise reduction potential of the monomer and can therefore result in inconsistent monomer consumption and other side reactions. The disparity between monomer conversion and polymer yield suggests that the formation of lower molecular weight oligomers and polymers were excluded by the isolation procedure. This was also consistent with the broad D inferred from GPC.

The final step in the optimisation table was to increase reaction time to get a high isolated polymer yield. Entry 14, 15, and 16 shows the result for reactions run for 60, 120, and 240 minutes. Entry 16 resulted in a 99% monomer conversion and an 87% isolated polymer yield. M_w and D show consistency across all three reactions under the same conditions. This uniformity was the result of polymer precipitation due to its insolubility at higher molecular weights.

Polymerisation kinetics

To further understand the mechanism of electrochemically induced ROP, the kinetics of the reaction were studied in detail. Monomer **4** was chosen for the kinetic study as it was used in the optimization study, and full characterisation data had been obtained. Using the previously optimised conditions (Table 2.2, entry 1), the polymerisation of monomer **4** was analysed by GPC and ^1H NMR spectroscopy. Over 2 hours, aliquots of 0.5 mL were taken from the reaction mixture (Scheme 2.7), concentrated under reduced pressure, and analysed by ^1H NMR spectroscopy. The integration of the resonance of the monomer to the electrolyte ($n\text{Bu}_4\text{NPF}_6$) was compared to calculate the conversion of the monomer. The aliquots were then dissolved in THF and analysed by GPC to compare changes in dispersity and molecular weight. The reaction was performed in triplicate, and the results were averaged.



Scheme 2.7: Reaction scheme (top). Aliquots of the reaction mixture over the course of the reaction (bottom).

Pseudo-first-order behaviour was observed during the reaction, which indicated a constant concentration of initiating species was being formed, followed by rapid polymerisation (Figure 2.14 A). Surprisingly, the M_w range of the polymeric material over 2 hours appeared relatively constant (Figure 2.14 B, C). This result could be explained by the precipitation observed in the electrochemical cell as the reaction proceeds (Figure 2.14). It was believed that the polymer precipitated at a particular chain length range in this reaction medium, preventing it from growing further. The M_w of the polymer produced was between 4000 g/mol and 5000 g/mol. While many applications require polymers with higher molecular weight, these polymers were still demonstrated to be useful in a number of applications, as described in the following chapter.

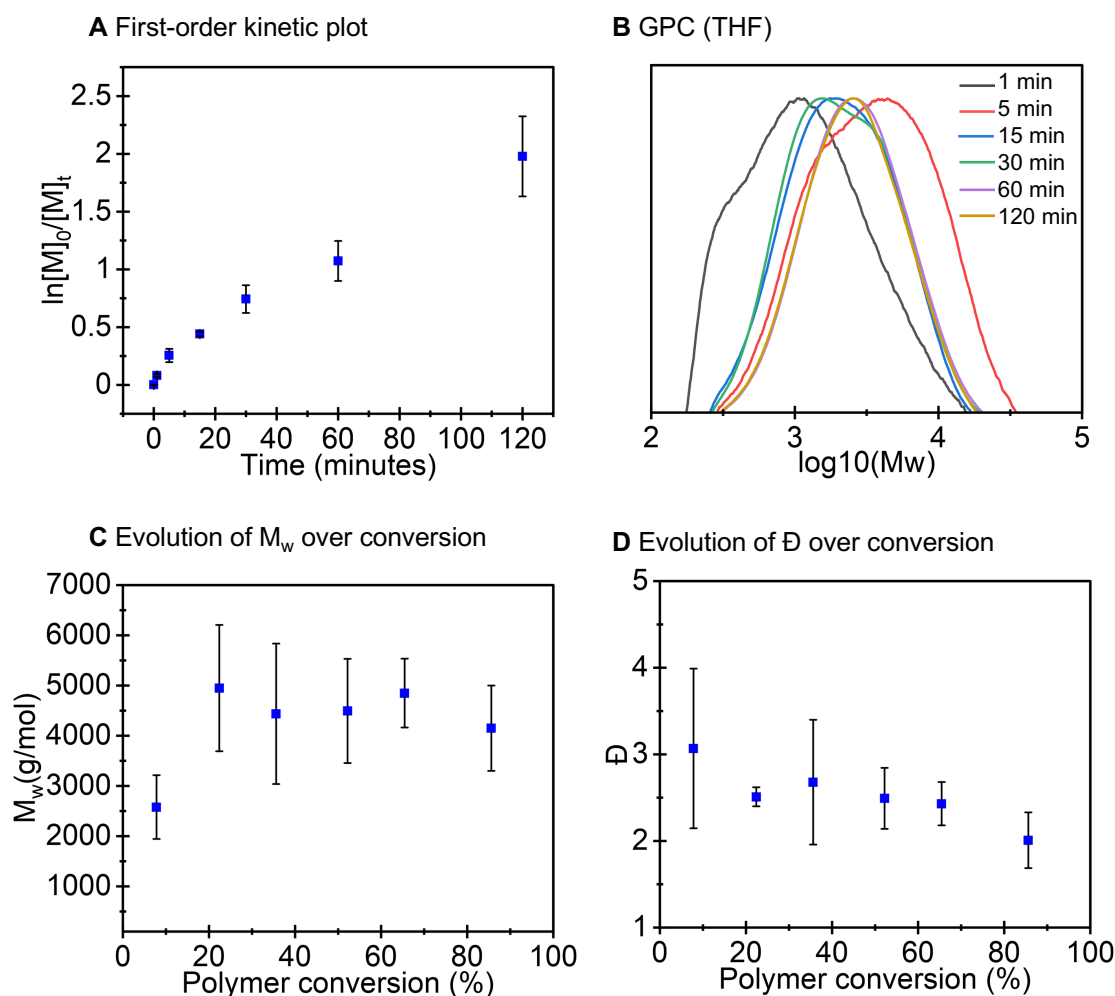


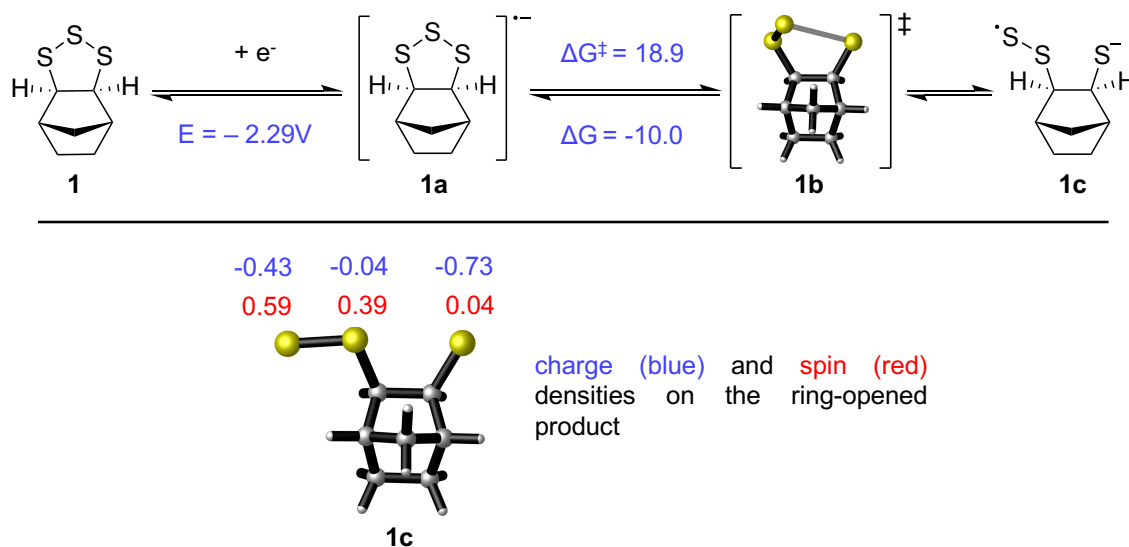
Figure 2.14: (A) Pseudo-first-order kinetic plot of monomer **4** consumption where $\ln[M]_0/[M]_t = k_1t$ ($[M]$ = monomer **4** concentration (M), t = time (minutes), k = first-order rate constant (M/min). (B) GPC (THF) of **poly-4** over 120 minutes of reaction time. (C) Evolution of the M_w of **poly-4** against **poly-4** conversion. (D) Evolution of \bar{D} of **poly-4** against **poly-4** conversion. All data was collected in triplicate.

The precipitation of the polymer provided three advantages to this method. First, a self-protection mechanism against reductive degradation of the polymer in the electrode double layer. In contrast to AROP, which consists of homogeneous chemical initiation that could react with and degrade the growing polymer chain. Second, the precipitation of the polymer at a particular chain length provided control over the polymer molecular weight. This could be utilised by changing the solubility of the polymer in solution using alternative solvents or increasing temperature. The third advantage of the polymer precipitation was an operationally simple purification: the precipitated polymer could be simply filtered away and the electrolyte can be recycled.

Polymerisation mechanism – DFT study

The polymerisation mechanism was studied using DFT calculations. Previously, DFT calculations were used to find the reduction potential of monomers **1**, **2**, **3**, and **4** and compare the values to those obtained experimentally (Table 2.1). The calculated reduction potential for monomer **1** (-2.29 V versus Fc/Fc^+) was consistent with the experimentally observed value (-2.22 V versus Fc/Fc^+) (Table 2.1). Due to its simple and symmetric structure compared to the non-symmetrical monomers **3** and **4**, monomer **1** was selected for subsequent DFT calculations.

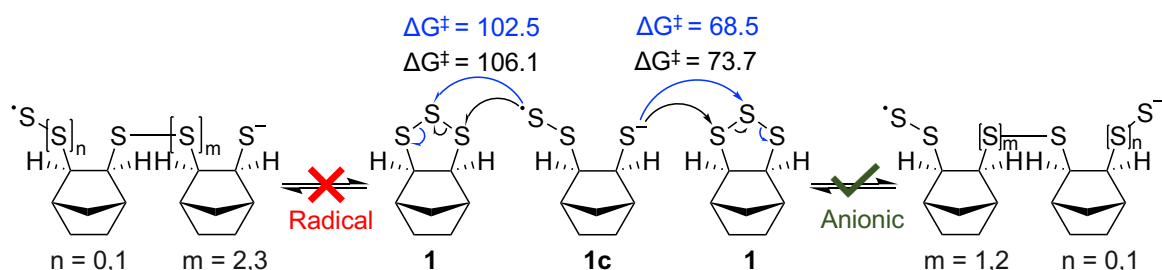
In the initiation step, the electrochemical reduction of monomer **1** results in the formation of the radical anion species **1a** (Scheme 2.8). The radical anion species **1a** does not spontaneously ring-open, but the Gibbs free energy barrier for it to do so was only 18.9 kJ/mol. After ring-opening of the reduced monomer, a formal negative charge was shown on the terminal monosulfide and a formal radical on the terminal disulfide. This depicts the computed spin- and charge-density distribution. However, both terminal sulfide species contained anionic and radical spin and charge density characteristics (Scheme 2.8).



Scheme 2.8: Initiation occurs by ring-opening of a radical anion **1a** formed by electrochemical reduction of monomer **1**. Gibbs free energy barriers and reaction energies (298 K, kJ/mol).

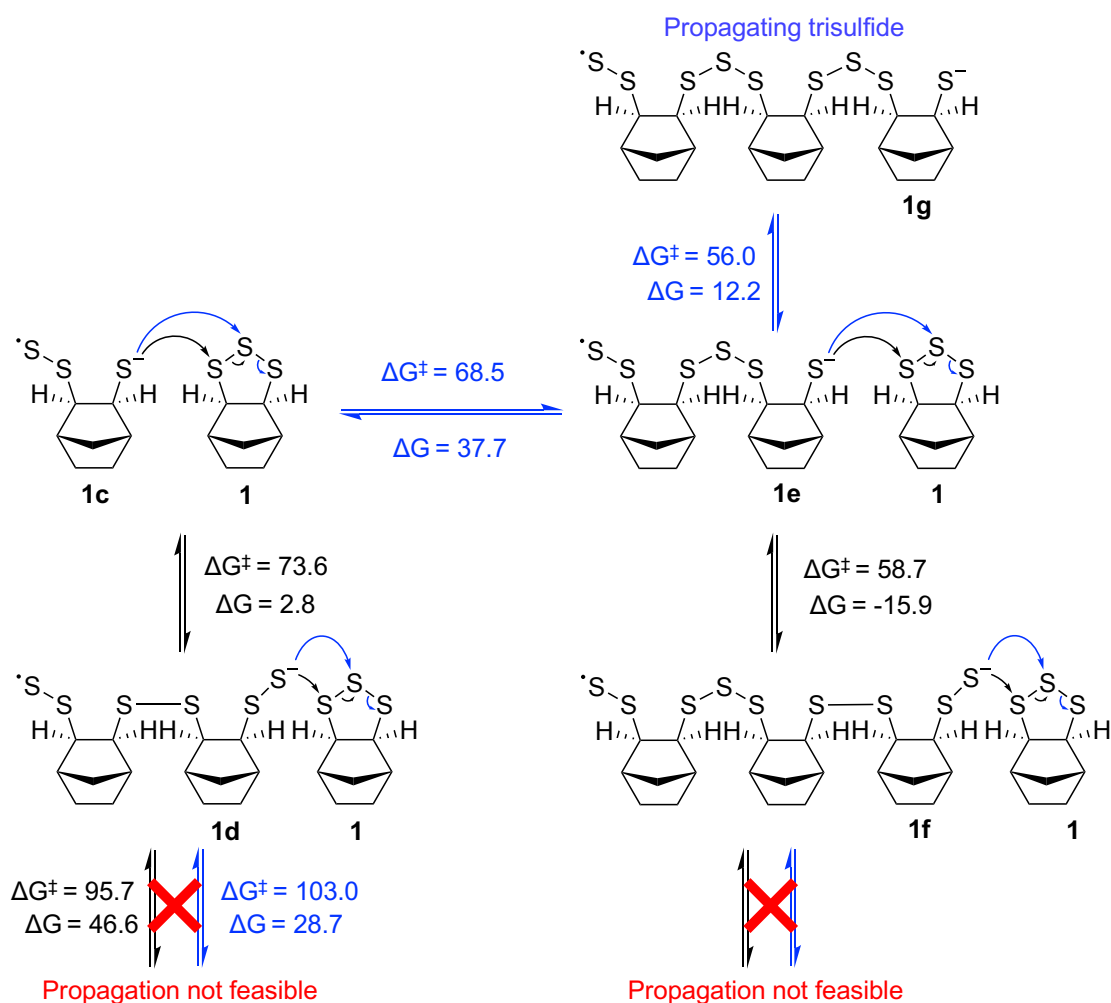
At this stage in the mechanism, inferring how the polymerisation will proceed without computational calculations was difficult. In theory, either terminal sulfur centre on intermediate **1c** or both might attack a neutral monomer, with attack by the terminal monosulfide represented as an AROP, and attack by the terminal disulfide represented as a radical ROP process (Scheme 2.9) Computational calculations revealed the attack by the monosulfide anion to be the considerably more

kinetically favoured pathway, resulting in AROP. Due to the significant difference in the kinetics of these two pathways, attack by the terminal disulfide terminus can be excluded from the proposed mechanism (Scheme 2.9).



Scheme 2.9: Propagation proceeds via AROP as the energy barrier to do so was more kinetically favoured compared to the radical pathway. Gibbs free energy barriers and reaction energies (298 K, kJ/mol).

Propagation occurred via the attack of a neutral monomer **1** by the monosulfide anion on **1c**, resulting in the ring-opening of the neutral monomer, forming a new S–S bond and a terminal sulfide anion (Scheme 2.10). The next computational investigation addressed which sulfur atom on the neutral monomer was attacked by the monosulfide anion. Attack of the terminal sulfur atom would lead to a disulfide linkage and a terminal disulfide anion **1d**, while the attack of the central sulfur atom would lead to a trisulfide linkage and a terminal monosulfide anion **1e**. Based on the calculated barriers and Gibbs free energy values, both pathways were likely to occur, with an approximate 8:1 preference for the latter. The next propagation step was investigated following four proposed pathways, where the two disulfide species from the first propagation step can attack either the terminal or central sulfur atom on a neutral monomer (Scheme 2.10). Attack by the terminal monosulfide anion to either the terminal or central sulfur atom on a neutral monomer was likely to occur, with the rate of attack at the central sulfur atom having a 3:1 kinetic preference. However, attack by the terminal disulfide anion was strongly kinetically and thermodynamically disfavoured, so these pathways can be ruled out.



Scheme 2.10: Proposed propagation mechanism. Gibbs free energy barriers and reaction energies (298 K, kJ/mol).

The formation of disulfide containing species **1d** and **1f** was likely to occur based on the calculations. The terminal disulfide anions were shown to be unreactive due to the high energy barrier, indicating that these species do not propagate further, and only the trisulfide-containing chain **1g** was able to propagate (Scheme 2.10). Consequently, the predominant repeat unit was calculated to be a trisulfide linkage. Interestingly, the computational calculations also revealed that the propagation reaction for all pathways was reversible at room temperature. Therefore, the unreactive disulfide-containing species formed would undergo backbiting, resulting in a monomer species that could re-enter a growing trisulfide chain. This provides a 'self-correction' mechanism that ensures the product consists of trisulfide units only.

Termination of the polymer chains was not investigated computationally. Based on the observation of polymer precipitation, kinetic data showing rapid polymerisation, and computational data showing reversible polymerisation, it was proposed that termination is caused by precipitation

of the polymer chain. Possible end groups could include sulfenic acid, sulfinate, or sulfonate species produced by the aerobic oxidation of the monosulfide anion or disulfide radical.

Polymerisation of other 1,2,3-trithiolane's

The polymerisation of monomers **1**, **2**, and **3** was targeted next. Monomers **1** and **3** were chosen for their functionality, which was applied in future experiments. This included polymer recycling and aqueous solubility of the polymer. The optimised conditions for monomer **4** were applied to these monomers and were reacted for 4 hours. Specifically, at a potential of -2.0 V versus Ag/AgCl at a monomer concentration of 0.04 M in an undivided ElectraSyn cell containing two glassy carbon electrodes. The supporting electrolyte was $n\text{Bu}_4\text{NPF}_6$ (0.1 M in acetonitrile, 15 mL). During the polymerisation, precipitate was observed for all monomers which was consistent with the observations for monomer **4**.

Poly-1 was isolated in a high yield of 83% (Figure 2.15 A). GPC analysis of the polymer in THF revealed a M_w of 6600 g/mol and a D of 3.08 (Figure 2.15 B). The polymer had a slightly higher M_w than **poly-4**, which had a M_w of 3890 g/mol and a D of 2.01 . This higher molecular weight may result from increased solubility in the electrolyte solution, leading to polymer precipitation at longer chain lengths.

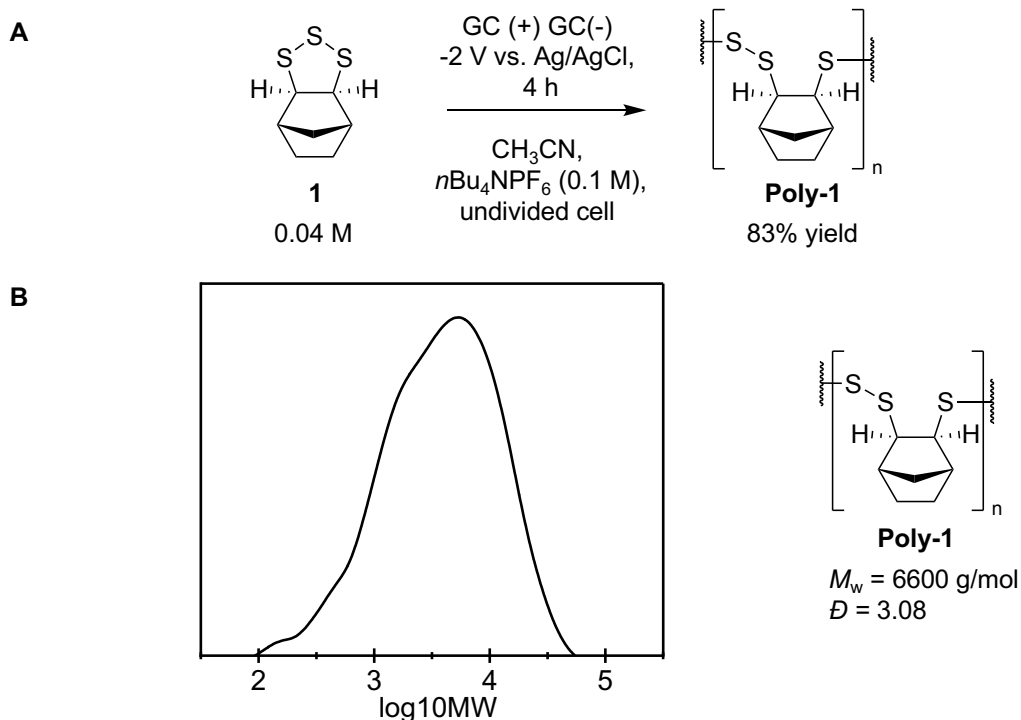


Figure 2.15: (A) Conditions for electrochemical polymerisation of monomer **1**. (B) GPC (THF) trace of **poly-1**.

^1H NMR spectroscopy of **poly-1** revealed broad peaks, consistent with polymeric material (Figure 2.16). In the ^1H NMR spectrum of **poly-1**, the broad signals appear to be split into separate peaks. For example, the proton signals adjacent to the C–S bond in **poly-1** at 3.3–3.7 ppm appear as three signals, whereas the proton signal adjacent to the C–S bond in monomer **1** was a distinct signal at 3.6 ppm (Figure 2.16). The separating of peaks in the ^1H NMR spectrum of **poly-1** could be caused by differences in polymer chain lengths. This was reflected in the broad dispersity of **poly-1** found by GPC analysis (Figure 2.15 B).

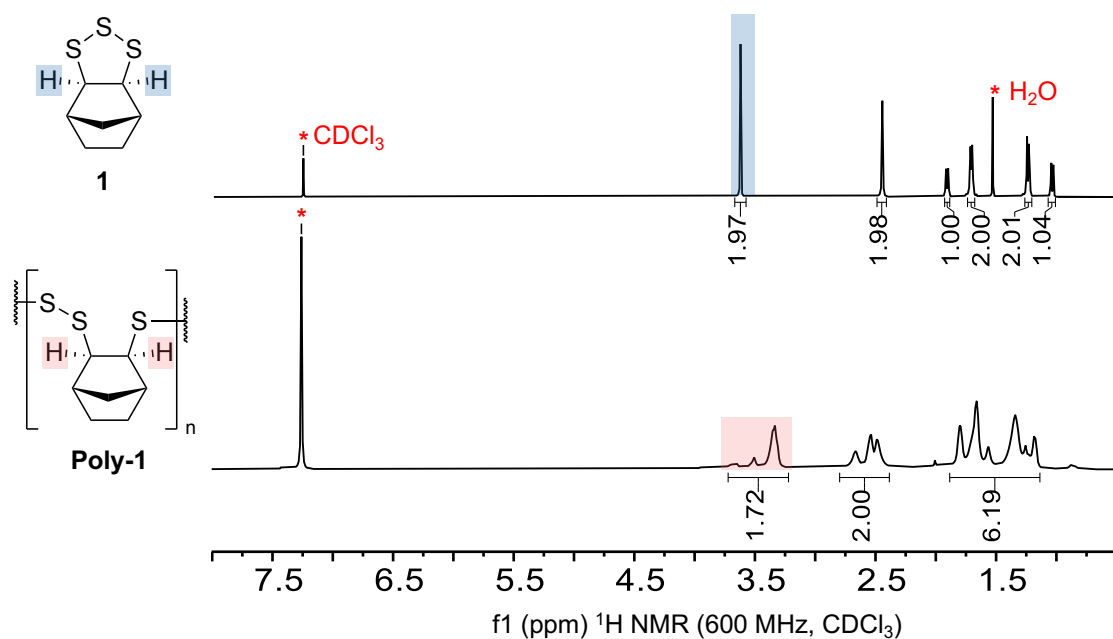


Figure 2.16: ^1H NMR spectra of monomer **1** (top) and poly-**1** (bottom).

The polymerisation of monomer **3** resulted in a moderate yield of 59% (Figure 2.17 A). The carboxylic acid functionality was tolerated under the polymerisation conditions. This was significant as it demonstrated the method's specificity to 1,2,3-trithiolane reduction. ^1H NMR spectroscopy analysis of poly-**3** in DMSO-*d*₆ revealed a signal at $\delta = 12.3$ ppm, consistent with the resonance of a carboxylic acid proton (Figure 2.17 C). This was also supported by FTIR analysis, which showed a strong carbonyl peak at 1697 cm^{-1} in the polymer spectrum, consistent with the monomer peak at 1686 cm^{-1} (Figure 2.17 B).

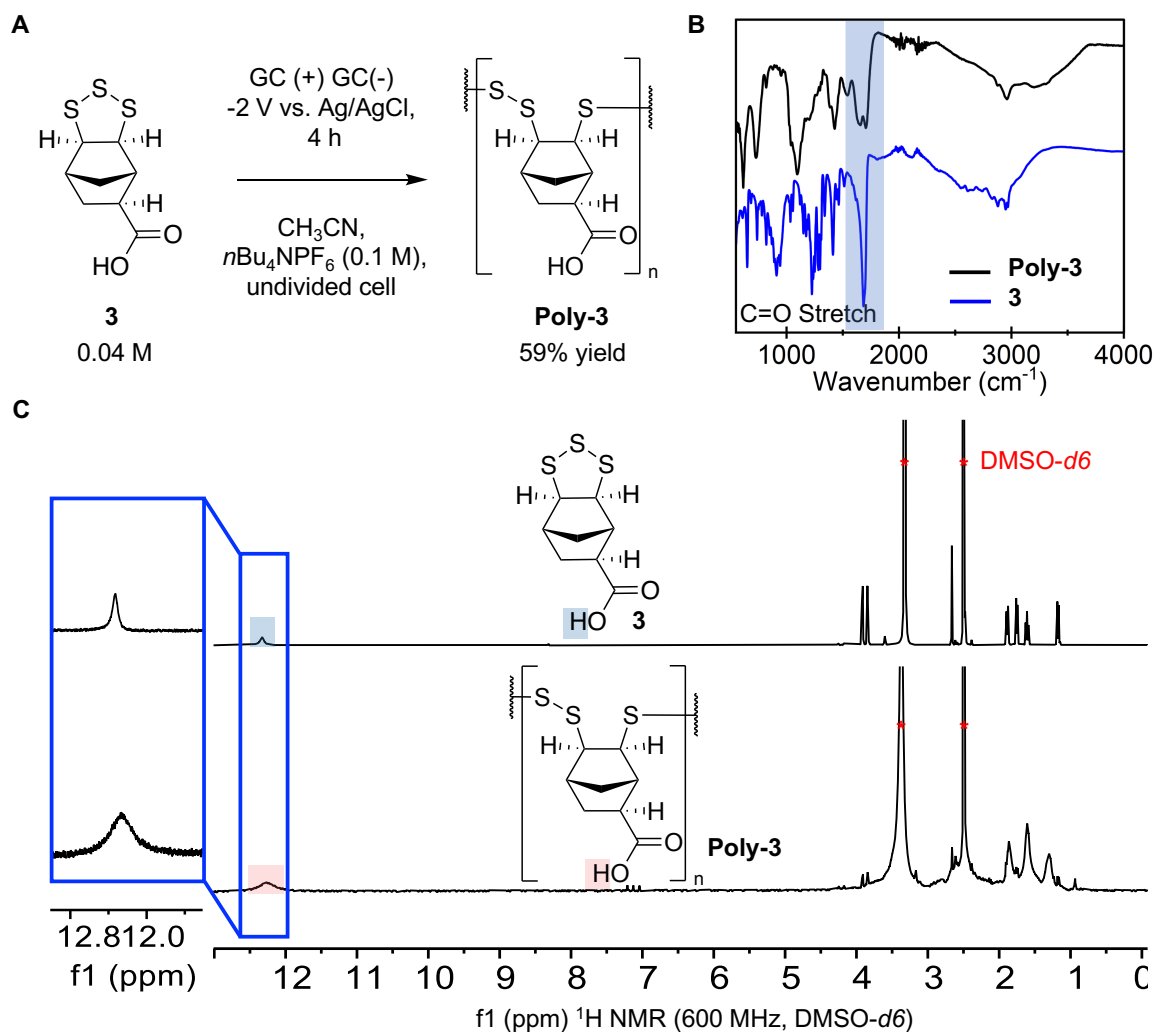


Figure 2.17: (A) Conditions for electrochemical polymerisation of monomer **3**. (B) FTIR spectra of monomer **3** and **poly-3**. (C) ¹H NMR spectrum of monomer **3** (top) and **poly-3** (bottom) in DMSO-*d*₆ shows carboxylic proton signal at $\delta = 12.3$ ppm.

Poly-3 was insoluble in THF and chloroform. **Poly-3** was designed to enhance solubility in aqueous solutions, which was achieved by adding one molar equivalent of NaOH per acid group, resulting in **Na-poly-3** (Figure 2.18).

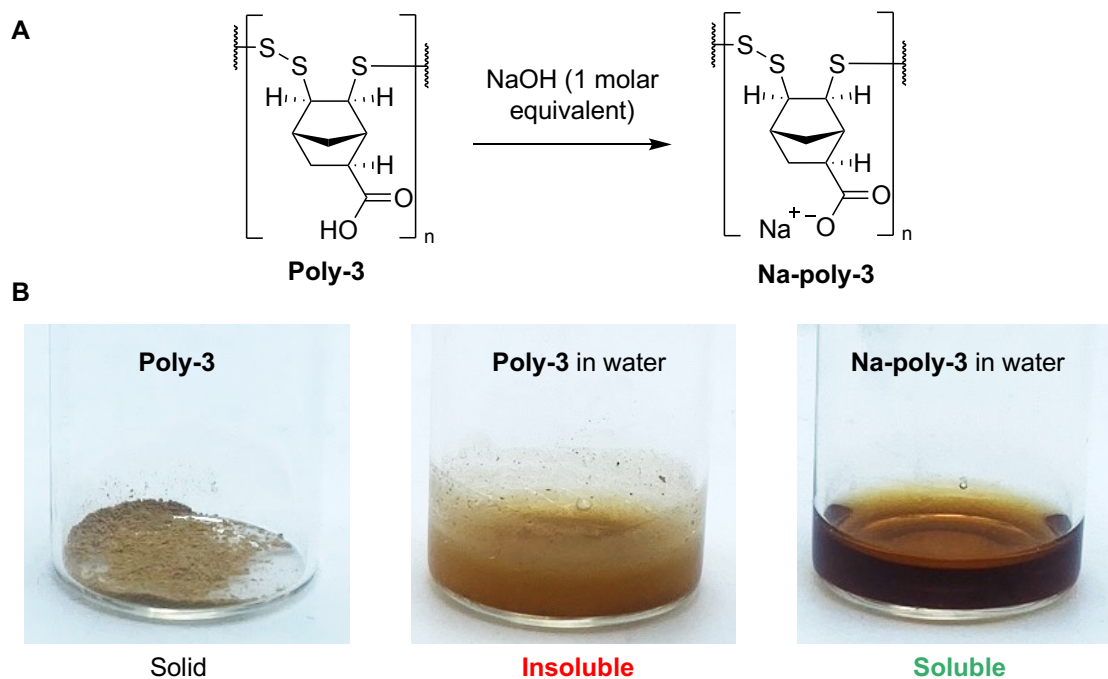


Figure 2.18: (A) conversion of **poly-3** to **Na-poly-3** by addition of 1 mol equiv. of NaOH per carboxylic acid. (B) solubility of **poly-3** and **Na-poly-3** in water.

Na-poly-3 was analysed with aqueous GPC resulting in a M_w of 8600 g/mol and a D of 1.31 (Figure 2.19). The molecular weight of this polymer was not comparable with the other poly(trisulfides) because they had been determined using different eluents and calibrated with different standards. Interestingly, the GPC trace had revealed a bimodal distribution. This might have been a result of greater solubility of the monomer and polymer in acetonitrile, which led to the formation of a higher molecular weight fraction. The lower molecular weight fraction might have arisen from the decreased monomer concentration at a higher conversion. This polymer was designed to be water soluble which was achieved by preparing the sodium carboxylate polymer **Na-poly-3** (Figure 2.18). There had been very few reports of high sulfur content water-soluble polysulfides in the literature. Jenkins and co-workers used high temperature inverse vulcanisation to produce a water-soluble polysulfide from sulfur and a charged comonomer, diallyl dimethylammonium chloride.^[24] Hasell and co-workers recently reported the copolymerisation, under mild reaction conditions, of sulfur and an anionic surfactant, sodium allyl sulfonate, producing a water soluble polysulfide.^[25] **Na-poly-3** offers advantages over polysulfide produced directly from the copolymerisation of organic monomer with elemental sulfur. This was because **Na-poly-3** is pure, has a known sulfur rank, and C-S stereochemistry. Moreover, this polymer demonstrated significant advancements in the sorption of valuable metals in aqueous media, which were investigated in the next chapter.

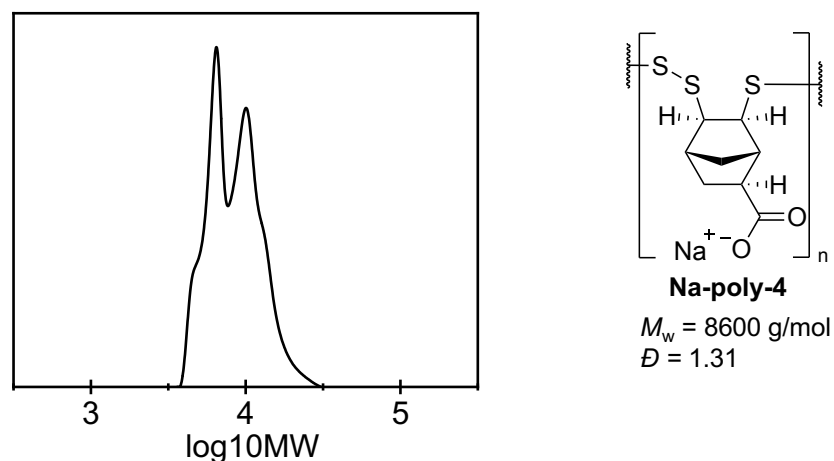


Figure 2.19: GPC (1:1 methanol: water) trace of **Na-poly-3**.

Next, the polymerisation of monomer **2** containing a pentathiolane group had been targeted. Initially, it was hypothesised that reduction and ROP of the five-membered sulfur ring would lead to a polymer with a repeating unit of five sulfur atoms (Figure 2.20 A). This would have resulted in the ability to further control sulfur rank and produce a polymer with a higher sulfur content. While applying a reductive potential of -2.0 V versus Ag/AgCl to monomer **2**, aliquots of the reaction mixture had been taken at 0, 2, and 4 hours and analysed by ^1H NMR spectroscopy (Figure 2.20 B). Before the reaction had begun, a clean spectrum had been observed, only containing the electrolyte and monomer **2**. However, at 2 hours, the proton signals for **2** had decreased by 85% while a signal appeared at 3.6 ppm corresponding to the resonance of monomer **1**. At 4 hours, the proton signal for monomer **1** had decreased by 50%, indicating its consumption leading to the formation of the **poly-1**. This indicated that the reduction of the monomer **2** leads to a desulfurisation event and the production of monomer **1**. This did not align with the original hypothesis but can be viewed as advantageous. If trace amounts of monomer **2** had been present in the monomer solution, they would have been converted into monomer **1** before addition to the growing polymer chain.

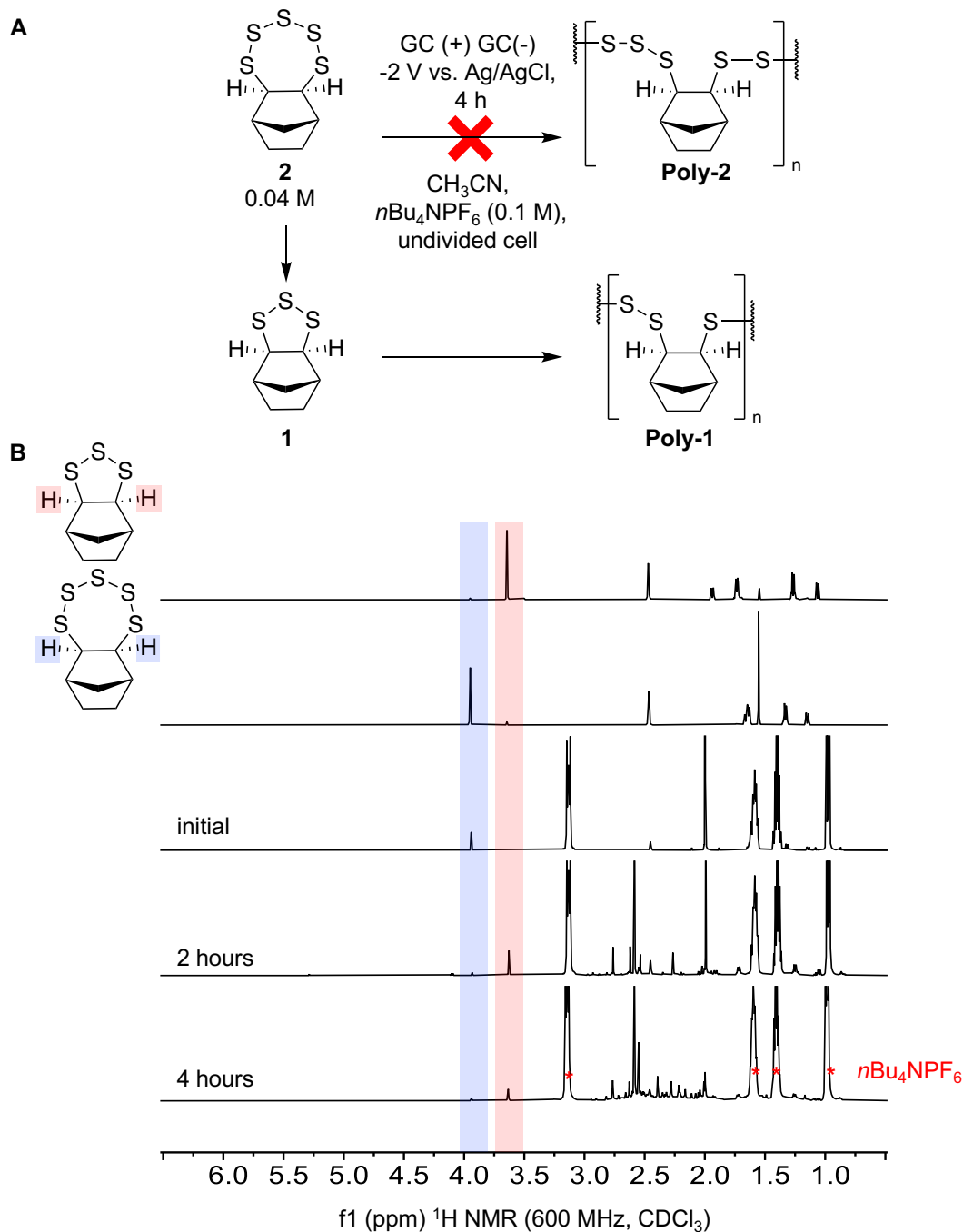


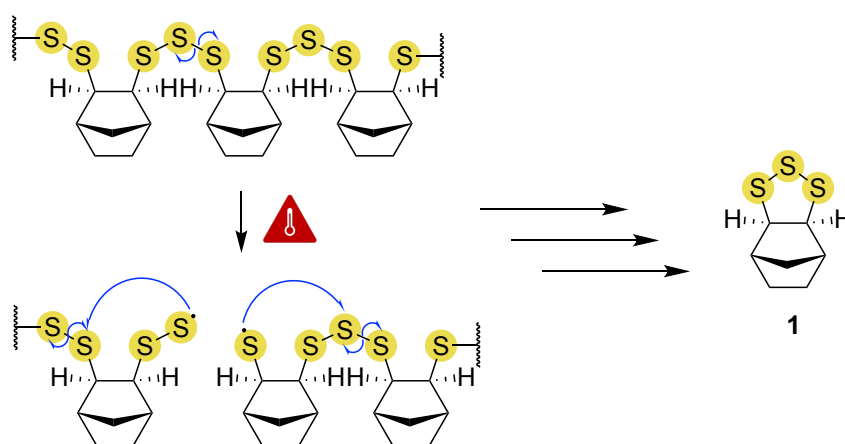
Figure 2.20: (A) It was hypothesised that reduction of monomer **2** would lead to **poly-2**. This hypothesis was shown to be incorrect and a desulfurisation event occurs instead forming monomer **1** and subsequently **poly-1**. (B) ^1H NMR spectra comparing proton signals of monomer **1** and monomer **2** during polymerisation of monomer **2** over 4 hours.

Thermal depolymerisation

Given the increasing environmental challenge posed by plastic pollution and the accumulation of legacy materials, it had been important that the production of new sulfur polymers

did not exacerbate this issue. Currently, recycling polysulfides produced by the copolymerisation of elemental sulfur and organic monomers had been challenging due to their poor solubility, lack of homogeneity and undefined sulfur rank. Our aim was to take advantage of the well-defined poly(trisulfides) to develop a method to recycle them efficiently.

The disassembly and reassembly of S–S covalent bonds were known to occur under high temperature and have been utilised for polysulfide repair.^[26-28] Following this principle, thermal recycling of the poly(trisulfides) back to the original monomer was investigated. **Poly-1** was chosen to investigate recycling methods due to its simple and symmetric structure. It was envisioned that simply heating the polymer would induce homolytic S–S bond cleavage in the trisulfide backbone, followed by radical backbiting to regenerate monomer **1** (Scheme 2.10).



Scheme 2.11: Proposed depolymerisation mechanism involving thermally induced homolytic cleavage of S–S bonds of **poly-1**, followed by backbiting to reform monomer **1**.

To test this hypothesis, **poly-1** was analysed by thermogravimetric analysis (TGA) coupled with GC-MS. At temperatures of 100 °C, 140 °C, 160 °C, and 170 °C the volatile species formed during TGA were analysed by GC-MS (Figure 2.21). The TGA analysis revealed the onset mass loss from the polymer at temperatures above 140 °C, with quantitative mass loss after heating to temperatures >210 °C. Remarkably, between 140 °C and 160 °C, only one signal corresponding to monomer **1** was observed by GC-MS. Above 160 °C, trace signals of norbornene and carbon disulfide were detected, indicating the thermal degradation of **poly-1**.

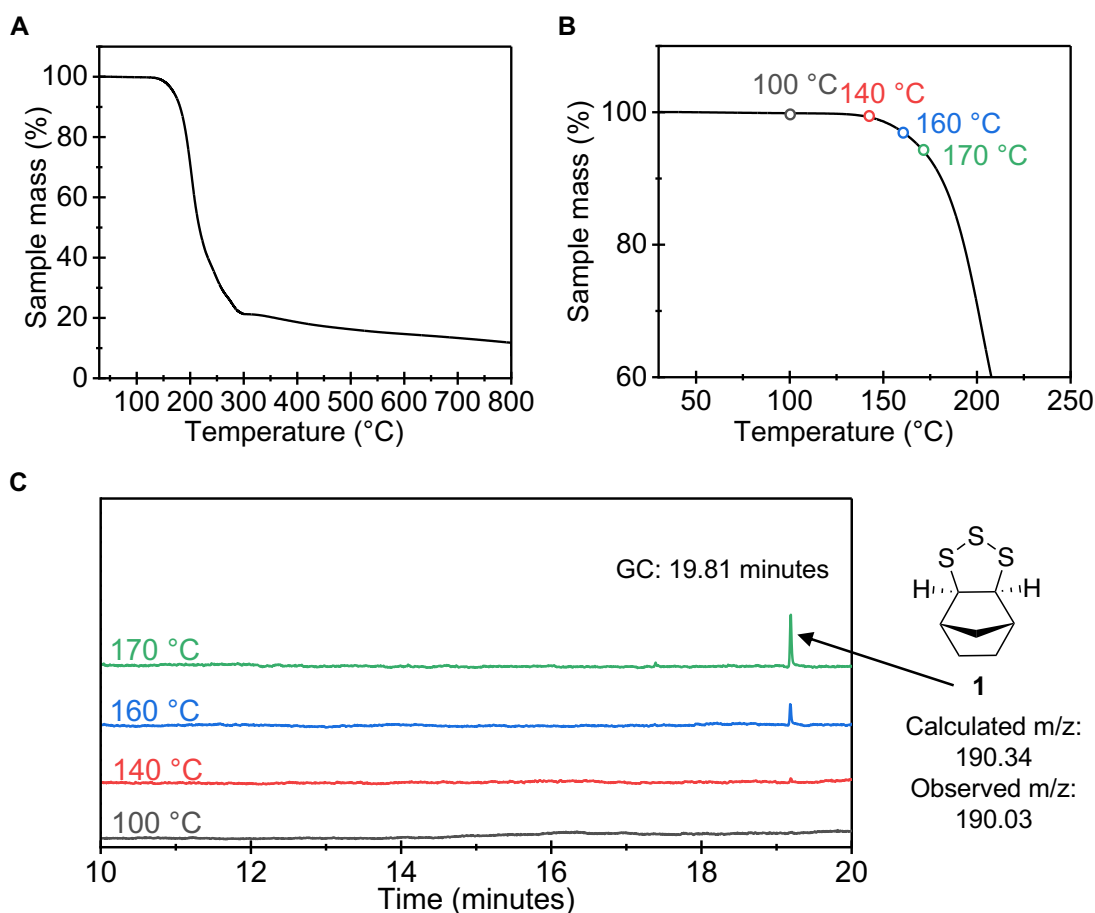


Figure 2.21: (A) TGA of **poly-1**. (B) Zoomed in TGA of **poly-1** showing an onset of mass loss above 140 °C. (C) GC-data of off-gas generated in TGA analysis indicating a single product (monomer **1**) was formed when **poly-1** was heated between 140 °C and 160 °C.

The following recycling method was developed with simplicity and low waste output as key design features. Given the volatility of monomer **1**, direct distillation was investigated as a method for purification and recovery of recycled monomer. A short path distillation apparatus was charged with neat polymer and heated at 150 °C under reduced pressure (1 mbar) for 4 hours (Figure 2.22). During the reaction, a yellow oil was observed in the condenser and collection vial. The distilled yellow oil was analysed by ^1H NMR without any further purification, revealing a highly pure monomer regenerated in a high yield of 72% (Figure 2.22). This experiment demonstrates that poly(trisulfides) can be thermally recycled with high yield and purity via this simple method. Importantly, this method creates a closed-loop system for the repeated recycling of **poly-1** without compromising its chemical and physical properties.

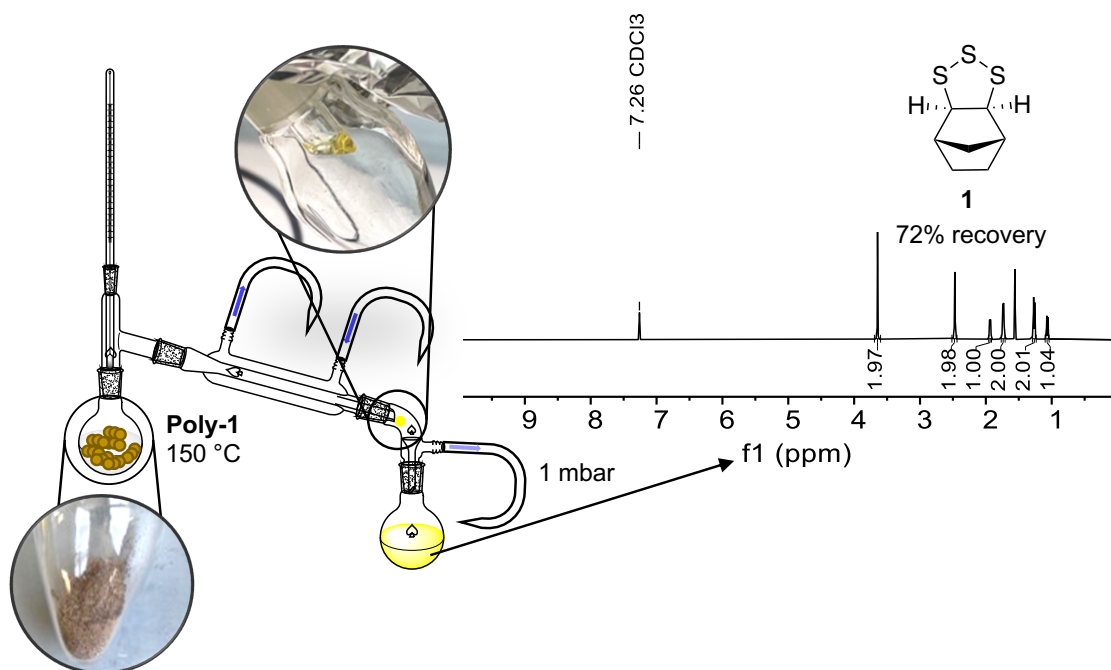


Figure 2.22: Vacuum distillation of **Poly-1** undergoing thermal recycling. ^1H NMR analysis of yellow oil reveals highly pure monomer **1** as the product.

Conclusion

In this chapter, an alternative method to produce polysulfides was developed by harnessing electrochemistry. This study presents the first report of electrochemically initiated ROP of 1,2,3-trithiolanes. The reaction proceeds safely and rapidly at ambient temperature, providing sulfur-rich polymers with a well-defined sulfur rank of three. The electrochemical method was more robust than analogous AROP, potentially motivating further exploration and adoption of this polymerisation technique. Insight into the mechanism was gained through kinetic studies and DFT calculations, revealing an intriguing self-correcting mechanism that favours propagation of the target trisulfide linkage. Thermal depolymerisation of the poly(trisulfides) was shown, resulting in the regeneration of the monomer in high purity.

Moreover, as the monomers were prepared directly from elemental sulfur, this shows a complementary strategy for conversion of excess elemental sulfur generated in the petroleum industry into value-added products. Unlike inverse vulcanisation, however, the electrochemical polymerisation was much milder and offers better control of sulfur rank.

Publication that resulted from the research in this chapter

Electrochemical synthesis of poly(trisulfides)

Pople, J. M. M.; Nicholls, T. P.; Pham, L. N.; Bloch, W. M.; Lisboa, L. S.; Perkins, M. V.; Gibson, C. T.; Coote, M. L.; Jia, Z.; Chalker, J. M. J. *Am. Chem. Soc.* 2023, 145, 11798-11810

Experimental details

General Considerations

Materials: Sulfur was purchased from Sigma-Aldrich (reagent grade, powder, purified by refining, 100 mesh particle size). Dicyclopentadiene, bicyclo[2.2.1]hept-2-ene (norbornene), *exo*-5-norbornenecarboxylic acid, dimethyl disulfide, dimethyl trisulfide, and nickel(II) chloride hexahydrate were purchased from Sigma-Aldrich. Silica gel was purchased from Sigma-Aldrich (technical grade, pore size 60 Å, 230-400 mesh particle size, 40-63 µm particle size).

NMR Spectroscopy: Proton nuclear magnetic resonance spectra (¹H NMR) and carbon-13 nuclear magnetic resonance spectra (¹³C NMR) were recorded on a 600 MHz Bruker spectrometer operating at 600 MHz and 151 MHz, respectively. All chemical shifts are quoted on the δ scale referencing residual solvent peaks (¹H NMR: δ = 7.26 for CDCl₃); (¹³C NMR: δ = 77.16 for CDCl₃); (¹H NMR: δ = 4.65 for D₂O). NMR spectra were assigned using correlation spectroscopy (COSY), heteronuclear multiple quantum coherence (HMQC) and heteronuclear multiple bond coherence (HMBC). Chemical shift values are reported in parts per million, ¹H-¹H coupling constants are reported in hertz and multiplicity is abbreviated as; s = singlet, d = doublet, m = multiplet, ap.= apparent.

Infrared (IR): Spectra were recorded using a FTIR Perkin Elmer Frontier spectrometer between 4000 and 500 cm⁻¹. Samples were analysed on a Perkin Elmer Universal ATR Sampling Accessory.

CHNS elemental analysis: Elemental analysis was performed by combustion analysis at the Chemical Analysis Facility at Macquarie University Analytical & Fabrication Facility.

Gas chromatography–mass spectrometry (GC-MS): GC-MS was carried out on an Agilent 7890A GC system fitted with an Agilent 5975C inert XL EI/CL MSD triple-axis detector and Agilent 7693 autosampler. The column used was an Agilent J&W HP-4ms GC Column, 30 m, 0.25 mm, 0.25 µm, 7-inch cage (19091S-433). The initial temperature of 100 °C was held for 3 minutes before ramping to 200 °C at a rate of 5 °C/min and then ramped to 250 °C at a rate of 20 °C/min.

The gas flow rate (helium) was 1.2 mL/min. The injection volume was 1 μ L with a 60:1 split ratio. The total run time was 25.5 minutes.

High-resolution mass spectrometry (HRMS): HRMS were recorded on a Waters Synapt HDMS Q-ToF by electrospray ionization (ESI) or a Perkin Elmer, AxION, DSA-ToF by atmospheric-pressure chemical ionization (APCI) and were reported as the observed molecular ion in positive or negative mode.

Raman spectroscopy: Raman spectra was collected using a Witec alpha300R Raman microscope at excitation laser wavelengths of 532 nm and 785 nm with a 40X objective (numerical aperture 0.6). The grating used was 600 grooves/mm which gives a spectral resolution of approximately 3 to 4 wavenumbers. The x-axis was calibrated to the 520.6 wavenumber peak for silicon. Approximately ten Raman spectra were collected on each sample with the integration time per spectra typically between 10 to 20 seconds with 2 to 3 accumulations.

Thermogravimetric analysis (TGA): TGA was carried out on a Perkin Elmer TGA800. Samples of 5-10 mg were heated between 30-800 $^{\circ}$ C at varied temperature rates under a flow of nitrogen.

Thermogravimetric analysis coupled with gas chromatography mass spectrometry (TGA-GC-MS): TGA-GC-MS was carried out on a Perkin Elmer TGA800 coupled to a Perkin Elmer Clarus 680 with a Perkin Elmer Clarus Sq 8 T mass spectrometer. The column used was a Perkin Elmer Elite-5MS GC column 30 m, 0.25 mm, 0.25 μ m. The initial temperature of 40 $^{\circ}$ C was held for 8 minutes before ramping to 250 $^{\circ}$ C at a rate of 15 $^{\circ}$ C/min. The gas flow rate was 1 mL/min. The total run time was 23 minutes.

IKA ElectraSyn[®]: Unless otherwise indicated, all polymer syntheses were conducted using an IKA ElectraSyn[®] 2.0. Electrodes were purchased from IKA and used as received. Between uses, glassy carbon electrodes were sonicated in chloroform, polished with Al₂O₃ powder (0.05 μ m) and washed with Mili-Q water and acetone. Standard caps and 20 mL vials were used unless otherwise stated. Reference electrodes were filled with fresh 3 M aq. KCl and washed with chloroform and distilled water after use. Reference electrodes were stored in 3 M aq. KCl between use.

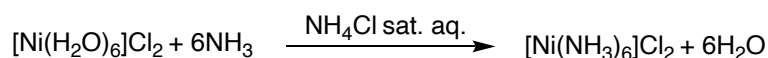
X-ray Crystallography: Single crystals were mounted in paratone-N oil on a nylon loop. X-ray diffraction data was collected at 100(2) K on the MX-1 and MX-2 beamlines of the Australian Synchrotron.^[29-30] Structures were solved by direct methods using SHELXT and refined with SHELXL and ShelXle as a graphical user interface.^[31] All non-hydrogen atoms were refined anisotropically, and hydrogen atoms were included as invariants at geometrically estimated positions.

Electrochemical characterisation: Cyclic voltammetry (CV) and chronoamperometry (CA) were performed on a Gamry Interface 1010E potentiostat (Warminster, PA, USA) using a standard three-electrode cell equipped with working electrode (glassy carbon disk electrode, 3 mm), a counter electrode (coiled platinum wire) and a reference electrode (Ag/AgCl, 3 M aq. KCl). The glassy carbon working electrode with a diameter of 3 mm was polished with Al₂O₃ power (0.05 μm) and washed with Mili-Q water and acetone before use.

Gel permeation chromatography (GPC): GPC of **poly-1** and **poly-4** was performed using a Shimadzu Prominence UPLC fitted with two Aglient columns (PLgel MiniMix-C (5 μm)) and a matching Aglient guard column (MiniMix-C) and a Shimadzu refractive index detector (RID-10 A, λ = 240 nm). The analysis was performed with a mobile phase of HPLC grade THF and an oven temperature of 40 °C. The flow rate was set to 1.00 mL/min. Injection volume was 10 μL. Polystyrene standards were used for calibration. GPC of **poly-3** was performed on a Shimadzu Prominence liquid chromatography system (Kyoto, Japan) coupled with a Shimadzu differential refractive index (RID-20A, λ = 633 nm), using 1:1 v/v MeOH:water as the mobile phase (50 °C) and two Aglient columns (PL aquagel-OH MIXED-M (8 μm), PL aquagel-OH 20 (5 μm)). A flow rate of 0.8 mL/min was applied. Column calibration curves were obtained using Dextran (Polymer Standards Service GmbH).

Synthesis of nickel catalyst

Synthesis of hexaamminenickel(II) chloride



In a 25 mL beaker, open to air, nickel (II) chloride hexahydrate (5.0 g, 21.0 mmol) was dissolved in deionised water (3.4 mL) with sonication. Ammonium chloride (sat. aq., 5 mL) was added. Concentrated ammonia solution (28-30% aq., 10 mL) was added to the solution forming a deep violet colour. The resulting mixture was cooled to 0 °C to crystallise for 1 hour. The crystals were collected by vacuum filtration, washing twice with 0 °C ammonia solution (28-30% aq., 2 mL) and

then with ethanol (10 mL). The crystals were dried under reduced pressure to deliver a violet solid (3.201 g, 66% yield) and used without further purification. **FTIR (neat, cm^{-1}):** 3338, 3185, 1607, 1164, 674. **UV-vis (λ_{MAX} , nm):** 359, 590. **MP:** 196-204 °C (decomp. purple to yellow)

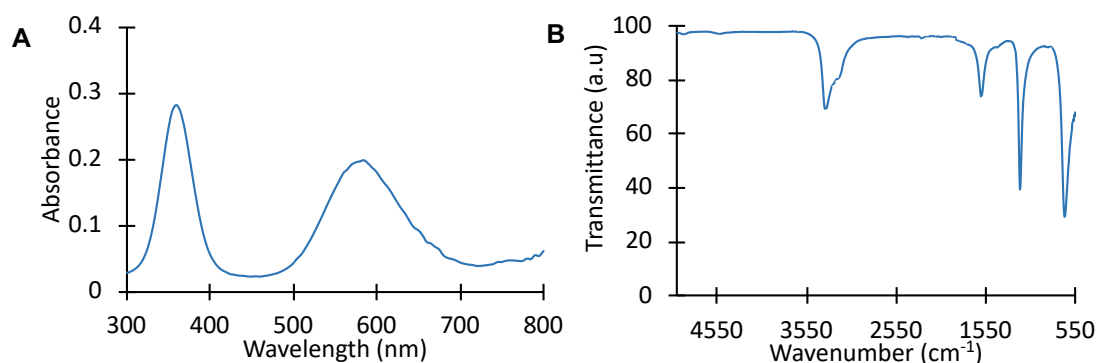
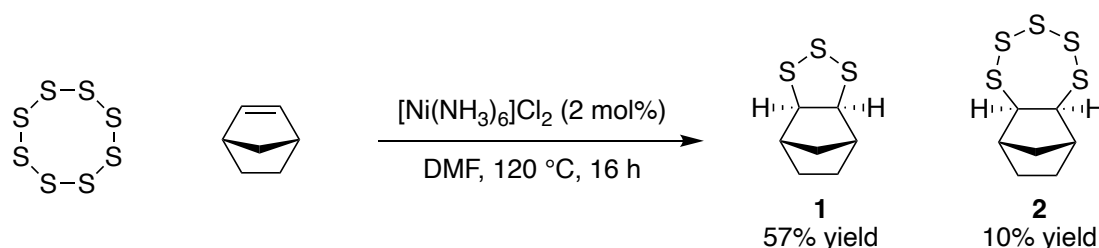


Figure S2.1: (A) UV-vis spectrum of hexaamminenickel (II) chloride (17 mM, 2.5% aqueous NH_3), 2.5% aqueous NH_3 was used as a blank. (B) FTIR spectrum of hexaamminenickel (II) chloride.

Synthesis of cyclic sulfide monomers

Synthesis of norbornane trisulfide 1 and norbornane pentasulfide 2



The following method was adapted from the literature.^[32] A 25 mL round bottom flask was equipped with a reflux condenser and a stir bar, and then norbornene (500 mg, 5.3 mmol) and DMF (5 mL) were added. Elemental sulfur (510 mg, 2.0 mmol S_8) and $[\text{Ni}(\text{NH}_3)_6]\text{Cl}_2$ (23 mg, 0.1 mmol) were then added, and the resulting reaction mixture was heated to 120 °C. After stirring for 16 hours the mixture was allowed to cool to room temperature before the solids were removed by filtration over a thin layer (~1 cm) of silica gel. The silica gel was washed with hexane (3 x 10 mL). Deionized water (10 mL) was added to the filtrate, the layers were separated, and the organic fraction was washed with deionized water (2 x 10 mL). The organic layer was collected, dried (Na_2SO_4), filtered, and concentrated under reduced pressure. Purification by flash chromatography over silica gel (hexane) delivered a yellow oil which formed crystals when dissolved in a small amount of hexane and cooled to 0 °C. The colourless crystals were collected by filtration to deliver monomer **2** (0.07 g, 10% yield). The filtrate was collected, and the solvent was evaporated to deliver monomer **1** as a yellow oil (0.85 g, 86% yield) containing minor impurities of monomer **2**.

To collect monomer **1** as a pure compound, norbornene (20.0 g, 0.21 mol), elemental sulfur (20.4 g, 809 mmol S₈) and [Ni(NH₃)₆]Cl₂ (920 mg, 4.0 mmol) were refluxed at 120 °C in DMF (50 mL). After 16 hours the mixture was allowed to cool to room temperature before the solids were removed by filtration over a thin layer (~1 cm) of silica gel. The silica gel was washed with hexane (3 x 100 mL). Deionized water (100 mL) was added to the filtrate, the layers were separated, and the organic fraction was washed with deionized water (2 x 100 mL). The organic layer was collected, dried (Na₂SO₄), filtered, and concentrated under reduced pressure. Monomer **1** was purified by distillation under a vacuum of 0.78 mbar at 165 °C, to deliver monomer **1** as a yellow oil (23.2 g, 57% yield) that was pure based on NMR analysis.

Monomer **1**: **¹H NMR (600 MHz, CDCl₃):** δ 3.64 (ap. d, *J* = 1.8 Hz, 2H), 2.47-2.44 (m, 2H), 1.94-1.92 (m, 1H), 1.75-1.71 (m, 2H), 1.29-1.24 (m, 2H), 1.08-1.04 (m, 1H). **¹³C NMR (151 MHz, CDCl₃):** δ 69.9, 40.8, 32.4, 27.7. **FTIR (neat, cm⁻¹):** 2952, 2869, 1468, 1446, 1310, 1298. **Elemental analysis:** found C, 44.2%; H, 5.51%; N, 0%; S, 50.43%. C₇H₁₀S₃ requires C, 44.07%; H, 5.30%; N, 0%; S, 50.53%.

Monomer **2**: **¹H NMR (600 MHz, CDCl₃):** δ 3.95 (ap. d, *J* = 1.9 Hz, 2H), 2.47-2.45 (m, 2H), 1.67-1.61 (m, 2H), 1.35-1.30 (m, 2H), 1.16-1.13 (m, 1H). **¹³C NMR (151 MHz, CDCl₃):** δ 75.7, 44.1, 35.7, 28.0. **Mp:** 104-107 °C. **FTIR (neat, cm⁻¹):** 2974, 2932, 2932, 1654, 1380, 1085, 1046, 879. **Elemental analysis:** found C, 33.17%; H, 3.83%; N, 0%; S, 63.09%. C₇H₁₀S₅ requires C, 33.04%; H, 3.96%; N, 0%; S, 63.00%. Note: single crystals suitable for X-ray diffraction analysis were produced by dissolving monomer **2** in the minimum amount of hot chloroform followed by a few drops of hexane and allowing to crystallize at room temperature under atmospheric conditions.

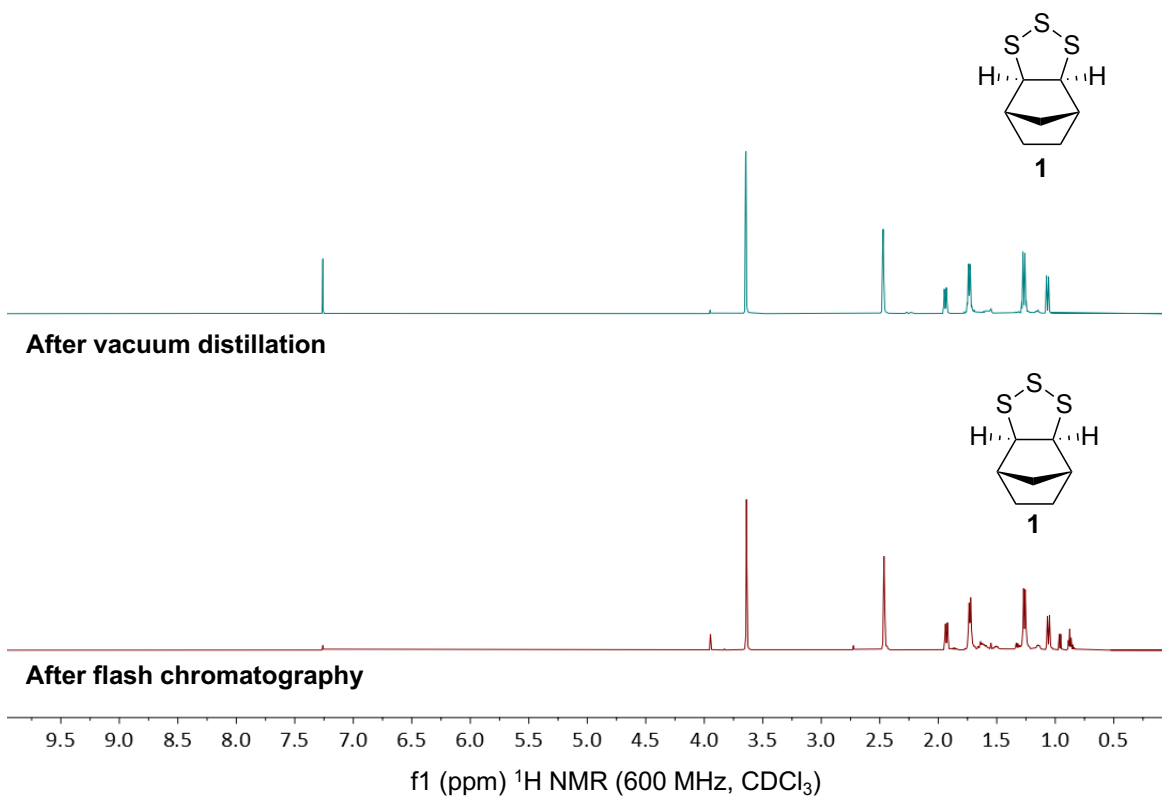


Figure S2.2: ^1H NMR spectra (600 MHz, CDCl_3) of monomer **1** after vacuum distillation (top) and after flash chromatography (silica gel, eluent: hexane).

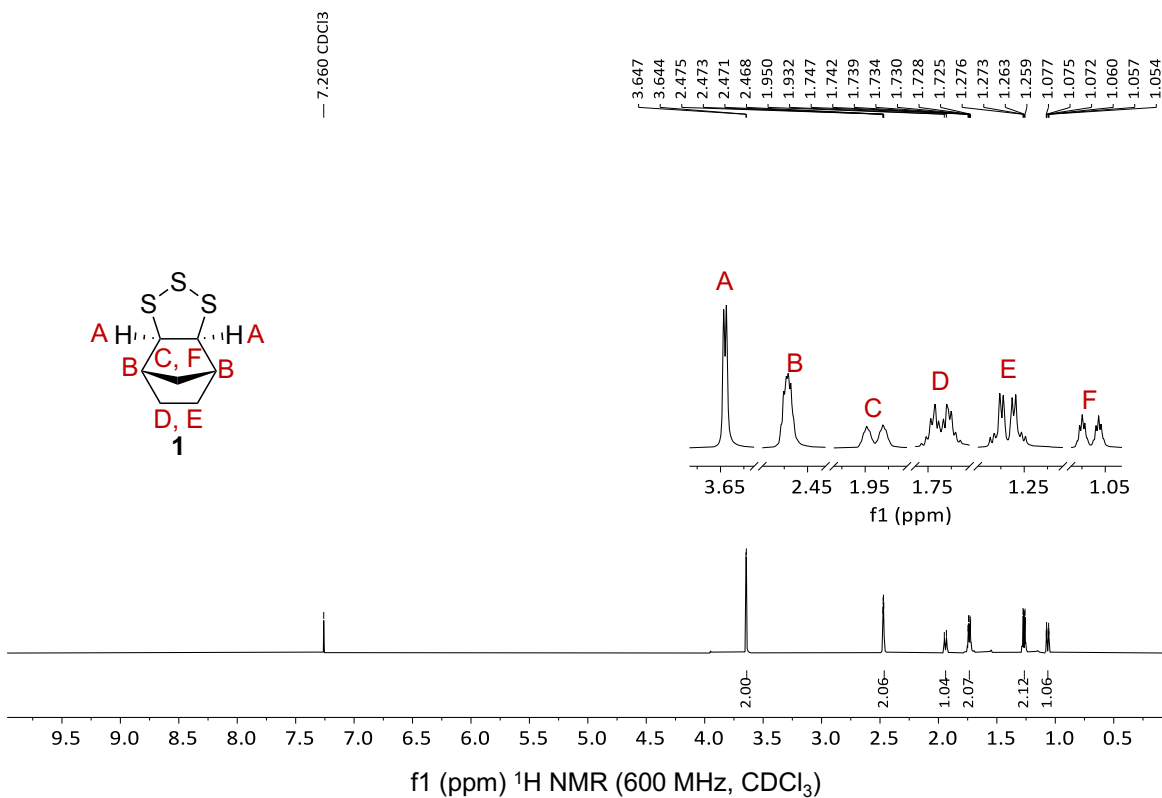


Figure S2.3: ^1H NMR spectrum (600 MHz, CDCl_3) of monomer **1** after vacuum distillation.

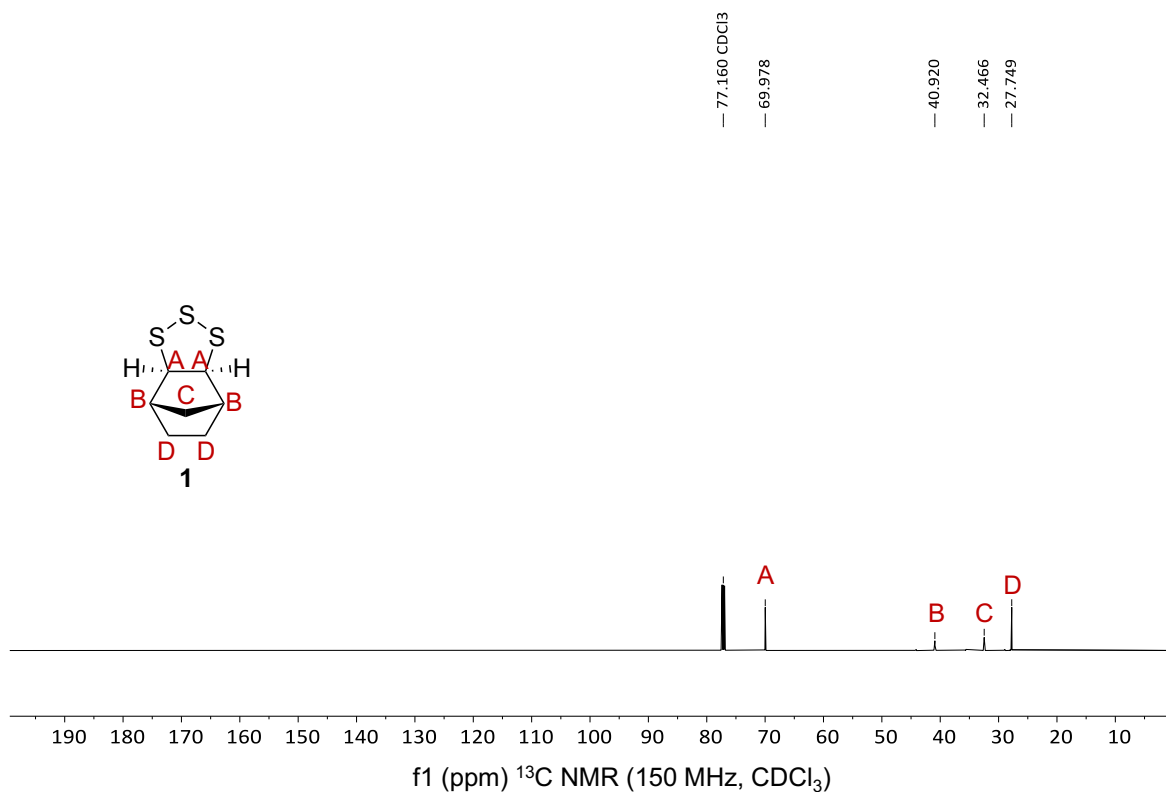


Figure S2.4: ^{13}C NMR spectrum (150 MHz, CDCl_3) of monomer **1** after vacuum distillation.

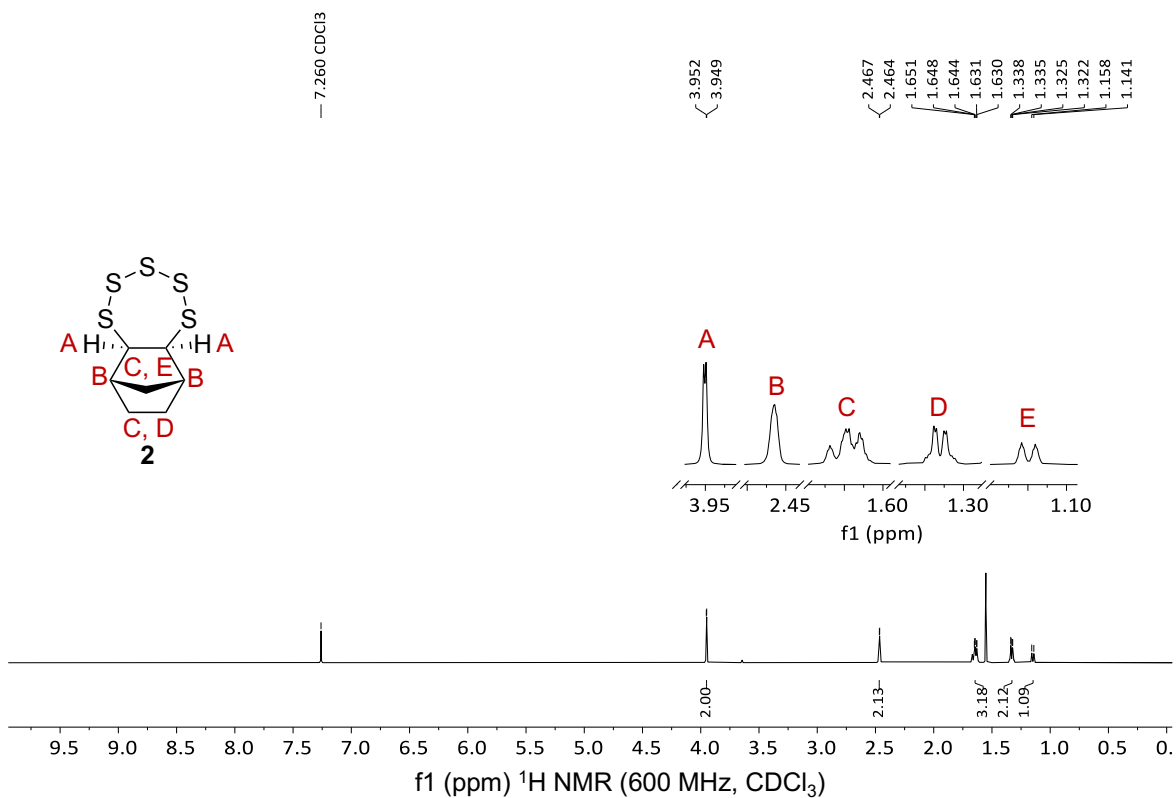


Figure S2.5: ^1H NMR spectrum (600 MHz, CDCl_3) of monomer **2** after flash chromatography (silica gel, eluent: hexane).

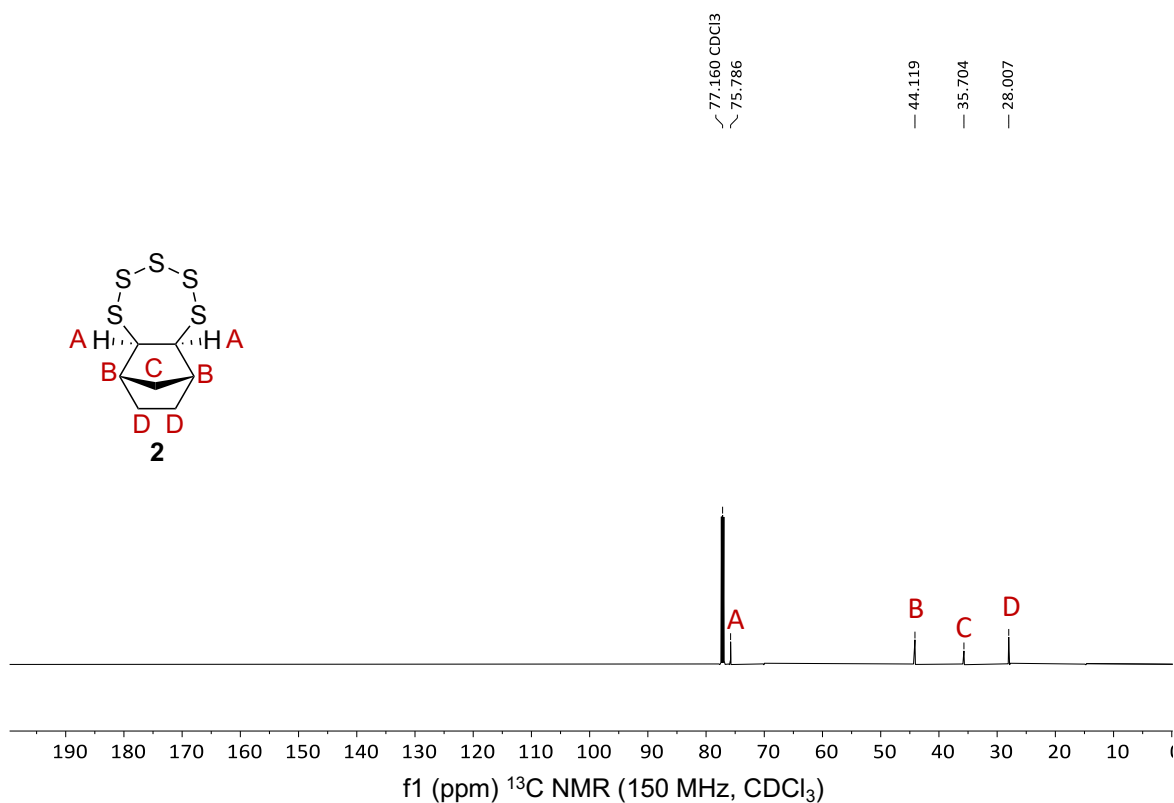


Figure S2.6: ^{13}C NMR spectrum (150 MHz, CDCl_3) of monomer **2** after flash chromatography (silica gel, eluent: hexane).

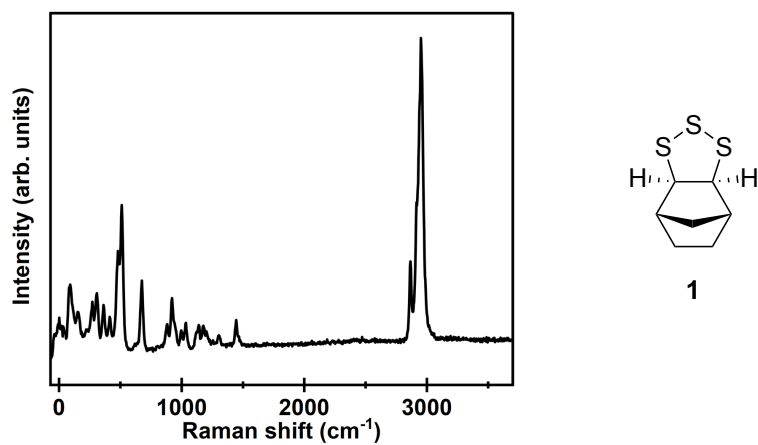


Figure S2.7: Raman spectrum of monomer **1** after vacuum distillation. Excitation laser wavelength of 532 nm. S-S peak observed between 450-540 cm^{-1} .

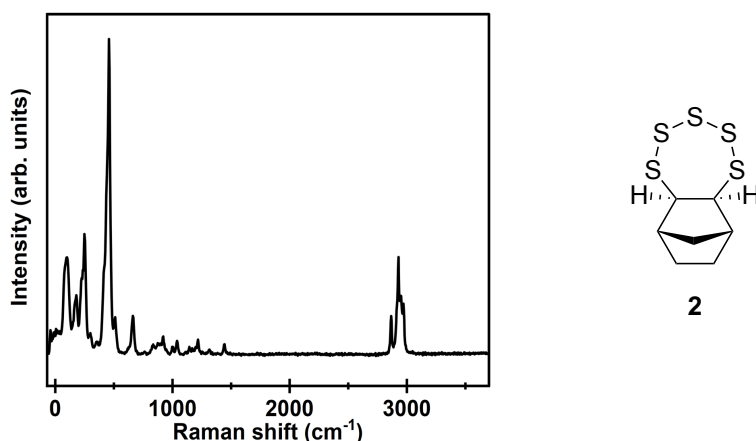
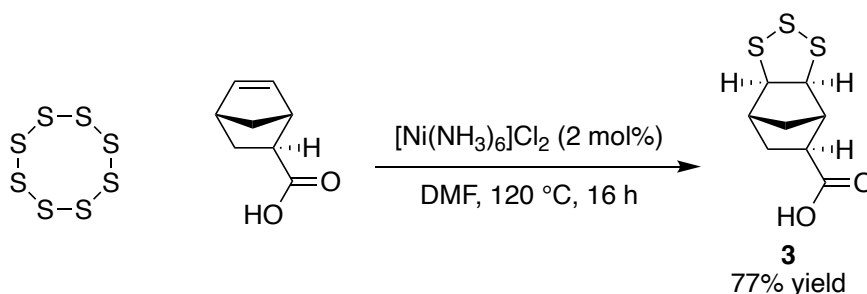


Figure S2.8: Raman spectrum of monomer **2** after flash chromatography (silica gel, eluent: hexane). Excitation laser wavelength of 532 nm. S–S peak observed between 425–475 cm^{-1} .

*Synthesis of norbornane trisulfide carboxylic acid **3***



The following method was adapted from the literature.^[32] To a 100 mL round bottom flask equipped with a stir bar, *exo*-5-norbornenecarboxylic acid (1.00 g, 7.2 mmol) and DMF (10 mL) were added. Elemental sulfur (670 mg, 2.7 mmol, S₈) and [Ni(NH₃)₆]Cl₂ (31 mg, 0.1 mmol) were then added, and the resulting reaction mixture was heated to 120 °C. After 16 hours, the mixture was allowed to cool to room temperature before the solids were removed by filtration over a thin layer (~1 cm) of silica gel. The silica gel was washed with hexane (3 x 20 mL). Deionized water (20 mL) was added to the filtrate, the layers were separated, and the organic fraction was washed with deionized water (2 x 20 mL). The organic fraction was collected, dried (Na₂SO₄), filtered and concentrated under reduced pressure. Purification by flash chromatography over silica gel (hexane: ethyl acetate (1:1)) delivered monomer **3** as a pale-yellow solid (1.3 g, 77% yield). **¹H NMR (600 MHz, CDCl₃):** δ 3.74–3.69 (m, 2H), 2.81 (ap. s, 1H), 2.56–2.54 (m, 1H), 2.51–2.47 (m, 1H), 2.15–2.10 (m, 1H), 2.03–1.98 (m, 1H), 1.68–1.62 (m, 1H), 1.36–1.32 (m, 1H). **¹³C NMR (151 MHz, CDCl₃):** δ 179.5, 69.3, 45.0, 40.7, 32.3, 31.0. **Mp:** 139–141 °C. **FTIR (neat, cm⁻¹):** 2952, 2874, 2122, 1689, 1410, 1285, 1224, 908. **Elemental analysis:** found C, 41.27%; H, 4.32%; N, 0%; S, 44.28%. C₈H₁₀O₂S₃ requires C, 41.00%; H, 4.30%; N, 0; S, 41.04%. **HRMS (ESI):** C₈H₉O₂S₃ [M–H][–], Calculated: 232.9764, Found 232.9748. Note: single crystals suitable for X-ray diffraction analysis were produced by

dissolving monomer **3** in the minimum amount of hot chloroform. A few drops of hexane were added, and the solution was cooled to 0 °C for 30 minutes forming fine yellow crystals.

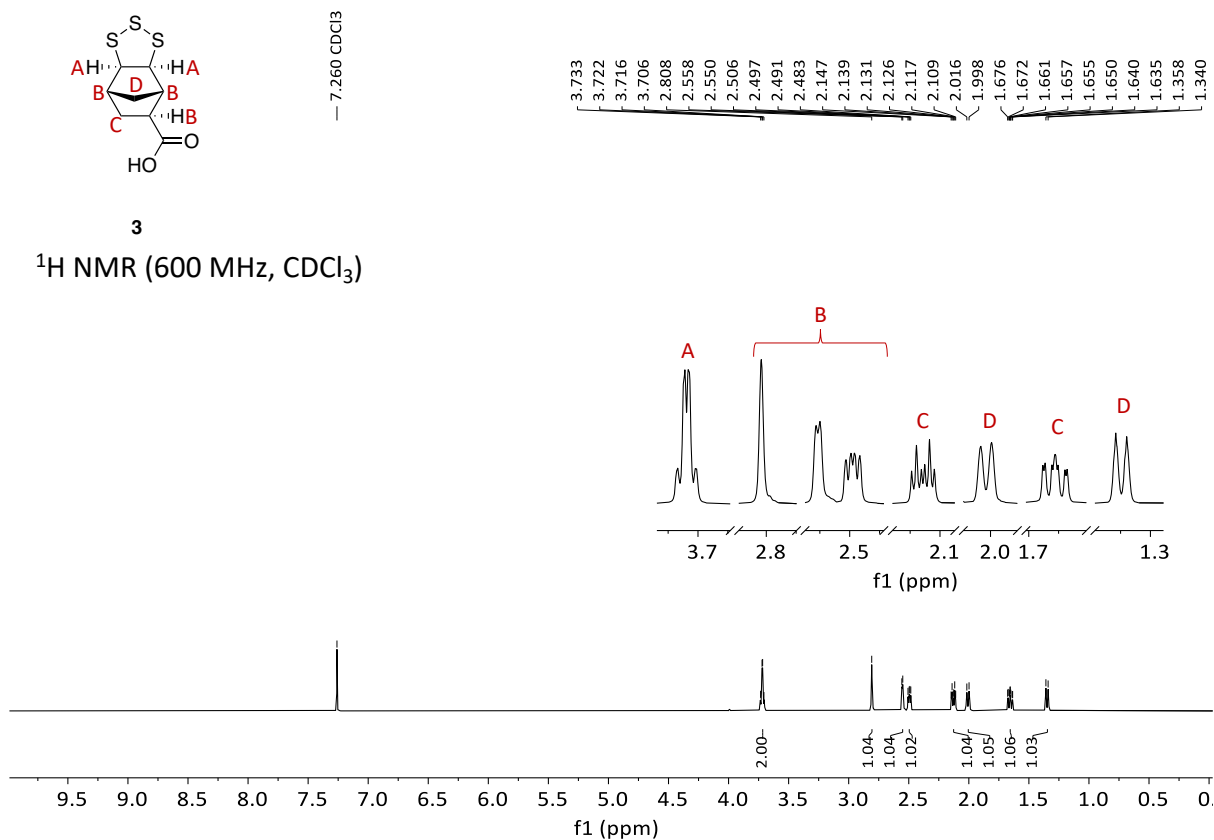


Figure S2.9: ^1H NMR spectrum (600 MHz, CDCl_3) of monomer **3** after flash chromatography (silica gel, eluent: hexane: ethyl acetate (1:1)).

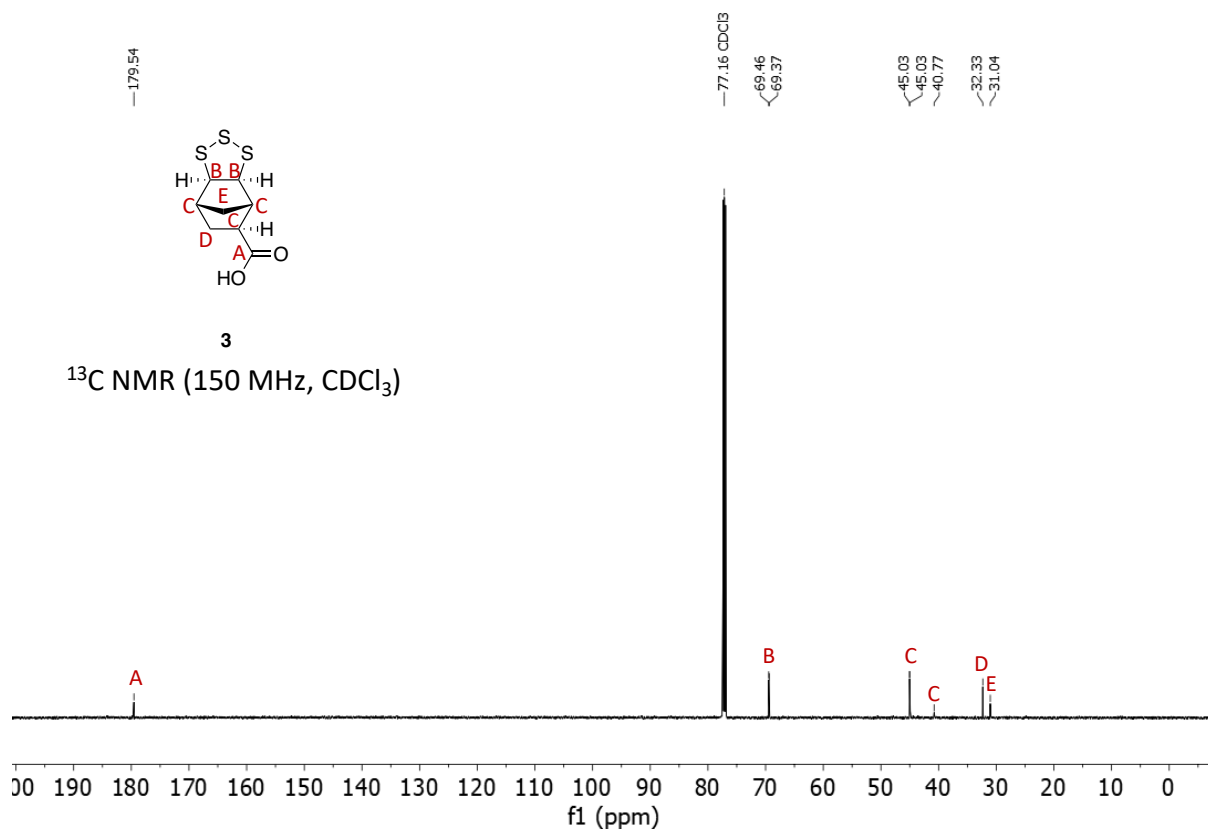


Figure S2.10: ¹³C NMR spectrum (150 MHz, CDCl₃) of monomer **3** after flash chromatography (silica gel, eluent: hexane: ethyl acetate (1:1)).

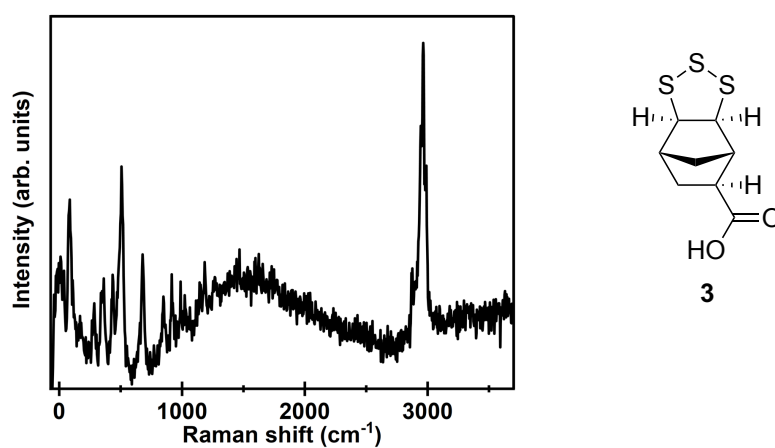
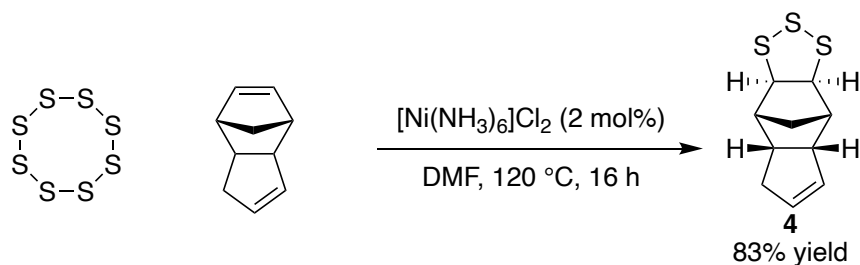


Figure S2.11: Raman spectrum of monomer **3** after flash chromatography (silica gel, eluent: hexane: ethyl acetate (1:1)). Excitation laser wavelength of 532 nm. S-S peak observed between 465-540 cm⁻¹.

Synthesis of dicyclopentadiene trisulfide 4



The following method was adapted from the literature.^[32] To a 100 mL round bottom flask equipped with a reflux condenser and a stir bar, dicyclopentadiene (1.00 g, 7.6 mmol) and DMF (10 mL) were added. Elemental sulfur (730 mg, 2.8 mmol, S₈) and [Ni(NH₃)₆]Cl₂ (33 mg, 0.3 mmol) were then added, and the resulting reaction mixture was heated to 120 °C. After 16 hours the mixture was allowed to cool to room temperature before the solids were removed by filtration over a thin layer (~1 cm) of silica gel. The silica gel was washed with hexane (3 x 20 mL). Deionized water (20 mL) was added to the filtrate, the layers were separated, and the organic fraction was washed with deionized water (2 x 20 mL). The organic layer was collected, dried (Na₂SO₄), filtered and concentrated under reduced pressure. Purification by flash chromatography over silica gel (hexane) delivered monomer **4** as a highly viscous yellow oil (1.92 g, 83% yield) which formed a waxy solid over time. **¹H NMR (600 MHz, CDCl₃):** δ 5.74-5.70 (m, 1H), 5.62-5.59 (m, 1H), 3.69 (ap. ddd, *J* = 17.0, 7.1, 1.9 Hz, 2H), 3.30-3.24 (m, 1H), 2.72-2.66 (m, 1H), 2.61 (ap. d, *J* = 5.1 Hz, 1H), 2.39-2.26 (m, 3H), 2.10 (ap. d, *J* = 10.3 Hz, 1H), 1.32-1.30 (m, 1H). **¹³C NMR (151 MHz, CDCl₃):** δ 132.3, 130.9, 66.3, 62.8, 52.1, 45.3, 43.8, 40.6, 35.8, 31.8. **Mp:** 67-70 °C. **FTIR (neat, cm⁻¹):** 3038, 2944, 2885, 2845, 1457, 1268, 947, 678. **Elemental analysis:** found C, 52.40%; H, 5.11%; N, 0%; S, 43.30%. C₁₀H₁₂S₃ requires C, 52.59%; H, 5.30%; N, 0%; S, 42.11%. Note: single crystals suitable for X-ray diffraction analysis were produced by dissolving monomer **4** in the minimum amount of hot hexane and leaving to recrystallize at room temperature forming fine yellow crystals.

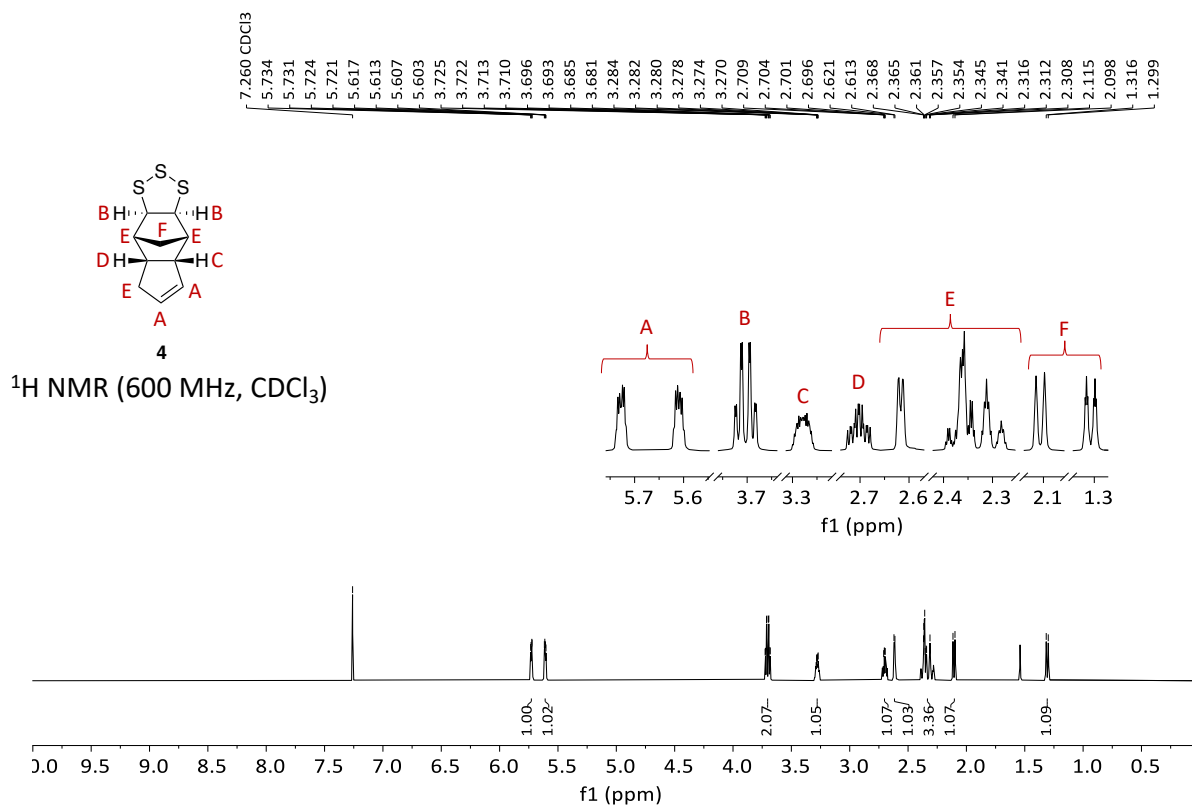


Figure S2.12: ¹H NMR spectrum (600 MHz, CDCl₃) of monomer **4** after flash chromatography (silica gel, eluent: hexane).

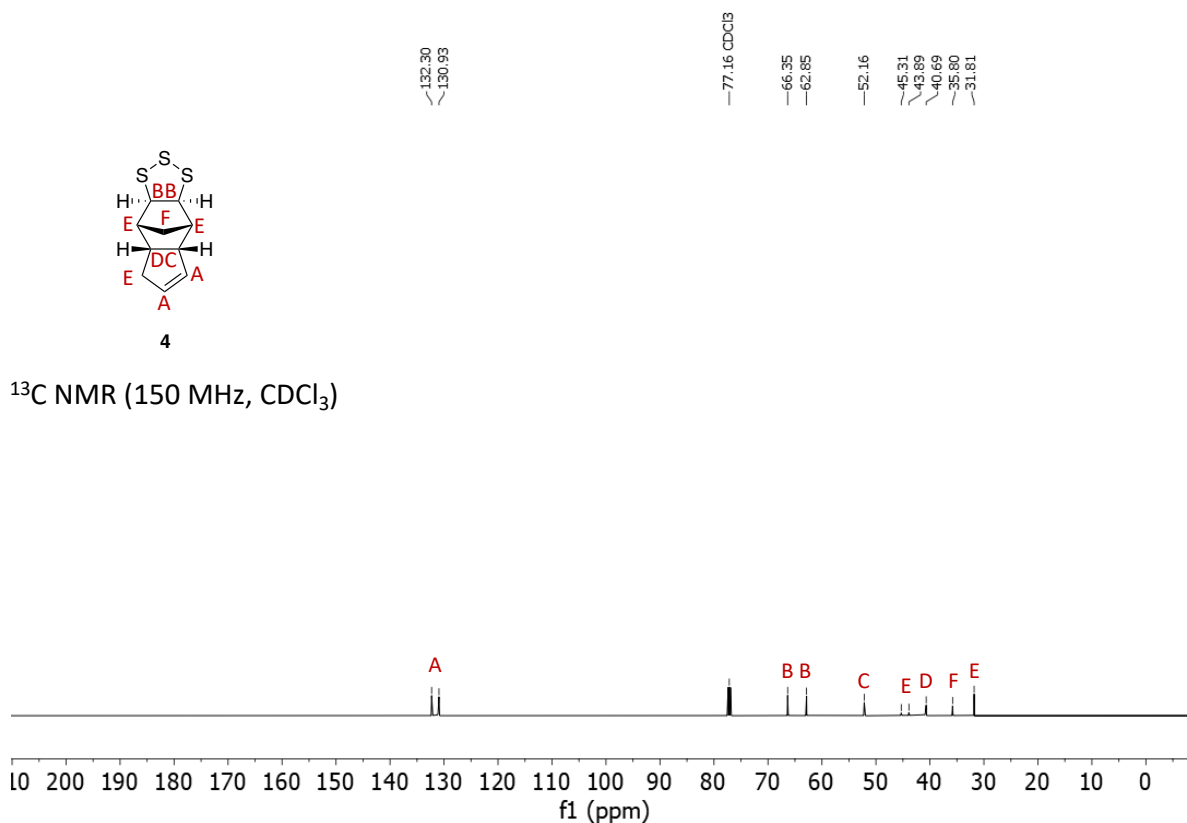


Figure S2.13: ^{13}C NMR spectrum (150 MHz, CDCl_3) of monomer 4 after flash chromatography (silica gel, eluent: hexane).

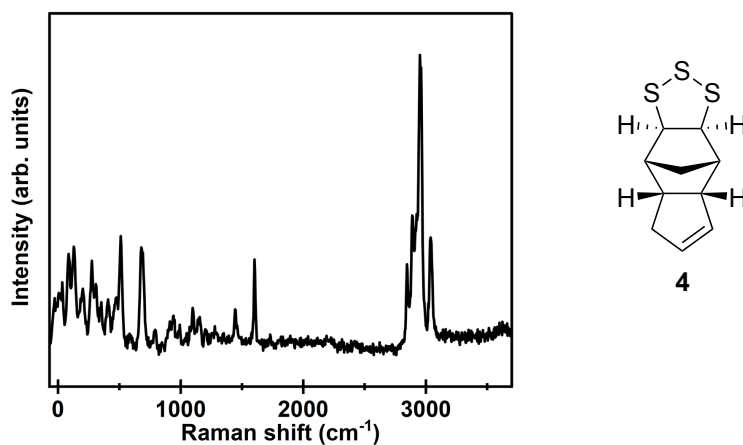


Figure S2.14: Raman spectrum of monomer 4 after flash chromatography (silica gel, eluent: hexane). Excitation laser wavelength of 532 nm. S–S peak observed between 480–540 cm^{-1} .

Sulfur rank comparison by Raman spectroscopy

S–S peaks in the Raman spectra were compared across all monomers (1–4). Raman signals of linear dimethyl disulfide and dimethyl trisulfide were also compared to the Raman signals produced by the cyclic sulfide monomers (1–4) to ascertain any differences between cyclic and linear trisulfides.

Knowing the Raman response of these monomers and small molecules is useful as it can provide information for correlating sulfur rank to specific signals that arise from the S–S bonds.

The 532 nm laser was used to analyse the monomer and small molecule samples as it gave good quality spectra with relatively high signal to noise ratio. For the polymer samples, fluorescence was significant for the 532 nm laser and yielded spectra with no interpretable Raman peaks. The 785 nm was also used to analyse the polymer samples to obtain spectra with reduced fluorescence but, as occurred with the 532 nm laser, no spectra with interpretable Raman peaks were observed. These results are consistent with research by Hasell and coworkers who analysed several sulfur polymers using a range of laser wavelengths (532 nm, 785 nm, 1064 nm) and found some were unable to be analysed with Raman spectroscopy due to significant fluorescence.⁷

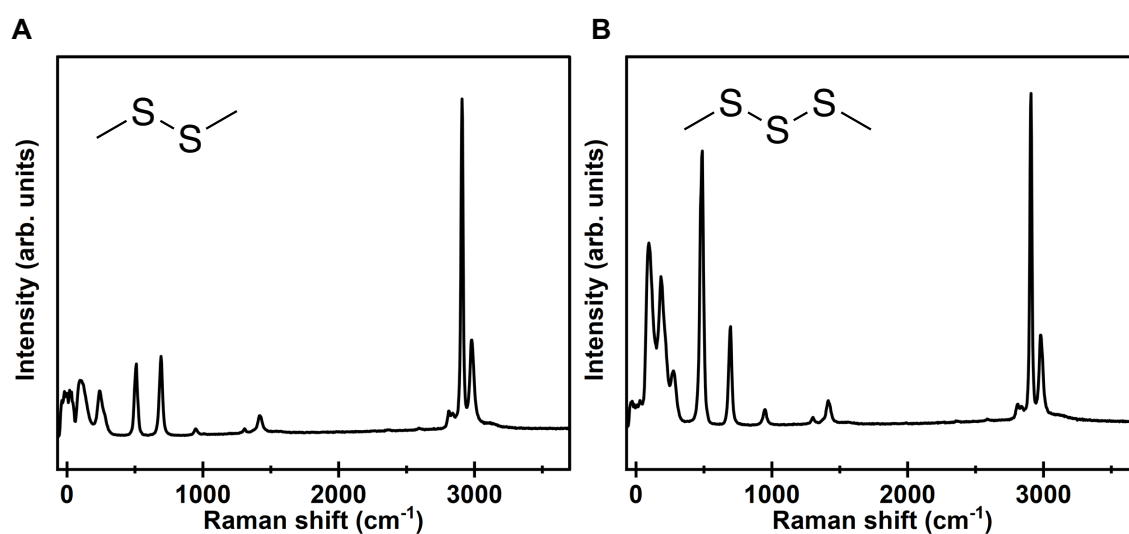


Figure S2.15: Raman spectra of (A) dimethyl disulfide (S–S peak observed between 480-535 cm^{-1}) and (B) dimethyl trisulfide (S–S peak observed between 450-510 cm^{-1}). Excitation laser wavelength of 532 nm.

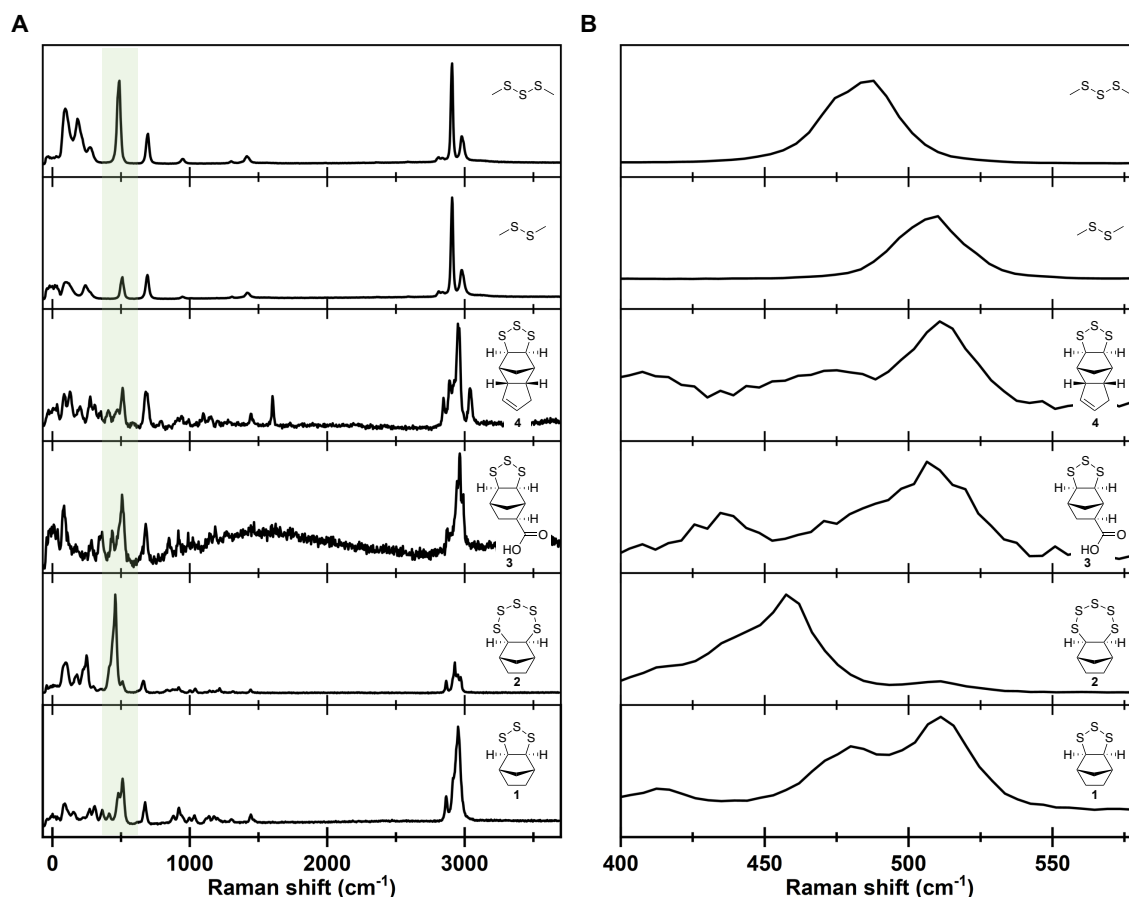


Figure S2.16: (A) Raman spectra of monomers **1**, **2**, **3**, **4**, dimethyl disulfide and dimethyl trisulfide. The highlighted region corresponds to key S–S bond signals. (B) Raman spectra within the highlighted S–S bond signals obtained using a laser wavelength of 532 nm. Subtle differences in the S–S region were observed for the linear and cyclic polysulfide molecules. For instance, the signal at 500–550 cm^{-1} in the cyclic monomers **1**, **3**, and **4** is distinct from the dimethyl trisulfide: a linear polysulfide with a signal at 420–500 cm^{-1} . The S–S signal for the cyclic pentasulfide **2** can also be distinguished from all of these trisulfides. However, due to fluorescence, the location of the S–S signal in the polymers could not be ascertained.

X-ray crystallographic data

Single crystals were mounted in paratone-N oil on a nylon loop. X-ray diffraction data for monomers **1**, **3** and **4** was collected at 100(2) K on the MX-1 and MX-2 beamlines of the Australian Synchrotron.^[29-30] Structures were solved by direct methods using SHELXT and refined with SHELXL and ShelXle as a graphical user interface.^[31] All non-hydrogen atoms were refined anisotropically, and hydrogen atoms were included as invariants at geometrically estimated positions.

Table S2.1: X-ray experimental data

Monomer	4	2	3
CCDC number	2215950	2215951	2215949
Empirical formula	C ₁₀ H ₁₂ S ₃	C ₇ H ₁₀ S ₅	C ₈ H ₁₀ O ₂ S ₃
Formula weight	228.38	254.45	234.34
Crystal system	Orthorhombic	Monoclinic	Monoclinic
Space group	Pca2 ₁	P2 ₁ /n	P2 ₁ /c
<i>a</i> (Å)	11.927(2)	10.056(2)	12.681(3)
<i>b</i> (Å)	11.489(2)	10.883(2)	6.2710(13)
<i>c</i> (Å)	14.940(3)	10.281(2)	12.456(3)
α (°)	90	90	90
β (°)	90	115.66(3)	105.89(3)
γ (°)	90	90	90
Volume (Å ³)	2047.2(7)	1014.2(4)	952.7(4)
<i>Z</i>	8	4	4
Density (calc.) (Mg/m ³)	1.482	1.666	1.634
Absorption coefficient (mm ⁻¹)	0.672	1.083	0.739
F(000)	960	528	488
Crystal size (mm ³)	0.18 x 0.11 x 0.05	0.18 x 0.15 x 0.12	0.22 x 0.13 x 0.12
θ range for data collection (°)	1.772 to 28.310	2.367 to 28.418	1.670 to 27.869
Reflections collected	62323	16760	15386
Observed reflections [R(int)]	5092 [0.1139]	2058 [0.0220]	1840 [0.0367]
Goodness-of-fit on F ²	1.032	1.092	1.045
R ₁ [I > 2 σ (I)]	0.0774	0.0235	0.0343
wR ₂ (all data)	0.2124	0.0676	0.0952
Largest diff. peak and hole (e.Å ⁻³)	1.373 and -0.466	0.327 and -0.407	0.519 and -0.442
Data / restraints / parameters	5092 / 169 / 235	2058 / 0 / 109	1840 / 0 / 120

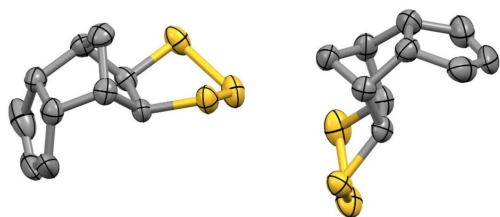


Figure S2.17: The asymmetric unit of monomer **4** with all non-hydrogen atoms shown as ellipsoids at the 50% probability level.



Figure S2.18: The asymmetric unit of monomer **2** with all non-hydrogen atoms shown as ellipsoids at the 50% probability level.

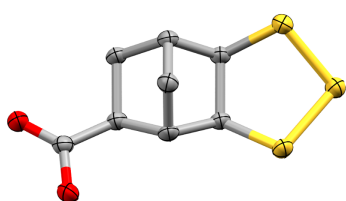
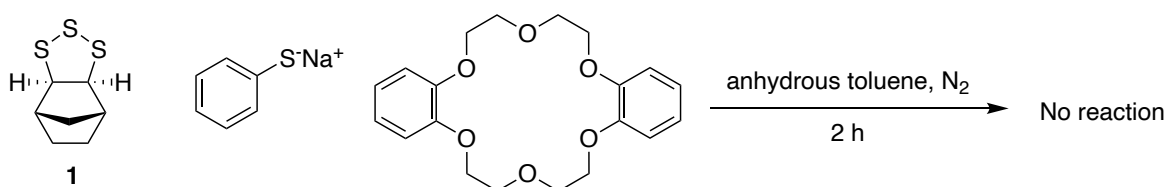


Figure S2.19: The asymmetric unit of monomer **3** with all non-hydrogen atoms shown as ellipsoids at the 50% probability level.

Anionic polymerisation

Attempted anionic polymerisation of monomer 1



The following method was adapted from the literature.^[33-34] A flame dried 25 mL two neck round bottom flask was fitted with a rubber septum (top neck), a stir bar and a glass stopper (side neck). Monomer **1** (400 mg, 2.1 mmol) was added to the flask via the side neck. Using a needle via the rubber septum, the round bottom flask was evacuated of air and filled with nitrogen. This was repeated 3 times. In a separate flame dried 1.5 mL GPC vial, sodium thiophenolate (3.7 mg, 0.028 mmol) and dibenzo-18-crown-6 (10.1 mg, 0.028 mmol) were added under a constant flow of nitrogen gas and the reaction mixture was maintained under an atmosphere of nitrogen. Anhydrous toluene (1 mL) was then added to both the round bottom flask and the GPC vial and stirred. The contents of the GPC vial were then added to the round bottom flask via syringe and stirred at room temperature. After 2 hours the reaction was quenched with benzyl bromide (23 μ L, 0.21 mmol). The

resulting solution was added dropwise into methanol (10 mL), turning the mixture cloudy. The cloudy solution become clear after 1 hour. After this time, the solvent was removed under reduced pressure to deliver a yellow oil which was analysed by GPC (THF) and ^1H NMR spectroscopy. Only unreacted monomer **1** was observed and no evidence of polymerisation was obtained.

A Monomer **1**



B Crude reaction mixture

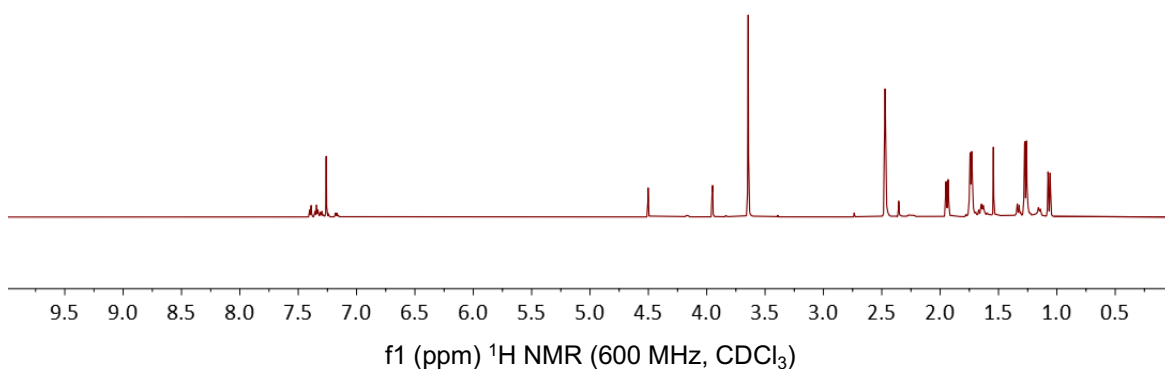


Figure S2.19: (A) ^1H NMR spectrum (600 MHz, CDCl_3) of monomer **1**. (B) ^1H NMR (600 MHz, CDCl_3) of crude reaction mixture, no polymer observed.

Electrochemical characterisation

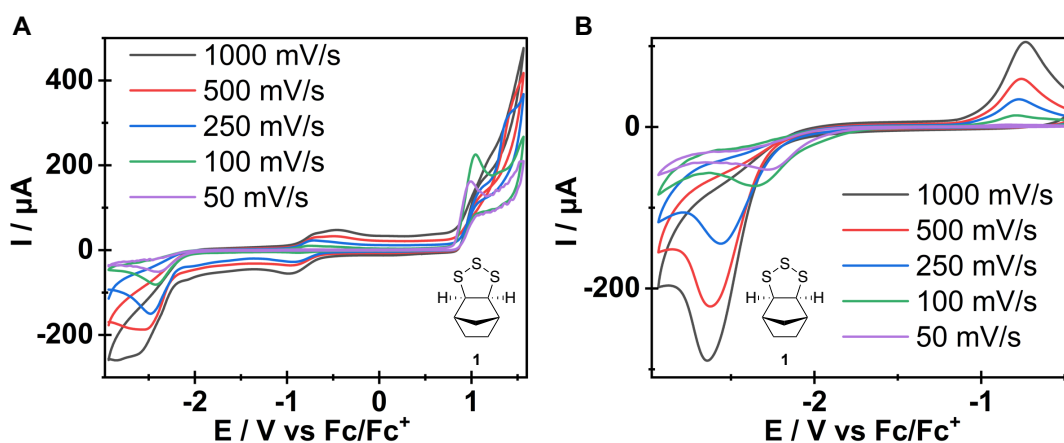


Figure S2.20: Cyclic voltammograms of monomer **1** (5 mM), $n\text{Bu}_4\text{NPF}_6$ (0.1 M in MeCN, 10 mL)

at different scan rates (50, 100, 250, 500 and 1000 mV/s), third scan. a) scanned from -2.9 to $+1.6$ V versus Fc/Fc^+ , b) scanned from -2.9 to -0.4 V versus Fc/Fc^+ .

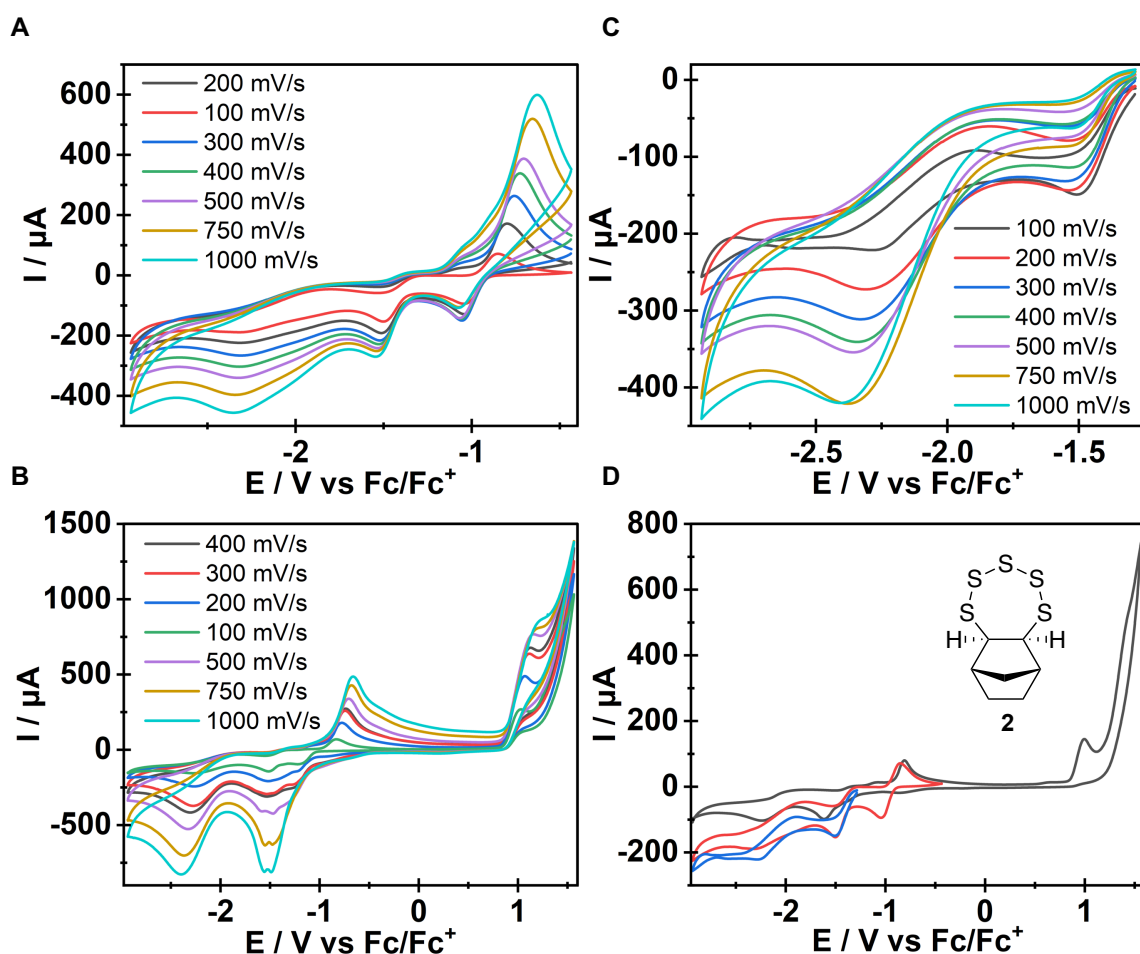
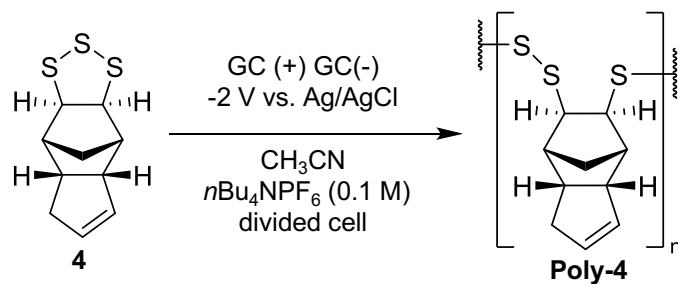


Figure S2.21: Cyclic voltammograms of monomer **2** (5 mM), $n\text{Bu}_4\text{NPF}_6$ (0.1 M in MeCN, 10 mL) at different scan rates (100, 200, 300, 400, 500, 750 and 1000 mV/s), third scan. a) scanned from -2.9 to 1.6 V versus Fc/Fc^+ , b) scanned from -2.9 to 1.6 V versus Fc/Fc^+ , c) scanned from -2.9 to -1.3 V versus Fc/Fc^+ , d) overlay of different scan ranges at 100 mV/s scan rate.

Electrochemical polymerisation

Divided cell experiment: constant potential



Electrochemical polymerisation of monomer **4** was run under standard constant potential conditions for 4 hours at a monomer concentration of 0.04 M (456 mg, 2.00 mmol) in a divided cell (25 mL in each chamber). Chambers were separated by dialysis film (MWCO 1000 Da). The dialysis film was used as an ion-permeable membrane so as to obtain sufficient current in the reaction. Electrochemical polymerisation was conducted using a Gamry Interface 1010E. After 4 hours, resulting solution from each chamber was collected in separate vials where solvent was removed under reduced pressure before analysis by ^1H NMR spectroscopy. Precipitate (36 mg) was observed in the solution from the chamber containing the working electrode, which was then analysed by GPC (THF).

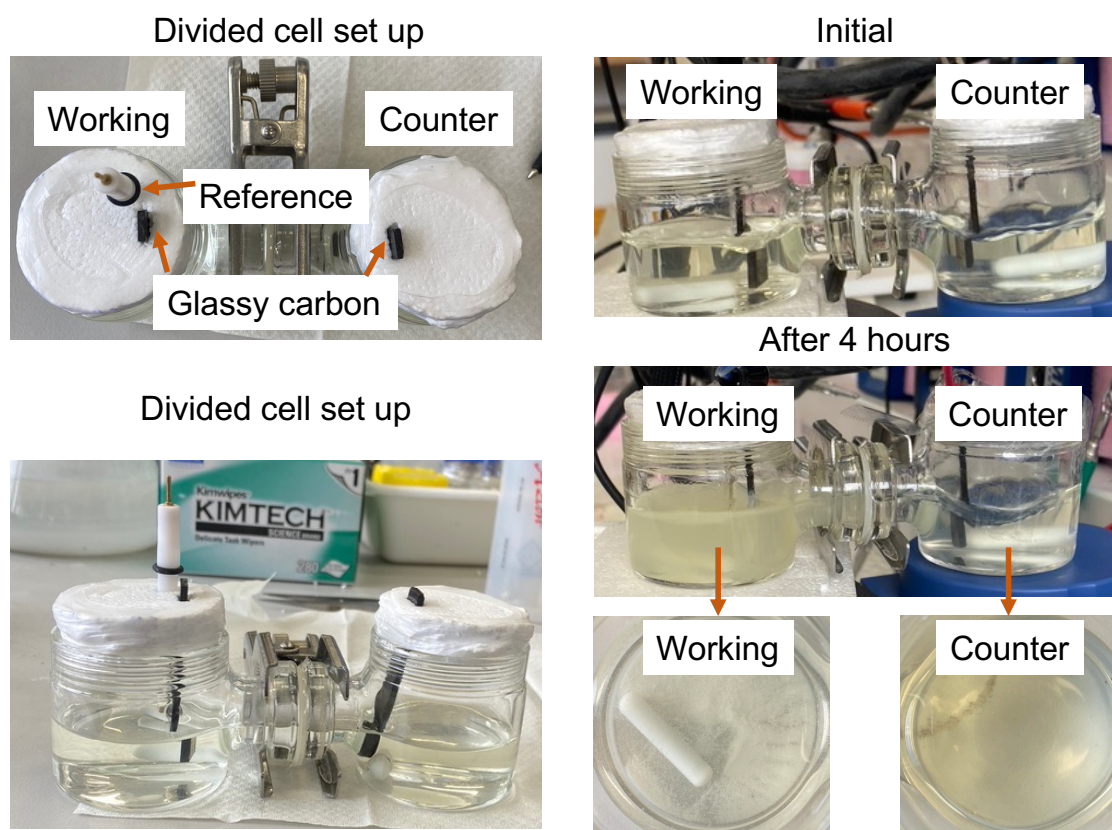


Figure S2.21: Images of divided cell set up (left), initial reaction solutions (top right) and solutions after reacting for 4 hours (bottom right). Polymer precipitate was only observed in the working chamber, which is consistent with initiation by cathodic reduction.

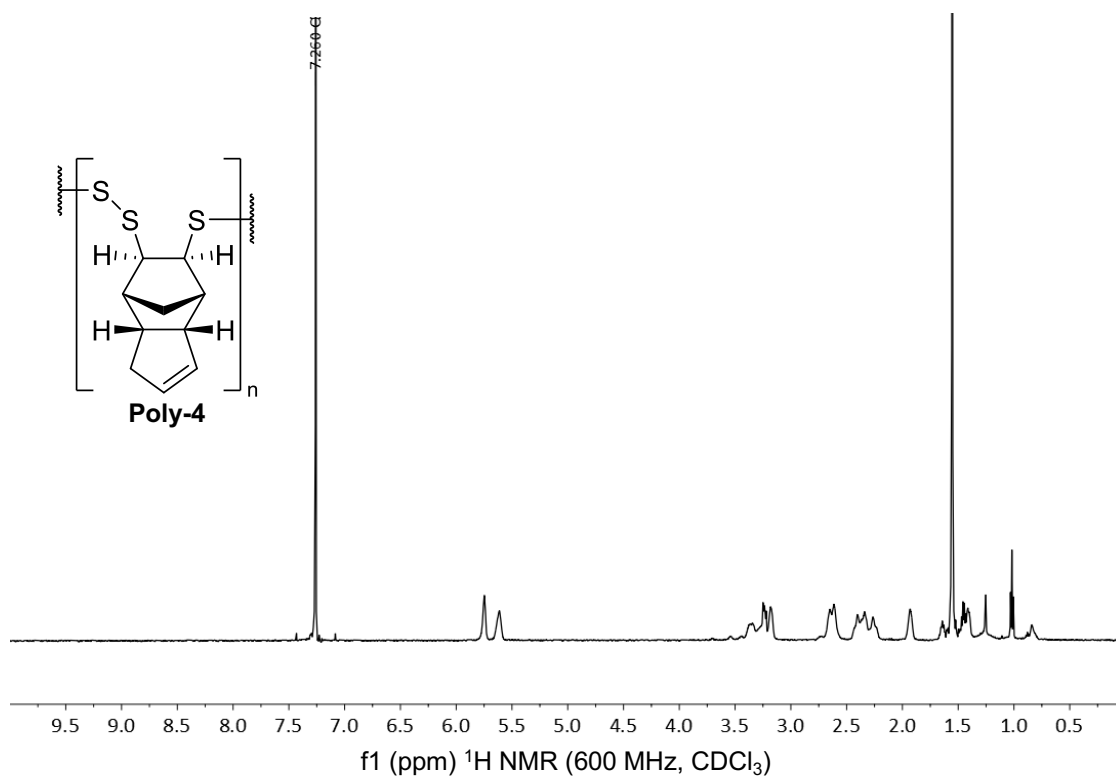


Figure S2.22: ^1H NMR spectrum (600 MHz, CDCl_3) of **poly-4** collected from the working chamber after using the divided cell configuration.

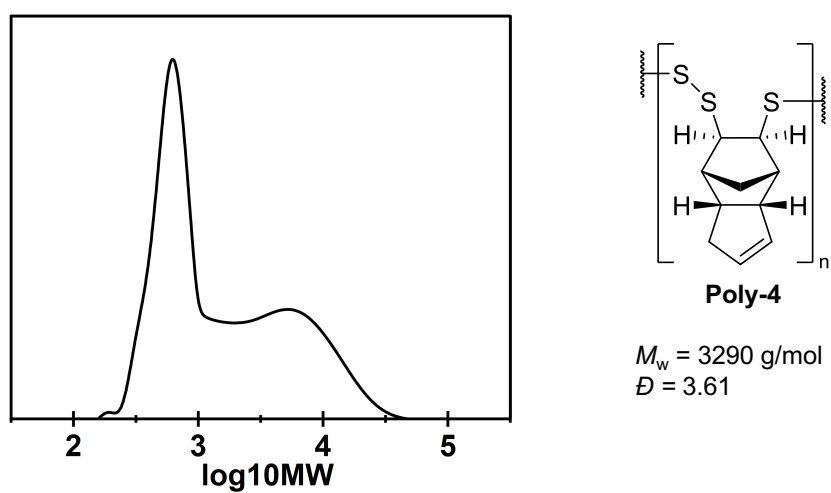
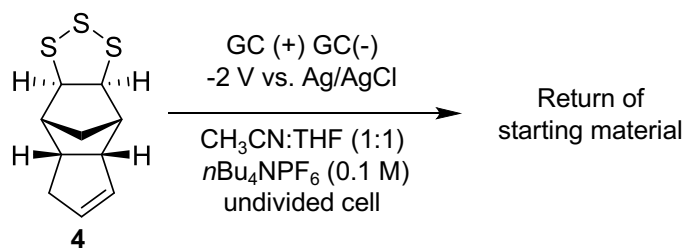


Figure S2.23: GPC (THF) of precipitate from working chamber.

The molecular weight is similar to the undivided cell, so oxidative depolymerisation or degradation is not a concern. The molecular weight is likely determined by the solubility of the polymer, with the product precipitating over the course of the reaction.

Mixed solvent experiment



THF was included in the solvent system in an attempt to improve solubility of the polymer product and increase molecular weight. However, the electrochemical polymerisation was not compatible with this solvent system, likely due to the increased resistance of the reaction medium in comparison to pure acetonitrile:

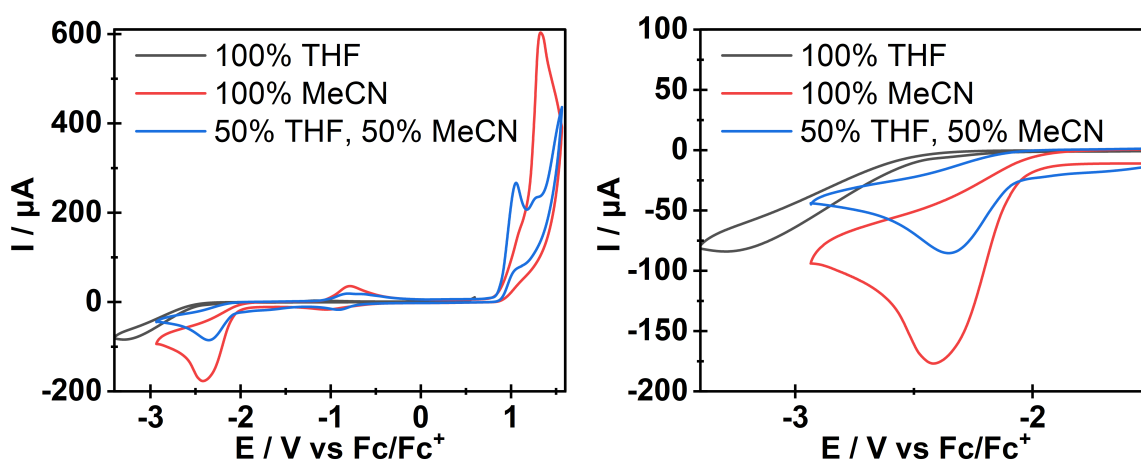


Figure S2.24: Cyclic voltammograms of monomer **4** (5 mM) at 100 mV/s, $n\text{Bu}_4\text{NPF}_6$ (0.1 M in solvent, 10 mL) in different solvent systems, third scan. Decreased reduction peak current was observed in the mixed solvent system (50% THF, 50% MeCN) when compared to 100% MeCN.

Electrochemical polymerisation of monomer **4** was run under standard constant potential conditions in a mixed solvent system (1:1, MeCN:THF) for 8 hours at a monomer concentration of 0.04 M (134 mg, 0.59 mmol). At every time interval (0, 1, 5, 15, 30, 60, 120) an aliquot (0.5 mL) was taken from the cell and transferred into a 10 mL vial and concentrated under reduced pressure. The remaining solid was redissolved in chloroform-*d* (0.7 mL) and analysed by ^1H NMR spectroscopy. No reaction was observed over 2 hours, indicating the electrochemical polymerisation is not compatible with this solvent system.

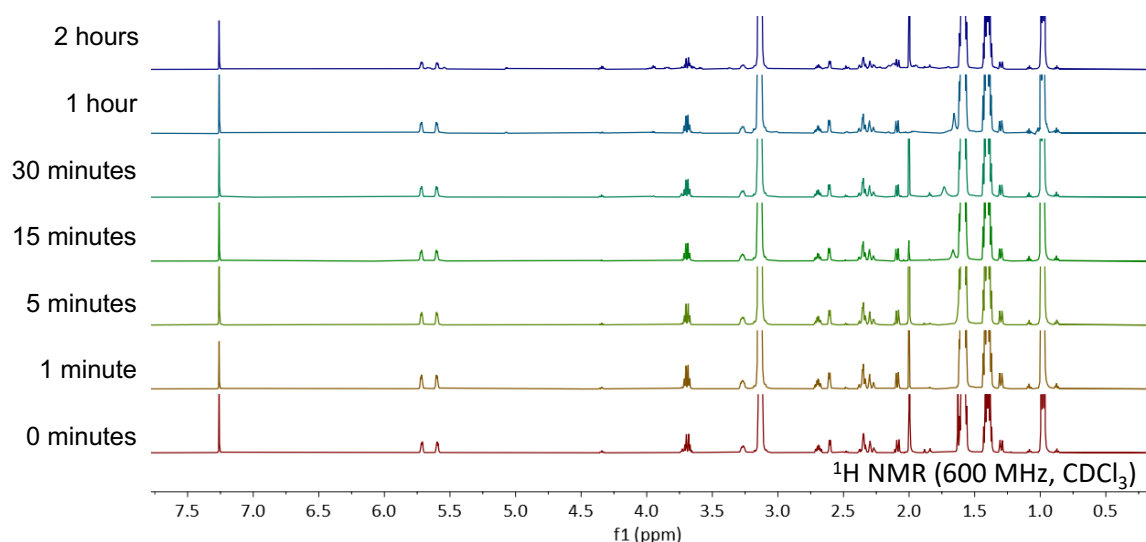


Figure S2.25: $^1\text{H NMR}$ spectrum (600 MHz, CDCl_3) of reaction solution over time.

Polymerisation optimisation

Standard ElectraSyn[®] method: constant current

An ElectraSyn[®] vial (20 mL) was charged with monomer (0.59 mmol), $n\text{Bu}_4\text{NPF}_6$ (580 mg, 0.1 M), acetonitrile (15 mL) and a small stir bar resulting in a 0.04 M concentration of monomer. Two glassy carbon electrodes were fitted to the ElectraSyn[®] lid. After sonicating the ElectraSyn[®] vial until the monomer was dissolved in solution, the lid was fitted to the vial and connected to the ElectraSyn[®]. A constant current of 10 mA was applied for the desired time, stirring at 1500 rpm.

Standard ElectraSyn[®] method: constant potential

An ElectraSyn[®] vial (20 mL) was charged with monomer (0.59 mmol), $n\text{Bu}_4\text{NPF}_6$ (580 mg, 0.1 M), acetonitrile (15 mL) and a small stir bar resulting in a 0.04 M concentration of monomer. Two glassy carbon electrodes and an Ag/AgCl (3 M aq. KCl) reference electrode were fitted to the ElectraSyn[®] lid. After sonicating the ElectraSyn[®] vial until the monomer was dissolved in solution, the lid was fitted to the vial and connected to the ElectraSyn[®]. A constant potential of -2.0 V versus Ag/AgCl (3 M aq. KCl) was applied for the desired time, stirring at 1500 rpm.

ElectraSyn[®] polymerisation note

Polymer in solution can obstruct the working or counter electrode. This can affect the current, which can lead to variations in electron equivalents (F/mol) and yield for reactions under otherwise identical conditions. For this reason, electrodes are thoroughly cleaned and polished as described in the general consideration section. This minimizes polymer build up on the electrodes.

Standard polymer workup

The reaction mixture was transferred from the ElectraSyn® vial to a round bottom flask, washing the electrodes with chloroform to get full transfer of the polymer to the flask (the polymer is soluble in chloroform). The resulting solution was concentrated under reduced pressure. The remaining solid was redissolved in 10 mL of chloroform (sonicated if required) and transferred to a 50 mL centrifuge tube. Acetonitrile (30 mL) was added to the centrifuge tube to precipitate the polymer and was vortexed to mix. The solution was centrifuged at 5000 rpm for 5 minutes. The supernatant was decanted, and the solid was redissolved in chloroform (10 mL). Acetonitrile (30 mL) was added to the centrifuge tube and vortexed to mix. The solution was centrifuged for 5 minutes (5000 rpm). The supernatant was decanted, and the solid was redissolved in chloroform (10 mL). This process was repeated a third time, and the solid polymer was collected.

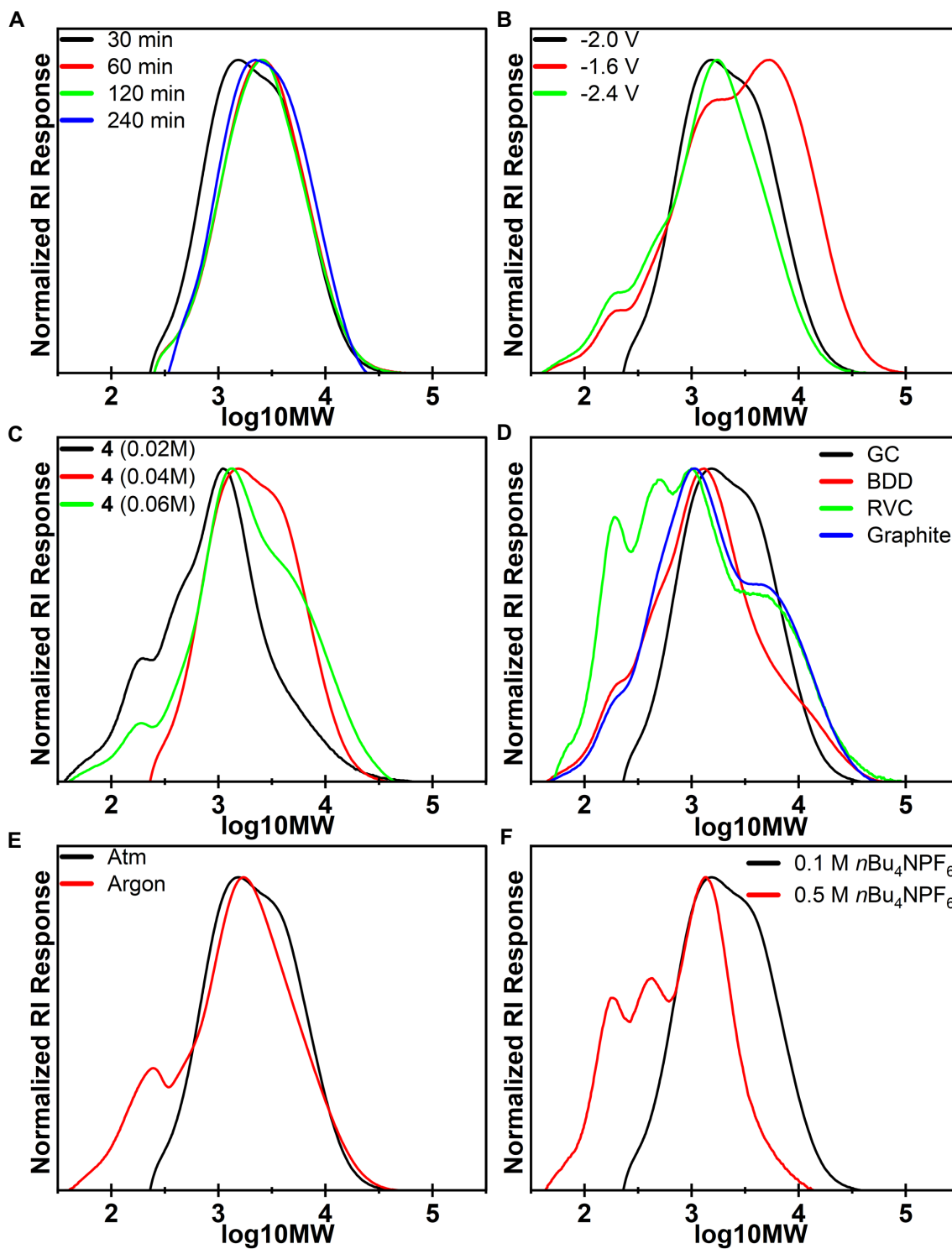


Figure S2.26: GPC (THF) of monomer 4 polymerisations under standard constant potential conditions with variations from standard conditions described, (A) different reaction duration, (B) reactions run at different applied potential, (C) reactions run at different monomer 4 concentration, (D) reactions with different working and counter electrode material (glassy carbon (GC), boron

doped diamond (BDD), reticulated vitreous carbon (RVC)), (E) reactions run under different atmospheres (air vs argon), (F) reactions run with different electrolyte concentration.

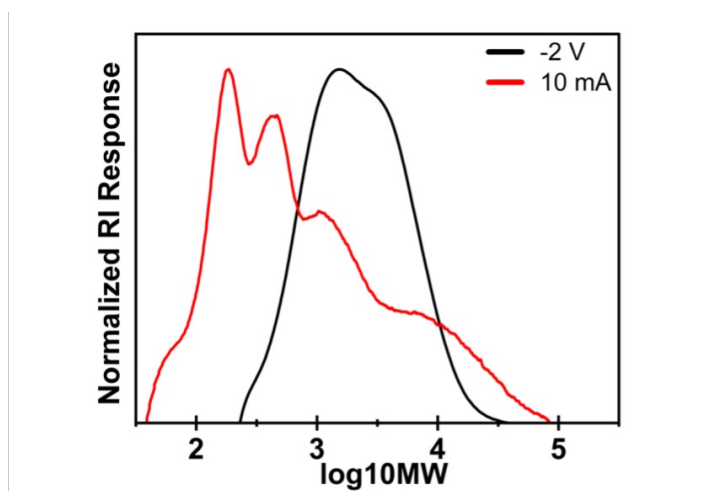
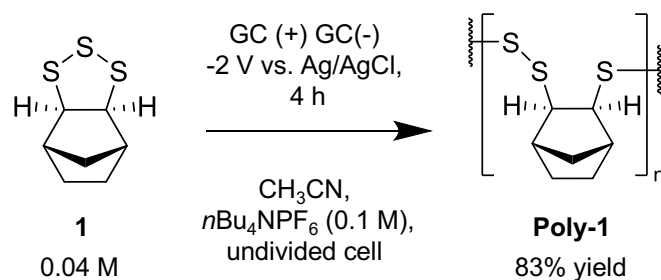


Figure S2.27: GPC (THF) of monomer **4** polymerisations under constant current (10 mA) and constant potential of -2.0 V versus Ag/AgCl (3 M aq. KCl).

Poly-1 characterisation



The following analysis of **poly-1** was conducted on polymer produced under standard constant potential conditions and worked up using standard polymer workup conditions.

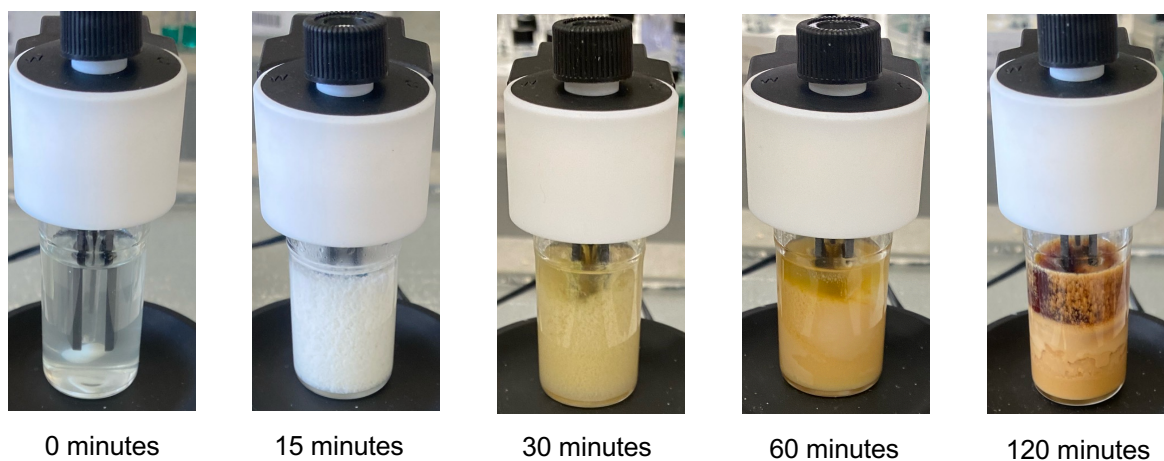


Figure S2.28: Monomer **1** (112 mg, 0.59 mmol) polymerisation over 2 hours under standard constant potential conditions forming **poly-1** (reaction was continued for 4 hours). After standard polymer workup, **poly-1** was collected as a light brown solid (93 mg, 83% yield).

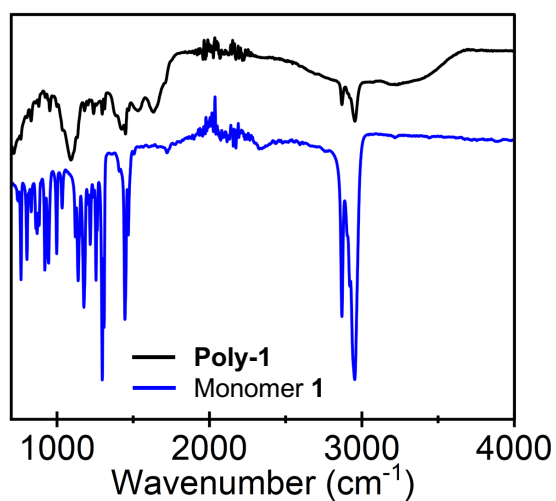


Figure S2.29: FTIR spectrum (neat) of **poly-1** and monomer **1**.

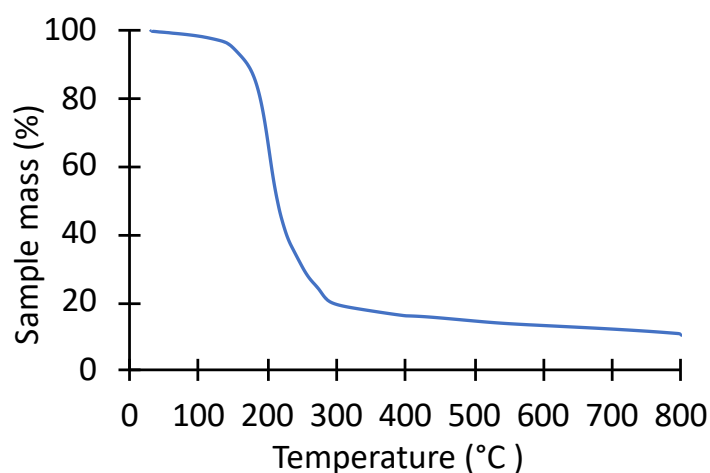


Figure S2.30: TGA of **poly-1** between 30-800 °C at a temperature ramp rate of 5 °C/min from 30-400 °C and then 20 °C/min from 400-800 °C under a flow of nitrogen. Between 100-300 °C there is a mass loss of 78%.

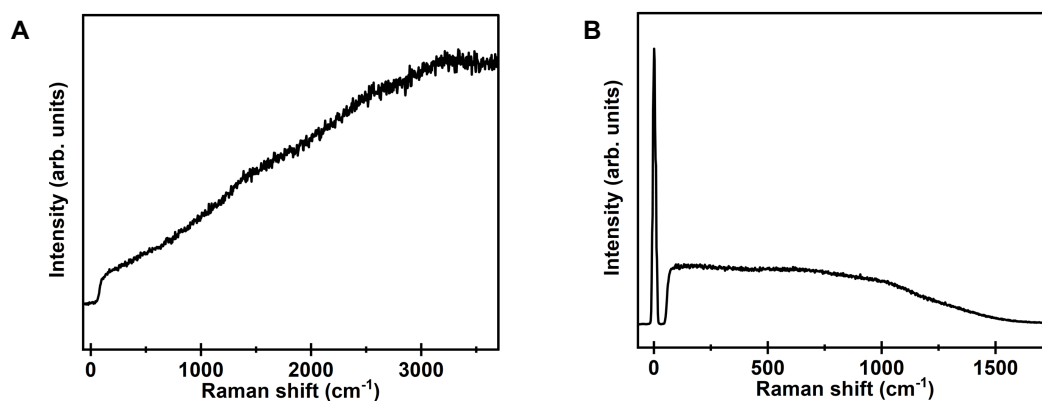
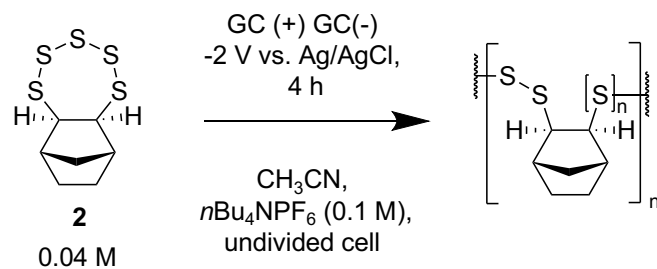


Figure S2.31: Raman spectra of **poly-1**. (A) excitation laser wavelength of 532 nm, (B) excitation laser wavelength of 785 nm.

Poly-2 characterisation

The following analysis of **poly-2** was conducted on polymer produced under standard constant potential conditions and worked up using standard polymer workup conditions.



Monomer **2** (187 mg, 0.73 mmol) polymerisation over 4 hours under standard constant potential conditions. After standard polymer workup, **poly-2** was collected as a dark brown solid (68 mg, 36% yield). **Poly-2** was insoluble in THF and chloroform.

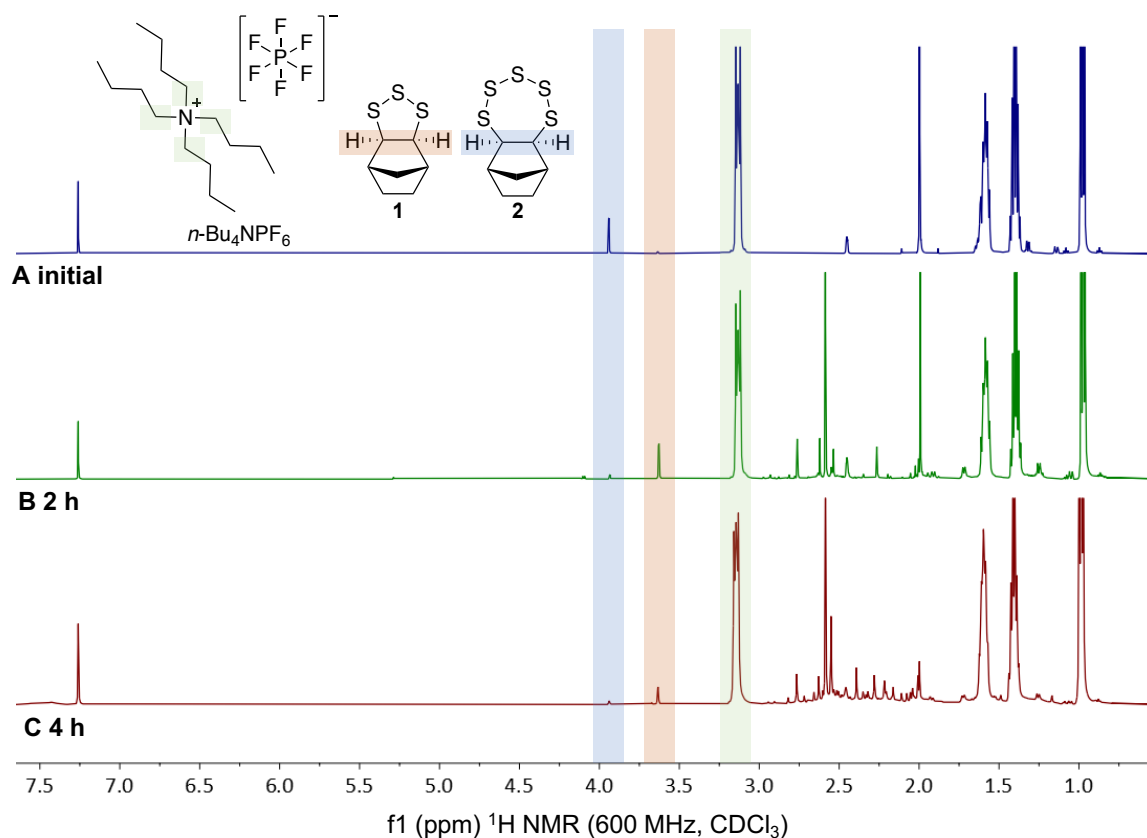
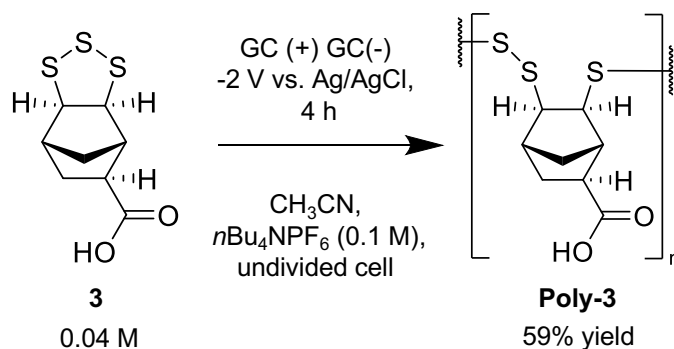


Figure S2.32: $^1\text{H NMR}$ spectra (600 MHz, CDCl_3) comparing amount of cyclic sulfide monomers **1** and **2** and $n\text{Bu}_4\text{NPF}_6$ signals (see highlighted resonances) during polymerisation of monomer **2**. (A) 0.5 mL aliquot of crude reaction mixture taken before potential applied, ratio of monomer **1**: $n\text{Bu}_4\text{NPF}_6$ is 1:159, ratio of monomer **2**: $n\text{Bu}_4\text{NPF}_6$ is 1:7, (B) 0.5 mL aliquot of crude reaction mixture taken 2 hours into reaction, ratio of monomer **1**: $n\text{Bu}_4\text{NPF}_6$ is 1:5, ratio of monomer **2**: $n\text{Bu}_4\text{NPF}_6$ is 1:52, (C) 0.5 mL aliquot of crude reaction mixture taken 4 hours into reaction, ratio of monomer **1**: $n\text{Bu}_4\text{NPF}_6$ is 1:10, ratio of monomer **2**: $n\text{Bu}_4\text{NPF}_6$ is 1:150.

Poly-3 characterisation

The following analysis of **poly-3** was conducted on polymer produced under standard constant potential conditions and worked up using standard polymer workup conditions.



Monomer **3** (193 mg, 0.82 mmol) polymerisation over 4 hours under standard constant potential conditions. After standard polymer workup, **poly-3** was collected as a brown solid (115 mg, 59 % yield). **Poly-3** was poorly soluble in methanol and chloroform.

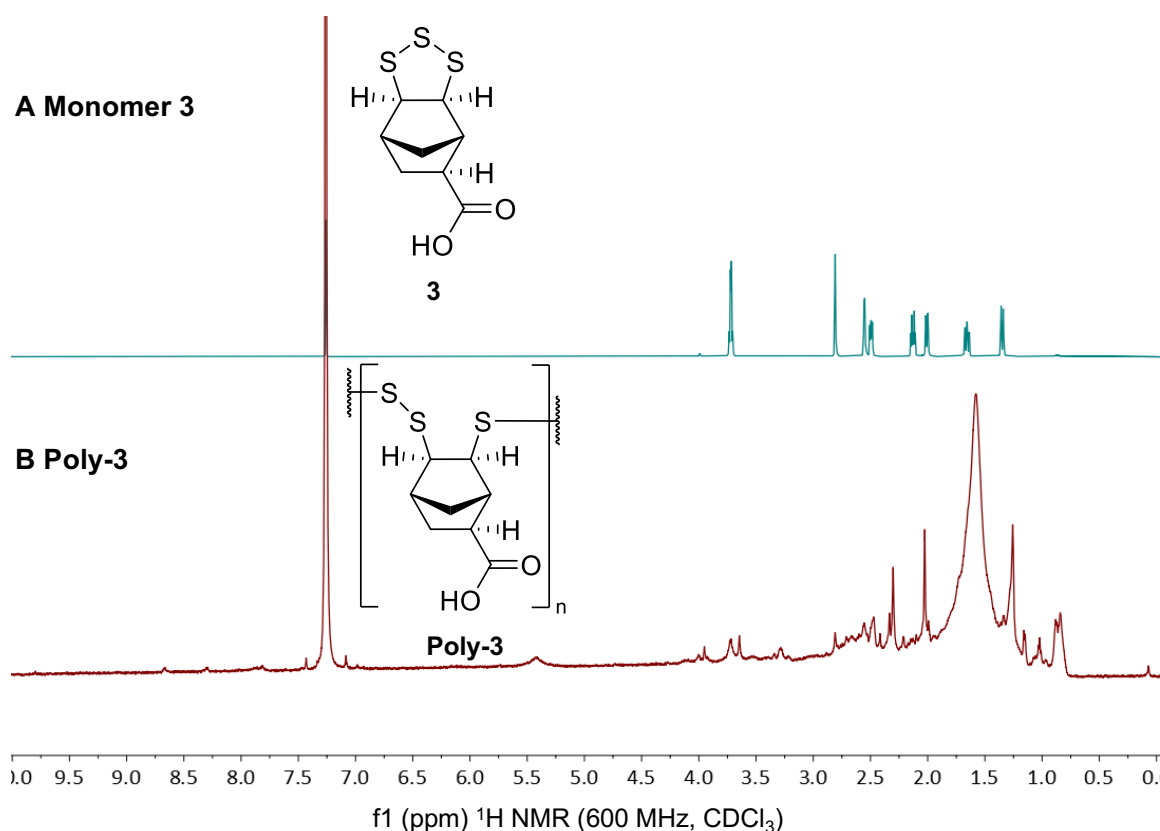


Figure S2.33: (A) ¹H NMR spectrum (600 MHz, CDCl₃) of monomer **3**, (B) ¹H NMR (600 MHz,

CDCl_3) of **poly-3**. Note that **poly-3** is only sparingly soluble, so this experiment is only to illustrate that monomer **3** was consumed in the reaction.

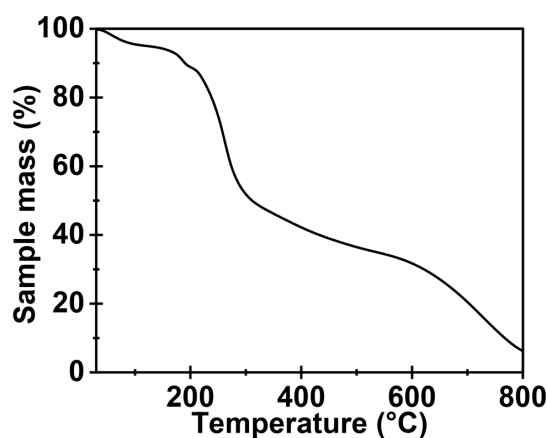


Figure S2.35: TGA of **poly-3** between 30-800 °C at a temperature ramp rate of 5 °C/min from 30-400 °C and then 20 °C/min from 400-800 °C under a flow of nitrogen. Between 30-200 °C there is a mass loss of 12%. Between 200-400 °C there is a mass loss of 46%. Between 400-800 °C there is a mass loss of 32%.

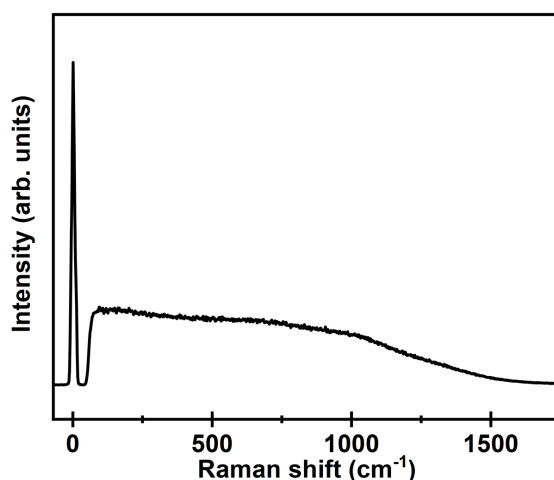
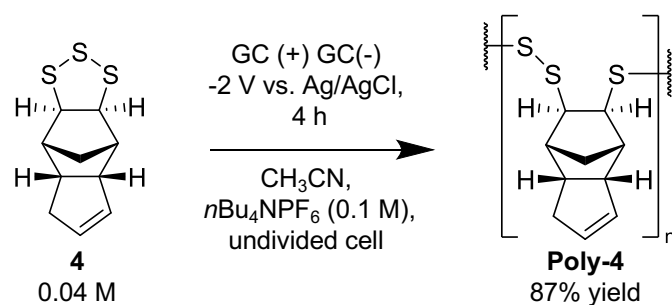


Figure S2.36: Raman spectra of **poly-3** with excitation laser wavelength of 785 nm. Fluorescence was also observed using a laser of 532 nm.

Poly-4 characterisation

The following analysis of **poly-4** was conducted on polymer produced under standard constant potential conditions (4 h) and worked up using standard polymer workup conditions.



Monomer **4** (134 mg, 0.59 mmol) polymerisation over 2 hours under standard constant potential conditions forming **poly-4** (reaction was continued for 4 hours). After standard polymer workup, **poly-4** was collected as a brown solid (116 mg, 87% yield).

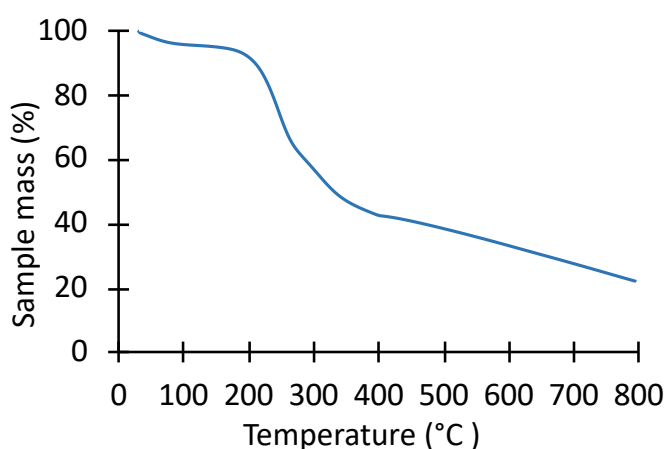


Figure S2.38: TGA of **poly-4** between 30-800 °C at a temperature ramp rate of 5 °C/min from 30-400 °C and then 20 °C/min from 400-800 °C under a flow of nitrogen. Between 30-200 °C there is a mass loss of 4.8%. Between 200-400 °C there is a mass loss of 51%. Between 400-800 °C there is a mass loss of 20%.

LiAlH₄ reduction of poly-4

Poly-4 (234 mg) and LiAlH₄ (97 mg, 2.55 mmol) were added to a flame-dried two neck 25 mL round bottom flask containing a magnetic stir bar. The flask was evacuated of air and refilled with nitrogen gas. Anhydrous THF (7 mL) was added dropwise with stirring. The resulting reaction mixture was stirred under a nitrogen atmosphere for 24 hours. HCl (1 M aq., 10 mL) was then added dropwise to quench the remaining reducing agent. After stirring for a further 5 minutes, hexane (10 mL) was added and stirred for 5 minutes. The layers were separated, and the aqueous layer was washed with hexane (3 x 10 mL). The organic fractions were combined and concentrated under reduced pressure to deliver compound **5** (176 mg). ¹H NMR and gas chromatography mass spectrometry revealed the yellow oil to be compound **5**. ¹H NMR (600 MHz, CDCl₃): δ 5.71-5.67

(m, 1H), 5.57-5.53 (m, 1H), 3.35-3.31 (m, 1H), 3.24-3.19 (m, 1H), 3.13-3.08 (m, 1H), 2.61-2.54 (m, 1H), 2.37-2.14 (m, 5H), 2.08-2.03 (m, 1H), 1.82-1.76 (m, 1H), 1.44-1.38 (m, 1H).

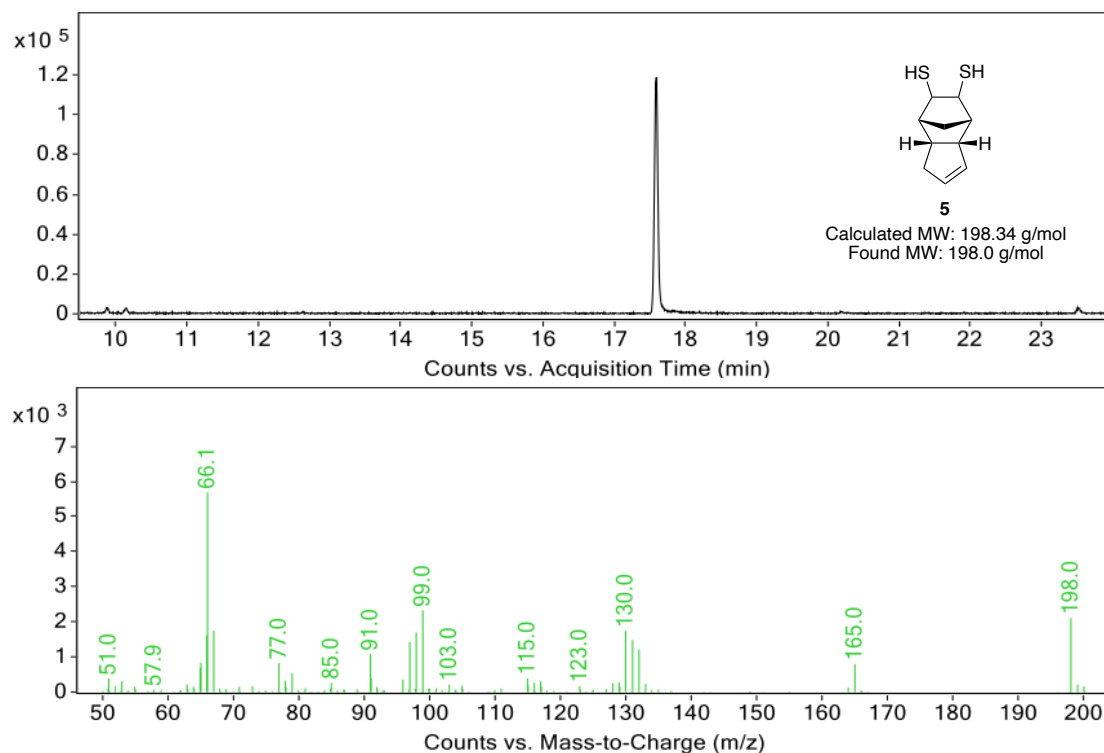


Figure S2.39: (Top) Gas chromatogram taken from organic fraction, mass spectrum of peak at 17.6 minutes is consistent with calculated mass of compound **5**. (Bottom) Mass spectrum of peak at 17.6 minutes.

Monomer **4** polymerisation kinetics

Electrochemical polymerisation of monomer **4** was run under standard constant potential conditions for 2 hours at a monomer concentration of 0.09 M (300 mg, 1.31 mmol). At every time interval (0, 1, 5, 15, 30, 60, 120 minutes) an aliquot (0.5 mL) was taken from the cell and transferred into a 10 mL vial and concentrated under reduced pressure. The remaining solid was redissolved in chloroform-*d* (0.7 mL) and analysed by ¹H NMR spectroscopy. The sample was then transferred to a 2 mL microcentrifuge tube and acetonitrile (1 mL) was added to precipitate the polymer. The solution was centrifuged in a small benchtop centrifuge for 1 minute. The supernatant was decanted, and the solid was redissolved in chloroform (0.5 mL) before repeating the above precipitation/centrifugation process 2 more times. The remaining solid was then dissolved in tetrahydrofuran (2 mL) and analysed by GPC (THF). These reactions were run in triplicate.

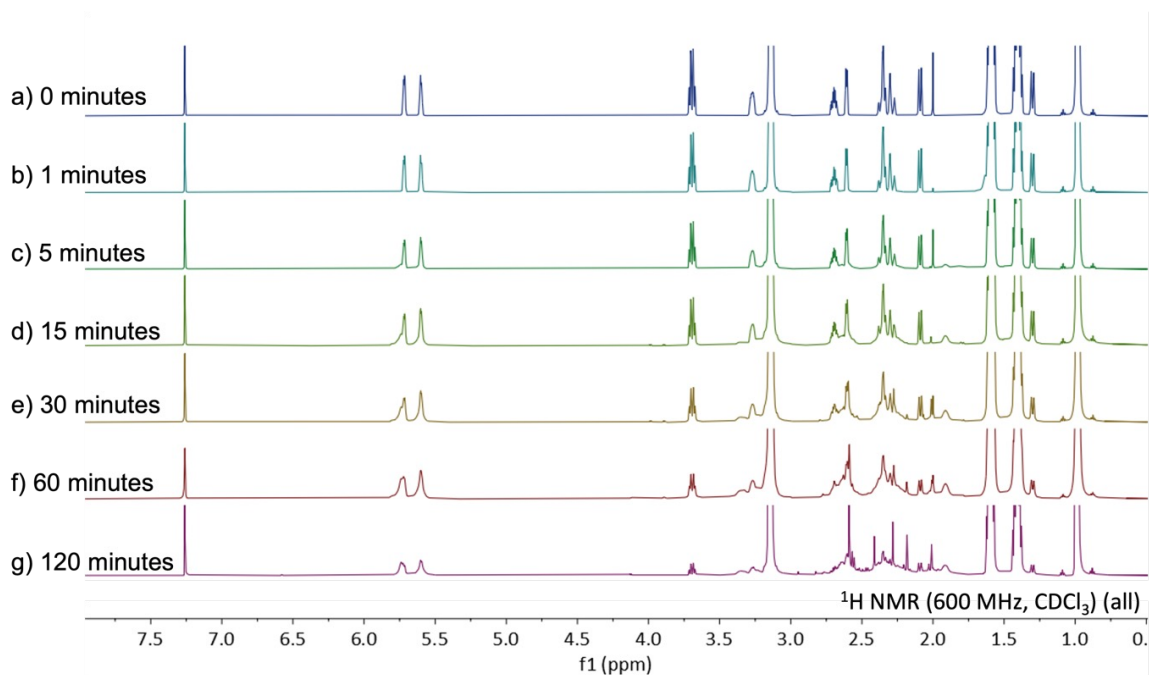


Figure S2.40: ^1H NMR spectra (600 MHz, CDCl_3) of monomer **4** polymerisation comparing consumption of monomer and production of polymer over time, a) initial solution before potential applied, b) 1 minute into reaction, c) 5 minutes into reaction, d) 15 minutes into reaction, e) 30 minutes into reaction, f) 60 minutes into reaction and g) 120 minutes into reaction.

^1H NMR (600 MHz, CDCl_3)

30 minutes

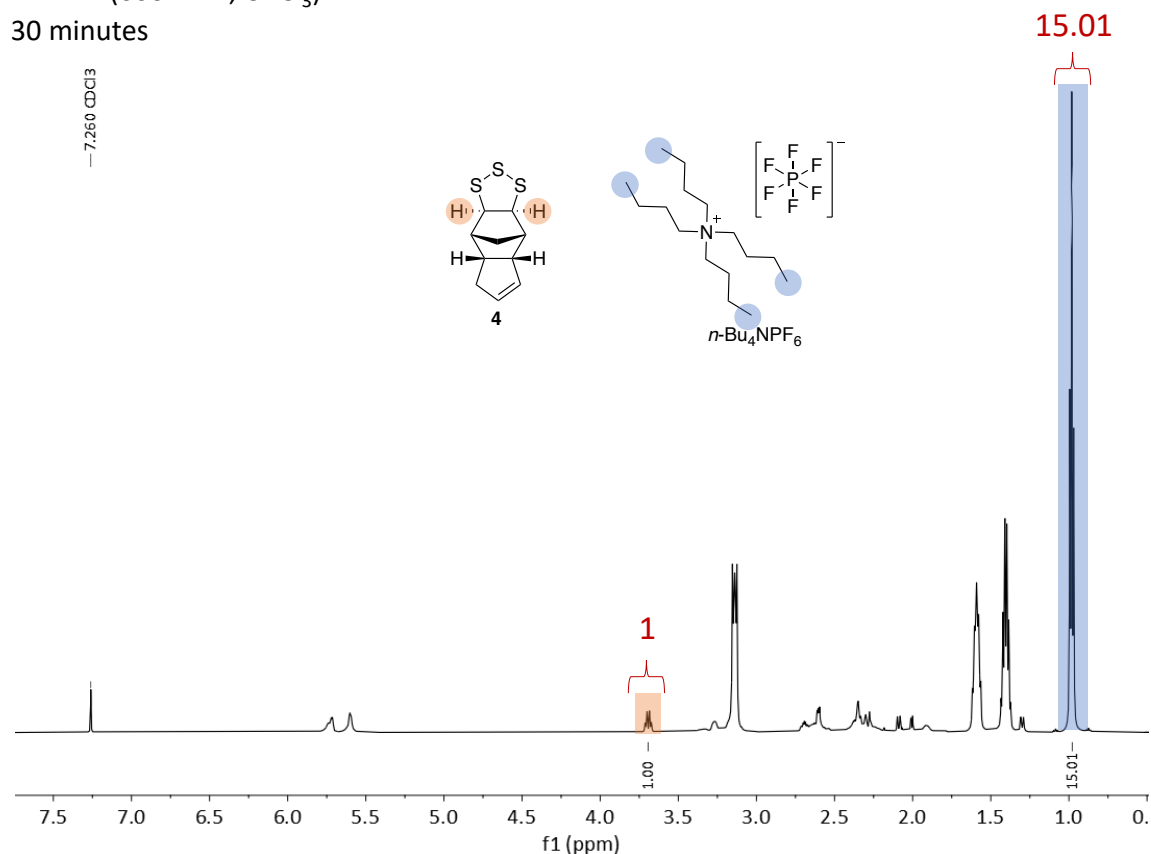


Figure S2.41: ^1H NMR (600 MHz, CDCl_3) of monomer **4** polymerisation at 30 minutes comparing integration of monomer and $n\text{Bu}_4\text{NPF}_6$ CH_3 signals (see highlighted protons). The integration of these peaks was used to calculate monomer **4** consumption over time.

Table S2.2: Summary at different time points during electrochemical polymerisation under standard constant potential conditions.

Time (minutes)	M_n (g/mol)	M_w (g/mol)	\bar{D}
1	850 ± 40	2580 ± 630	3.07 ± 0.92
5	1970 ± 500	4950 ± 1260	2.50 ± 0.01
15	1640 ± 70	4440 ± 1400	2.67 ± 0.72
30	1780 ± 170	4490 ± 1030	2.49 ± 0.35
60	1990 ± 100	4850 ± 680	2.42 ± 0.25
120	2010 ± 130	4150 ± 850	2.00 ± 0.32

Computational studies

Computational Procedures

Standard density functional theory (DFT) calculations were performed using the Gaussian 16 software package.^[35] Geometry optimizations and frequency calculations were performed at the wB97XD^[36]/6-31+G(d,p)^[37] level of theory, using SMD^[38] to implicitly model the acetonitrile solvent environment, and improved energies were then obtained via wB97XD^[36]/def2TZVPD^[39] single point calculations. All stationary points were confirmed as global rather than merely local minima via systematic conformational searching, and all transition states were confirmed via IRC calculations using the default HPC algorithm in Gaussian. Gibbs free energies in acetonitrile solution at 298.15 K of all species were calculated using the direct method^[40] in which ideal gas partition functions are evaluated using the solution-phase geometries and frequencies, and then corrected to a standard state of 1 M. Redox potentials were evaluated using the Nernst equation, using the electron convention based on Fermi-Dirac^[41] statistics to calculate the Gibbs free energy of the electron, and a value of 4.964 V^[42] for the corresponding potential of the Fc/Fc⁺ reference electrode. Values were compared with the corresponding experimental values to benchmark the accuracy of the calculations.

Table S2.3: Energy components (Hartree, 298.15K) used to calculate redox potentials of monomers.^a

Species	oxidation state	E ^b	E	ZPE	TC	TS	H	G
	-1	-1467.50830	-1467.34402	0.16085	0.00826	0.04607	-1467.33730	-1467.38034
	0	-1467.41224	-1467.23838	0.16266	0.00762	0.04366	-1467.24007	-1467.28069
	-1	-1656.11431	-1655.87959	0.17612	0.01116	0.05400	-1655.92514	-1655.97610
	0	-1656.01627	-1655.77189	0.17778	0.01055	0.05164	-1655.82605	-1655.87466
	-1	-1583.02112	-1582.82494	0.20171	0.01020	0.05040	-1582.80733	-1582.85470
	0	-1582.92467	-1582.71888	0.20352	0.00958	0.04813	-1582.70969	-1582.75478
	-1	-2263.94102	-2263.70682	0.16464	0.01138	0.05373	-2263.76310	-2263.81380
	0	-2263.83672	-2263.59205	0.16633	0.01052	0.05028	-2263.65798	-2263.70523

^aUnless stated otherwise, calculations performed at the wB97XD/6-31+G(d,p) level of theory using SMD to model the acetonitrile solvent environment. E is the total DFT energy, ZPE is the zero-point vibrational energy, TC is the thermal correction to the enthalpy, H is the total enthalpy, TS is the temperature times the total entropy, and G is the total Gibbs free energy in solution and includes a correction for change of state from 1atm to 1M. ^b Calculated with

wB97XD/def2TZVPD//wB97XD/6-31+G(d,p) using SMD to model the acetonitrile solvent environment.

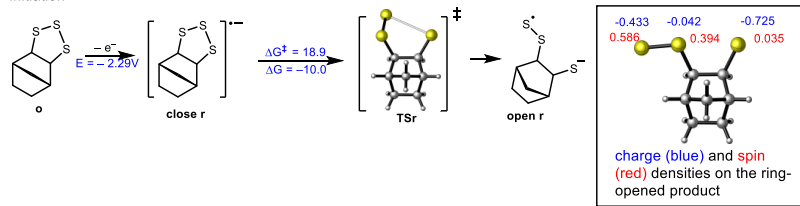
Table S2.4: Total Gibbs free energy (kJ/mol) of all species in study of polymerisation propagation mechanism depicted in the scheme below.^a

Species	E ^b	E	ZPE	TC	TS	H	G
close r	-1467.50830	-1467.34402	0.16085	0.00826	0.04607	-1467.33730	-1467.38034
open r	-1467.51039	-1467.34391	0.16039	0.00855	0.04762	-1467.33956	-1467.38416
o	-1467.41224	-1467.23838	0.16266	0.00762	0.04366	-1467.24007	-1467.28069
inter o	-1467.38223	-1467.20546	0.16216	0.00788	0.04449	-1467.21030	-1467.25176
open so	-1467.34664	-1467.17931	0.16024	0.00858	0.04703	-1467.17593	-1467.21993
to	-1467.34411	-1467.17623	0.16072	0.00851	0.04813	-1467.17300	-1467.21810
open to	-1467.34606	-1467.17869	0.16037	0.00857	0.04808	-1467.17524	-1467.22029
inter to	-1467.34443	-1467.17743	0.16027	0.00864	0.04856	-1467.17364	-1467.21916
d1	-2934.90986	-2934.60032	0.32327	0.01871	0.07385	-2934.56599	-2934.63680
d2	-2934.92351	-2934.58553	0.32377	0.0193	0.07497	-2934.57858	-2934.65050
d3	-2934.92556	-2934.58748	0.32430	0.01906	0.07291	-2934.58031	-2934.65019
d4	-2934.90646	-2934.57025	0.32357	0.01924	0.07424	-2934.56176	-2934.63297
t1	-4402.35050	-4401.84155	0.48746	0.02978	0.09824	-4401.83137	-4401.92657
t2	-4402.36082	-4401.85244	0.48765	0.02994	0.09899	-4401.84134	-4401.93729
t3	-4402.35834	-4401.85139	0.48794	0.02967	0.09773	-4401.83884	-4401.93354
t4	-4402.35433	-4401.84617	0.48736	0.02876	0.09358	-4401.83632	-4401.92687
tetra	-5869.77326	-5868.52127	0.65066	0.04037	0.12267	-5869.08035	-5869.19998
TSr	-1467.50417	-1467.33863	0.16010	0.00776	0.04559	-1467.33442	-1467.37698
TSo	-1467.32326	-1467.15285	0.16093	0.00754	0.04394	-1467.15291	-1467.19381
TSso 1	-1467.34509	-1467.17802	0.15963	0.00795	0.04528	-1467.17562	-1467.21786
TSso 2	-1467.34674	-1467.17915	0.16071	0.00776	0.04473	-1467.17638	-1467.21808
TSsto 1	-1467.34365	-1467.17616	0.16045	0.00769	0.04549	-1467.17362	-1467.21608
TSsto 2	-1467.34193	-1467.17473	0.16037	0.00765	0.04548	-1467.17201	-1467.21446
TSd1	-2934.90986	-2934.57291	0.32327	0.01871	0.07385	-2934.56599	-2934.63680
TSd2	-2934.91275	-2934.57544	0.32321	0.01858	0.07275	-2934.56907	-2934.63879
TSd3	-2934.90005	-2934.56167	0.32347	0.01848	0.07128	-2934.55621	-2934.62446
TSd4	-2934.89984	-2934.56079	0.32317	0.01858	0.07267	-2934.55621	-2934.62584
TSst1	-4402.33388	-4401.82482	0.48657	0.02925	0.09675	-4401.81617	-4401.90989
TSst2	-4402.33290	-4401.82463	0.48694	0.02922	0.09703	-4401.81486	-4401.90886
TSst3	-4402.33111	-4401.82290	0.48728	0.02902	0.09540	-4401.81292	-4401.90528
TSst4	-4402.33433	-4401.82621	0.48728	0.02910	0.09503	-4401.81606	-4401.90806
TSst	-5869.75905	-5869.07868	0.65050	0.03966	0.11992	-5869.06700	-5869.18388

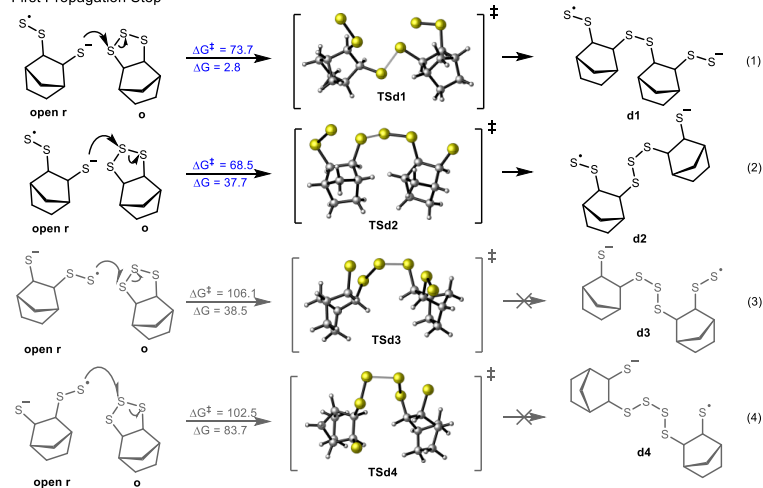
^aUnless stated otherwise, calculations performed at the wB97XD/6-31+G(d,p) level of theory using SMD to model the acetonitrile solvent environment. E is the total DFT energy, ZPE is the zero-point vibrational energy, TC is the thermal correction to the enthalpy, H is the total enthalpy, TS is the temperature times the total entropy, and G is the total Gibbs free energy in solution and includes a correction for change of state from 1atm to 1M. ^b Calculated with

wB97XD/def2TZVPD//wB97XD/6-31+G(d,p) using SMD to model the acetonitrile solvent environment.

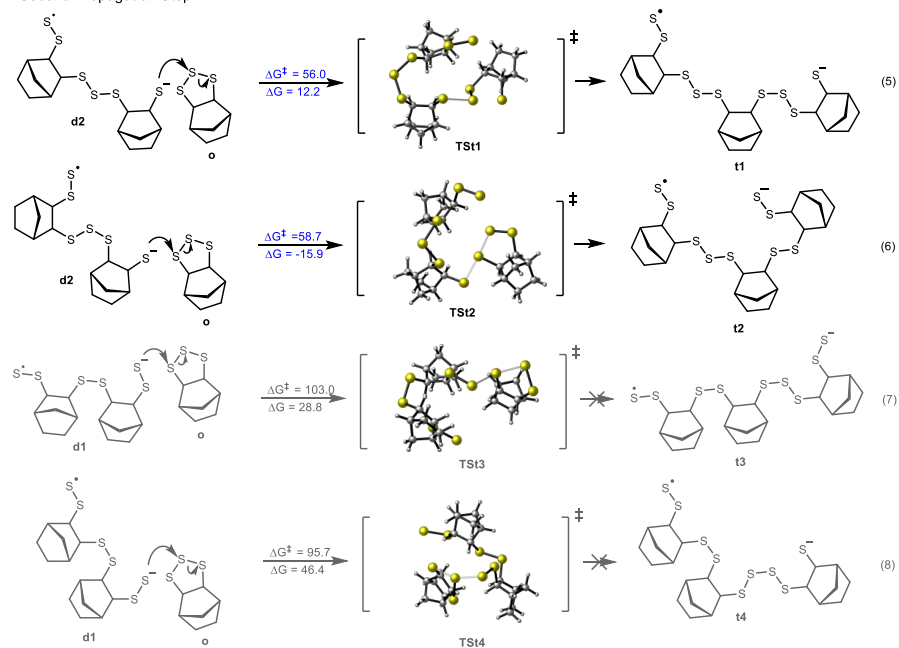
Initiation



First Propagation Step



Second Propagation Step



Third Propagation Step

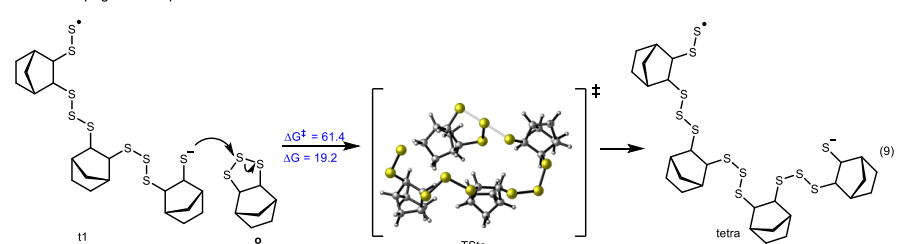


Figure S2.41: Gibbs free barriers and reaction energies (298 K, kJ mol^{-1}) for the ring opening of the reduced and neutral norbornene trisulfide in acetonitrile, and subsequent attack of the ring-opened reduced species on the neutral monomer. The inset shows the charge (blue) and spin (red) densities on the sulfur atoms in the ring-opened reduced species.

TGA-GC-MS investigation

Poly-1 was investigated at different temperatures using thermogravimetric analysis coupled with gas chromatography-mass spectrometry (TGA-GC-MS). This technique was used to optimise the temperature required for the recycling of **poly-1** to monomer **1**.

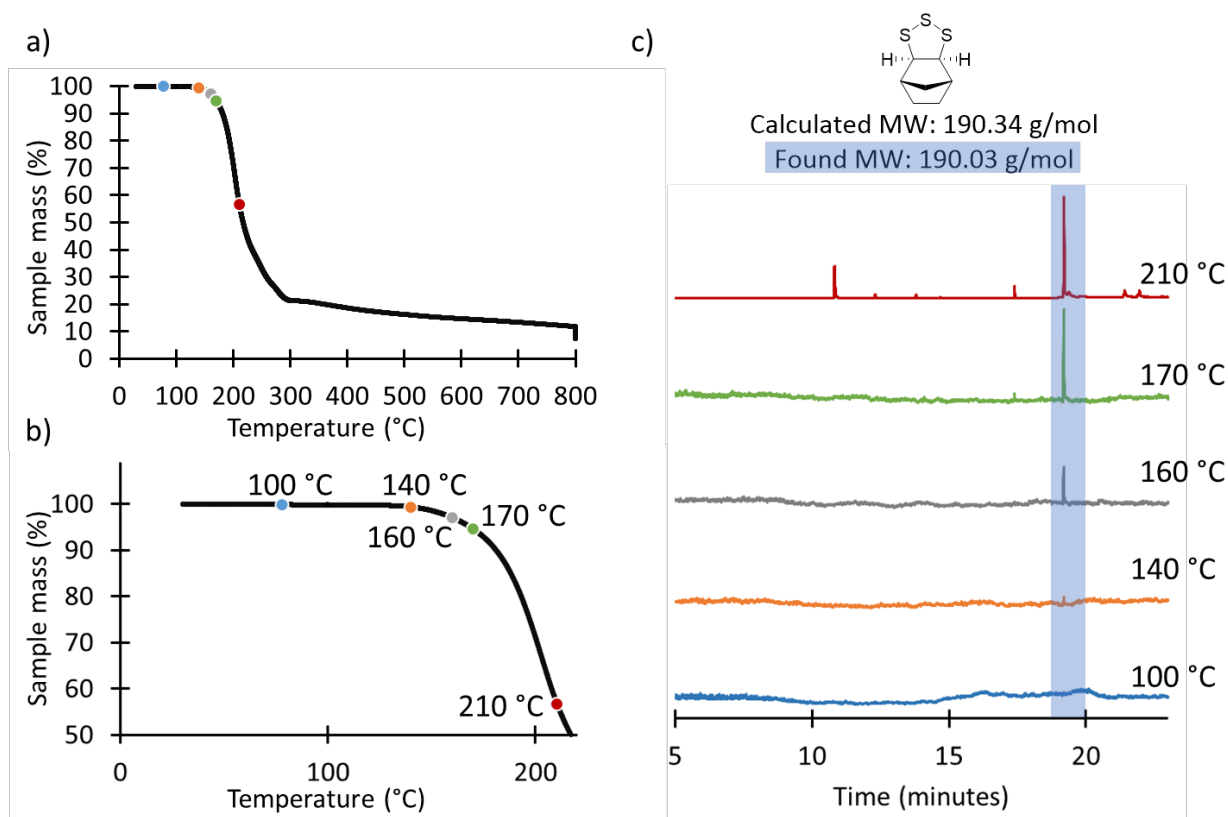


Figure S2.42: Monomer **1** generation from **poly-1** at different temperatures using TGA-GC-MS a) TGA of **poly-1** heated from 30-300 °C at a temperature ramp rate of 5 °C/min, then from 300-800 °C at a temperature ramp rate of 50 °C/min and then a 10-minute hold at 800 °C under a flow of nitrogen, b) TGA of **poly-1** showing the temperature points that were sampled for gas chromatography mass spectrometry (GC-MS) analysis, c) Gas chromatograms collected from the TGA of **poly-1** at 100, 140, 160, 170 and 210 °C. Decomposition of polymer was observed at 210 °C.

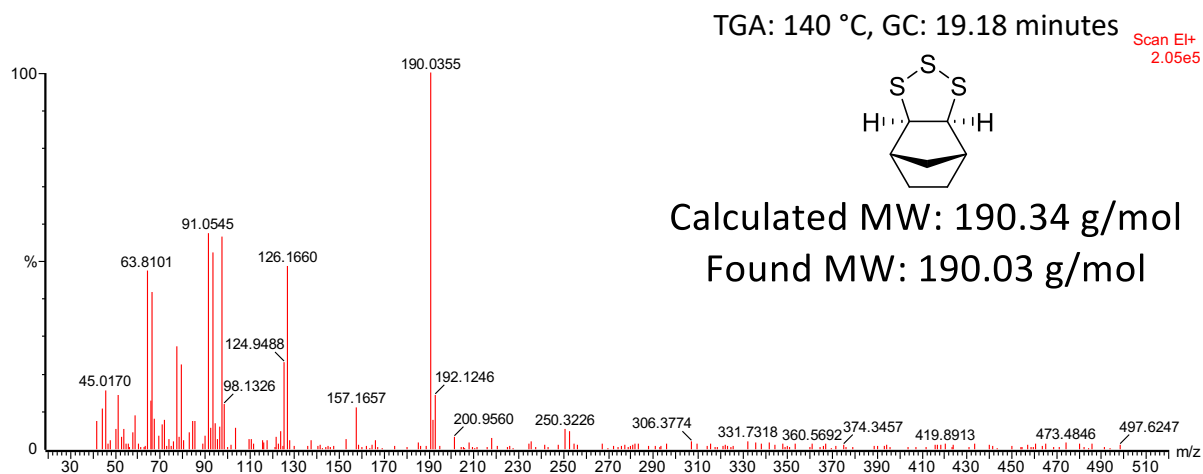


Figure S2.43: Mass spectrum of volatile products evolved from the TGA of the thermal decomposition of **poly-1** at 140 °C (19.18 minutes). Mass spectrum is consistent with the mass of monomer **1**.

Thermal depolymerisation of **poly-1**

Poly-1 recycling: 190 °C

Poly-1 (178 mg) was heated at 190 °C under a reduced pressure of 1 mbar using a short-path distillation apparatus. After 18 hours yellow oil was observed in the condenser and the remaining polymer had become dark in colour. A yellow oil was collected by washing the condenser with hexane (5 x 10 mL). The fractions were combined and concentrated under reduced pressure to deliver monomer **1** (54 mg, 30% yield). ¹H NMR analysis revealed the yellow oil to be monomer **1**. The remaining polymer (87 mg, 49% yield) was analysed by NMR spectroscopy and GPC (THF).

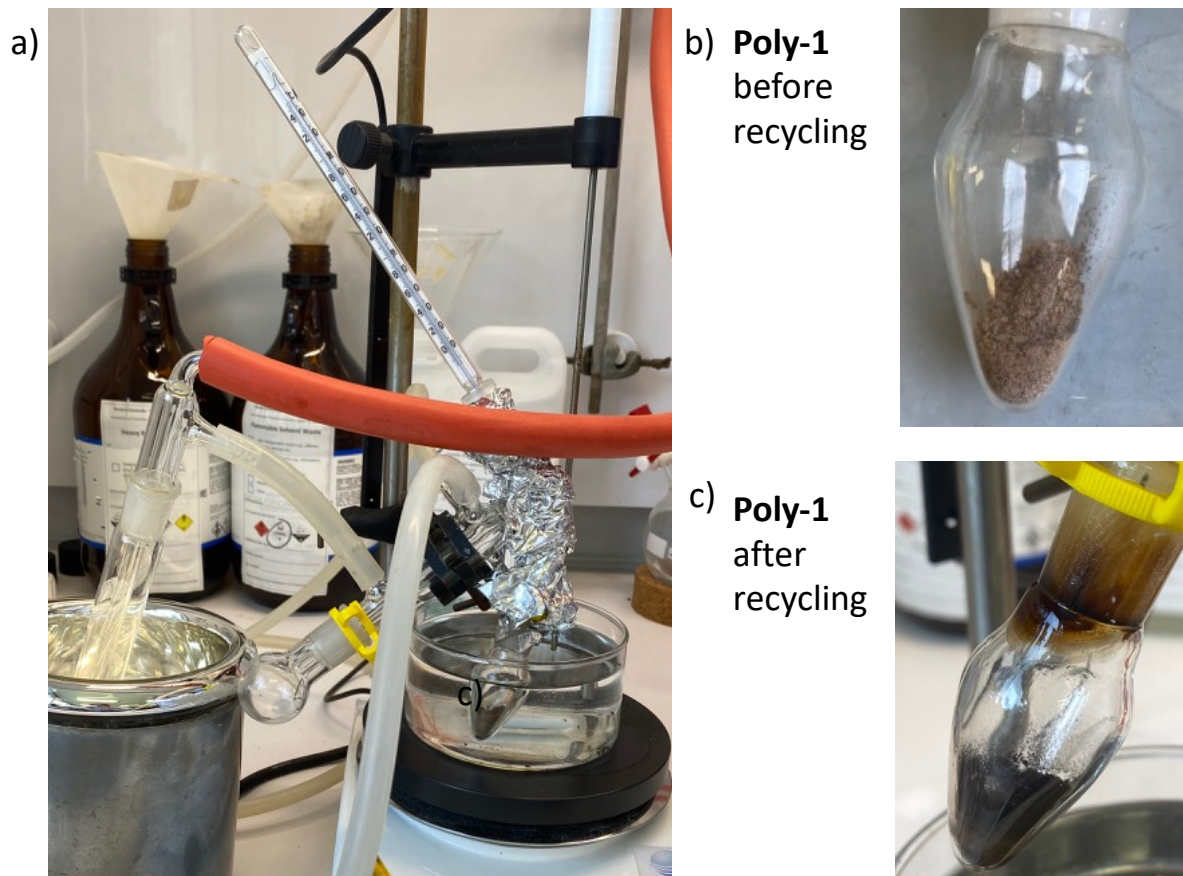


Figure S2.44: a) Vacuum distillation set up, b) **poly-1** before thermal recycling , c) **poly-1** after thermal recycling.

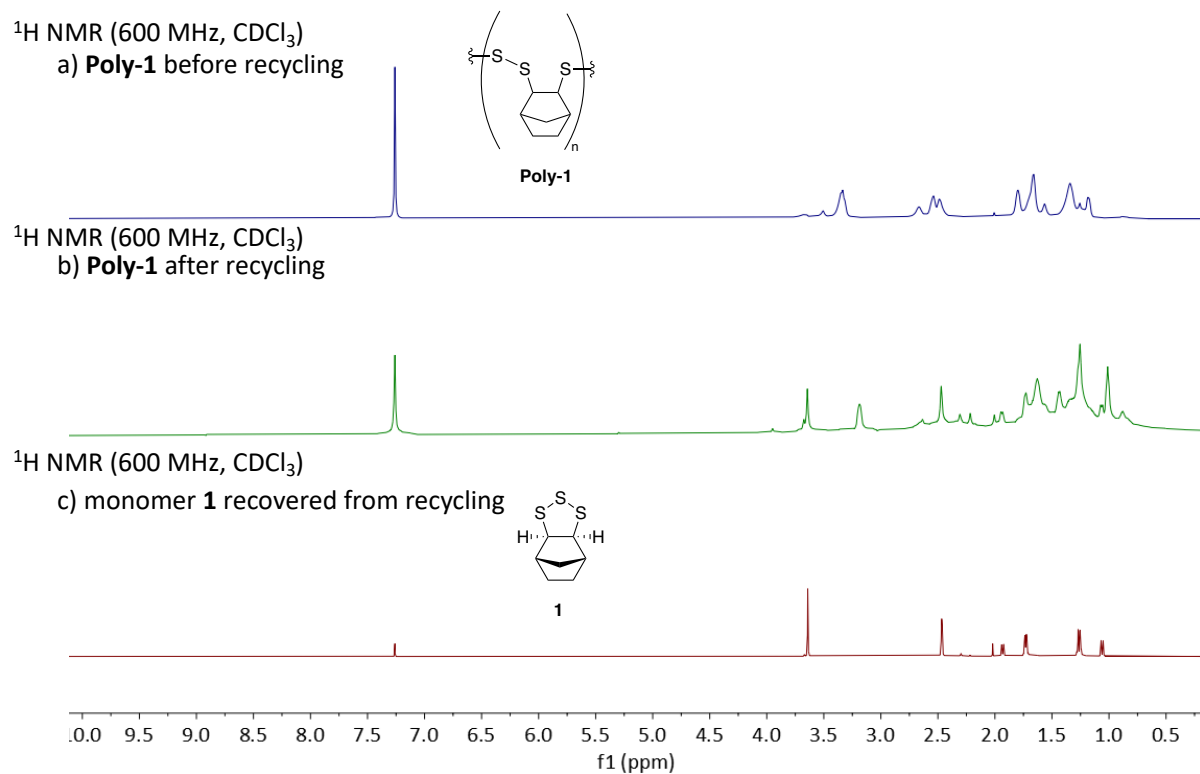


Figure S2.45: ¹H NMR (600 MHz, CDCl₃) of a) **poly-1** before thermal recycling experiment, b) **poly-1** after thermal recycling experiment and c) yellow oil collected from the thermal recycling of **poly-1**, Peaks are consistent with monomer **1**.

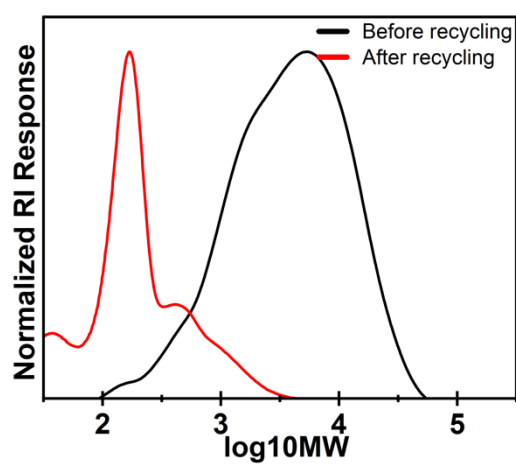


Figure S2.46: GPC (THF) of **poly-1** before thermal recycling and after thermal recycling.

Poly-1 (low molecular weight) recycling: 150 °C

The following **poly-1** recycling was performed on a low molecular weight ($M_w = 1060$ g/mol) sample.

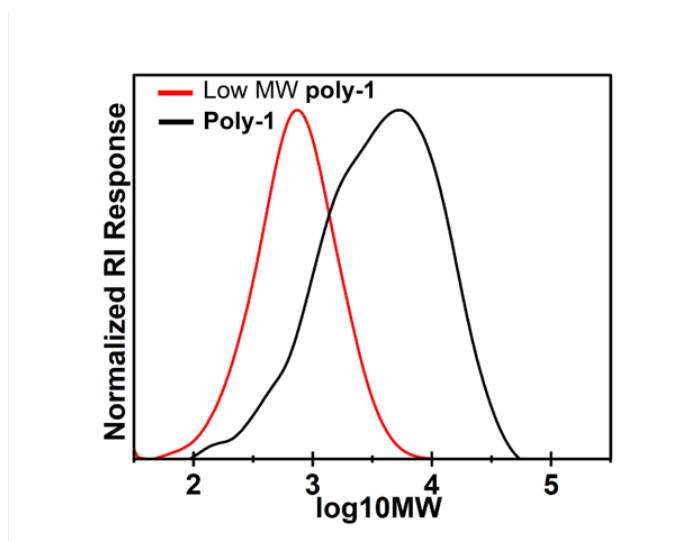


Figure S2.47: GPC (THF) of standard **poly-1** compared to a low molecular weight sample of **poly-1** collected through selective centrifugation.

Poly-1 (50 mg) was heated at 150 °C under a reduced pressure of 1 mbar using a short-path distillation apparatus. After 4 hours yellow oil was observed in the condenser. The yellow oil was collected by washing the condenser with hexane (5 x 10 mL). The fractions were combined and concentrated under reduced pressure to deliver monomer **1** (36 mg, 72% yield). ^1H NMR analysis revealed the yellow oil to be monomer **1**.

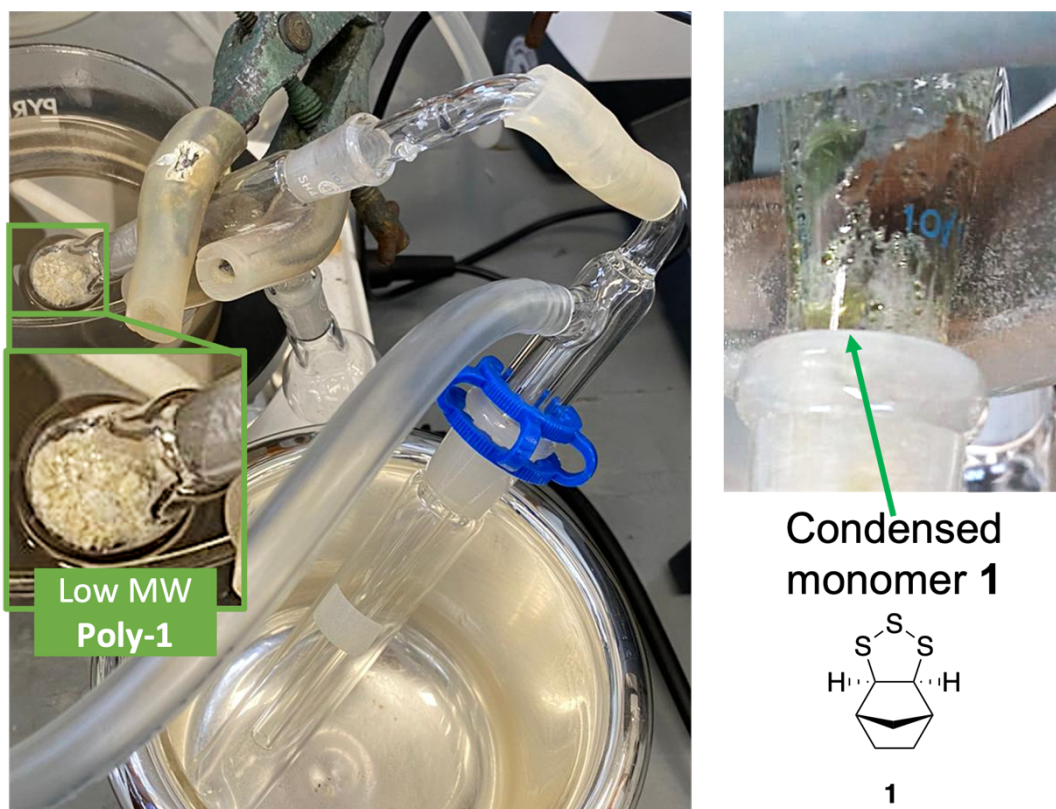


Figure S2.48: Vacuum distillation set up showing light color of low MW **poly-1** (left), yellow oil (monomer **1**) condensed on the inside of distillation adaptor after 4 hours at 150 °C under a reduced pressure of 1 mbar (right).

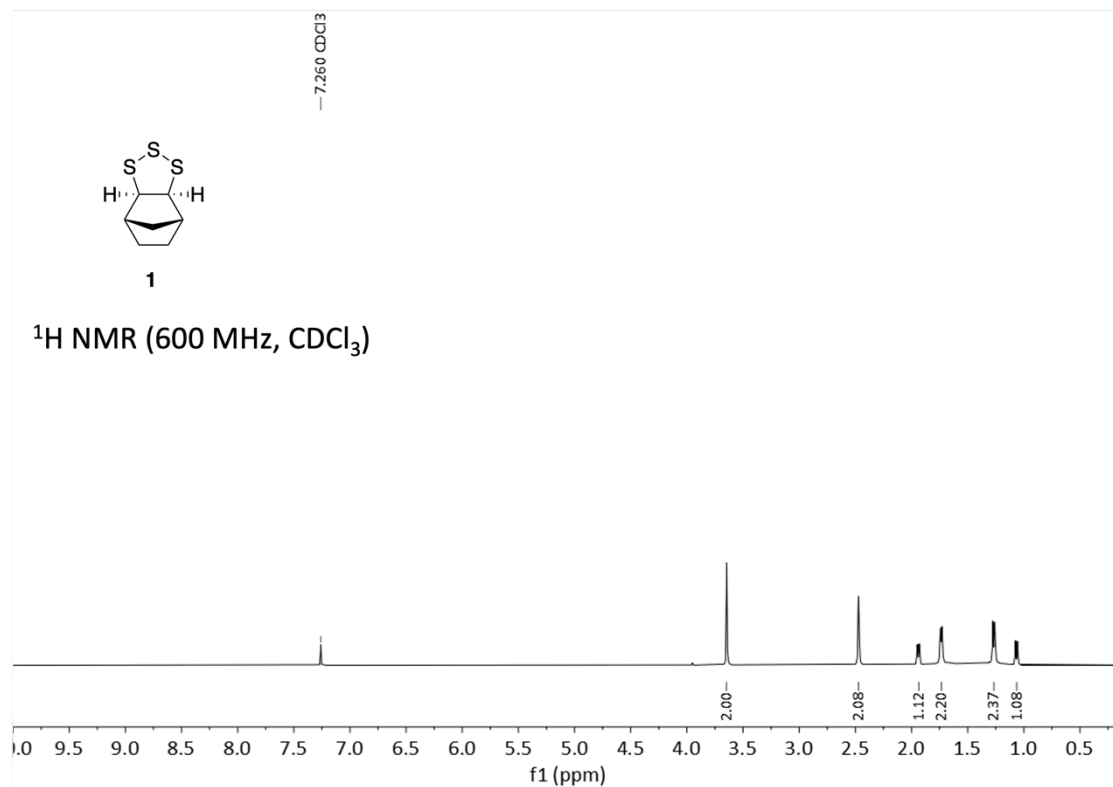


Figure S2.49: ^1H NMR spectrum (600 MHz, CDCl_3) of yellow oil collected from the vacuum distillation. Peaks are consistent with monomer **1**

Poly-3 thermal depolymerisation (neat)

Poly-3 (20 mg) was heated to 170 °C for 6 hours. Chloroform was then used to extract recycled monomer (2 mg, 10%). The polymer appeared to also undergo other reactions and appeared black, which may be the result of condensation or other degradation pathways due to the carboxylic acid:

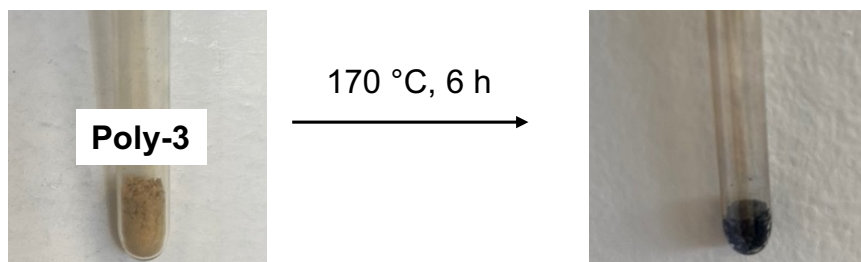
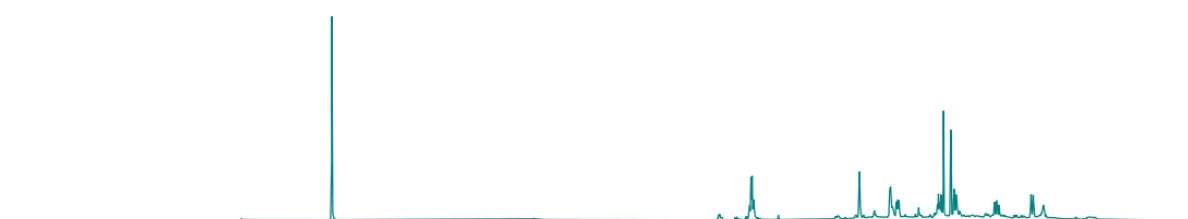


Figure S2.50: **Poly-3** change in colour after heating.

^1H NMR (600 MHz, CDCl_3)
Monomer **3** recovered from recycling experiment



^1H NMR (600 MHz, CDCl_3)
Pure monomer **3**

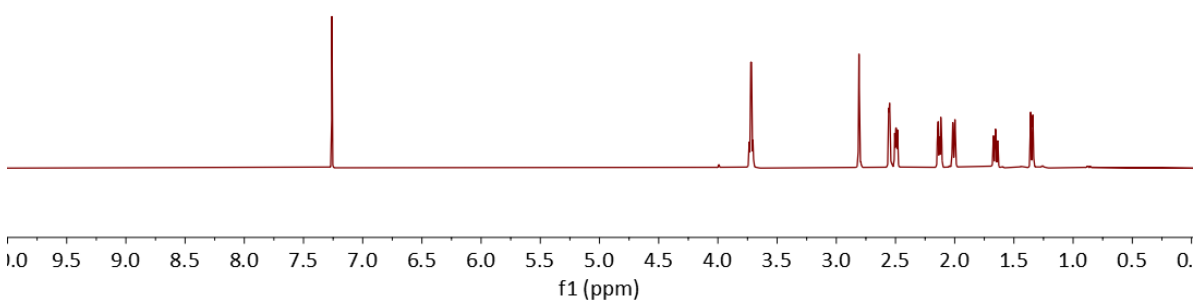


Figure S2.51: ^1H NMR spectra (600 MHz, CDCl_3) of monomer **3** recovered from recycling experiment (top) and a monomer **3** reference spectrum (bottom).

References

- [1] W. J. Chung, J. J. Griebel, E. T. Kim, H. Yoon, A. G. Simmonds, H. J. Ji, P. T. Dirlam, R. S. Glass, J. J. Wie, N. A. Nguyen, *Nature chemistry* **2013**, *5*, 518-524.
- [2] M. Mann, B. Zhang, S. J. Tonkin, C. T. Gibson, Z. Jia, T. Hasell, J. M. Chalker, *Polymer Chemistry* **2022**, *13*, 1320-1327.
- [3] J. Bao, K. P. Martin, E. Cho, K.-S. Kang, R. S. Glass, V. Coropceanu, J.-L. Bredas, W. O. N. Parker, Jr., J. T. Njardarson, J. Pyun, *Journal of the American Chemical Society* **2023**, *145*, 12386-12397.
- [4] D. J. Parker, H. A. Jones, S. Petcher, L. Cervini, J. M. Griffin, R. Akhtar, T. Hasell, *Journal of Materials Chemistry A* **2017**, *5*, 11682-11692.
- [5] J. J. Griebel, G. Li, R. S. Glass, K. Char, J. Pyun, *Journal of Polymer Science Part A: Polymer Chemistry* **2015**, *53*, 173-177.
- [6] X. Wu, J. A. Smith, S. Petcher, B. Zhang, D. J. Parker, J. M. Griffin, T. Hasell, *Nature communications* **2019**, *10*, 647.
- [7] L. He, J. Yang, H. Jiang, H. Zhao, H. Xia, *Industrial & Engineering Chemistry Research* **2023**, *62*, 9587-9594.
- [8] J. Jia, J. Liu, Z.-Q. Wang, T. Liu, P. Yan, X.-Q. Gong, C. Zhao, L. Chen, C. Miao, W. Zhao, *Nature Chemistry* **2022**, *14*, 1249-1257.
- [9] L. E. Apodaca, Mineral Commodity Summaries, **January, 2022**.
- [10] H. Leuchs, *Berichte der deutschen chemischen Gesellschaft* **1906**, *39*, 857-861.
- [11] F. S. Dainton, T. R. E. Devlin, P. A. Small, *Transactions of the Faraday Society* **1955**, *51*, 1710-1720.
- [12] F. Sanda, T. Endo, *Journal of Polymer Science Part A: Polymer Chemistry* **2001**, *39*, 265-276.
- [13] O. Nuyken, S. D. Pask, *Polymers* **2013**, *5*, 361-403.
- [14] J. E. McIntyre, *Synthetic fibres: nylon, polyester, acrylic, polyolefin*, Taylor & Francis US, **2005**.
- [15] M. Bednarek, *Progress in Polymer Science* **2016**, *58*, 27-58.
- [16] A. Kisanuki, Y. Kimpara, Y. Oikado, N. Kado, M. Matsumoto, K. Endo, *Journal of Polymer Science Part A: Polymer Chemistry* **2010**, *48*, 5247-5253.
- [17] Y. Liu, Y. Jia, Q. Wu, J. S. Moore, *Journal of the American Chemical Society* **2019**, *141*, 17075-17080.
- [18] T. Baran, A. Duda, S. Penczek, *Journal of Polymer Science: Polymer Chemistry Edition* **1984**, *22*, 1085-1095.

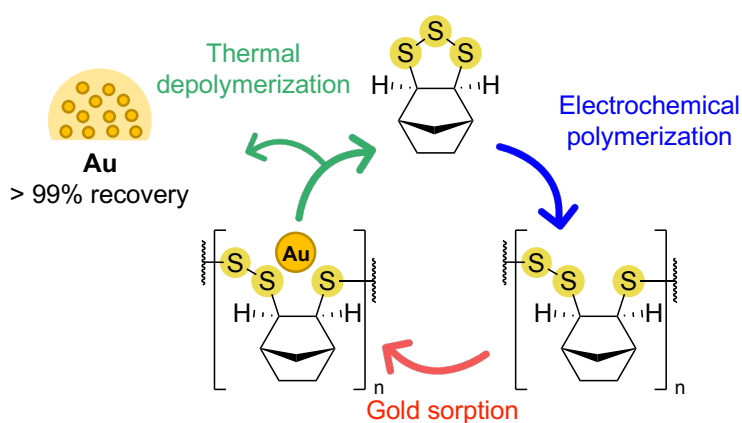
- [19] C. Schotten, T. P. Nicholls, R. A. Bourne, N. Kapur, B. N. Nguyen, C. E. Willans, *Green Chemistry* **2020**, *22*, 3358-3375.
- [20] P. D. Bartlett, T. Ghosh, *The Journal of Organic Chemistry* **1987**, *52*, 4937-4943.
- [21] S. Poulain, S. Julien, E. Duñach, *Tetrahedron letters* **2005**, *46*, 7077-7079.
- [22] A. K. Mann, L. S. Lisboa, S. J. Tonkin, J. R. Gascooke, J. M. Chalker, C. T. Gibson, *Angewandte Chemie International Edition* **2024**, *63*, e202404802.
- [23] L. J. Dodd, C. Lima, D. Costa-Milan, A. R. Neale, B. Saunders, B. Zhang, A. Sarua, R. Goodacre, L. J. Hardwick, M. Kuball, T. Hasell, *Polymer Chemistry* **2023**, *14*, 1369-1386.
- [24] M. L. Eder, C. B. Call, C. L. Jenkins, *ACS Applied Polymer Materials* **2022**, *4*, 1110-1116.
- [25] J. J. Dale, M. W. Smith, T. Hasell, *Advanced Functional Materials* **2024**, *n/a*, 2314567.
- [26] J. J. Griebel, N. A. Nguyen, S. Namnabat, L. E. Anderson, R. S. Glass, R. A. Norwood, M. E. Mackay, K. Char, J. Pyun, *ACS Macro Letters* **2015**, *4*, 862-866.
- [27] Y. Xin, H. Peng, J. Xu, J. Zhang, *Advanced Functional Materials* **2019**, *29*, 1808989.
- [28] S. J. Tonkin, C. T. Gibson, J. A. Campbell, D. A. Lewis, A. Karton, T. Hasell, J. M. Chalker, *Chemical Science* **2020**, *11*, 5537-5546.
- [29] N. P. Cowieson, D. Aragao, M. Clift, D. J. Ericsson, C. Gee, S. J. Harrop, N. Mudie, S. Panjekar, J. R. Price, A. Riboldi-Tunncliffe, *Journal of synchrotron radiation* **2015**, *22*, 187-190.
- [30] D. Aragão, J. Aishima, H. Cherukuvada, R. Clarcken, M. Clift, N. P. Cowieson, D. J. Ericsson, C. L. Gee, S. Macedo, N. Mudie, *Journal of synchrotron radiation* **2018**, *25*, 885-891.
- [31] G. M. Sheldrick, *Acta Crystallographica Section A: Foundations and Advances* **2015**, *71*, 3-8.
- [32] S. Poulain, S. Julien, E. Duñach, *Tetrahedron Lett.* **2005**, *46*, 7077-7079.
- [33] T. Baran, A. Duda, S. Penczek, *Macromol. Chem. Phys.* **1984**, *185*, 2337-2346.
- [34] T. Baran, A. Duda, S. Penczek, *J. Polym. Sci., Polym. Chem. Ed.* **1984**, *22*, 1085-1095.
- [35] M. J. T. Frisch, G. W.; Schlegel, H. B.; Scuseria, G. E.; Robb, M. A.; Cheeseman, J. R.; Scalmani, G.; Barone, V.; Petersson, G. A.; Nakatsuji, H.; Li, X.; Caricato, M.; Marenich, A. V.; Bloino, J.; Janesko, B. G.; Gomperts, R.; Mennucci, B.; Hratchian, H. P.; Ortiz, J. V.; Izmaylov, A. F.; Sonnenberg, J. L.; Williams-Young, D.; Ding, F.; Lipparini, F.; Egidi, F.; Goings, J.; Peng, B.; Petrone, A.; Henderson, T.; Ranasinghe, D.; Zakrzewski, V. G.; Gao, J.; Rega, N.; Zheng, G.; Liang, W.; Hada, M.; Ehara, M.; Toyota, K.; Fukuda, R.; Hasegawa, J.; Ishida, M.; Nakajima, T.; Honda, Y.; Kitao, O.; Nakai, H.; Vreven, T.; Throssell, K.; Montgomery, J. A., Jr.; Peralta, J. E.; Ogliaro, F.; Bearpark, M. J.; Heyd, J. J.; Brothers, E. N.; Kudin, K. N.; Staroverov, V. N.; Keith, T. A.; Kobayashi, R.; Normand, J.; Raghavachari, K.; Rendell, A. P.; Burant, J. C.; Iyengar, S. S.; Tomasi, J.; Cossi, M.;

- Millam, J. M.; Klene, M.; Adamo, C.; Cammi, R.; Ochterski, J. W.; Martin, R. L.; Morokuma, K.; Farkas, O.; Foresman, J. B.; Fox, D. J, *Gaussian 16, Revision C.01, Gaussian, Inc., Wallingford CT* **2016**.
- [36] B. O. Al Sasi, A. Demirbas, *Petroleum Science and Technology* **2016**, *34*, 1550-1555.
- [37] a. Petersson, A. Bennett, T. G. Tensfeldt, M. A. Al-Laham, W. A. Shirley, J. Mantzaris, *The Journal of chemical physics* **1988**, *89*, 2193-2218.
- [38] A. V. Marenich, C. J. Cramer, D. G. Truhlar, *The Journal of Physical Chemistry B* **2009**, *113*, 6378-6396.
- [39] D. Rappoport, F. Furche, *The Journal of chemical physics* **2010**, *133*.
- [40] R. F. Ribeiro, A. V. Marenich, C. J. Cramer, D. G. Truhlar, *The Journal of Physical Chemistry B* **2011**, *115*, 14556-14562.
- [41] I. M. Alecu, J. Zheng, Y. Zhao, D. G. Truhlar, *Journal of chemical theory and computation* **2010**, *6*, 2872-2887.
- [42] M. Namazian, C. Y. Lin, M. L. Coote, *Journal of chemical theory and computation* **2010**, *6*, 2721-2725.

Chapter 3

Large scale electrochemical synthesis of poly(trisulfides) and their applications

Linear poly(trisulfides) are valuable polymers due to their linear structure, processability and recyclability. This chapter explores the scaling up of electrochemical poly(trisulfide) synthesis as well as their applications, including gold sorption and recovery, silver sorption and release, copper binding and precipitation from water, and thermal curing to crosslink the polymer. Validating the multi-gram production of poly(trisulfides) is vital for their use in these applications.



Acknowledgments

Lynn Lisboa for help in the copper binding experiment

Introduction

The development of scalable methods for polysulfide synthesis is essential for their use in applications. Polysulfide synthesis typically relies on high temperatures to generate reactive molten sulfur, which can be crosslinked with organic comonomers to form stable polymeric materials through a process known as inverse vulcanisation.^[1] Inverse vulcanisation, even on a small scale, can lead to hazardous run-away reactions.^[2-3] This risk is amplified as the process is scaled up due to enhanced mass and heat transfer issues. Another challenge of polysulfide synthesis via inverse vulcanisation is the limited understanding of the polysulfide structure, which consists of a range of sulfur ranks, poorly controlled C–S bond stereochemistry, and undesired by products within the polysulfide network.^[4] Recent studies have sought to better understand the structure of inverse vulcanised polysulfides using solid-state ¹³C NMR spectroscopy and degradation studies.^[4-5] However, there is still limited control over the polysulfide structure regarding C–S stereochemistry and sulfur rank. Additionally, polysulfides produced via inverse vulcanisation are typically insoluble in organic solvents, complicating processing and characterisation by solution-based methods.

In contrast, poly(trisulfides) made through electrochemical ring-opening polymerisation are produced at room temperature, have well-defined C–S stereochemistry and sulfur rank, and are solvent processable. Key poly(trisulfides) produced in the previous chapter also show unique properties in polymer recycling and water solubility. Poly(trisulfide), **poly-1**, containing a symmetric norbornane backbone underwent thermal depolymerisation, resulting in a high recovery of the pure monomer. Poly(trisulfide), **poly-3**, containing a carboxylic acid functional group was found to be water-soluble when deprotonated with NaOH.

Poly(trisulfide) synthesis was previously conducted in a commercially available electrochemical reactor (ElectraSyn), which provided reproducible products using standardised equipment (Figure 3.1 A). The ElectraSyn consists of a potentiostat, electrochemical cell, and comes with a range of electrode options. The largest cell for this electrochemical reactor had a volume of 20 mL, producing up to 200 mg of poly(trisulfide) at a time. To scale up the reaction, a GAMRY potentiostat was used as it can conduct electrochemical reactions on external electrochemical cells (Figure 3.1 B). These electrochemical cells can be tailored to the requirements for electrode size and reactor volume. The ability to change these features is important for the design of a large-scale electrochemical reactor.

A ElectraSyn

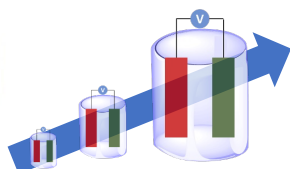


Standardized parts

Easily reproducible

Small volume (20 mL)

B GAMRY potentiostat



Large reaction volumes

More challenging to reproduce

Figure 3.1: (A) ElectraSyn potentiostat and complementary electrodes. (B) GAMRY potentiostat which can be used to run electrochemical reactions on different cell volumes.

When scaling up the electrochemical synthesis of poly(trisulfides), several challenges were anticipated, and the process was not expected to scale up linearly. One of these issues is the decrease in mass transfer as the reactor scale is increased in batch.^[6] Maintaining the electrode surface area to reactor volume ratio was important to preserve efficiency. As size of the batch reactor increases, the distance between the electrodes increases, leading to increased resistance.^[7] This could lead to issues such as ohmic drop if the distance between the reference electrode and working electrode was too great.^[8] These potential challenges are commonly faced when scaling up electrochemical reactions. Therefore, several scale-up steps were conducted and assessed to determine the optimal conditions for a large-scale synthesis of poly(trisulfides).

Continuous flow reactors offer scaled production of poly(trisulfides) with decreased mass transfer issues, enhanced cell conductivity, and high surface area to reaction volume ratio, as the cell volume can remain small while a large volume of reagent is passed through.^[9] Therefore, poly(trisulfide) synthesis was investigated using a continuous flow process. However, poly(trisulfide) synthesis in continuous flow comes with its own challenges due to the production of polymer precipitate, which could lead to blockages in the flow lines.

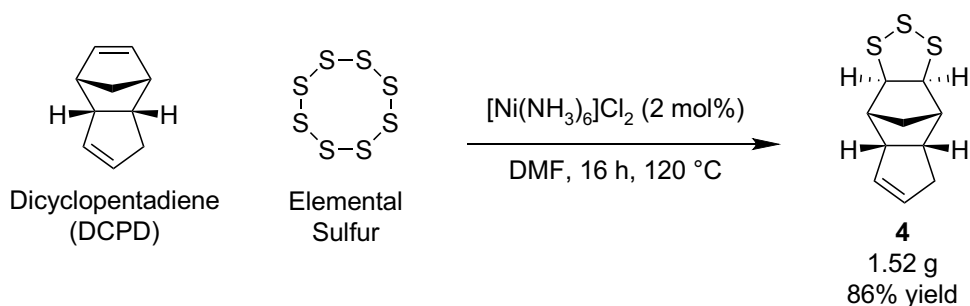
With these potential challenges in mind, batch and continuous flow processes were investigated to scale-up the electrochemical production of poly(trisulfides). A large electrochemical batch reactor was designed to produce the poly(trisulfides) on a scale 125 times what was achieved in the ElectraSyn. In the process of designing a large-scale electrochemical reactor, alternative cost-

effective electrode materials were investigated. Using a continuous flow electrochemical cell, the electrochemical polymerisation was validated in a continuous flow process. With reliable access to poly(trisulfide) materials, several applications were then explored. These includes gold sorption and recovery, silver sorption and release, copper binding and precipitation from water, and thermal curing to achieve crosslinking.

Results and discussion

Large scale monomer synthesis

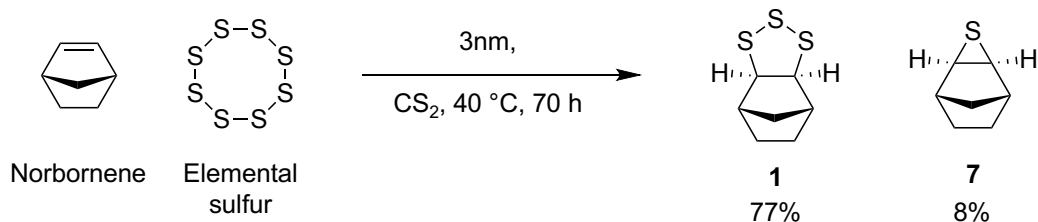
In the previous chapter, a small library of 1,2,3-trithiolane monomers were synthesised following a literature-reported procedure.^[10] This synthesis employs a nickel catalyst, $[\text{Ni}(\text{NH}_3)_6]\text{Cl}_2$ (2 mol%) to activate elemental sulfur at 120 °C in DMF, resulting in its addition to strained C=C double bonds in norbornene derivatives. Specifically, the synthesis of **4** was conducted by heating dicyclopentadiene (1.00 g, 7.6 mmol), elemental sulfur (730 mg, 2.3 mmol), and $[\text{Ni}(\text{NH}_3)_6]\text{Cl}_2$ (33 mg, 0.3 mmol) in DMF (10 mL) at 120 °C for 16 hours (Scheme 3.1). After purification, monomer **4** was obtained in high purity with a yield of 86 % (1.52 g).



Scheme 3.1: Synthesis of monomer **4** on a 1 g scale.

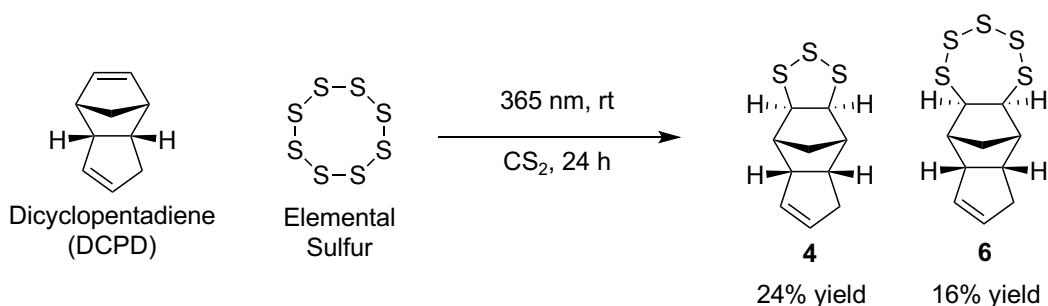
The synthesis of monomer **4** was then scaled up from 1 g to 20 g of dicyclopentadiene, using the same equivalents of elemental sulfur and nickel catalyst while reducing the amount of solvent by 50%. After purification, monomer **4** was recovered in high purity with a yield of 72% (25.6 g). This reaction demonstrated that the monomer synthesis could be scaled up in batch.

An alternative method to activate sulfur is through UV irradiation.^[11] Inoue and coworkers demonstrated the photochemical addition reaction of sulfur to olefins, forming 1-thiolanes and 1,2,3-trithiolanes (Scheme 3.2).^[11]



Scheme 3.2: Photochemical addition reaction of sulfur to norbornene.^[11]

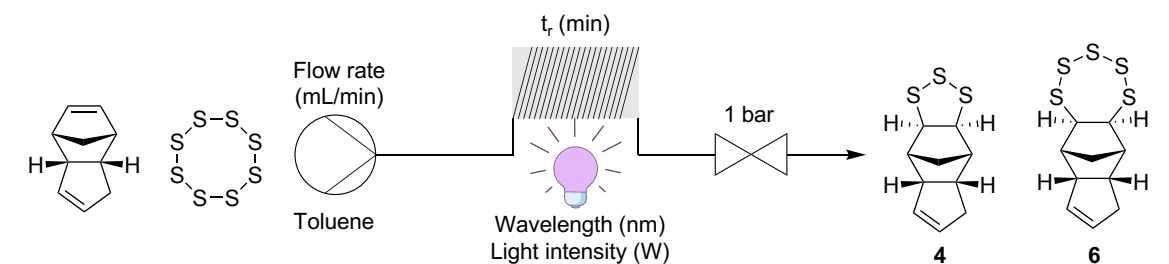
A complementary procedure to Inoue's work was then investigated for the synthesis of monomer **4** in CS₂ using a 365 nm light for 24 hours (Scheme 3.3). Crude ¹H NMR analysis of the reaction mixture showed a 24% conversion to monomer **4** and a 16% conversion to monomer **6**.



Scheme 3.3: Photochemical addition reaction of sulfur to dicyclopentadiene.

Photochemical synthesis of 1,2,3-trithiolanes offers milder reaction conditions compared to the thermal reaction. To facilitate the large-scale production, a continuous flow process was investigated with the aim of optimising reaction conditions for the production of monomer **4** in significant quantities. A challenge of reacting sulfur in continuous flow was its low solubility in organic solvents, with sulfur being most soluble in CS₂, benzene, and toluene.^[12] Insoluble particles in solution could cause blockages in the system and must be avoided. Therefore, a low concentration solution of sulfur (33 mM, toluene) was prepared and maintained at a temperature of 60 °C. Toluene was selected as the solvent because CS₂ has a low boiling point and benzene is hazardous.

A stock solution of dicyclopentadiene (78 mM) and sulfur (33 mM) was prepared in toluene and heated to 60 °C while stirring for 30 minutes to dissolve the sulfur. The stock solution was then filtered to remove any insoluble material and maintained at 60 °C while in the flow reactor reservoir. The solution was passed through a photochemical reactor illuminated with LEDs under different reaction conditions including temperature, flow rate, wavelength and lamp power (Table 3.1). Each reaction solution was then collected, dried under reduced pressure, and purified by column chromatography, resulting in three fractions. The first was the unreacted dicyclopentadiene, the second fraction was a mixture of monomer **4** and **6**, and the last fraction was an unknown byproduct. The mass of unreacted dicyclopentadiene was used to calculate reaction conversion.

Table 3.1: Summary of photochemical synthesis of **4** in continuous flow.

	Temperature (°C)	Residence time (min)	Wavelength (nm)	Light intensity (W)	Conversion (%)	Yield 4 (%)	Yield 6 (%)
1	80	1.25	365	226	62	8	3
2	80	1.25	455	226	0	0	0
3	60	1.25	365	226	95	11	5
4	60	2.5	365	226	92	22	9
5	60	10	365	226	97	7	8
6	60	2.5	365	22.6	95	12	3

Entry 1 was conducted at 80 °C under 365 nm (226 W) irradiation at a residence time of 1.25 minutes. This resulted in a 62% conversion of dicyclopentadiene, an 8% yield of **4**, and a 3% yield of **6**. Although the yield was low, the reaction time was drastically shorter compared to the 24-hour batch reaction, which yielded a 40% mixture of **4** and **6**.

In entry 2, the reaction was conducted at a wavelength of 455 nm (100 W). This resulted in no conversion of the starting material, indicating that 455 nm light was not effective. It was interesting that no reaction occurred under 455 nm irradiation, as sulfur absorbs visible light at this wavelength as indicated by UV-Vis spectroscopy.^[13] Furthermore, recent work by Quan and coworkers describe the photochemical crosslinking of sulfur (S₈) and dicyclopentadiene under irradiation at 455 nm, neat.^[13]

The reaction temperature was then decreased to 60 °C resulting in an increase in conversion, but no significant change to the yield of monomers **4** and **6** (entry 3). It was proposed that the lower reaction temperature favours the conversion of dicyclopentadiene and elemental sulfur to an unknown byproduct.

Next, the flow rate was slowed to increase the residence time from 1.25 minutes (entry 3) to 2.5 minutes (entry 4) and 10 minutes (entry 5). All 3 reactions showed high conversion and little difference in the yield of monomers **4** and **6**. Entry 4, which had a residence time of 2.5 minutes, showed the highest yields for monomers **4** (22%) and **6** (9%).

Overall, the yields of the cyclic sulfide monomers remained low while the conversion of dicyclopentadiene was high. It was then hypothesised that the high intensity irradiation (226 W) was favouring the production of the unknown byproduct. To test this, the light intensity was decreased to 22.6 W at 365 nm (entry 6). However, there was no significant change to either conversion or yield of monomers **4** and **6**.

To understand the reaction further, the unknown byproduct was investigated. ^1H NMR spectroscopy of the third fraction eluted from the column chromatography of entry 1 shows broad peaks consistent with polymeric material (Figure 3.2). This fraction represented the primary product (83%) of the photochemical reaction. It was hypothesised that during the photochemical reaction of sulfur and dicyclopentadiene, a polymeric material was formed from the ring-opening polymerisations of monomers **4** and **6** which were first produced in the reaction. This fascinating finding was studied in detail in the next chapter.

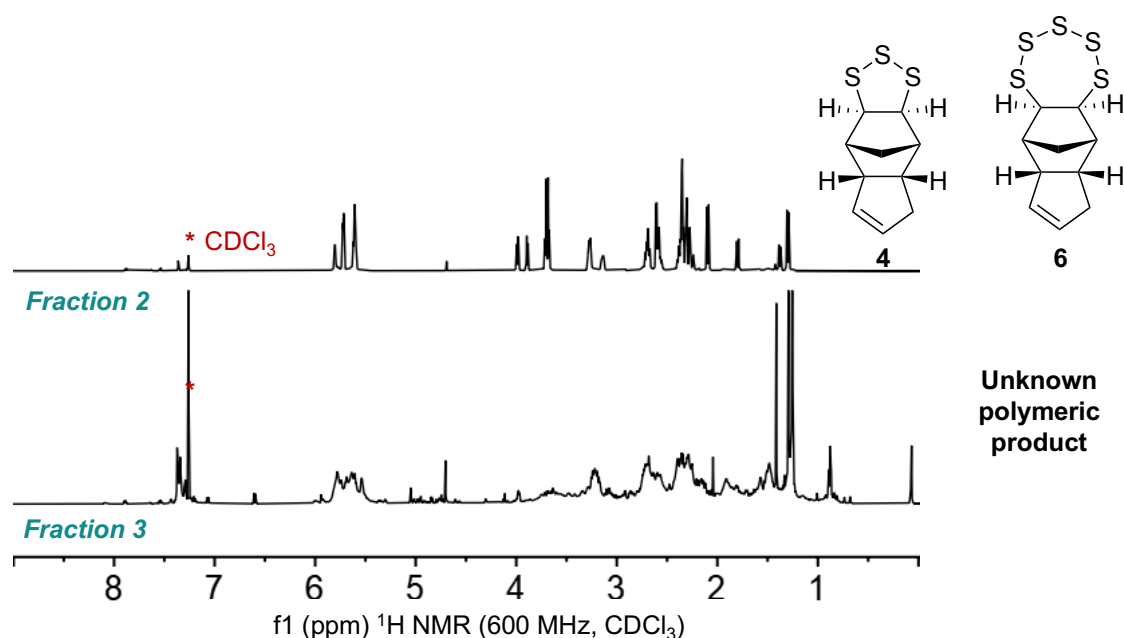


Figure 3.2: ^1H NMR spectra of column fractions 2 and 3 from the photochemical reaction of sulfur and dicyclopentadiene (entry 1).

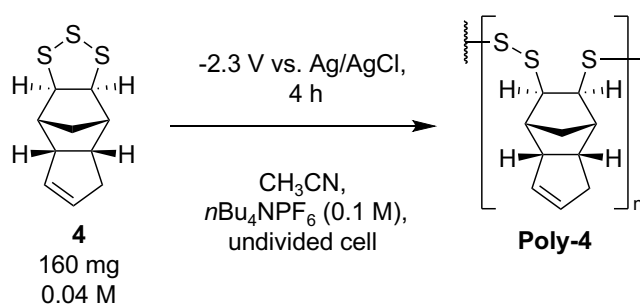
Alternative carbon-based electrode materials

Alternative carbon-based electrodes were evaluated for their effectiveness during the electrochemical polymerisation of 1,2,3-trithiolane monomer **4**. Glassy carbon electrodes were used previously for the synthesis of poly(trisulfides). However, a pair of glassy carbon electrodes (0.8 cm x 5 cm) cost \$352 AUD. Therefore, the large-scale batch reactor, which would require larger electrodes to account for the increase in reagents, would be very costly. This was why alternative

carbon-based materials, graphite and carbon felt, which were lower in cost, have been investigated. A pair of graphite electrodes (0.8 cm x 5 cm) cost \$78 AUD and high purity carbon felt (10 cm x 10 cm) could be purchased at \$10 AUD and easily cut to a desired size.

The selected electrodes, glassy carbon (2 x 0.8 cm x 5 cm), graphite (2 x 0.8 cm x 5 cm), and carbon felt (2 x 0.8 cm x 5 cm) were each investigated in a 20 mL electrochemical cell. The cells were charged with monomer **4** (160 mg, 0.7 mmol) in a 0.1 M *n*Bu₄NPF₆ solution (584 mg in acetonitrile, 15 mL). A constant potential of -2.3 V versus Ag/AgCl (3 M aq. KCl) was applied to each reaction for 4 hours while stirring at 1500 rpm. After each reaction, the solutions were worked-up by successive dissolution in chloroform (10 mL) and precipitation with acetonitrile (30 mL). The resulting suspension was centrifuged at 5000 rpm for 5 minutes, forming a pellet of the precipitate. The supernatant was decanted, and the process was repeated three times to purify the polymer from the electrolyte and the remaining monomer. Analysis by GPC and ¹H NMR spectroscopy was conducted to determine conversion, isolated yield, weight average molecular weight (*M*_w) and dispersity (*D*) (Table 3.2).

Table 3.2: Summary of alternative carbon-based electrode material used in the synthesis of **poly-4**.



	Electrode material	Conversion (%)	Yield (%)	<i>M</i> _w (g/mol)	<i>D</i>
1	Glassy carbon	64	33	3300	2.4
2	Graphite	>99	83	3400	2.4
3	Carbon felt	>99	94*	5800	5.6

*Yield is not accurate due to the presence of carbon felt fibers in the isolated polymer product.

The first electrode material, glassy carbon, resulted in a conversion of 64% and an isolated polymer yield of 33% (entry 1). The isolated polymer had a *M*_w of 3300 g/mol with a *D* of 2.4 (entry 1).

Graphite electrodes were investigated next, resulting in a conversion of >99% and an 83% isolated yield (entry 2). The isolated polymer had a *M*_w of 3400 g/mol with a *D* of 2.4, similar to the polymer produced using the glassy carbon electrodes (entry 1). The weak physical properties of graphite, combined with the rapid stirring and formation of precipitate in the pores of the electrode,

led to cracking and breaking of the electrode (Figure 3.3 A). Due to this issue, graphite electrodes were not studied further.

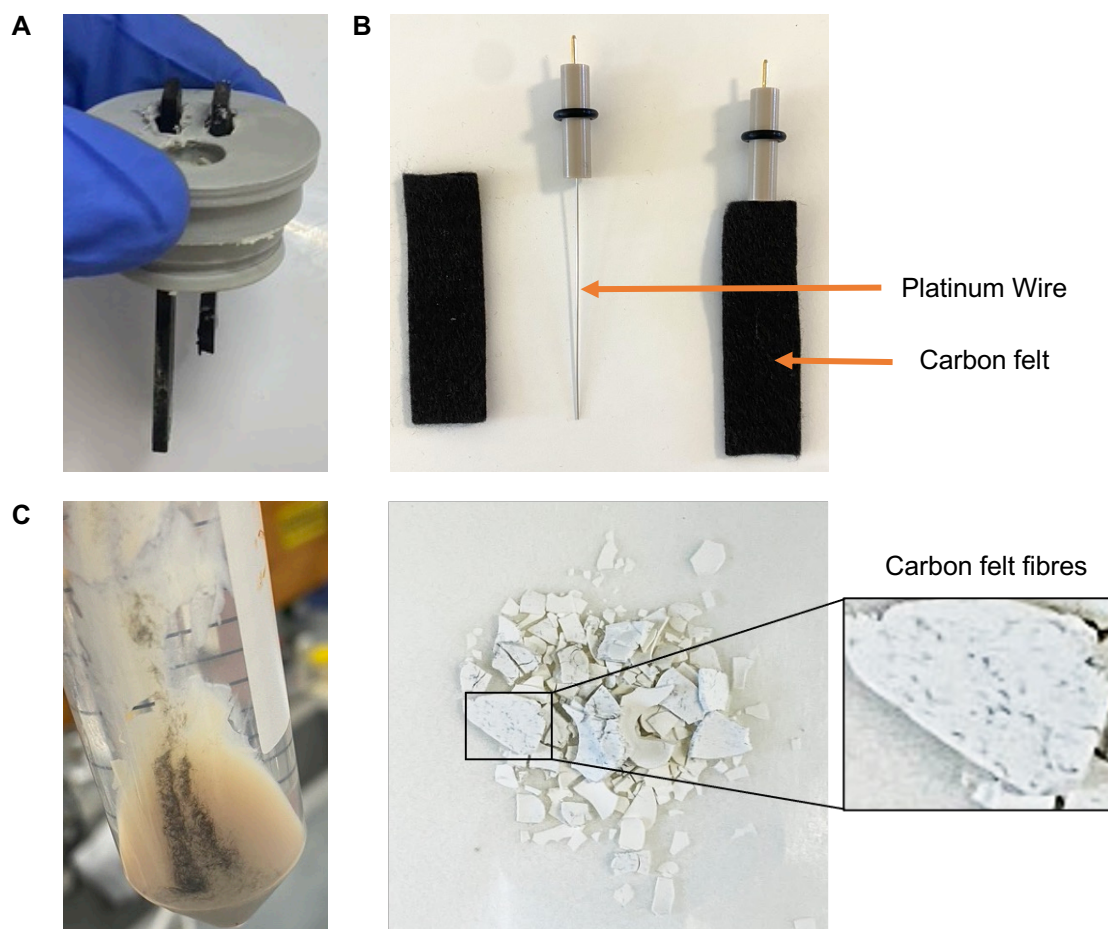


Figure 3.3: (A) Broken graphite electrode after reaction in Table 2, entry 2. (B) Platinum wire electrode embedded into the middle of the carbon felt electrode. (C) Carbon felt fibres within the polymer precipitate.

Carbon felt was studied next due to its low cost. Additionally, as a woven fabric, carbon felt should not crack during the reaction. Another advantage of carbon felt was it could be purchased in large sheets and easily cut to size. To keep the carbon felt supported and connected during the reaction, a platinum wire was threaded through the centre of the electrode (Figure 3.3 B). The reaction resulted in a conversion of >99% (entry 3). Like graphite, carbon felt also has a much higher surface area compared to glassy carbon, contributing to the high conversion. The isolated polymer had a broad D of 5.6 and a M_w of 5800 g/mol. Due to the woven structure of the carbon felt, small fibres were released into the reaction mixture (Figure 3.3 C). This was disadvantageous as it contaminates the isolated polymer. However, using filtration or centrifugation, a large majority of the carbon fibres could be removed from the final product. With that said, some polysulfide applications may benefit from the presence of a small amount of carbon felt fibres. For example, as

cathode materials in lithium sulfur batteries, the carbon fibre would act as a conducting additive in the formulation of sulfur polymer cathodes.

Alternative carbon-based electrodes could be used to produce poly(trisulfides) more effectively than glassy carbon and at a significantly lower cost. However, glassy carbon electrodes have the advantage of high durability and do not contaminate the solution, resulting in a clean polymer product. Carbon felt electrodes were very cost effective and could be cut to the desired shape on demand. They were highly effective at converting 1,2,3-trithiolane monomers into poly(trisulfides). However, it was important to note that carbon fibre electrodes contaminate the polymer with small fibres. Despite this, carbon felt was used as the electrode material for the scale-up reactions due to its low cost and ease of customisation.

Scale-up in batch

When scaling up electrochemical reactions, it was important to note that the reaction might not scale up linearly due to challenges related to mass transfer. Therefore, the scaling up of the reaction was performed in several steps: from 160 mg to 1.0 g, then to 6.8 g, and finally to a 20 g scale, which represents a 125-fold increase from the original reaction scale.

As the scale of each reaction increased, so did the size of the reaction vessel. (Figure 3.4 A). For the scaled-up reactions, larger carbon felt electrodes were positioned on the inside edges of the beaker (Figure 3.4 B). To connect the carbon felt electrodes to the potentiostat, a platinum wire electrode was embedded into the centre of the carbon felt and secured on the side of the beaker (Figure 3.4 B). The stirring speed was reduced from 1500 rpm to 400 rpm to minimize disruption to the ends of the electrode which were not secured.

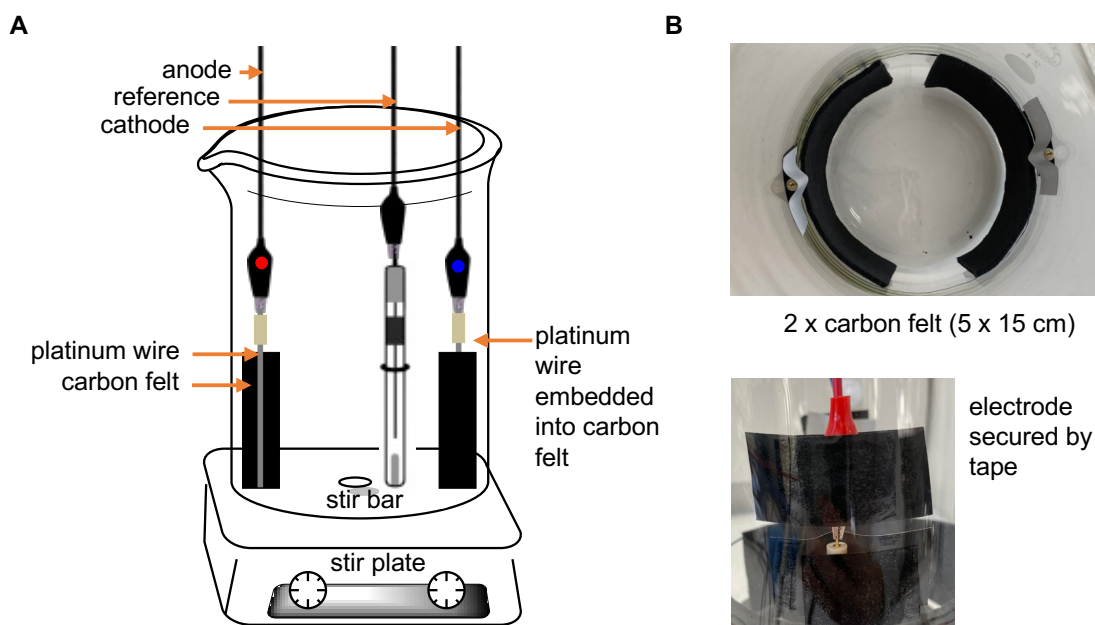
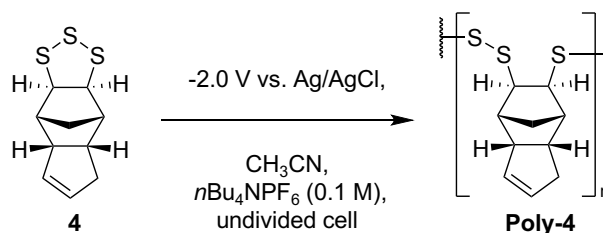


Figure 3.4: (A) Diagram of batch reactor (B) Carbon felt electrodes positioned on the inside wall of the batch reactor. Carbon felt electrodes were embedded with a platinum wire electrode which was secured onto the inside wall using tape.

For each scale-up test, an aliquot (0.5 mL) of the crude product was taken at the end of the reaction, concentrated under reduced pressure, and analysed by ^1H NMR spectroscopy to determine the conversion of monomer **4**. In this analysis, the integration of the resonances of **4** were compared with those of the electrolyte ($n\text{Bu}_4\text{NPF}_6$). Each reaction was then worked up, and the purified polymer was characterised by GPC to determine M_w and \mathcal{D} (Table 3.3).

Table 3.3: Summary of batch polymerisation results at different reaction volumes.



	Mass of 4 (g)	Concentration (M)	Reaction time (hours)	Electrode size (cm)	Conversion (%)	M_w (g/mol)	\mathcal{D}
1	1	0.04	3	5 x 6	87	3200	2.9
2	6.8	0.06	4	5 x 15	56	4000	3.6
3*	20	0.18	24	5 x 15	88	22000	1.9

*polymerisation conducted at 30 °C

For the first scale-up step, the mass of monomer **4** was increased from 160 mg to 1.0 g. To account for the additional mass of monomer, carbon felt electrodes were cut to a larger size (6 cm x

5 cm), resulting in an increased surface area (Figure 3.5 A). The goal of increasing the electrode surface area was to achieve high monomer conversion on a similar timescale to the previous reactions (160 mg, 4 h). The concentration of monomer **4** was kept the same as in previous reactions (0.04 M), resulting in a reaction volume of 100 mL. The reaction was conducted in a 120 mL beaker, with the carbon felt electrodes positioned on each side of the beaker walls (Figure 3.5 A). The beaker was also fitted with a reference electrode, and a constant potential of -2.0 V versus Ag/AgCl (3 M aq. KCl) was applied for 3 h, stirring at 400 rpm. During the reaction, formation of precipitate was observed in solution and on the carbon felt electrodes (Figure 3.5 B). After 3 hours, an aliquot (0.5 mL) of the crude reaction mixture was taken and analysed by ^1H NMR spectroscopy resulting in a monomer conversion of 87% (Table 3.3). This high conversion was comparable with the previous 160 mg scale reaction, which achieved $>99\%$ conversion in 4 hours.

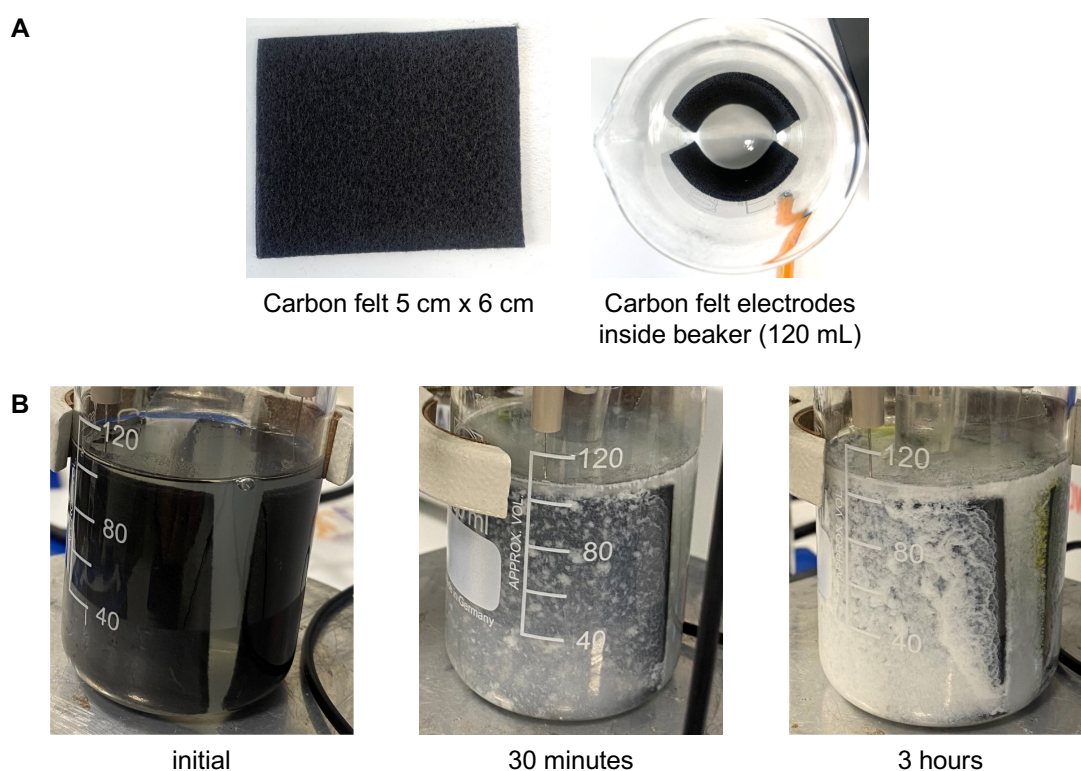


Figure 3.5: (A) Carbon felt electrodes (2 x 5 cm x 6 cm) cut and positioned inside beaker. (B) Formation of precipitate in solution during the reaction.

When transferring the reaction solution from a beaker to a round-bottom flask for work-up, precipitated polymer was observed adhering to the fibres of the electrodes. Washing the electrodes with chloroform helped dissolve the polymer, allowing it to be transferred from the reaction vessel. After evaporating the solvent under reduced pressure, the polymer was worked up through serial dissolution in chloroform (10 mL) and precipitation with acetonitrile (30 mL). The resulting suspension was centrifuged at 5000 rpm for 5 minutes, forming a pellet of the precipitate. The

supernatant was decanted, and the process was repeated 3 times to purify the polymer (0.9 g) from the electrolyte and the remaining monomer. It was important to note that the polymer was contaminated with a small amount of carbon felt fibres. GPC analysis of the isolated polymer showed a M_w of 3200 g/mol and a broad D of 2.9 (Figure 3.6).

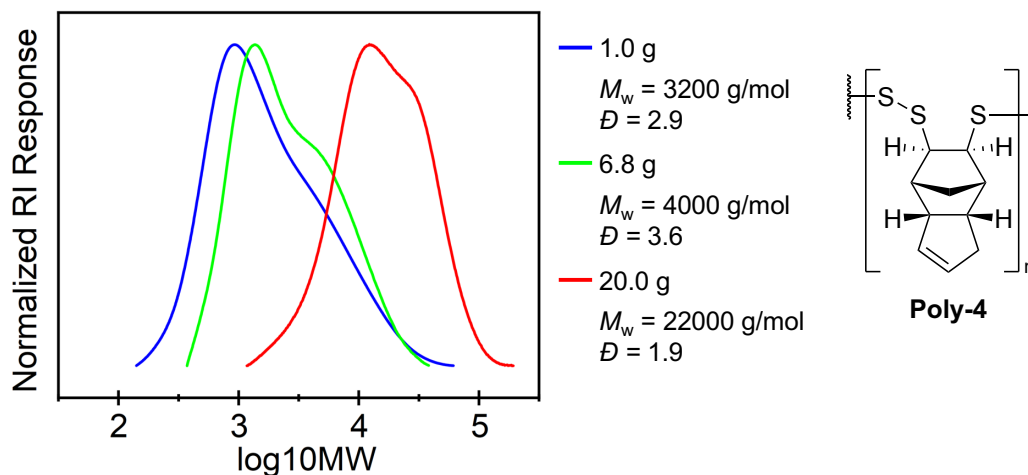


Figure 3.6: GPC (THF) of purified **poly-4** from batch reactions.

Scaling up the electrochemical synthesis of poly(trisulfides) from 160 mg to 1.0 g (6.25-fold increase), while maintaining the same monomer concentration (0.04 M) proved successful and resulted in a high monomer conversion of 87% after 3 hours (Table 3.3). Increasing the electrode surface area likely facilitated in a comparable reaction rate to the 160 mg scale, as there was a larger surface area for monomer reduction/ polymer initiation to occur.

The next step was to scale the reaction to a multi-gram (6.8 g) scale. For this experiment, a 2 L beaker was used. The carbon felt electrodes were cut to a larger size again (5 cm x 15 cm) to account for the increased amount of monomer. The concentration of the reaction was also increased from 0.04 M to 0.06 M. This resulted in a solution volume of 500 mL. Once the reaction solution was added to the beaker, approximately 1 cm of the carbon felt electrodes was not submerged in solution (Figure 3.7). The beaker was fitted with a reference electrode, and a constant potential of -2.0 V versus Ag/AgCl (3 M aq. KCl) was applied for 4 h, stirring at 400 rpm. After 4 hours, ^1H NMR spectroscopy of the crude reaction solution indicated 56% conversion of monomer **4**. The decrease in monomer conversion after 4 hours compared to the 1 g (87% conversion, 3 h) and 160 mg (>99% conversion, 4 h) was likely due to the increased amount of monomer and lower electron equivalents being delivered to the reaction mixture from the electrodes. GPC analysis of the purified polymer (3.7 g) resulted in a M_w of 4000 g/mol and a broad D of 3.6 (Figure 3.6).

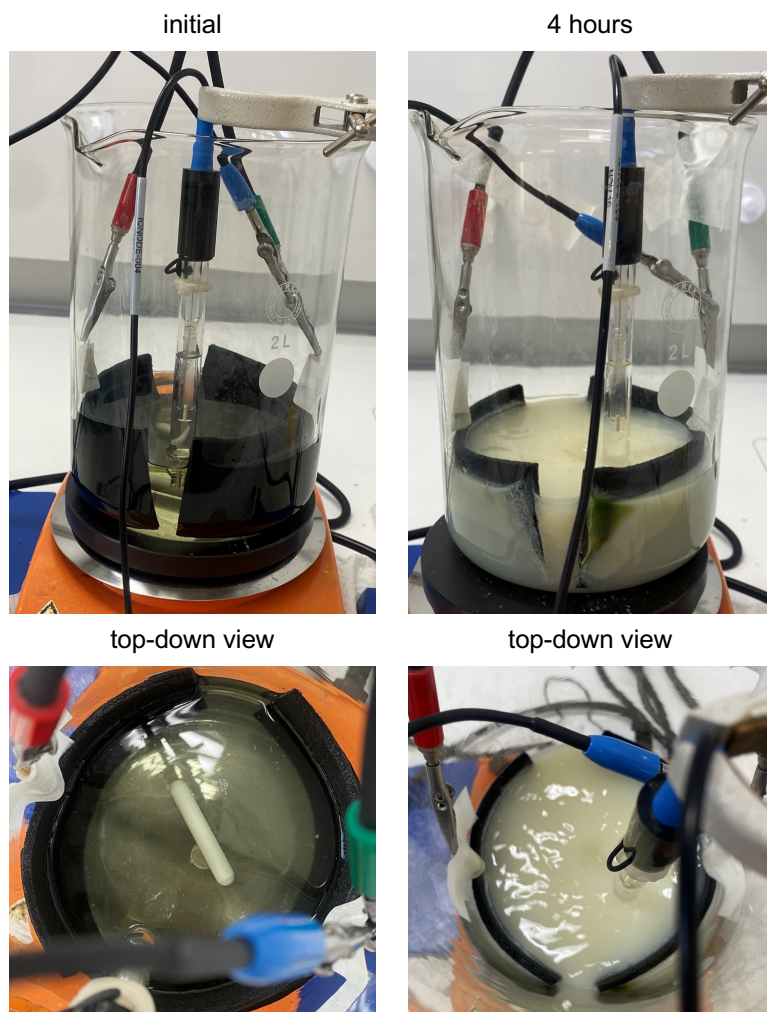


Figure 3.7: Electrochemical polymerisation of **4** (6.8 g, 0.06 M) conducted in a 2 L beaker.

Scaling up the electrochemical synthesis of poly(trisulfides) to a multigram scale resulted in a decrease in conversion compared to the 1.0 g and 160 mg scale reactions. This suggests that for larger-scale reactions, both the reaction time and the electrode surface area need to be increased to accommodate for the amount of monomer. Changing the monomer concentration from 0.04 M to 0.06 M showed no significant change in the molecular weight of the purified polymer. It was hypothesised that a more substantial change in monomer concentration would more significantly impact the molecular weight. A higher concentration of monomer molecules in solution would promote a higher rate of propagation. Additionally, higher monomer concentration reduced the need for excessive electrolyte and allows for the use of smaller reaction vessels. These considerations were crucial when scaling up a reaction. However, the solubility of monomer **4** in the electrolyte solution remains a limiting factor in this process.

The final scale-up reaction was performed with 20 g of monomer **4**, representing a 125-fold increase from the original reaction scale (Figure 3.8 A). To minimize electrolyte usage, the reaction

volume was maintained at 500 mL, which resulted in a monomer **4** concentration of 0.18 M. To prevent the monomer from precipitating out of solution, the reaction was maintained at 30 °C (Figure 3.8 B). Two carbon felt electrodes (5 cm x 15 cm) were positioned on either side of a 2 L beaker, and a reference electrode was positioned in the centre of the beaker. A constant potential of -2.0 V versus Ag/AgCl (3 M aq. KCl) was applied for 24 h, stirring at 400 rpm. Aliquots (0.5 mL) of the reaction were taken over the 24 hours and analysed by ^1H NMR spectroscopy to determine the conversion (Figure 3.8 C). The conversion was constant for the first 15 hours, and then slowed between 15 and 24 hours. This trend was anticipated, as the buildup of polymer in solution and on the electrode surface hindered monomer access to the electrode double layer. Additionally, the decline in monomer concentration in solution led to reduced polymer chain growth.

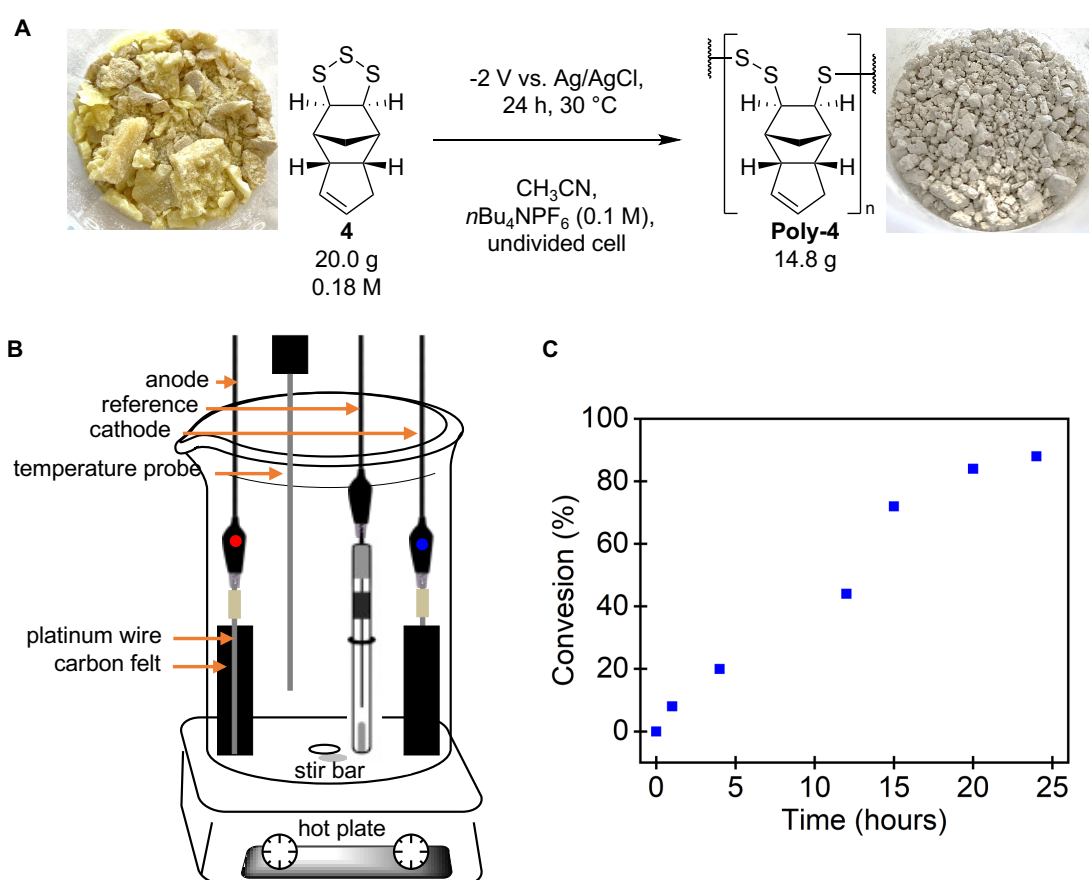


Figure 3.8: (A) Reaction scheme for the polymerisation of 20 g of monomer **4**. (B). Diagram of updated batch reactor including temperature probe. (C) Conversion of monomer **4** over the reaction period.

After 24 hours, the reaction achieved a high monomer conversion of 88% (Table 3.3). The reaction solution was then transferred to a 1 L round-bottom flask, and the electrodes were washed with chloroform to ensure full transfer of the polymer to the flask, as the polymer was soluble in chloroform. The resulting solution was evaporated under reduced pressure. The remaining solid was

redissolved in 100 mL of chloroform by stirring at 40 °C for 1 hour. Acetonitrile (200 mL) was added to precipitate the polymer while stirring. The polymer was collected by filtration. The filtered polymer was then redissolved in 100 mL of chloroform, and the precipitation process was repeated two more times to remove unreacted monomer and electrolyte. The resulting polymer (14.8 g) was characterised by GPC, resulting in a M_w of 22000 g/mol and a D of 1.9 (Figure 3.6). The increase in molecular weight compared to the previous reactions was attributed to the increase in monomer concentration and the elevated reaction temperature, both of which promote the growth of longer polymer chains. The elevated temperature was also thought to increase the solubility of the polymer, allowing higher molecular weight to be attained before polymer precipitation.

Through three stages of scale-up, it was shown that the electrochemical ring-opening polymerisation of poly(trisulfides) could be transferred from the ElectraSyn potentiostat on a 160 mg scale to an external potentiostat and run on a multigram scale (20.0 g). By increasing the surface area of the electrodes, a greater amount of monomer could be converted in the same time frame. Alternative carbon-based electrode, carbon felt, was used as a substitute to glassy carbon for the polymerisation. This substitution could significantly lower the cost of developing large-scale electrochemical batch reactors. To account for the increase in reagents and associated mass transfer challenges, increased reaction time was needed to achieve high monomer conversion. Another variable explored was increasing monomer concentration to reduce the amount of electrolyte required for a reaction. To keep the monomer in solution at higher concentration, the temperature needed to be increased. The combined increase in monomer concentration and temperature resulted in an increase in polymer molecular weight, which was expected. This section demonstrates that the electrochemical ring-opening polymerisation of poly(trisulfides) could be conducted on a scale 125 times larger than previously shown. This validated that the process could be scaled in batch to produce large quantities of poly(trisulfides) for use in applications which are described later in this chapter.

Electrolyte recovery

One challenge for the large-scale production of poly(trisulfides) is the expensive electrolyte needed for the process, consisting of $n\text{Bu}_4\text{NPF}_6$ (0.1 M) dissolved in acetonitrile. Due to the solubility limitations of the monomer **4** in the electrolyte, a large volume of electrolyte solution was required for the reaction. Consequently, it was important that the electrolyte could be recovered and reused post-reaction. During polymerisation, no evidence of side reactions had been observed. Therefore, remaining monomer and the electrolyte could be recovered and reused without the loss of any reagents.

The first step in the recovery process involves collecting acetonitrile, achieved through a straightforward evaporation and condensation process. In this case, a rotary evaporator was used post-reaction to recover acetonitrile. The resulting solid containing unreacted monomer **4** and $n\text{Bu}_4\text{NPF}_6$ was washed with hexane, dissolving the monomer, which was separated from the solid electrolyte via filtration (Figure 3.9). Finally, the solid electrolyte was recrystallised from hot ethanol, yielding a white, needle-like crystalline product (91% recovery). This product was characterised by ^1H NMR spectroscopy, which shows a very clean spectrum for $n\text{Bu}_4\text{NPF}_6$ (Figure 3.9).

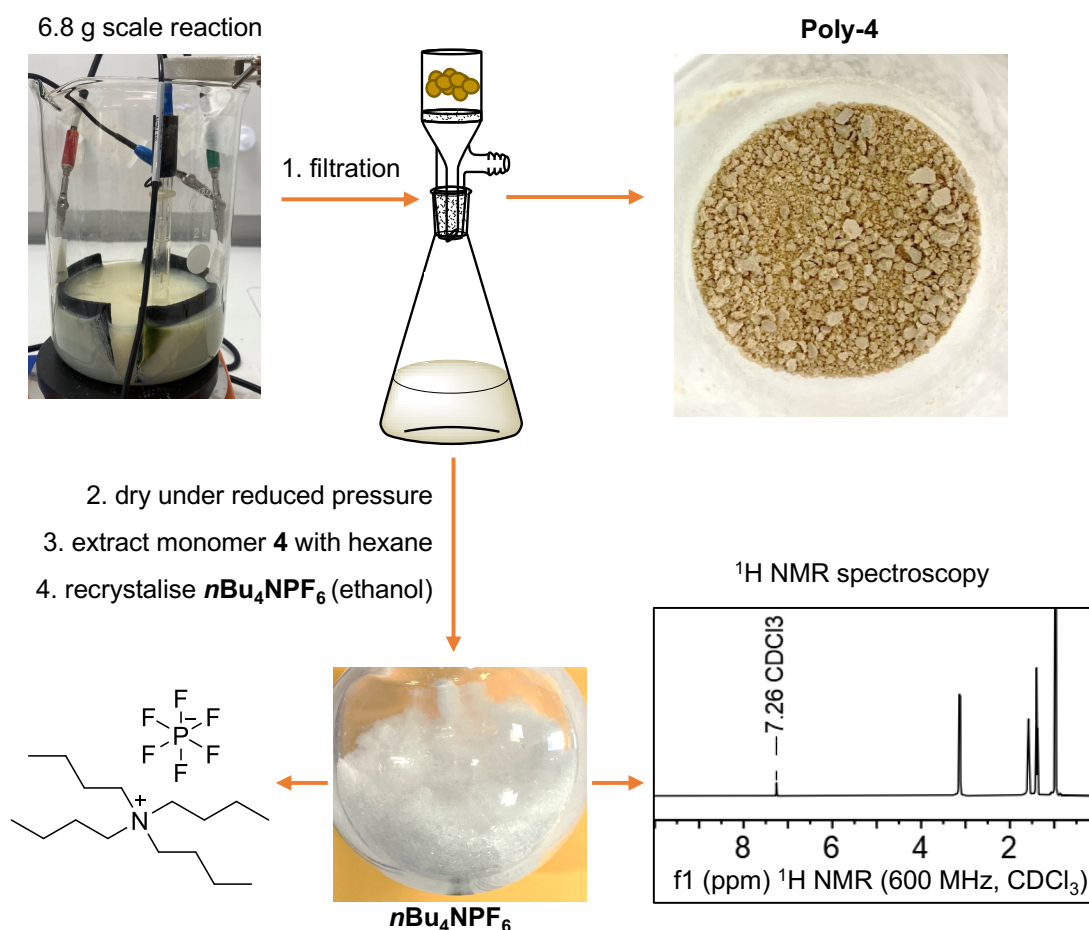


Figure 3.9: Purification of the electrolyte salt, $n\text{Bu}_4\text{NPF}_6$ from a 6.8 g scale reaction.

The purification of $n\text{Bu}_4\text{NPF}_6$ described above provides a method to recycle the electrolyte used in the poly(trisulfide) synthesis. In a practical application, the electrolyte would not need to be purified to such an extent. Instead, the electrolyte would simply need to be separated from the polymer and then recharged with more monomer. This process could be achieved by directly filtering out the polymer, adding additional monomer to the filtrate, and subsequent reaction initiation. Optimisation of this process would further minimise the use of expensive and hazardous solvents and electrolyte during the large-scale synthesis and purification of poly(trisulfides).

Scale-up in continuous flow

Another method to scale up the electrochemical ring-opening polymerisation of 1,2,3-trithiolanes was through a continuous flow process. In this section, the transition from a batch process to a continuous flow process was explored. To achieve this goal, an electrochemical flow cell was used (Figure 3.10). The flow cell contains two glassy carbon electrodes separated by a flow channel. A small hole allowed a reference electrode to be placed between the two other electrodes to make a three-electrode cell. Flow lines were connected to the inlet and outlet points of the cell, and the electrolyte solution containing monomer **4** was pumped through. While the solution was being pumped, the electrodes, which were connected to a potentiostat, had a constant potential applied to initiate the polymerisation.

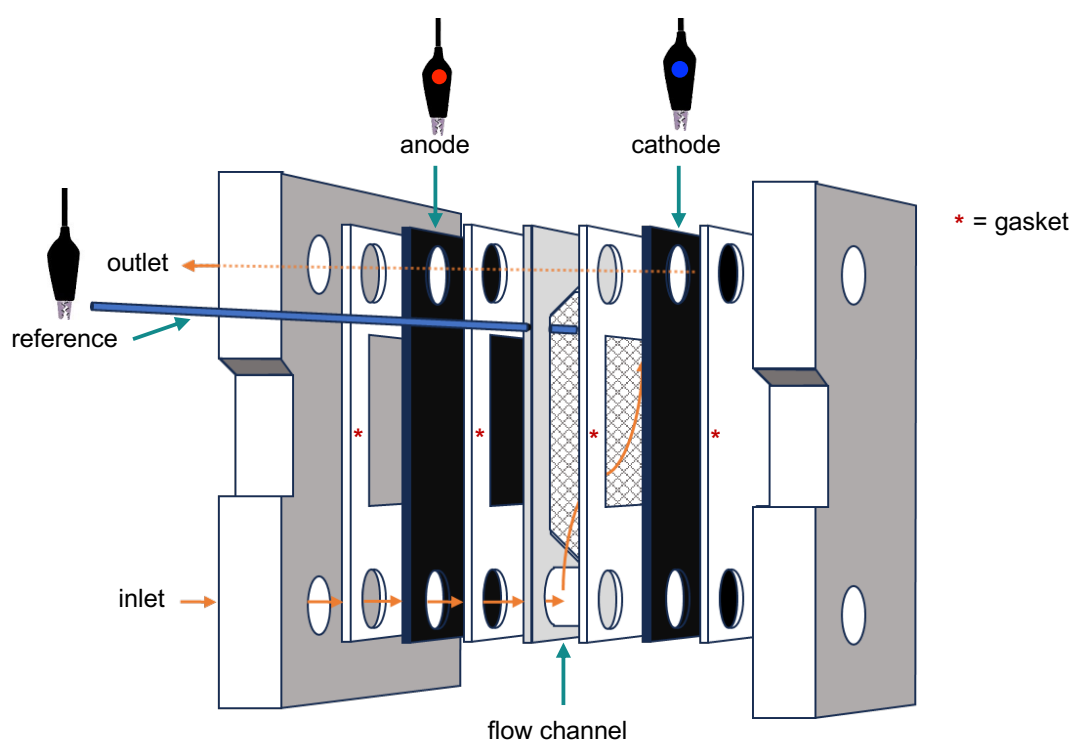
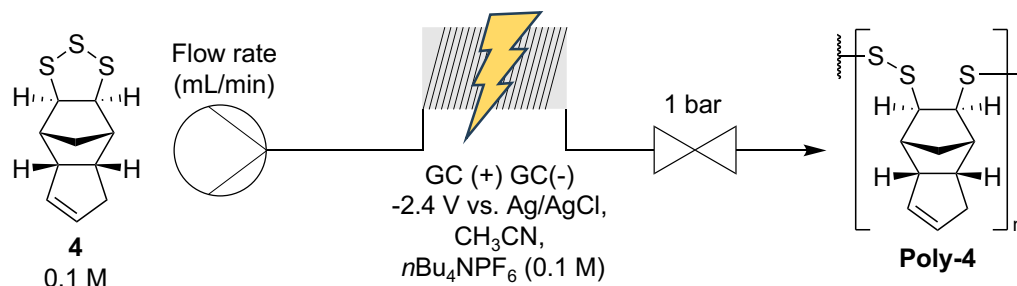


Figure 3.10: Electrochemical flow cell containing a glassy carbon anode and cathode and a Ag/AgCl reference electrode.

A solution of monomer **4** (456 mg, 2.0 mmol, 0.1 M) and $n\text{Bu}_4\text{NPF}_6$ (774 mg, 2.0 mmol, 0.1 M) in acetonitrile (20 mL) was prepared. The flow lines and flow cell were first filled with a blank electrolyte solution of $n\text{Bu}_4\text{NPF}_6$ (0.1 M) in acetonitrile. A constant potential of -2.4 V versus Ag/AgCl was applied to the cell, and then monomer solution was passed through at a flow rate of 0.5 mL/min , resulting in a residence time of 8 minutes. After the solution had fully passed through the reactor, it was collected and concentrated under reduced pressure before analysis by $^1\text{H NMR}$.

spectroscopy, resulting in a monomer **4** conversion of 55% (Table 3.4). The crude product was analysed by GPC, resulting in a M_w of 7500 g/mol with a narrow D of 1.2 (Table 3.4).

Table 3.4: Electrochemical polymerisation of **4** in continuous flow under different flow rates.



Flow rate (mL/min)	Residence time (min)	Conversion (%)	M_w (g/mol)	D
0.5	8	55	7500	1.2
2	2	32	5100	2.5

The flow cell was opened after the reaction, revealing polymer build up on the electrode surfaces (Figure 3.11). Discolouration could also be observed on the PTFE spacers (Figure 3.11). The build-up of polymer in the flow cell was a major disadvantage as it reduces monomer interaction with the electrode surface and could lead to blockages. To mitigate this issue the flow rate was increased to 2 mL/min (residence time of 2 minutes) to prevent polymer build-up in the cell. This adjustment resulted in a decrease in conversion to 32% and a decrease in M_w to 5100 g/mol (Table 3.4). When the cell was opened for inspection, there was a reduction in build-up observed. However, a significant amount of polymer build up was still present, which would lead to blockages if run for an extended period of time.

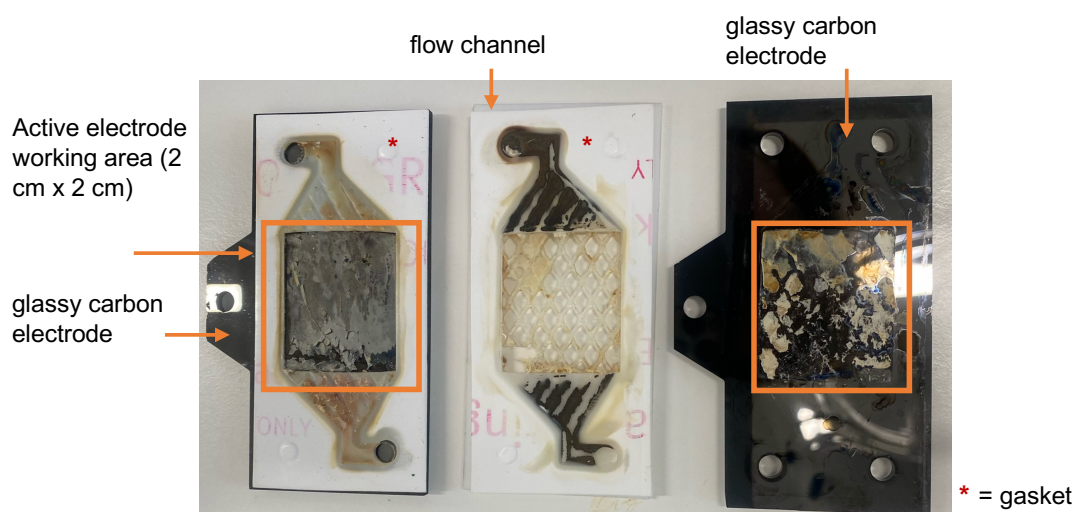


Figure 3.11: Build up on the electrode surfaces in the flow cell after reaction.

Transferring the batch electrochemical polymerisation to a continuous flow process proved successful for the production of poly(trisulfides). Continuous flow electrochemical polymerisation offers improved mass transfer and decreased resistance due to the decreased interelectrode gap. However, due to the precipitation event which occurs during the reaction, the flow cell becomes obstructed with precipitated polymer, which could lead to blockages when run for an extended period of time. Future optimisation of the polymerisation in continuous flow will focus on using larger flow tubing, lower monomer concentrations, and higher flow rates to prevent blockages.

Applications of electrochemically generated poly(trisulfides)

The purpose of scaling up the synthesis of poly(trisulfides) was to validate their production for use in specialised applications. The successful scale-up of poly(trisulfide) synthesis had been demonstrated on a 125 times scale using a large-scale batch reactor. The production of poly(trisulfides) was also validated using a continuous flow process. As shown in Chapter 2, a range of poly(trisulfides) could be produced electrochemically, each with different functionalities (Figure 3.12). In this next section, these functionalities were exploited in several applications.

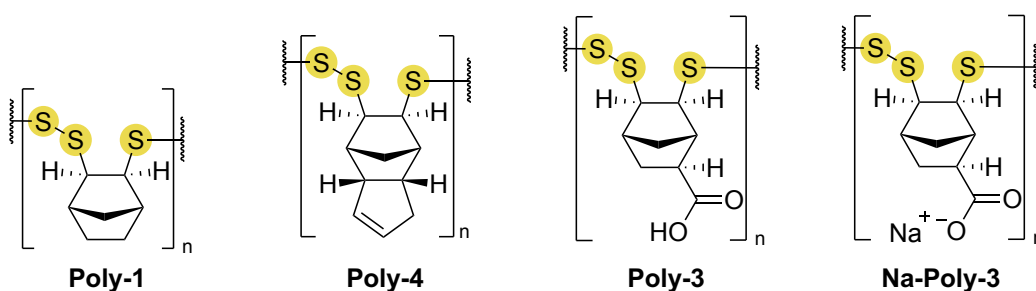


Figure 3.12: Library of poly(trisulfides) produced via electrochemical ring-opening polymerisation.

Gold sorption and recovery

Gold plays an important role in our society as a commodity and currency, and its use in science and medicine. Methods of obtaining gold include small-scale gold mining,^[14] formal commercial gold mining,^[14] electronic waste recycling,^[15] and industrial and medical waste scavenging.^[16] An increase in demand for safe and sustainable gold recovery has led to an increase of research in the area. One way to achieve safe and sustainable gold recovery is through readily available, affordable, non-toxic gold sorbents. Polysulfides made by inverse vulcanisation and related processes have shown promise in this area.^[17] However, polysulfide sorbents are often pyrolysed or chemically degraded to recover high purity gold. We hypothesised that **poly-1** would act as an effective gold sorbent which could later be depolymerised and recovered rather than undergoing pyrolysis or chemical degradation to recover the gold. This provides a potentially sustainable and safer solution for the recovery of gold.

Polysulfides have been reported to have a high affinity for gold due to their sulfur content.^[17] It was proposed that the linear poly(trisulfides) made by electrochemical polymerisation would also have a high affinity for gold. To test our hypothesis, **poly-1** (200 mg) was added to an aqueous solution of AuCl₃ in water (100 ppm Au³⁺) (Figure 3.13 A). Au³⁺ was used as a model gold species, as this oxidation state is formed with some oxidative lixivants.^[18] After end-over-end rotation of the mixture for 12 hours at ambient temperature, the concentration of gold remaining in solution was measured by atomic absorption spectroscopy (AAS). **Poly-1** captured 97% of gold from solution. The polymer-bound gold (**poly-1-Au**) was recovered by centrifugation and its surface was then characterised using energy dispersive X-ray (EDX) spectroscopy (Figure 3.13 B). Gold was observed across the polymer surface which was consistent with the coordination of the trisulfide to the gold salt.

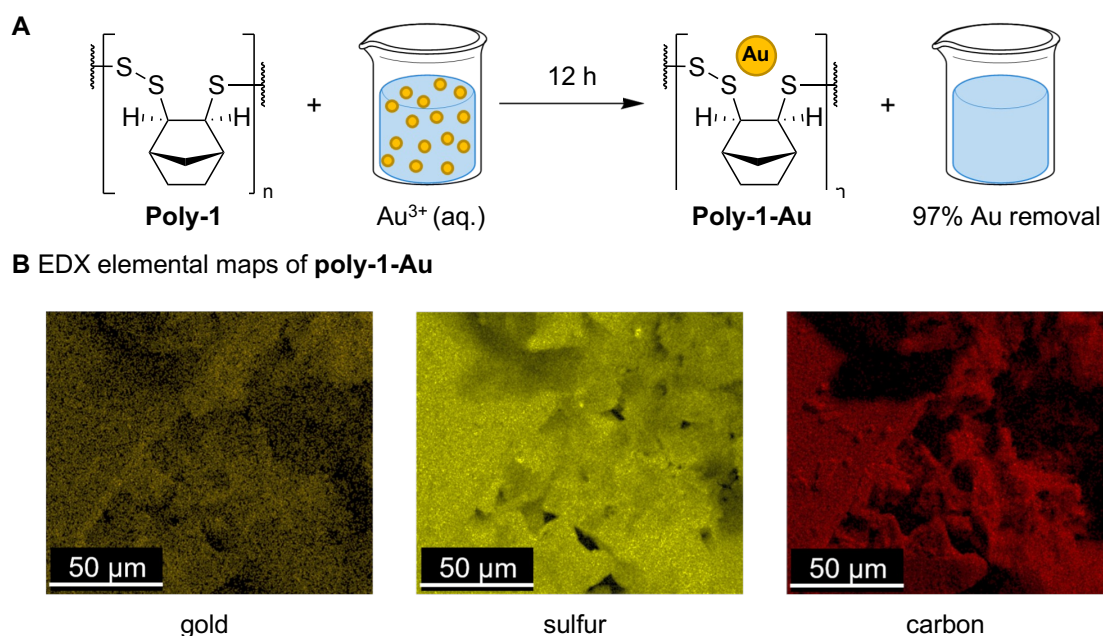
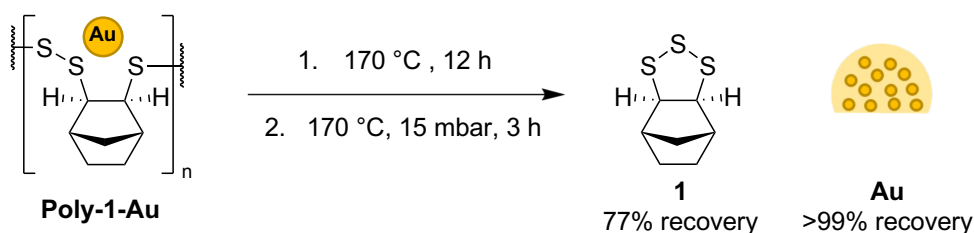


Figure 3.13: (A) **Poly-1** (200 mg) was added to a 10 mL aqueous solution of AuCl₃ (100 ppm in Au³⁺). After rotating for 12 h, 97% of the gold had been removed from the solution. (B) Energy dispersive X-ray (EDX) spectroscopy of the isolated **poly-1-Au**. Gold, sulfur, and carbon were all collocated across the polymer.

Next, the recyclability of **poly-1-Au** was investigated. **Poly-1-Au** was heated in a short path distillation apparatus at 170 °C for 12 hours to depolymerise and recover the monomer. After this time, the pressure was reduced to 15 mbar for a further 3 hours to separate the regenerated monomer from the gold (Scheme 3.4). Monomer **1** was recovered in a high yield of 70% with high purity shown by ¹H NMR spectroscopy. The gold concentrate was then subjected to analytical digestion with aqua regia followed by analysis by AAS which indicated quantitative recovery of gold from the original solution.



Scheme 3.4: Heating the complex formed from the polymer and gold (**poly-1-Au**) resulted in depolymerisation and reformation of monomer **1**. The gold remained behind and was recovered in quantitative yield.

This experiment shows **poly-1** was an efficient and recyclable alternative to other polysulfides used for gold recovery. With a good yield of the recovered monomer, more sorbents could be prepared and reused, resulting in a promising concept in gold sorption from leachates encountered in mining and electronic waste recycling.

Silver sorption and release

Polysulfides made by inverse vulcanisation have recently been explored for their antibacterial activity against Gram-positive and Gram-negative bacteria.^[19] The use of silver as an antibacterial agent has also been studied extensively.^[20] Silver coordination polymers are widely used for antibacterial treatment due to their high biocompatibility, biodegradability, and low toxicity.^[21] Here, it was hypothesised that **poly-1** would act as a binding site and carrier for silver, for potential dual-mode biocide activity. Trisulfide groups occur naturally in living organisms and are reservoirs for critical forms of sulfur in the human body.^[22] Therefore, **poly-1** has the potential to be biocompatible and biodegradable due to the well-defined trisulfide linkages.

The coordination of silver to **poly-1** was measured by adding **poly-1** (200 mg) to an aqueous solution of AgNO_3 in water (100 ppm Ag^+) and measuring the decrease in silver concentration by AAS (Figure 3.14 A). The resulting polymer-bound silver (**poly-1-Ag**) was recovered by centrifugation and was characterised by EDX spectroscopy which showed the presence of silver across the polymer surface (Figure 3.14 B).

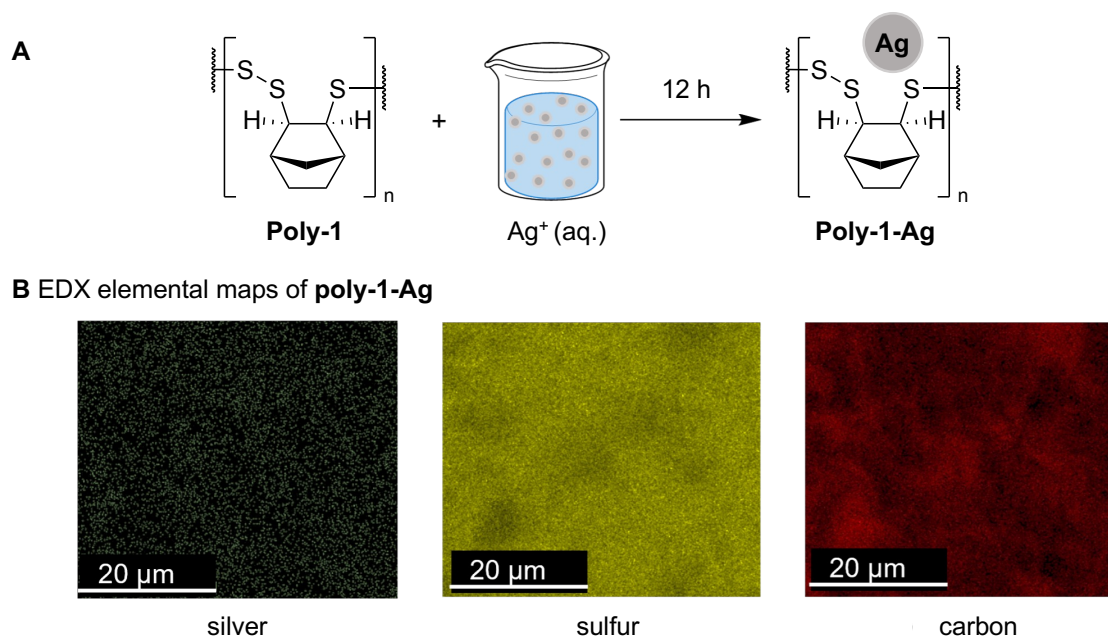
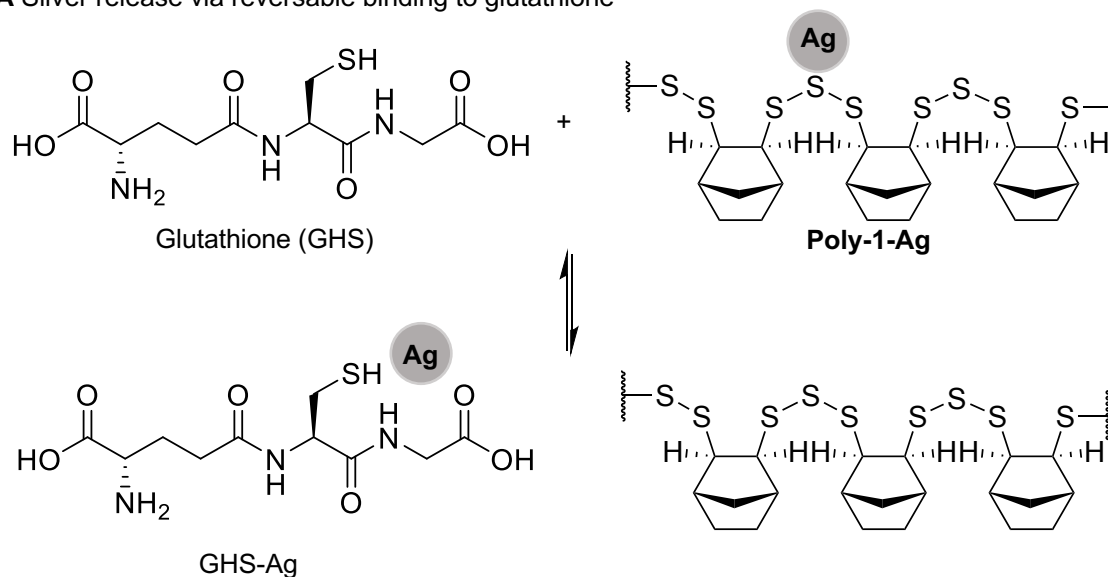


Figure 3.14: (A) **Poly-1** (200 mg) was added to a 10 mL aqueous solution of AgNO_3 in water (100 ppm Ag^+). (B) Energy dispersive X-ray (EDX) spectroscopy of the isolated **poly-1-Ag**. Silver, sulfur, and carbon were all collocated across the polymer.

Next, it was envisioned the release of the silver coordinated to **poly-1-Ag** could occur either by reversible binding to sulfur or degradation of the polymer under mild reducing conditions (Figure 3.15). Both hypotheses were tested by measuring the release of silver from **poly-1-Ag** in an aqueous phosphate buffer saline solution using AAS. One solution containing **poly-1-Ag** was spiked with 10 mM glutathione while the other solution remained reducing agent free. Glutathione (GHS) is an abundant intracellular small molecule thiol which acts as an antioxidant.^[23] This was the logic behind using glutathione as a reducing agent as it has the potential to reduce S–S bonds in the polymer, releasing silver (Figure 3.15 B).

A Silver release via reversible binding to glutathione



B Silver release via polymer reduction

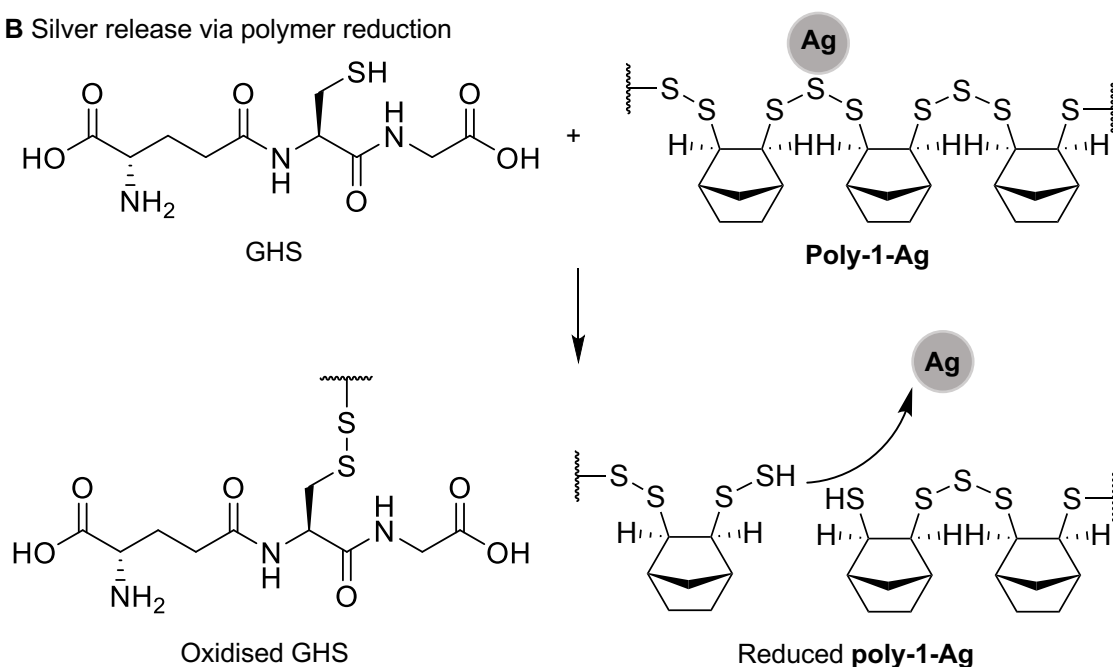


Figure 3.15: Hypothesised mechanisms of silver release. (A) Reversible binding. (B) Polymer reduction.

The release of silver from **poly-1-Ag** in the presence and absence of GHS was measured by AAS over 24 hours (Figure 3.16). At 0.5 hours the concentration of silver released from **poly-1-Ag** was three times greater in the presence of GHS. However, from 0.5 to 24 hours, the concentration of silver released from **poly-1-Ag** in the presence of GHS does not increase significantly. In contrast, the concentration of silver released in the absence of GHS had a steady rate across the 24 hours. This indicates GHS competes for silver bound to the polymer surface resulting in a more rapid rate of release in the first 0.5 hours compared to the unassisted reversible binding of silver to the polymer

surface. After 24 hours, the concentration of silver released from **poly-1-Ag** in the absence of GHS was comparable to silver released in the presence of GHS. This indicates that as silver diffuses away from the polymer in solution, more silver was released from the polymer surface to maintain the reversible equilibrium.

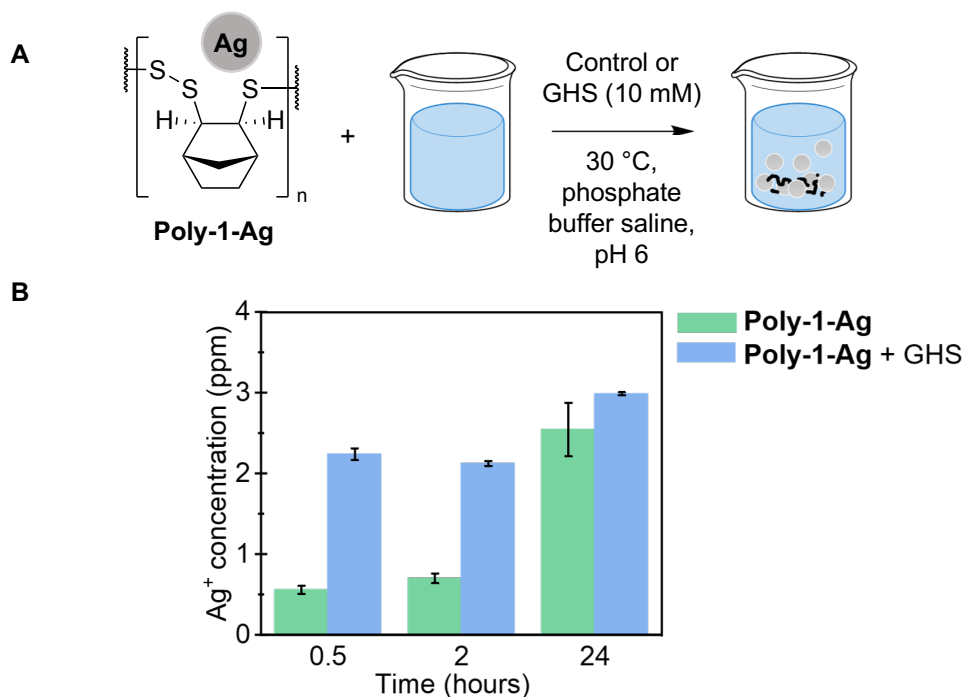


Figure 3.16: (A) **Poly-1-Ag** in phosphate buffer saline with and without the presence of GHS (10 mM). (B) Release of silver from **poly-1-Ag** over 24 hours in the presence and absence of GHS.

To investigate the mechanism by which GHS increases the rate of silver released in the first 0.5 hours, GPC was used to determine the effect of 10 mM of GHS on **poly-1**. There was no significant change to the M_w or D compared to a control sample of **poly-1** (Figure 3.17). This suggests the glutathione does not cause polymer breakdown under these conditions, but rather competes for the binding of silver. The amount of silver released from **poly-1-Ag** over 24 hours was found to be 3.5% in the presence of GHS and 3% in the absence of GHS.

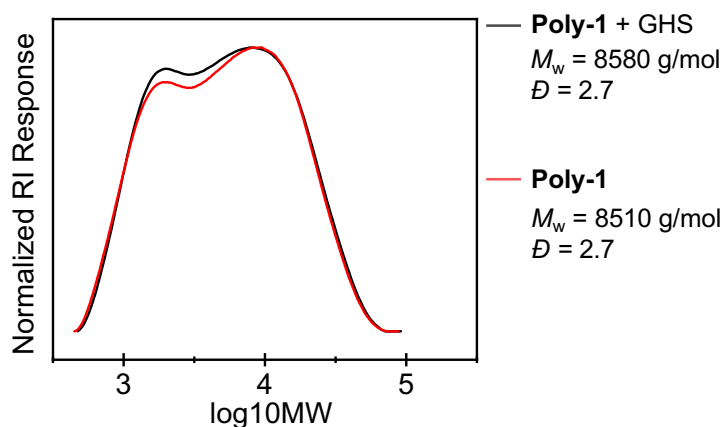


Figure 3.17: GPC (THF) trace of **poly-1** with and without the addition of 10 mM GHS.

These results suggest that **poly-1** has the potential to act as a dual acting biocide material. The polymer was both the vehicle for silver and a biocide itself; the silver was released slowly by reversible binding to the polysulfide. As these materials gain interest for their biological activity, it is important to have control over the polymer structure for medical applications. Through electrochemically induced ring-opening polymerisation of 1,2,3-trithiolanes, we maintain control of polymer structure and sulfur rank, providing linear poly(trisulfide).

Copper binding

Polysulfides are known to bind to metals such as mercury and gold due to their high sulfur content. To enhance the ability of polysulfides to bind to metals, **poly-3** was designed to have carboxylic acid functionality to provide another site to coordinate to metals such as copper. Carboxylic acids could be converted to charged carboxylates that improve the water solubility of the polymer due to their ionic nature as well as improve metal binding by providing additional and stronger donor sites. Carboxylates are commonly used donor sites for coordination with metals such as copper,^[24] and ionic polymers can have improved water solubility which may improve metal binding in aqueous solutions.^[25]

To test this hypothesis, **poly-1**, **poly-3**, and **poly-4** were selected and their ability to bind to Cu(II) was investigated. **Poly-3** was also deprotonated by the addition of 1.0 mol equivalent of NaOH per carboxylic acid group to provide the water-soluble **Na-poly-3** which was also tested for Cu(II) binding. The four polymers were studied for their Cu(II) binding abilities using a 0.5:1 and 1:1 CuSO₄-to-monomer ratio in water. After 1 hour, the results indicated that **Na-poly-3** displayed the best Cu binding properties of the polymers tested with an 89% copper removal for the 0.5:1 copper-to-monomer ratio (Figure 3.18 A). The other polymers, which were not soluble in water, removed less than 33% of the Cu(II) present (Figure 3.18 A). The higher copper ratio of 1:1 also

showed that **Na-poly-3** had the highest affinity to Cu in solution with a removal of 51% while the remaining polymers showed a binding less than 40%. It was suspected that the improved binding of Cu to **Na-poly-3** was a result of the combination of improved interaction with the metals in water afforded by its solubility, as well as the presence of carboxylate groups that serve as ligands for copper. The binding percentages measured suggest that two carboxylate groups bind to one Cu metal. This form of binding causes cross-linking between polymer chains and precipitation of the polymer as a gel (Figure 3.18 B). This precipitation mechanism is useful when considering the use of **Na-poly-3** as a flocculant in copper recovery processes or remediation applications. The ability of polysulfides to bind other metals besides gold^[17] and mercury^[26] is also an important capability for multi-metal binding required in remediation, mining, and metal recycling.^[27]

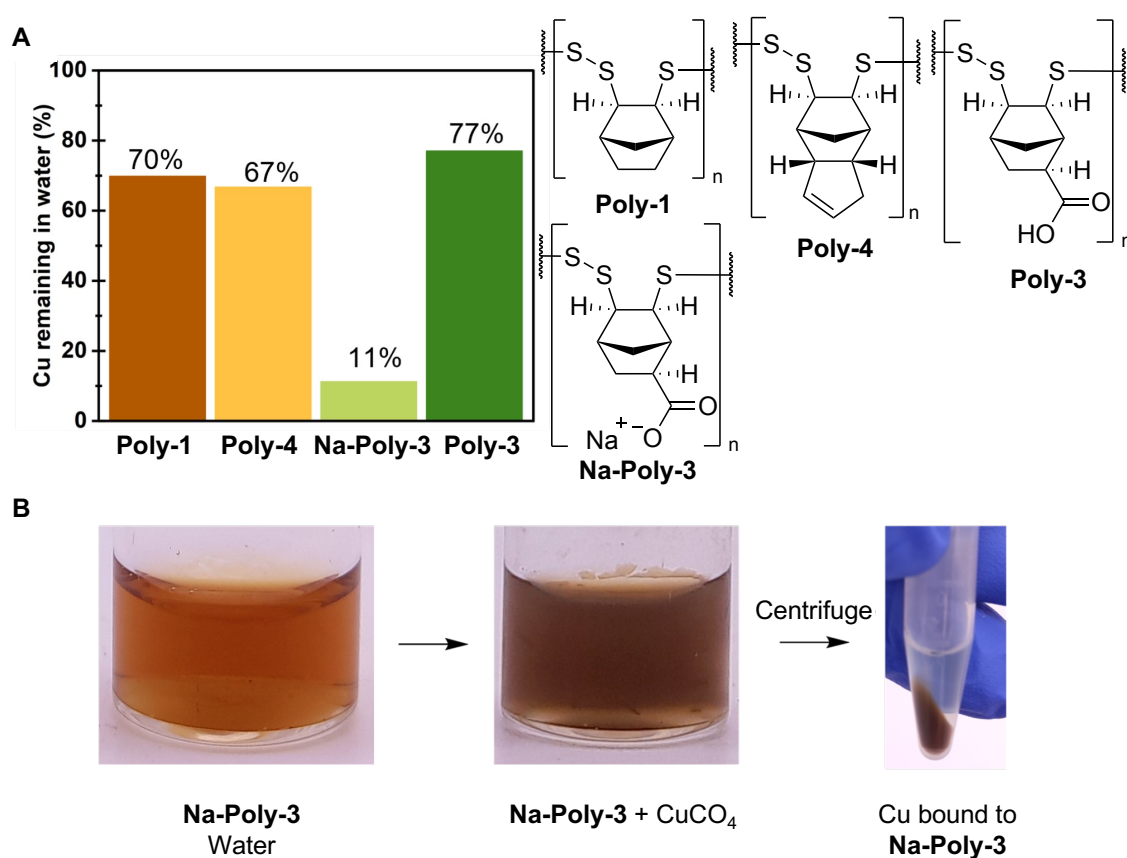


Figure 3.18: (A) Copper sorption plot showing Cu remaining in solution of 0.5:1 Cu(II)-to-monomer ratios after 1 hour of agitation. (B) Images showing fully soluble **Na-poly-3** in H₂O, the addition of CuSO₄ caused precipitation of the polymer as a gel, while simultaneously removing Cu from solution.

Thermal curing

Thermal curing of sulfur-dicyclopentadiene oligomers was shown to induce crosslinking resulting in a solvent resistant polysulfide.^[5] This same principle was applied to **poly-4** which was cured at high temperature to test if cross-linking would provide a material that was more chemically and thermally robust than the linear polymer. This route also would provide a safe method for the synthesis and curing of sulfur-dicyclopentadiene copolymers that are prone to runaway reactions when produced through inverse vulcanisation.^[3]

Poly-4 (250 mg) was cured at 190 °C for 6 hours, which caused it to turn from brown to black (Figure 3.19). Some regenerated monomer **4** was also isolated (10% recovery) by extraction with hexane after the curing process. This was likely caused by backbiting in the polymer chain after S–S bond cleavage. This supports the proposal of reactive sulfur bonds in the polymer which may crosslink with the unreacted alkene on dicyclopentadiene.

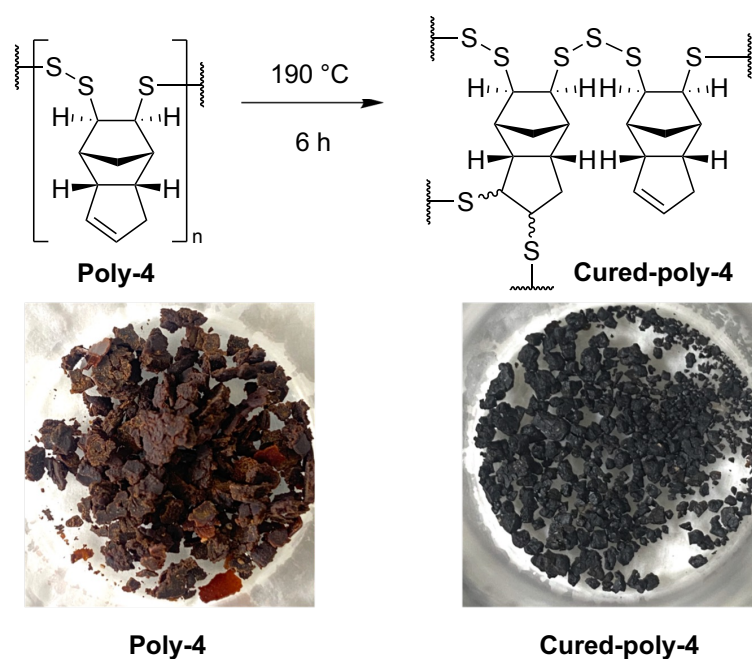


Figure 3.19: Poly-4 before and after curing at 190 °C for 6 hours.

The thermal stability of the remaining **cured-poly-4** (90%) was studied using TGA which shows a distinct change in initial mass loss at 235 °C compared to **poly-4** which begins to lose mass at 180 °C (Figure 3.20 A). For **cured-poly-4**, cross-linking prevents this depolymerisation and monomer volatilisation, which translates to higher thermal stability. Additionally, solvent stability studies showed **cured-poly-4** was insoluble in THF and chloroform, whereas **poly-4** was soluble in both solvents (Figure 3.20 B). An increase in thermal stability and decrease in solubility was

consistent with cross-linking during thermal curing due to S–S bond scission and addition of thiyl radicals to the alkene in **cured-poly-4**.^[5]

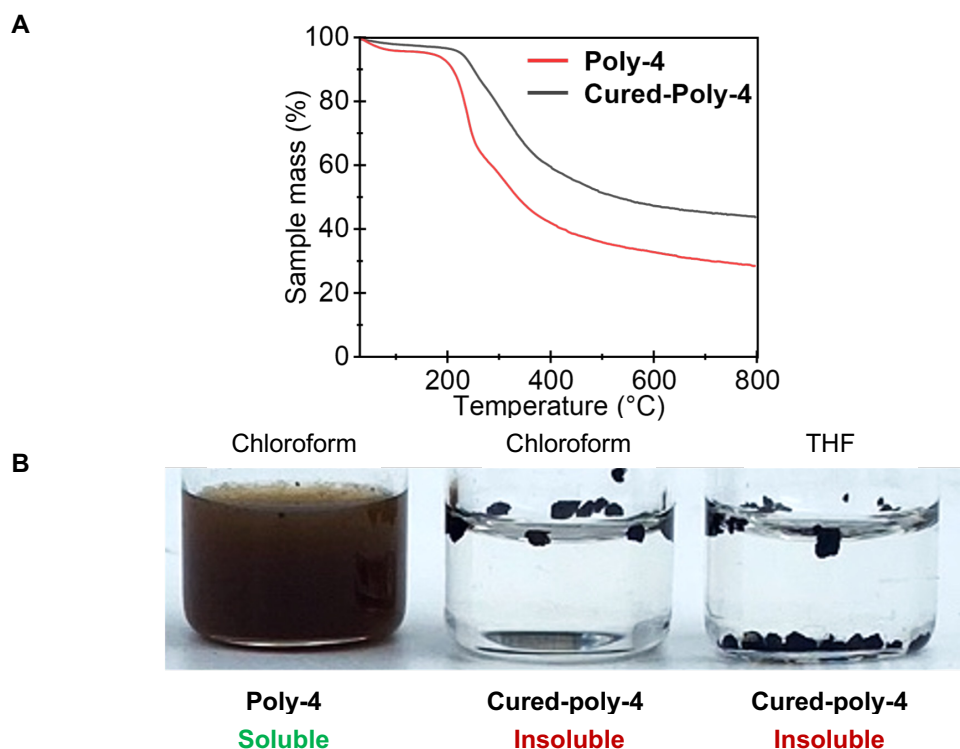


Figure 3.20: (A) TGA comparing **poly-4** and **cured-poly-4**. Less mass loss was observed for **cured-poly-4**, which was attributed to cross-linking. Carbonisation was observed for both samples after heating to 800 °C. (B) **poly-4** (10 mg) and **cured-poly-4** (10 mg) in 1 mL of either chloroform or THF. **Cured-poly-4** was insoluble in chloroform and THF.

Conclusion

In this chapter, methods to scale-up poly(trisulfide) synthesis were investigated so that these polymers could be evaluated in a variety of applications. First, the synthesis of 1,2,3-trithiolane monomers was progressed from a 1 g scale, resulting in an 83% yield, to a 20 g scale in a 72% yield while reducing the solvent use by 50%. The photochemical synthesis of 1,2,3-trithiolanes was also explored in continuous flow. An intriguing finding from the UV reactions was the formation of polymeric material as a by-product. This finding was explored in detail in the next chapter.

Next, large-scale electrochemical batch reactors were designed with considerations given towards the use of cost-effective electrode material. It was shown that the electrochemical synthesis of poly(trisulfides) could be conducted on a scale 125 times larger than had been previously demonstrated. However, an increase in reaction time from 4 hours to 24 hours was required. To account for the increased use of electrolyte material when scaling-up in batch, electrolyte recovery

was conducted on a 6.8 g batch reaction and resulted in a 91% recovery yield. ¹H NMR spectroscopy of the recovered electrolyte showed high purity and no evidence of electrolyte degradation. These achievements demonstrated that the electrochemical synthesis of poly(trisulfides) could be scaled up as required without the waste of electrolyte material.

A continuous flow process to electrochemically synthesise poly(trisulfides) was also validated as a potential scale-up method. It was shown that a conversion of 55% could be achieved with a residence time of 8 minutes. However, build-up of polymer in the flow cell was observed, leading to obstruction. Therefore, scale-up in continuous flow still requires optimisation and development.

The poly(trisulfide) products were used in several high-value applications including gold sorption and recovery, silver sorption and release, copper binding and precipitation from water and thermal curing to achieve crosslinking. By scaling up electrochemical poly(trisulfide) synthesis, a key step has been achieved in deploying these polymers in a number of applications of potential commercial value.

Publication that resulted from the research in this chapter

Electrochemical synthesis of poly(trisulfides)

Pople, J. M. M.; Nicholls, T. P.; Pham, L. N.; Bloch, W. M.; Lisboa, L. S.; Perkins, M. V.; Gibson, C. T.; Coote, M. L.; Jia, Z.; Chalker, J. M., *J. Am. Chem. Soc.* **2023**, *145*, 11798-11810.

Experimental details

General considerations

Materials: Sulfur was purchased from Sigma-Aldrich (reagent grade, powder, purified by refining, 100 mesh particle size). Dicyclopentadiene and nickel(II) chloride hexahydrate were purchased from Sigma-Aldrich. Silica gel was purchased from Sigma-Aldrich (technical grade, pore size 60 Å, 230-400 mesh particle size, 40-63 µm particle size). Glassy carbon and graphite electrodes were purchased from IKA. Micro Flow Cell was purchased from Electrocell.

NMR Spectroscopy: Proton nuclear magnetic resonance spectra (¹H NMR) were recorded on a 600 MHz Bruker spectrometer operating at 600 MHz. All chemical shifts are quoted on the δ scale referencing residual solvent peaks (¹H NMR: δ = 7.26 for CDCl₃). Chemical shift values are reported in parts per million, ¹H¹H coupling constants are reported in hertz and multiplicity is abbreviated as; s = singlet, d = doublet, m = multiplet, ap.= apparent.

Scanning Electron Microscopy (SEM) with Energy Dispersive X-ray (EDX): SEM/EDX images were obtained using a FEI Inspect F50 SEM fitted with a EDAX energy dispersive X-ray detector. Samples were sputter coated with silver metal (10 nm thickness) before analysis.

Thermogravimetric analysis (TGA): TGA was carried out on a Perlin Elmer TGA800. Samples of 5-10 mg were heated between 30-800 °C at varied temperature rates under a flow of nitrogen.

Potentiostat: Chronoamperometry (CA) experiments were performed on a Gamry Interface 1010E potentiostat (Warminster, PA, USA).

Atomic absorption spectroscopy (AAS): AAS was performed on a GBC SavantAA using an Au (242.8 cm⁻¹) hollow cathode lamp.

Gel permeation chromatography (GPC): GPC analysis was performed using a Waters 2695 separations module, using two Agilent columns (PLgel MiniMix-C (5 µm)) and a matching Agilent guard column (MiniMix-C) and a Waters 410 refractive index detector. All samples were eluted in THF at a flow rate of 0.2 mL/min. Calibration was performed using narrow distribution polystyrene

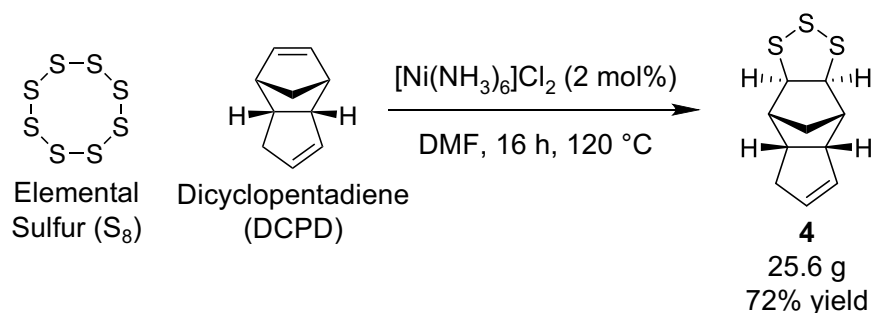
standards ($D < 1.1$) ranging from 500 to 2 million g/mol. Samples were prepared by dissolving in THF (2 mg/mL) followed by filtration using a 0.45 μm PTFE syringe filter before analysis.

Flow chemistry apparatus: All flow reactions were conducted on a commercially available Vapourtec RS-200 system comprising an R2C+ pump module.

Continuous flow photoreactor: A Vapourtec R-Series system with R2C+ pump module was used to pump solutions through a coil of PFA tubing (10 mL). The coil was fitted to a Uniqsis Polar Bear Plus FlowTM which was used to control the temperature of the reaction mixture. A Uniqsis PhotoSynTM provided LED irradiation (365 nm). The back pressure of the system was controlled using a Vapourtec SF-10 reagent pump operating in pressure controller mode.

Large scale monomer synthesis

Monomer 4 synthesis – 20 g scale



The following method was adapted from the literature.^[10] A 250 mL round bottom flask equipped with a reflux condenser and stir bar was charged with dicyclopentadiene (20.0 g, 151 mmol), elemental sulfur (14.6 g, 56 mol) and $[\text{Ni}(\text{NH}_3)_6]\text{Cl}_2$ (0.7 g, 3 mmol), and DMF (100 mL). The resulting reaction mixture was heated to 120 °C for 16 hours while stirring. After 16 hours the mixture was allowed to cool to room temperature before the solids were removed by filtration over a thin layer (~1 cm) of silica gel. The silica gel was washed with hexane (3 x 50 mL). Deionized water (100 mL) was added to the filtrate, the layers were separated, and the organic fraction was washed with deionized water (2 x 100 mL). The organic layer was collected, dried (Na_2SO_4), filtered and concentrated under reduced pressure. Purification by flash chromatography over silica gel (hexane) delivered monomer 4 as a highly viscous yellow oil (25.6 g, 72% yield) which formed into a yellow crystalline product. ¹H NMR (600 MHz, CDCl_3): δ 5.74-5.70 (m, 1H), 5.62-5.59 (m, 1H), 3.69 (ap. ddd, $J = 17.0, 7.1, 1.9$ Hz, 2H), 3.30-3.24 (m, 1H), 2.72-2.66 (m, 1H), 2.61 (ap. d, $J = 5.1$ Hz, 1H), 2.39-2.26 (m, 3H), 2.10 (ap. d, $J = 10.3$ Hz, 1H), 1.32-1.30 (m, 1H).

— 7.26 CDCl₃

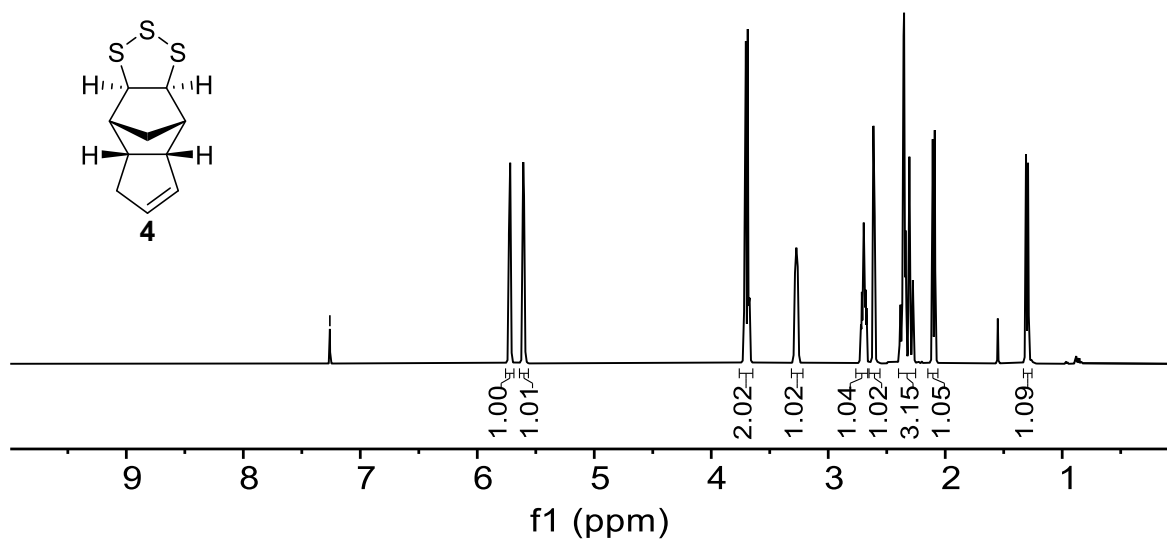
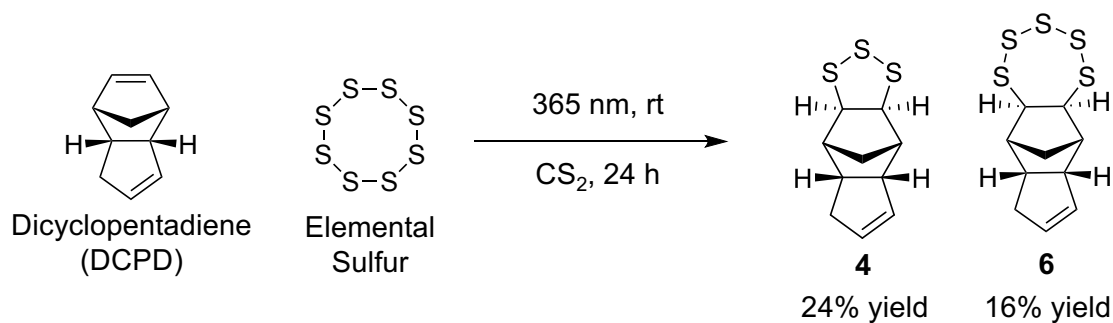


Figure S3.1: ¹H NMR (600 MHz, CDCl₃) of crystalline product (4).

Photochemical monomer 4 synthesis – batch



The following method was adapted from the literature.^[11] A 20 mL vial equipped with a stir bar was charged with dicyclopentadiene (1.0 g, 7.6 mmol), elemental sulfur (1.1 g, 34.3 mmol), and CS₂ (10 mL). The solution was then irradiated by a 365 nm light for 24 hours while stirring. The reaction solution was then concentrated under reduced pressure and analysed by ¹H NMR spectroscopy (CDCl₃).

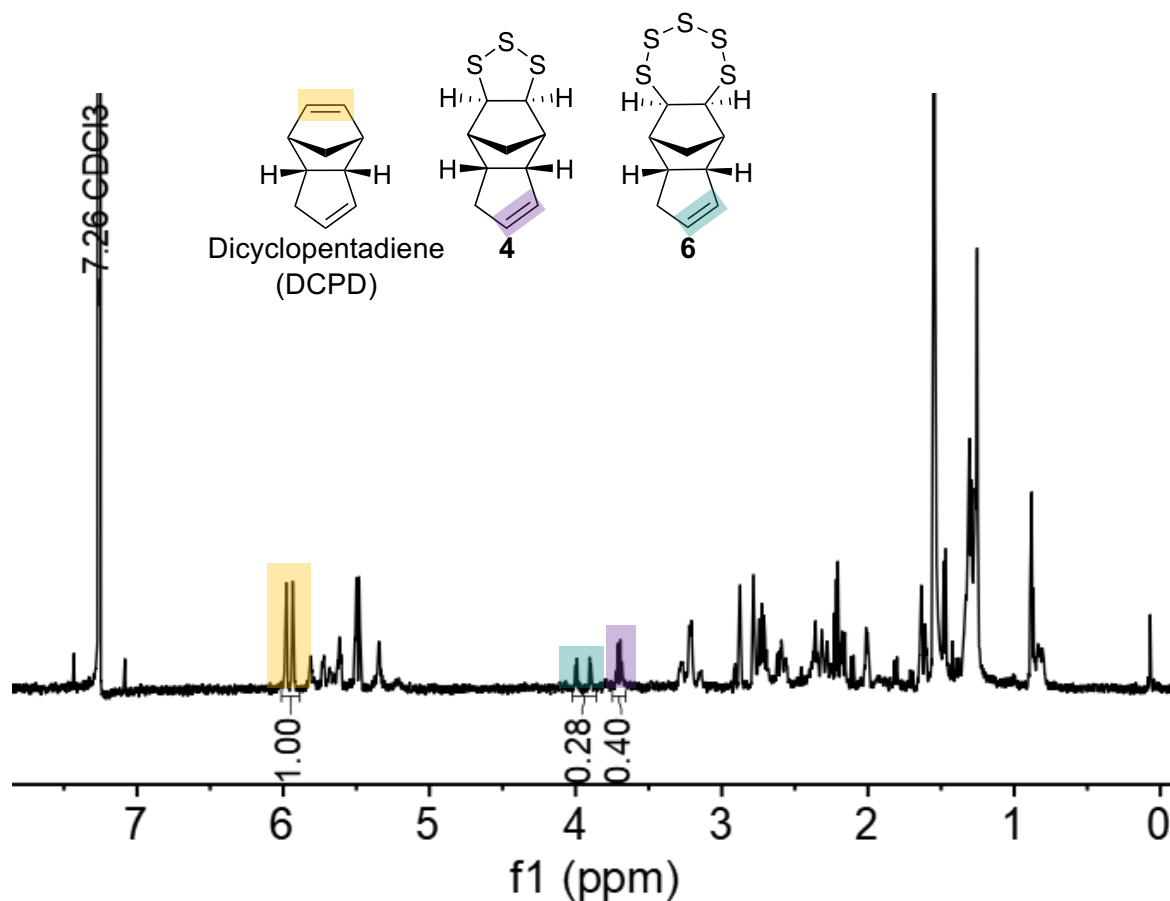
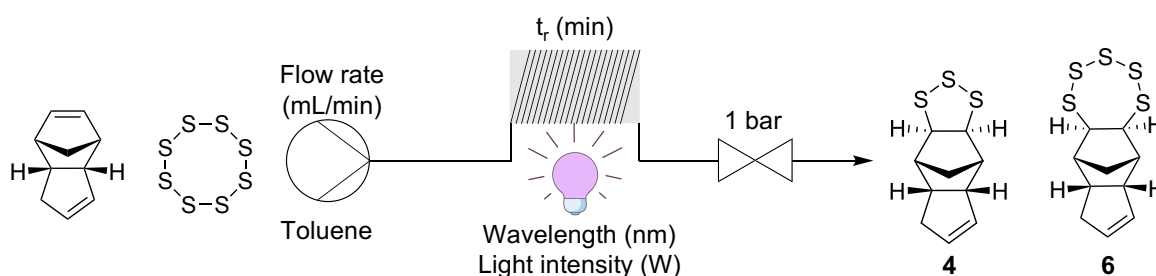


Figure S3.2: ^1H NMR (600 MHz, CDCl_3) of crude reaction solution. Integration of dicyclopentadiene, to **4** and **6** proton signals are highlighted and used to calculate the conversions.

Photochemical monomer **4** synthesis – continuous flow

General procedure



A stock solution was prepared by combining dicyclopentadiene (1.0 g, 7.8 mmol, 78 mM), elemental sulfur (0.8 g, 3.3 mmol, 33 mM) and toluene (100 mL). A stir bar was added, and the stock solution was stirred at 60 °C for 30 minutes to dissolve the elemental sulfur. After filtering the stock solution, it was kept at 60 °C to keep everything solubilised. For each reaction, 8 mL was passed through a

photochemical reactor illuminated with light-emitting diodes under different conditions including temperature, flow rate, wavelength and lamp power (Table S3.1). The solutions were concentrated under reduced pressure and purified by flash chromatography over silica gel (100% hexane – 100% ethyl acetate) delivering dicyclopentadiene as the first eluent and a mixture of **4** and **6** as the second eluent.

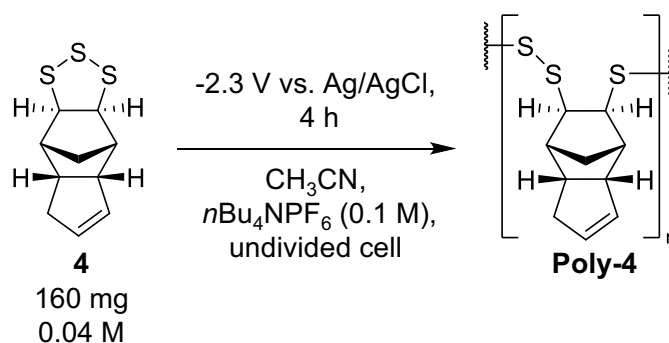
Table S3.1: Summary of photochemical synthesis of **4** in continuous flow, differing temperature, residence time, wavelength and lamp power.

	Temperature (°C)	Residence time (min)	Wavelength (nm)	Light intensity (W)	Conversion (%)	Yield 4 (%)	Yield 6 (%)
1	80	1.25	365	226	62	8	3
2	80	1.25	455	226	0	0	0
3	60	1.25	365	226	95	11	5
4	60	2.5	365	226	92	22	9
5	60	10	365	226	97	7	8
6	60	2.5	365	22.6	95	12	3

Alternative carbon-based electrode material for the synthesis of poly-**4**

A set of glassy carbon (0.8 x 5 cm), graphite (0.8 x 5 cm) and carbon felt (0.8 x 5 cm) electrodes were used for the polymerisation of **4** using the conditions detailed below.

General procedure



An electrochemical cell was charged with **4** (160 g, 0.7 mmol, 0.04 M), $n\text{Bu}_4\text{NPF}_6$ (584 mg, 0.1 M), acetonitrile (15 mL) and a small stir bar. A constant potential of -2.3 V vs. Ag/AgCl, 3 M aq. KCl) was applied for 4 hours, mixing at 1500 rpm. After 4 hours, an aliquot (0.5 mL) of the reaction mixture was taken, concentrated under reduced pressure, and analysed by ^1H NMR spectroscopy to determine conversion of monomer **4**. The remaining solution was transferred to a round bottom

flask, washing the electrodes with chloroform. The resulting solution was concentrated under reduced pressure. The remaining solid was redissolved in 10 mL of chloroform and transferred to a 50 mL centrifuge tube. Acetonitrile (30 mL) was added to the centrifuge tube to precipitate the polymer and was vortexed to mix. The solution was centrifuged at 5000 rpm for 5 minutes. The supernatant was decanted, and the solid was redissolved in chloroform (10 mL). Acetonitrile (30 mL) was added to the centrifuge tube and vortexed to mix. The solution was centrifuged for 5 minutes (5000 rpm). The supernatant was decanted, and the solid was redissolved in chloroform (10 mL). This process was repeated a third time, and the solid polymer was collected and analysed by GPC and ^1H NMR spectroscopy.

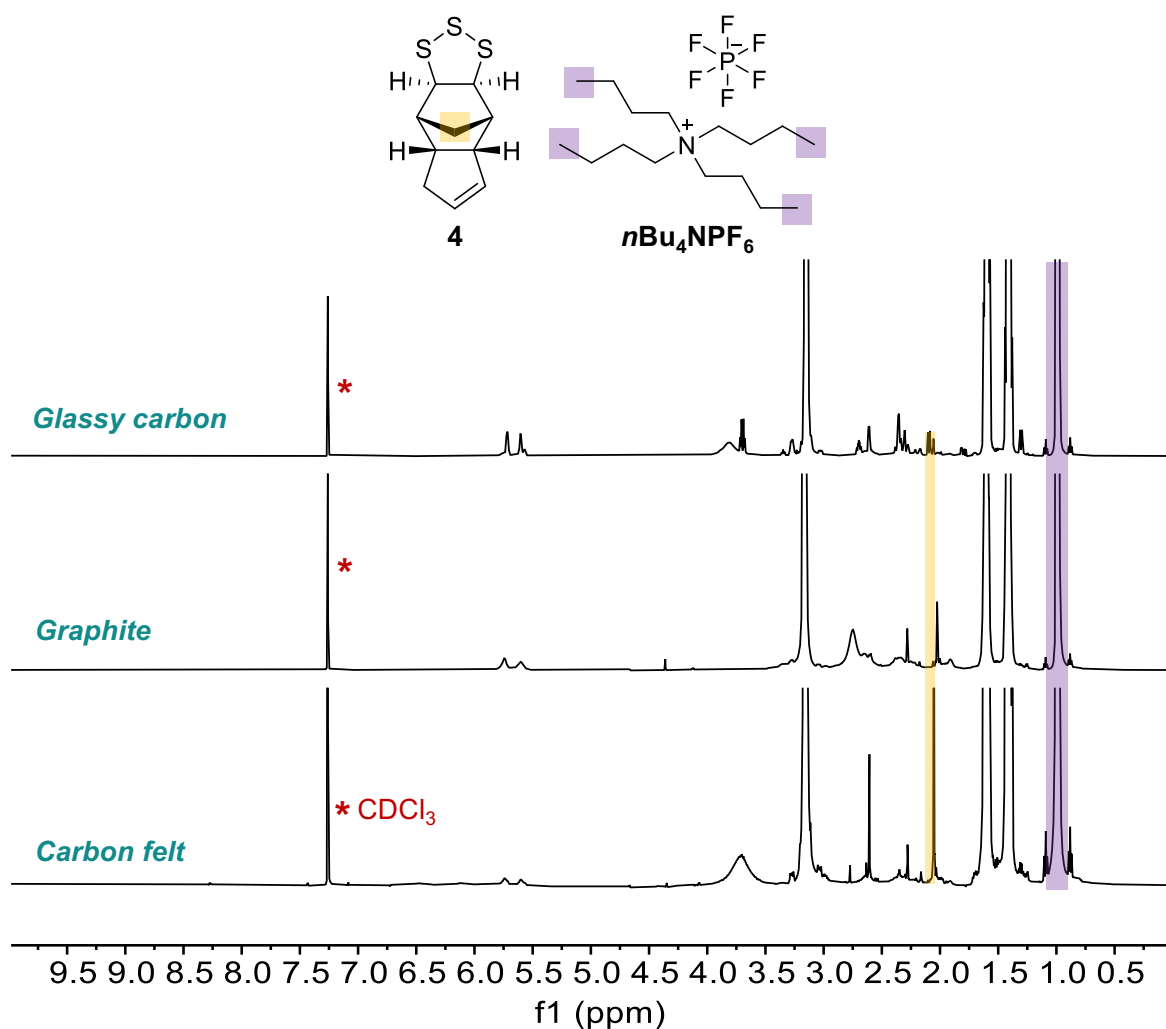


Figure S3.3: ^1H NMR (600 MHz, CDCl_3) of crude reaction mixture. Integration of **4** and $n\text{Bu}_4\text{NPF}_6$ proton signals are highlighted and used to calculate the conversion of **4**.

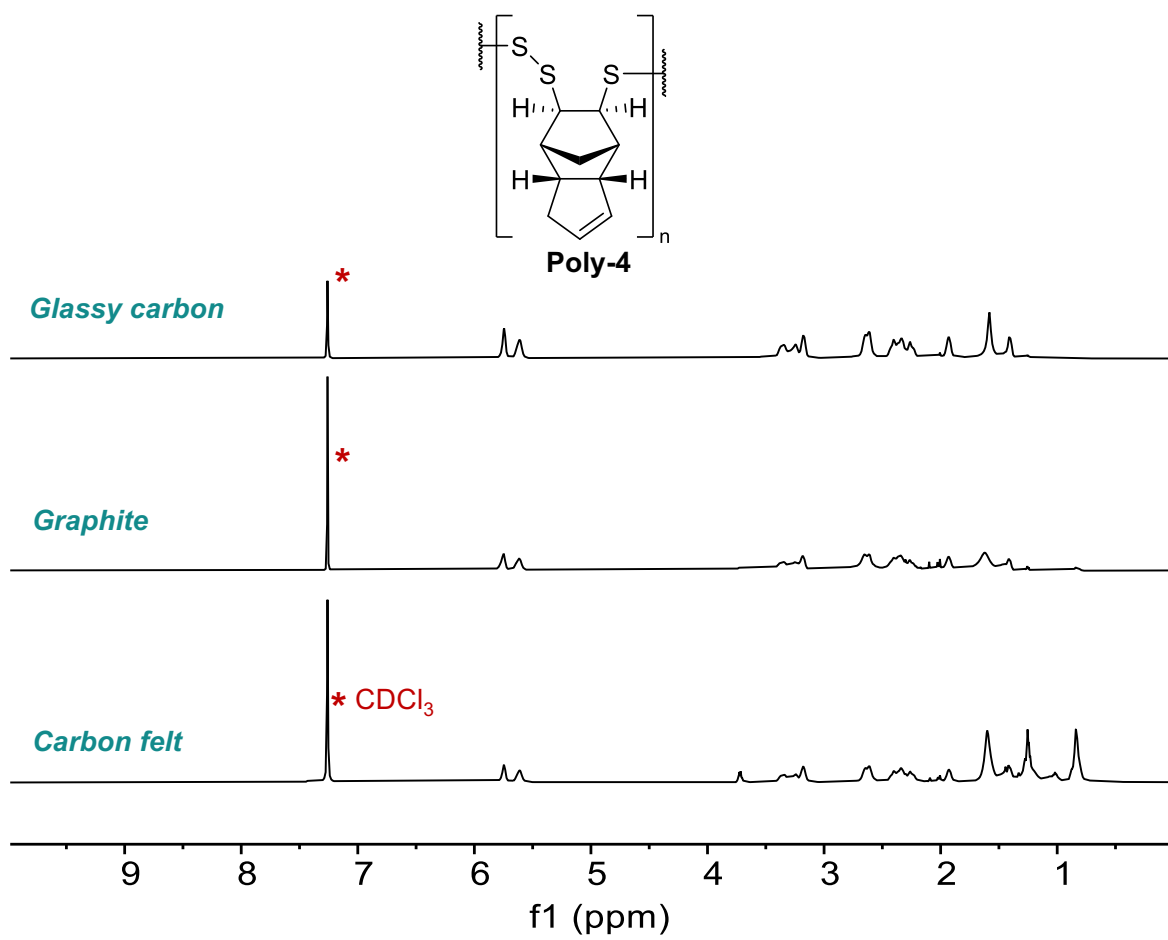


Figure S3.4: ¹H NMR (600 MHz, CDCl₃) of purified poly-4.

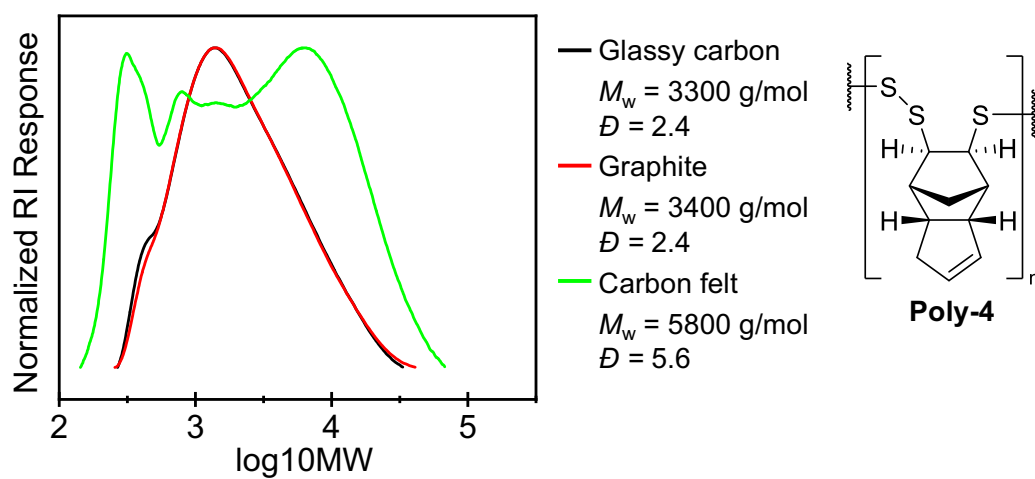
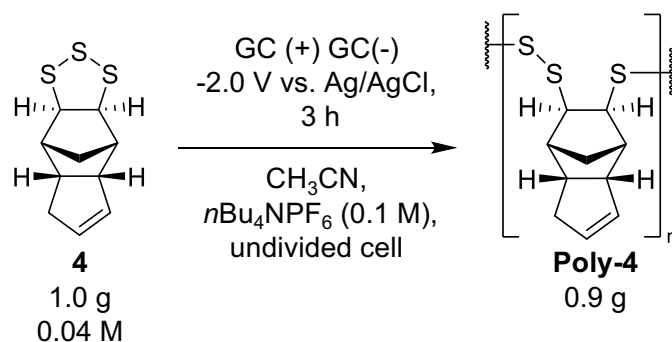


Figure S3.5: GPC (THF) of purified poly-4.

Scale-up of electrochemical polymerisation in batch

Batch poly-4 synthesis – 1 g



A glass beaker (120 mL) was charged with **4** (1.03 g, 4.4 mmol, 0.04 M), *n*Bu₄NPF₆ (3.8 g, 9.8 mmol, 0.1 M), acetonitrile (100 mL) and a stir bar. Two carbon felt pieces (5 cm x 6 cm) were positioned on each side of the inside beaker walls. A platinum wire was inserted into each piece of carbon to allow for connection to the potentiostat. A Ag/AgCl (3 M aq. KCl) reference electrode held by a clamp was placed into the centre of the beaker. A constant potential of -2.0 V versus Ag/AgCl (3 M aq. KCl) was applied for 3 h, stirring at 400 rpm. An aliquot (0.5 mL) of the crude reaction mixture was taken, concentrated under reduced pressure, and analysed by ¹H NMR spectroscopy to determine monomer conversion (87%). The reaction mixture was then transferred to a round bottom flask, washing the electrodes with chloroform to get full transfer of the polymer to the flask (the polymer was soluble in chloroform). The resulting solution was concentrated under reduced pressure. The remaining solid was redissolved in 10 mL of chloroform and transferred to a 50 mL centrifuge tube. Acetonitrile (30 mL) was added to the centrifuge tube to precipitate the polymer and was vortexed to mix. The solution was centrifuged at 5000 rpm for 5 minutes. The supernatant was decanted, and the solid was redissolved in chloroform (10 mL). Acetonitrile (30 mL) was added to the centrifuge tube and vortexed to mix. The solution was centrifuged for 5 minutes (5000 rpm). The supernatant was decanted, and the solid was redissolved in chloroform (10 mL). This process was repeated a third time, and the solid polymer was collected (0.9 g, contains carbon felt impurities).

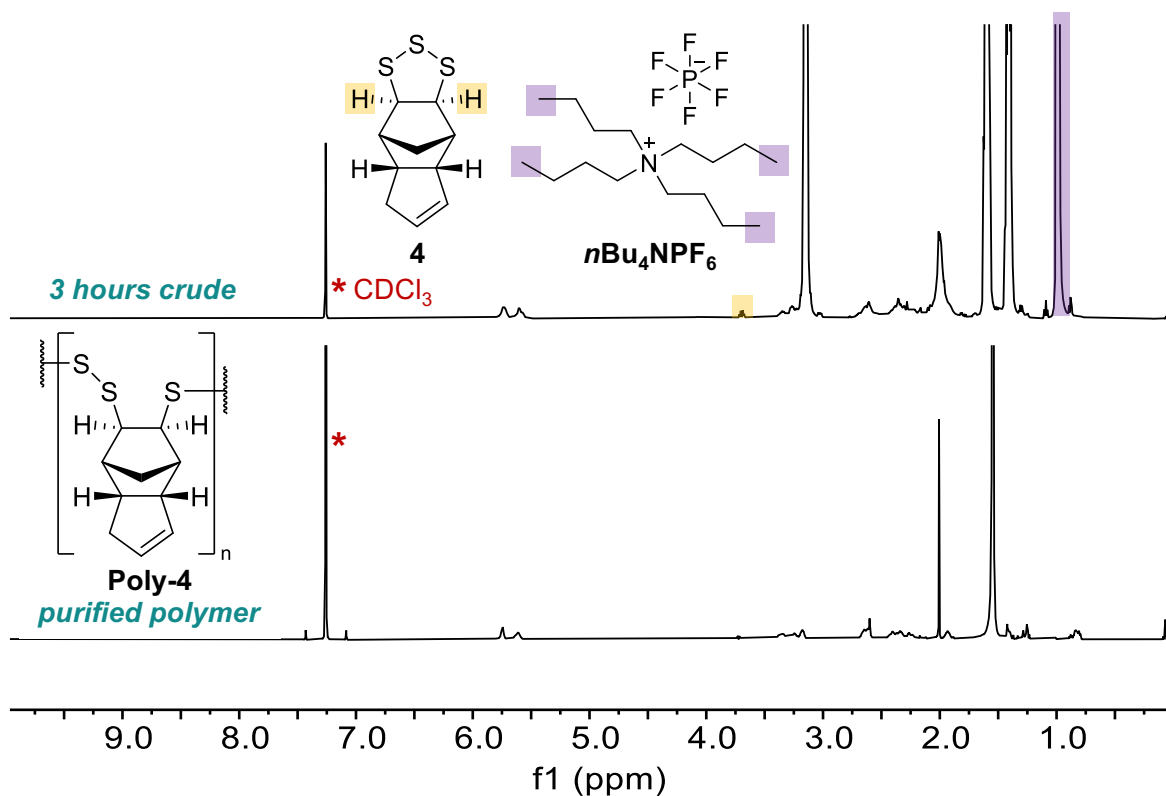


Figure SI 3.6: Top: ^1H NMR (600 MHz, CDCl_3) of crude reaction mixture taken after 4 hours. Integration of **4** and $n\text{Bu}_4\text{NPF}_6$ proton signals are highlighted and used to calculate the conversion of **4**. Bottom: ^1H NMR (600 MHz, CDCl_3) of purified **poly-4**.

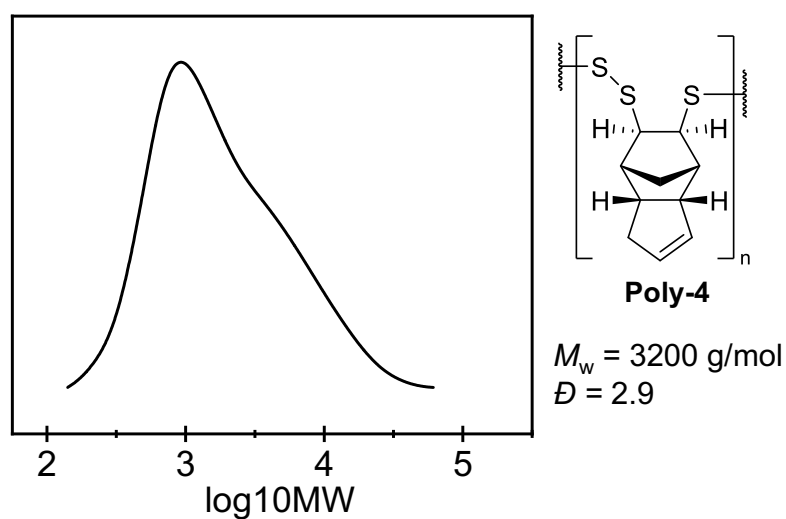
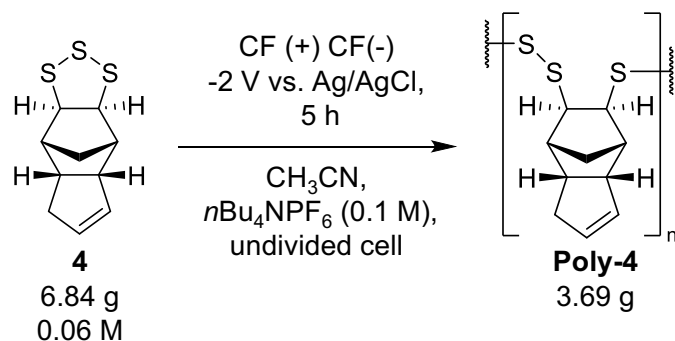


Figure SI 3.7: GPC (THF) of purified **poly-4**.

Batch poly-4 synthesis – 6.8 g



A glass beaker (2 L) was converted to an electrochemical cell. Two carbon felt pieces (5 cm x 15 cm) were positioned on each side of the inside beaker walls. A platinum wire was inserted into each piece of carbon felt to allow for connection to the potentiostat. A Ag/AgCl (3 M aq. KCl) reference electrode held by a clamp was placed into the centre of the beaker. The beaker was charged with **4** (6.84 g, 30 mmol, 0.06 M), $n\text{Bu}_4\text{NPF}_6$ (19.4 g, 50.0 mmol, 0.1 M), acetonitrile (500 mL) and a stir bar. The solution was stirred at 400 RPM. A constant potential of -2.0 V versus Ag/AgCl (3 M aq. KCl) was applied for 4 h. An aliquot (0.5 mL) of the crude reaction mixture was taken, concentrated under reduced pressure, and analysed by ^1H NMR spectroscopy to determine monomer conversion (56%). The reaction mixture was then transferred to a 1L round bottom flask, washing the electrodes with chloroform to get full transfer of the polymer to the flask (the polymer was soluble in chloroform). The resulting solution was concentrated under reduced pressure. The remaining solid was redissolved in 100 mL of chloroform by stirring at 40 °C for 1 hour. Acetonitrile (200 mL) was added to precipitate the polymer while stirring. The polymer was purified by filtration. The filtered polymer was then redissolved in 100 mL of chloroform and the precipitation process was repeated two more times to remove unreacted monomer and electrolyte from the polymer. The resulting polymer (3.69 g, containing carbon felt impurities) was characterised by ^1H NMR spectroscopy (CDCl_3) and GPC (THF).

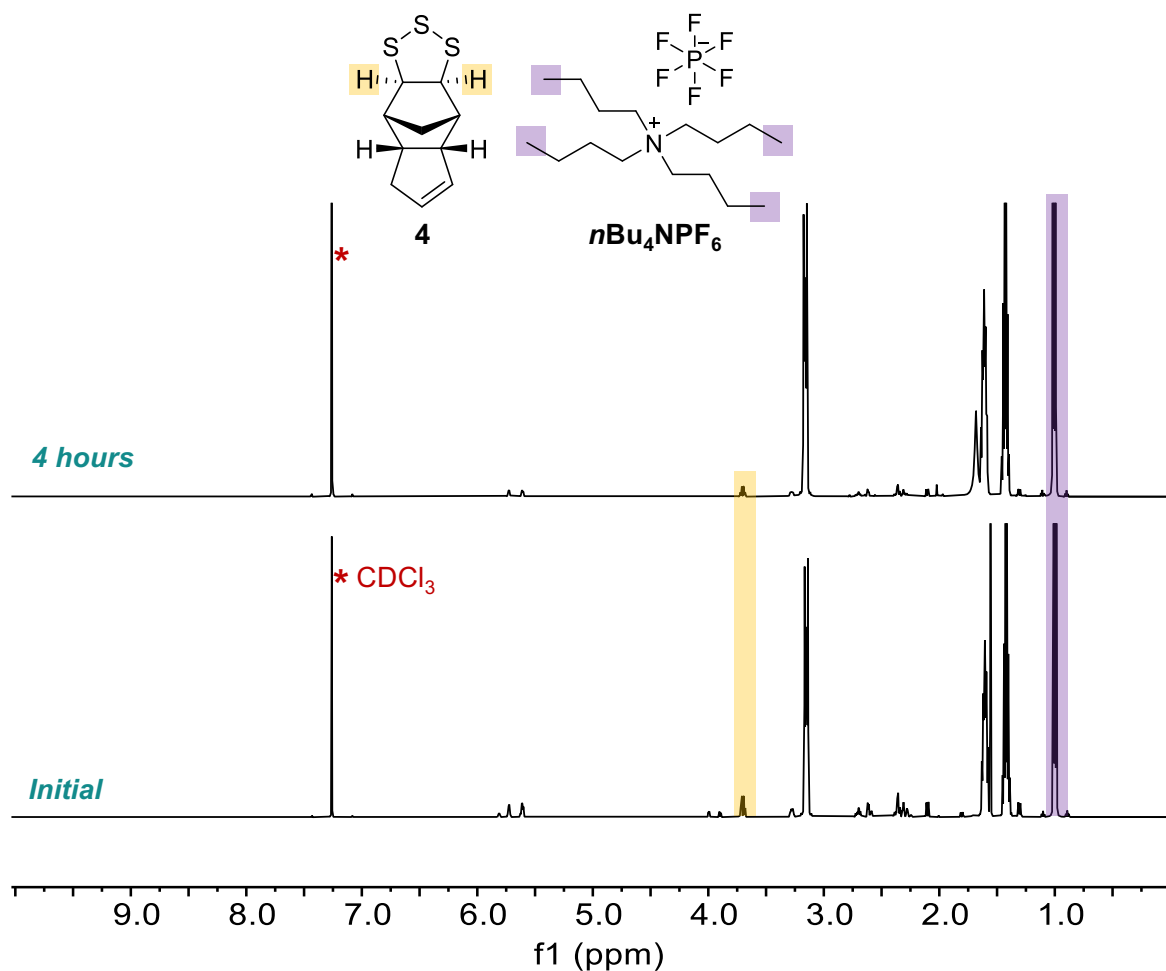


Figure S3.8: ^1H NMR (600 MHz, CDCl_3) of initial solution after all reagent was fully dissolved (bottom). ^1H NMR (600 MHz, CDCl_3) of crude reaction mixture taken after 4 hours. Integration of **4** and $n\text{Bu}_4\text{NPF}_6$ proton signals are highlighted and used to calculate the conversion of **4**.

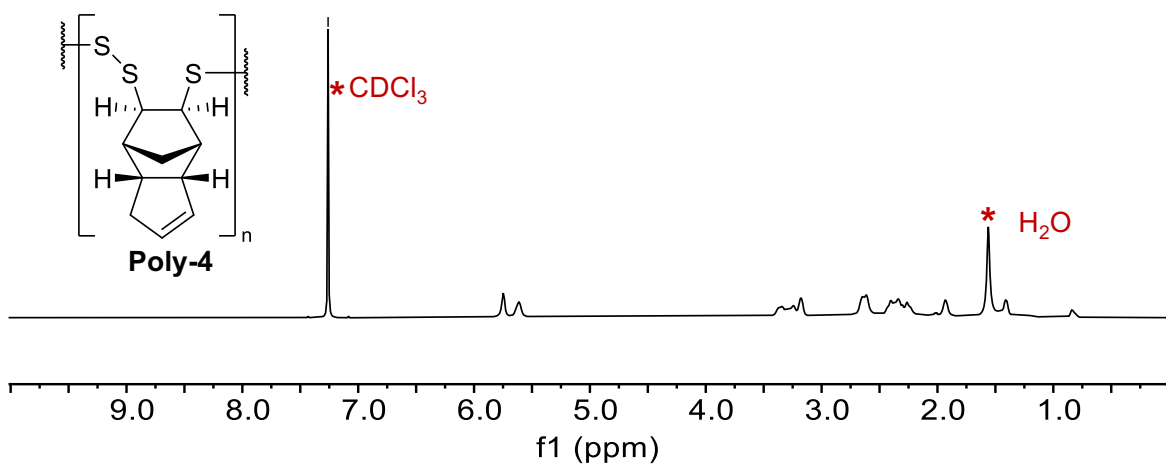


Figure S3.9: ^1H NMR (600 MHz, CDCl_3) of purified **poly-4**.

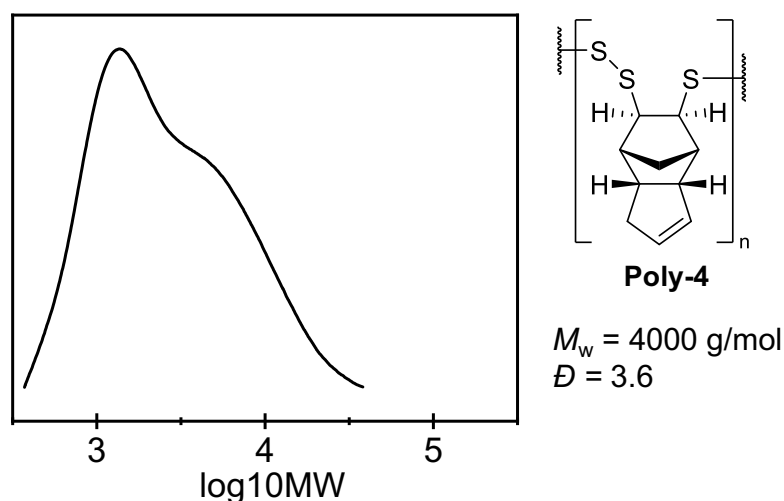


Figure S3.10: GPC (THF) of purified **poly-4**.

Batch poly-4 synthesis – 20 g

A glass beaker (2 L) was converted to an electrochemical cell. Two carbon felt pieces (5 cm x 15 cm) were positioned on each side of the inside beaker walls. A platinum wire was inserted into each piece of carbon felt to allow for connection to the potentiostat. A Ag/AgCl (3 M aq. KCl) reference electrode held by a clamp was placed into the centre of the beaker. The beaker was charged with **4** (20.0 g, 87.7 mmol, 0.18 M), $n\text{Bu}_4\text{NPF}_6$ (19.4 g, 50.0 mmol, 0.1 M), acetonitrile (500 mL) and a stir bar. The solution was stirred at 400 RPM at 30 °C for the duration for the reaction. A constant potential of -2.0 V versus Ag/AgCl (3 M aq. KCl) was applied for 24 h. Aliquots (0.5 mL) of the crude reaction mixture was taken at 0, 1, 4, 12, 15, 20, and 24 hours, concentrated under reduced pressure, and analysed by ^1H NMR spectroscopy to determine monomer conversion. At 24 hours, monomer conversion was found to be 88%. The reaction mixture was then transferred to a 1L round bottom flask, washing the electrodes with chloroform to get full transfer of the polymer to the flask (the polymer was soluble in chloroform). The resulting solution was concentrated under reduced pressure. The remaining solid was redissolved in 100 mL of chloroform by stirring at 40°C for 1 hour. Acetonitrile (200 mL) was added to precipitate the polymer while stirring. The polymer was purified by filtration. The filtered polymer was then redissolved in 100 mL of chloroform and the precipitation process was repeated two more times to remove unreacted monomer and electrolyte from the polymer. The resulting polymer (14.8 g, containing carbon felt impurities) was characterised by ^1H NMR spectroscopy (CDCl_3) and GPC (THF).

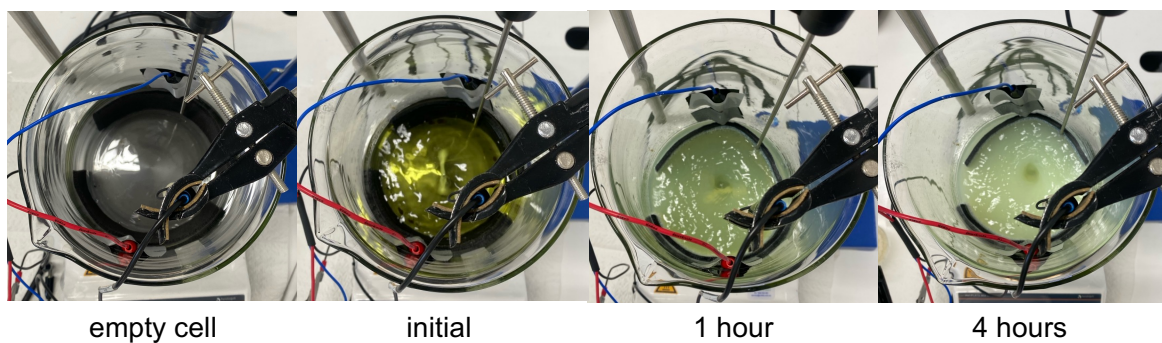


Figure S3.11: Top view of electrochemical cell before addition of reagents, before a potential was applied, and after a potential of -2.0 V versus Ag/AgCl (3 M aq. KCl) was applied for 1 and 4 hours.

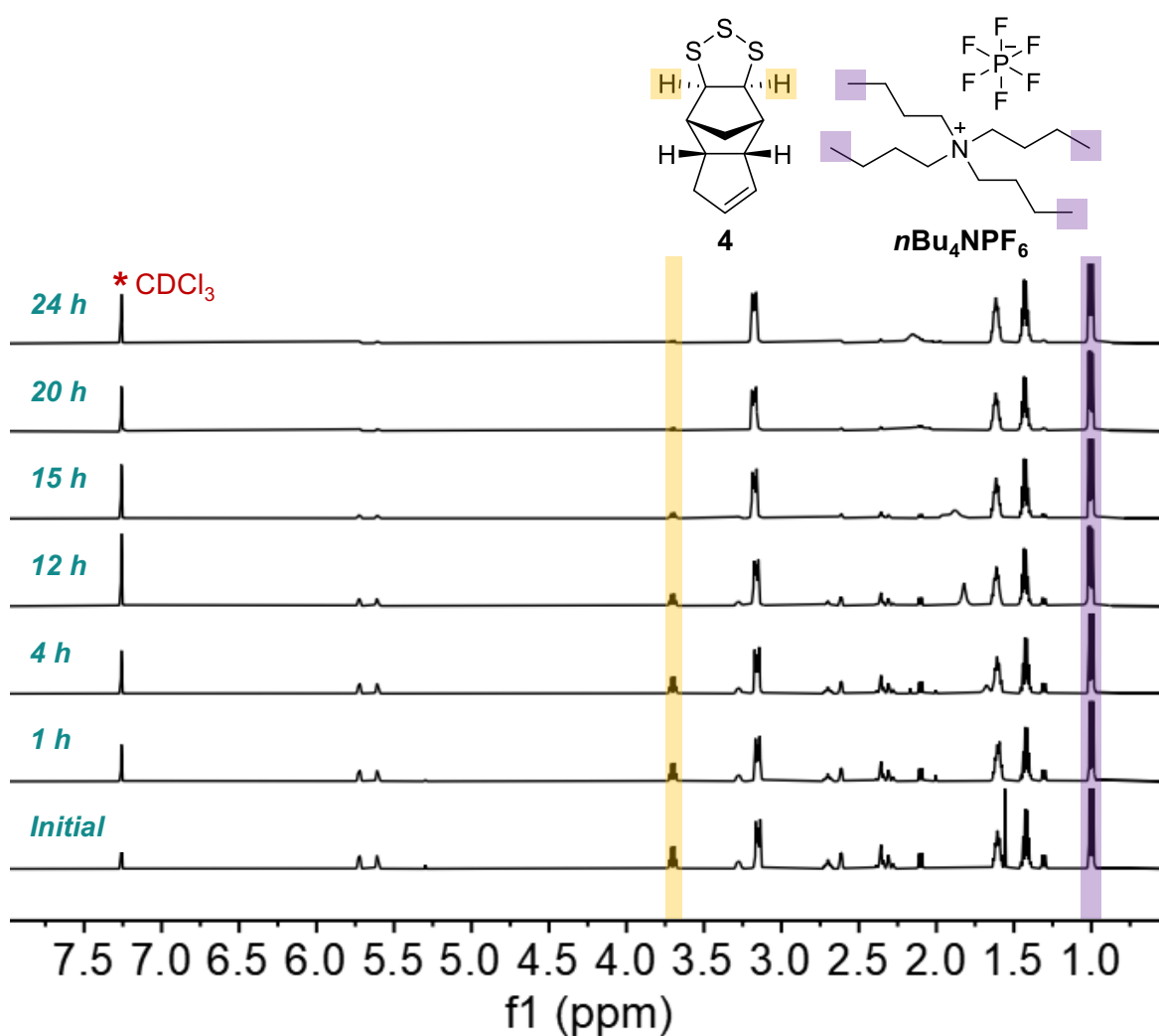


Figure S3.12: ¹H NMR (600 MHz, CDCl₃) of crude reaction at 0, 1, 4, 12, 15, 20, and 24 hours. Integration of **4** and *n*Bu₄NPF₆ proton signals are highlighted and used to calculate the conversion of **4**.

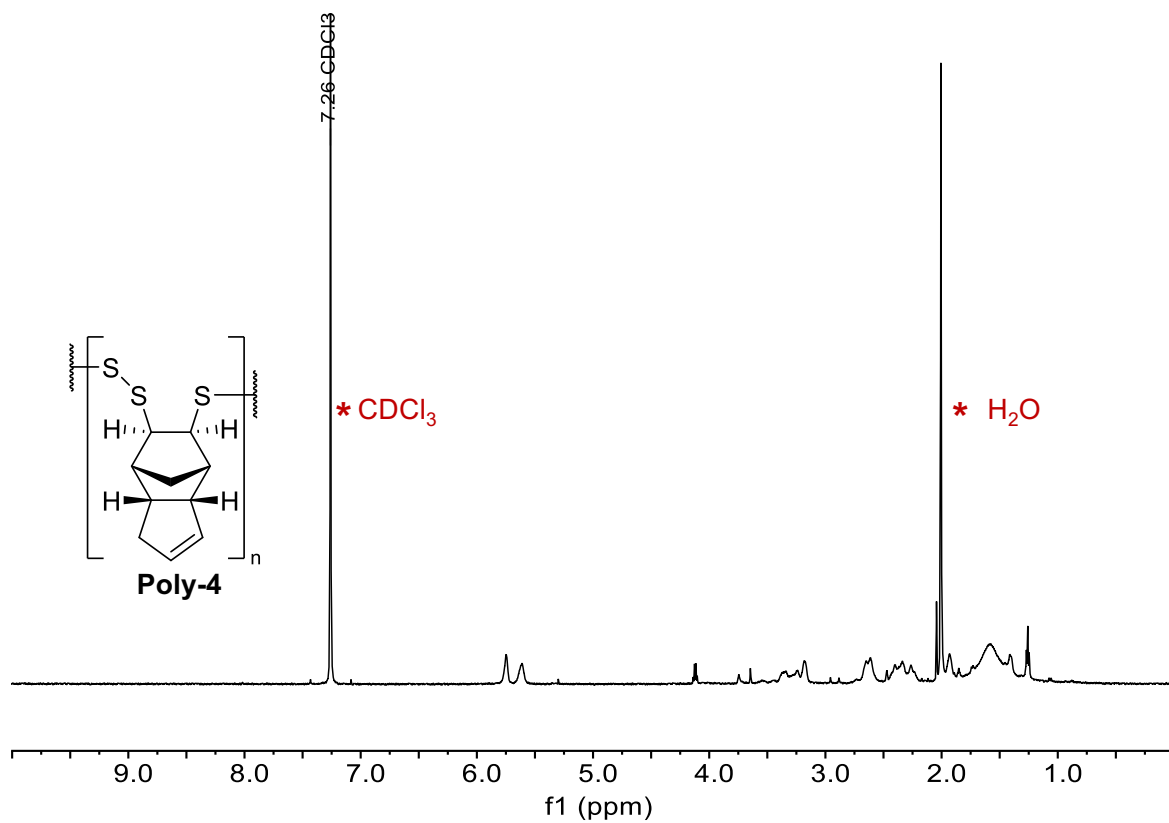


Figure S3.13: ^1H NMR (600 MHz, CDCl_3) of purified **poly-4**.

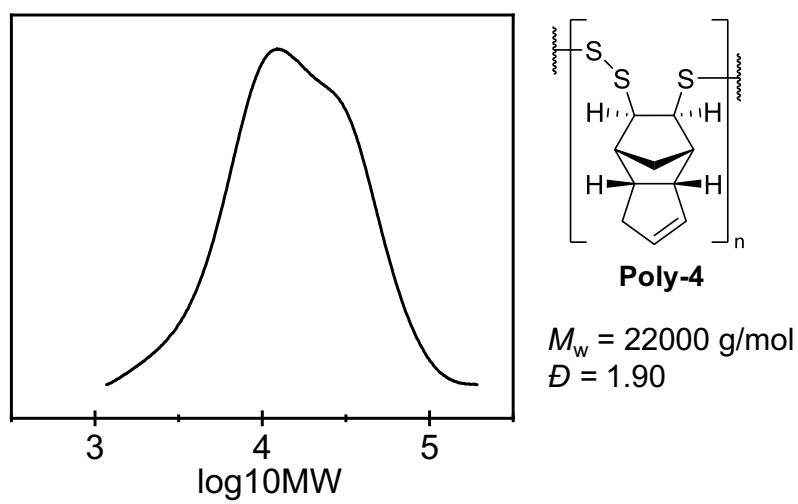


Figure S3.14: GPC (THF) of purified **Poly-4**.

Electrolyte recovery

Electrolyte purification was performed on the filtrate from the 6.8 g polymerisation reaction. After the polymer was collected by filtration the filtrate containing unreacted **4** and $n\text{Bu}_4\text{NPF}_6$ was collected and dried under reduced pressure. Monomer **4** was extracted from $n\text{Bu}_4\text{NPF}_6$ by washing the crude product with hexane (3 x 50 mL). The resulting $n\text{Bu}_4\text{NPF}_6$ was purified through recrystallisation with hot ethanol which returned a white crystalline product (17.6 g, 91% recovery) and was characterised by ^1H NMR spectroscopy (CDCl_3).

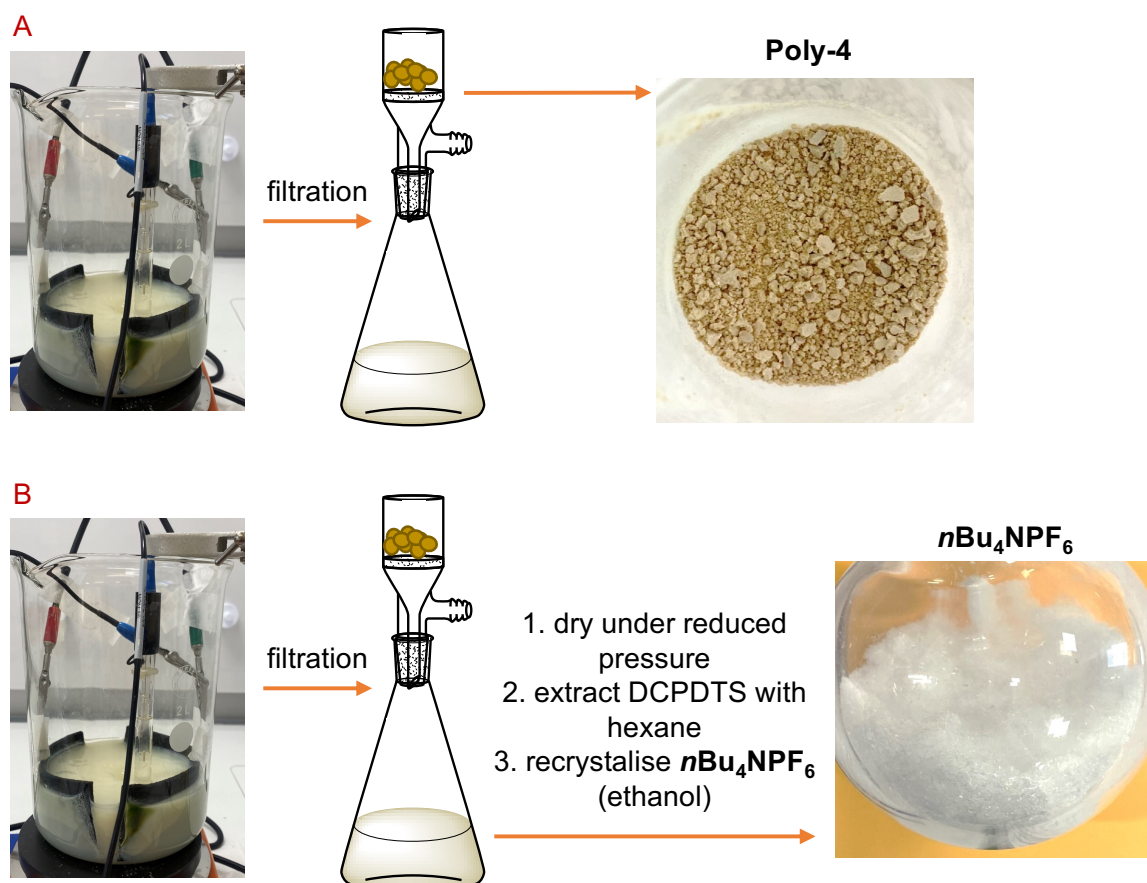


Figure S3.15: A: **Poly-4** purification via filtration. B: purification of electrolyte ($n\text{Bu}_4\text{NPF}_6$) from filtrate.

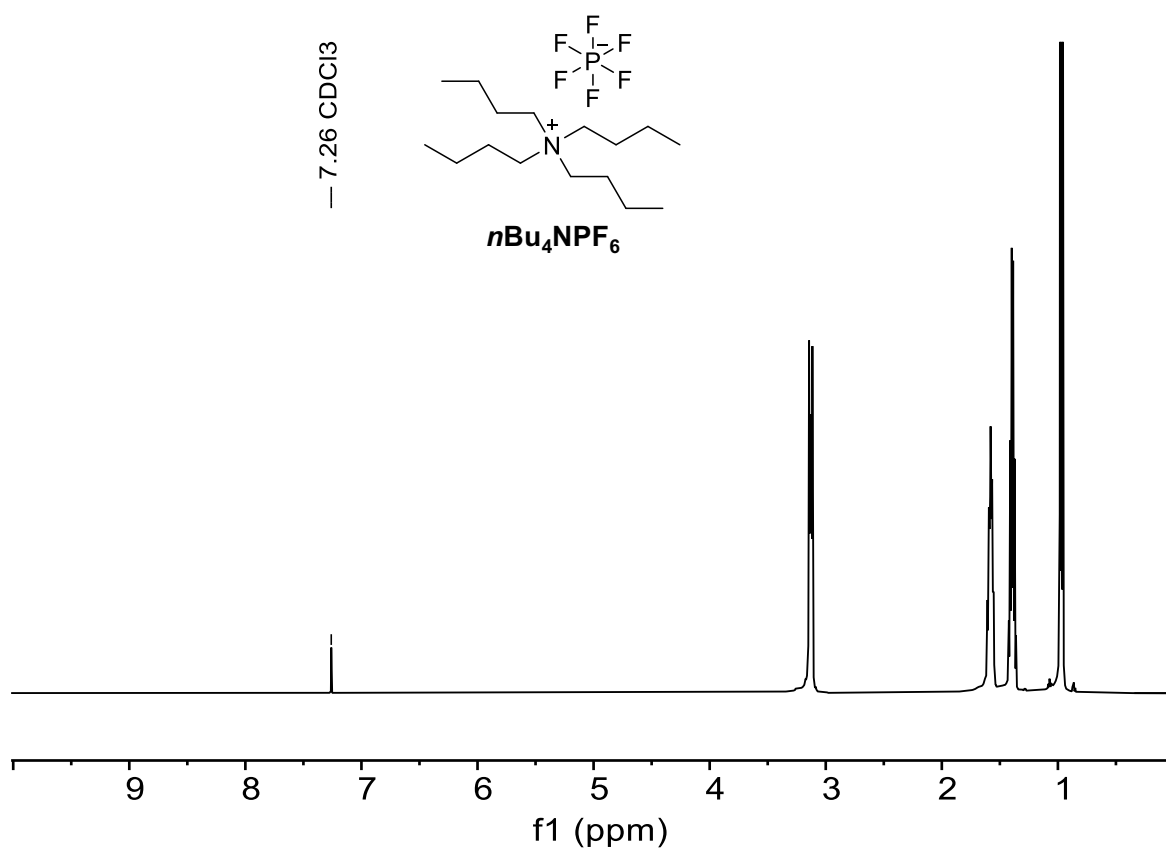
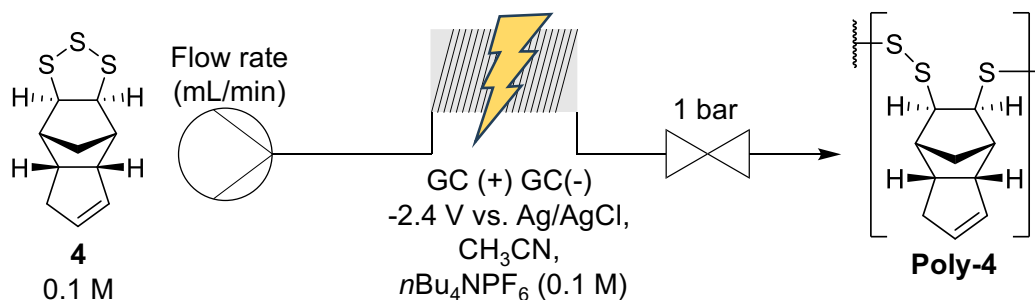


Figure S3.16: ^1H NMR (600 MHz, CDCl_3) of purified $n\text{Bu}_4\text{NPF}_6$.

Scale-up of electrochemical polymerisation in continuous flow

General procedure



A solution of **4** (456 mg, 2.0 mmol, 0.1 M) and $n\text{Bu}_4\text{NPF}_6$ (774 mg, 2.0 mmol, 0.1 M) in acetonitrile (20 mL) was pumped through the continuous flow electrochemical cell. The reactor was under a constant potential of -2.4 V versus Ag/AgCl. After the solution had fully passed through the reactor, it was collected and concentrated under pressure before analysis by ^1H NMR spectroscopy (CDCl_3) and GPC (THF).

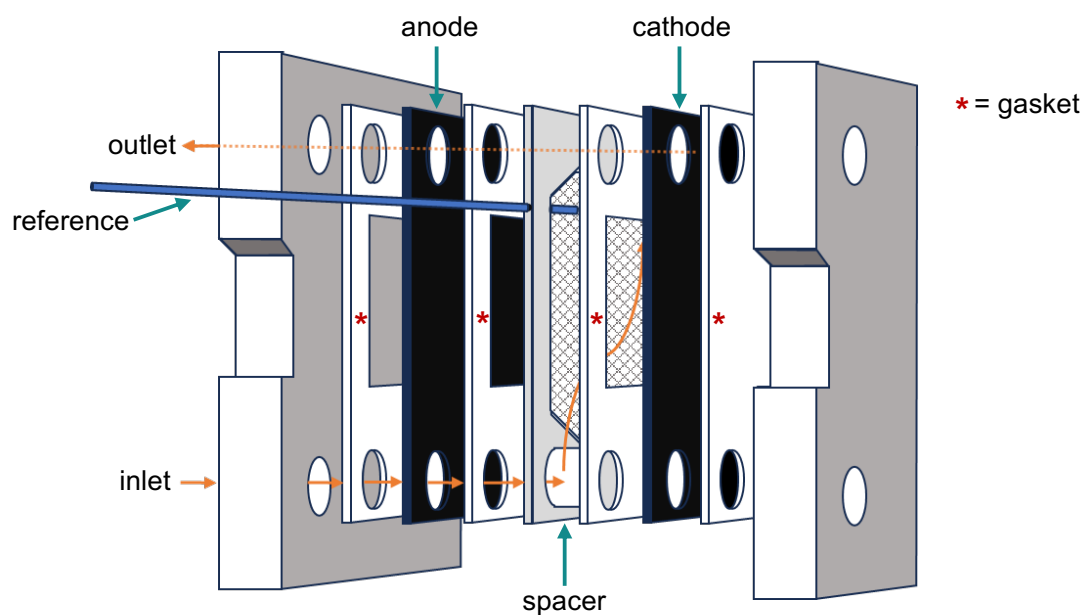


Figure S3.17: Schematic illustration of the electrochemical reactor. Gaskets and spacer are made from PTFE. Anode and cathode are gassy carbon. The internal volume of the reactor was 4 mL.

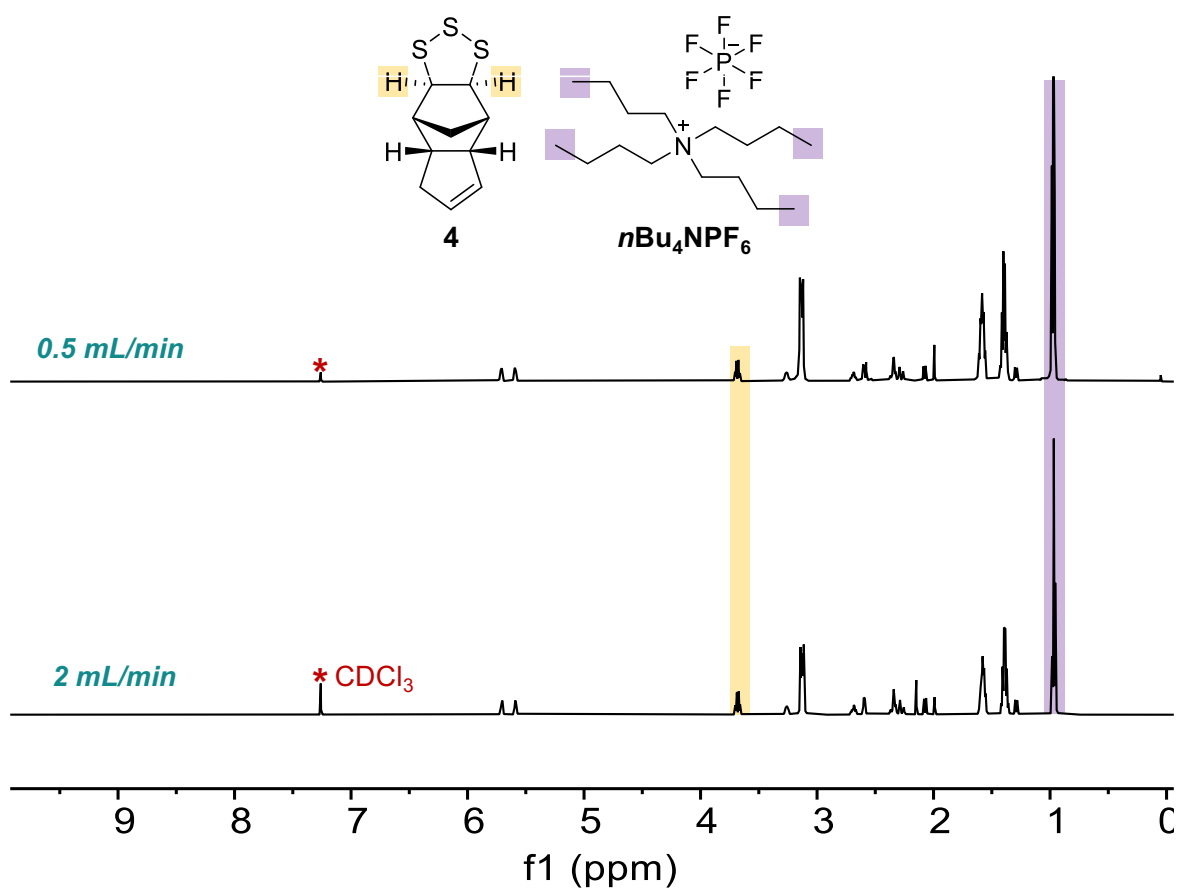


Figure S3.18: ^1H NMR (600 MHz, CDCl_3) of crude reaction mixture taken after reacting in continuous flow at a flow rate of 0.5 mL/min (top) and 2 mL/min (bottom). Integration of **4** and $n\text{Bu}_4\text{NPF}_6$ proton signals are highlighted and used to calculate the conversion of **4**.

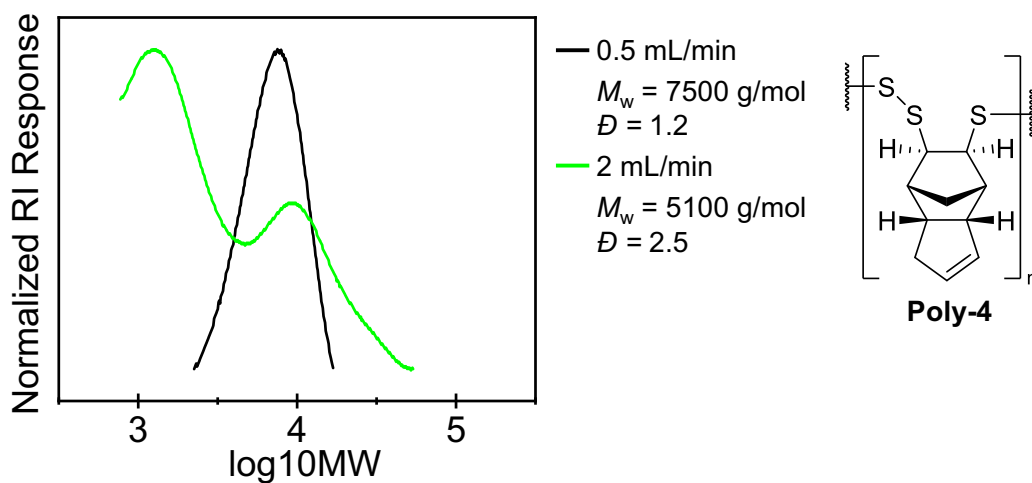


Figure S3.19: GPC (THF) of crude **poly-4** produced at different flow rates.

A Polymer build up after a flow rate of 0.5 mL/min



B Polymer build after a flow rate of 2 mL/min

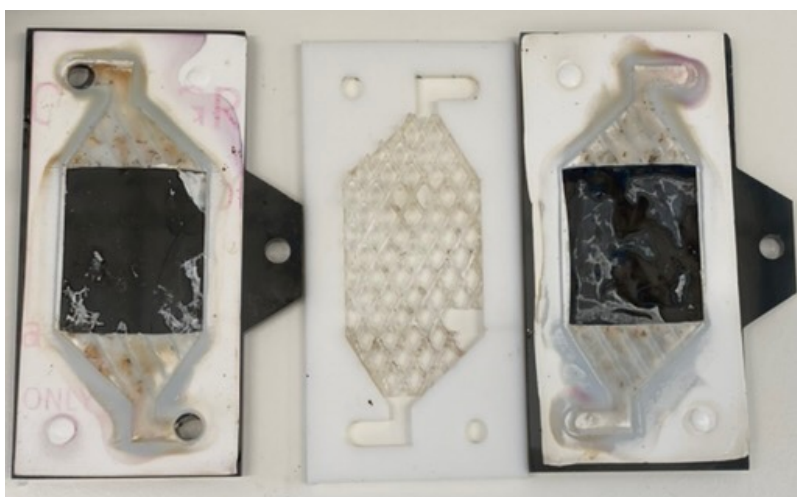


Figure S3.20: Polymer build up on the electrode surfaces in the flow cell after reaction.

Applications

Gold sorption and recovery

Gold(III) sorption

A stock solution (25 mL) of 100 ppm aqueous gold solution was prepared by diluting a gold standard (gold in hydrochloric acid 1 mg/L) in Milli-Q water. This solution was added to 2 separate 15 mL centrifuge tubes. The following experiments were then prepared:

- 1) Control: sample of 10 mL aqueous gold solution (100 ppm)
- 2) **Poly-1:** 200 mg of **poly-1** and 10 mL aqueous gold solution (100 ppm)

After the samples were prepared, they were rotated at 25 RPM for 12 hours. 2 mL aliquots were taken from the samples and centrifuged for 5 minutes on a small benchtop centrifuge. The supernatant was then collected and analyzed by atomic absorption spectroscopy (AAS). Sample concentrations were determined based on a series of gold calibration standards.

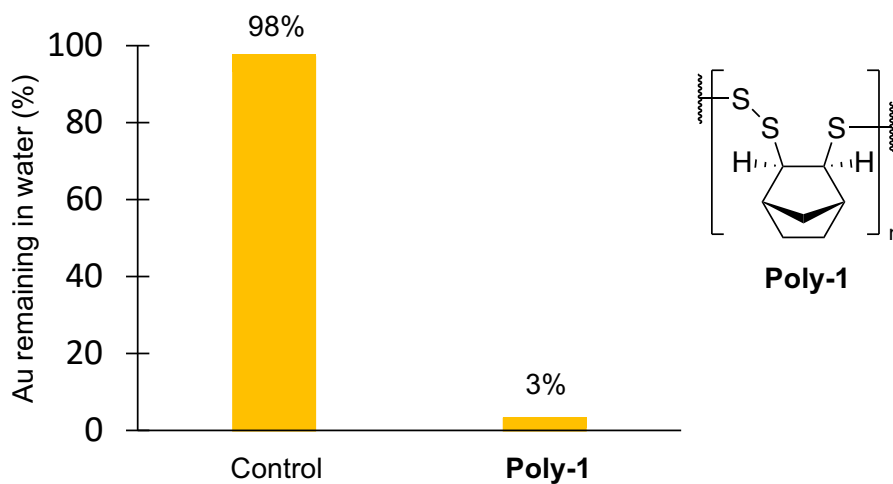


Figure S3.21: Gold sorption plot. Control shows 98% gold remaining in solution and **poly-1** shows 3% gold remaining in solution based on AAS calibration standards.

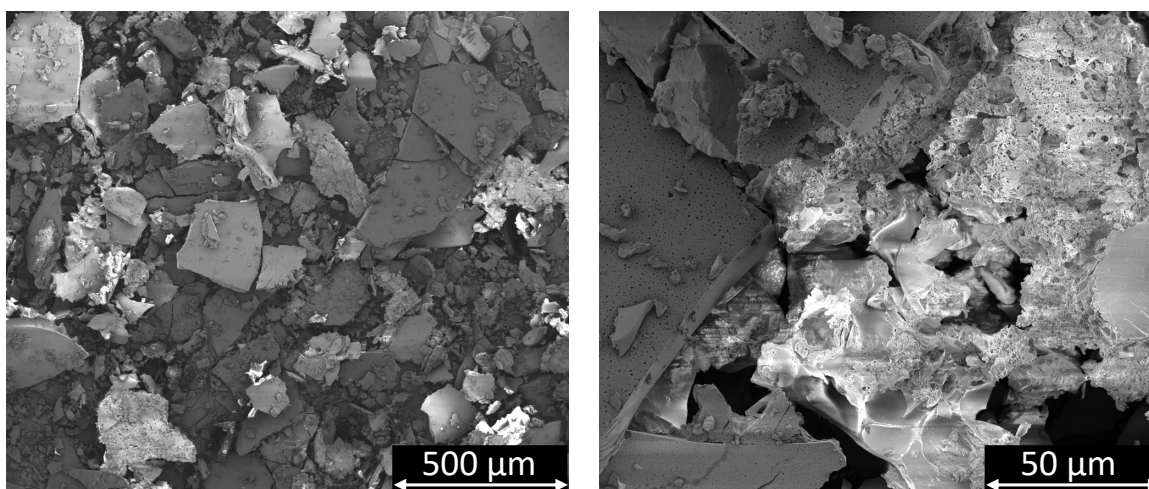


Figure S3.22: Scanning electron microscope (SEM) images of **poly-1-Au** after Au sorption experiment prepared by dusting dried sample on carbon tape and then coating the sample in 10 nm of platinum.

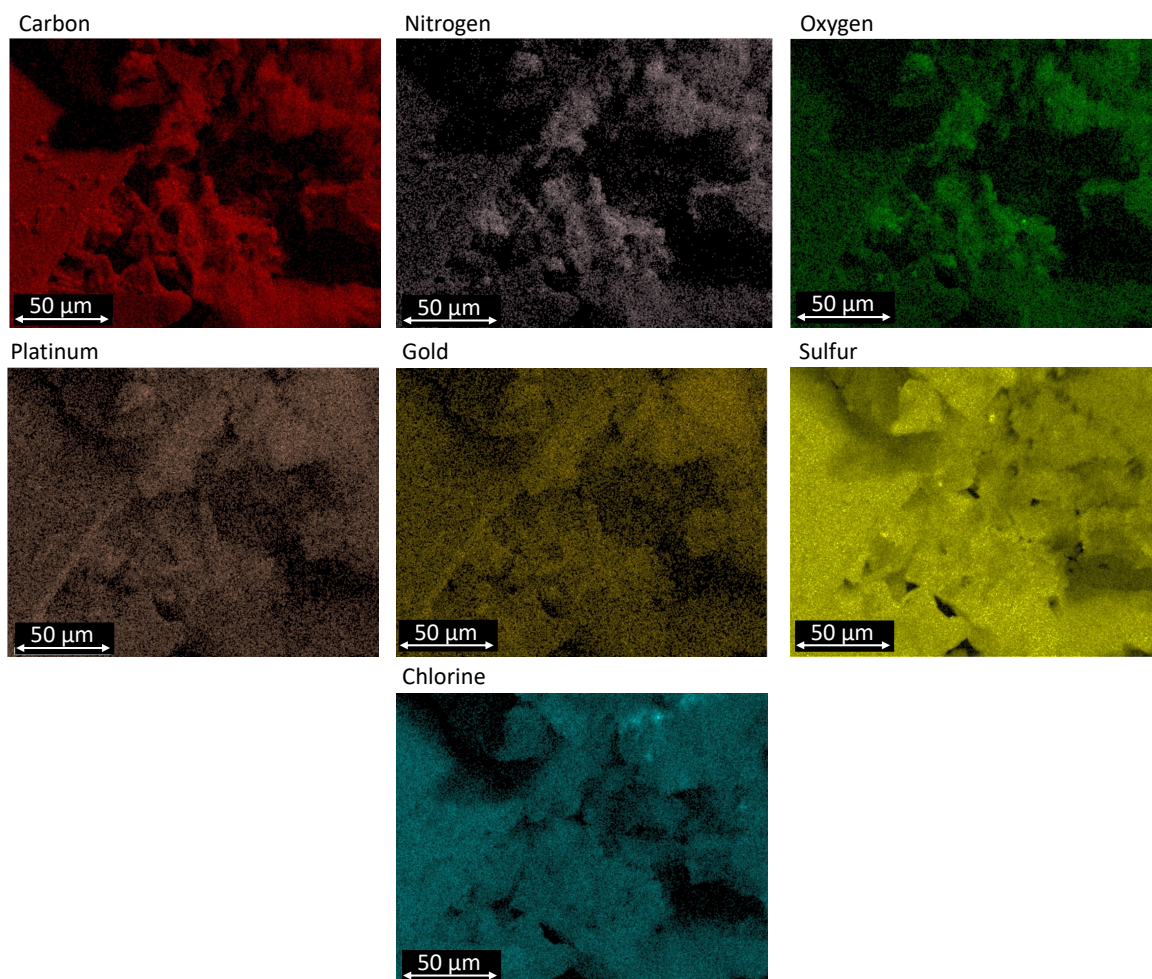


Figure S3.23: Scanning electron microscopy (SEM) with energy dispersive X-ray (EDX) characterisation of **poly-1-Au** after Au sorption experiment.

Polymer recycling and monomer recovery

Poly-1-Au (104 mg) was heated at 170 °C under atmospheric pressure for 14 hours in a short-path distillation apparatus. A reduced pressure of 15 mbar was then applied for 3 hours at 170 °C. The distillate was collected by washing the receiving flask and the condenser with hexane (5 x 10 mL). The fractions were combined and concentrated under reduced pressure to deliver monomer **1** (72 mg, 70% yield). ¹H NMR spectra data was consistent for that previously observed for monomer **1**.

A Distillation flask under atm at 170 °C



B Receiving flask under 15 mbar at 170 °C

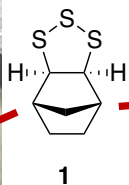
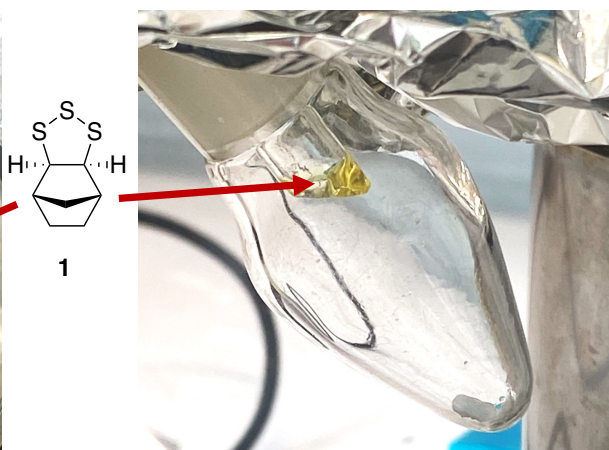


Figure S3.24: Recovery of monomer **1** from the recycling of **poly-1** before and after applied vacuum at 170 °C, a) yellow oil (monomer **1**) condensing in distillation flask under atmospheric pressure, b) yellow oil (monomer **1**) condensing in condenser and dripping into receiving flask after applying a reduced pressure of 15 mbar.

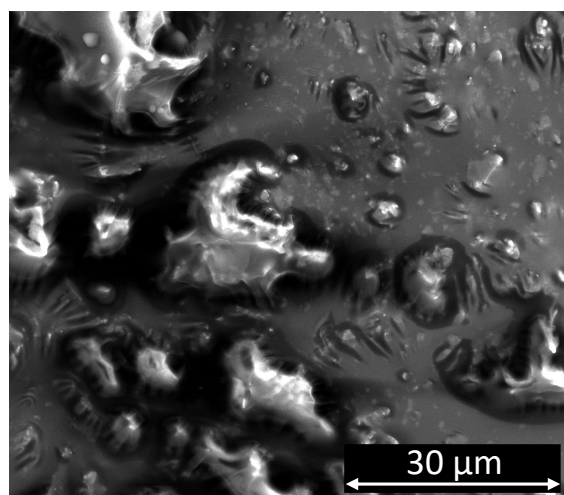
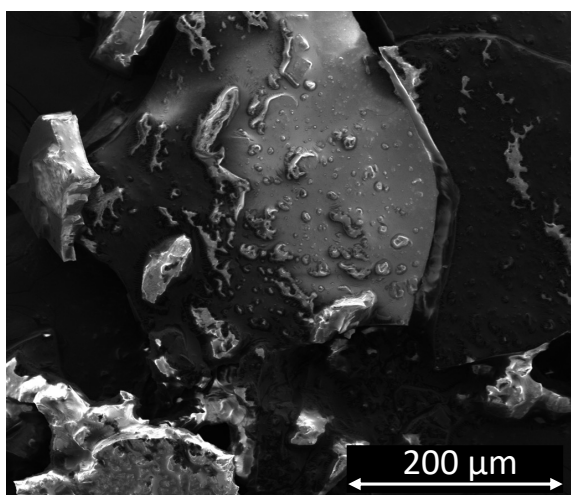


Figure S3.25: Scanning electron microscope (SEM) images of **Poly-1-Au** remaining in the distillation flask prepared by dusting dried sample on carbon tape and then coating the sample in 10 nm of platinum.

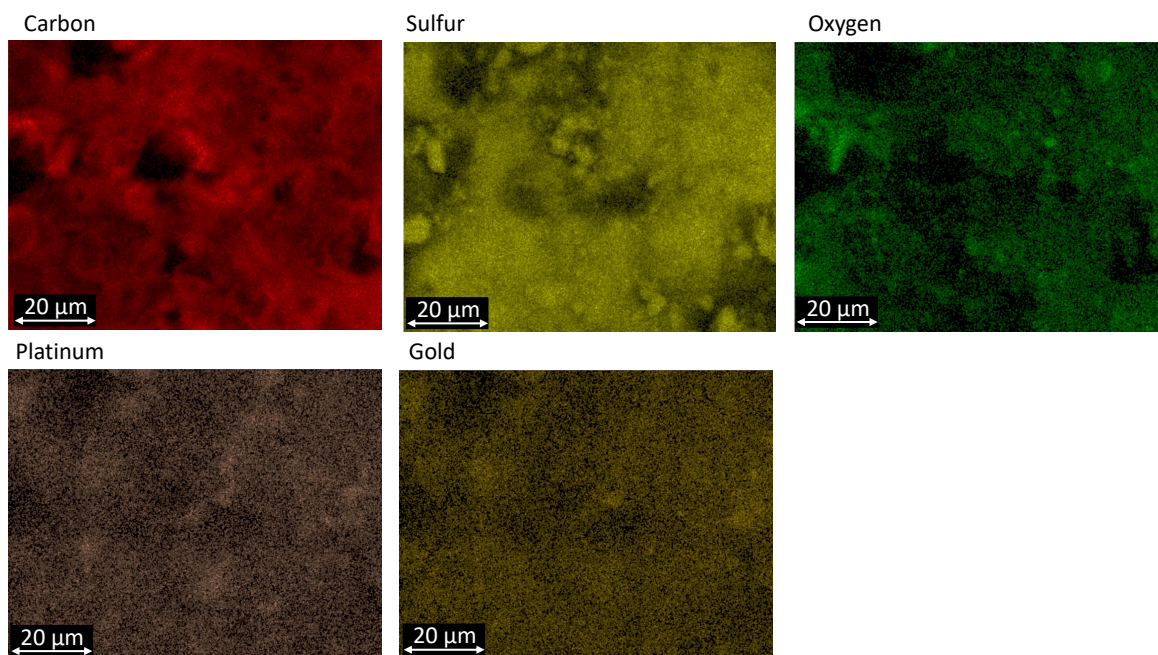


Figure S3.26: Scanning electron microscopy (SEM) with energy dispersive X-ray (EDX) characterisation of **poly-1-Au** remaining in the distillation flask showing individual element maps.

Quantification of gold recovery

The remaining **poly-1-Au** (32 mg) from the previous experiment was suspended in aqua regia (3:1 HCl/HNO₃, 10 mL) and stirred at room temperature for 18 hours. An aliquot (200 μL) was taken and diluted to 2 mL with milli-Q water. The solution was then transferred to a 2 mL Eppendorf tube and centrifuged on a small bench top centrifuge for 1 minute. The supernatant was then collected and analysed immediately by atomic absorption spectroscopy (AAS) resulting in a gold concentration of 5.36 ± 0.04 ppm. Sample concentration was determined based on a series of gold calibration standards prepared by diluting a gold standard (gold in hydrochloric acid 1 mg/L) in Milli-Q water. Back calculation was performed to determine the mass of gold remaining in the distillation flask (0.530 ± 0.004 mg). The expected amount of gold was 0.500 mg, which indicates excellent mass balance.

Silver sorption and release

Silver sorption

A stock solution (25 mL) of 100 ppm aqueous silver solution was prepared by diluting a silver standard (silver in nitric acid 1 mg/L) in Mili-Q water. This solution was added to a 15 mL centrifuge tubes. The following experiment was then prepared:

1) 68 mg of **poly-1** and 10 mL aqueous silver solution (100 ppm)

After the sample was prepared, it was rotated at 25 RPM for 6 hours. A 2 mL aliquot was taken from the sample and centrifuged for 5 minutes on a small benchtop centrifuge. The supernatant was then collected and analysed by atomic absorption spectroscopy (AAS) resulting in a 30% decrease in silver concentration (70 ppm) from the solution. Sample concentration was determined based on a series of silver calibration standards.

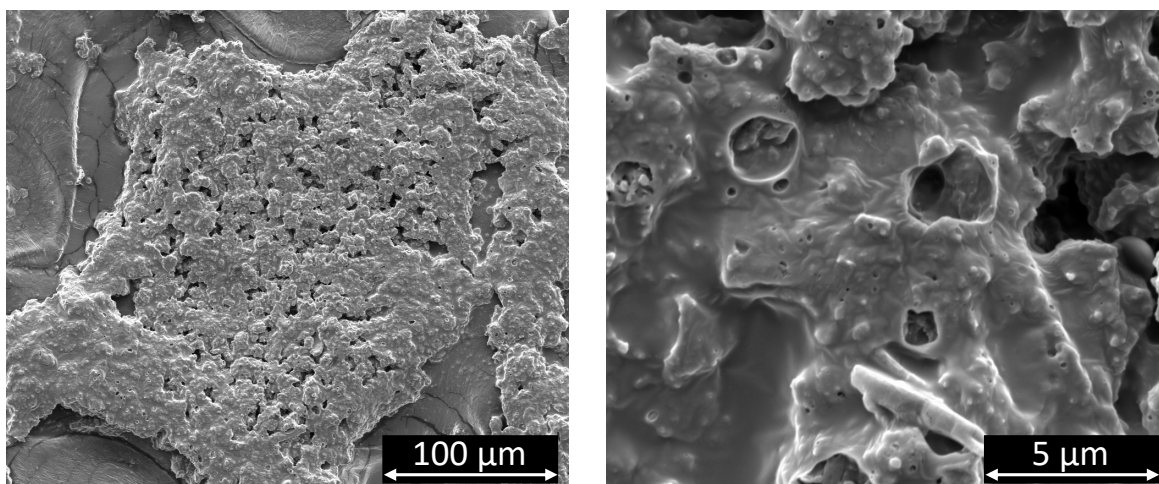


Figure S3.27: Scanning electron microscope (SEM) images of **poly-1** prepared by dissolving polymer in chloroform and dropping onto carbon tape and allowing to evaporate. Sample was then coated with 10 nm of platinum.

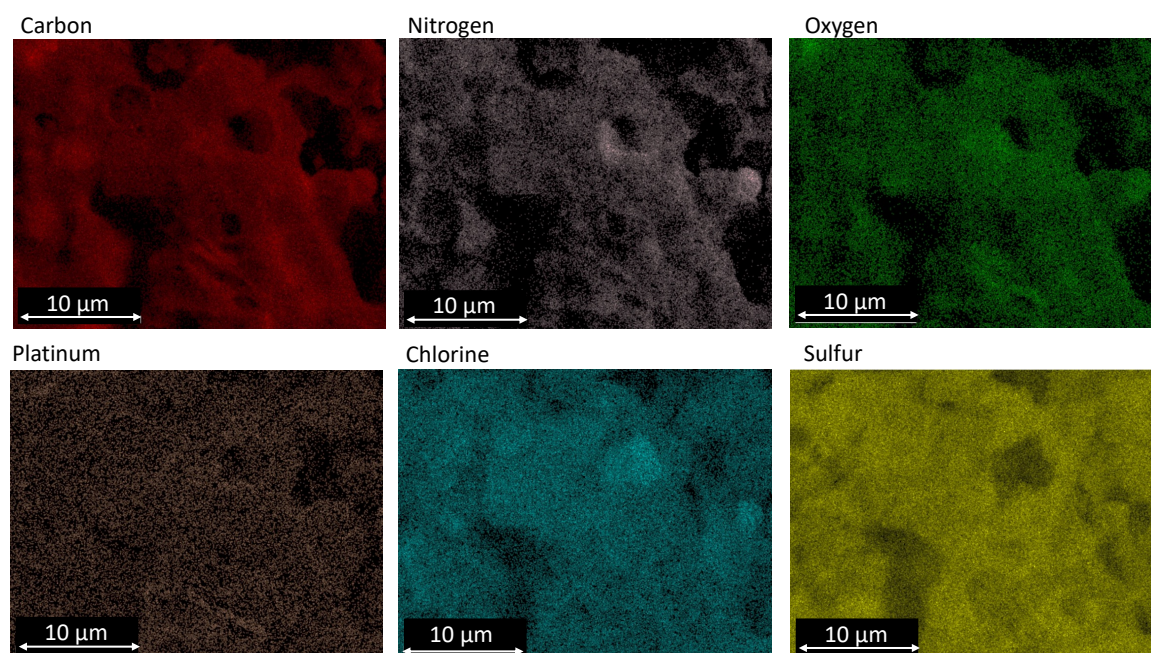


Figure S3.28: Scanning electron microscopy (SEM) with energy dispersive X-ray (EDX) characterisation of **poly-1** showing individual element maps.

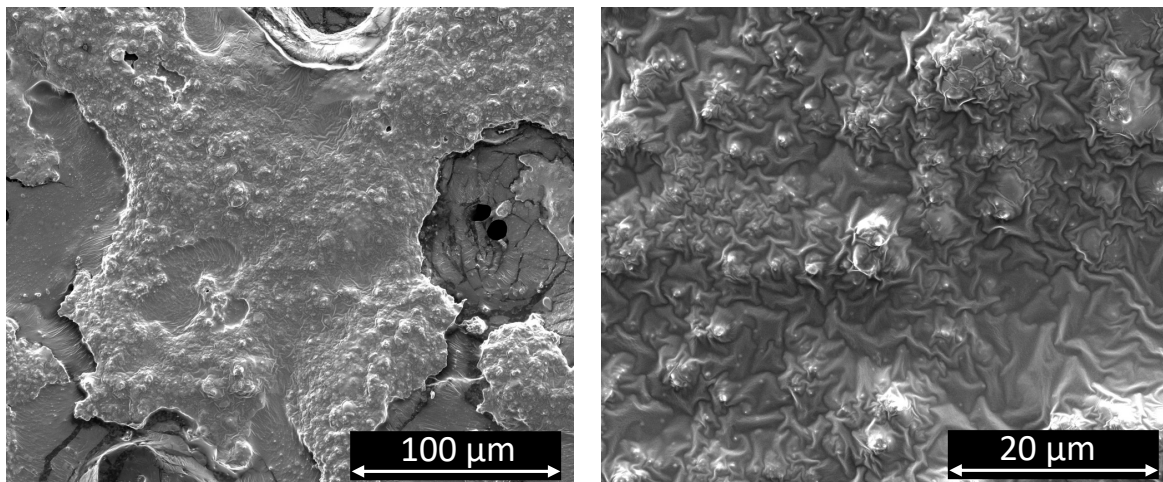


Figure S3.29: Scanning electron microscope (SEM) images of **poly-1-Ag** prepared by drying **poly-1-Ag**, then redissolving in chloroform and dropping onto carbon tape and allowing to evaporate. Sample was then coated with 10 nm of platinum.

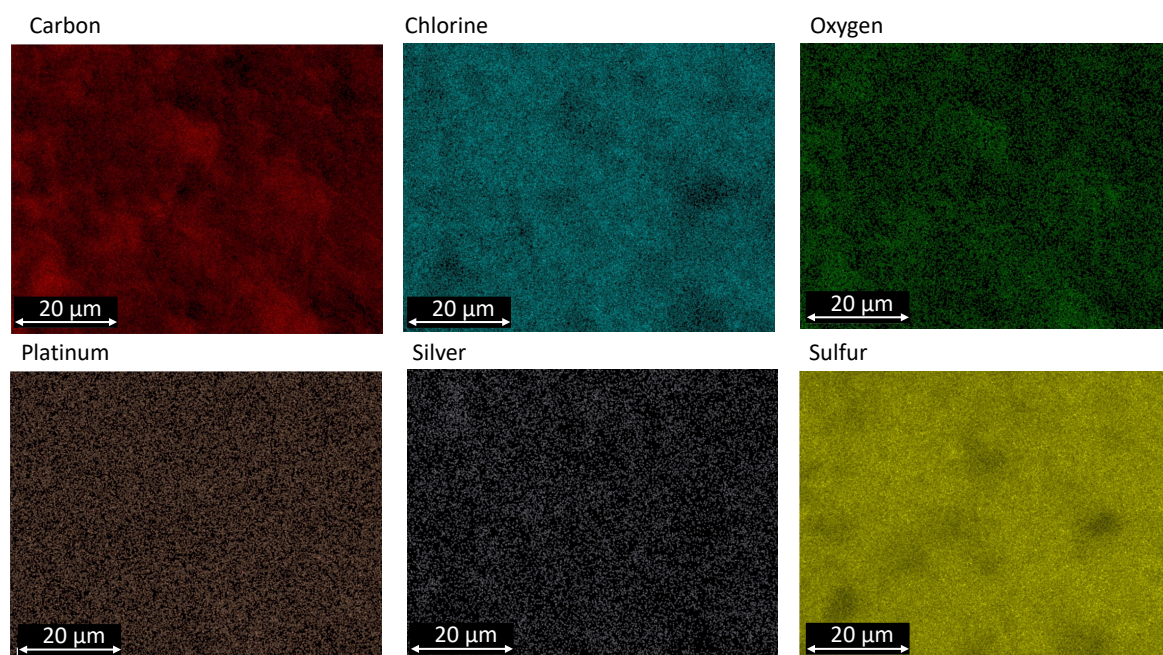


Figure S3.30: Scanning electron microscopy (SEM) with energy dispersive X-ray (EDX) characterisation of **poly-1-Ag** showing individual element maps.

Silver release

In 2 mL Eppendorf tubes the following experiments were prepared:

- 1) Control (Ag): 10 mg of **poly-1-Ag** and 2 mL of aqueous phosphate buffer saline (pH 6).
- 2) Control: 10 mg of **poly-1** and 2 mL of aqueous phosphate buffer saline (pH 6).
- 3) Glutathione (Ag): 10 mg **poly-1-Ag** and 2 mL of glutathione solutions (10 mM of glutathione in aqueous phosphate buffer saline (pH 6)).
- 4) Glutathione: 10 mg **poly-1** and 2 mL of glutathione solutions (10 mM of glutathione in aqueous phosphate buffer saline (pH 6)).

Solutions were placed in a thermal shaker at 30 °C for 24 hours. Aliquots (0.5 mL) were taken from each sample at 0.5 hours, 2 hours, and 24 hours diluted with H₂O to 2 mL before samples were centrifuged for 5 minutes on a small benchtop centrifuge. The supernatant was then collected and analysed immediately by atomic absorption spectroscopy (AAS). Sample concentration was determined based on a series of silver calibration standards.

Copper binding

A stock solution of CuSO₄•5H₂O (102.8 mg, 1.00 mL, 0.412 M) and a stock solution of NaOH (9.24 mg, 1.00 mL, 0.231 M) was prepared.

Sample preparation for 0.5:1 Cu(II)/monomer ratio

An aqueous solution of **Na-poly-3** was prepared by suspending **poly-3** (5.00 mg) in H₂O (0.882 mL) followed by the addition of stock NaOH solution (92.3 µL). The resulting mixture was sonicated until the polymer was dissolved (~5 min). Aqueous suspensions of **poly-1** (5.00 mg, 0.968 mL), **poly-3** (5.00 mg, 0.974 mL), **poly-4** (5.00 mg, 0.973 mL) were also prepared.

Sample preparation for 1:1 Cu(II)/monomer ratio

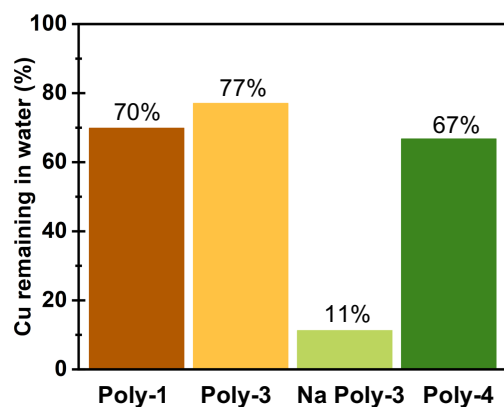
An aqueous solution of **Na-poly-3** was prepared by suspending **poly-3** (5.00 mg) in H₂O (0.856 mL) followed by the addition of stock NaOH solution (92.3 µL). The resulting mixture was sonicated until the polymer was dissolved (~5 min). Aqueous suspensions of **poly-1** (5.00 mg, 0.936 mL), **poly-3** (5.00 mg, 0.945 mL), **poly-4** (5.00 mg, 0.948 mL) were also prepared.

Stock CuSO₄•5H₂O was added to the prepared polymer mixtures to give a total volume of 1.00 mL. The solutions were agitated using a Grant-bio Thermo shaker (1000 RPM, 1 h). The samples were then centrifuged for 5 min using a small benchtop centrifuge and the supernatant collected for analysis by atomic absorption spectroscopy (AAS). The concentration of copper in the supernatant solution was determined using standard addition and a series of copper calibration standards.

Table S3.2: Results for Cu(II) sorption studies for **poly-1**, **poly-3**, **Na-poly-3** and **poly-4**.

	Cu:Monomer	Initial [Cu] (ppm)	Final [Cu] (ppm)	Cu removal (%)	Capacity (mg/g)
Poly-1	0.5:1	834	584	30	50.3
	1:1	1670	1106	34	112
Poly-3	0.5:1	678	453	33	45.1
	1:1	1357	842	38	103
Na poly-3	0.5:1	678	77	89	120
	1:1	1357	660	51	139
Poly-4	0.5:1	696	537	23	31.9
	1:1	1392	839	40	111

A 0.5:1 Cu(II)/monomer



B 0.5:1 Cu(II)/monomer

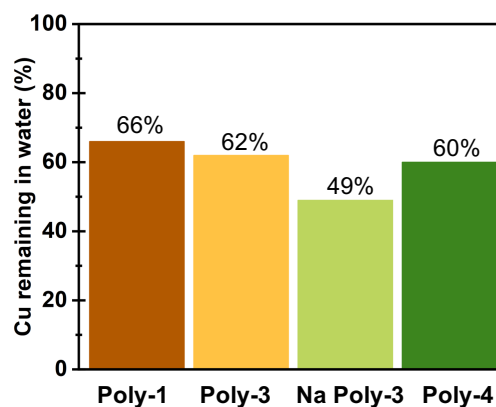


Figure S3.31: Copper sorption graphs after 1 hour, left: 0.5 equivalents of Cu(II) added per monomer within the polymer **poly-1**, **poly-3**, **Na-poly-3** and **poly-4**, right: 1 equivalent of Cu(II) added per monomer within the polymer **poly-1**, **poly-3**, **Na-poly-3** and **poly-4**.

Thermal curing

Poly-4 (250 mg) and a small stir bar were added to a 25 mL flask. The flask was heated to 190 °C. After 6 hours the remaining polymer had a mass of 225 mg (90% recovered polymeric material). This cured polymer was insoluble in chloroform and THF and black in color. A yellow oil was also produced, which collected on the walls of the flask. This material was extracted with hexane and concentrated under reduced pressure. ¹H NMR analysis revealed this material was monomer **4**, generated by thermal depolymerisation (23 mg, 10% isolated yield).

— 7.260 CDCl₃

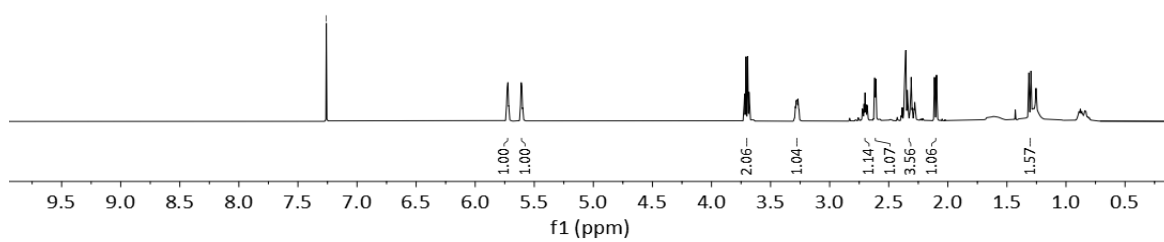
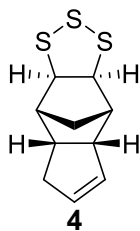


Figure S3.32: ¹H NMR spectrum of monomer **4**, formed by thermal depolymerisation during curing. The monomer was isolated by extraction with hexane.

References

- [1] W. J. Chung, J. J. Griebel, E. T. Kim, H. Yoon, A. G. Simmonds, H. J. Ji, P. T. Dirlam, R. S. Glass, J. J. Wie, N. A. Nguyen, *Nature chemistry* **2013**, *5*, 518-524.
- [2] J. J. Griebel, G. Li, R. S. Glass, K. Char, J. Pyun, *Journal of Polymer Science Part A: Polymer Chemistry* **2015**, *53*, 173-177.
- [3] D. J. Parker, H. A. Jones, S. Petcher, L. Cervini, J. M. Griffin, R. Akhtar, T. Hasell, *Journal of Materials Chemistry A* **2017**, *5*, 11682-11692.
- [4] J. Bao, K. P. Martin, E. Cho, K.-S. Kang, R. S. Glass, V. Coropceanu, J.-L. Bredas, W. O. N. Parker, Jr., J. T. Njardarson, J. Pyun, *Journal of the American Chemical Society* **2023**, *145*, 12386-12397.
- [5] M. Mann, B. Zhang, S. J. Tonkin, C. T. Gibson, Z. Jia, T. Hasell, J. M. Chalker, *Polymer Chemistry* **2022**, *13*, 1320-1327.
- [6] T. Noël, Y. Cao, G. Laudadio, *Accounts of Chemical Research* **2019**, *52*, 2858-2869.
- [7] A. Sulaymon, A. Abbar, *Electrolysis* **2012**, *17*.
- [8] S. C. Perry, C. P. de León, F. C. Walsh, *Journal of The Electrochemical Society* **2020**, *167*, 155525.
- [9] S. Maljuric, W. Jud, C. O. Kappe, D. Cantillo, *Journal of Flow Chemistry* **2020**, *10*, 181-190.
- [10] S. Poulain, S. Julien, E. Duñach, *Tetrahedron letters* **2005**, *46*, 7077-7079.
- [11] S. Inoue, T. Tezuka, S. Oae, *Phosphorus and Sulfur and the Related Elements* **1978**, *4*, 219-221.
- [12] Y. Ren, H. Shui, C. Peng, H. Liu, Y. Hu, *Fluid phase equilibria* **2011**, *312*, 31-36.
- [13] J. Jia, J. Liu, Z.-Q. Wang, T. Liu, P. Yan, X.-Q. Gong, C. Zhao, L. Chen, C. Miao, W. Zhao, *Nature Chemistry* **2022**, *14*, 1249-1257.
- [14] L. J. Esdaile, J. M. Chalker, *Chemistry—A European Journal* **2018**, *24*, 6905-6916.
- [15] M. D. Rao, K. K. Singh, C. A. Morrison, J. B. Love, *RSC advances* **2020**, *10*, 4300-4309.
- [16] N. Ferronato, V. Torretta, *International journal of environmental research and public health* **2019**, *16*, 1060.
- [17] X. Wu, J. A. Smith, S. Petcher, B. Zhang, D. J. Parker, J. M. Griffin, T. Hasell, *Nature communications* **2019**, *10*, 647.
- [18] S. La Brooy, H. Linge, G. Walker, *Minerals Engineering* **1994**, *7*, 1213-1241.
- [19] R. A. Dop, D. R. Neill, T. Hasell, *ACS Applied Materials & Interfaces* **2023**, *15*, 20822-20832.

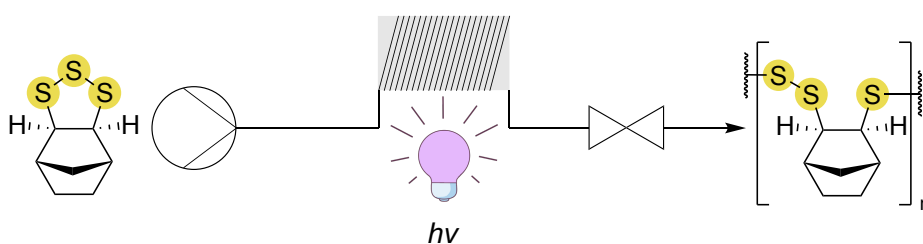
- [20] G. Franci, A. Falanga, S. Galdiero, L. Palomba, M. Rai, G. Morelli, M. Galdiero, *Molecules* **2015**, *20*, 8856-8874.
- [21] W. Zhang, G. Ye, D. Liao, X. Chen, C. Lu, A. Nezamzadeh-Ejehieh, M. S. Khan, J. Liu, Y. Pan, Z. Dai, *Molecules* **2022**, *27*, 7166.
- [22] E. M. Brown, N. B. Bowden, *ACS Omega* **2022**, *7*, 11440-11451.
- [23] T. Ida, T. Sawa, H. Ihara, Y. Tsuchiya, Y. Watanabe, Y. Kumagai, M. Suematsu, H. Motohashi, S. Fujii, T. Matsunaga, *Proceedings of the National Academy of Sciences* **2014**, *111*, 7606-7611.
- [24] G. Deacon, R. Phillips, *Coordination chemistry reviews* **1980**, *33*, 227-250.
- [25] M. L. Eder, C. B. Call, C. L. Jenkins, *ACS Applied Polymer Materials* **2022**, *4*, 1110-1116.
- [26] J. M. Chalker, M. Mann, M. J. Worthington, L. J. Esdaile, *Organic Materials* **2021**, *3*, 362-373.
- [27] F. G. Müller, L. S. Lisboa, J. M. Chalker, *Advanced Sustainable Systems* **2023**, *7*, 2300010.

Chapter 4

Photochemical synthesis of poly(trisulfides) in continuous flow

In this chapter, the photochemical initiated ring-opening polymerisation of 1,2,3-trithiolane monomers was revisited with new methods that featured improved molecular weight control.

Given the need for safe and sustainable methods of polysulfide synthesis, photochemical polymerisation can be carried out under ambient conditions without any chemical additives. By applying a continuous flow photochemical reactor, precise control of poly(trisulfide) molecular weight was achieved. For the first time, high molecular weight poly(trisulfides) were produced using photochemical initiation. Additionally, poly(trisulfide) syntheses in continuous flow offered the potential for upscale production. Photodegradation of poly(trisulfides) demonstrated a new method of polymer recycling. The discovery of photodegradable high sulfur content polymers opens up exciting new applications for this class of materials.



Acknowledgments

Thomas Nicholls and Harshal Patel for help with upscaling and photodegradation experiments

Harshal Patel for synthesising tetrasulfide ($n\text{Pr}_2\text{S}_4$) and Raman analysis

Sam Tonkin for optimised monomer **10** synthesis

Witold Bloch for X-ray crystallography

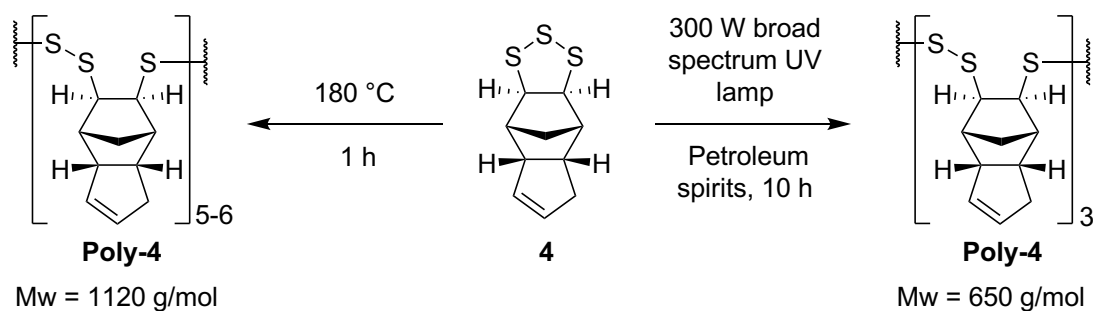
Introduction

With growing interest in sustainable and safe methods of polysulfide synthesis for applications such as gold sorbents^[1] and lenses for infrared thermal imaging,^[2] research in this area continues to expand. Currently, high temperature inverse vulcanisation is the preferred method of polysulfide synthesis due to its operational simplicity and wide comonomer scope, allowing for the production of a large library of polysulfides.^[3] However, the dangers associated with inverse vulcanisation, such as runaway reactions and the production of toxic H_2S gas, make upscaling polysulfide synthesis challenging.^[4-5] Polysulfides are useful in many applications and made from low-cost feedstocks due to the enormous stockpiles of unused elemental sulfur from the petroleum industry.^[6] A key challenge enroute to commercialisation of polysulfides lies in addressing the safety issues associated with their synthesis, which becomes increasingly hazardous at large scales.

One recent method developed by Quan and coworkers is the photochemically initiated polymerisation of sulfur and organic crosslinkers conducted at ambient temperature.^[7-8] This method of polysulfide synthesis avoids the dangers associated with inverse vulcanisation while yielding materials analogous to those produced by the conventional inverse vulcanisation process.^[7] While this new technique is still in its infancy, its use is limited by several key challenges. A major challenge is the scalability of the reaction. The authors demonstrate that in batch reactions on a scale less than 1 gram, the photochemical polymerisation is not homogeneous, with different products formed at different locations in the reaction vessel.^[7] This challenge is likely to be exacerbated as the reaction is scaled up. Another challenge is the production of ill-defined polysulfides with unknown sulfur rank, undefined C–S stereochemistry, and unreacted elemental sulfur. These are challenges commonly encountered when elemental sulfur is directly added during polymerisation, resulting in ill-defined and difficult to process products. In Chapter 2, this challenge was addressed through the polymerisation of well-defined monomers that acted as sulfur carriers, leading to the production of processable poly(trisulfides).

The synthesis of poly(trisulfides) through photochemical ring-opening polymerisation of well-defined 1,2,3-trithiolane monomers was previously reported by Emsley and Griffiths in 1980.^[9]

In this brief study, Emsley and Griffiths initiated the polymerisation of monomer **4** both thermally (180 °C) and photochemically (300 W broad spectrum UV lamp) (Scheme 4.1).^[9]



Scheme 4.1: Photochemical and thermal polymerisation of monomer **4**.^[9]

Research on the thermodynamics of 1,2,3-trithiolane polymerisation conducted by Penczek and co-workers showed that above its ceiling temperature (70 °C), the equilibrium favours the formation of the monomer over the formation of polymeric material.^[10] The ceiling temperature is an important property to understand for polymers as it indicates the temperature in which the rate of polymerisation and depolymerisation are equal. Therefore, it is not surprising that Emsley and Griffiths report low molecular weight material for the thermal polymerisation of **4**.^[9]

The photochemical production of **poly-4** resulted in a polymer molecular weight of 650 g/mol after 10 hours, which is approximately three repeating monomer units (Scheme 4.1). We hypothesised that the light could break S–S bonds in the monomer and polymer product, which could explain the oligomeric products. In contrast, the electrochemical polymerisation of 1,2,3-trithiolane monomers is unique in that the initiation event only occurs at the electrode double layer, allowing for chain growth in solution without further reductive degeneration of the S–S bonds in the polymer backbone. The electrochemical polymerisation of monomer **4** was reported to produce polymers with a weight average molecular weight (M_w) of up to 22000 g/mol.

In this chapter, the photochemical polymerisation of 1,2,3-trithiolanes was revisited to provide a new, rationally-designed process for making these polymers with higher molecular weight. A key aspect was the use of continuous flow processes to photochemically initiate polymerisation and prevent polymer degradation. Photochemical polymerisation of 1,2,3-trithiolanes has many benefits over previous methods. It does not require the addition of chemical initiators which are used in anionic polymerisation and it is conducted under ambient conditions.^[10] Compared to the electrochemical polymerisation of 1,2,3-trithiolanes, photochemical polymerisation could be conducted in a broad range of solvents and does not require costly electrolytes. The photochemical polymerisation of 1,2,3-trithiolanes was explored by first understanding the polymerisation in a batch reactor. Then using a continuous flow process, the controlled production of poly(trisulfides)

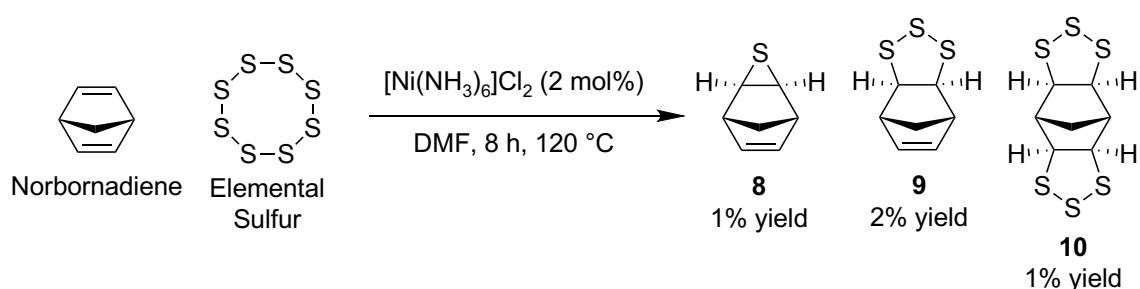
with a broad range of molecular weights was demonstrated. This synthesis was conducted open to atmosphere and allowed the multi-gram production of poly(trisulfides), which is necessary for their use in several applications.

Results and Discussion

Monomer synthesis

Monomers **1** and **4** were synthesised according to the procedure described in Chapter 2. More specifically, the synthesis of *exo*-1,2,3-trithiolane monomers was conducted through the reaction of the strained alkene bond on norbornene derivatives with elemental sulfur at 120 °C in DMF. The reaction was catalysed by the addition of $[\text{Ni}(\text{NH}_3)_6]\text{Cl}_2$ (2 mol%). For monomer **1**, the crude product was purified solely through vacuum distillation instead of column chromatography followed by vacuum distillation. This was a much simpler purification method and reduces the need for excess organic solvents used during column chromatography.

Using analogous reaction conditions monomers **8**, **9**, and **10** were synthesised through the reaction of sulfur and norbornadiene, which contains two reactive alkene bonds (Scheme 4.2). The synthesis resulted in very low yields for all monomers, with most of the product consisting of a polymeric material formed from sulfur and norbornadiene. Further optimisation of the reaction conditions was conducted to increase the yield of monomer **10** from 1% to 9%. The reaction time was increased to 24 hours, and the stoichiometry of the reaction was adjusted to have 6 sulfur atoms per norbornadiene molecule and changing the solvent to a 1:1 ratio of DMF and toluene. Under these optimised reaction conditions, the purification of monomer **10** was performed via recrystallisation.



Scheme 4.2: Reaction of sulfur and norbornadiene forming monomer **8**, **9**, and **10**.

Monomers **9** and **10** were crystalline solids, and their structures were determined unambiguously by single crystal X-ray diffraction (Figure 4.1). The monomers were isolated as the *exo*-isomers in which the C–S bonds have a *cis* relationship on the same face as the bridgehead methylene group. The synthesis of monomer **10** had been previously reported using an exotic sulfur

transfer reagent, S₁₀.^[11] However, this is the first instance the structure of **10** had been reported by single crystal X-ray diffraction.

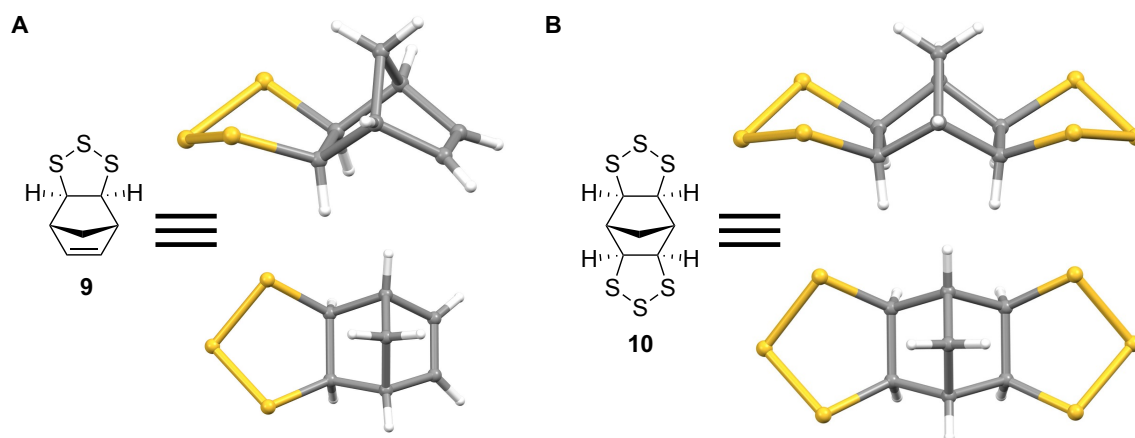
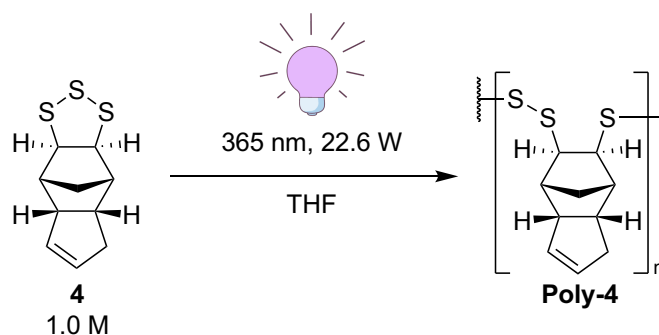


Figure 4.1: (A) X-ray crystal structure of monomer **9**. (B) X-ray crystal structure of monomer **10**.

Photochemical polymerisation in batch

Emsley and Griffiths observed that photochemical polymerisation of monomer **4** by UV irradiation (broad spectrum UV lamp, 300 W) led to the precipitation of low molecular weight oligomers (630 g/mol) from petroleum spirits after 10 hours.^[9] It was hypothesised that this was due to the homolytic cleavage of S–S bonds in the monomer and polymer, causing the polymer to break down as it forms, resulting in high conversion of the monomer and low polymer molecular weight.

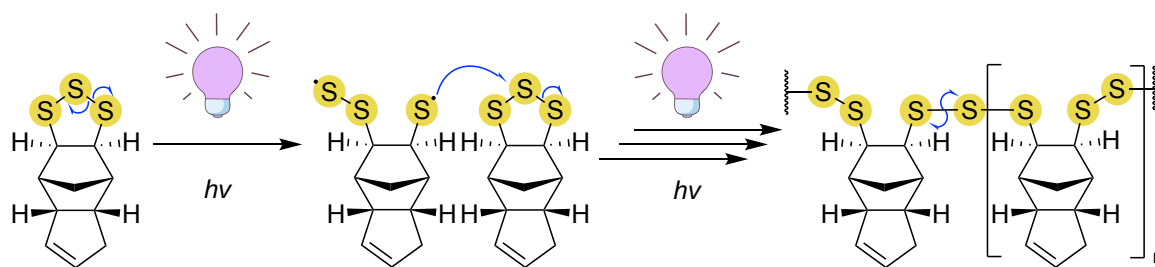
To test this hypothesis, a stock solution of monomer **4** (1.0 M, THF) was irradiated with UV light (365 nm LEDs, 22.6 W). The conversion of the monomer and molecular weight of the polymer was analysed at different time points (Table 4.1). At each time interval, a GC-MS vial containing the monomer solution was removed from the photochemical irradiation, the solvent was evaporated under reduced pressure, and the remaining material was analysed by ¹H NMR spectroscopy (CDCl₃) and GPC (THF).

Table 4.1: Summary of photochemical polymerisation of monomer **4** in batch.

	Time (minutes)	M_w (g/mol)	\mathcal{D}	Conversion (%)
1	3	22800	1.5	6
2	6	16500	2.2	9
3	12	13400	1.7	16
4	24	10800	1.5	26
5	60	5300	1.4	36
6	120	2200	1.2	45

Conversion of monomer **4** was determined by ^1H NMR spectroscopy (CDCl_3) by integrating the monomer proton signal against the polymer. Conversion of the monomer proceeded steadily over the first 24 minutes (entry 1-4). Between 24 and 120 minutes, the rate of monomer conversion decreases, reaching a final conversion of 45% after 2 hours (entry 6). A reduction in the conversion rate was expected as the concentration of the monomer decreases.

GPC analysis at 3 minutes shows a M_w of 22800 and a dispersity (\mathcal{D}) of 1.5 while having a conversion of 6% (entry 1). Subsequent time points show a decrease in M_w as time and conversion increase, with a final M_w of 2200 g/mol at 120 minutes (entry 6). These results clearly show a trend and support the hypothesis that UV irradiation induces polymerisation and also breaks down the polymer chains, resulting in an increased conversion and a decreased molecular weight. These results were also consistent with the low molecular weight (630 g/mol) observed by Emsley and Griffiths for the UV polymerisation of monomer **4** over ten hours.^[9] It is likely that higher molecular weight polymer chains formed initially and then broke down by photochemical scission of the S–S bonds in the polymer as the reaction proceeded (Scheme 4.3).



Scheme 4.3: Proposed polymer chain formation and breakdown during the photochemical polymerisation of 1,2,3-trithiolanes.

A change in reaction colour from yellow (6 minutes) to orange (24 minutes) to pink (120 minutes) was observed during the reaction (Figure 4.2). This observation was not noted in the work by Emsley and Griffiths, who reported the formation of a white precipitate.^[9] It was apparent that the polymer had greater solubility in THF compared to petroleum spirits, which was why it does not precipitate out of solution. It was not clear what caused the change in colour in solution. However, after purification, the polymer appears white.

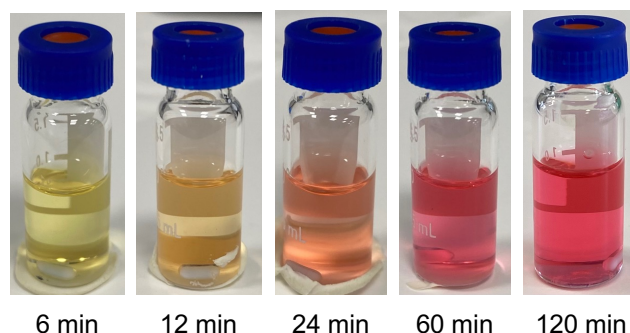
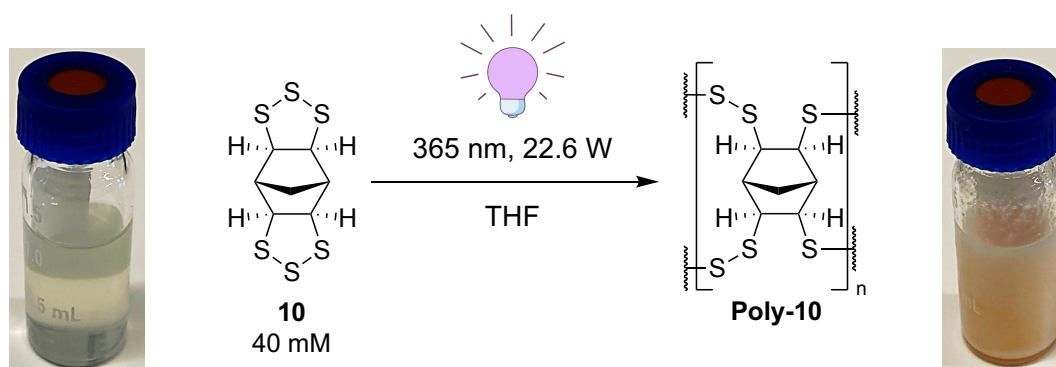


Figure 4.2: Change in reaction solution colour during UV irradiation of monomer **4**.

As a way to generate crosslinked polymers, monomer **10** was investigated, as it consists of two 1,2,3-trithiolane groups. Crosslinking polysulfides leads to greater chemical and thermal stability^[12] and the dynamic S–S bonds in the network can be used to make repairable polymers.^[13] However, one drawback of crosslinked polysulfides is their reduced solubility in organic solvents compared to linear polysulfides making characterisation by solution based methods challenging.^[12, 14] Therefore, it was proposed that monomer **10** could be used in small quantities in a copolymerisation with **4** to provide a crosslinked polysulfide network.

The photochemical polymerisation of pure monomer **10** was first investigated to determine if it could polymerise. Specifically, monomer **10** (40 mM, THF) was irradiated with UV light (365 nm, 22.6 W) for 1 hour. After 1 hour, the solution appeared cloudy, and a precipitate had formed (Scheme 4.4). The solvent was removed under reduced pressure leaving behind an off-white powder which was insoluble in chloroform and THF contrasting with **poly-4** which was soluble in both

solvents. The insolubility of the product supports the hypothesised crosslinked structure of **poly-10**. ^1H NMR spectroscopy (CDCl_3) and GPC (THF) analysis were performed on the product to detect the presence of starting material. Both analysis techniques showed no presence of polymer or monomer **10**, suggesting the production of a highly crosslinked polysulfide. This positive result supported the hypothesis that monomer **10** acts as a crosslinker during photochemical polymerisation.



Scheme 4.4: Photochemical polymerisation of monomer **10** in batch forming a precipitated product.

Next, photochemical copolymerisation of monomer **4** and **10** was investigated as a method to make crosslinked polysulfide networks. Monomer **4** (0.7 M, THF) and monomer **10** were combined in a 10:1 molar ratio and irradiated with UV light (365 nm, 22.6 W). During the reaction, the formation of precipitate was observed, as well as a change in solution colour (Figure 4.3). At each time point a GC-MS vial containing the monomer solution was removed from the UV irradiation, the solvent was removed under reduced pressure and the remaining material was analysed by ^1H NMR spectroscopy (CDCl_3) and GPC (THF).

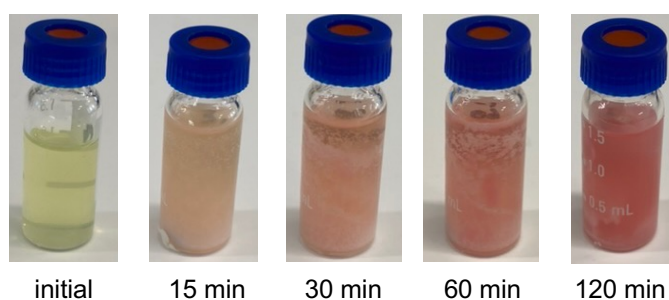
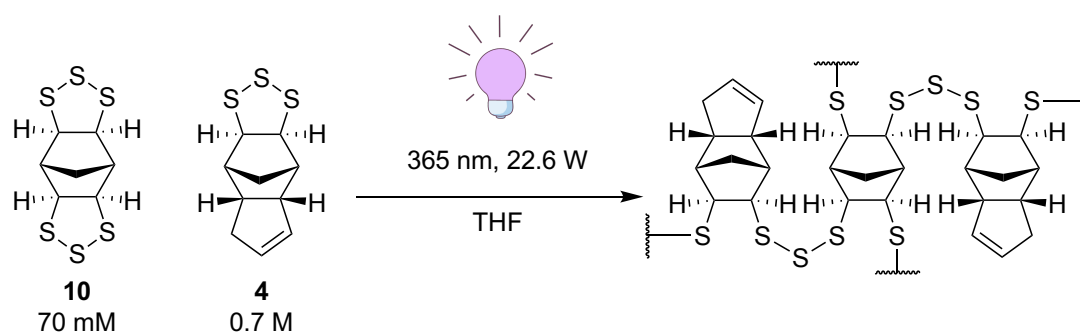


Figure 4.3: Precipitation and change in reaction solution colour during UV irradiation of monomer **4** and **10**, with a 10:1 molar ratio of monomers used in this experiment.

At 120 minutes (Table 4.2, entry 4) the conversion of monomer **4** was 59% which was higher than the conversion of monomer **4** at 120 minutes without the presence of monomer **10** (45%, Table 4.1, entry 6). The M_w drops from 10450 g/mol at 15 minutes (entry 1) to 2600 g/mol at 120 minutes

(entry 4), indicating the breakdown of polymer chains to lower molecular weight species was still occurring. When preparing the crude samples for characterisation, the entire sample was not fully soluble in THF or chloroform. Therefore, characterisation was only performed on the soluble portion, which was likely not crosslinked, explaining why the results were similar to the photochemical polymerisation of monomer **4** in batch without the addition of monomer **10**. The insoluble fraction potentially consists of crosslinked monomer **10** and monomer **4**.

Table 4.2: Summary of photochemical polymerisation of monomer **4** with 10 mol% monomer **10** in batch.



	Time (min)	M_w (g/mol)	\bar{D}	Conversion (%)
1	15	10450	1.9	23
2	30	6800	1.8	33
3	60	4200	1.6	45
4	120	2600	1.4	59

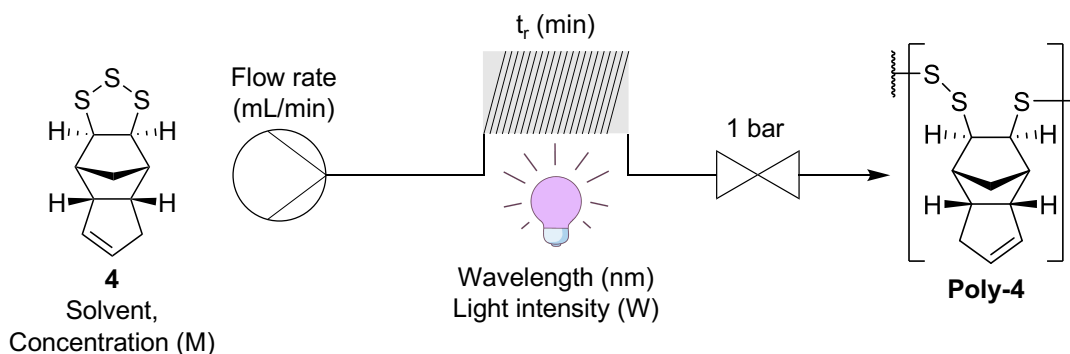
Studies on the structure of the insoluble precipitate have not yet been conducted. However, further characterisation by solid state ^{13}C NMR and degradation studies could be employed to characterise the structure of the insoluble product. These are common methods for characterising the structure of insoluble polysulfides.^[15]

Through the batch photochemical polymerisation of monomer **4**, **poly-4** with a M_w of 22800 g/mol was synthesised at 3 minutes under UV irradiation. However, these long polymer chains were quickly destroyed by the same UV irradiation, leading to smaller oligomeric fragments ($M_w = 2200$ g/mol after 120 minutes). The photochemical polymerisation of monomer **10** was shown to produce an insoluble product, suggesting the formation of a crosslinked polysulfide. The addition of monomer **10** to the photochemical polymerisation of monomer **4** was proposed to generate polysulfide networks by photochemical ring-opening polymerisation. The formation of insoluble product suggests that this may have indeed occurred.

Photochemical polymerisation in continuous flow – monomer 4

By monitoring the photochemical polymerisation of 1,2,3-trithiolane monomers in batch, it was demonstrated that long polymer chains ($M_w > 20,000$ g/mol) form. However, the challenge with photochemical polymerisation in batch was that the UV irradiation also causes the breakdown of long polymer chains into small polymer fragments, presumably via the photolysis of the S–S bonds in the polymer.

Using a continuous flow photochemical reactor, the residence time of the solution within the reactor can be controlled, and also the amount of time the solution was exposed to light irradiation. It was hypothesised that with this control, the molecular weight can be subsequently controlled and tuned. Specifically, it was thought that the light could initiate ring-opening polymerisation by cleavage of the S–S bond in the monomer. The polymer, as it is formed, is then pumped through the reactor into a collection vessel. This way, the irradiation time of the polymer was predicted to be reduced in comparison to batch and therefore minimise polymer degradation. To investigate this hypothesis, monomer **4** was subjected to photochemical polymerisation in a continuous flow photochemical reactor (Scheme 4.5). Other variables were also investigated, including wavelength, solvent, light intensity, temperature, and concentration. After each reaction, the crude product was concentrated under reduced pressure and analysed by ^1H NMR spectroscopy (CDCl_3) and GPC (THF). Integration of the monomer proton signals against the polymer was used to determine monomer conversion.



Scheme 4.5: Photochemical polymerisation of monomer **4** in continuous flow.

Wavelength

The first variable investigated was the wavelength of light used to irradiate the monomer and induce ring-opening polymerisation. UV-vis analysis of monomer **4** shows a strong absorption band between 200 nm and 400 nm (Figure 4.4). It was therefore hypothesised that irradiation within this range would lead to high reactivity.

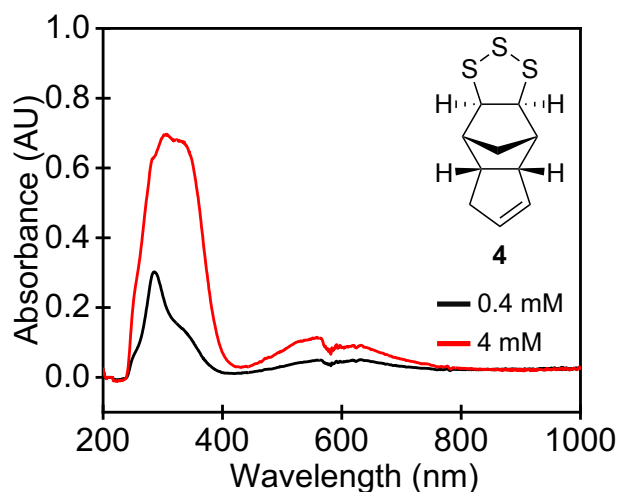


Figure 4.4: UV-vis spectra of monomer **4** (0.4 mM and 4 mM, THF).

Monomer **4** (5 mL, 0.10 M, toluene) was passed through a photochemical reactor and irradiated with LEDs (365 nm, 226 W or 455 nm, 100 W) at 21 °C. The reaction solution was passed through at a flow rate of 4 mL/min, resulting in a residence time of 2.5 minutes. As a control, the stock solution was also passed through the photochemical reactor without irradiation.

The control confirmed that no reaction was occurring in the photoreactor without irradiation, as evidenced by ^1H NMR and GPC analysis. Irradiation at 365 nm resulted in a monomer conversion of 76%, while irradiation at 455 nm resulted in a monomer conversion of 16%. These results were consistent with the UV-vis spectrum of monomer **4** which shows greater absorption at 365 nm compared to 455 nm (Figure 4.4). GPC analysis of the solution irradiated at 365 nm shows a M_w of 1300 g/mol, while the solution irradiated at 455 nm had a M_w of 11600 g/mol (Figure 4.5). It was likely that the high absorbance at 365 nm, coupled with the high power used, resulted in the formation of longer polymer chains which were rapidly broken down into smaller fragments. This in turn resulted in a high conversion of monomer and production of low molecular weight polymers. In contrast, the low absorbance at 455 nm resulted in low conversion and the formation of higher molecular weight polymers.

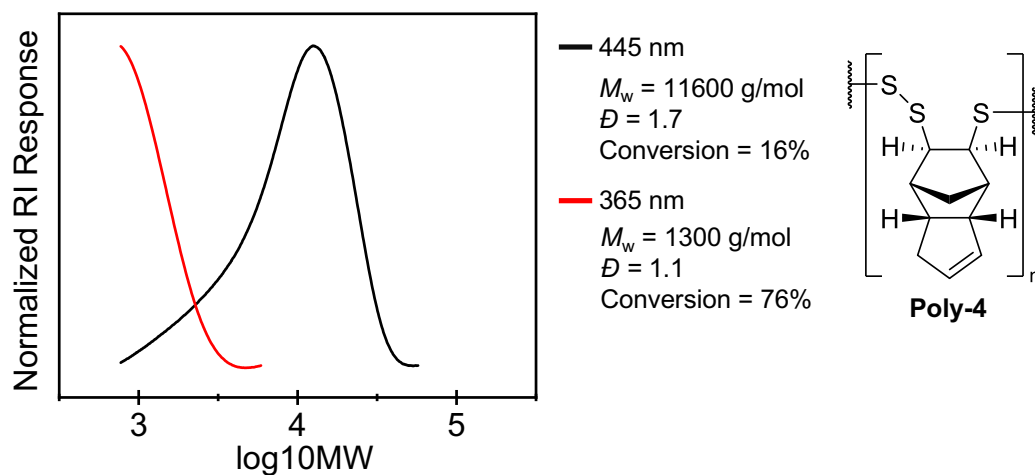


Figure 4.5: GPC (THF) of **poly-4** produced using different wavelengths of light.

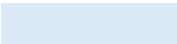
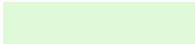
Solvent

In comparison to the electrochemical polymerisation of 1,2,3-trithiolanes, the photochemical polymerisation can tolerate a greater range of solvents. This was because the solvent used in electrochemical polymerisation must be stable under the electrochemical conditions applied to the reaction, limiting the choice of solvent. Acetonitrile was used as the solvent in the electrochemical polymerisation of 1,2,3-trithiolanes due to its electrochemical stability at a wide range of potentials. However, the polymer had low solubility in acetonitrile, causing it to precipitate from solution, thereby limiting its chain growth and molecular weight. In the following photochemical polymerisation experiments, a library of solvents with varying poly(trisulfide) solubility was explored.

For each reaction, a stock solution of monomer **4** (0.04 M) was prepared in the following solvents: chloroform, ethyl acetate, hexane, tetrahydrofuran, acetone, toluene, 2-propanol, dichloromethane, methanol, dimethylformamide, acetonitrile and diethyl ether (Table 4.3). The concentration was selected to match that used in the electrochemical polymerisation of 1,2,3-trithiolanes for comparison purposes. For each reaction, the stock solution of monomer **4** (3 mL) was passed through a photochemical reactor and irradiated with 365 nm LEDs (226 W, 21 °C) at a flow rate of 4 mL/min, resulting in a residence time of 2.5 minutes.

Table 4.3: Photochemical polymerisation of monomer **4** in different solvents.

	Solvent	M_w (g/mol)	\bar{D}	Conversion (%)
1	Hexane	1800	1.2	71
2	2-Propanol	1200	1.1	80
3	Methanol	2000	1.3	80
4	Acetonitrile	2500	1.5	83
5	Diethyl Ether	1500	1.2	78
6	Ethyl Acetate	1300	1.1	80
7	Acetone	1300	1.1	44
8	Dimethylformamide (DMF)	1400	1.1	63
9	Toluene	1400	1.1	67
10	Dichloromethane	1700	1.2	70
11	Tetrahydrofuran	1500	1.1	71
12	Chloroform	1800	1.2	71

 Low solubility  High solubility

All solvents resulted in a moderate to high conversion, with the lowest monomer conversion of 44% from acetone (entry 7). Also, all solvents resulted in low molecular weight oligomeric material, with the highest M_w of 2500 g/mol from the reaction in acetonitrile (entry 4). The molecular weight of **poly-4** produced via electrochemical polymerisation results in a M_w of around 4500 g/mol at a concentration of 0.04 M. The lower molecular weight reported from the photochemical reactions was likely due to the exposure of the polymer product to the high intensity UV irradiation, which was hypothesised to cause breakdown of the S–S bonds in the polymer product. In the electrochemical polymerisation, the polymer was protected from further S–S bond reduction in the backbone, as the site of reaction was localised to the electrode double layer. When the monomer was first reduced at the electrode double layer, it diffuses away, allowing for chain growth before precipitation. In contrast, the polymer in the photoreactor was continuously exposed to UV irradiation.

The following solvents: hexane, 2-propanol, methanol, acetonitrile, diethyl ether, ethyl acetate, acetone and DMF, exhibited medium to low solubility for **poly-4** (entry 1-8). Therefore, the polymer precipitates out of solution as it passes through the photochemical reactor. Precipitation of the polymer out of solution can lead to blockages in the flow tubing and limits the potential molecular weight of the polymer. For toluene, dichloromethane, THF and chloroform, the polymer remained fully soluble (entry 9-12). Using these solvents for further optimisation would allow for the production of higher molecular weight polymers. Additionally, high-concentration monomer solutions can be easily prepared. For the following reactions, THF was selected as the solvent

because it resulted in the highest monomer conversion of 71% compared to the other solubilising solvents (entry 11).

Light intensity

The wavelength and solvent optimisation experiments were conducted using a high power (226 W) in the photochemical flow reactor. This resulted in high conversion but low molecular weight. It was hypothesised that the strong light intensity applied to the reaction caused the breakdown of formed polymer chains, resulting in a low molecular weight product. Therefore, it was proposed that lowering the light intensity would lead to the production of higher molecular weight polymers. It was also hypothesised that lowering the light intensity would lead to a decrease in monomer conversion. To compensate for this, the flow rate of the reaction was decreased to increase the residence time.

To test these hypotheses, a stock solution of monomer **4** (1.0 M) in THF (10 mL) was prepared. For each reaction, 2 mL of the stock solution was passed through a photochemical reactor and irradiated with 365 nm LEDs (226 W, 113 W or 22.6 W, 21 °C). The reaction solution was passed through at a flow rate of 0.5 mL/min, resulting in a residence time of 20 minutes. GPC analysis showed that the first hypothesis was supported: lower irradiation power leads to higher molecular weight polymers (Figure 4.6). Irradiation at 226 W with a residence time of 20 minutes resulted in an oligomeric product that was too low in molecular weight to be detected by GPC. At 113 W the M_w was 1400 g/mol and at 22.6 W the M_w was 3000 g/mol (Figure 4.6).

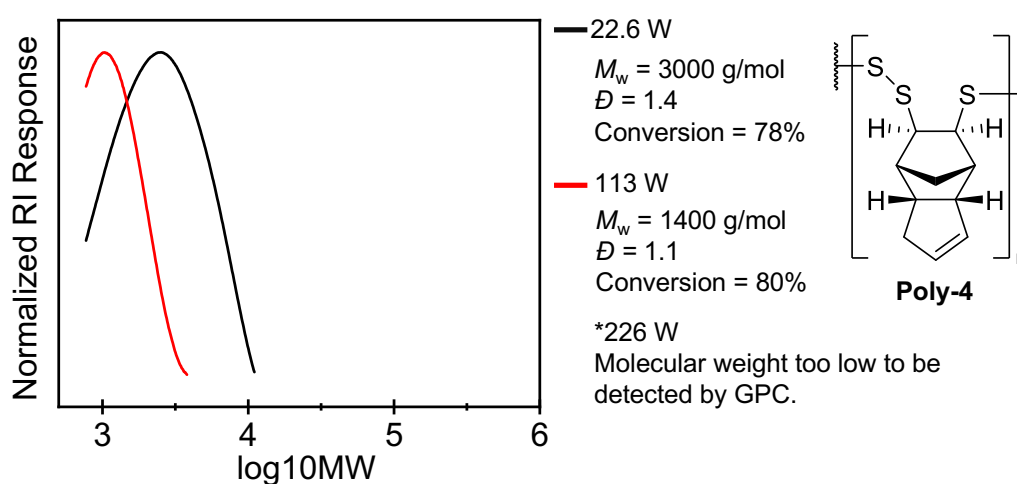


Figure 4.6: GPC (THF) of **poly-4** produced under different intensities of UV irradiation.

There was no significant difference in the monomer conversion for the reactions conducted at 22.6 W and 113 W (Figure 4.6). This indicates a similar amount of monomer converted by the UV irradiation, but fewer of the S-S bonds in the backbone of the polymer were broken down due

to the lower intensity UV irradiation. Therefore, the increase in residence time was not necessary to account for the difference in light intensity. However, increasing the residence time does lead to further breakdown in the polymer chains resulting in a lower molecular weight while only increasing monomer conversion slightly. For the following reactions, a light intensity of 22.6 W was used as it results in higher molecular weight polymers and does not significantly affect monomer conversion.

Temperature

Next, the effect of temperature on the photochemical polymerisation was investigated. The temperature range was controlled by the Polar Bear Plus FlowTM temperature control system, and the volatility of the solvents had to be considered. Therefore, temperatures of 60 °C and -13 °C were selected and compared to the reaction at ambient temperature (21 °C). It was hypothesised that higher temperatures would result in more rapid propagation.

A stock solution of monomer **4** (1.0 M) in THF (10 mL) was prepared. For each reaction, 2 mL of the stock solution was passed through a photochemical reactor and irradiated with 365 nm LEDs (22.6 W). The reaction solution was passed through at a flow rate of 0.5 mL/min, resulting in a residence time of 20 minutes. Contrary to the hypothesis, the greatest monomer conversion was observed at -13 °C (80%), followed by 21 °C (78%), and then 60 °C (52%) (Figure 4.7). GPC results also showed that the reaction at -13 °C produced the highest molecular weight, followed by 21 °C, with 60 °C producing the lowest molecular weight (Figure 4.7).

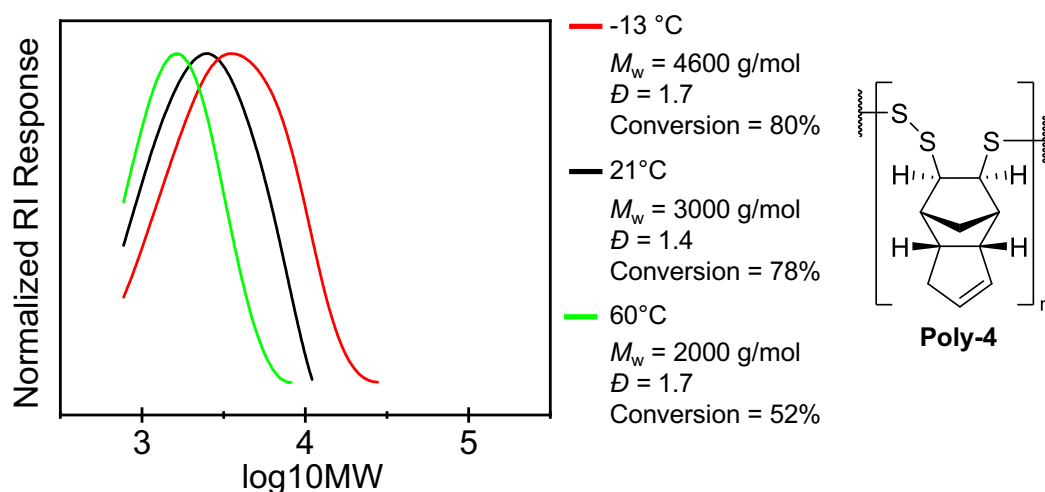


Figure 4.7: GPC (THF) of **poly-4** produced at different temperatures.

The results showed the opposite trend from the previous reactions, where higher conversion typically led to a lower molecular weight. Therefore, at lower temperatures, higher conversion was achieved along with the highest molecular weight. Based on these results, it was proposed that the

increase in temperature favours depolymerisation and formation of the monomer. Although the reaction at -13 °C produced the highest conversion and molecular weight, it requires significant energy to cool the photochemical reactor to such a low temperature. Consequently, subsequent reactions were conducted at 21 °C.

Concentration

The effect of monomer concentration was investigated next. Monomer **4** exhibits high solubility in THF, allowing for the preparation of stable solutions up to 2.0 M. It was hypothesised that increasing the monomer concentration would result in higher molecular weights due to the greater availability of monomer for chain growth. Conversely, it was expected that monomer conversion would decrease with increasing concentration.

A range of stock solutions of monomer **4** in THF were prepared: 0.1 M, 0.5 M, 1.0 M, 1.5 M, and 2 M. Each stock solution (10 mL) was passed through a photochemical reactor illuminated with 365 nm LEDs (22.6 W, 21 °C) at a flow rate of 4 mL/min, resulting in a residence time of 2.5 minutes. Increasing the monomer concentration from 0.1 M to 0.5 M resulted in a M_w increase from 2600 g/mol to 9600 g/mol (Table 4.4). This demonstrates that higher concentrations led to an increase in molecular weight. From 0.5 M to 1.0 M, there was another significant increase in M_w from 9600 g/mol to 13900 g/mol (Table 4.4). However, at concentrations of 1.0 M, 1.5 M, and 2 M, there was little change in the GPC trace, indicating that the relationship between concentration and molecular weight had reached a limit (Table 4.4). Therefore, a concentration of 1.0 M was selected for subsequent reactions.

Table 4.4: Photochemical polymerisation of monomer **4** at different concentrations.

	Concentration (M)	M_w (g/mol)	\bar{D}	Conversion (%)
1	0.1	2600	1.4	58
2	0.5	9600	1.9	52
3	1.0	13900	1.9	28
4	1.5	15600	1.5	26
5	2.0	14300	1.6	23

Flow rate

The last variable of interest was the flow rate. It was hypothesised that a faster flow rate would lead to higher molecular weight polymers. The rationale behind this hypothesis was that

reduced exposure to UV irradiation decreases the likelihood of polymer breakdown, with the goal of having just enough light to initiate polymerisation.

Using a 1.0 M solution of monomer **4** in THF, 2 mL was passed through a photochemical reactor and irradiated with 365 nm LEDs (22.6 W, 21 °C) at different flow rates (0.5 mL/min, 1.0 mL/min, 2 mL/min, 4 mL/min, and 6 mL/min). The GPC traces for these reactions shows a clear correlation between flow rate and molecular weight (Figure 4.8).

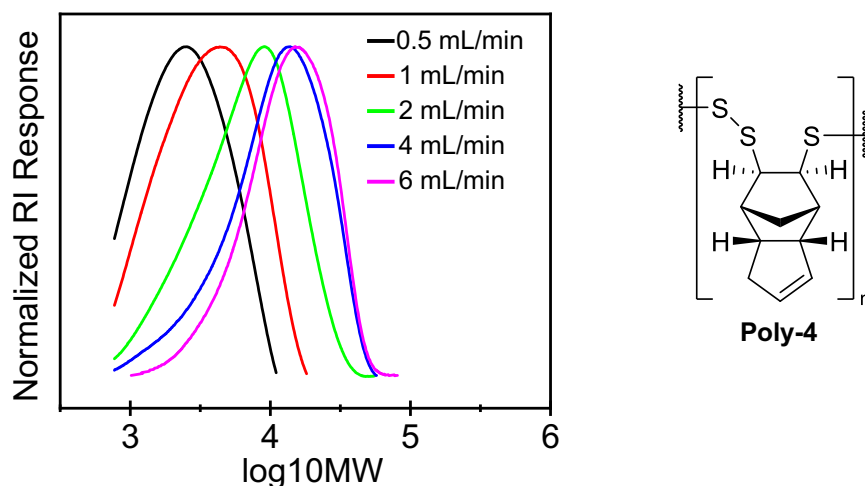


Figure 4.8: GPC (THF) of **poly-4** produced at different flow rates.

At 0.5 mL/min, the solution had a residence time of 20 minutes, leading to a low M_w of 3000 g/mol and a conversion of 78% (Table 4.5, entry 1). As the flow rate was increased, the residence time decreases, resulting in reduced UV irradiation, a higher molecular weight, and lower conversion. At 6 mL/min, the solution had a short residence time of 1.6 minutes, leading to a high M_w of 15900 g/mol and a conversion of 32% (Table 4.5, entry 5).

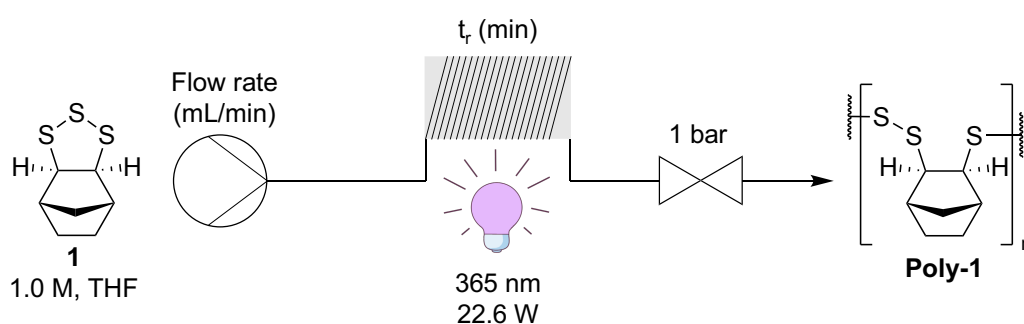
Table 4.5: Photochemical polymerisation of monomer **4** at different flow rates.

	Flow rate (mL/min)	Residence time (min)	M_w (g/mol)	\bar{D}	Conversion (%)
1	0.5	20	3000	1.4	78
2	1	10	4500	1.6	65
3	2	5	8700	1.8	59
4	4	2.5	13900	1.9	28
5	6	1.6	15900	1.8	32

These experiments demonstrate clear control over the molecular weight of the polymers. However, the drawback of synthesising high molecular weight polymers was the lower conversion values. It was important to note that low conversion does not imply a loss of monomer. Therefore, for reactions with low conversion, the monomer can be isolated and reacted again to produce more polymer. Strategies to achieve this are discussed in the poly(trisulfide) preparation section below.

Photochemical polymerisation in continuous flow – monomer 1

Photochemical polymerisation of monomer **1** was then investigated in continuous flow (Scheme 4.6). It was hypothesised that monomer **1** would perform similarly to monomer **4**. The effect of monomer concentration and flow rate was investigated, as these variables had the most significant impact on the polymer molecular weight in the studies of **poly-4**.



Scheme 4.6: Photochemical polymerisation of monomer **1** in continuous flow.

Concentration

The effect of concentration was first investigated, with monomer **1** having greater solubility in THF compared to monomer **4**. A range of stock solutions of monomer **1** in THF were prepared (1.0 M, 3.8 M, and 5.0 M). Each stock solution (2 mL) was passed through a photochemical reactor and irradiated with 365 nm LEDs (22.6 W, 21 °C) at 6 mL/min, resulting in a residence time of 1.6 minutes. As anticipated, increasing the monomer concentration from 1.0 M to 3.8 M resulted in a change of M_w from 11500 g/mol to 16500 g/mol (Figure 4.9). However, at the concentration of 5.0 M the M_w decreased to 13060 g/mol. This indicated that a limit had been reached where increasing the monomer concentration no longer led to increased molecular weight.

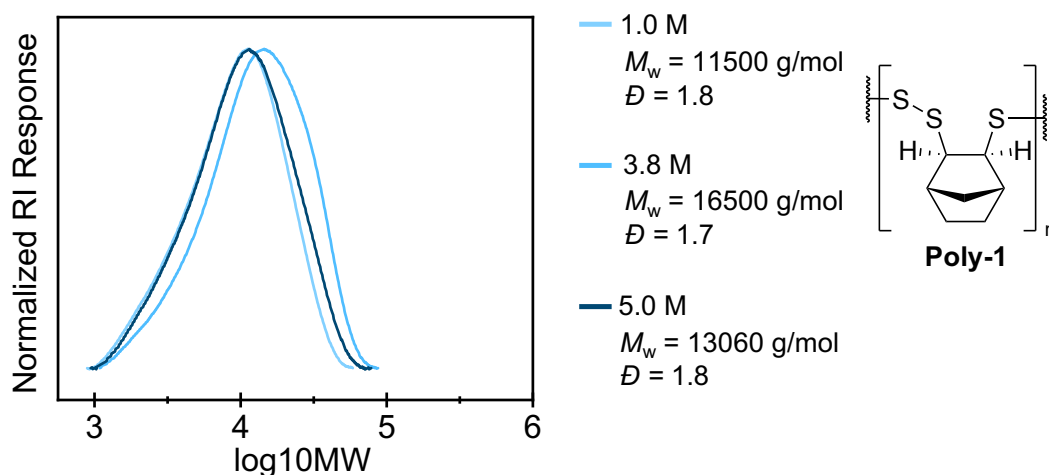


Figure 4.9: GPC (THF) of **poly-1** produced at different concentrations.

Flow rate

Next, the effect of flow rate was investigated on the photochemical polymerisation of monomer **1**. For each flow rate, 10 mL of monomer **1** (1.0 M, THF) was passed through a photochemical reactor and irradiated with 365 nm LEDs (22.6 W, 21 °C) at different flow rates (1 mL/min, 4 mL/min, and 10 mL/min.). The GPC of the crude solutions shows an increase in molecular weight as the flow rate increases, with a M_w of 1700 g/mol at 1 mL/min, 4800 g/mol at 4 mL/min, and 13800 g/mol at 10 mL/min (Figure 4.10). These results were consistent with the trends observed for the photochemical polymerisation of monomer **4**.

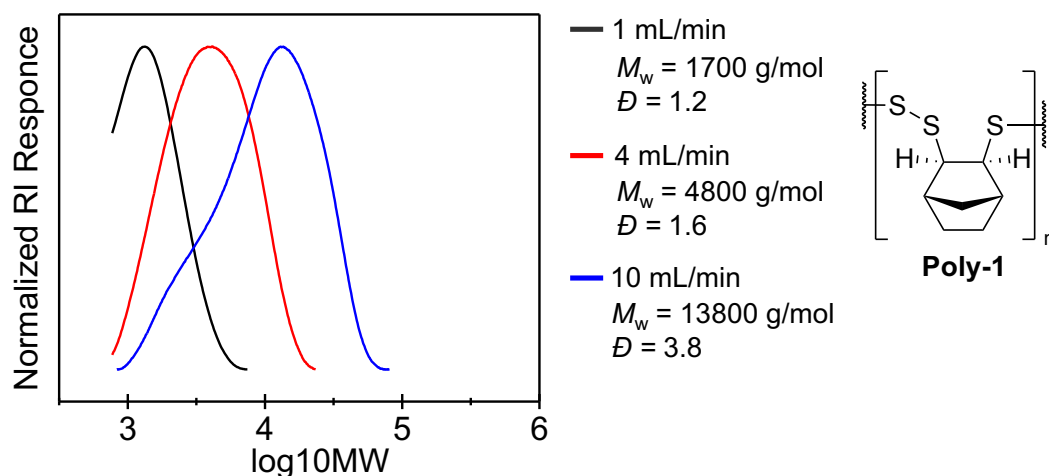


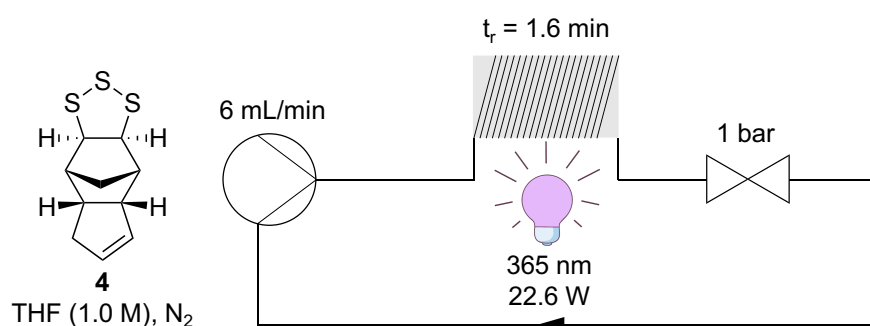
Figure 4.10: GPC (THF) of **poly-1** produced at different flow rates.

Recirculation under an inert atmosphere

The initiation event for the photochemical ring-opening polymerisation of 1,2,3-trithiolanes differs from the previously studied electrochemical initiation in Chapter 2, suggesting different

polymerisation mechanism and kinetics. In order to understand the mechanism and kinetics for the photochemical polymerisation, several experimental studies have been conducted.

First, a recirculation experiment was conducted under an inert atmosphere. In this experiment, the reaction solution passes through the flow tubing, entering and exiting the photochemical reactor multiple times during the reaction time (Scheme 4.7). This setup exposes the solution to intermittent UV irradiation while it was circulated through the system. The reaction was conducted under an inert atmosphere to prevent the possible oxidation of the polymer chain end groups. It was hypothesised the on/off effect of the UV irradiation would allow for the high conversion of monomer while minimizing the photodegradation of the formed polymer chains.



Scheme 4.7: Recirculation of continuous flow photochemical polymerisation of monomer 4.

A solution of monomer 4 (1.0 M, THF, 20 mL) was prepared and purged with nitrogen for 5 minutes. A stir bar and the monomer solution were transferred to a 2-neck round bottom flask under a nitrogen atmosphere. One neck was blocked with a rubber septum, while the other neck contained the inlet tube and was sealed. The flow tubing (previously filled with anhydrous THF) were loaded with the monomer solution until the solution reached the outlet. The outlet tube was then transferred to the second neck on the round bottom flask and resealed, ensuring no dilution by THF from the system. The solution was then passed through the photochemical reactor and irradiated with 365 nm LEDs (22.6 W, 21 °C) at a flow rate of 6 mL/min. An aliquot (0.1 mL) of the recirculating solution was taken at 3, 6, 9, 12, 16, 24, 48, 85 and 125 minutes, concentrated under reduced pressure and analysed by ¹H NMR spectroscopy (CDCl₃) and GPC (THF) to determine monomer conversion, *M_w* and *D* (Table 4.6).

Table 4.6: Summary of results from recirculated polymerisation of monomer 4.

	Time (minutes)	M_w (g/mol)	\bar{D}	Conversion (%)
1	3	13200	1.7	18
2	6	10900	1.8	32
3	9	9100	1.8	46
4	12	8000	1.8	57
5	16	6100	1.7	67
6	24	4400	1.6	68
7	48	2600	1.4	72
8	85	1800	1.2	73
9	125	1300	1.1	81
10	Purified	1500	1.1	-

At 3 minutes, the conversion of monomer 4 was 18%, with a M_w of 13200 g/mol (Table 4.6, entry 1). Within the first 12 minutes, the conversion rapidly increases to 57% with a M_w 8000 g/mol (Figure 4.11 A). However, between 16 minutes to 125 minutes, the rate of conversion dropped, and the molecular weight continued to decline, reaching 1300 g/mol at 125 minutes at a conversion of 81% (Table 4.6, entry 9). This clearly indicates that the recirculation of the solution through the photochemical reactor causes the continued breakdown of the polymer chains as shown by the GPC trace (Figure 4.11 B). This was consistent with the findings when the reaction was run in batch, where continued exposure to UV irradiation led to the formation and breakdown of polymer chains and increased monomer conversion. Therefore, intermittent light irradiation at this rate does not significantly decrease the photodegradation of the polymer chains. With that said, the results in Figure 4.11 B clearly indicate that **poly-4** can be photochemically degraded. This opens up the potential for new applications where polymer degradation is triggered by light.

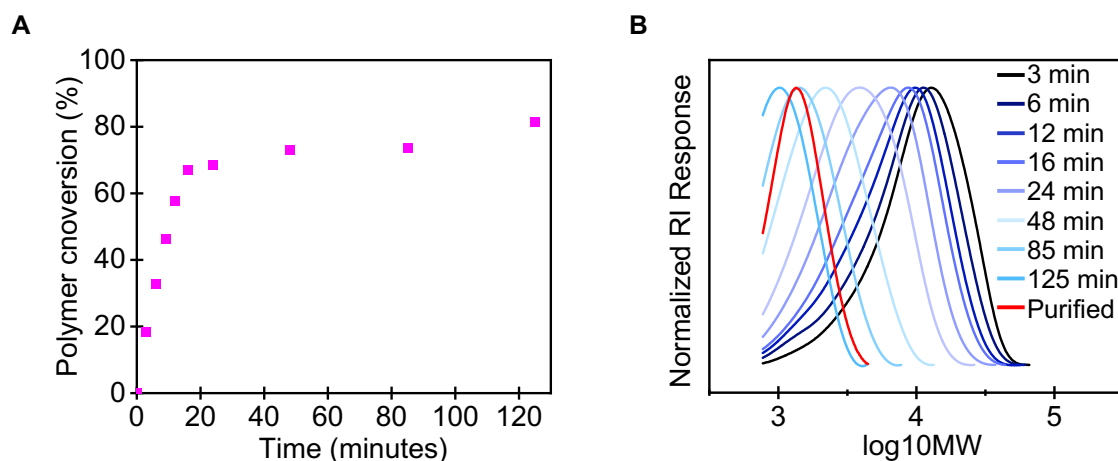
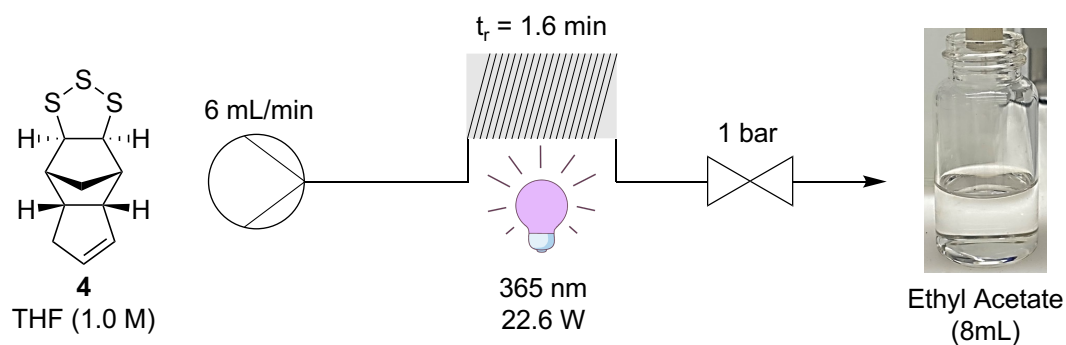


Figure 4.11: (A) Polymer conversion over time during the recirculation experiment. (B) GPC (THF) taken at each time point.

Future experiments are focussed on reactor designs that allow for the precipitation of the polymer product and then re-circulation of unreacted monomer through the photochemical reactor. In this way, the polymer product is isolated and not resubjected to irradiation that will break its S–S bonds. Relatedly, batch reactions are also underway to test if the polymerisation can be done with pulsed light and in solvents that dissolve the monomer but not the polymer product. Here, the goal is to initiate polymerisation and then have the product precipitate, so it is then protected from photochemical breakdown. The light pulses will be designed to operate at the frequencies so that irradiation causes initiation of the monomer and then polymer growth and precipitation occur in the absence of irradiation.

Direct precipitation of polymer after UV-irradiation

Next, direct precipitation of the polymer after UV irradiation was investigated to determine if there was a change in polymer molecular weight compared to a sample that was not precipitated directly. The purpose of this experiment was to understand if the polymerisation is living after it had exited the photochemical reactor. To precipitate the polymer directly, a 20 mL vial containing ethyl acetate (8 mL) was positioned at the outlet (Scheme 4.8). When the irradiated solution exits the flow tubing, it will go directly into the ethyl acetate and precipitate. It was proposed that this direct precipitation of the potentially living polymer solution would terminate polymerisation, and therefore have an effect on the molecular weight and \bar{D} .



Scheme 4.8: Direct precipitation of **poly-4** after UV irradiation.

A solution of monomer **4** (1.0 M, THF, 8 mL) was passed through the photochemical reactor and irradiated with 365 nm LEDs (22.6 W, 21 °C) at a flow rate of 6 mL/min, resulting in a residence time of 1.6 minutes. As the irradiated solution exited the outlet tubing into ethyl acetate, it instantly formed a cloudy precipitate. The precipitated polymer was filtered and washed with ethyl acetate (3 x 10 mL), then collected and dried under reduced pressure (296 mg, 16%). The polymer was analysed by ^1H NMR spectroscopy (CDCl_3) and GPC (THF).

GPC analysis of the precipitate showed a M_w of 12300 g/mol and a \mathcal{D} of 1.7 (Figure 4.12). Compared to polymerisation of monomer **4** under the same reaction conditions without precipitation in the collection vessel, the difference in molecular weight was not significant (Figure 4.12).

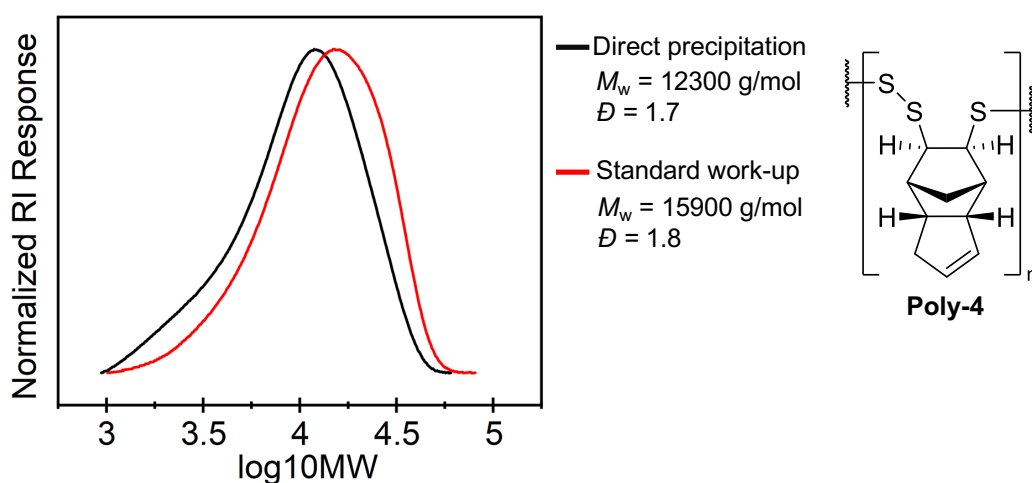
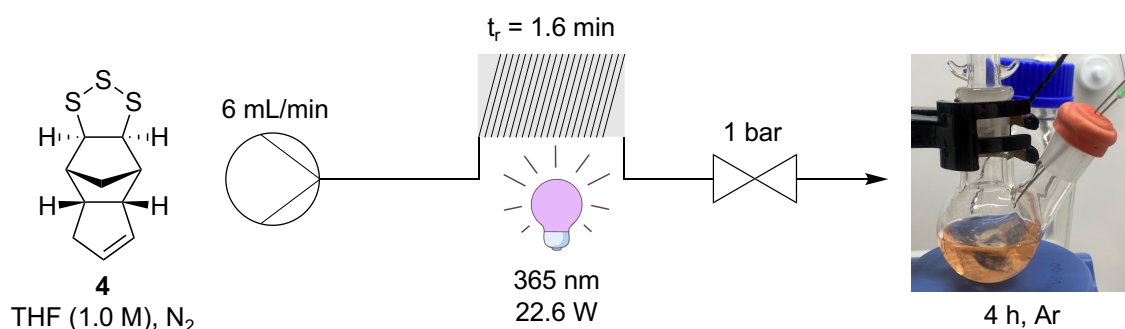


Figure 4.12: GPC (THF) of **poly-4** directly precipitated after UV irradiation in continuous flow and **poly-4** subjected to the standard work-up procedure after UV irradiation in continuous flow.

Reactivity of poly-4 after UV irradiation under an inert atmosphere

The next experiment conducted was to further investigate the activity of the polymer as it exits the flow reactor. To do this, the reaction was kept under an inert atmosphere and collected in a separate vessel as it exits the flow reactor after irradiation (Scheme 4.9). The solution was then maintained under an inert atmosphere and investigated for changes in conversion and molecular weight over time. It was hypothesised that if the polymerisation was living, changes in conversion and molecular weight will occur as the reaction solution is kept under an inert atmosphere.



Scheme 4.9: Collection of UV irradiated monomer 4 under an inert atmosphere.

A solution of monomer 4 (1.0 M, THF, 8 mL) was purged with nitrogen for 5 minutes and then passed through the photochemical reactor and irradiated with 365 nm LEDs (22.6 W, 21 °C) at a flow rate of 6 mL/min, resulting in a residence time of 1.6 minutes. The outlet was connected to a 2-neck round bottom flask containing a stir bar. The other neck was stopped with a rubber septum containing an argon stream and a vent. After the mixture had completely passed into the round bottom flask, aliquots (0.1 mL) were taken at 3, 9, 24 and 240 minutes through the rubber septum, concentrated under reduced pressure, and analysed by ¹H NMR spectroscopy (CDCl₃) and GPC (THF).

GPC analysis of the irradiated solution under inert atmosphere shows no change in molecular weight over the 4-hour period (Figure 4.13). ¹H NMR spectroscopy of the solution also showed no change in monomer conversion over the 4 hours. These results support the theory that the reaction is not living as it exits the flow reactor. This indicates that the termination event is rapid even under an inert atmosphere. Overall, these experiments suggest a mechanism that involves photochemical initiation, rapid polymerisation, and termination in the flow reactor.

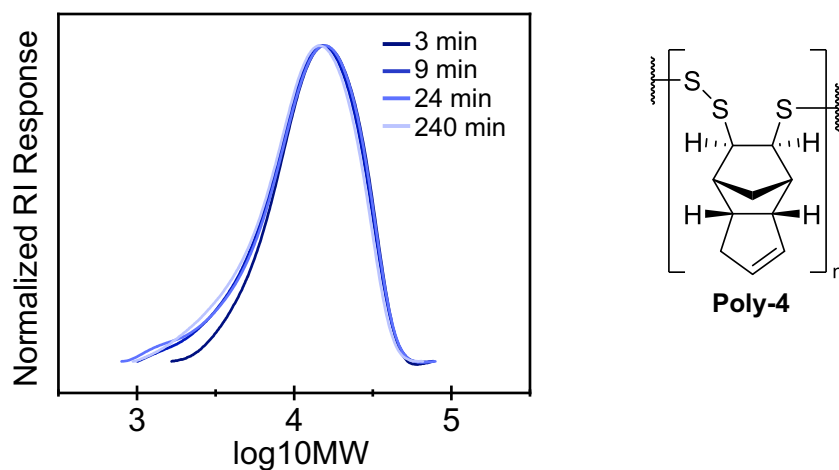
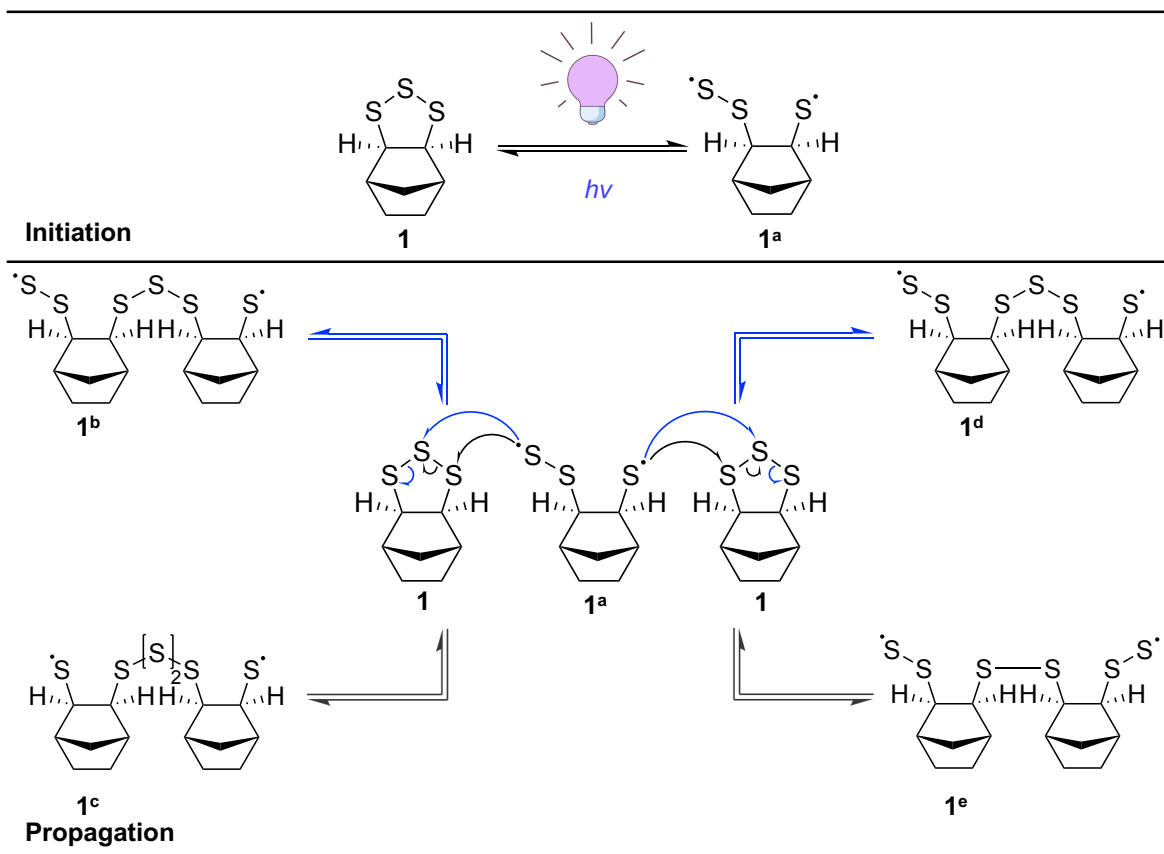


Figure 4.13: GPC of aliquots taken over 4 hours.

Proposed mechanism and structure

We propose the UV initiated polymerisation of 1,2,3-trithiolane monomers proceeded via radical ring-opening polymerisation. Homolytic cleavage of S–S bonds occurs through UV irradiation, leading to thiyl radicals.^[7] Therefore, it was proposed that the ring-opening of monomer **1** will form the diradical species **1^a**, which could then propagate through four pathways: disulfide radical attack on a monomer at the centre or terminal sulfur atom, or monosulfide radical attack on a monomer at the centre or terminal sulfur atom (Scheme 4.10). Without computational studies on the energy barriers for each pathway, the most likely pathway could not be determined. Based on degradation studies conducted on **poly-4**, the C–S bond stereochemistry remained intact, indicating no C–S bond cleavage occurred during UV polymerisation.



Scheme 4.10: Proposed initiation and propagation of 1,2,3-trithiolane monomer **1**.

Recent work by the Hassel group has demonstrated that Raman spectroscopy can be used to distinguish sulfur ranks.^[16] Therefore, Raman spectroscopy was conducted on **poly-1**, as well as monomer **1**, $n\text{Pr}_2\text{S}_2$, $n\text{Pr}_2\text{S}_3$, and $n\text{Pr}_2\text{S}_4$ (Figure 4.14). Subtle differences in the S–S signals of monomer **1**, $n\text{Pr}_2\text{S}_2$, $n\text{Pr}_2\text{S}_3$, and $n\text{Pr}_2\text{S}_4$ were used as references. Monomer **1** and $n\text{Pr}_2\text{S}_3$ both contain trisulfide groups; however, the cyclic trisulfide (monomer **1**) has two signals in the S–S region at 475 cm^{-1} and 512 cm^{-1} , while the linear trisulfide ($n\text{Pr}_2\text{S}_3$) has one signal in the S–S region at 488 cm^{-1} . The spectrum of **poly-1** shows one signal, which is consistent with its proposed linear structure. Although the signal at 491 cm^{-1} for **poly-1** is broad, its shift is consistent with that of a linear trisulfide bond. Shoulders on the peak at 491 cm^{-1} indicate the presence of minor amounts of disulfide or tetrasulfide linkages; however, the major signal suggest the polymer primarily has repeating units of three sulfur atoms.

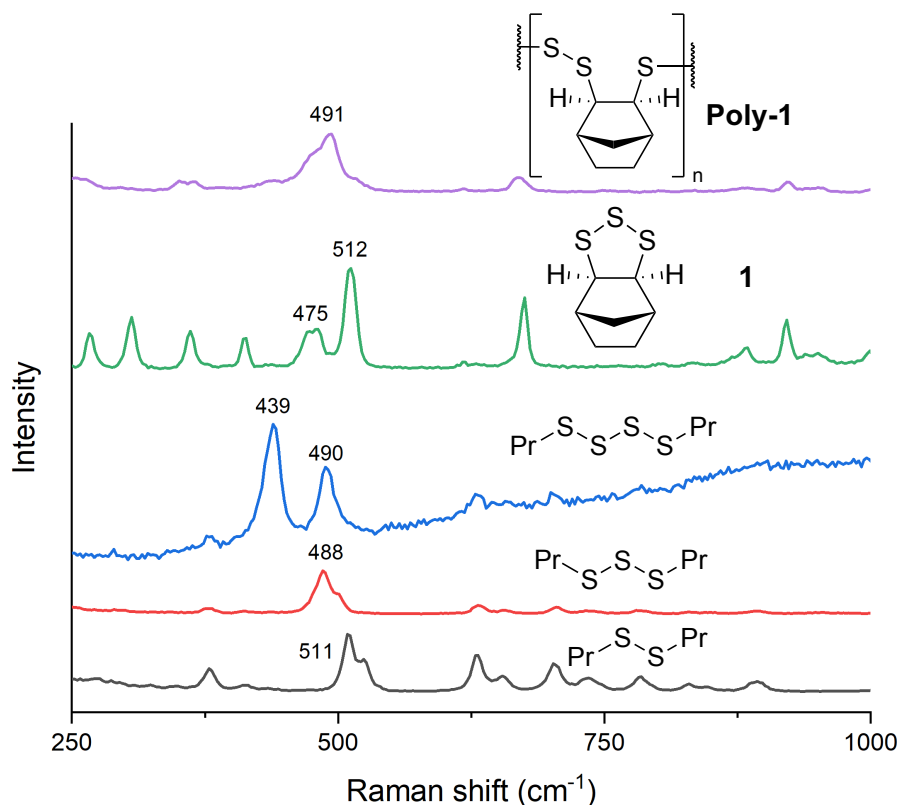


Figure 4.14: Raman spectra of **poly-1**, monomer **1**, $n\text{Pr}_2\text{S}_2$, $n\text{Pr}_2\text{S}_3$, and $n\text{Pr}_2\text{S}_4$.

Termination of the polymer chains has not yet been investigated. Possible modes of termination include the recombination of two radical end groups or aerobic oxidation of the radical sulfide to a sulfenic acid, sulfinic acid, or sulfonate (Figure 4.15).

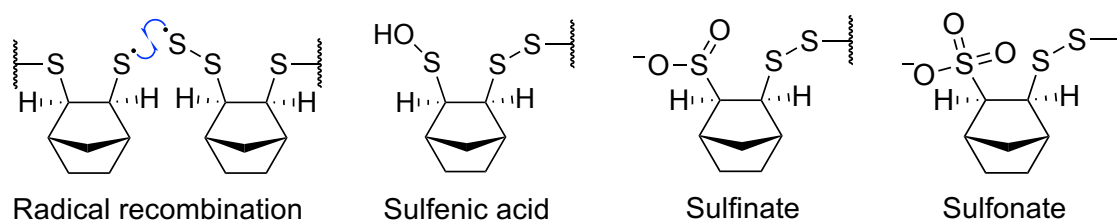


Figure 4.15: Proposed termination species

Thermal depolymerisation

The thermal depolymerisation of photochemically synthesised **poly-1** was investigated next. The ability to recycle these compounds is a key feature, therefore it is important to demonstrate the depolymerisation of photochemically produced poly(trisulfides). Thermal depolymerisation of electrochemically synthesised **poly-1** resulted in good yields of highly pure monomer **1**. As the polymer was heated above its ceiling temperature, the equilibrium favours depolymerisation and the

formation of the monomer.^[10] The clean depolymerisation was attributed to the polymers linear structure.

To investigate the thermal depolymerisation, photochemically synthesised **poly-1** (0.96 g, $M_w = 13800$ g/mol, $D = 1.9$) was heated at 180 °C under high vacuum (1-10 mbar) using a short-path distillation apparatus (Figure 4.15 A). After 3 hours, a yellow oil was observed in the collection chamber. A sample of the yellow oil was analysed by ¹H NMR spectroscopy, which revealed the oil to be highly pure monomer **1** (0.78 g, 81%) (Figure 4.15 B).

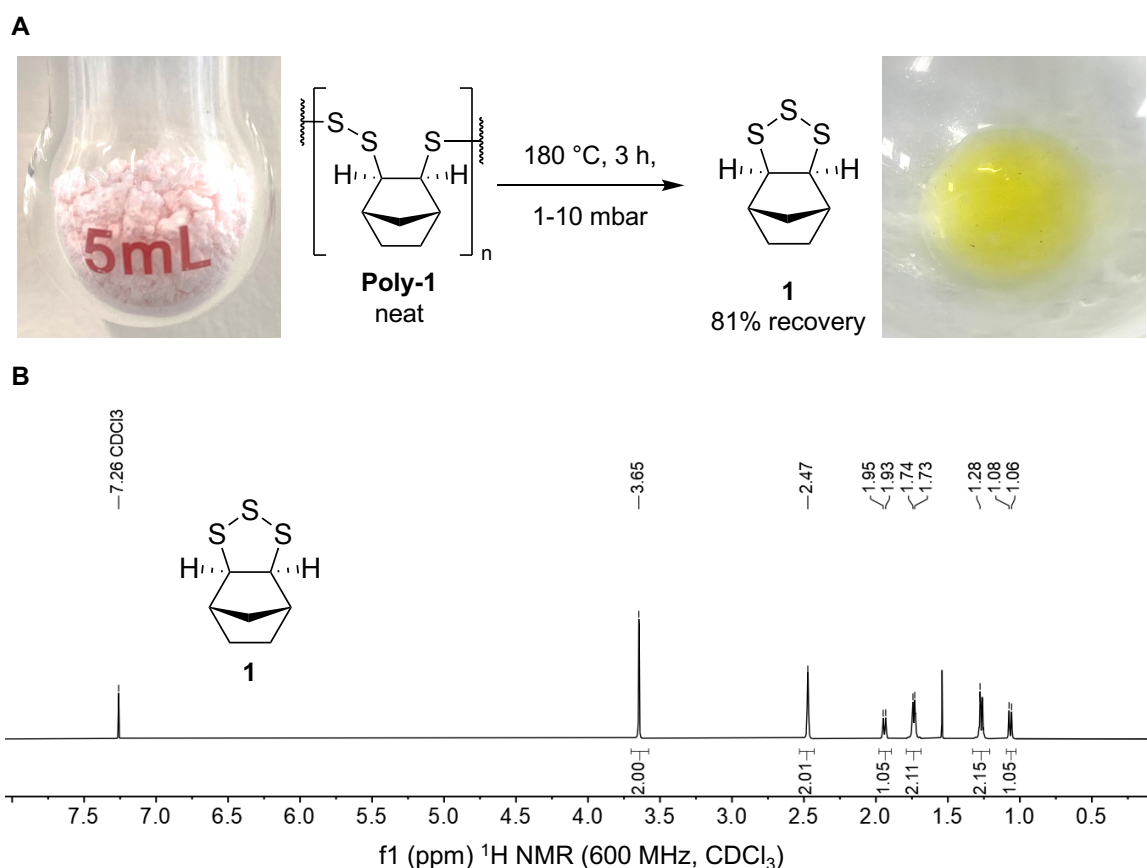


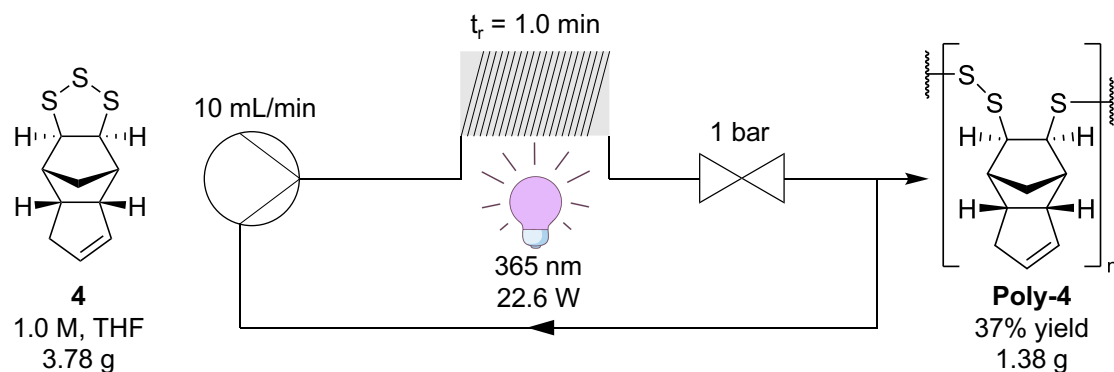
Figure 4.15: (A) Thermal depolymerisation reaction. (B) ¹H NMR spectrum of monomer **1** recovered from the thermal depolymerisation of **poly-1**.

The high yield (81%) of monomer **1** recovered from the thermal depolymerisation of photochemically polymerised **poly-1** showed the polymer can be chemically recycled in good yield with high purity. Therefore, the photochemically synthesised polymer can be used in closed loop applications, such as a recyclable gold sorbent.

Large scale preparation of poly(trisulfides) in continuous flow

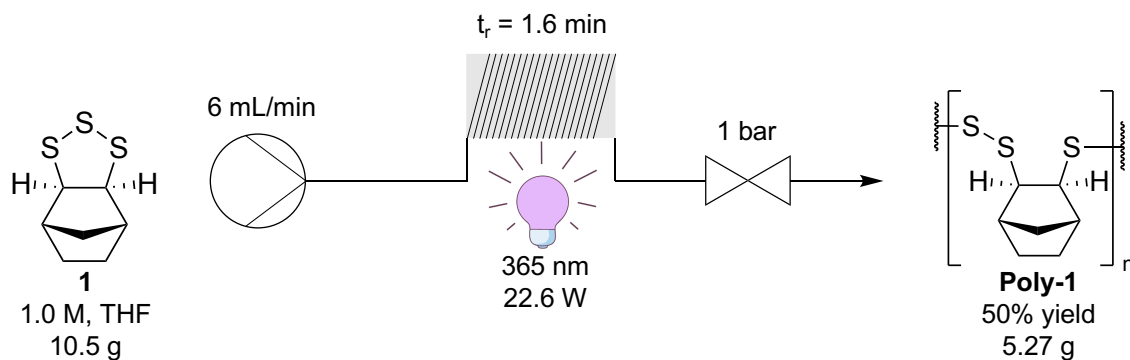
A key advantage of continuous flow photochemical polymerisation is the ability to readily scale up production. Continuous flow synthesis can be scaled up without the challenges typically associated with scaling up batch reactions, such as heat and mass transfer issues. In this section, the multigram synthesis of poly(trisulfides) is demonstrated in continuous flow. The reactions are run at high concentration (1.0 M) with short residence times (1 to 1.6 minutes), making the process highly efficient. Although the yields of the reaction in continuous flow are low when producing high molecular weight polymers, there is no loss of reagents. Therefore, the monomer can be passed through the flow reactor multiple times, resulting in no reagent waste.

Poly-4 was prepared in continuous flow via the addition of monomer to the reaction solution to maintain concentration (Scheme 4.11). This was done to show the unpolymerized monomer in the solution can be passed through the flow reactor multiple times in order to increase output. Specifically, monomer **4** (1.0 M, 10 mL, THF) was passed through a photochemical reactor and irradiated with 365 nm LEDs (22.6 W, 21 °C) at 10 mL/min, resulting in a residence time of 1 minute. The reaction solution was collected, concentrated under reduced pressure and redissolved in chloroform (5 mL). Ethyl acetate (15 mL) was added to precipitate the polymer, which was collected by filtration. The filtrate was concentrated under reduced pressure and then charged with additional monomer **4** and THF, resulting in a solution of monomer **4** (1.0 M, 10 mL, THF). This process was repeated 6 times resulting in 1.38 g (37% yield) of **poly-4** with a $M_W = 8200$ g/mol, $D = 1.7$.



Scheme 4.11: Preparation of **poly-4** in continuous flow.

Poly-1 was then prepared in continuous flow (Scheme 4.12). For this synthesis, a larger stock solution was prepared (55 mL, 1.0 M, THF). The solution was passed through a photochemical reactor irradiated with 365 nm LEDs (22.6 W, 21 °C) at 6 mL/min, resulting in a residence time of 1.6 minutes. After collection and purification, **poly-1** was recovered at a yield of 50% (5.27 g) with a $M_W = 5600$ g/mol and a $D = 1.8$.



Scheme 4.12: Preparation of **poly-1** in continuous flow.

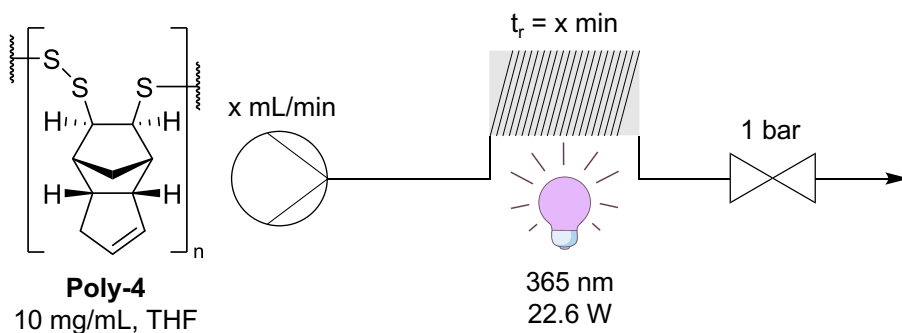
To put this into perspective, it took 63 minutes to produce 1 g of **poly-1**. Therefore, using one reactor, 24 g of polymer can be produced in a day. The benefit of scaling up a process in continuous flow is parallel reactors can be applied to meet a demand without the loss of optimal reaction conditions that are often lost in upscaled batch processing.

Photodegradation of poly(trisulfides)

There are several examples of photodegradable polymers in the literature that are highly beneficial in applications such as biomedicines,^[17] degradable films,^[18] and recyclable polymers.^[19] Lu and co works have shown that poly(sulfide selenide)s exhibit excellent photodegradability, which can be employed in applications such as photo-stimulated and responsive smart materials.^[20] Polysulfides produced through inverse vulcanisation have been shown to be photosensitive, resulting in rapid modifications using low-power lasers in the visible and infrared wavelength regions.^[21] These photosensitive polysulfides have shown application in lithography and erasable information storage.^[21]

Throughout this chapter, experimental results have supported the hypothesis that polymer chains formed during the photochemical polymerisation of 1,2,3-trithiolane monomers are cleaved with continued UV irradiation. To test this hypothesis, pure **poly-4** was irradiated with UV light under continuous flow and its molecular weight and structure were analysed using GPC (THF) and ¹H NMR spectroscopy (CDCl₃).

A solution of **poly-4** (509 mg, $M_w = 9800 \text{ g/mol}$, $D = 1.6$) in THF (50 mL) was prepared and passed through a photochemical reactor and irradiated with 365 nm LEDs (21 °C, 22.6 W) at 10 mL/min (residence time = 1 minute) and 0.5 mL/min (residence time = 20 minutes) (Scheme 4.13). Under both reaction conditions, the molecular weight of **poly-4** drastically decreased to a level undetectable by GPC, providing clear evidence of photodegradation.



Scheme 4.13: Photodegradation of **poly-4** in continuous flow.

^1H NMR spectroscopy of the crude products show a broadening of signals between 1.75 ppm and 2.75 ppm and sharp signals appearing at 4 ppm and at 5.75 ppm (Figure 4.16). The broadening of the peaks was likely due to the formation of a range of oligomeric species. The peaks at 4 ppm and 5.75 ppm are shifted compared to the monomer **4** signals. The formation of small amounts of monomer **4** was also observed. Further analysis on these breakdown products is currently underway to determine their structure.

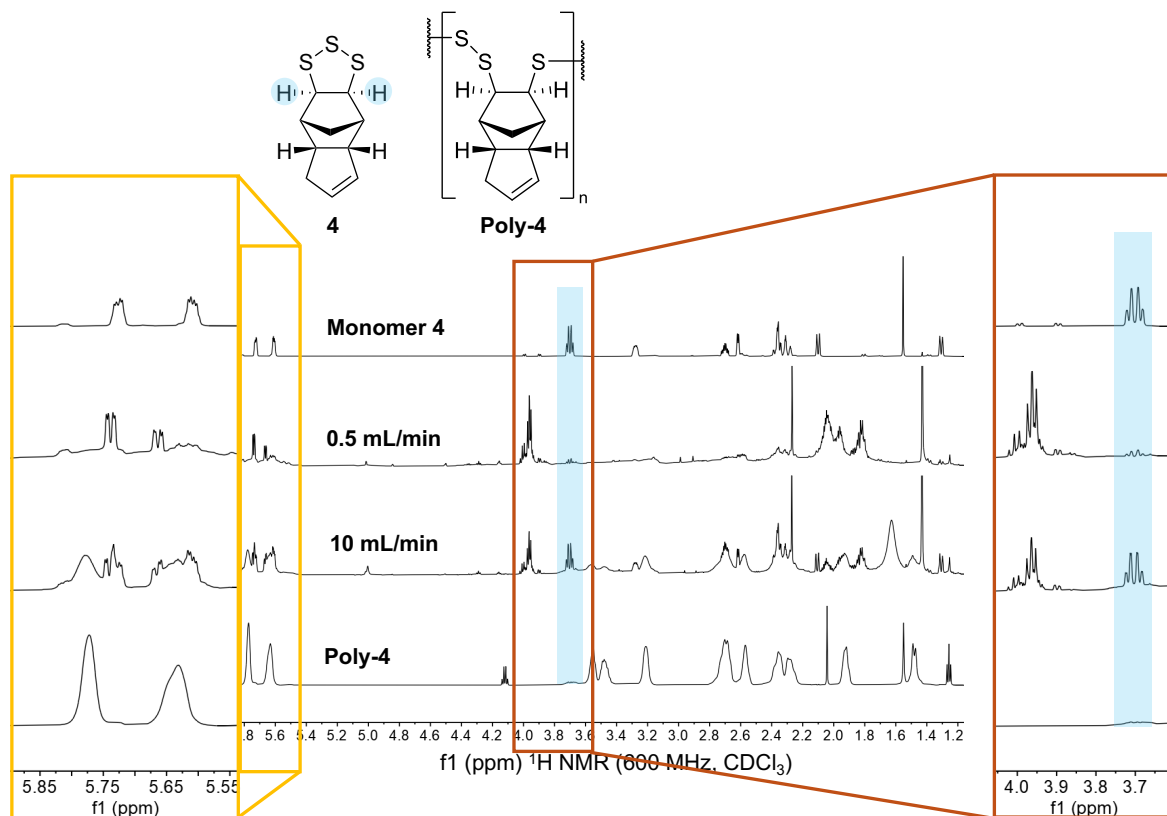


Figure 4.16: ^1H NMR spectra of **poly-4** and **poly-4** after photodegradation under different conditions.

The photodegradation of **poly-1** was also investigated in batch, yielding analogous results. After just 5 minutes of irradiation with 365 nm LEDs (21 °C, 22.6 W), the polymer M_w decreased from 7800 g/mol to 1200 g/mol. ^1H NMR spectroscopy of the photodegraded product after 60 minutes showed the presence of sharp peaks consistent with monomer **1** (Figure 4.17). This is an exciting result as it demonstrates the potential for recycling of poly(trisulfides) back to their monomer units using light irradiation alone.

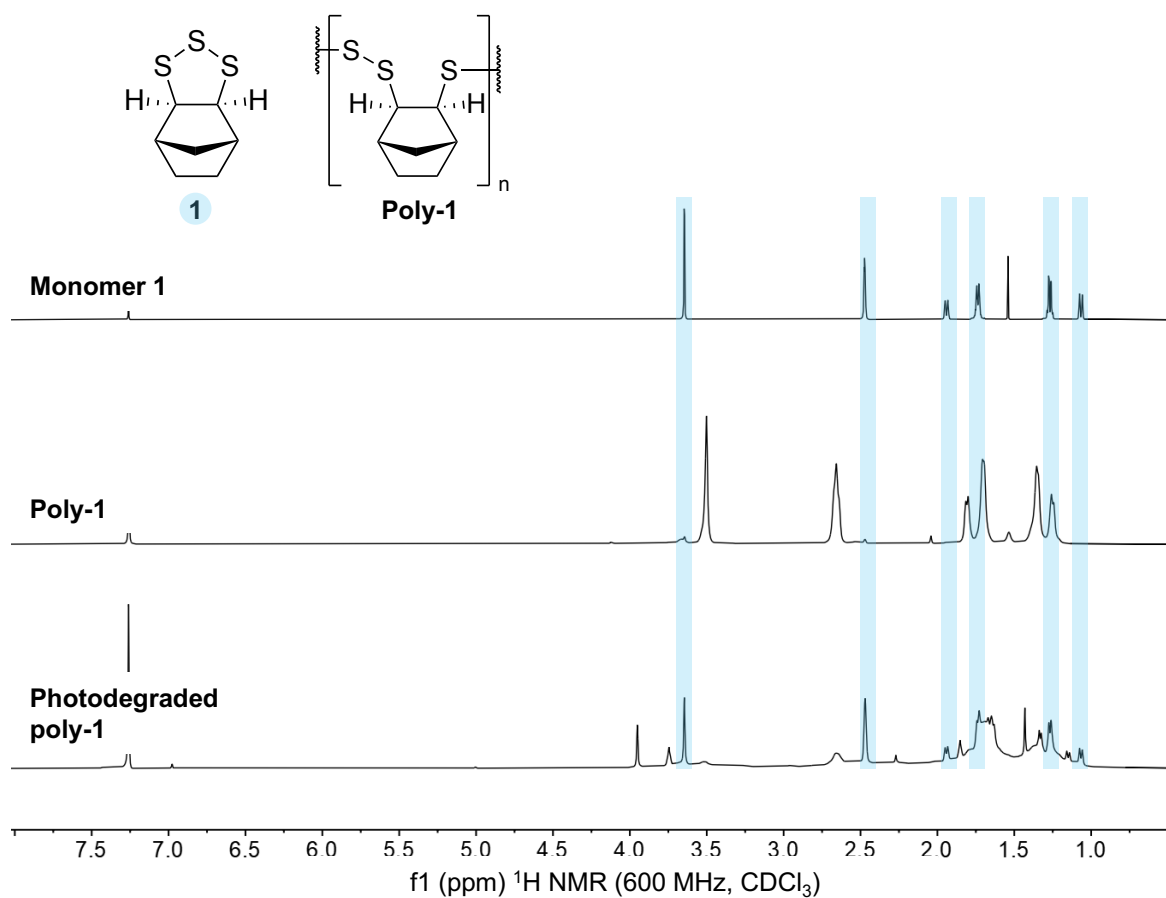


Figure 4.17: ^1H NMR spectra of **poly-1** before and after photodegradation.

UV irradiation of poly(trisulfides) demonstrated the rapid breakdown of polymer molecular weight to small oligomeric species and the regeneration of monomer. This exciting result has potential use in several applications, including UV-degradable coatings for controlled release of cargo, photolithographic modifications, and photochemical depolymerisation and recycling.

Conclusion

In this chapter, the photochemical polymerisation of 1,2,3-trithiolanes was studied. In batch reactions, an intriguing phenomenon was revealed: long polymer chains were formed first, but continued irradiation resulted in polymer degradation. With this understanding, a continuous flow photochemical reactor was used to irradiate 1,2,3-trithiolane monomers under short and controlled periods of irradiation to initiate polymerisation and reduce the amount of polymer breakdown. This resulted in the ability to precisely control the molecular weight. Additionally, a continuous flow process allowed for the production of poly(trisulfides) on a multi-gram scale, which is important for studying their potential applications. The production of sulfur-rich polymers using UV irradiation alone is a significant advantage over other synthetic methods as it can be done safely under ambient conditions without the need for additional chemical reagents.

The photodegradation of the key poly(trisulfides) showed rapid degradation to low molecular weight species. Photodegradable sulfur-rich polymers have potential widespread application in photodegradable films and coatings. Exploration of these applications is currently underway.

Experimental details

General considerations

Materials: Sulfur was purchased from Sigma-Aldrich (reagent grade, powder, purified by refining, 100 mesh particle size). Dicyclopentadiene, bicyclo[2.2.1]hept-2-ene (norbornene), and bicyclo[2.2.1]hepta-2,5-diene (norbornadiene) were purchased from Sigma-Aldrich. Silica gel was purchased from Sigma-Aldrich (technical grade, pore size 60 Å, 230-400 mesh particle size, 40-63 µm particle size).

NMR Spectroscopy: Proton nuclear magnetic resonance spectra (¹H NMR) were recorded on a 600 MHz Bruker spectrometer operating at 600 MHz. All chemical shifts are quoted on the δ scale referencing residual solvent peaks (¹H NMR: δ = 7.26 for CDCl₃); (¹³C NMR: δ = 77.16 for CDCl₃). Chemical shift values are reported in parts per million, ¹H¹H coupling constants are reported in hertz and multiplicity is abbreviated as; s = singlet, d = doublet, m = multiplet, ap.= apparent.

UV-Vis Spectroscopy: UV-Vis spectroscopy was performed on a Thermo Fisher Evolution Array UV-Visible Photodiode Spectrophotometer using a quartz cuvette. Sample concentration (0.004 M - 0.04 M) in THF.

Scanning Electron Microscopy (SEM) with Energy Dispersive X-ray (EDX): SEM/EDX images were obtained using a FEI Inspect F50 SEM fitted with a EDAX energy dispersive X-ray detector. Samples were sputter coated with silver metal (10 nm thickness) before analysis.

Gel permeation chromatography (GPC): GPC analysis was performed using a Waters 2695 separations module, using two Agilent columns (PLgel MiniMix-C (5 µm)) and a matching Agilent guard column (MiniMix-C) and a Waters 410 refractive index detector. All samples were eluted in THF at a flow rate of 0.2 mL/min. Calibration was performed using narrow distribution polystyrene standards (*D* < 1.1) ranging from 500 to 2 million g/mol. Samples were prepared by dissolving in THF (2 mg/mL) followed by filtration using a 0.45 µm PTFE syringe filter before analysis.

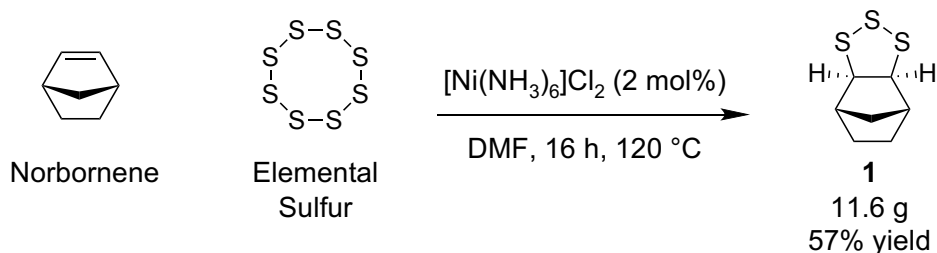
Flow chemistry apparatus: All flow reactions were conducted on a commercially available Vapourtec RS-200 system comprising an R2C+ pump module.

Continuous flow photoreactor: A Vapourtec R-Series system with R2C+ pump module was used to pump solutions through a coil of PFA tubing (10 mL). The coil was fitted to a Uniqsis Polar Bear Plus FlowTM which was used to control the temperature of the reaction mixture. A Uniqsis

PhotoSyn™ provided LED irradiation (365 nm). The back pressure of the system was controlled using a Vapourtec SF-10 reagent pump operating in pressure controller mode.

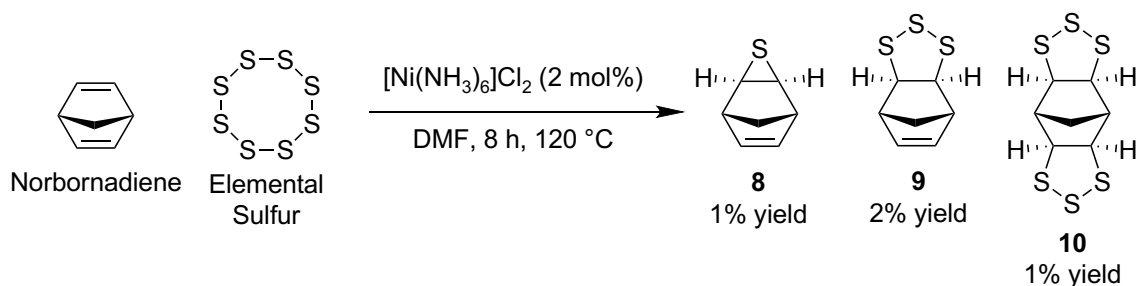
Monomer synthesis

Monomer 1



The following method was adapted from the literature.^[22] A 250 mL round bottom flask was equipped with a reflux condenser and a stir bar, and then norbornene (26.7 g, 284 mmol) and DMF (250 mL) were added. Elemental sulfur (27.3 g, 107 mmol S₈) and [Ni(NH₃)₆]Cl₂ (496 mg, 2.14 mmol) were then added, and the resulting reaction mixture was heated to 120 °C. After stirring for 16 hours the mixture was allowed to cool to room temperature before the solids were removed by filtration over a thin layer (~1 cm) of silica gel. The silica gel was washed with hexane (3 x 100 mL). Deionized water (100 mL) was added to the filtrate, the layers were separated, and the organic fraction was washed with deionized water (2 x 100 mL). The organic layer was collected, dried (Na₂SO₄), filtered, and concentrated under reduced pressure. Purification by distillation under a vacuum of 0.78 mbar at 165 °C (oil bath temperature) delivered monomer **1** as a yellow oil (11.6 g, 57% yield). ¹H NMR (600 MHz, CDCl₃): δ 3.64 (s, 2H), 2.47 (s, 2H), 1.93 (d, *J* = 10.4 Hz, 1H), 1.74 (d, *J* = 8.1 Hz, 2H), 1.27 (d, *J* = 7.8 Hz, 2H), 1.07 (d, *J* = 10.5 Hz, 1H). ¹³C NMR (151 MHz, CDCl₃): δ 70.0, 40.9, 32.5, 27.8.

Monomers 8, 9, 10



The following method was adapted from the literature.^[22] A 50 mL round bottom flask was equipped

with a reflux condenser and a stir bar, and then norbornadiene (10.0 g, 108 mmol) and DMF (100 mL) were added. Elemental sulfur (10.5 g, 41 mmol S₈) and [Ni(NH₃)₆]Cl₂ (424 mg, 1.8 mmol) were then added, and the resulting reaction mixture was heated to 120 °C. After stirring for 8 hours the mixture was allowed to cool to room temperature before the solids were removed by filtration over a thin layer (~1 cm) of silica gel. The silica gel was washed with hexane (3 x 100 mL). Deionized water (1000 mL) was added to the filtrate, the layers were separated, and the organic fraction was washed with deionized water (2 x 100 mL). The organic layer was collected, dried (Na₂SO₄), filtered, and concentrated under reduced pressure. Purification by flash chromatography over silica gel (hexane) delivered a yellow oil which formed crystals over time. The crystals were collected to deliver monomer **9** (401 mg, 2% yield). The remaining oil contained monomer **8** (133 mg, 1% yield) with impurities of monomer **9**. A later eluent delivered a yellow brown oil of mixed products which delivered monomer **10** (306 mg, 1% yield). when dissolved in a small amount of hexane and cooled to 0 °C.

Monomer **9**: ¹H NMR (600 MHz, CDCl₃): δ 6.38 (s, 2H), 4.05 (m, 2H), 2.90 (s, 2H), 2.47 (d, *J* = 9.0 Hz, 1H), 1.71 (d, *J* = 9.0 Hz, 1H). ¹³C NMR (151 MHz, CDCl₃): δ 139.37, 70.81, 46.22, 43.31.

Monomer **10**: ¹H NMR (600 MHz, CDCl₃): δ 3.85 (s, 4H), 2.65 (s, 2H), 2.00 (s, 2H). ¹³C NMR (151 MHz, CDCl₃): δ 68.88, 45.56, 27.94.

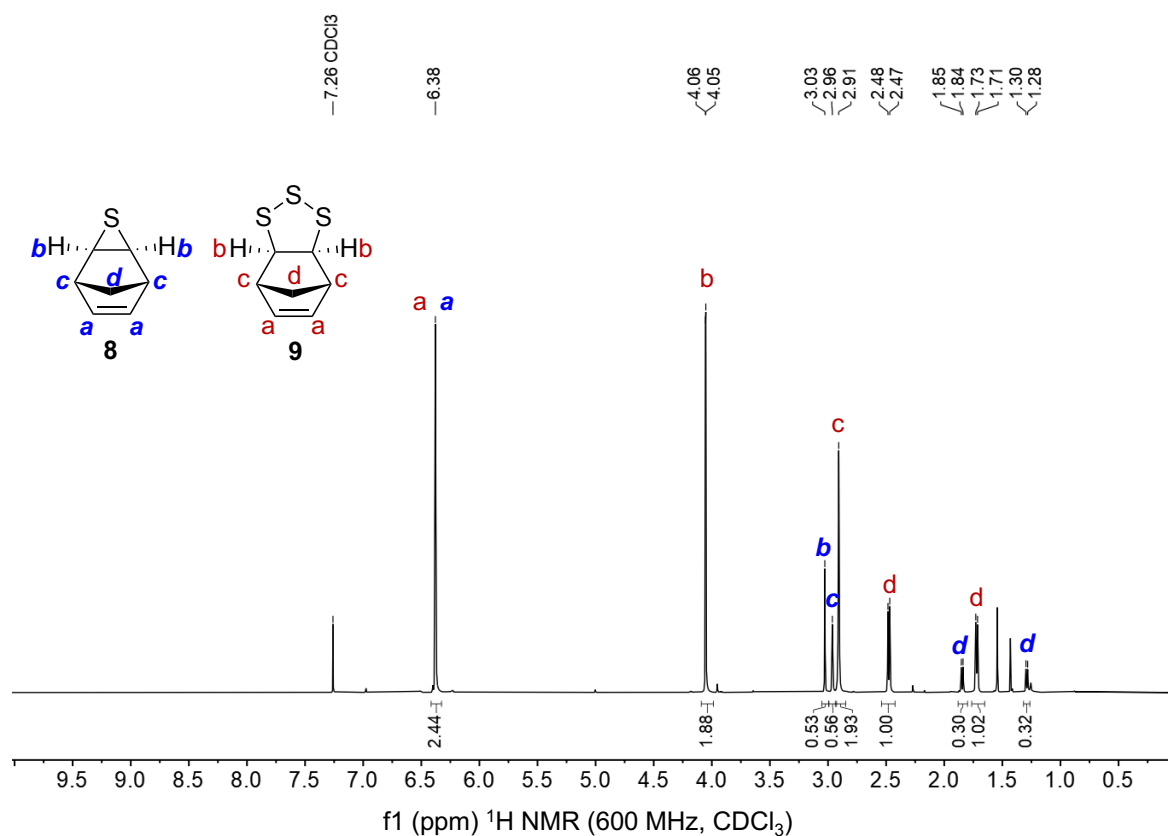


Figure S4.1: ^1H NMR spectrum (600 MHz, CDCl_3) of monomer **8** and **9** mixture.

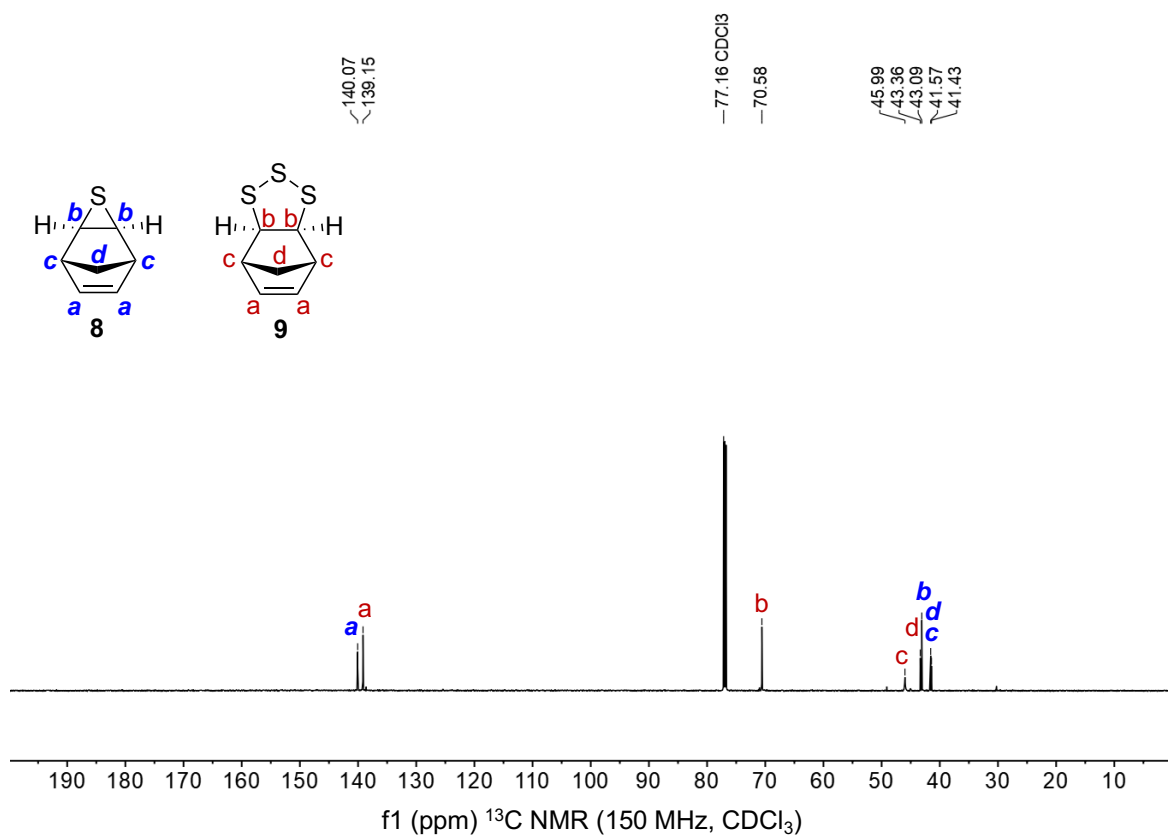


Figure S4.2: ^{13}C NMR spectrum (150 MHz, CDCl_3) of monomer **8** and **9** mixture.

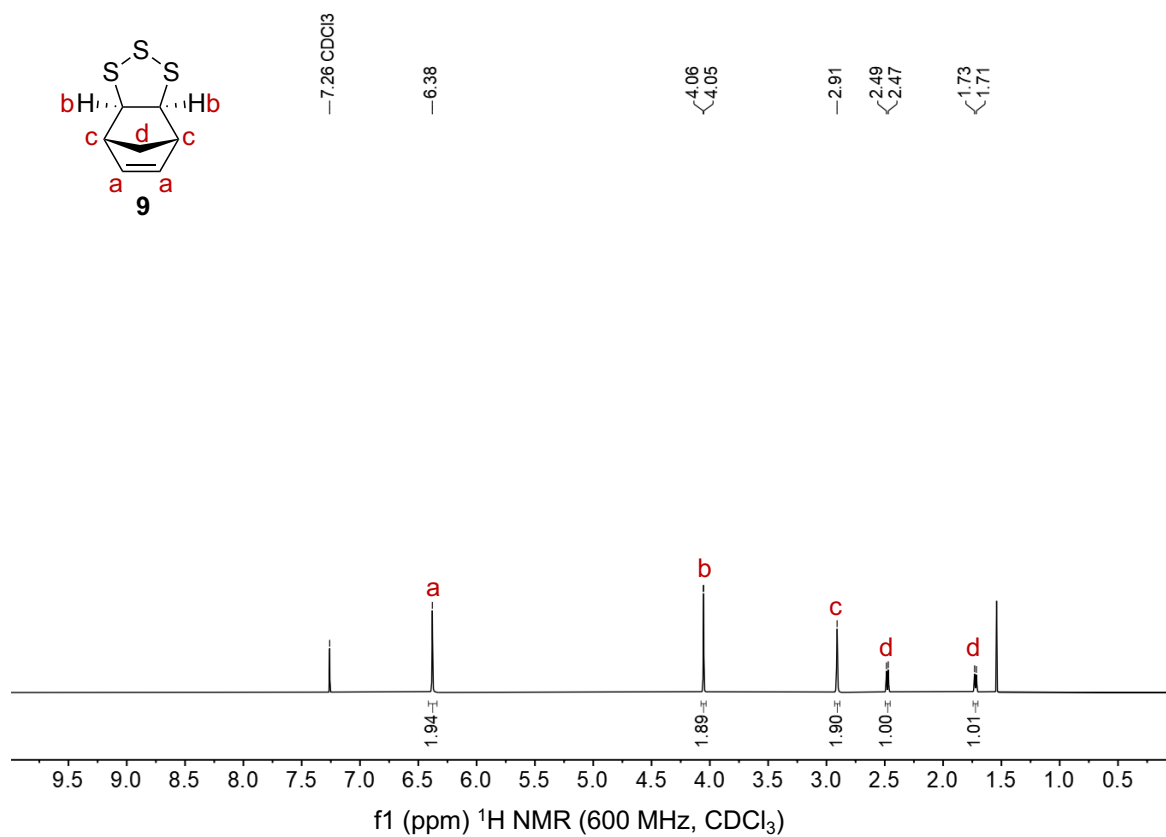


Figure S4.3: ^1H NMR spectrum (600 MHz, CDCl_3) of monomer **9**.

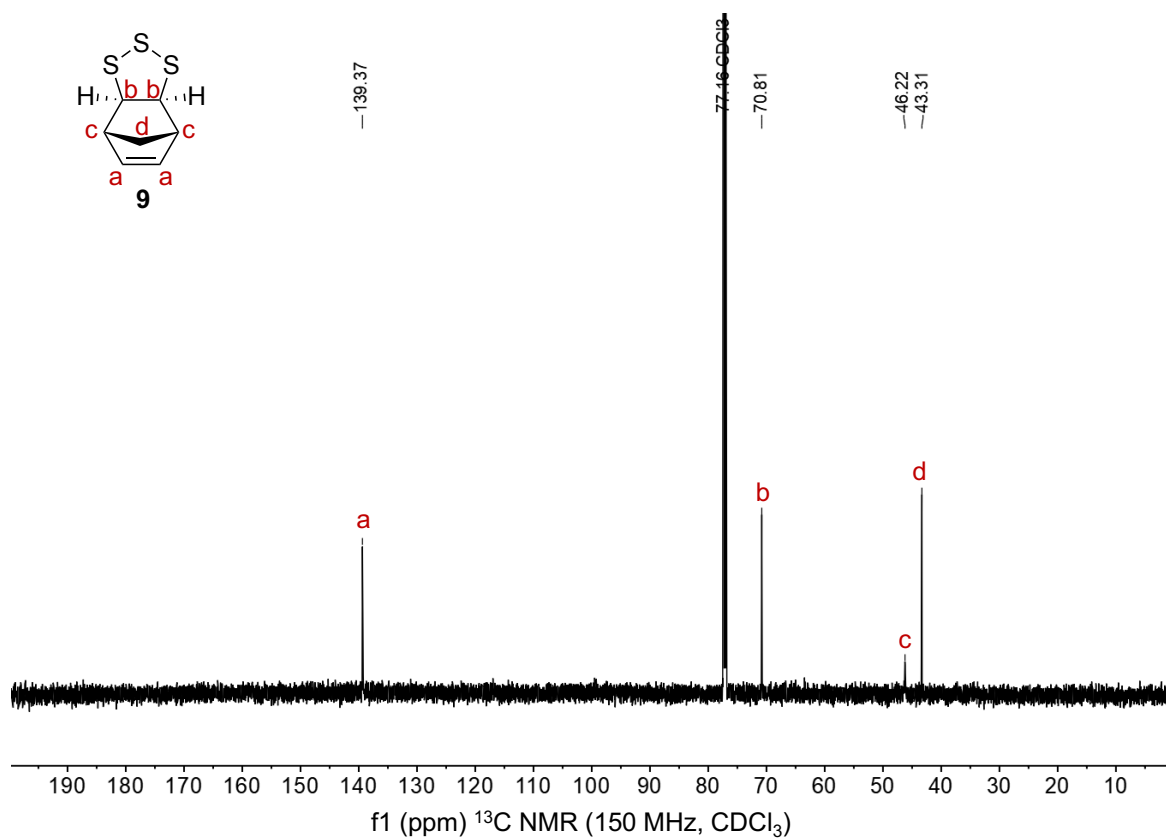


Figure S4.4: ^{13}C NMR spectrum (150 MHz, CDCl_3) of monomer **9**.

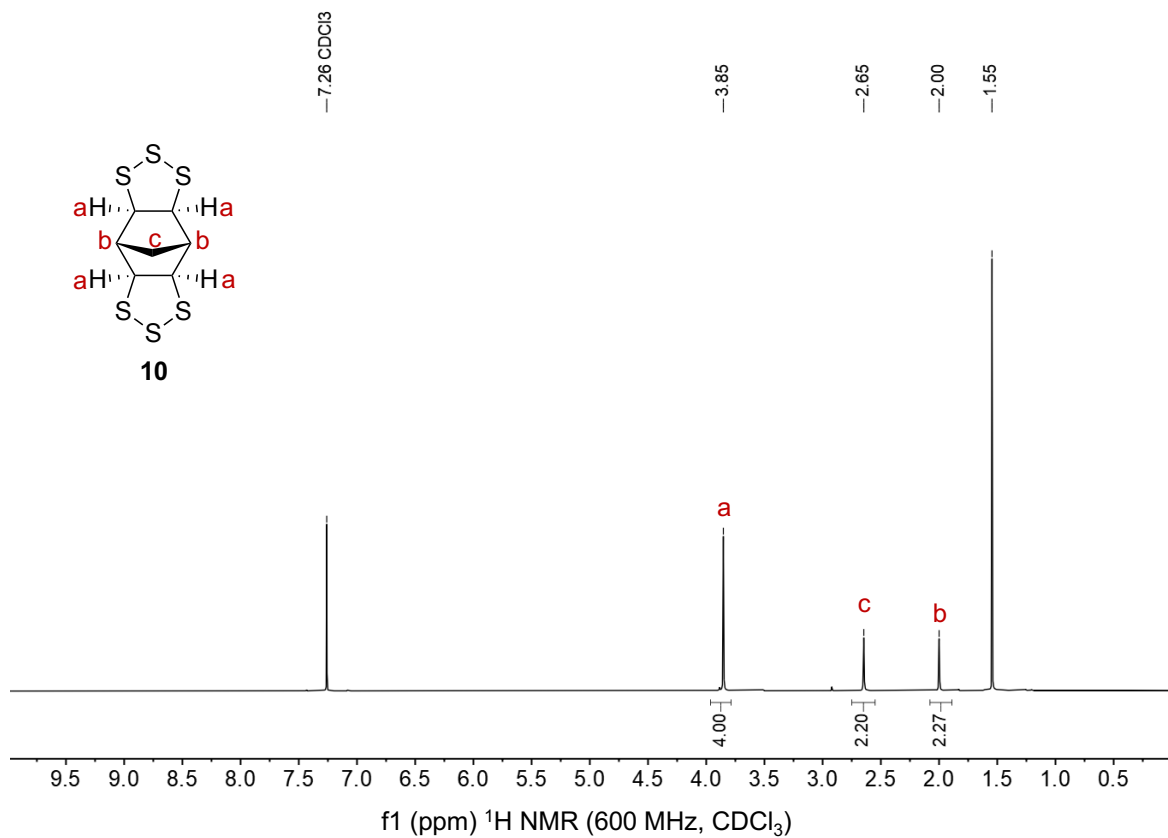


Figure S4.5: ^1H NMR spectrum (600 MHz, CDCl_3) of monomer **10**.

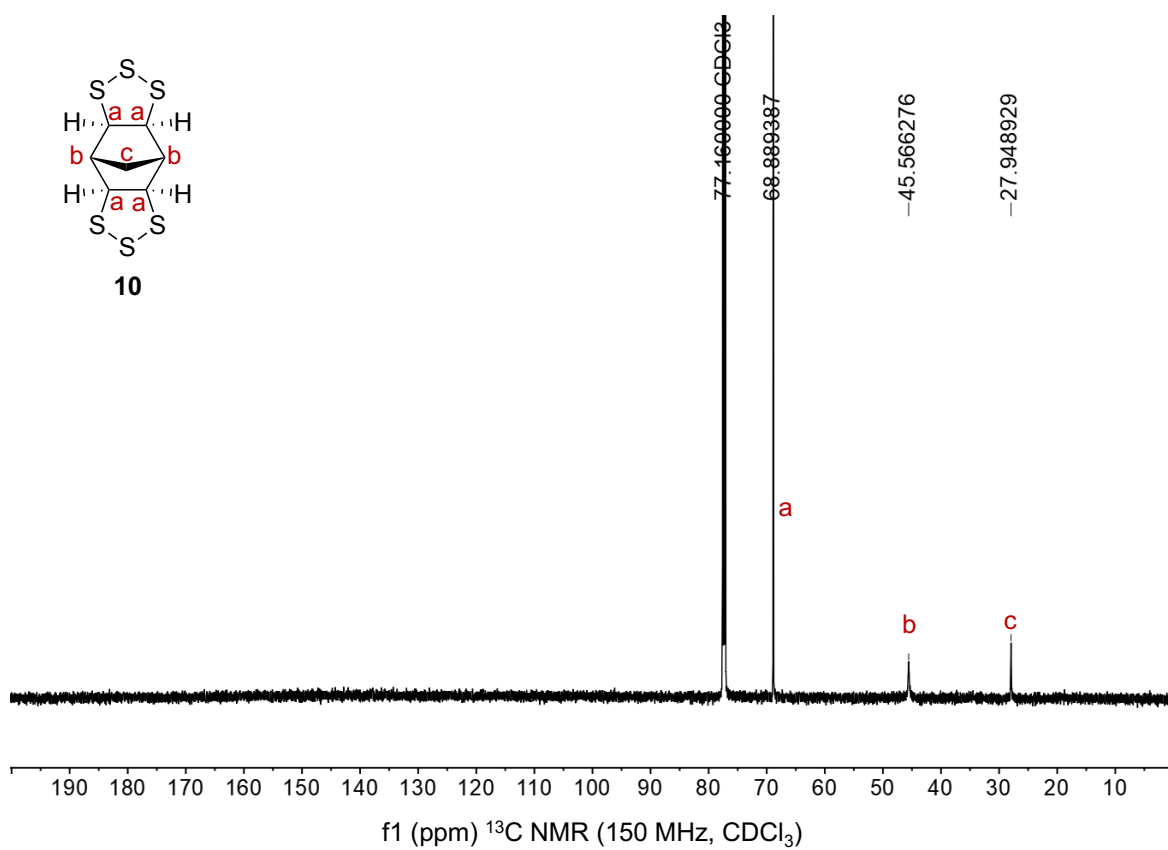


Figure S4.6: ^{13}C NMR spectrum (150 MHz, CDCl_3) of monomer **10**.

Monomer 10 – optimised synthesis

The following optimised synthesis of monomer **10** was developed by another group member, Sam Tonkin. A 250 mL round bottom flask was equipped with a reflux condenser and a stir bar. It was then charged with elemental sulfur (9.45 g, 36 mmol S₈), [Ni(NH₃)₆]Cl₂ (228 mg, 1 mmol), norbornadiene (4.53 g, 49 mmol), toluene (50 mL) and DMF (50 mL). The resulting reaction mixture was heated to 120 °C. After stirring for 24 hours the mixture was poured into a baker containing hexane (250 mL) and distilled water (250 mL). The solution was filtered over Celite. The filtrate was washed with distilled water (3 x 250 mL). The organic layer was collected, dried (MgSO₄) and filtered. The filtrate was left for 24 hours while monomer **4** crystallized out of solution. A maximum yield of monomer **10** of 9% was obtained using these conditions.

X-ray crystallographic data

Single crystals were mounted in paratone-N oil on a nylon loop. X-ray diffraction data for monomer **9** and monomer **10** was collected at 100(2) K on the MX-1 and MX-2 beamlines of the Australian Synchrotron.^[23-24] Structures were solved by direct methods using SHELXT^[25] and refined with SHELXL^[25] and ShelXle^[26] as a graphical user interface. All non-hydrogen atoms were refined anisotropically, and hydrogen atoms were included as invariants at geometrically estimated positions.

Table S4.1: X-ray experimental data

Monomer	9	10
CCDC number	2289708	2289709
Empirical formula	C7H8S3	C7H8S6
Formula weight	188.31	284.49
Crystal system	Orthorhombic	Monoclinic
Space group	Pbcn	P21/c
<i>a</i> (Å)	42.045(8)	6.7640(14)
<i>b</i> (Å)	7.7730(16)	13.008(3)
<i>c</i> (Å)	9.6930(19)	12.204(2)
<i>a</i> (°)	90	90
<i>b</i> (°)	90	100.82(3)
<i>g</i> (°)	90	90
Volume (Å ³)	3167.8(11)	1054.7(4)
<i>Z</i>	16	4
Density (calc.) (mg/m ³)	1.579	1.792
Absorption coefficient (mm ⁻¹)	0.849	1.243
F(000)	1568	584
Crystal size (mm ³)	0.17 x 0.15 x 0.12	0.25 x 0.21 x 0.18
q range for data collection (°)	0.969 to 27.882	2.310 to 27.882
Reflections collected	46785	15666
Observed reflections [R(int)]	3673 [0.0385]	2510 [0.0538]
Goodness-of-fit on F ²	1.105	1.080
R1 [>2s(I)]	0.0300	0.0301
wR2 (all data)	0.0806	0.0768
Largest diff. peak and hole (e.Å ⁻³)	0.388 and -0.389	0.614 and -0.530
Data / restraints / parameters	3673 / 0 / 181	2510 / 0 / 119

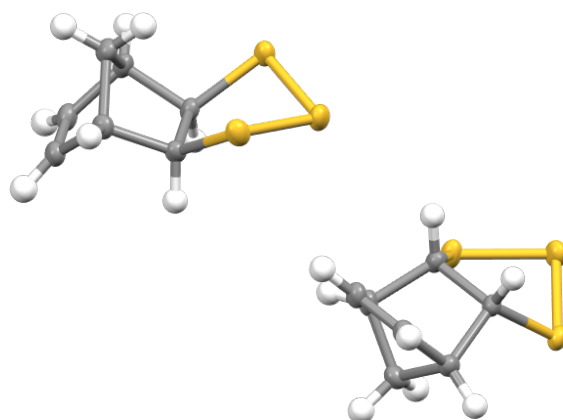


Figure S4.7: The asymmetric unit of monomer **9** with all non-hydrogen atoms shown as ellipsoids at the 50% probability level.

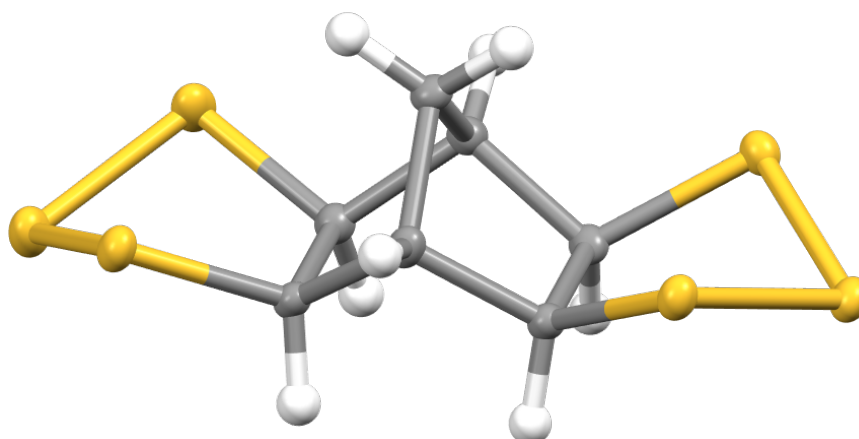
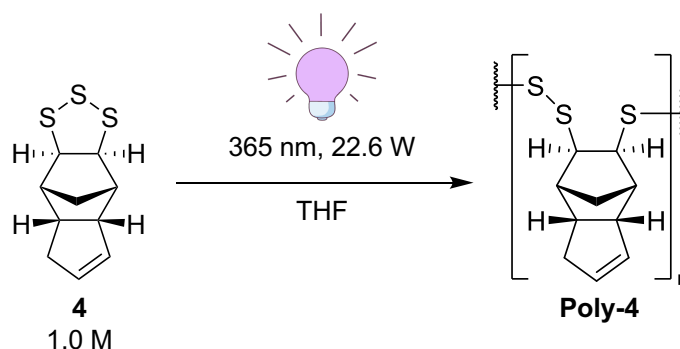


Figure S4.8: The asymmetric unit of monomer **10** with all non-hydrogen atoms shown as ellipsoids at the 50% probability level.

Photochemical polymerisation in batch

Monomer 4



A stock solution of monomer **1** (2.28 g, 10 mmol, 1 M) in THF (10 mL) was prepared. Eight GC-MS vials with stir bars were prepared containing 1 mL of the stock solution. The vials were then placed onto a stir plate inside of the Uniqsis PhotoSynTM photoreactor. The vials were placed so they were facing the UV lights at a uniform distance. Stirred samples were irradiated with UV light (365 nm, 22.6 W). At 0, 3, 6, 12, 24, 60 and 120 minutes, the light was turned off shortly and a vial was taken out. The solution in the vial was concentrated under reduced pressure and analysed by ¹H NMR spectroscopy (CDCl₃) and GPC (THF).

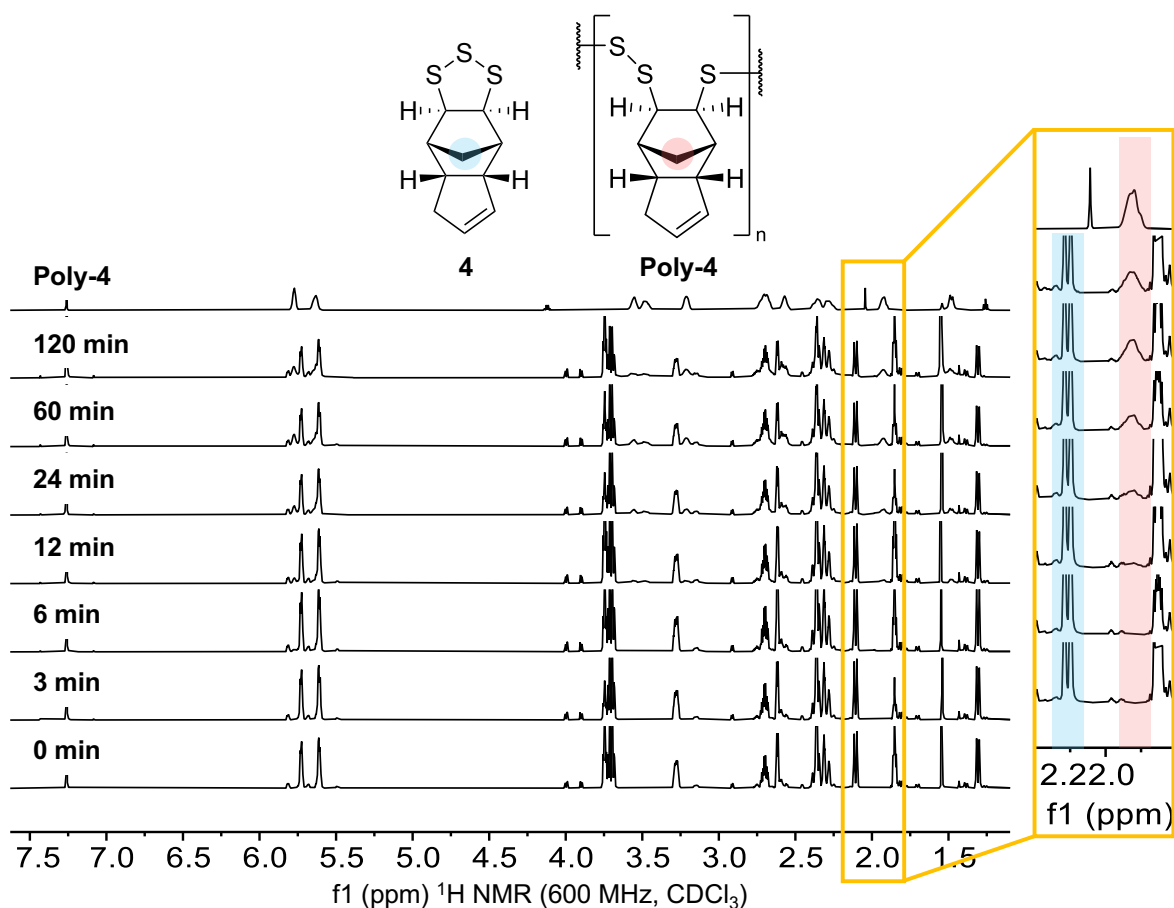


Figure S4.9: ¹H NMR spectra (600 MHz, CDCl₃) of photochemical polymerisation of monomer **4** (1.0 M, THF) in batch at different time points. The highlighted peaks of monomer **4** and **poly-4** were used to calculate conversion.

The solvent was removed under reduced pressure leaving an off-white powder. The powder was insoluble in chloroform and THF.

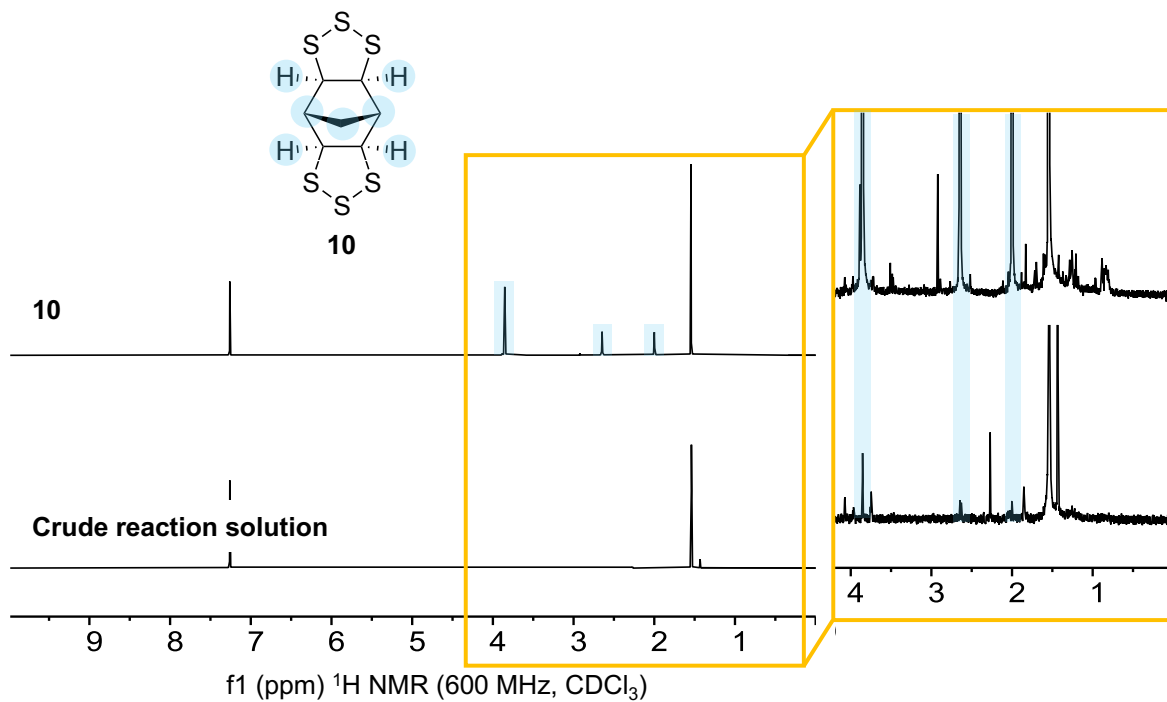


Figure S4.11: ¹H NMR spectrum (600 MHz, CDCl₃) of photochemical polymerisation of monomer **10** (40 mM, THF) in batch after 1 hour showing no presence of soluble material.

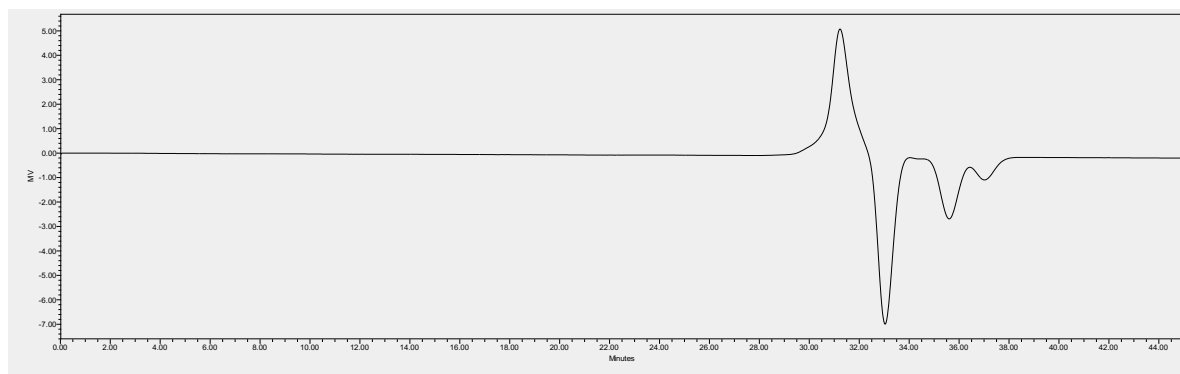
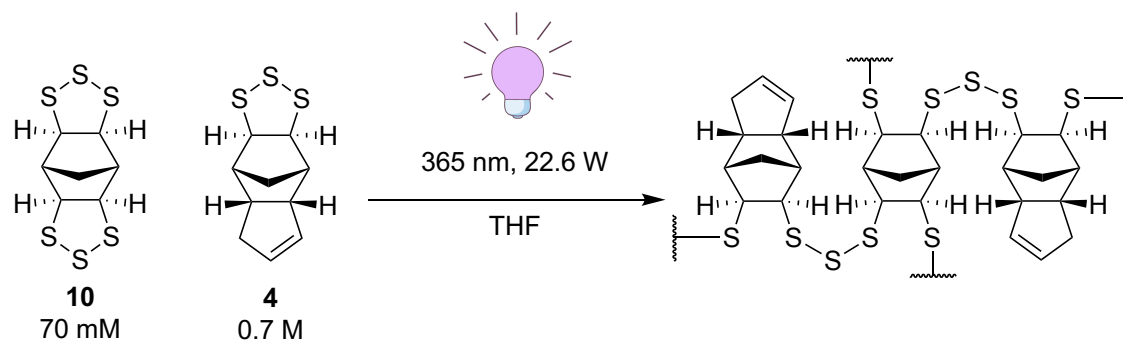


Figure S4.12: GPC (THF) trace of product. No signal observed indicating no soluble material.

Monomer **10** and **4**



A stock solution of monomer **4** (2.28 g, 10 mmol, 1 M) in THF (10 mL) was prepared. A stock solution of monomer **10** (134 mg, 0.5 mmol, 0.2 M) in THF (2.5 mL) was prepared. Four GC-MS vials with stir bars were prepared containing 1 mL of monomer **4** stock solution and 0.5 mL of monomer **10** stock solution. The vials were then placed onto a stir plate inside of the Uniqsis PhotoSynTM photoreactor. The vials were placed so they were facing the UV lights at a uniform distance. Stirred samples were irradiated with UV light (365 nm, 22.6 W). At 15, 30, 60 and 120 minutes, the light was turned off shortly and a vial was taken out. The solution in the vial was concentrated under reduced pressure and analysed by ¹H NMR spectroscopy (CDCl₃) and GPC (THF).

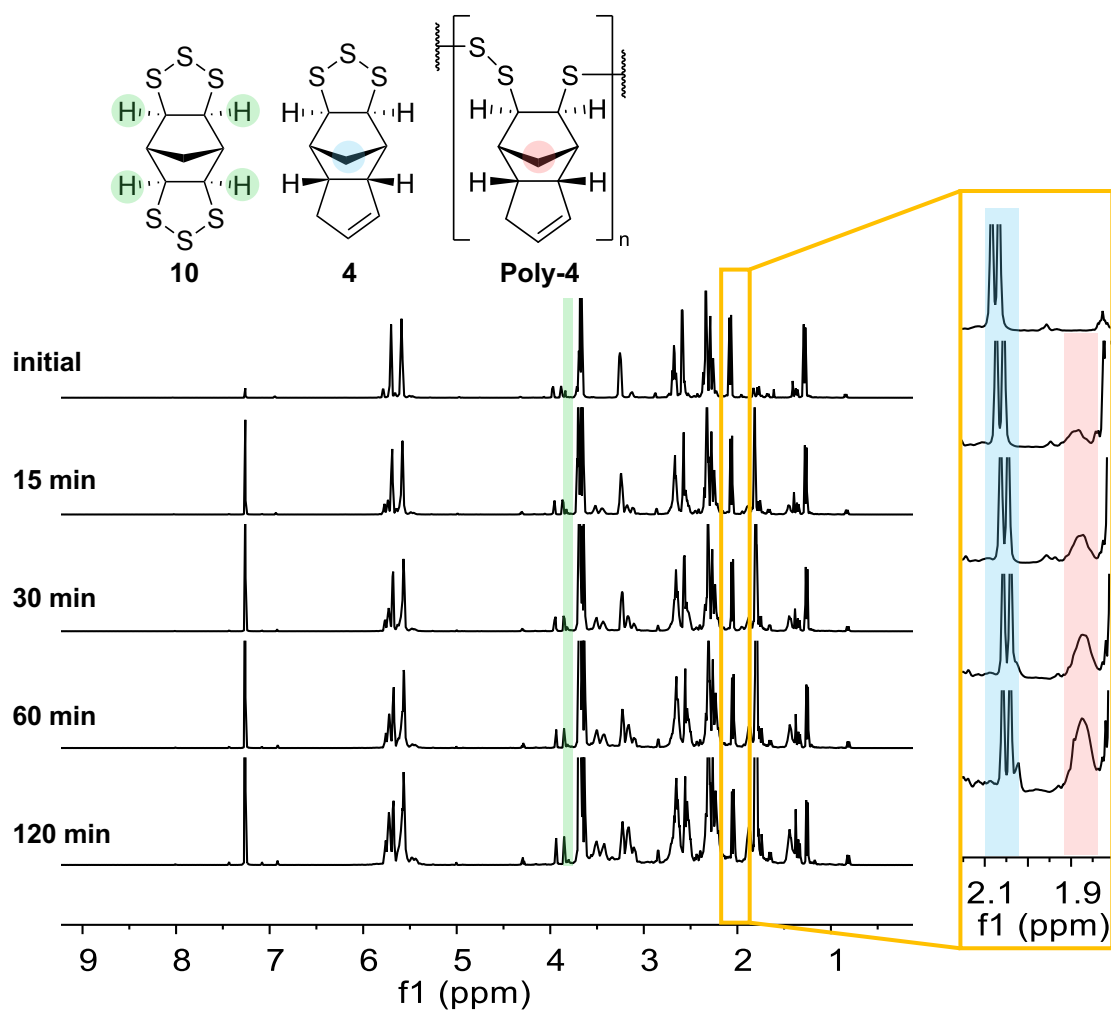


Figure S4.13: ^1H NMR spectra (600 MHz, CDCl_3) of photochemical polymerisation of monomer **4** (0.7 M, THF) and monomer **10** (70 mM, THF) in batch at different time points. The highlighted peaks of monomer **4** and **poly-4** were used to calculate conversion.

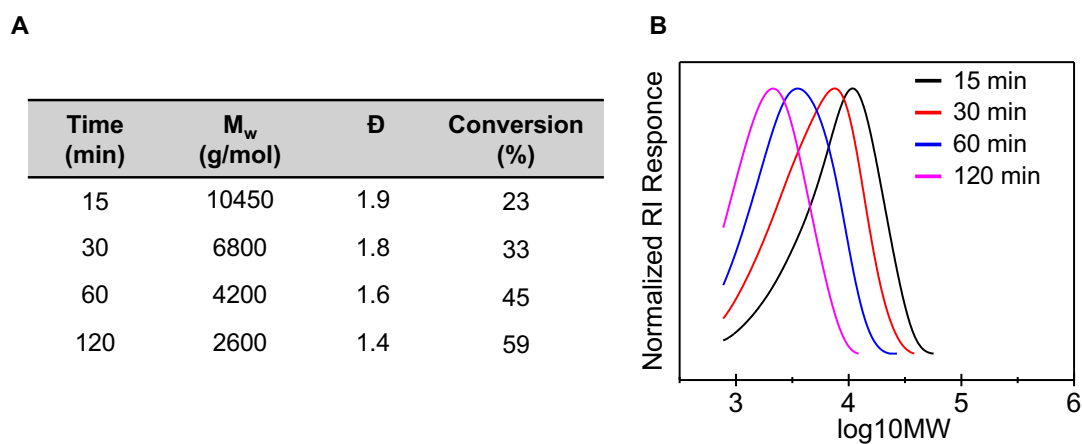
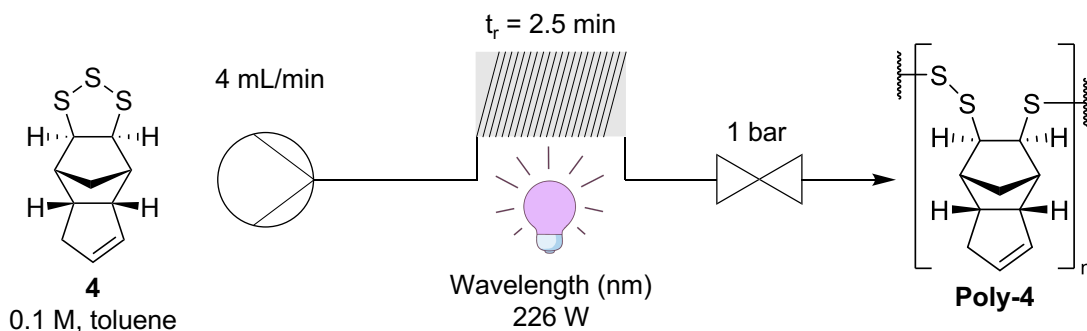


Figure S4.14: (A) Summary of ^1H NMR and GPC data for the photochemical polymerisation of

monomer **4** and monomer **10** at differing time points. (B) GPC (THF) of the photochemical polymerisation of monomer **4** and monomer **10** at differing time points.

Photochemical polymerisation in continuous flow – monomer **4**

Wavelength



A stock solution of monomer **4** (1.2 g, 5 mmol, 0.1 M) in toluene (50 mL) was prepared. For each reaction, 5 mL was passed through perfluoroalkoxyalkanes (PFA) tubing (10 mL, 21 °C) at a flow rate of 4 mL/min with irradiation from LEDs (365 nm, 226 W or 455 nm, 100 W) and backpressure regulation at 1 bar. The residence time for the reaction was 2.5 minutes. The product was collected in a glass vial (20 mL) and the solvent was removed under reduced pressure. The crude product was analysed by ^1H NMR spectroscopy (CDCl_3) and GPC (THF).

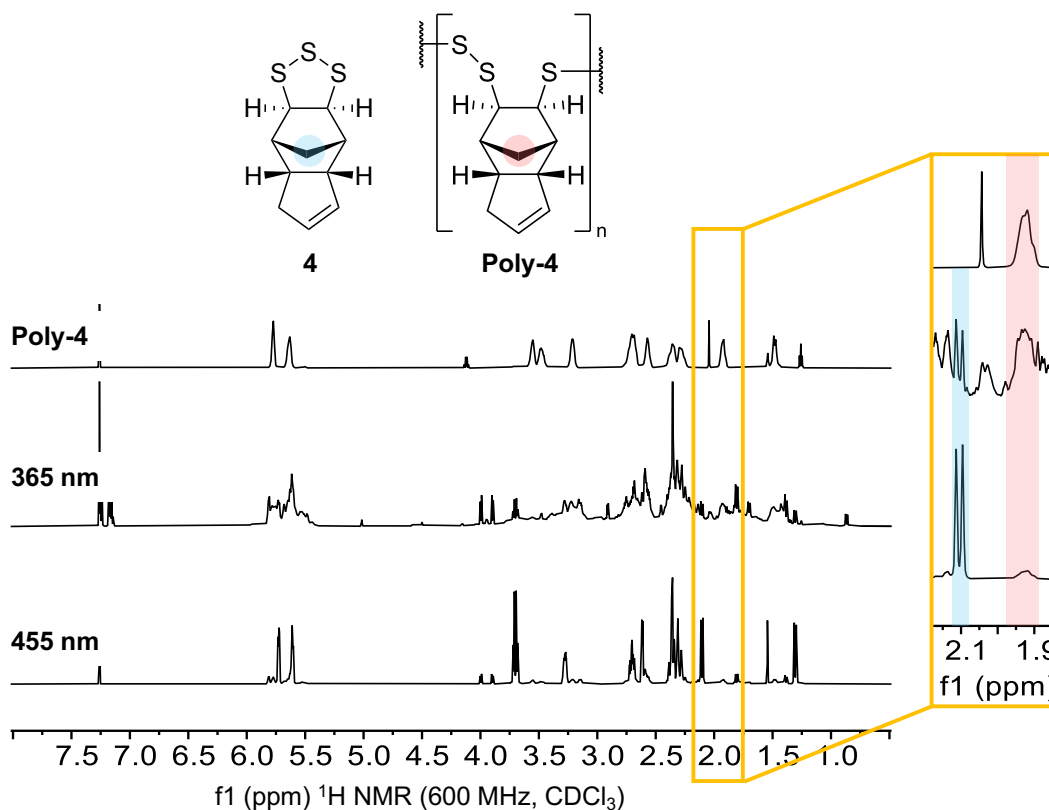


Figure S4.15: ^1H NMR spectra (600 MHz, CDCl_3) of photochemical polymerisation of monomer **4** in continuous flow at different wavelengths of light irradiation. The highlighted peaks of monomer **4** and **poly-4** were used to calculate conversion.

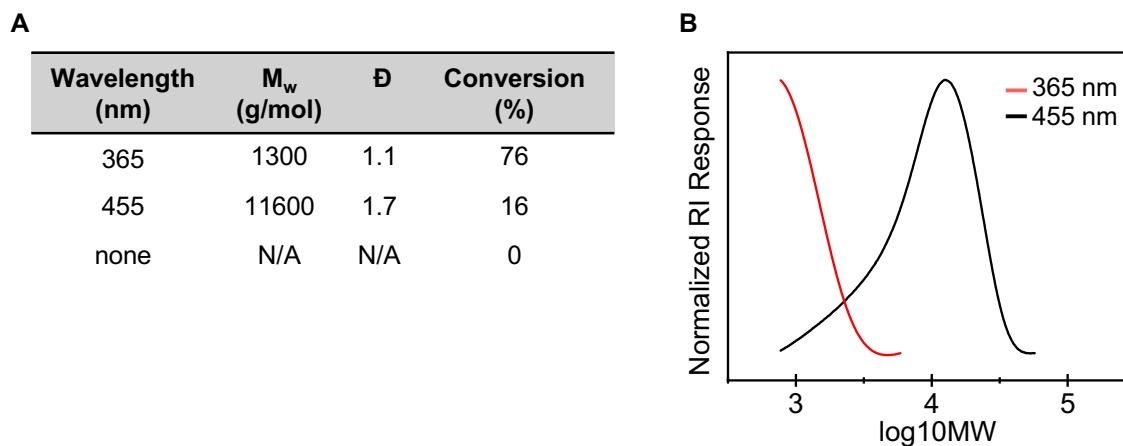
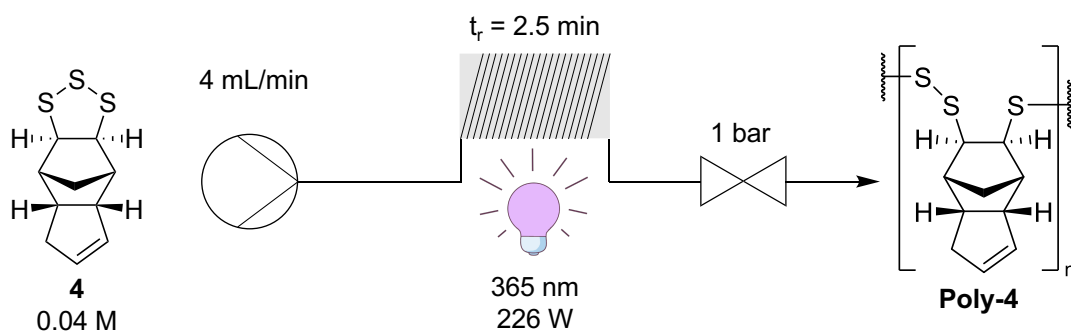


Figure S4.16: (A) Summary of ^1H NMR and GPC data for the photochemical polymerisation of monomer **4** at different wavelengths. (B) GPC (THF) of the photochemical polymerisation of monomer **4** at different wavelengths.

Solvent



For each of the following solvents a stock solution of monomer **4** (137 mg, 0.6 mmol, 15 mL, 0.04 M) was prepared: chloroform, ethyl acetate, hexane, tetrahydrofuran, acetone, toluene, 2-propanol, dichloromethane, methanol, dimethylformamide, acetonitrile and diethyl ether. For each reaction, 3 mL was passed through perfluoroalkoxyalkanes (PFA) tubing (10 mL, 21 °C) at a flow rate of 4 mL/min with irradiation from LEDs (365 nm, 226 W) and backpressure regulation at 1 bar. The residence time for the reaction was 2.5 minutes. The product was collected in a vial (20 mL) and the solvent was removed under reduced pressure. The crude product was analysed by ^1H NMR spectroscopy (CDCl_3) and GPC (THF).

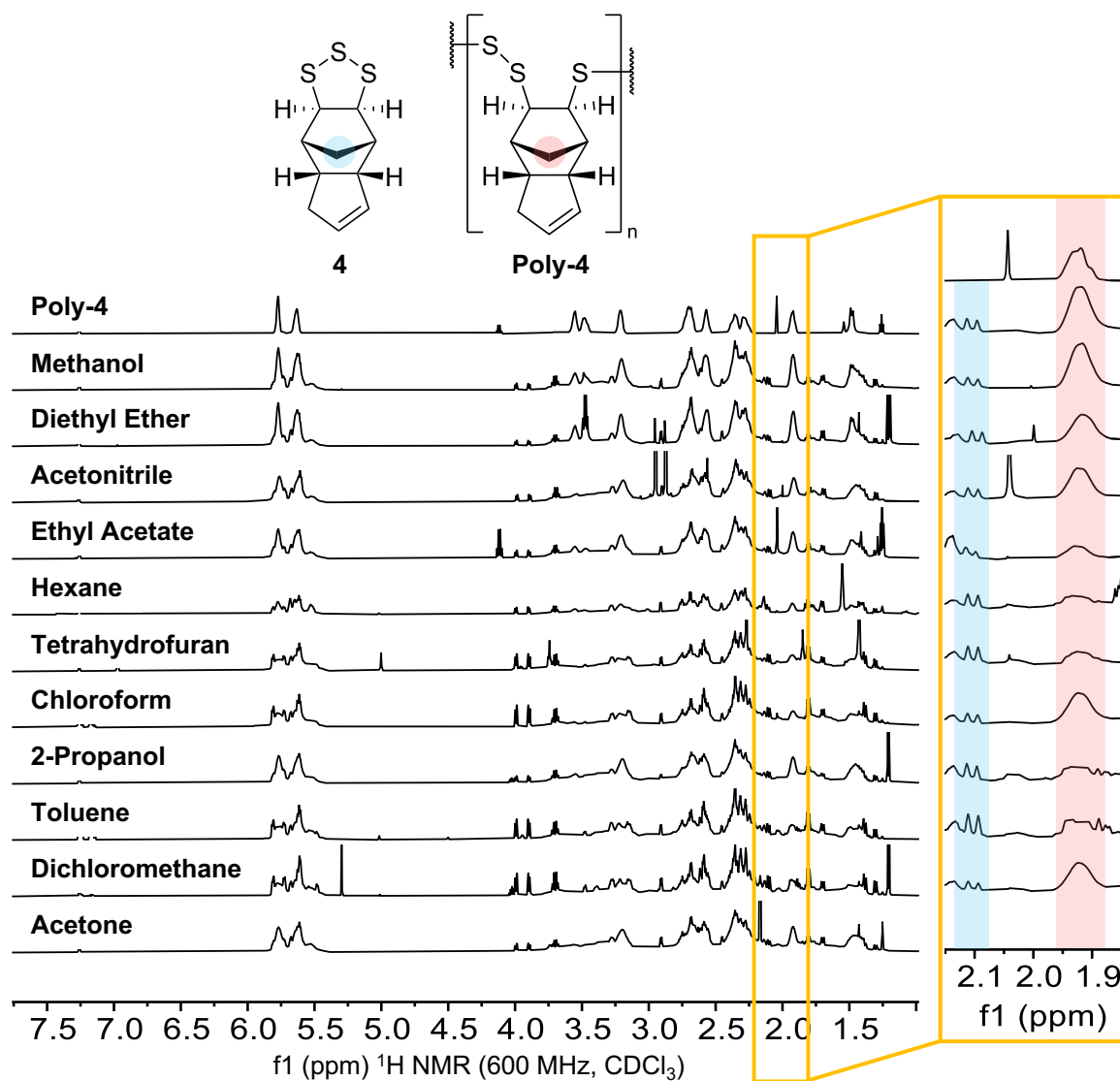


Figure S4.17: ^1H NMR spectra (600 MHz, CDCl_3) of photochemical polymerisation of monomer **4** in continuous flow in different solvents. The highlighted peaks of monomer **4** and **poly-4** were used to calculate conversion.

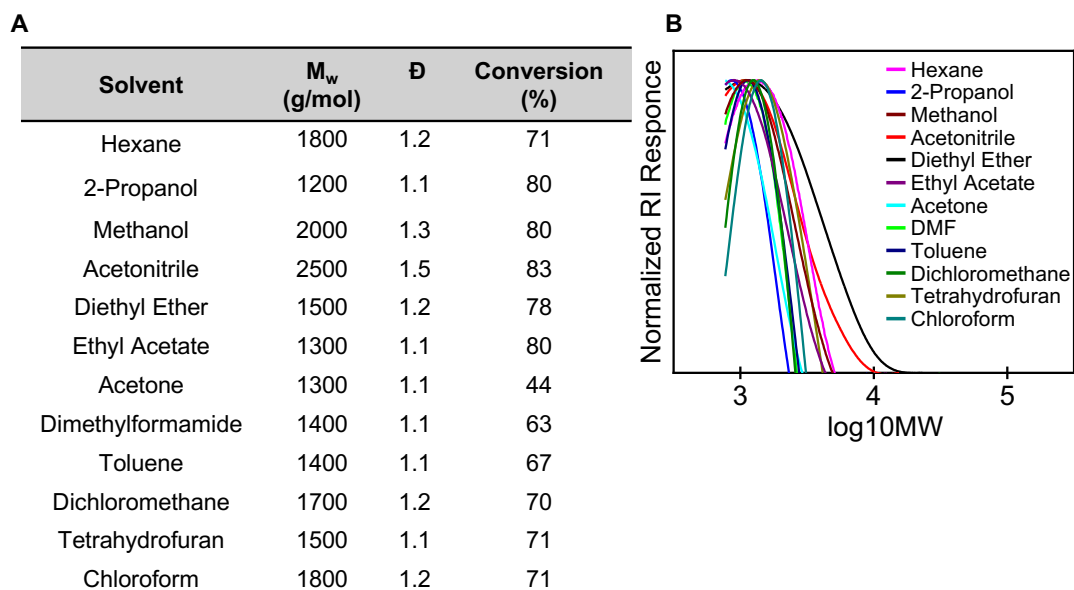
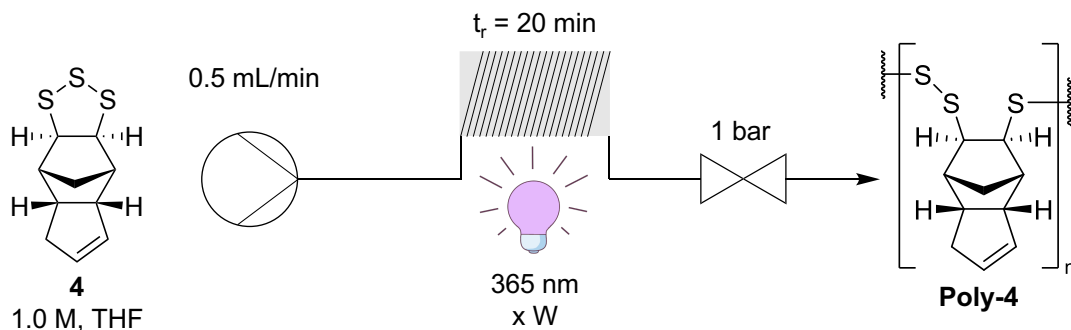


Figure S4.18: (A) Summary of ^1H NMR and GPC data for the photochemical polymerisation of monomer **4** in different solvents. (B) GPC (THF) of the photochemical polymerisation of monomer **4** in different solvents.

Light intensity



A stock solution of monomer **4** (2.28 g, 10 mmol, 1.0 M) in THF (10 mL) was prepared. For each reaction, 2 mL was passed through perfluoroalkoxyalkanes (PFA) tubing (10 mL, 21 °C) at a flow rate of 0.5 mL/min with irradiation from LEDs (365 nm, 226 W or 113 W or 22.6 W) and backpressure regulation at 1 bar. The residence time for the reaction was 20 minutes. The product was collected in a vial (20 mL) and the solvent was removed under reduced pressure. The crude product was analysed by ^1H NMR spectroscopy (CDCl_3) and GPC (THF).

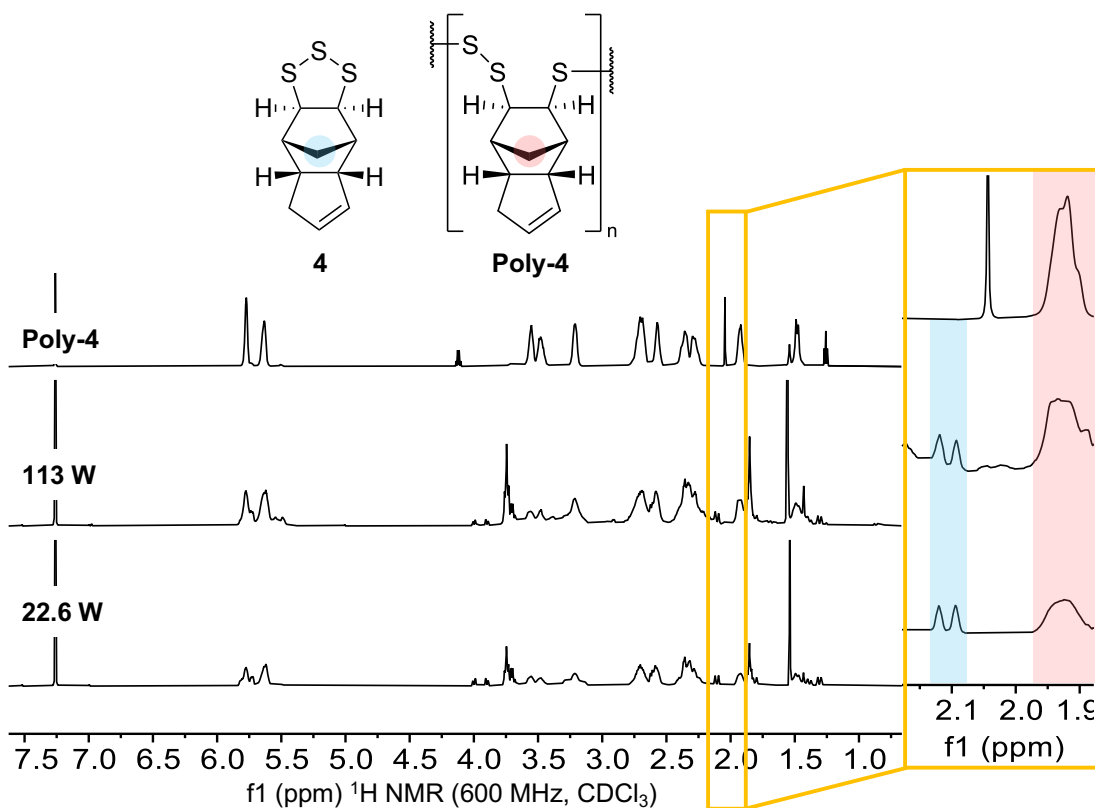


Figure S4.19: ¹H NMR spectra (600 MHz, CDCl₃) of photochemical polymerisation of monomer **4** in continuous flow at different light intensities. The highlighted peaks of monomer **4** and **poly-4** were used to calculate conversion.

A

Light intensity (W)	M _w (g/mol)	Đ	Conversion (%)
22.6	3000	1.4	78
113.0	1400	1.1	80

B

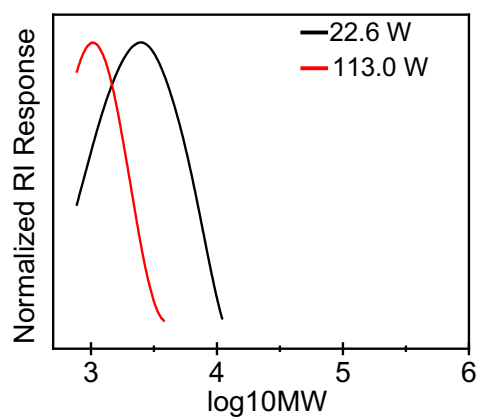
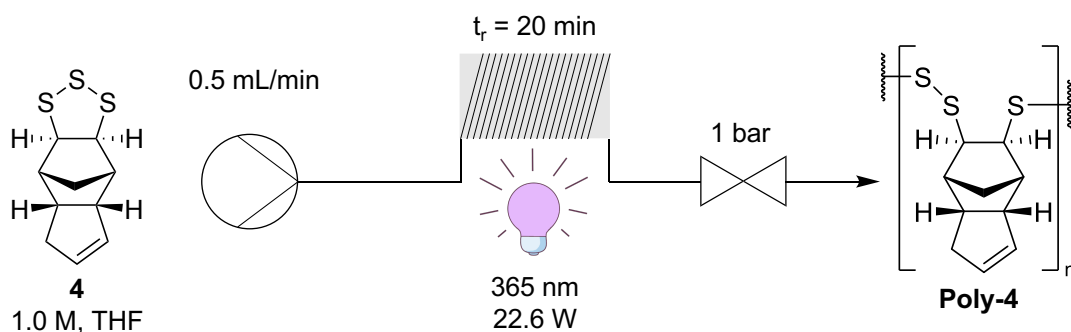


Figure S4.20: (A) Summary of ¹H NMR and GPC data for the photochemical polymerisation of monomer **4** at different light intensities. (B) GPC (THF) of the photochemical polymerisation of monomer **4** at different light intensities.

Temperature



A stock solution of monomer **4** (2.28 g, 10 mmol, 1.0 M) in THF (10 mL) was prepared. For each reaction, 2 mL was passed through perfluoroalkoxyalkanes (PFA) tubing (10 mL, -13 °C, 21 °C, or 60 °C) at a flow rate of 0.5 mL/min with irradiation from LEDs (365 nm, 22.6 W) and backpressure regulation at 1 bar. The residence time for the reaction was 20 minutes. The product was collected in a vial (20 mL) and the solvent was removed under reduced pressure. The crude product was analysed by ^1H NMR spectroscopy (CDCl_3) and GPC (THF).

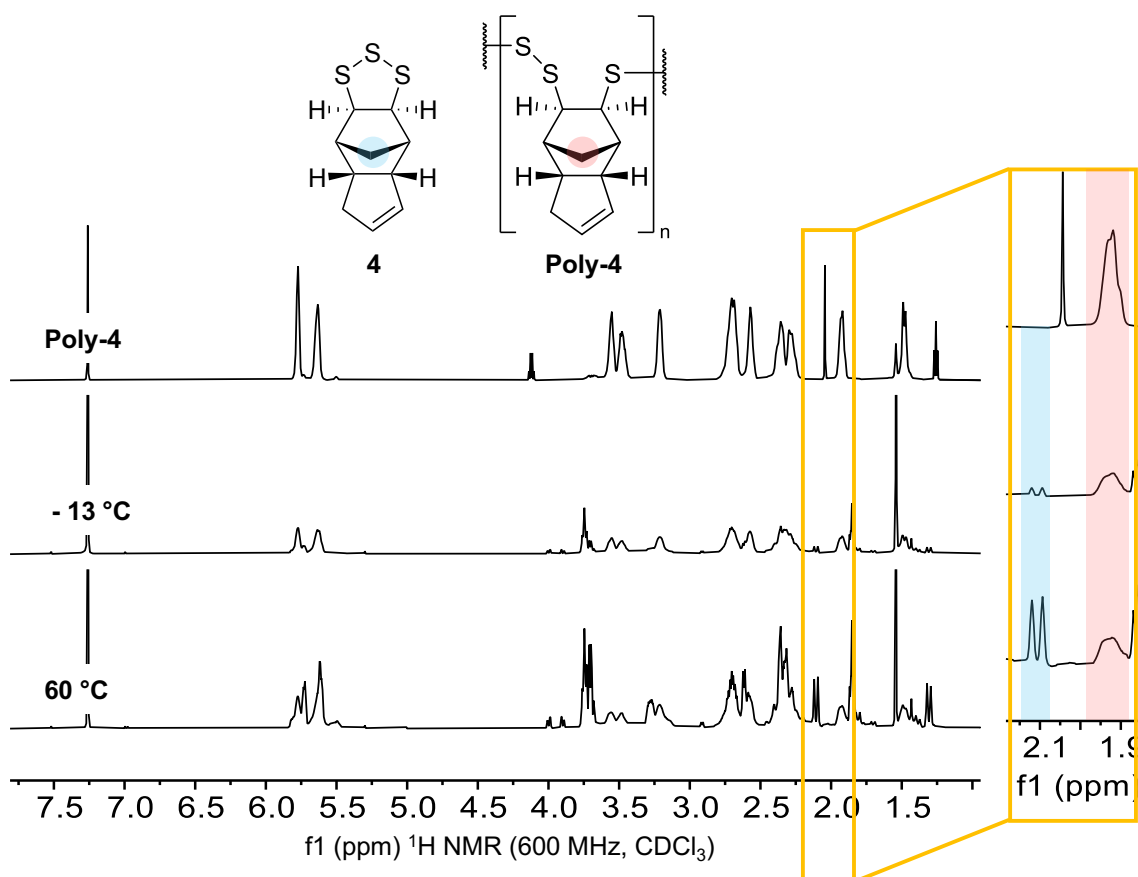


Figure S4.21: ^1H NMR spectra (600 MHz, CDCl_3) of photochemical polymerisation of monomer **4** in continuous flow at different temperatures. The highlighted peaks of monomer **4** and **poly-4** were used to calculate conversion.

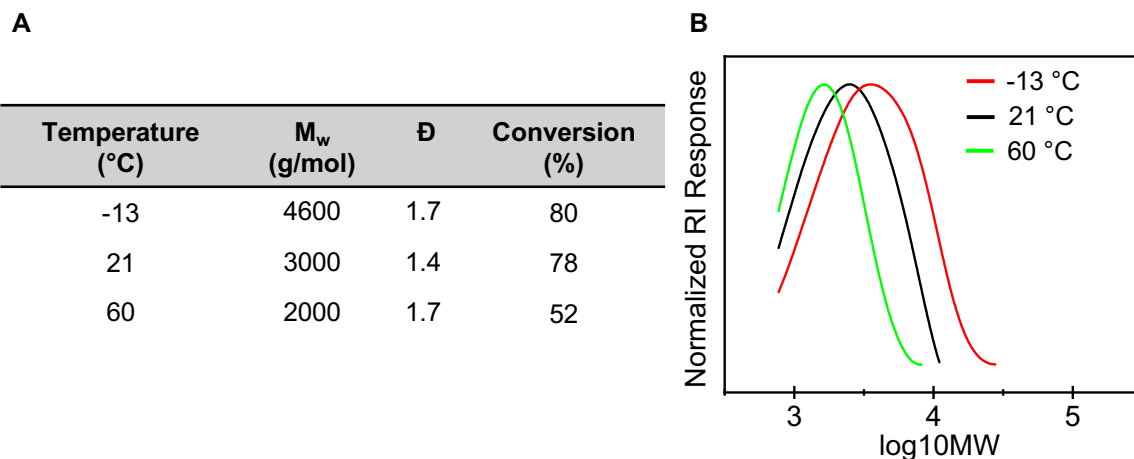
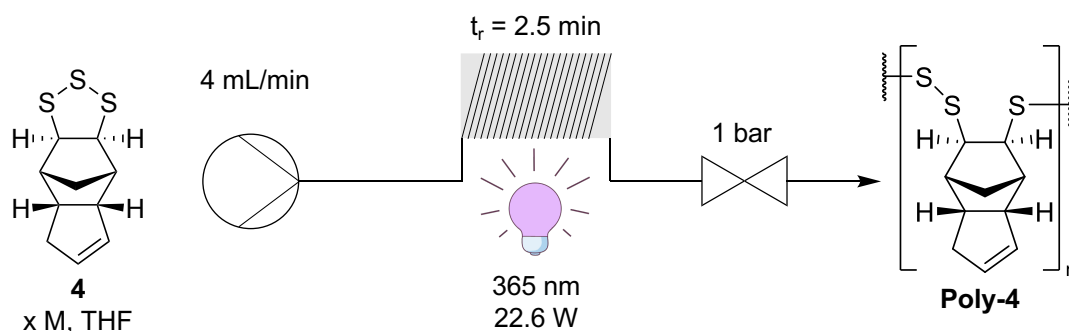


Figure S4.22: (A) Summary of ^1H NMR and GPC data for the photochemical polymerisation of monomer **4** at different temperatures. (B) GPC (THF) of the photochemical polymerisation of monomer **4** at different temperatures.

Concentration



The following stock solutions of monomer **4** were prepared in THF (10 mL): 0.1 M (228 mg, 1 mmol), 0.5 M (1.14 g, 5 mmol), 1.0 M (2.28 g, 10 mmol), 1.5 M (3.42 g, 15 mmol), and 2.0 M (4.56 g, 20 mmol). For each reaction, 10 mL was passed through perfluoroalkoxyalkanes (PFA) tubing (10 mL, 21 °C) at a flow rate of 4 mL/min with irradiation from LEDs (365 nm, 22.6 W) and backpressure regulation at 1 bar. The residence time for the reaction was 2.5 minutes. The product was collected in a vial (20 mL) and the solvent was removed under reduced pressure. The crude product was analysed by ^1H NMR spectroscopy (CDCl_3) and GPC (THF).

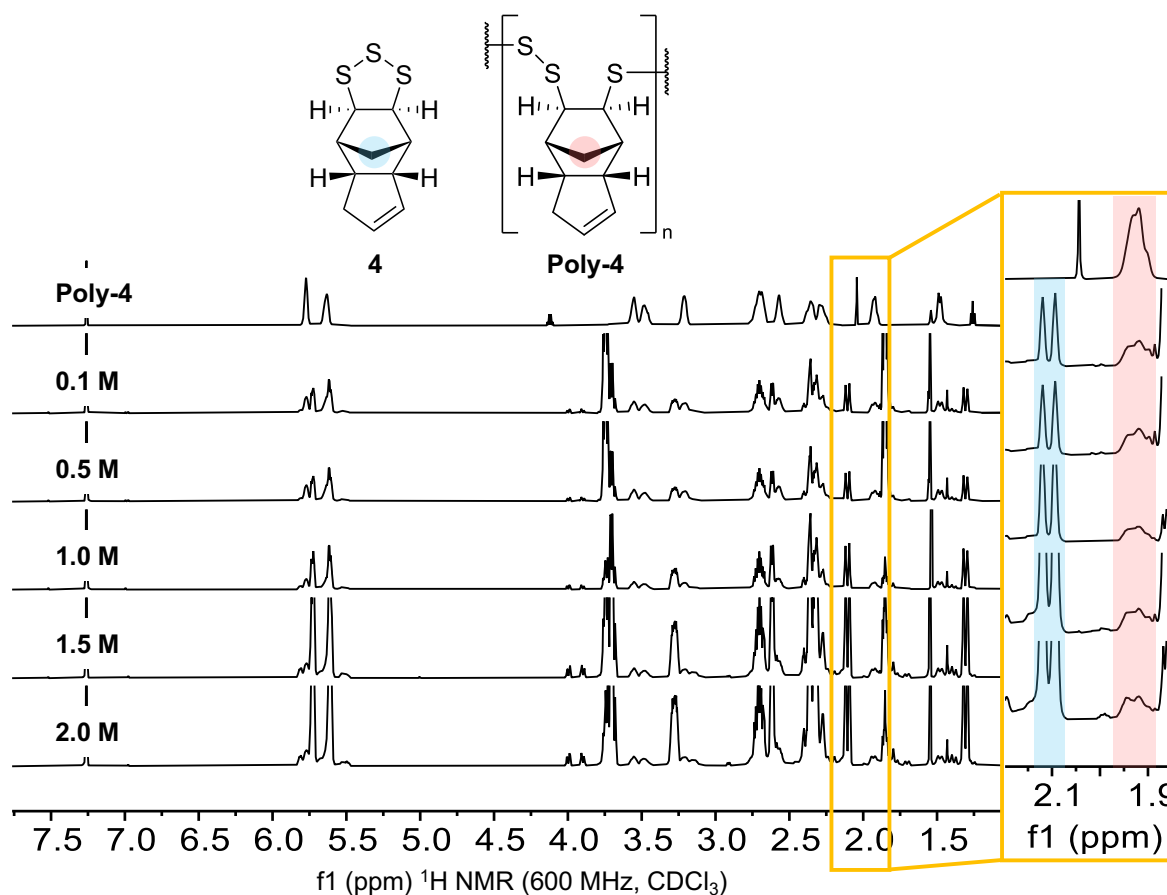


Figure S4.23: ^1H NMR spectra (600 MHz, CDCl_3) of photochemical polymerisation of monomer **4** in continuous flow at different concentrations. The highlighted peaks of monomer **4** and **poly-4** were used to calculate conversion.

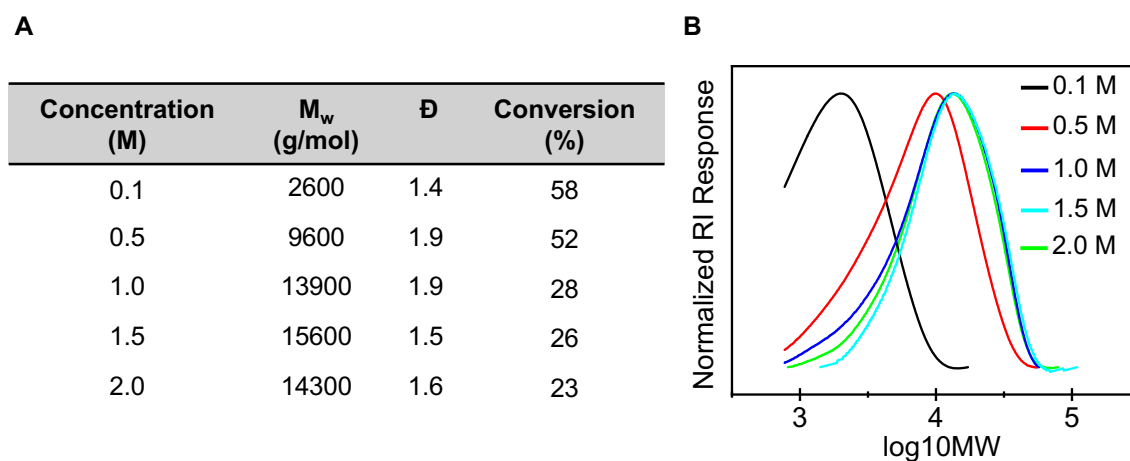
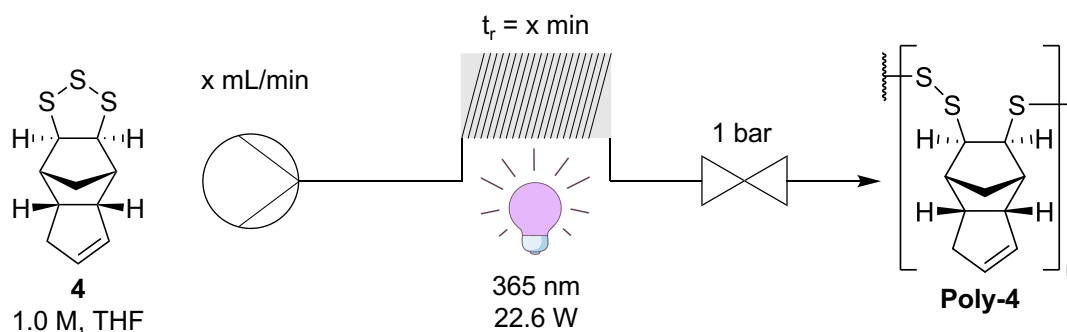


Figure S4.24: (A) Summary of ^1H NMR and GPC data for the photochemical polymerisation of monomer **4** at different concentrations. (B) GPC (THF) of the photochemical polymerisation of monomer **4** at different concentrations.

Flow rate



A stock solution of monomer **4** (2.28 g, 10 mmol, 1.0 M) in THF (10 mL) was prepared. For each reaction, 2 mL was passed through perfluoroalkoxyalkanes (PFA) tubing (10 mL, 21 °C) at different flow rates and backpressure regulation at 1 bar. The product was collected in a vial (20 mL) and the solvent was removed under reduced pressure. The crude product was analysed by ^1H NMR spectroscopy (CDCl_3) and GPC (THF).

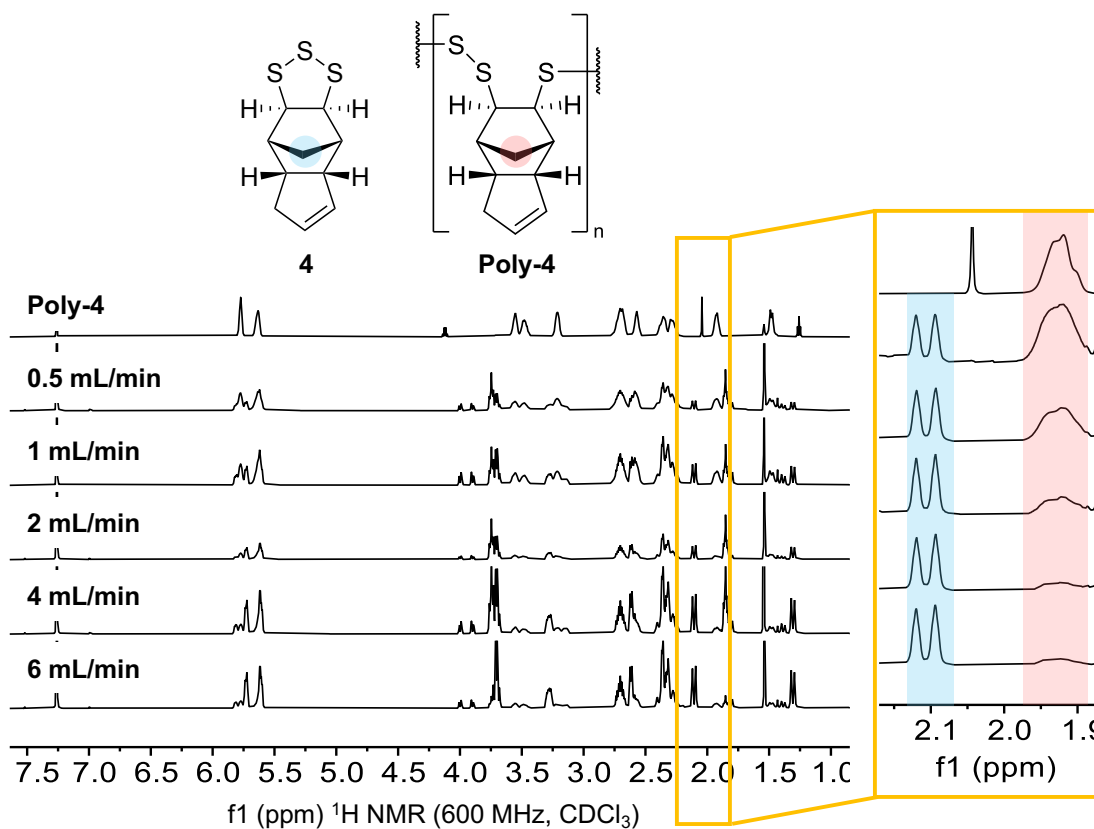


Figure S4.25: ^1H NMR spectra (600 MHz, CDCl_3) of photochemical polymerisation of monomer **4** in continuous flow at different flow rates. The highlighted peaks of monomer **4** and **poly-4** were used to calculate conversion.

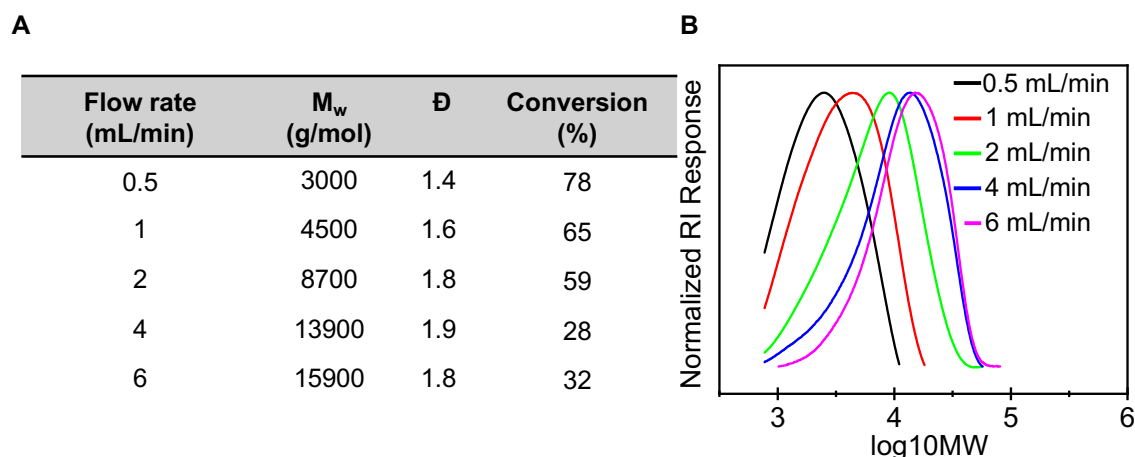
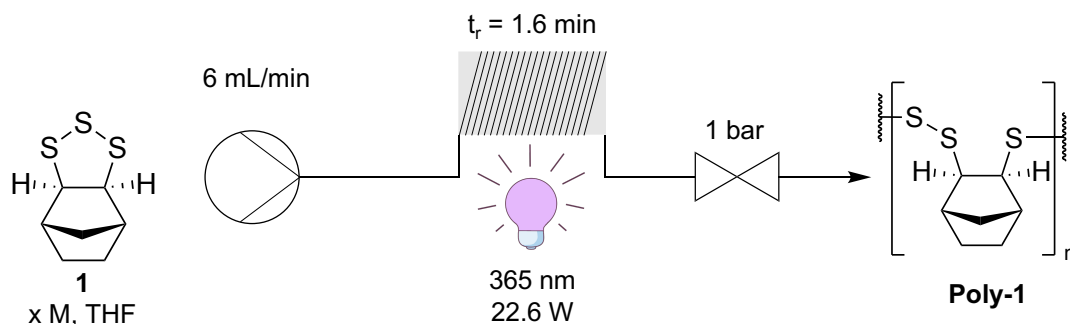


Figure S4.26: (A) Summary of ^1H NMR and GPC data for the photochemical polymerisation of monomer **4** at different flow rates. (B) GPC (THF) of the photochemical polymerisation of monomer **4** at different flow rates.

Photochemical polymerisation in continuous flow – monomer **1**

Concentration



The following stock solutions of monomer **1** were prepared in THF (2 mL): 1.0 M (380 mg, 2 mmol), 3.8 M (1.44 g, 7.5 mmol), 5.0 M (1.89 g, 10 mmol). For each reaction, 1.5 mL was passed through perfluoroalkoxyalkanes (PFA) tubing (10 mL, 21 °C) at a flow rate of 6 mL/min with irradiation from LEDs (365 nm, 22.6 W) and backpressure regulation at 1 bar. The residence time for the reaction was 1.6 minutes. The product was collected in a vial (20 mL) and the solvent was removed under reduced pressure. The crude product was analysed by ^1H NMR spectroscopy (CDCl_3) and GPC (THF).

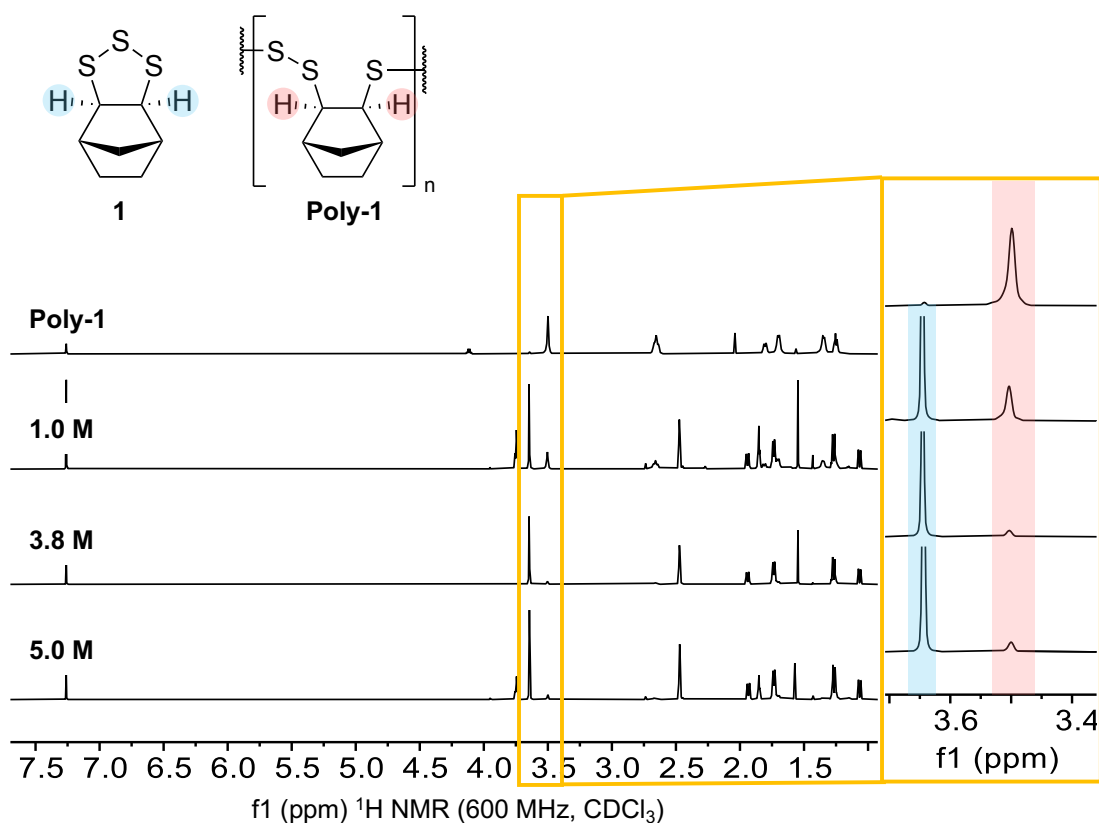


Figure S4.27: ¹H NMR spectra (600 MHz, CDCl₃) of photochemical polymerisation of monomer **1** in continuous flow at different concentrations. The highlighted peaks of monomer **1** and **poly-1** were used to calculate conversion.

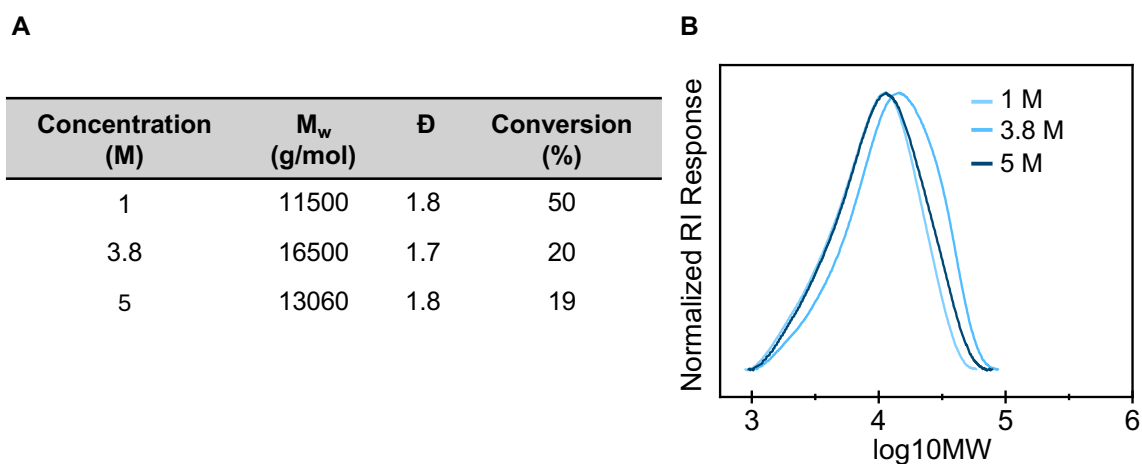
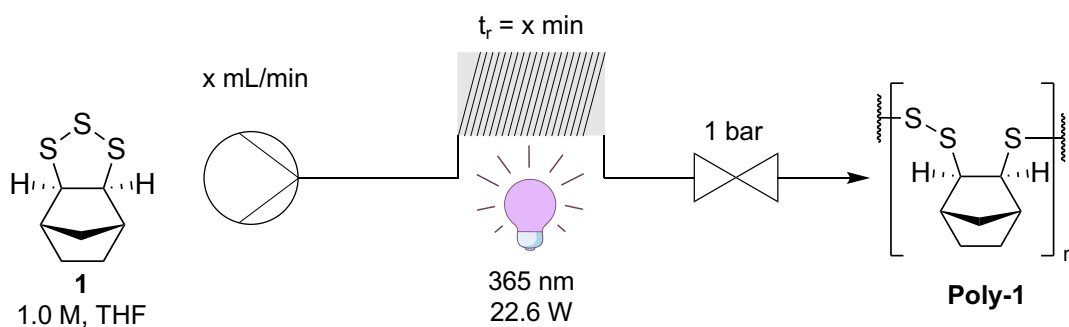


Figure S4.28: (A) Summary of ¹H NMR and GPC data for the photochemical polymerisation of monomer **1** at different concentrations. (B) GPC (THF) of the photochemical polymerisation of monomer **4** at different flow rates.

Flow rate



A stock solution of monomer **1** (9.5 g, 50 mmol, 1.0 M) in THF (50 mL) was prepared. For each reaction, the total stock solution was passed through perfluoroalkoxyalkanes (PFA) tubing (10 mL, 21 °C) with irradiation from LEDs (365 nm, 22.6 W) at different flow rates and backpressure regulation at 1 bar. The product was collected in a round bottom flask (100 mL) and the solvent was removed under reduced pressure. Chloroform (10 mL) was added to re-dissolve the solids and then ethyl acetate (40 mL) was added to precipitate the polymer product and remove it from the unreacted monomer **1** via filtration. The unreacted monomer **1** was collected by evaporating the filtrate under reduced pressure. The unreacted monomer **1** was redissolved in THF to make a concentration of 1.0 M. For each flow rate, this process was repeated 1-5 times. The purified polymer from each flow rate was analysed by ^1H NMR spectroscopy (CDCl_3) and GPC (THF).

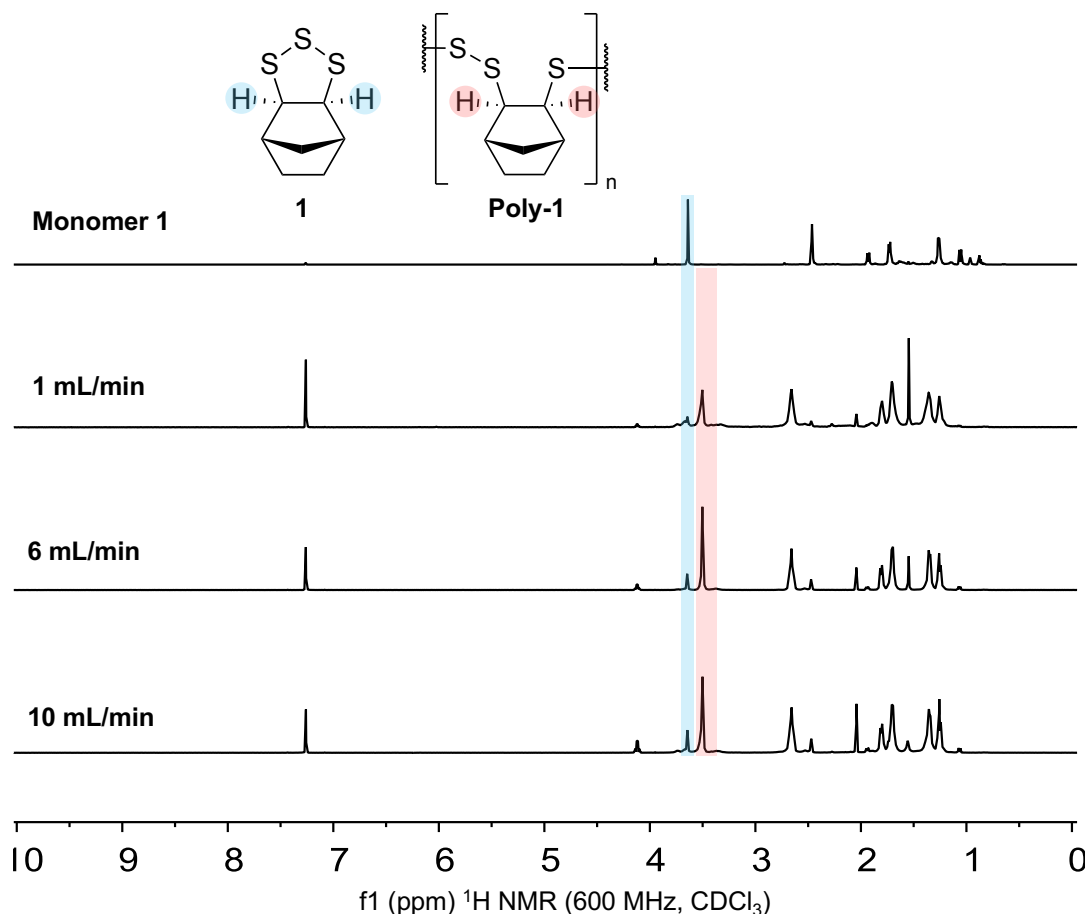


Figure S4.29: ^1H NMR spectra (600 MHz, CDCl_3) poly-**1** produced by photochemical polymerisation of monomer **1** in continuous flow at different flow rates.

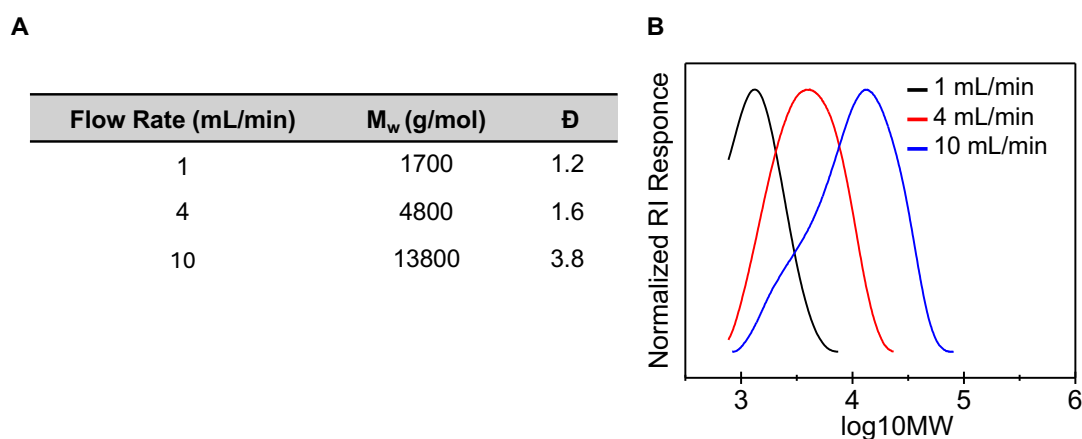
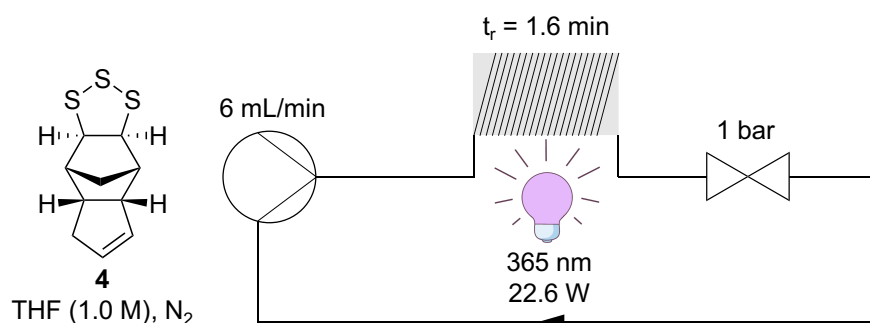


Figure S4.30: (A) Summary of ^1H NMR and GPC data for the photochemical polymerisation of monomer **1** at different flow rates. (B) GPC (THF) of the photochemical polymerisation of monomer **1** at different flow rates.

Recirculation under an inert atmosphere



A solution of monomer **4** (4.56g, 20 mmol, 1.0 M) in THF (20 mL) was prepared and purged with nitrogen (5 minutes). A stir bar and the monomer solution were transferred to a 2-neck round bottom flask under a nitrogen atmosphere. One neck was blocked with a rubber septum, while the other neck contained the inlet tube and was sealed with aluminium foil. The through perfluoroalkoxyalkanes (PFA) tubing (10 mL, 21 °C) (previously filled with dry THF) were loaded with the monomer solution until the solution reached the outlet. The outlet tube was then transferred to the second neck on the bound bottom flask and resealed with aluminium foil. This meant that the monomer solution was not diluted with the THF that was already in the system. The solution then circulated and irradiated from LEDs (365 nm, 22.6 W) at a flow rate of 6 mL/min (residence time = 1.6 minutes) and backpressure regulation at 1 bar. At 3, 6, 9, 12, 16, 24, 48, 85 and 125 minutes, an aliquot (0.10 mL) of the recirculating solution was taken from the 2-neck round bottom flask, concentrated under reduced pressure and analysed by ¹H NMR spectroscopy (CDCl₃) and GPC (THF). After 125 minutes, the flow system was fully unloaded of the reaction mixture. Ethyl acetate (20 mL) was added to the mixture causing the polymer to precipitate. The polymer was filtered and washed with ethyl acetate (3 x 10 mL). The precipitated polymer was then redissolved in chloroform (5 mL) and precipitated with ethyl acetate (20 mL) before purification by filtration a second time (1.19 g, 25%).

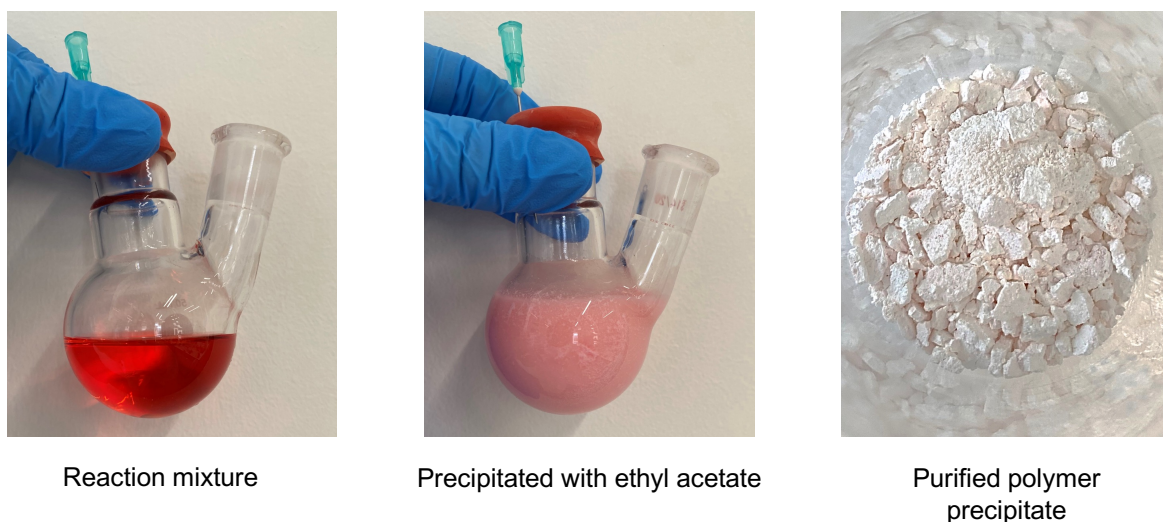


Figure S4.31: Work up of reaction solution.

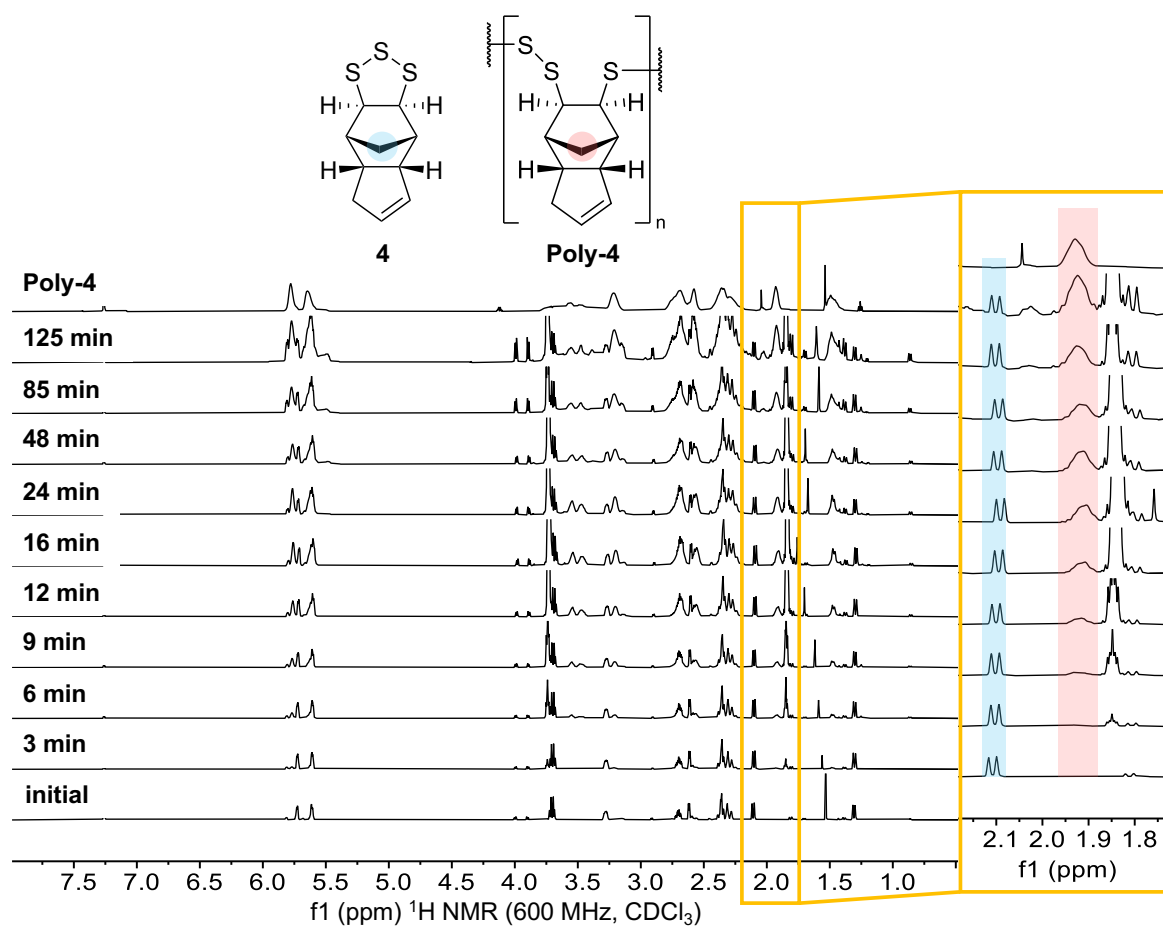


Figure S4.32: $^1\text{H NMR}$ spectra (600 MHz, CDCl_3) of photochemical polymerisation of monomer **4** (1.0 M, THF, N_2) recirculated under continuous flow. The highlighted peaks of monomer **4** and **poly-4** were used to calculate conversion.

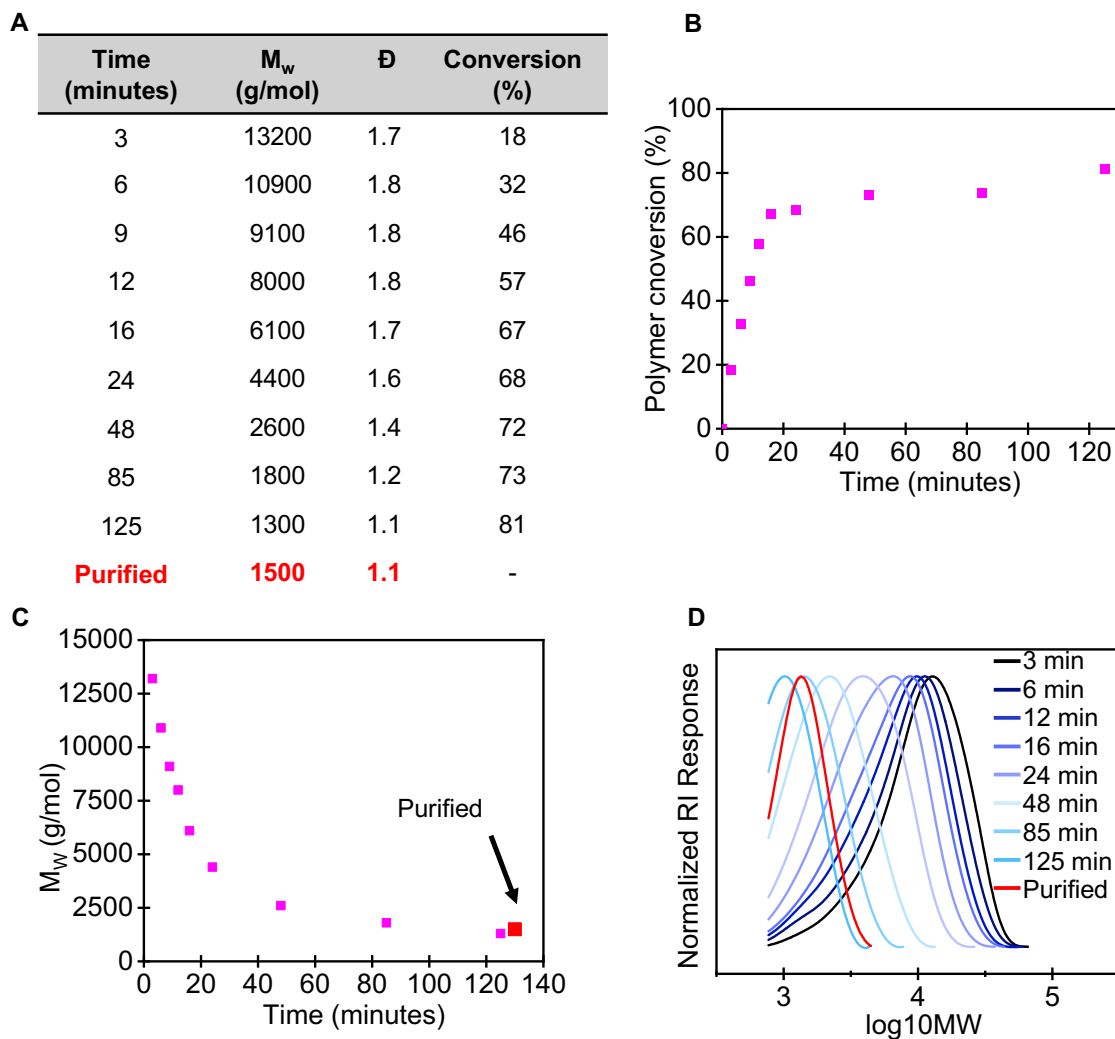
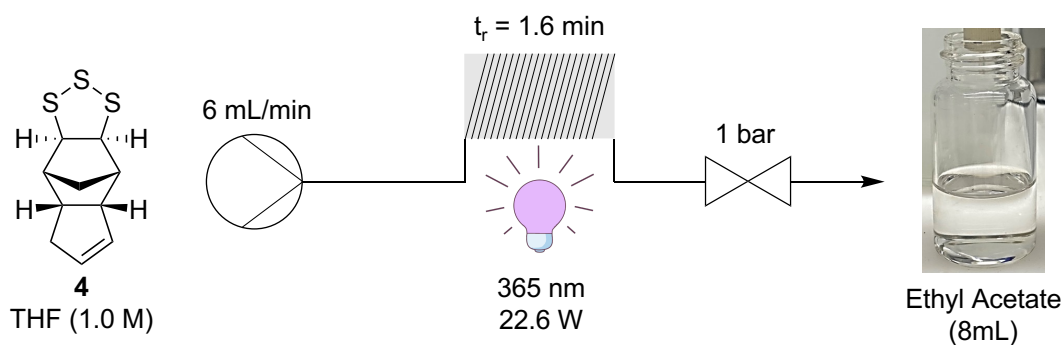


Figure S4.33: (A) Summary of ^1H NMR and GPC data for the photochemical polymerisation of monomer **4** recirculated under continuous flow. (B) Graph showing polymer conversion trend over time. (C) Graph showing polymer molecular weight trend over time. (D) GPC (THF) of the photochemical polymerisation of monomer **4** recirculated under continuous flow.

Direct precipitation of polymer after UV-irradiation



A stock solution of monomer **4** (2.28 g, 10 mmol, 1.0 M) in THF (10 mL) was prepared. 8mL was passed through perfluoroalkoxyalkanes (PFA) tubing (10 mL, 21 °C) at a flow rate of 6 mL/min with irradiation from LEDs (365 nm, 22.6 W) and backpressure regulation at 1 bar. The residence time for the reaction was 1.6 minutes. The product was collected in a vial (20 mL) containing ethyl acetate (8 mL), causing the polymer to precipitate. The precipitate was purified by filtration and wash with ethyl acetate (3 x 10 mL). The precipitated polymer was then dried under vacuum (296 mg, 16%). The polymer product was analysed by ^1H NMR spectroscopy (CDCl_3) and GPC (THF).



Figure S4.34: Direct precipitation of reaction solution in ethyl acetate.

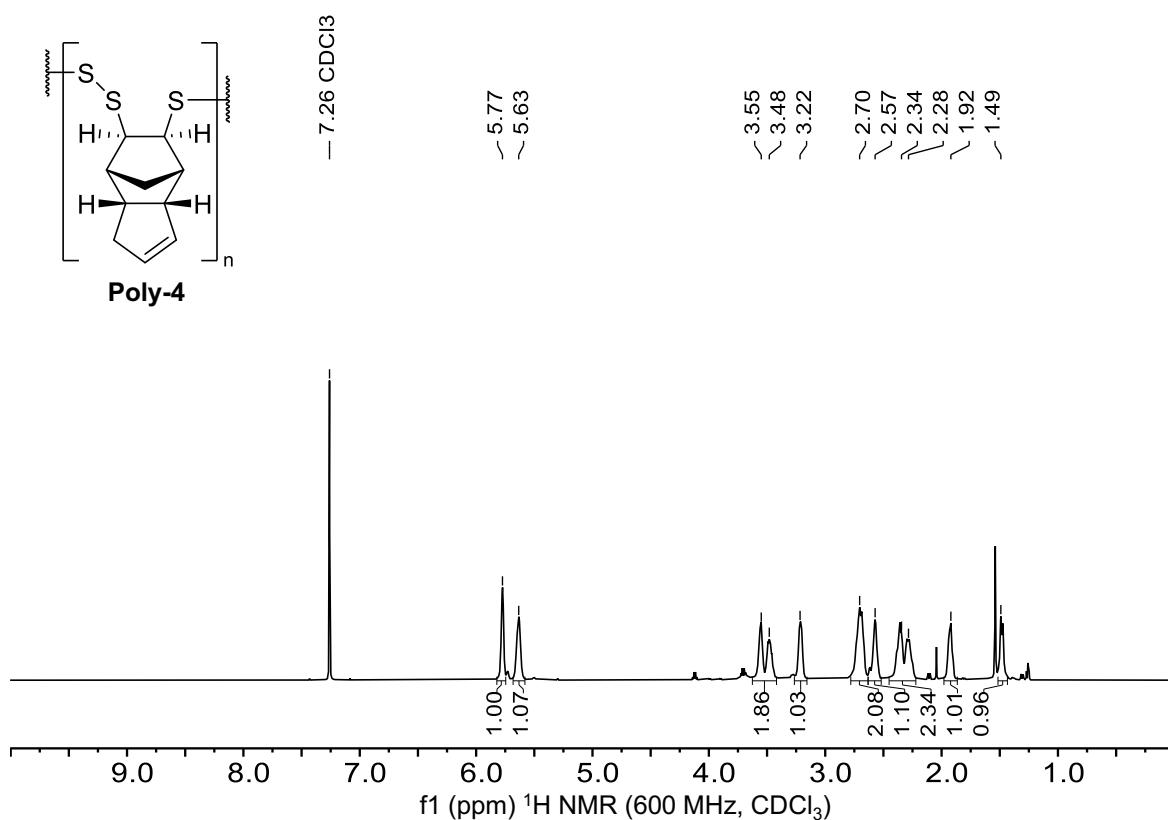


Figure S4.35: ^1H NMR spectra (600 MHz, CDCl_3) of **poly-4** directly precipitated at continuous flow outlet.

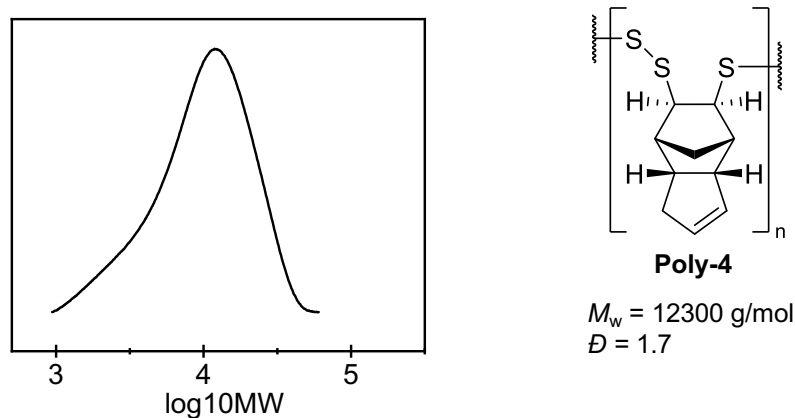
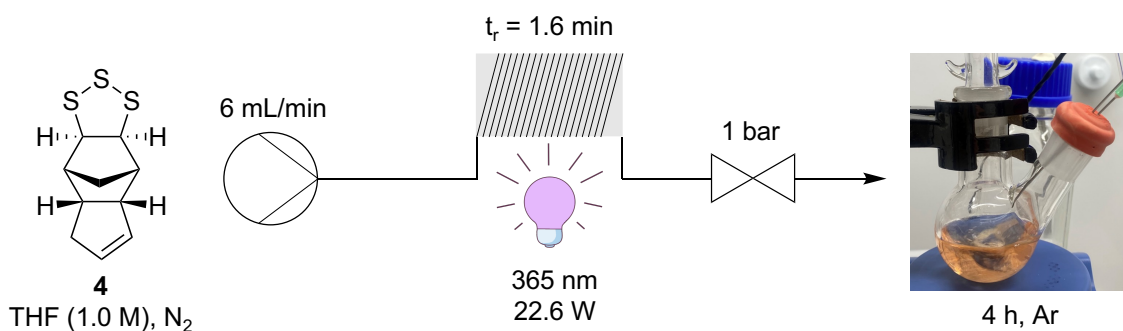


Figure S4.36: GPC (THF) of **poly-4** directly precipitated at continuous flow outlet.

Reactivity of **poly-4** after UV irradiation under an inert atmosphere



A solution of monomer **4** (2.28 g, 10 mmol, 1.0 M) in THF (10 mL) was prepared and purged with nitrogen (5 minutes). 8 mL was passed through perfluoroalkoxyalkanes (PFA) tubing (10 mL, 21 °C) at a flow rate of 6 mL/min with irradiation from LEDs (365 nm, 22.6 W) and backpressure regulation at 1 bar. The residence time for the reaction was 1.6 minutes. The product was collected in a sealed 2-neck round bottom flask containing a stir bar. The other neck was stopped with a rubber septum containing an argon stream and a vent. After the mixture had completely passed into the round bottom, an aliquot (0.1 mL) taken at 3, 9, 24 and 240 minutes from the 2-neck round bottom flask, concentrated under reduced pressure and analysed by ^1H NMR spectroscopy (CDCl_3) and GPC (THF). Ethyl acetate (20 mL) was added to the remaining mixture causing the polymer to precipitate. The polymer was filtered and washed with ethyl acetate (3 x 10 mL). The precipitated polymer was then collected and dried under vacuum (276 mg, 15%).

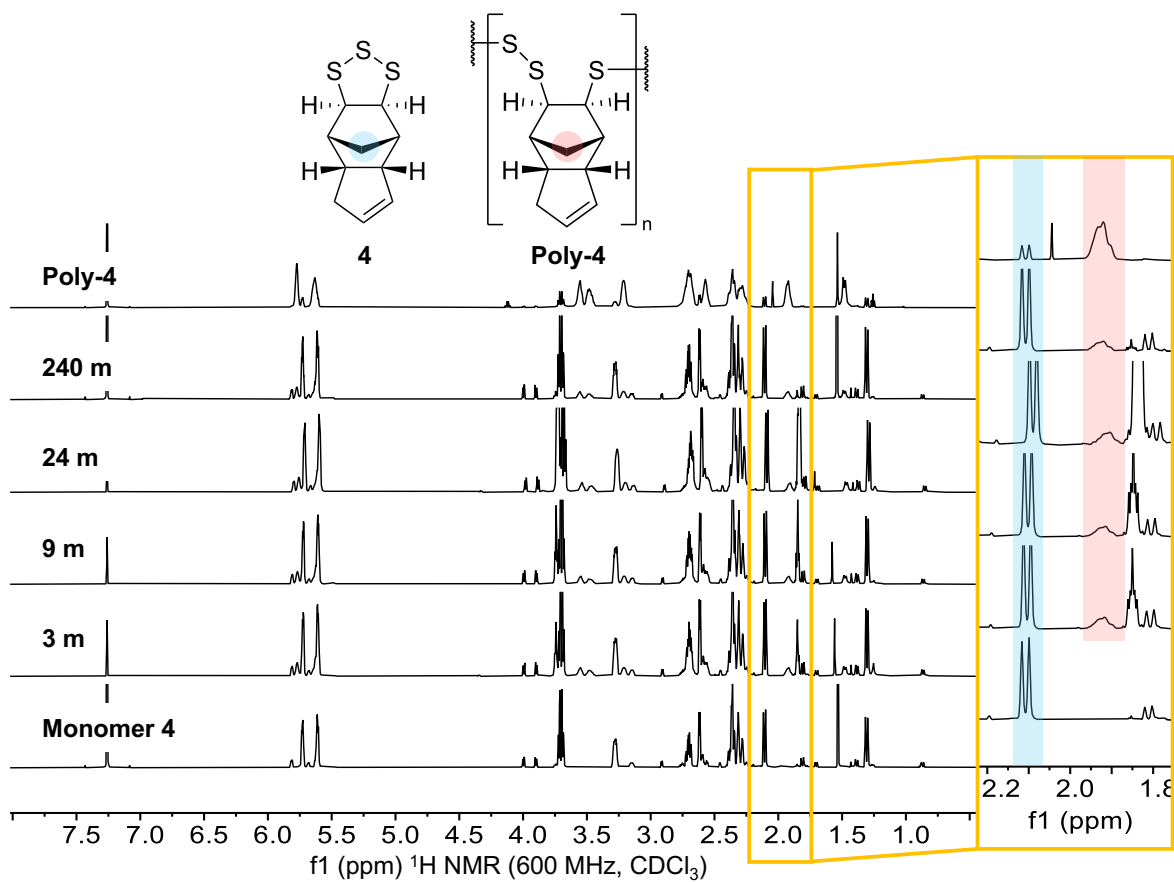


Figure S4.37: ^1H NMR spectra (600 MHz, CDCl_3) of **poly-4** after photochemical polymerisation in continuous flow. The highlighted peaks of monomer **4** and **poly-4** were used to calculate conversion.

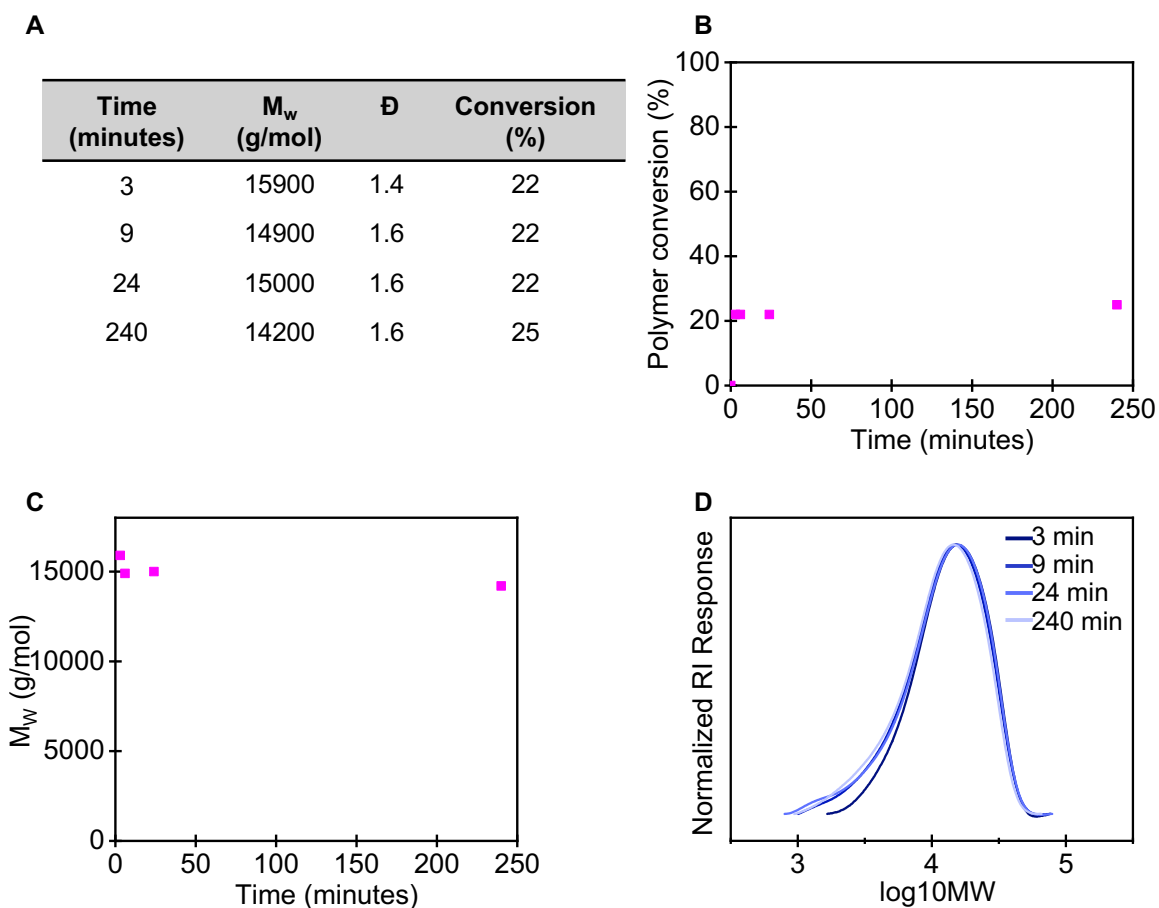
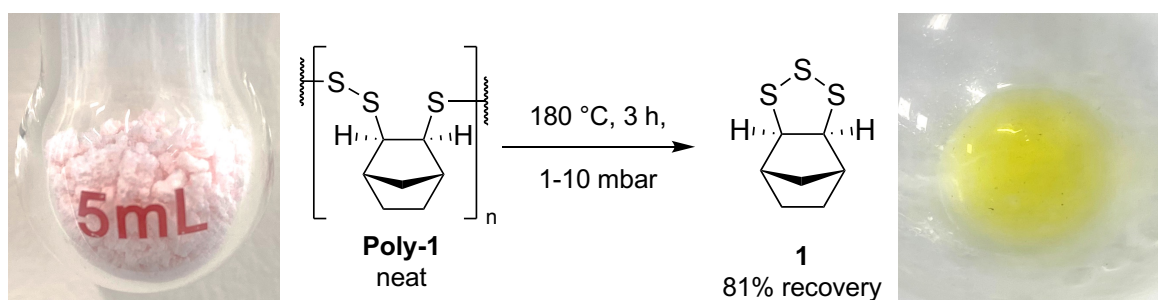


Figure S4.38: (A) Summary of ^1H NMR and GPC data for the reactivity of **poly-4** after photochemical polymerisation in continuous flow. (B) Graph showing polymer conversion trend over time. (C) Graph showing polymer molecular weight trend over time. (D) GPC (THF) of **poly-4** after photochemical polymerisation in continuous flow.

Thermal depolymerisation



Poly-1 (0.96 g , $M_w = 13800\text{ g/mol}$, $\bar{D} = 1.9$) was heated at $180\text{ }^\circ\text{C}$ under high vacuum ($1\text{-}10\text{ mbar}$) using a short-path distillation apparatus. After 3 hours, a yellow oil was observed in the collection

chamber. A sample of the yellow oil was analysed by ^1H NMR spectroscopy which revealed the oil to be highly pure monomer **1** (0.78 g, 81%).

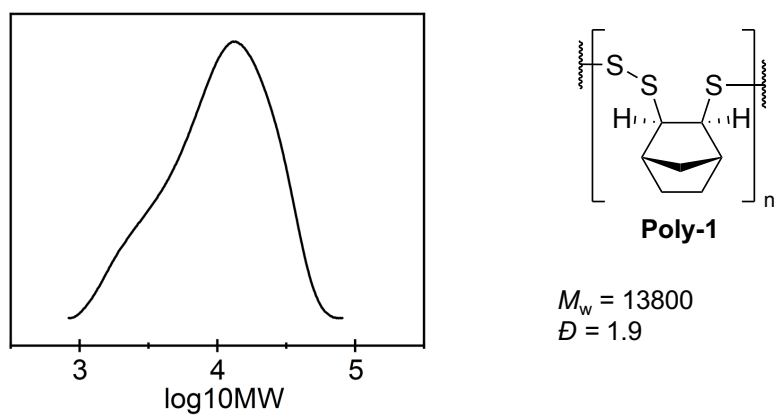


Figure S4.39: GPC (THF) of **poly-1** before undergoing thermal recycling.

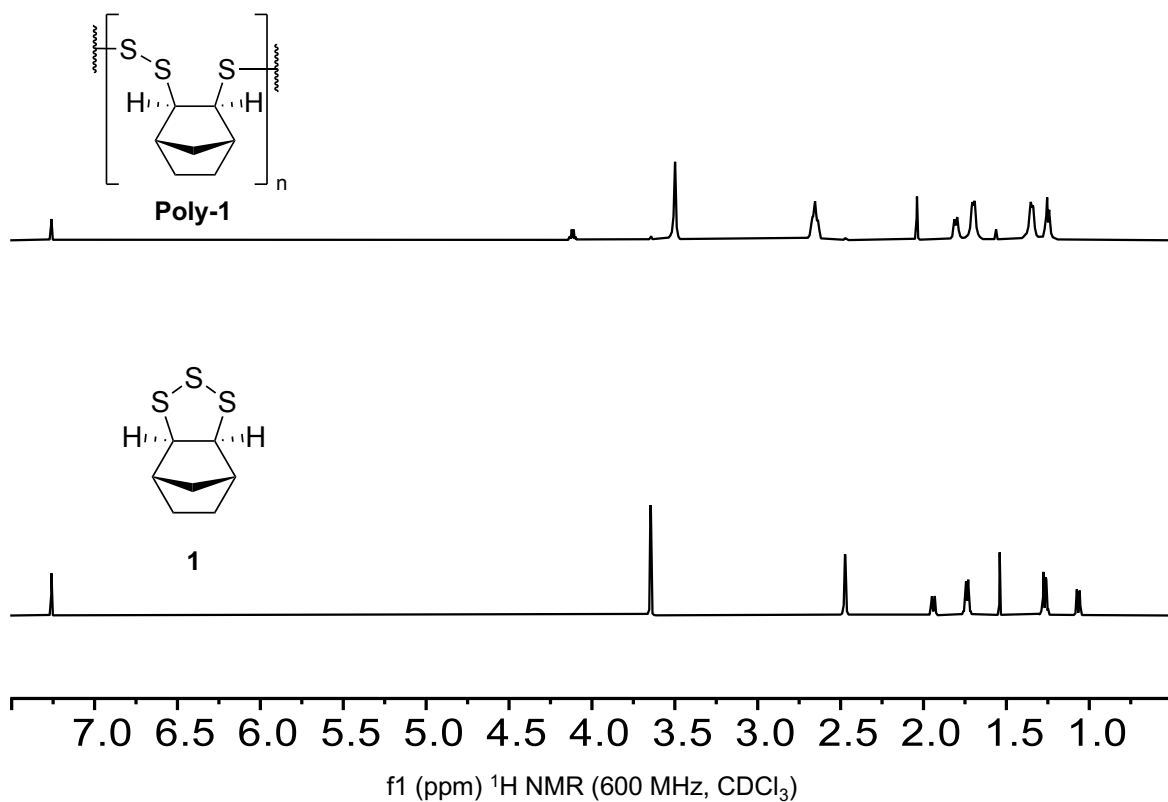
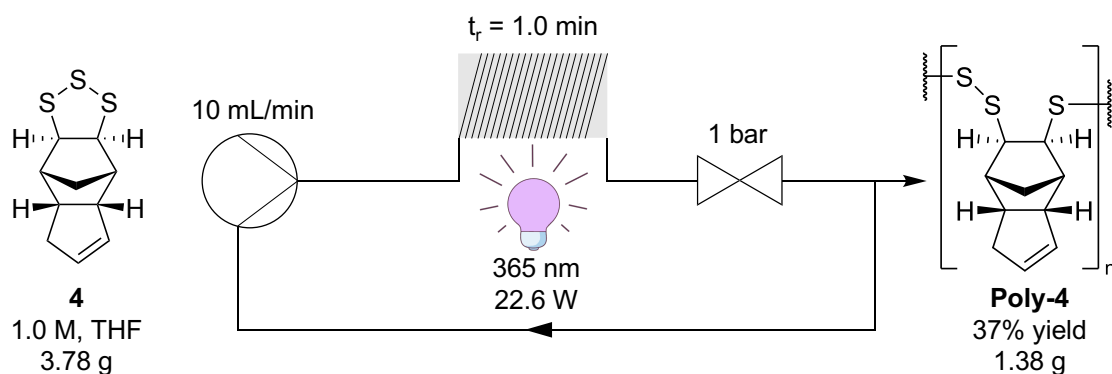


Figure S4.40: ^1H NMR spectrum (600 MHz, CDCl_3) of **poly-1** before undergoing thermal recycling

(top). ^1H NMR spectrum (600 MHz, CDCl_3) of monomer **1** recovered from the thermal recycling of **poly-1** (bottom).

Large scale preparation of poly(trisulfides) in continuous flow

Poly-4



A solution of monomer **4** (2.28 g, 10 mmol, 1.0 M) in THF (10 mL) was prepared. The solution was passed through perfluoroalkoxyalkanes (PFA) tubing (10 mL, 21 °C) at a flow rate of 10 mL/min with irradiation from LEDs (365 nm, 22.6 W) and backpressure regulation at 1 bar. The residence time for the reaction was 1.0 minutes. The product was collected in a 20 mL vial. The product was concentrated under reduced pressure and redissolved in chloroform (5 mL). Ethyl acetate (15 mL) was added to precipitate the polymer which was collected by filtration. The filtrate was concentrated under reduced pressure and its mass was recorded (1.96 g). The concentrated filtrate was then charged with monomer **4** (316 mg) and THF (10 mL) resulting in a 1.0 M solution. The process was repeated 6 times. The collected polymer was combined and redissolved in chloroform (20 mL), ethyl acetate (60 mL) was added to precipitate the polymer which was collected by filtration and dried under vacuum resulting in 1.38 g of **poly-1**. The polymer was analysed by ^1H NMR (CDCl_3) and GPC (THF).

Amount of monomer **4** added after each reaction: #2 (316 mg), #3 (321 mg), #4 (283 mg), #5 (170 mg), #6 (414 mg). Total monomer added (3.78 g). Total polymer yield (37%). Monomer recovered (1.88 g, 49%). Monomer recovered from filtrate from combined polymer purification (0.51 g, 13 %).

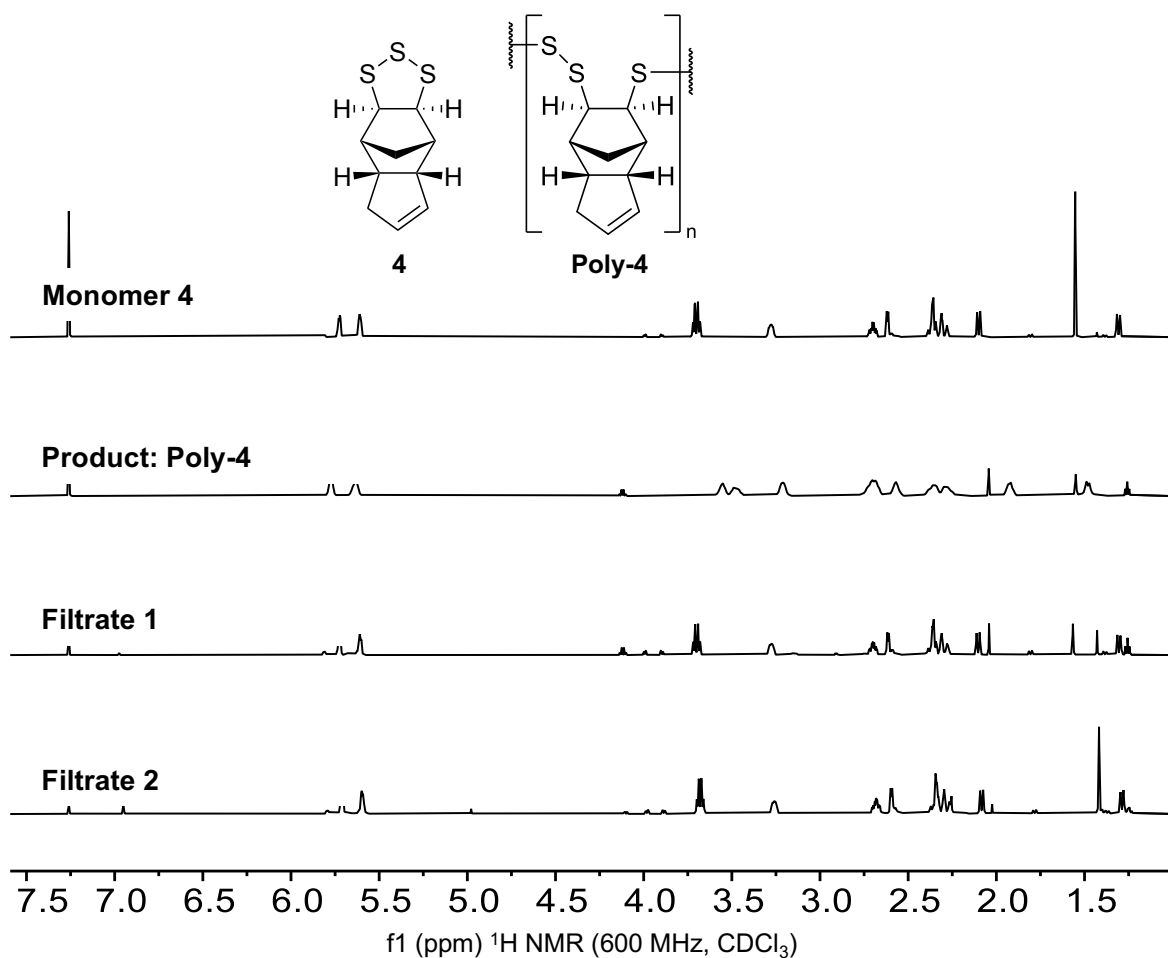


Figure S4.41: ^1H NMR spectra (600 MHz, CDCl_3) of monomer before polymerisation, final combined polymer product, concentrated filtrate after polymer extraction #6 (49%) and concentrated filtrate after final combined polymer extraction (13%).

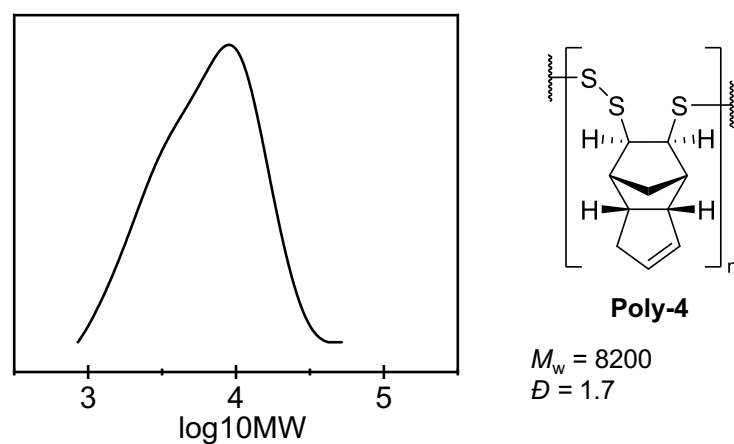
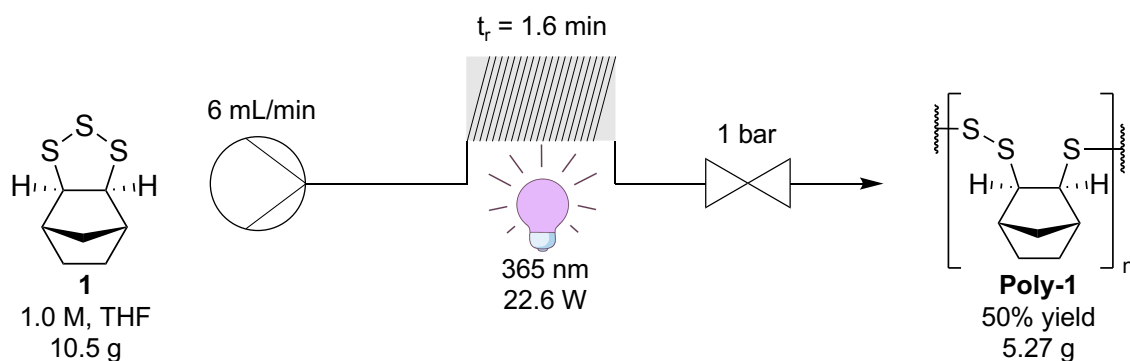


Figure S4.42: GPC (THF) of combined **poly-4**.

Poly-1



A solution of monomer **1** (10.54 g, 55 mmol, 1.0 M) in THF (55.4 mL) was prepared. The solution was passed through perfluoroalkoxyalkanes (PFA) tubing (10 mL, 21 °C) at a flow rate of 6 mL/min with irradiation from LEDs (365 nm, 22.6 W) and backpressure regulation at 1 bar. The residence time for the reaction was 1.6 minutes. The product was collected in a 100 mL round-bottomed flask. The product was concentrated under reduced pressure and redissolved in chloroform (10 mL). Ethyl acetate (40 mL) was added to precipitate the polymer which was collected by filtration. The filtrate was concentrated under reduced pressure to recovery unreacted monomer **1** (3.87 g). The polymer collected by filtration was redissolved in chloroform (5 mL) and precipitated 3 times with ethyl acetate to deliver **poly-3** as a white powder (5.27 g, 50%).

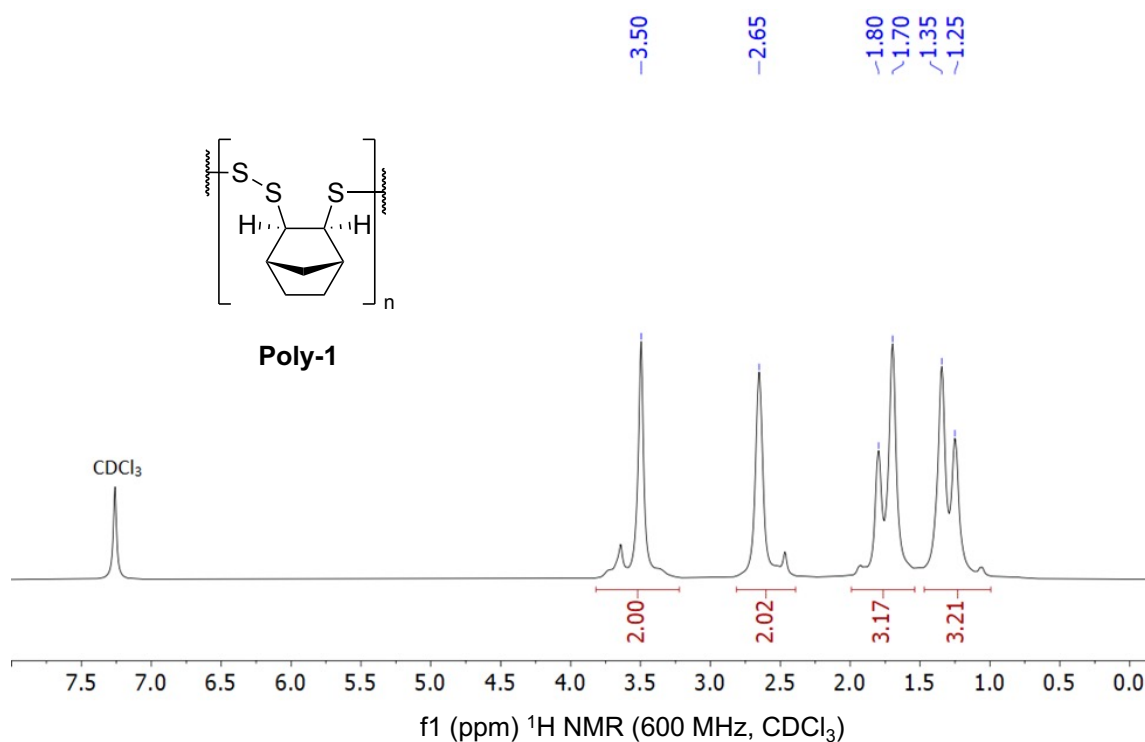


Figure S4.43: ¹H NMR spectra (600 MHz, CDCl₃) of **poly-1**.

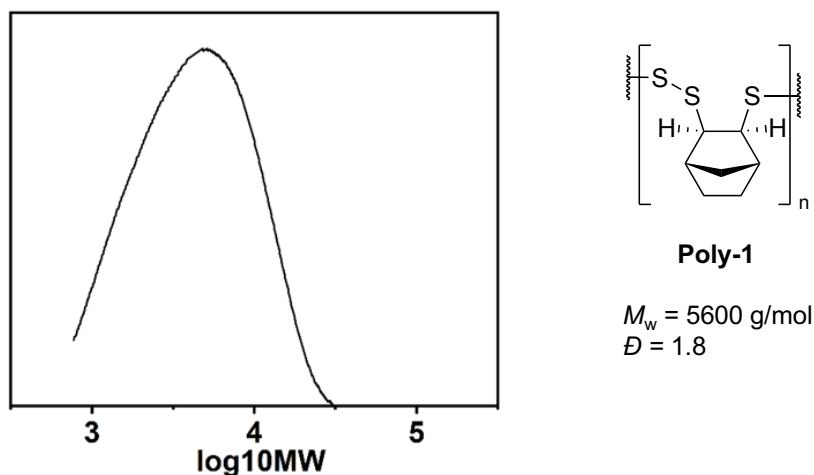


Figure S4.44: GPC (THF) of poly-1.

LiAlH₄ Degradation

Poly-4 (234 mg, $M_w = 12100$ g/mol, $D = 1.7$) and LiAlH₄ (104 mg, 2.74 mmol) were added to a flame-dried two neck 25 mL round bottom flask containing a magnetic stir bar. The flask was evacuated of air and refilled with nitrogen gas. Anhydrous THF (12 mL) was added dropwise with stirring. The resulting reaction mixture was stirred under a nitrogen atmosphere for 12 hours. HCl (3 M aq., 5 mL) was then added dropwise to quench the remaining reducing agent. After stirring for a further 5 minutes, hexane (10 mL) was added and stirred for 5 minutes. The solution was filtered, and the organic layer was separated. The organic layer was washed with H₂O (3 x 10 mL). The organic fraction was dried (Na₂SO₄), filtered and concentrated under reduced pressure. ¹H NMR and gas chromatography mass spectrometry revealed the yellow oil to be the dithiol product **5** (150 mg, 64%).

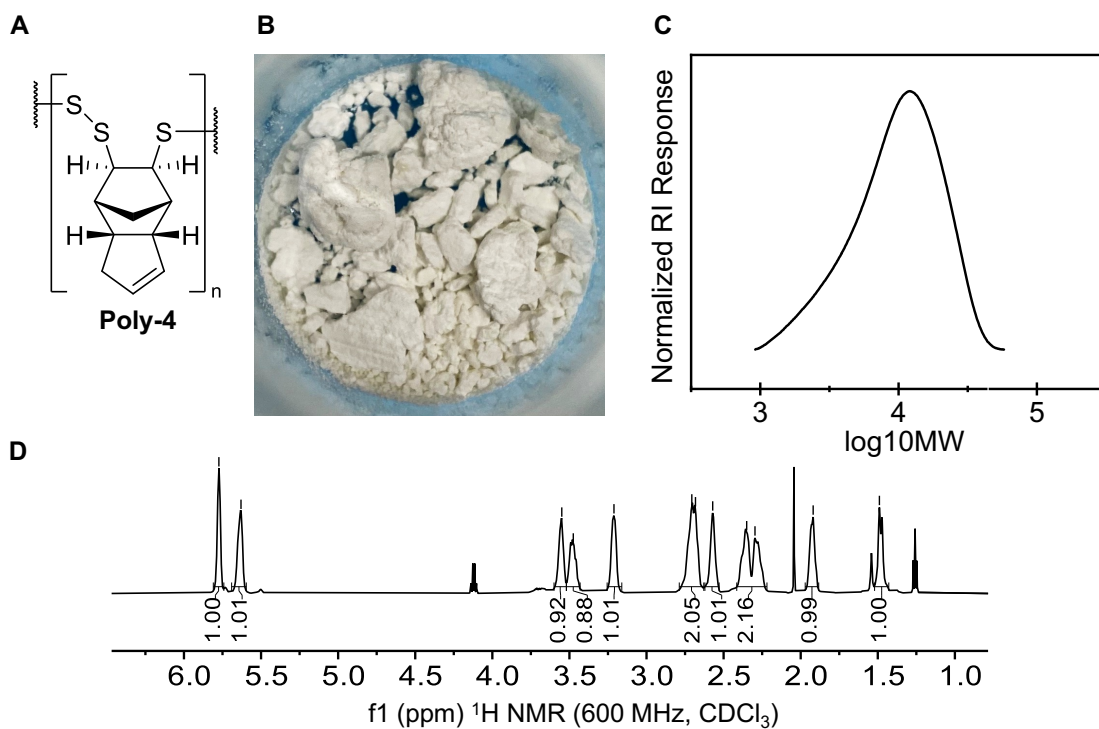


Figure S4.45: (A) Poly-4. B) image of Poly-4. C) GPC (THF) of Poly-4. D) ^1H NMR spectrum of Poly-4.

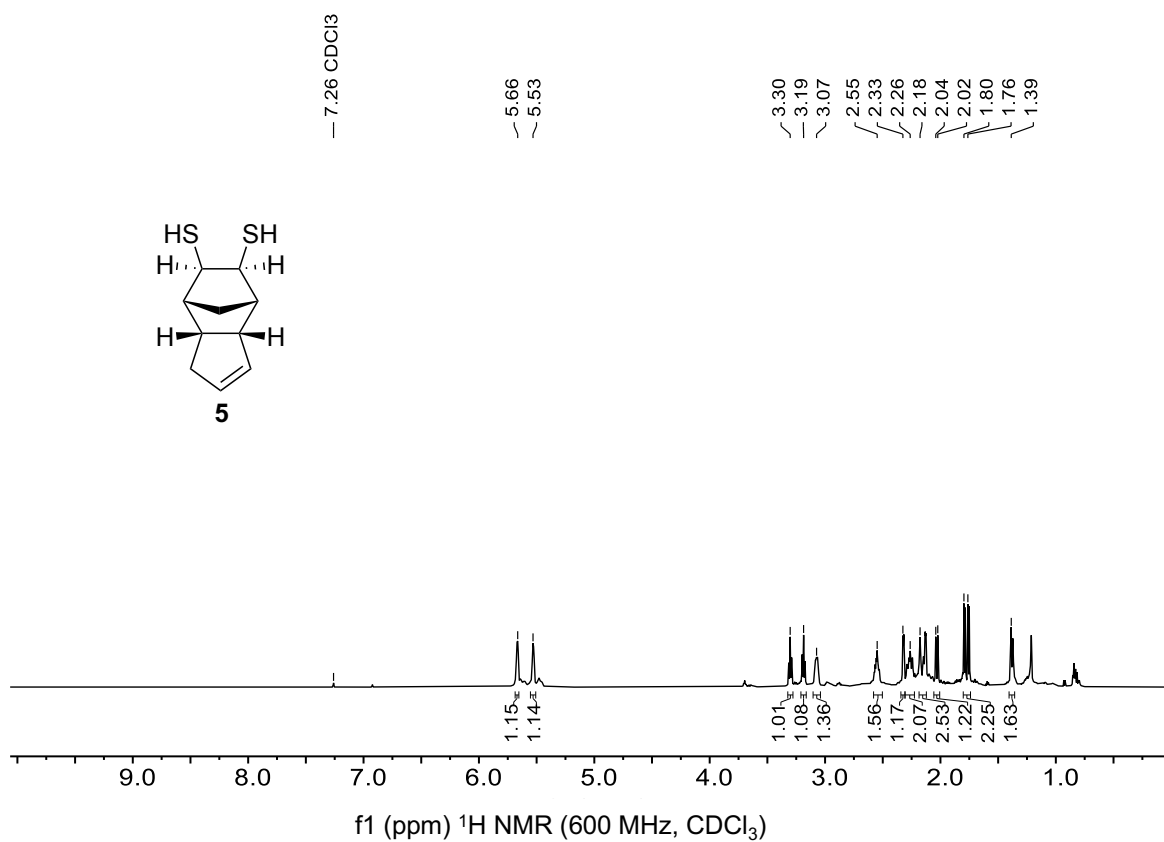


Figure S4.46: ^1H NMR spectrum (600 MHz, CDCl_3) of reduction product.

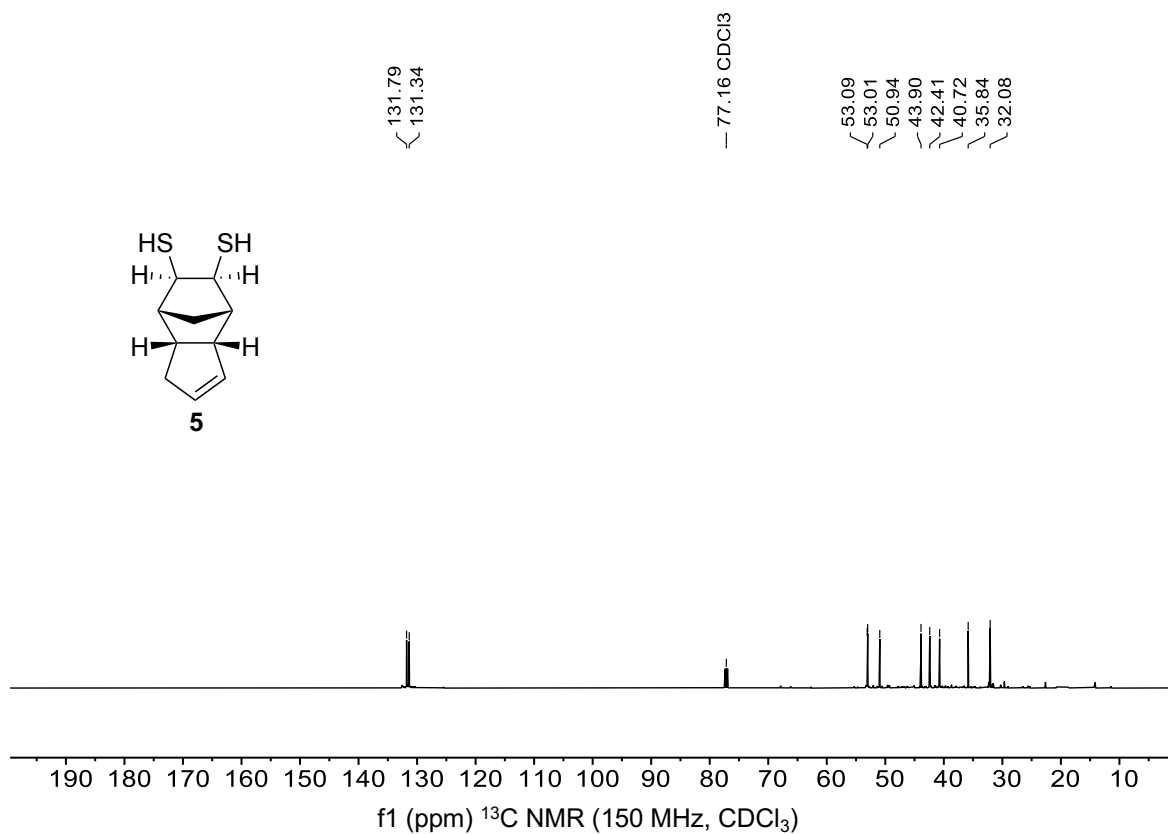


Figure S4.47: ^{13}C NMR spectrum (150 MHz, CDCl_3) of reduction product.

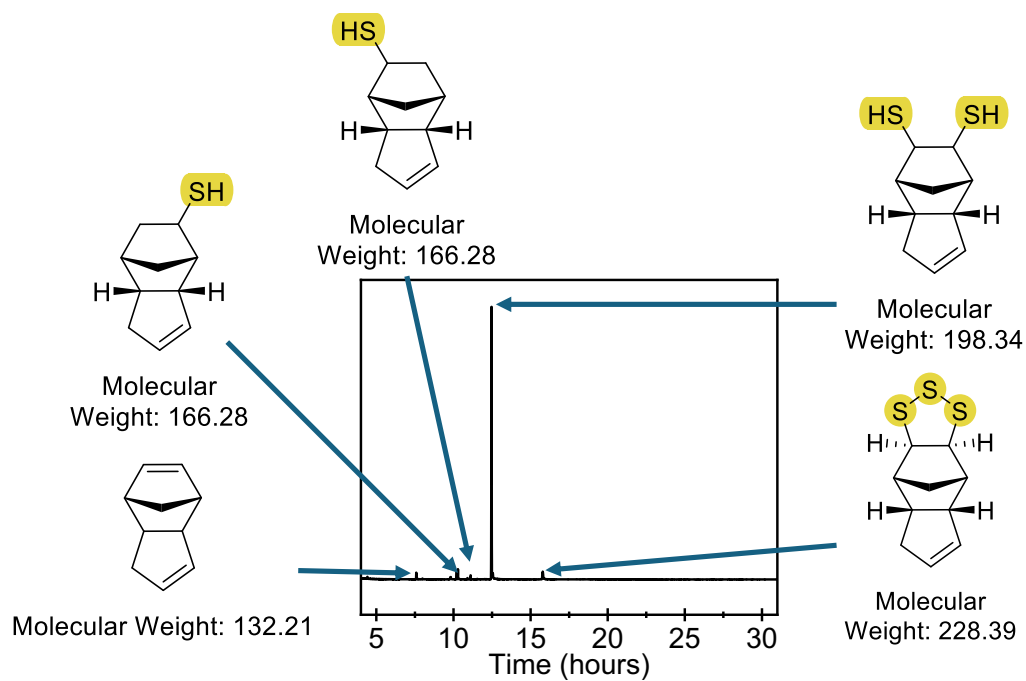
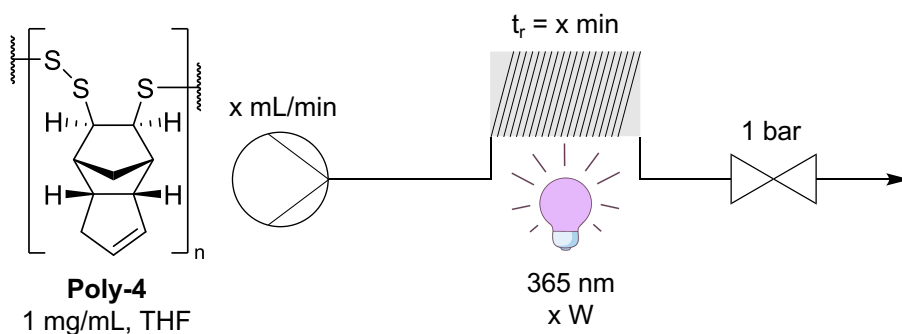


Figure S4.48: Gas chromatogram of reduction product.

Photodegradation

Continuous flow - *poly-4*



A solution of **poly-4** (509 mg, $M_w = 9200 \text{ g/mol}$, $D = 1.6$) in THF (50 mL) was prepared. For each reaction, 1 mL of the stock solution was passed through perfluoroalkoxyalkanes (PFA) tubing (10 mL, 21 °C) at different flow rates with irradiation from LEDs (365 nm, 22.6 W) and backpressure regulation at 1 bar. The product was collected in a 20 mL vial, concentrated under reduced pressure and analysed by $^1\text{H NMR}$ (CDCl_3) and GPC (THF). The product was so low in molecular weight it could not be detected by GPC.

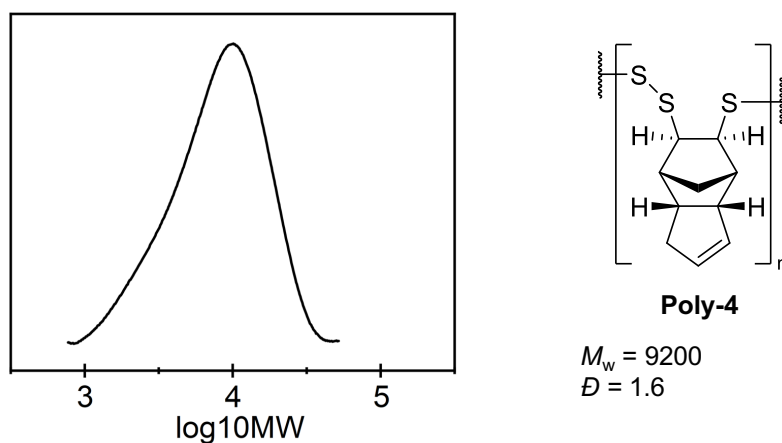


Figure S4.49: GPC (THF) of **poly-4** before photodegradation.

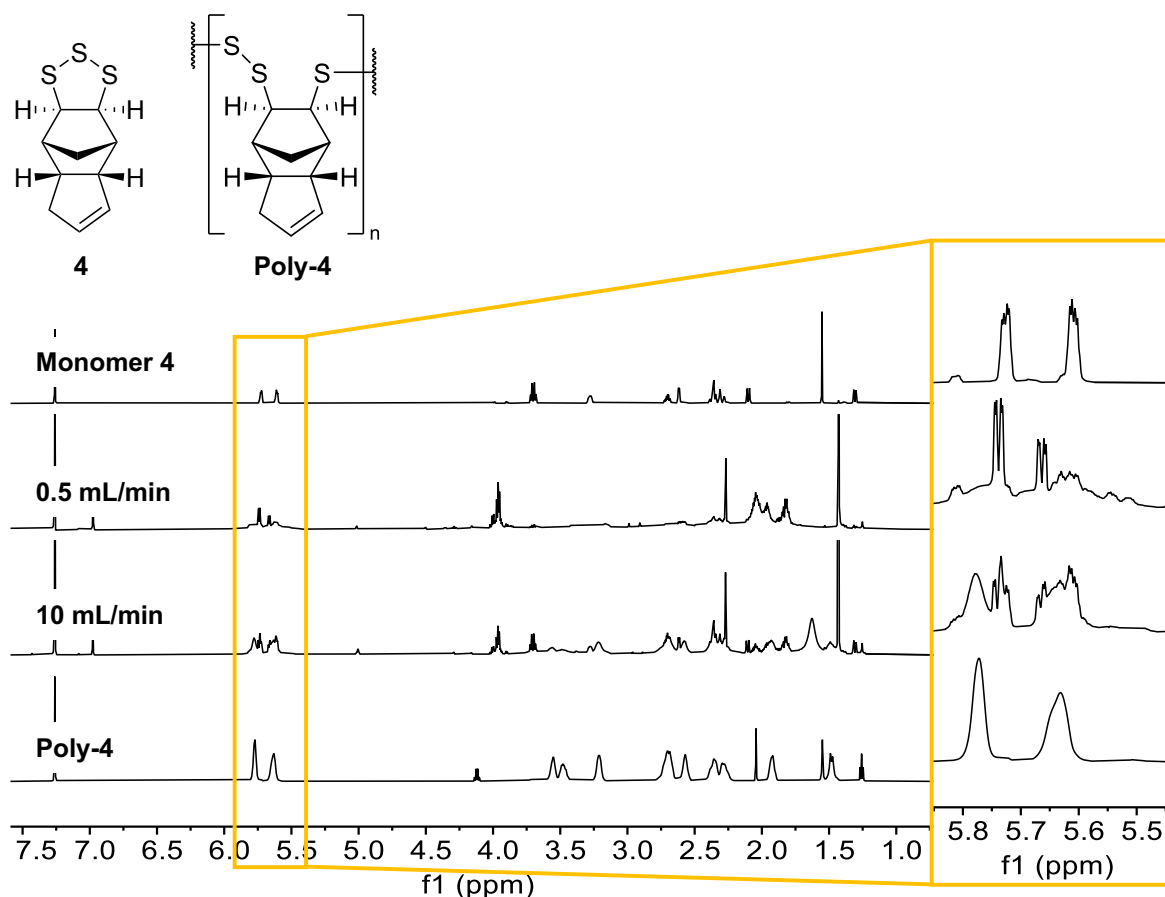
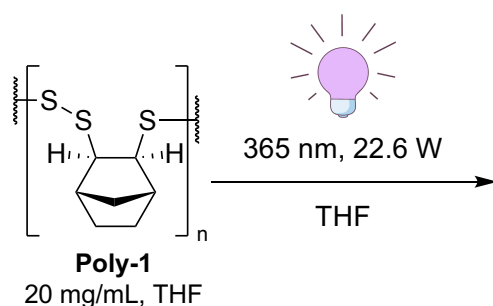


Figure S4.50: ^1H NMR spectra (600 MHz, CDCl_3) of **poly-4** before photodegradation and after photodegradation at different flow rates.

Batch - poly-1



A solution of **poly-1** (20 mg, $M_w = 7800 \text{ g/mol}$, $D =$) in THF (1 mL) was prepared in a GC-MS vial. The solution was sonicated to aid in polymer dispersion. The vial was placed onto a stir plate inside of the Uniqsis PhotoSynTM photoreactor. The sample was irradiated with UV light (365 nm, 22.6 W), and a 50 μL aliquot was taken at 0, 5, 20 and 60 minutes and analysed by GPC (THF). At 60 minutes, the solution was concentrated under reduced pressure and analysed by ^1H NMR spectroscopy (CDCl_3).

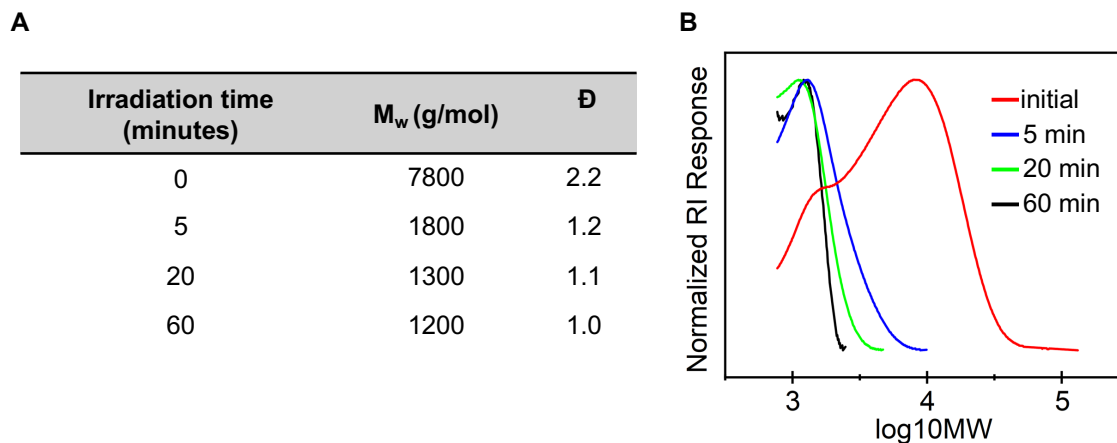


Figure S4.51: (A) Summary of GPC data for the degradation of **poly-1** at different time points. (B) GPC (THF) of **poly-1** before photodegradation and after photodegradation at different time points.

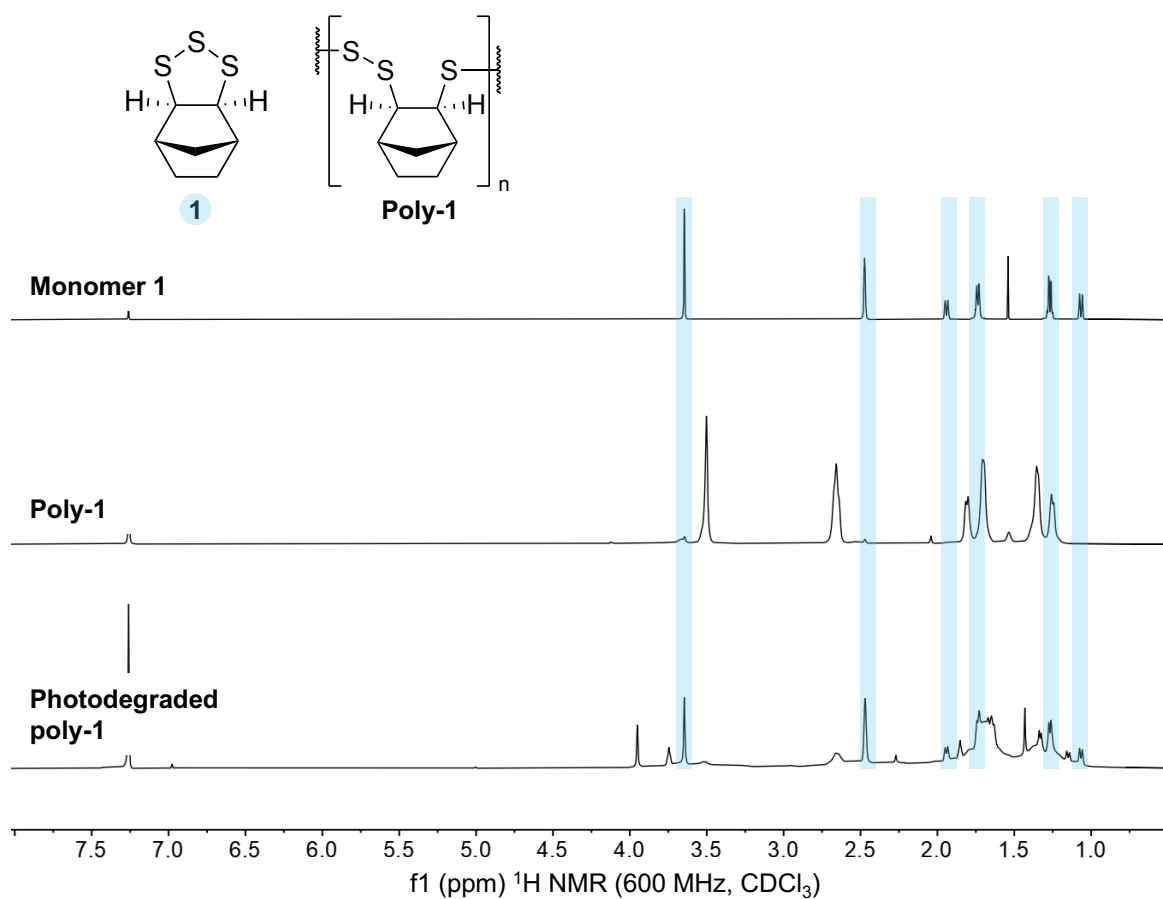


Figure S4.52: ^1H NMR spectra (600 MHz, CDCl_3) of **poly-1** before photodegradation and after photodegradation.

References

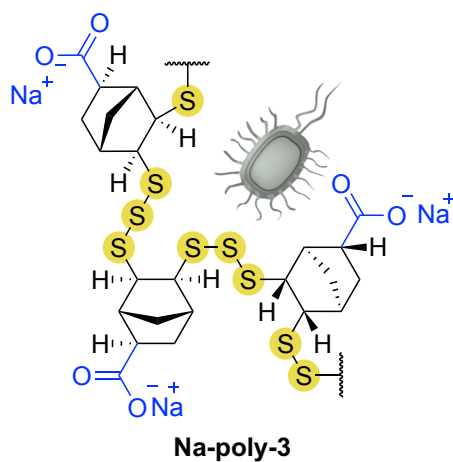
- [1] M. M. a. J. M. Chalker, *Vol. WO2020198778.*, **2019**.
- [2] S. J. Tonkin, L. N. Pham, J. R. Gascooke, M. R. Johnston, M. L. Coote, C. T. Gibson, J. M. Chalker, *Advanced Optical Materials* **2023**, *11*, 2300058.
- [3] W. J. Chung, J. J. Griebel, E. T. Kim, H. Yoon, A. G. Simmonds, H. J. Ji, P. T. Dirlam, R. S. Glass, J. J. Wie, N. A. Nguyen, *Nature chemistry* **2013**, *5*, 518-524.
- [4] D. J. Parker, H. A. Jones, S. Petcher, L. Cervini, J. M. Griffin, R. Akhtar, T. Hasell, *Journal of Materials Chemistry A* **2017**, *5*, 11682-11692.
- [5] J. J. Griebel, G. Li, R. S. Glass, K. Char, J. Pyun, *Journal of Polymer Science Part A: Polymer Chemistry* **2015**, *53*, 173-177.
- [6] G. Kutney, *Sulfur: history, technology, applications and industry*, Elsevier, **2023**.
- [7] J. Jia, J. Liu, Z.-Q. Wang, T. Liu, P. Yan, X.-Q. Gong, C. Zhao, L. Chen, C. Miao, W. Zhao, *Nature Chemistry* **2022**, *14*, 1249-1257.
- [8] J. Jia, P. Yan, S. D. Cai, Y. Cui, X. Xun, J. Liu, H. Wang, L. Dodd, X. Hu, D. Lester, *European Polymer Journal* **2024**, *207*, 112815.
- [9] J. Emsley, D. W. Griffiths, *Phosphorus and Sulfur and the Related Elements* **1980**, *9*, 227-230.
- [10] T. Baran, A. Duda, S. Penczek, *Journal of Polymer Science: Polymer Chemistry Edition* **1984**, *22*, 1085-1095.
- [11] P. Lesté-Lasserre, D. N. Harpp, *Tetrahedron letters* **1999**, *40*, 7961-7964.
- [12] M. Mann, B. Zhang, S. J. Tonkin, C. T. Gibson, Z. Jia, T. Hasell, J. M. Chalker, *Polymer Chemistry* **2022**, *13*, 1320-1327.
- [13] J. J. Griebel, N. A. Nguyen, S. Namnabat, L. E. Anderson, R. S. Glass, R. A. Norwood, M. E. Mackay, K. Char, J. Pyun, *ACS Macro Letters* **2015**, *4*, 862-866.
- [14] C. W. H. Rajawasam, O. J. Dodo, M. A. S. N. Weerasinghe, I. O. Raji, S. V. Wanasinghe, D. Konkolewicz, N. De Alwis Watuthanthrige, *Polymer Chemistry* **2024**, *15*, 219-247.
- [15] J. Bao, K. P. Martin, E. Cho, K.-S. Kang, R. S. Glass, V. Coropceanu, J.-L. Bredas, W. O. N. Parker, Jr., J. T. Njardarson, J. Pyun, *Journal of the American Chemical Society* **2023**, *145*, 12386-12397.
- [16] L. J. Dodd, C. Lima, D. Costa-Milan, A. R. Neale, B. Saunders, B. Zhang, A. Sarua, R. Goodacre, L. J. Hardwick, M. Kuball, T. Hasell, *Polymer Chemistry* **2023**, *14*, 1369-1386.
- [17] G. Pasparakis, T. Manouras, P. Argitis, M. Vamvakaki, *Macromolecular Rapid Communications* **2012**, *33*, 183-198.
- [18] J. Wang, J. Xie, C. Zong, X. Han, J. Zhao, S. Jiang, Y. Cao, A. Fery, C. Lu, *ACS Applied Materials & Interfaces* **2017**, *9*, 37402-37410.

- [19] C. Hu, M. Zhao, Q. Li, Z. Liu, N. Hao, X. Meng, J. Li, F. Lin, C. Li, L. Fang, S. Y. Dai, A. J. Ragauskas, H. J. Sue, J. S. Yuan, *ChemSusChem* **2021**, *14*, 4260-4269.
- [20] T.-J. Yue, X.-Y. Fu, J. Zhang, Y.-G. Zhou, W.-M. Ren, X.-B. Lu, *Macromolecules* **2024**, *57*, 1319-1327.
- [21] A. K. Mann, L. S. Lisboa, S. J. Tonkin, J. R. Gascooke, J. M. Chalker, C. T. Gibson, *Angewandte Chemie International Edition* **2024**, *63*, e202404802.
- [22] S. Poulain, S. Julien, E. Duñach, *Tetrahedron Lett.* **2005**, *46*, 7077-7079.
- [23] N. P. Cowieson, D. Aragao, M. Clift, D. J. Ericsson, C. Gee, S. J. Harrop, N. Mudie, S. Panjekar, J. R. Price, A. Riboldi-Tunnicliffe, *Journal of synchrotron radiation* **2015**, *22*, 187-190.
- [24] D. Aragão, J. Aishima, H. Cherukuvada, R. Clarken, M. Clift, N. P. Cowieson, D. J. Ericsson, C. L. Gee, S. Macedo, N. Mudie, *Journal of synchrotron radiation* **2018**, *25*, 885-891.
- [25] G. M. Sheldrick, *Acta Crystallographica Section A: Foundations and Advances* **2015**, *71*, 3-8.
- [26] C. B. Hübschle, G. M. Sheldrick, B. Dittrich, *Journal of applied crystallography* **2011**, *44*, 1281-1284.

Chapter 5

Antimicrobial and antifungal activity of poly(trisulfides)

*This chapter assessed the antimicrobial and antifungal activity of poly(trisulfides), marking the first exploration of the biocidal properties of high sulfur content polymers with a linear structure and a known sulfur rank of three. The first example of a water-soluble high sulfur content polymer, which is advantageous for determining dose to activity relationships is presented. Poly(trisulfides) exhibited greater activity against Gram-positive bacteria compared to Gram-negative bacteria. Na-poly-3 had a minimum inhibitory concentration (MIC) for *S. aureus* at $\leq 256 \mu\text{g/mL}$ and for *C. albicans* at $\leq 16 \mu\text{g/mL}$, highlighting its potential as a biocide or fungicide.*



Acknowledgments

Tom Hasell and Jo Fothergill for hosting me in their labs

Ocean Clarke for training and help running MIC/MBC experiments

Introduction

A recent area of interest for high sulfur content polymers is their application in biological fields.^[1-2] Sulfur-containing compounds have a long history of use as therapeutics, antioxidants, and biocides. For instance, diallyl trisulfide, found in garlic, has been used medicinally for thousands of years.^[3] Polysulfide compounds, commonly found in living organisms, aid in regulating redox balance due to their antioxidant properties.^[4] Naturally occurring thiol containing molecules, such as glutathione, are overproduced in human tumour cells.^[5] Therefore, polysulfides are often incorporated into drug delivery systems, as S–S bond scission occurs through nucleophilic attack by the thiol group in glutathione, facilitating tumour selective drug release.^[6-7]

Recently, high sulfur content polymers produced through inverse vulcanisation have shown antimicrobial properties. Deng and coworkers demonstrated that surfaces coated with poly(sulfur-diisopropenylbenzene) (poly(S-DIB)) were active against *Escherichia coli* (*E. coli*), resulting in the reduction of up to 72% *E. coli* growth (Figure 5.1).^[8] Since this 2018 study, several groups have investigated the antimicrobial activities of polysulfides produced with different organic crosslinkers, including dicyclopentadiene,^[9-10] perillyl alcohol,^[10-11] divinylbenzene,^[10] and urushiol.^[12] However, polysulfides produced through inverse vulcanisation are not well-defined and are insoluble in aqueous media, limiting the ability to understand their mechanism of action and their dose to activity relationship.

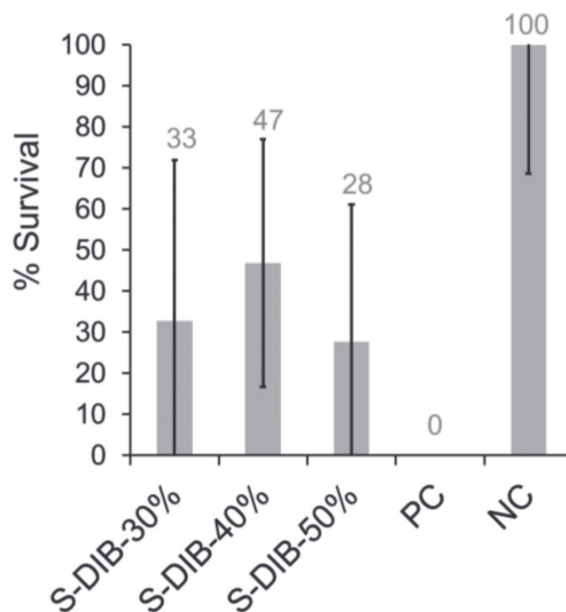
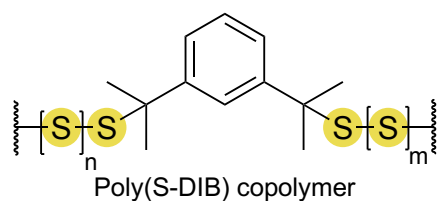


Figure 5.1: Antimicrobial activity of poly(S-DIB), relative to the positive control (silicon wafer with biocide) and the negative control (blank silicon wafer). From left 70 wt.% sulfur content, 60 wt.% sulfur content, 50 wt.% sulfur content poly(S-DIB), positive control and negative control. ^[8]
 © 2018, John Wiley and Sons. This image was reproduced under a Creative Commons License: CC BY 4.0.^[8]

To further understand the antimicrobial activity of high sulfur content polymers, linear poly(trisulfides) were investigated. These polymers contain no elemental sulfur, as they are synthesised from pure, well-defined, 1,2,3-trithiolane monomers. The water-soluble poly(trisulfides) will allow for precise calculation of the dosage required to achieve antimicrobial inhibition. Dosage is an important characteristic when comparing new antimicrobial agents to other new and existing biocides. The antifungal activity of poly(trisulfides) will also be investigated. This research into new antibiotics and antifungicides comes at a critical time where antimicrobial and antifungal resistance is growing.^[13-14] Gram-positive *Staphylococcus aureus* (*S. aureus*) and Gram-negative *E. coli* were selected to compare poly(trisulfide) activity against both types of bacteria. *S. aureus* and *E. coli* are clinically relevant, causing high numbers of blood stream infections in hospital patients, with some cases leading to death.^[15] The antifungal activity of poly(trisulfides) will also be investigated against *Candida albicans* (*C. albicans*), a fungus which is responsible for the leading cause of fungal infection related deaths.^[16]

Results and Discussion

Minimum inhibitory concentration

Minimum inhibitory concentration (MIC) is the lowest concentration ($\mu\text{g/mL}$) of an antimicrobial or antifungal agent that inhibits the *in vitro* growth of microorganisms, as determined by measurement of the optical density of the culture. Quantifying the amount of an antimicrobial or antifungal agent is crucial for assessing its activity, precisely dosing, and comparing against other antibiotics and antifungicides. To assess the MIC of a new compound, it must be soluble in aqueous media. Due to this requirement, MIC experiments had not previously been conducted on high sulfur content polymers because of their insolubility in aqueous media. Therefore, this study presents the first investigation of MIC for high sulfur content polymers that have a known sulfur rank and do not contain unreacted elemental sulfur.

Chapter 2 detailed the synthesis and characterisation of a water-soluble poly(trisulfide). **Na-poly-3** is an ideal candidate for MIC investigations due to its regular trisulfide structure and stereochemistry. **Na-poly-3** is produced through the deprotonation of **poly-3** with one molar equivalent of NaOH per carboxylic acid group (Figure 5.2). **Poly-3** synthesised through photochemical polymerisation (Figure 5.2 A, **UV-Na-poly-3**) and electrochemical polymerisation (Figure 5.2 B, **E-Na-poly-3**) were both investigated in the MIC study. It was proposed that both methods of polymerisation produce analogous polymeric structures. However, there might be subtle differences in the chain length and end group species, which could affect their activity. Monomer **3** was also deprotonated through the addition of one molar equivalent of NaOH, forming water soluble **Na-3** (Figure 5.2 C). **Na-3** was investigated in the MIC study to compare its activity to that of **Na-poly-3**. As a negative control, sodium polyacrylate (Figure 5.2 D) was investigated due to the presence of the carboxylate functional group connected to the backbone of the polymer chain, to determine if the carboxylate functional group played any role in antimicrobial or antifungal activity.

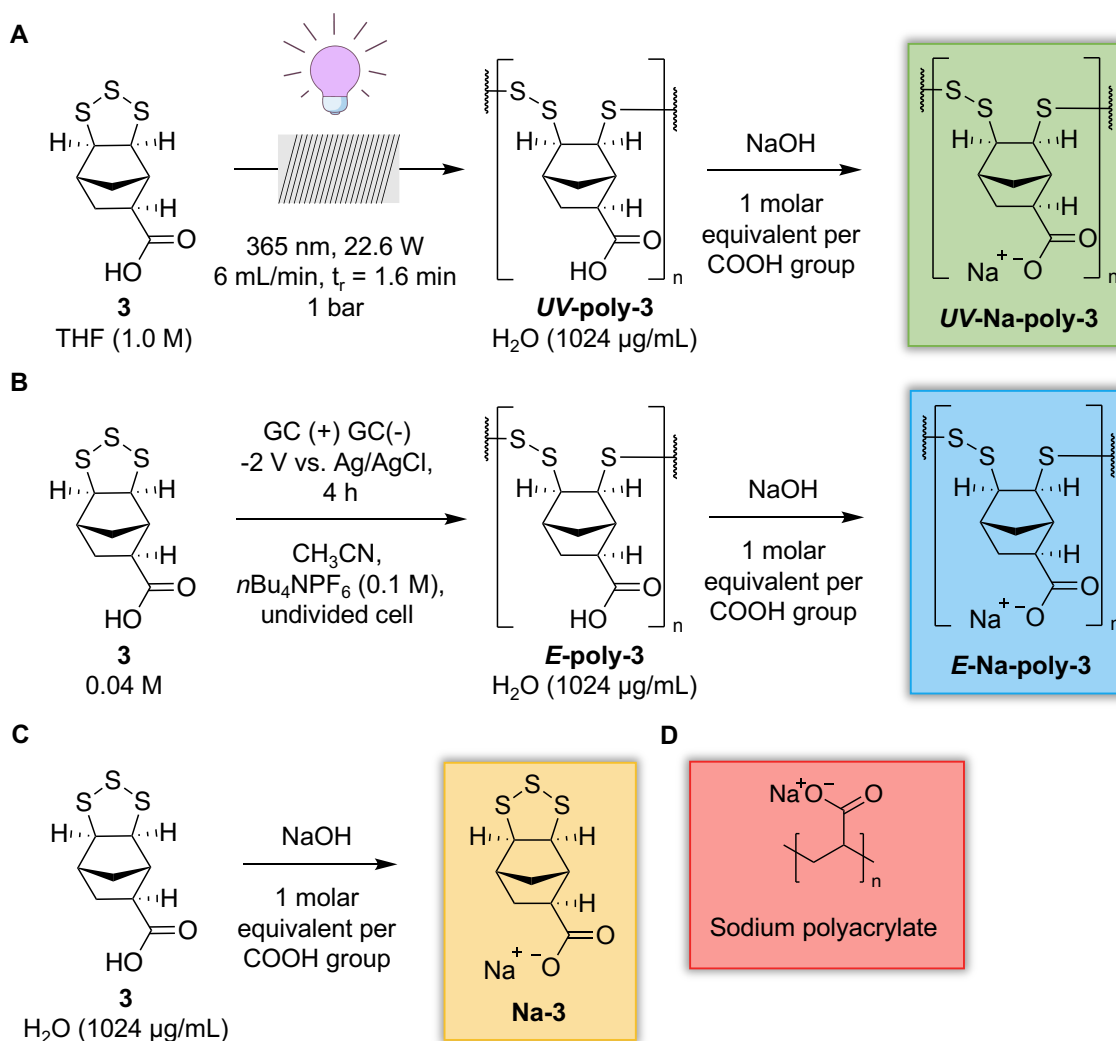


Figure 5.2: (A) Continuous flow photochemical synthesis of *UV-poly-3* followed by its deprotonation with NaOH forming *UV-Na-poly-3*. (B) Electrochemical synthesis of *E-poly-3* followed by its deprotonation with NaOH forming *E-Na-poly-3*. (C) Deprotonation of monomer **3** with NaOH forming **Na-3**. (D) Sodium polyacrylate purchased and used without further modification.

The MIC experiments were conducted on three cultures: *S. aureus*, *E. coli*, and *C. albicans*. First, each culture was streaked onto Luria-Bertani (LB) agar plates from a frozen stock and incubated overnight at 37 °C. A suspension for each culture was prepared in biological triplicates by collecting 3-5 colonies from the agar plate, suspending the colonies in LB broth, and incubating overnight at 37 °C with agitation. The cultures were normalised to 1×10^9 colony-forming units (CFU)/mL by measuring their optical density at 600 nm (OD_{600}). Each normalised culture was further diluted 1:100 in LB broth for *C. albicans* and Mueller Hinton (MHI) broth for *E. coli* and *S. aureus* before being dispensed onto a 96-well plate. For each culture, three technical replicates were plated per sample concentration. Samples *UV-Na-poly-3*, *E-Na-poly-3*, **Na-3**, and sodium

polyacrylate were plated at different concentrations ranging between 0 $\mu\text{g/mL}$ and 512 $\mu\text{g/mL}$. The wells containing no sample acted as a positive control to measure unaffected growth. The 96-well plates were then incubated at 37 $^{\circ}\text{C}$ for 20 hours, and their OD_{600} was recorded using a plate reader.

Figure 5.3 presents the relevant MIC results for *S. aureus*, showing a MIC of 16 $\mu\text{g/mL}$ for **UV-Na-poly-3**, 256 $\mu\text{g/mL}$ for **E-Na-poly-3**, and 512 $\mu\text{g/mL}$ for **Na-3**. Sodium polyacrylate showed no biocidal activity against *S. aureus*. These findings align with previous research indicating polysulfides produced through inverse vulcanisation can inhibit *S. aureus* growth on the surface of the materials.^[9-12] However, this study is the first to demonstrate a clear relationship between dose and activity. A MIC of 16 $\mu\text{g/mL}$ for **UV-Na-poly-3** is particularly noteworthy, achieving higher activity compared to common antibiotics such as oxacillin (MIC of 128 $\mu\text{g/mL}$), erythromycin (MIC of 32 $\mu\text{g/mL}$), and kanamycin (MIC of >32 $\mu\text{g/mL}$).^[17] Interestingly, **UV-Na-poly-3** exhibited greater activity against *S. aureus* compared to **Na-3**. Initially, it was hypothesised that the monomer would interact more effectively with the cell wall of *S. aureus* due to its smaller size, leading to greater activity. However, the polymer's superior activity over the monomer suggests that other factors are at play, which require further investigation to fully understand. Both electrochemically and photochemically synthesised **poly-3** performed comparably which is consistent with their similar structure.

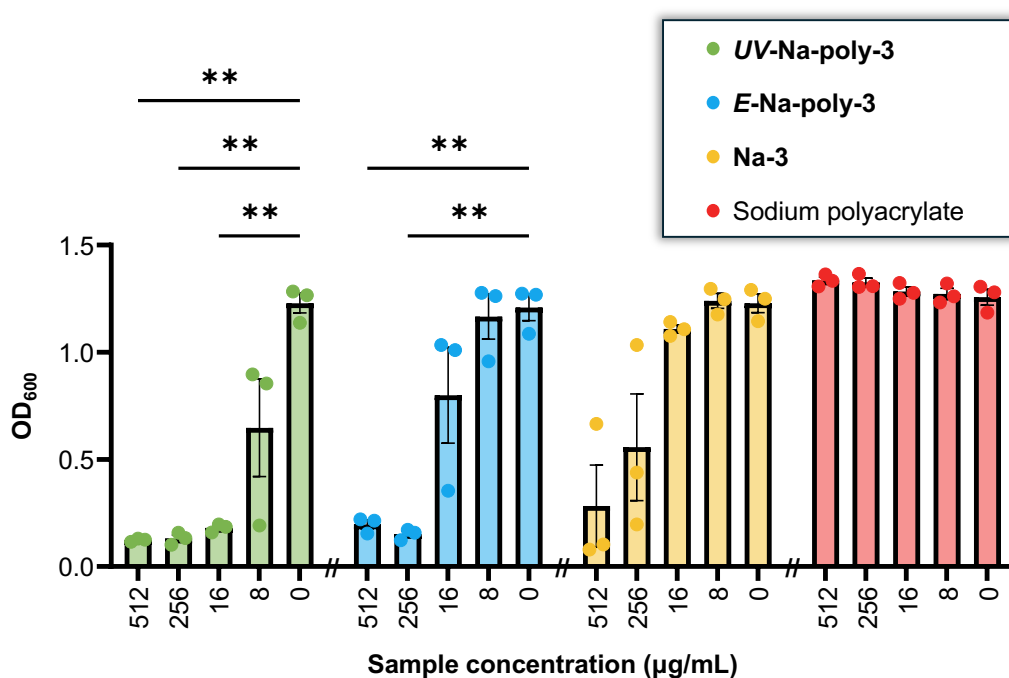


Figure 5.3: Absorbance of *Staphylococcus aureus* at 600 nm, in the presence of **UV-Na-poly-3**, **E-Na-poly-3**, **Na-3**, and sodium polyacrylate at 512 $\mu\text{g/mL}$, 256 $\mu\text{g/mL}$, 16 $\mu\text{g/mL}$, 8 $\mu\text{g/mL}$, and 0 $\mu\text{g/mL}$ (blank) during a 20-hour incubation period. Data represents the mean of three biological replicates ($n = 3$) and error bars show standard error of the mean. $**p \leq 0.01$.

Figure 5.4 shows the relevant MIC results for *E. coli*. Samples **UV-Na-poly-3**, **E-Na-poly-3**, and **Na-3** exhibited some inhibition of *E. coli* growth at 256 $\mu\text{g/mL}$ and 512 $\mu\text{g/mL}$ compared to the *E. coli* growth with no sample added. However, significant inhibition was only observed at 512 $\mu\text{g/mL}$ of **E-Na-poly-3**, and even then, it did not result in complete inhibition. To determine a MIC for *E. coli* using **Na-poly-3** or **Na-3**, the concentration would need to be investigated above 512 $\mu\text{g/mL}$. However, concentrations above 512 $\mu\text{g/mL}$ are generally not considered viable for new antibiotics. Sodium polyacrylate showed no activity against *E. coli*. The antimicrobial effect of polysulfides produced by inverse vulcanization on the surface growth of *E. coli* has been demonstrated by several groups.^[8-9, 12, 18] Although polysulfides show an antimicrobial effect against *E. coli*, the MIC investigation indicates this effect is not as strong compared to polysulfide antimicrobial activity against *S. aureus*.

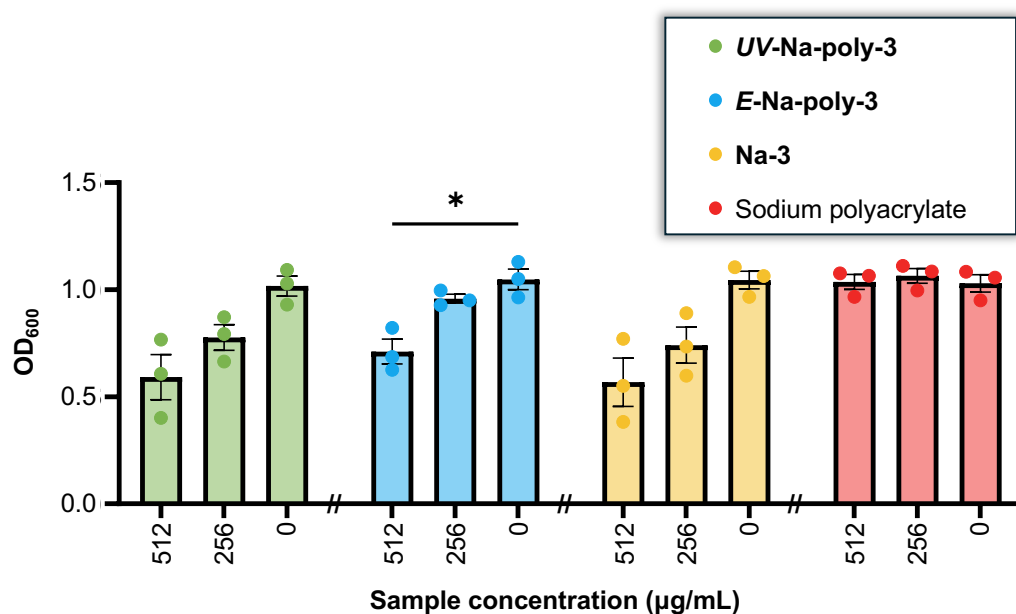


Figure 5.4: Absorbance of *Escherichia coli* at 600 nm, in the presence of **UV-Na-poly-3**, **E-Na-poly-3**, **Na-3**, and sodium polyacrylate at 512 $\mu\text{g/mL}$, 256 $\mu\text{g/mL}$, and 0 $\mu\text{g/mL}$ (blank) during a 20-hour incubation period. Data represents the mean of three biological replicates ($n = 3$) and error bars show standard error of the mean. $*p \leq 0.05$.

S. aureus is a Gram-positive bacterium, meaning it contains a single cell wall, whereas *E. coli* is a Gram-negative bacterium with both a cell wall and an outer membrane. Gram-positive bacteria, having a simpler cell barrier, are often more susceptible to biocides compared to Gram-negative bacteria, which possess a more complex cell barrier.^[19] Therefore, it is reasonable that **Na-poly-3** and **Na-3** exhibited a greater biocidal effect on *S. aureus* than on *E. coli*.

Figure 5.5 presents the relevant MIC results for *C. albicans*, showing a MIC of 8 $\mu\text{g/mL}$ for **UV-Na-poly-3**, 16 $\mu\text{g/mL}$ for **E-Na-poly-3**, and 256 $\mu\text{g/mL}$ for **Na-3**. Sodium polyacrylate showed no activity against *C. albicans*. The polymer exhibited higher activity compared to the monomer, a phenomenon warranting further investigation to understand the underlying reasons.

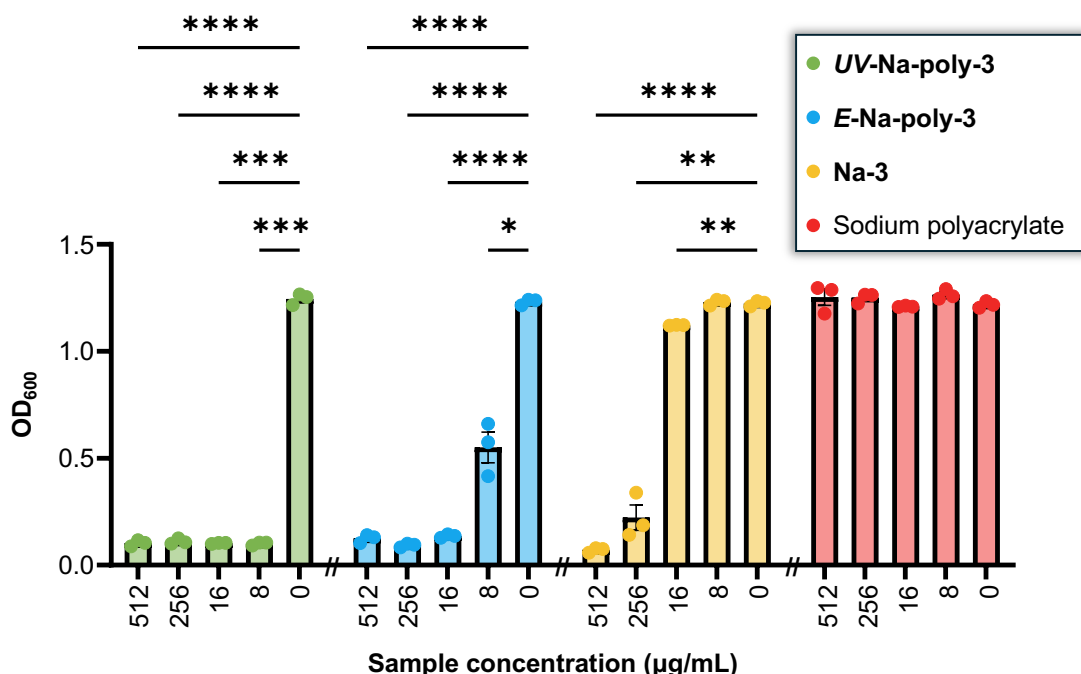


Figure 5.5: Absorbance of *Candida albicans* at 600 nm, in the presence of **UV-Na-poly-3**, **E-Na-poly-3**, **Na-3**, and sodium polyacrylate at 512 $\mu\text{g/mL}$, 256 $\mu\text{g/mL}$, 16 $\mu\text{g/mL}$, 8 $\mu\text{g/mL}$, and 0 $\mu\text{g/mL}$ (blank) during a 20-hour incubation period. Data represents the mean of three biological replicates ($n = 3$) and error bars show standard error of the mean. * $p \leq 0.05$, ** $p \leq 0.01$, *** $p \leq 0.001$, **** $p \leq 0.0001$.

Compared to the well-documented antibacterial properties of polysulfides, their antifungal effects have not been extensively explored in the literature, despite the current need for new fungicides. Shen and coworkers investigated the antifungal activity of sulfur-urushiol inverse vulcanised polymer surfaces.^[12] They found that this polymer inhibited up to 52% of the surface growth of *S. cerevisiae*, providing the first evidence of the antifungal activity of polysulfides produced via inverse vulcanisation.^[12] These findings align with the MIC values obtained in this study, which are remarkable for new antifungal agents. Typical antifungal agents such as ketoconazole and nystatin have MIC values for *C. albicans* around 4 $\mu\text{g/mL}$.^[20] Therefore, the MIC of 8 $\mu\text{g/mL}$ for **UV-Na-poly-3** is a significant result and should be investigated further as a potential new antifungal agent.

Several mechanisms have been proposed for the biocidal activity of high sulfur content polymers. One proposal suggests the presence of unreacted elemental sulfur within the matrix of polysulfides produced via inverse vulcanization.^[9, 21] However, this study demonstrated the antimicrobial and antifungal activity of poly(trisulfides) that do not contain elemental sulfur contaminants. It is known that small molecule sulfides, disulfides and trisulfides exhibit antimicrobial activity, which increases with higher sulfur rank.^[22-23] The increased activity is thought to be due to the weakening of S–S bonds as the sulfur rank increases. Weaker S–S bonds are more likely to react with other chemical species found in bacteria and fungi, inhibiting cell growth.^[9-10] This hypothesis is based on the thiol-disulfide exchange mechanisms which occurs within living organisms.^[4, 6-7, 24] However, the exact mechanism is still unknown and more research in the area is needed. This study is the first to investigate a high molecular weight poly(trisulfide) as a biocide, marking an important step in understanding the underlying mechanism of action.

Minimum bactericidal and fungicidal concentration

Minimum bactericidal/fungicidal concentration (MBC/MFC) is the lowest concentration ($\mu\text{g/mL}$) of an antimicrobial or antifungal agent required to kill a bacterium or fungus. MBC/MFC experiments are conducted after MIC experiments on the sample concentrations that showed complete inhibition of bacterial and fungal growth. An aliquot (10 μL) was taken from each well with no growth for each sample and spotted onto an LB agar plate in triplicates. The plates were incubated at 37 °C overnight. All concentrations for each strain showed growth, indicating that the polysulfides are inhibitory rather than bactericidal/fungicidal. This provides further insight for their activity, suggesting that they prevent the bacterium or fungus from growing rather than causing cell death.

Conclusion

This chapter explored the antimicrobial and antifungal activity of water-soluble poly(trisulfides). Both photochemically and electrochemically synthesised **Na-poly-3** showed similar activity, while the monomer **Na-3** showed slightly less activity against the strains investigated compared to the polymer. **Na-poly-3** had a MIC for *S. aureus* at $\leq 256 \mu\text{g/mL}$, while **Na-3** had a MIC for *S. aureus* at $512 \mu\text{g/mL}$. Both **Na-poly-3** and **Na-3** showed the reduction in the growth of *E. coli* but did not exhibit a MIC for *E. coli* at concentrations $\leq 512 \mu\text{g/mL}$. It was proposed that **Na-poly-3** and **Na-3** are more biocidal against *S. aureus* due to its singular cell wall compared to *E. coli*, which has a cell wall and an outer membrane. **Na-poly-3** had a MIC for *C. albicans* at $\leq 16 \mu\text{g/mL}$ while **Na-3** had a MIC for *C. albicans* at $256 \mu\text{g/mL}$. These low MIC values are promising for new fungicides, warranting further investigation.

Against all strains tested, **Na-poly-3** and **Na-3** did not lead to cell death, but rather inhibited the growth of the bacteria and fungi. This study demonstrates, for the first time, the relationship between dosage and activity for high sulfur content polymers using water-soluble poly(trisulfides) as biocides. Additionally, it is the first investigation of a high sulfur content polymer with a known stereochemistry and sulfur rank, examining its activity against bacteria and fungi. This important step advances our understanding of the mechanism of action and represents a significant milestone in this area of research, encouraging further study. Future research will look to investigating why the polymer is more active than the monomer. Poly(trisulfides) will also be investigated as antifungal and antimicrobial coatings or slow-release mechanism for medicinal and agricultural applications.

Experimental details

General materials, cultures and media

Luria–Bertani broth (Miller), LB agar, Mueller Hinton Broth and phosphate buffered saline (PBS) were purchased from Sigma-Aldrich. Methicillin-resistant *S. aureus* strain USA300, *E. coli* strain K12, *C. albicans* strain CAF 2.1 were cultured from frozen stocks stored at the University of Liverpool. **Poly-3** synthesised electrochemically under conditions and purification described chapter 2 was used. **Poly-3** synthesised photochemically in continuous flow under conditions and purification described chapter 3 was used. Monomer **3** synthesised under conditions and purification described chapter 2 was used.

Bacteria Preparation, Storage, and Enumeration

Glycerol stocks of *S. aureus* strain USA300, *E. coli* strain K12, and *C. albicans* strain CAF 2.1 were stored at $-80\text{ }^{\circ}\text{C}$ for long-term storage. For experimental use, frozen glycerol stocks of *S. aureus*, *E. coli*, and *C. albicans* were defrosted and streaked onto LB agar plates, which were then incubated overnight at $37\text{ }^{\circ}\text{C}$. Bacterial cultures were prepared by swabbing 3-5 colonies into 10 mL of LB broth, followed by overnight incubation at $37\text{ }^{\circ}\text{C}$ with agitation. Colony forming units (CFUs) were enumerated by serially diluting the cultures in PBS onto LB agar, using the Miles and Misra method. CFU/cm^2 and CFU/mL were calculated using the following equation:

$$\text{CFU}/\text{mL} = (\text{No. of colonies} \times \text{total dilution factor})/\text{volume of culture plated in mL}$$

Determination of minimum inhibitory concentration

Susceptibility to biocides was evaluated by determination of minimum inhibitory concentrations (MICs) using a 96-well plate and were assessed according to the European Committee on Antimicrobial Susceptibility Testing (EUCAST) guidelines, for an incubation period of 20 hours against *S. aureus* strain USA300 and *E. coli* strain K12, in LB medium and *C. albicans* strain CAF 2.1, in MHI medium. An initial OD_{600} of 0.1 ($\sim 5 \times 10^5$ CFU/mL) was used for the cell cultures prior to incubation. The OD_{600} was measured using a FLUOstar Omega microplate reader.

Statistical analysis

Statistical analysis was conducted by performing two-way ANOVAs, coupled with Dunnett's correction for multiple comparisons, using GraphPad Prism.

Minimum inhibitory concentration

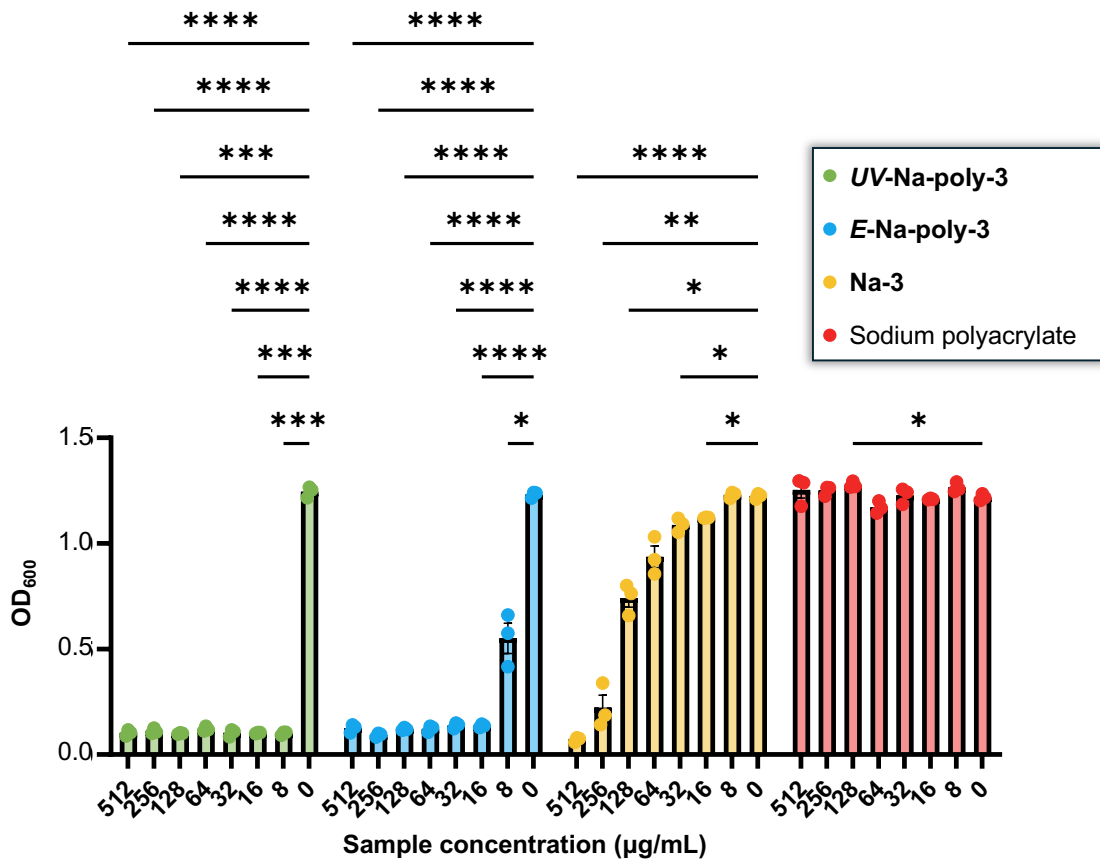


Figure S5.1: Absorbance of *Staphylococcus aureus* at 600 nm, in the presence of *UV-Na-poly-3*, *E-Na-poly-3*, *Na-3*, and sodium polyacrylate at 512 µg/mL, 256 µg/mL, 16 µg/mL, 8 µg/mL, and 0 µg/mL (blank) during a 20-hour incubation period. Data represents the mean of three biological replicates (n = 3) and error bars show standard error of the mean. *p ≤ 0.05, **p ≤ 0.01, ***p ≤ 0.001, ****p ≤ 0.0001.

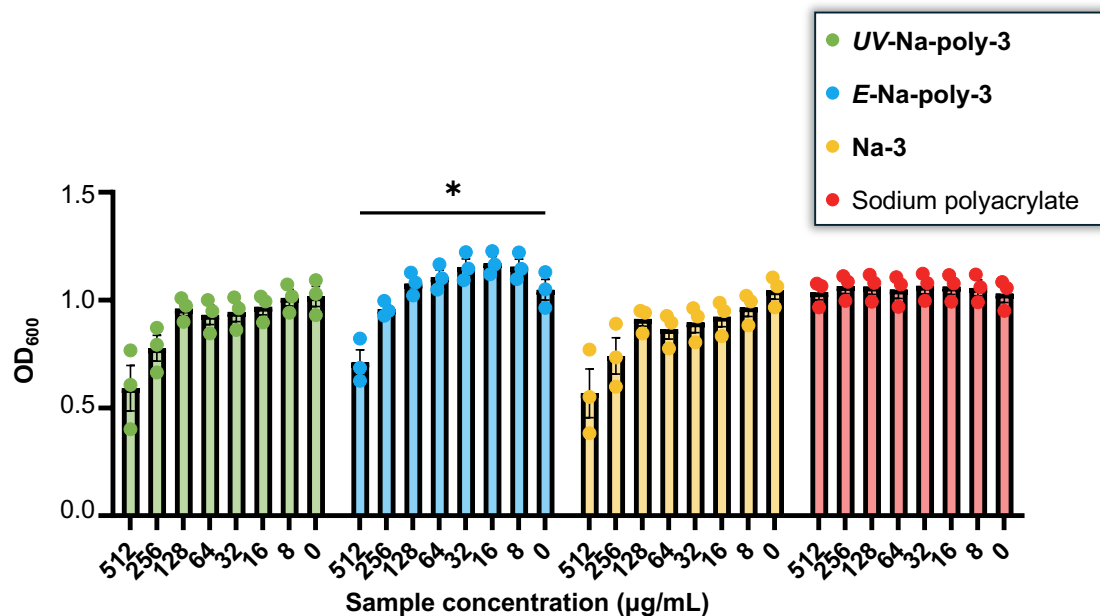


Figure S5.2: Absorbance of *Escherichia coli* at 600 nm, in the presence of *UV-Na-poly-3*, *E-Na-poly-3*, *Na-3*, and sodium polyacrylate at 512 µg/mL, 256 µg/mL, and 0 µg/mL (blank) during a 20-hour incubation period. Data represents the mean of three biological replicates (n = 3) and error bars show standard error of the mean. *p ≤ 0.05.

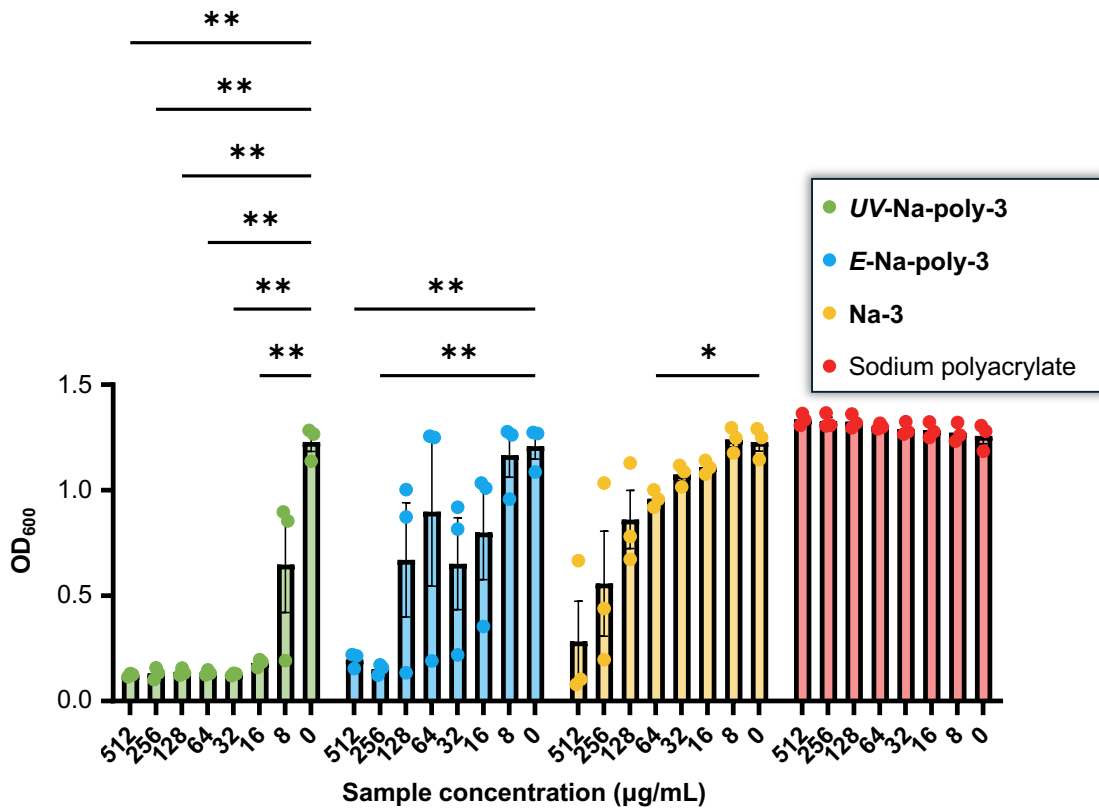


Figure S5.3: Absorbance of *Candida albicans* at 600 nm, in the presence of *UV-Na-poly-3*, *E-Na-poly-3*, *Na-3*, and sodium polyacrylate at 512 µg/mL, 256 µg/mL, 16 µg/mL, 8 µg/mL, and 0 µg/mL (blank) during a 20-hour incubation period. Data represents the mean of three biological replicates (n = 3) and error bars show standard error of the mean. *p ≤ 0.05, **p ≤ 0.01, ***p ≤ 0.001, ****p ≤ 0.0001.

References

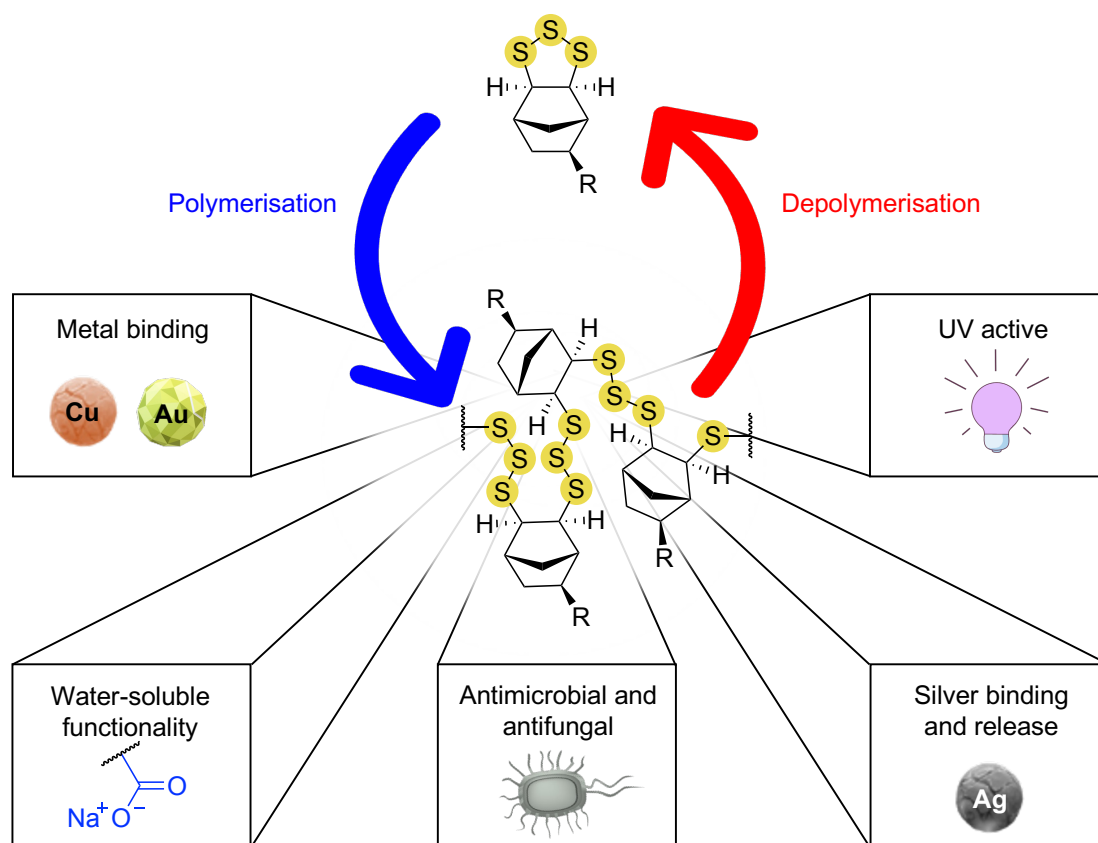
- [1] S. Lindahl, M. Xian, *Current Opinion in Chemical Biology* **2023**, *75*, 102325.
- [2] C. D. Vo, G. Kilcher, N. Tirelli, *Macromolecular Rapid Communications* **2009**, *30*, 299-315.
- [3] B. B. Petrovska, S. Cekovska, *Pharmacognosy reviews* **2010**, *4*, 106.
- [4] M. Ikeda, Y. Ishima, V. T. Chuang, M. Sakai, H. Osafune, H. Ando, T. Shimizu, K. Okuhira, H. Watanabe, T. Maruyama, *Molecules* **2019**, *24*, 1689.
- [5] A. A. Cluntun, M. J. Lukey, R. A. Cerione, J. W. Locasale, *Trends in cancer* **2017**, *3*, 169-180.
- [6] B. Sun, C. Luo, H. Yu, X. Zhang, Q. Chen, W. Yang, M. Wang, Q. Kan, H. Zhang, Y. Wang, *Nano letters* **2018**, *18*, 3643-3650.
- [7] Y. Yang, B. Sun, S. Zuo, X. Li, S. Zhou, L. Li, C. Luo, H. Liu, M. Cheng, Y. Wang, *Science advances* **2020**, *6*, eabc1725.
- [8] Z. Deng, A. Hoefling, P. Théato, K. Lienkamp, *Macromolecular Chemistry and Physics* **2018**, *219*, 1700497.
- [9] J. A. Smith, R. Mulhall, S. Goodman, G. Fleming, H. Allison, R. Raval, T. Hasell, *ACS Omega* **2020**, *5*, 5229-5234.
- [10] R. A. Dop, D. R. Neill, T. Hasell, *Biomacromolecules* **2021**, *22*, 5223-5233.
- [11] R. L. Upton, R. A. Dop, E. Sadler, A. M. Lunt, D. R. Neill, T. Hasell, C. R. Crick, *Journal of Materials Chemistry B* **2022**, *10*, 4153-4162.
- [12] H. Shen, H. Qiao, H. Zhang, *Chemical Engineering Journal* **2022**, *450*, 137905.
- [13] D. W. Denning, *European Journal of Hospital Pharmacy* **2022**, *29*, 109-112.
- [14] D. Limmathurotsakul, S. Dunachie, K. Fukuda, N. A. Feasey, I. N. Okeke, A. H. Holmes, C. E. Moore, C. Dolecek, H. R. van Doorn, N. Shetty, *The Lancet infectious diseases* **2019**, *19*, e392-e398.
- [15] M. E. De Kraker, P. G. Davey, H. Grundmann, B. S. Group, *PLoS medicine* **2011**, *8*, e1001104.
- [16] G. D. Brown, D. W. Denning, N. A. Gow, S. M. Levitz, M. G. Netea, T. C. White, *Science translational medicine* **2012**, *4*, 165rv113-165rv113.
- [17] D. R. Nair, J. Chen, J. M. Monteiro, M. Josten, M. G. Pinho, H.-G. Sahl, J. Wu, A. Cheung, *The Journal of Antibiotics* **2017**, *70*, 1009-1019.
- [18] J. Cubero-Cardoso, P. Gómez - Villegas, M. Santos-Martín, A. Sayago, Á. Fernández-Recamales, R. Fernández de Villarán, A. A. Cuadri, J. E. Martín-Alfonso, R. Borja, F. G. Feroso, R. León, J. Urbano, *Polymer Testing* **2022**, *109*, 107546.
- [19] I. Liaqat, A. N. Sabri, *Curr Microbiol* **2008**, *57*, 340-347.

- [20] A. Naeini, A. R. Khosravi, M. Chitsaz, H. Shokri, M. Kamlnejad, *Journal de Mycologie Médicale* **2009**, *19*, 168-172.
- [21] U. Münchberg, A. Anwar, S. Mecklenburg, C. Jacob, *Organic & biomolecular chemistry* **2007**, *5*, 1505-1518.
- [22] S.-m. Tsao, M.-c. Yin, *Journal of antimicrobial chemotherapy* **2001**, *47*, 665-670.
- [23] S. Ankri, D. Mirelman, *Microbes and infection* **1999**, *1*, 125-129.
- [24] T. Ida, T. Sawa, H. Ihara, Y. Tsuchiya, Y. Watanabe, Y. Kumagai, M. Suematsu, H. Motohashi, S. Fujii, T. Matsunaga, *Proceedings of the National Academy of Sciences* **2014**, *111*, 7606-7611.
- [25] C. W. S. Yeung, M. H. Periyah, J. Y. Q. Teo, E. T. L. Goh, P. L. Chee, W. W. Loh, X. J. Loh, R. Lakshminarayanan, J. Y. C. Lim, *Macromolecules* **2023**, *56*, 815-823.

Chapter 6

Conclusions and future work

This chapter concludes the research highlights from this thesis. Future work and applications in functional films, photolithography, adhesives and cathodes in lithium-sulfur batteries are also discussed.



Conclusions

The aim of this thesis was the development of well-defined polysulfides, a challenge that hampers certain applications of inverse vulcanisation. Specifically, this thesis aimed to develop polysulfides with a known sulfur rank, C–S stereochemistry, and structure. Another current issue of polysulfide synthesis through inverse vulcanisation are the dangers associated with the high-temperature method, which become more pronounced as the process is upscaled. This thesis aimed to develop methods of polysulfide synthesis which are safer and potentially scalable. The following summary illustrates ways in which these aims were achieved.

Chapter 2 described a novel method for the electrochemically induced ring-opening polymerisation of 1,2,3-trithiolane monomers. A library of 1,2,3-trithiolane monomers were synthesised through the reaction of elemental sulfur with the strained alkene bond on norbornene derivatives. Key monomers synthesised include a norbornene carboxylic acid 1,2,3-trithiolane and dicyclopentadiene 1,2,3-trithiolane, whose structures were confirmed unambiguously by single crystal X-ray diffraction. Having well-defined monomers with known C–S stereochemistry was important for the synthesis of well-defined polymers. Notably, the C–S bonds were not cleaved during this polymerisation, preserving this stereochemistry—an important contrast to inverse vulcanisation in which the C–S bonds are formed without stereochemical control. Several electrochemical characterisation techniques, including cyclic voltammetry and chronoamperometry, were conducted on the monomers to understand their redox chemistry. It was shown that the monomers undergo reduction at -2.2 V versus Fc/Fc^+ to form a radical anion intermediate that undergoes ring-opening. The ring-opened monomer can then attack another monomer, leading to polymerisation. Reductive degradation and analysis of a dicyclopentadiene poly(trisulfide) was conducted, revealing the alkene on the dicyclopentadiene 1,2,3-trithiolane remains intact during the polymerisation process. This demonstrated the polymerisation technique is chemoselective for the reduction of 1,2,3-trithiolane monomers and results in a linear polymer structure, which is advantageous for polymer solubility, characterisation, and processing. Kinetic and computational studies revealed the process proceeds rapidly via reduction to a radical anion, which then undergoes ring-opening polymerisation. An interesting computational finding demonstrated that the process has a unique ‘self-correction’ mechanism resulting in the selective formation of trisulfide links in the polymer backbone. Achieving a known sulfur rank of three is a milestone in polysulfide synthesis, as there have been very few reports of high sulfur content polymers with a known sulfur rank of three. Polysulfides with a known sulfur rank are valuable as they provide a mechanism to better understand the effects sulfur rank on polymer properties.

A key poly(trisulfide) containing a carboxylic acid functional group was shown to be water soluble via the addition of 1 molar equivalent of NaOH per acid group. This is the first time a water soluble, linear, high sulfur content polymer has been demonstrated in the literature, providing opportunities for enhanced applications in aqueous media in areas such as metal binding and biomedical fields. Another key poly(trisulfide) containing a symmetric norbornane backbone was shown to readily undergo thermal depolymerisation back to its monomer. Simple distillation was used to recover the monomer in high yield and purity. This is the first example of a fully recyclable high sulfur content polymer, which is an important issue to consider in the synthesis of new materials. This innovative method of polysulfide synthesis meets the aims of this thesis in making well-defined high sulfur content polymers at room temperature, with electricity being the sole energy source.

Chapter 3 demonstrated the scalability of poly(trisulfide) synthesis through the electrochemical ring-opening methods described in Chapter 2. By first investigating alternative cost-effective electrode materials, it was found that carbon felt was an excellent choice. Three progressively larger electrochemical cells were designed to optimise the multi-gram synthesis of poly(trisulfides). This approach addressed several challenges, including adjustment of electrode size, monomer solubility and mass transfer issues. As a result, the final electrochemical reactor successfully produced poly(trisulfides) on a scale 125 times larger than previously achieved. Additionally, the electrolyte required for the synthesis was shown to be recoverable, enhancing both the economics and sustainability of the process.

Several high value applications were explored for the first time using these poly(trisulfides). Notably, the poly(trisulfides) demonstrated effective gold recovery from aqueous solutions, offering a practical gold sorbent relevant to the mining and electronic waste recycling industries. Impressively, the gold bound poly(trisulfide) could undergo thermal depolymerisation, allowing the recovery of both the monomer and gold. This marked the first example of a recyclable polysulfide used in gold recovery applications. Furthermore, poly(trisulfides) were shown to bind and release silver, presenting opportunities for dual-action biocides. The water-soluble carboxylate poly(trisulfide) exhibited enhanced copper-binding capabilities and could precipitate out of solution after binding, revealing its potential as a flocculant for copper binding. Additionally, the thermal crosslinking of linear dicyclopentadiene poly(trisulfide) was explored to produce a material with increased thermal stability and solvent resistance over the corresponding linear polysulfide. The research presented in this chapter validates the feasibility for scaling up poly(trisulfide) synthesis through the electrochemical ring-opening of 1,2,3-trithiolane monomers while highlighting poly(trisulfides) versatility and potential for high-value applications. These findings contribute

significantly to the field of polysulfide synthesis, opening avenues for the safe and sustainable synthesis and applications of sulfur polymers.

Chapter 4 explored the synthesis of poly(trisulfides) through the photochemically induced ring-opening polymerisation of 1,2,3-trithiolane monomers. Initial batch reactions resulted in the rapid cleavage of long poly(trisulfide) chains, producing oligomeric material. By controlling the amount of light exposure to the solution through use of a continuous flow reactor, the molecular weight of the poly(trisulfides) could be easily controlled. By adjusting irradiation time, wavelength, light intensity, and monomer concentration, a range of polymer molecular weights—including high molecular weight poly(trisulfides)—was achieved. It was proposed that the mechanism proceeds via radical ring-opening polymerisation, which is different from the electrochemical mechanism. Despite this difference, the photochemically produced poly(trisulfide) was shown to consist of primarily three sulfur molecules per repeating unit using Raman analysis. Furthermore, a norbornane based poly(trisulfide) was shown to be thermally recyclable back to its monomer units in high yields, providing further evidence of their linear structure. The photochemical synthesis method, conducted at room temperature without the need for an inert atmosphere, resulted in mild, safe, and practical reaction conditions. Poly(trisulfide) synthesis in continuous flow was shown to have the potential for upscaled polymer production, which would be necessary when used in future applications. A particularly exciting discovery was the rapid photodegradation of the poly(trisulfides) upon re-exposure to light irradiation, suggesting new applications for photodegradable high sulfur content polymers. Through the re-discovery and adaptation of photochemical poly(trisulfide) synthesis, linear poly(trisulfides) were produced under mild reaction conditions. Not only does this method allow for the precise control of poly(trisulfide) molecular weight, but also introduced the possibility of creating photodegradable sulfur polymers, opening up new avenues for their applications.

Chapter 5 investigated the antimicrobial and antifungal properties of water-soluble poly(trisulfides). Both **Na-poly-3**, synthesised via photochemical and electrochemical methods, demonstrated similar effectiveness, whereas the monomer **Na-3** was slightly less active. **Na-poly-3** showed a minimum inhibitory concentration (MIC) of ≤ 256 $\mu\text{g/mL}$ against *S. aureus*, compared to 512 $\mu\text{g/mL}$ for **Na-3**. Both **Na-poly-3** and **Na-3** inhibited *E. coli* growth but did not show an MIC at concentrations ≤ 512 $\mu\text{g/mL}$. **Na-poly-3** and **Na-3** had greater biocidal activity against *S. aureus* compared to *E. coli*, likely due to *S. aureus* having a simpler cell wall compared to *E. coli*'s dual-layer structure. For *C. albicans*, **Na-poly-3** had a notably low MIC of ≤ 16 $\mu\text{g/mL}$, while **Na-3** had an MIC of 256 $\mu\text{g/mL}$, highlighting **Na-poly-3**'s potential as a fungicide.

Future work

The research presented in this thesis has made significant strides towards developing safe methods for polysulfide synthesis and producing recyclable, linear poly(trisulfides) with known structure, sulfur rank, and C–S stereochemistry. The primary aims were to enable the safe, multi-gram scale synthesis of polysulfides and to produce well-defined polysulfides to better understand, control, and optimise their properties. This was demonstrated through the synthesis of specific poly(trisulfides) with functionalities such as water solubility, linear structure, and sites for post-polymerisation modifications that aided in their applications.

With the successful development and validation of scalable synthesis methods for well-defined poly(trisulfides), further applications for these materials are being explored. These applications target areas where understanding and controlling the material's structure is essential, such as antimicrobial and antifungal materials and cathode materials for lithium-sulfur batteries. Currently, polysulfides are used in these applications, but their poorly defined structure limits the understanding of the underlying mechanisms of operation. By using linear poly(trisulfides), we can gain a deeper insight into these mechanisms.

Future experiments will be conducted to further control the photochemical synthesis of poly(trisulfides). This work will focus on reactor designs that allow the polymer to precipitate out of solution, potentially protecting it from further photodegradation. One reactor design of interest involves pulsed light irradiation at different frequencies to initiate polymerisation but reduce photodegradation.

A novel area of application introduced in this thesis are photodegradable poly(trisulfides). The photodegradation of poly(trisulfides) will be further explored in applications such as polymer recycling, controlled release of cargo, and in the selective photolithography of polysulfide films (Figure 6.1 A). Another application for the polys(trisulfide) is as thermally recyclable adhesive (Figure 6.1 B). These applications are already being investigated by our lab and collaborators. Continued research will explore new applications for poly(trisulfides), expanding their potential uses even further.

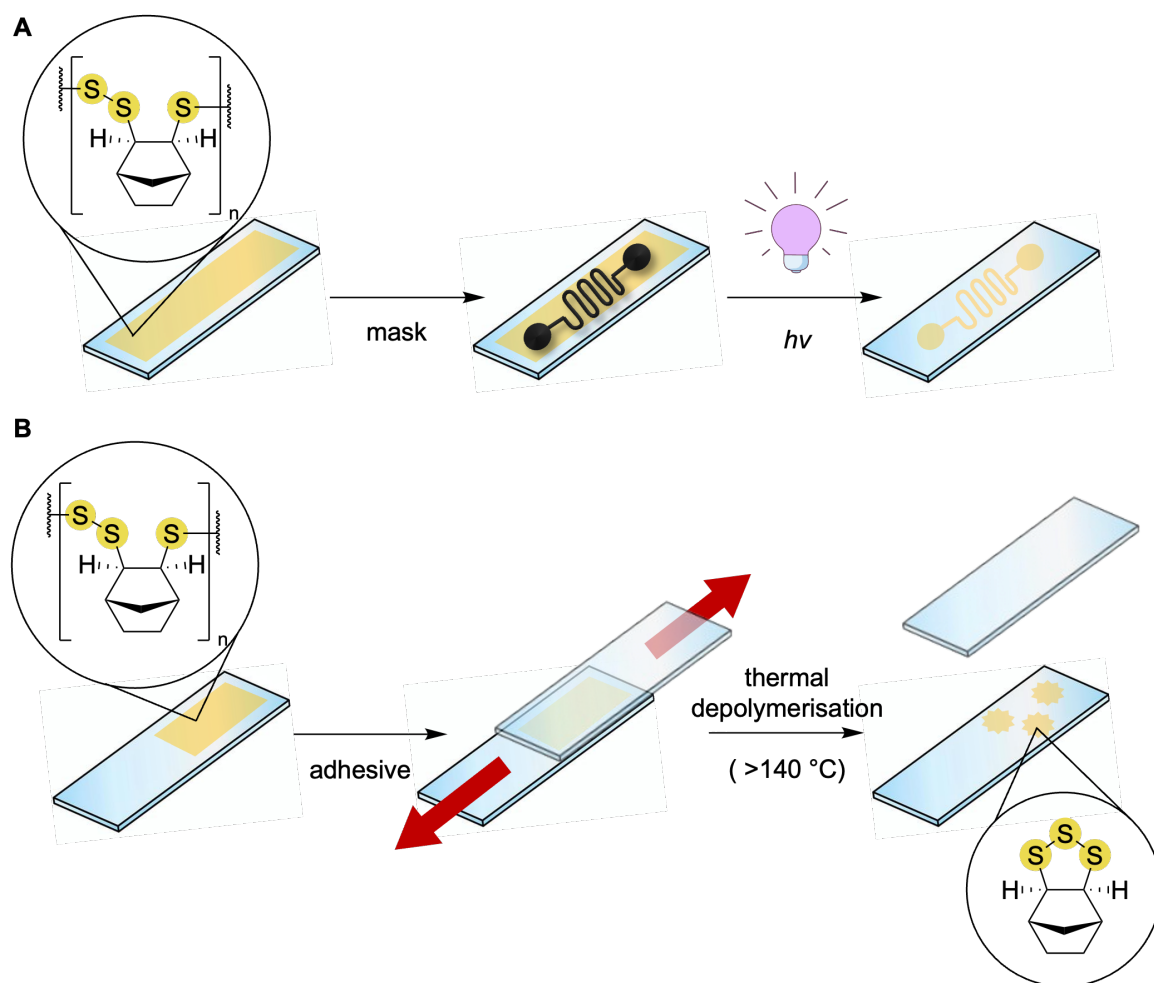


Figure 6.1: (A) Photoetching a poly(trisulfide) film. (B) Thermally recyclable poly(trisulfide) adhesive.